“OVIDIUS” UNIVERSITY OF CONSTANTZA
UNIVERSITATEA „OVIDIUS” CONSTANȚA

“OVIDIUS” UNIVERSITY ANNALS - CONSTANTZA
Year XII
(2010)

Series: CIVIL ENGINEERING

ANALELE UNIVERSITĂȚII „OVIDIUS”CONSTANȚA
ANUL XII
(2010)

Seria: CONSTRUCȚII

Ovidius University Press
2010

"OVIDIUS" UNIVERSITY ANNALS - CONSTANTZA
SERIES: CIVIL ENGINEERING
ANALELE UNIVERSITĂȚII „OVIDIUS" CONSTANȚA
SERIA: CONSTRUCȚII

Mail address: "OVIDIUS" University, Faculty of Civil Engineering,
124, Mamaia Blvd., 900527, RO., Constantza, Romania
E-mail:

ORDERING INFORMATION

The journal may be obtained by ordering at the "OVIDIUS" University, or on exchange basis with similar romanian or foreign institutions.
Revista poate fi procurată prin comandă la Universitatea „OVIDIUS", sau prin schimb de publicații cu instituții similare din țară și străinătate.
124, Mamaia Blvd., 900527, RO., Constantza, Romania

ISSN 1584-5990
© 2000 Ovidius University Press. All rights reserved.

TABLE OF CONTENTS

ISSN-1584-5990

Section IV. Hydraulics: theory and applications

Section V. Hydraulic Constructions

Section VI. Impact of climate change in water resources availability and crop productivity

Section VII. Integrated management of water and land resources

Section VIII. Irrigation and drainage

Section IX. Surface and groundwater hydrology

Section X. Civil engineering

Ovidius University Annals Series: Civil Engineering Volume 1, Issue 12, June 2010

A segmentation procedure to detect changes in hydro-meteorological time series

Pierre Hubert
UMR Sisyphe, Université P. & M. Curie, Paris, France
IAHS Secretary General

A possible cause of nonstationarity in time series is the existence of some abrupt modification of their statistical parameters, and especially of a sudden change of the mean. Series with such a change exhibit a strong temporal persistence, with high values of the Hurst coefficient, but with poor possibilities to fit any effective autoregressive model. Some classical tests enable us to find a unique possible change point of the mean and then to split the original nonstationary into two subseries. To go further and to explore multiple singularity models, a segmentation procedure of time series has been designed and implemented. This procedure yields the optimal (from a least squares point of view) partition of the original series into as many subseries as possible, all differences between the means of two contiguous segments remaining simultaneously significant. The segmentation procedure has been applied to many time series in different parts of the World and it appears as a useful and robust tool to detect changes in time series and to model in a simple way past hydro-climatological variability. A few applications, especially to semi-arid West Africa rainfall and discharge time series, will be presented.

ISSN-1584-5990

Scaling vs. non-stationarity in the water cycle: From the quest for finding underlying mechanisms to better estimators

Alin A. Carsteanu(1), Luis G. Escandon-Alcazar(2), Govindan T.E.(1), Jorge J. Castro(2)
(1) ESFM - IPN, Mexico City, Mexico
(2) Cinvestav - IPN, Mexico City, Mexico

Abstract:

Non-stationarity in time series is scale-related in an essential way, when there is no a-priori analytical description of the underlying process. Multifractal scaling, on the other hand, offers a consistent framework, compatible with prime principles, for the analysis of hydro-meteorological time series, and its phenomenological existence has been convincingly shown over the last few decades. However, the scaling behavior in hydro-meteorological time series reaches far beyond the scales where it can be explained by a straightforward frozen-field paradigm to G.I.

Taylor's hypothesis. The explanation for Taylor's transposition of turbulent statistics from the spatial to the temporal domain (and the other way around) is usually stated in terms of smaller features being advected by a large-scale transport velocity, while intrinsic temporal velocity fluctuations are slower than the corresponding inertial terms.

This phenomenology, however, can obviously not be extended beyond planetary spatial scales. Therefore we propose and analyze a 4-D space-time multifractal model, using different estimating tools, from classical scaling analysis to breakdown coefficients and run lengths.

ISSN-1584-5990

SECTION I

COASTAL ENGINEERING

Research on cohesive sediment Erodibility by flow Overview and application

Mohamed Amine BOUKHEMACHA, Khoudir MEZOUAR, Romeo CIORTAN

***Abstract*: Erosion of cohesive sediment by flow is a very complicated phenomenon occurring worldwide. Understanding and modeling of the erosion process are important for many issues such as the breaching of embankments or riverbank stability. In the last few decades, numerous studies have been done on the erosion of cohesive sediment by flow. Nevertheless, the factors affecting the erosion resistance of cohesive sediment are still not fully understood. In this paper an overview of the studies on the erosion susceptibility, erosion resistance, erosion threshold and the erosion rate of cohesive sediment by flow is presented. As application, a comparative study will be done using the experimental data of 9 soils. It was observed PSD based methods can be used to assess soil susceptibility to erosion. And even with the differences observed between the calculated values of the critical shear stress, the qualitative classification of soil erosion gave the same results.**

***Keywords:* Cohesive materials; erodibility; critical shear stress; soil erosion coefficient**

1. INTRODUCTION

Generally, sediment can be classified as cohesive and non-cohesive. The erodibility of non- cohesive sediment is mainly a function of the physical properties of the particles such as the size, shape, density, porosity and fall velocity; whereas the erosion resistance of cohesive sediment depends heavily on the strength of the cohesive bond binding the particles which makes the situation much more complex.

Internal erosion is one of the main causes of failure of hydraulic works (dams, dikes), and the topic of many ongoing research. The complexity of this phenomenon lies in its invisibility, since its initiation and continuation occur inside the structure. Knowing the sensitivity and speed with which soil can erode is a factor that could help in the detection and prediction of internal erosion.

2. INTERNAL EROSION

The internal erosion is a phenomenon that differs from surface erosion. However, its quantification is appreciated by a similar law. The erosion rate can be determined by an equation that can be written in two forms (Eq. 1): mass and volume.

Mohamed Amine BOUKHEMACHA, Technical University of Civil Engineering of Bucharest, Romania
Khoudir MEZOUAR, S.C. IPTANA S.A. Bucharest, Romania
Romeo CIORTAN, S.C. IPTANA S.A. Bucharest, Romania

ISSN-1584-5990

$$\dot{m} = C_e(\tau_t - \tau_c) \quad \text{ou :} \quad \dot{\varepsilon} = k_d(\tau_t - \tau_c) \quad (1)$$

Where, $\dot{m}$ and ($\dot{\varepsilon}$): erosion rate in the mass (volume) equation respectively, τ_t : hydraulic shear stress, τ_c : critical shear stress, C_e and (k_d) : coefficient of soil erosion for mass (volume) equation respectively. These equations apply in the case ($\tau_t > \tau_c$), if not the erosion rate is zero. These two equations are similar given the relationship between the two coefficients of soil erosion (Eq. 2). ρ_d : dry density of the soil.

$$C_e = \rho_d . k_d \quad (2)$$

2.1 Critical shear stress

The hydraulic shear stress is the stress applied on the soil surface under the flow action. The critical shear stress is the minimal hydraulic shear stress required to initiate erosion. Fell and Wan (2005) reported that in practice it is difficult to determine the initial shear constraint for a particular soil. Including the determination by laboratory tests as the *'hole erosion test'* by varying the hydraulic charge is expensive, and even then, this stress is not well defined.

Several studies have focused on finding a relationship between the critical shear stress and other soil properties (Dunn, 1959; Smerdon and Beasley 1961; Lyle and Smerdon, 1965; Reddi and Bonal, 1997; Torri et al., 1987, Mitchener and Torfs 1996; Julian and Torres 2006). In general, many formulas listed in Table 1, simple or complicated in the form, differ remarkably from one to another, and are all empirical with poor universality. Many of the formulas have only been tested against the experimental data of the authors themselves, some even without testing.

Table. 1 Summary of formulas of critical shear stress for cohesive sediment erosion

Author	Form of formula	Notation	Testing data	Limitations
Dunn (1959)	$\tau_c = 0.20 + \frac{(S_v + 180)}{1000}\tan(30 + 1.73 I_p)$ $\tau_c = 0.02 + \frac{(S_v + 180)}{1000}\tan(0.06 U_f)$ $\tau_c = 0.001(S_v + 180)\tan(30 + 1.73 I_p)$	S_v : Shear strength (psf), I_p : Plasticity index U_f : Percent of clay particles less than 0.06mm by weight		*Ip* is useful for predicting soil erodabiliy for soils with *Ip* between 5 to 16
Smerdon and Beasley (1961)	$\tau_c = 0.163(I_p)^{0.84}$ $\tau_c = 0.493 x 10^{0.0182 c'_p}$ $\tau_c = 10.2(D_r)^{-0.63}$ $\tau_c = 3.54 * 10^{-28.1 D_{50}}$	c'_p : percentage of clay by weight (%); D_{50} : mean particle size (m); D_r : dispersion ratio	Flume test, cohesive Missouri soil samples	

Mitchener and Torfs (1996)	$\tau_c = 0.015(\rho_s - 1000)^{0.73}$	ρ_s : sediment density	Artificial mixture of mud and sand	
Julian and Torres 2006	$\tau_c = 0.1 + 0.01779c_p + 0.0028(c_p)^2 - 2.34*10^{-5}(c_p)^3$	c_p : percentage of silt-clay particles less than 0.063mm by weight	Field measurement in the Sand River	
Cao and Du (1986)	$\tau_c = 0.7(\rho_d)^5$	ρ_d :sediment dry density	flume test, remoulded samples from the Yellow River, D_{50}=0.0039 mm	
Thorn and Parsons (1980)	$\tau_c = 5.42*10^{-6}(\rho_d)^{2.28}$		Remoulded samples from Grangemouth, Brisbane and Belawan	
Torri et al., (1987)	$\tau_c = \beta S_v$	β : coefficient, varying form 10^{-4} to $5*10^{-4}$	Laboratory flume on sandy loam, silty clay, clay	good results for soils with S_v less than 20 kPa
Briaud et al. (2001)	$\tau_c = D_{50}$	τ_c (Pa) D_{50} (mm)		Soils with D_{50} >0.1mm

2.2 Coefficient of soil erosion

Although simple relations between k_d and soil properties are not available (Hanson and Temple, 2002), Hanson and Simon (2001) proposed an empirical method for estimating *kd* if τ_c is known. They conducted 83 jet tests to determine τ_c and k_d for stream beds of highly erodible loess in the midwestern U.S. The beds were typically 50% to 80% silt-sized material with a τ_c range of 0.0 to 400 Pa and a k_d range of 0.001 to 3.75 cm3/N·s. The study found wide variation in the resistance parameters from the jet test results, but detected an inverse relation between τ_c and k_d, where k_d (cm^3/(N.s)) could be estimated as a function of τ_c (Pa):

$$k_d = 0.2.\tau_c^{-.05} \quad (3)$$

2.3 Soil erodibility

The assessment of soil erodibility can be done in terms of erosion speed using soil classifications from Wan and Fell (2004), Hanson and Simon (2001), Hanson (personal communication). Other methods evaluate the soil susceptibility to internal erosion using the PSD curve (Kenney and Lau, 1985; Istomnia, 1957).

Wan and Fell (2004) have proposed a soil classification (Tab. II) in terms of the erosion rate index, I_{HET}, given by (Eq. 4) taking C_e(s/m).

$$I_{HET} = -\log_{10}(C_e) \quad (4)$$

Groupe number	Erosion rate index	Description	Notation
1	<2	Extremely rapid	ED
2	2-3	Very rapid	VD
3	3-4	Moderately rapid	MD
4	4-5	Moderately slow	MS
5	5-6	Very slow	VS
6	>6	Extremely slow	ES

Table. 2 Qualitative terms for a representative erosion rate index (Wan and Fell 2004)

Hanson and Simon (2001) have proposed a quantitative classification of the soil erodibility similar to that proposed by Wan and Fell (2004).

Their classification identifies 5 groups, as it is illustrated in (Fig. 1); it uses soil's k_d and τ_c.

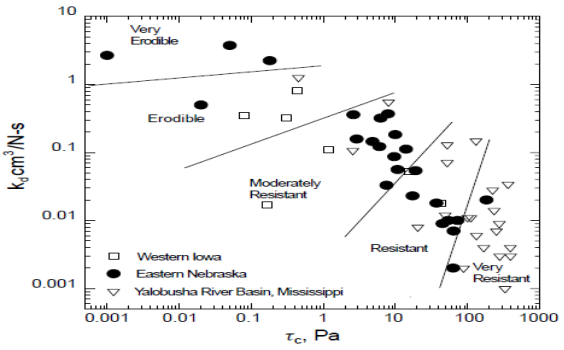

Fig. 1 Classification of soil erodibility for streambank (Hanson and Simon 2001)

Hanson (personal communication), proposed a classification into 6 groups based solely on the values of k_d, (Table 3).

Table. 3 Qualitative terms for a volume coefficient of soil erosion

vk_d (ft/hr/psf)	Description	Notation
>10	Extremely erodible	EE
1-10	Very erodible	VE
0.1-1	Moderately erodible	ME
0.01-0.1	Moderately resistant	MR
0.001-0.01	Very resistant	VR
<0.001	Extremely resistant	ER

Istomnia (1957) based on the particles size distribution (PSD), gave a classification of the soil erodibility based on the ***Uniformity coefficient*** U, given by the ratio D_{60} / D_{10} or D_{60} (D_{30}) particle diameter corresponding to 60% (10%) of passing respectively. Istomnia (1957) has given the following criteria:

- There is no internal erosion if U<10;

- There is a transition condition if $10<U<20$;
- Internal erosion is liable for $U>20$.

Kenney and Lau (1985) suggested a graphical method to assess the susceptibility of a soil to internal erosion based on the shape of the grading curve (Fig. 2). *F* is a masse fraction smaller than, *D* is the particle diameter and *H* is the masse fraction measured between particle size *D* and *4D*. The line $H=1.3D$ is the boundary existing between stable and unstable materials. The material has a high potential of internal erosion when its representing curves intercept with the boundary line.

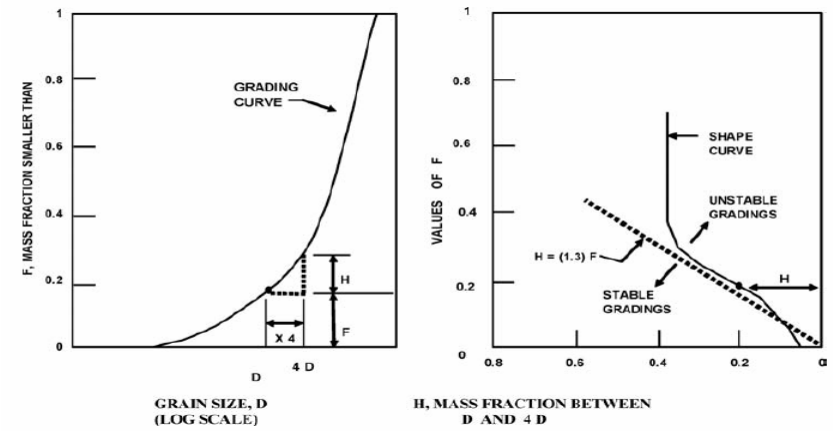

Fig. 2 Method describing the shape of grading curves (Kenney and Lau 1985)

3. Methods and experimental data

Soil erodibility and erosion speed assessments will be conducted on the experimental data of 9 different soils, using some of the various relations seen previously. To assess soil susceptibility to erosion there will be used those methods based on the PSD, and to evaluate soil erosion speed there will be used those applicable methods to evaluate the critical shear stress and then, the coefficient of soil erosion.

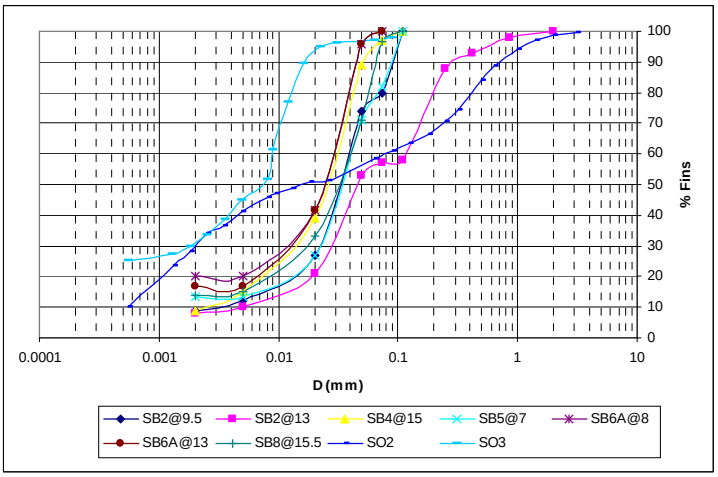

Fig. 3 PSD for the used soils

The available experimental data for the used materials are represented in (Table IV). These soils are fine or with a high fine fraction (clays and silts). The PSD curves of these materials are given in (Fig. 3).

Table. 4 Soils available experimental data

Soils	**SB2 @9.5**	**SB2 @13**	**SB4 @15**	**SB5 @7**	**SB6A @8**	**SB6A @13**	**SB8 @15.5**	**SO2**	**SO3**
USC	CL-ML	CL-ML	ML	ML	ML	CL-ML	CL	CL	CL
w%	14.7		28.9	22.6	25.6	26.5	31.0	18.4	14.0
LL	24.00	27.00	27.00	24.00	32.00	28.00	37.00	35.89	30.73
PI	5.00	6.00	4.00	2.00	7.00	7.00	15.00	24.05	13.89
G_s	2.66	2.65	2.65	2.65		2.69	2.67	2.53	2.65
ρ_d (g/cm 3)	1.59	1.51	1.44			1.55		1.75	1.83
Trovane (KPa)	62.24	59.85	35.91	23.94	47.88	65.84	35.91	88.25	34.32
D_{50} (mm)	0.034	0.044	0.024	0.033	0.023	0.023	0.032	0.018	0.008
D_{60} (mm)	0.049	0.12	0.03	0.04	0.03	0.03	0.04	0.09	0.009
D_{10} (mm)	0.0023	0.0030	0.0050					0.0006	
U	21	40	6					160	

4 RESULTS AND DISCUSSION

4.1 Soil susceptibility to erosion

Using Istomnia (1957) method to assess soil susceptibility to internal erosion, the available values of uniformity coefficient (Tab. IV), indicates that soil sample (SB4@15) is not susceptible to internal erosion, and for the 3 other samples (SB2@0.5, SB2@13 and SO2) internal erosion is liable.

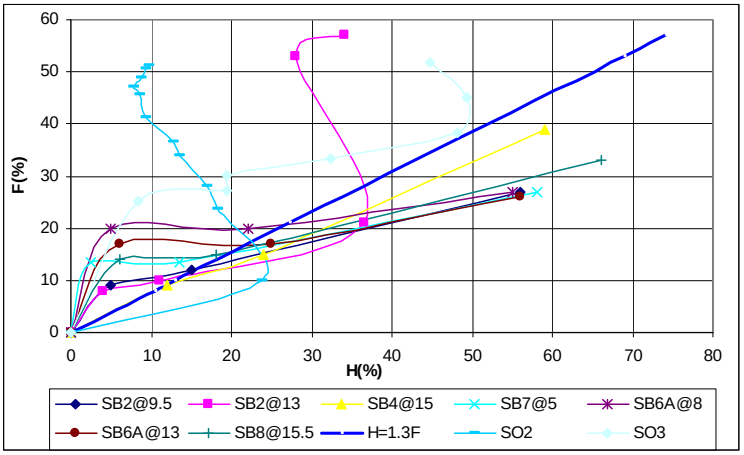

Fig. 4 Resulting grading curves with Kenney and Lau (1985) method

Kenney and Lau (1985) graphical method results are given in (Fig. 4). These results indicates that only soil sample (SB4@15), has not a high potential of internal erosion since its shape grading curves stays in the stable grading zone. The other soil samples have a high potential of internal erosion.

For the available data both methods, Istomnia (1957) and Kenney and Lau (1985), have given similar results, since they both assessed soil sample (SB4@15) as stable for internal erosion. The others samples, were assessed as unstable or with high potential for internal erosion.

Table. 5 Critical shear stress, soil erosion coefficient and erosion speed quantification for the used soils

Method	**Soils**									
	SB2 @9.5	**SB2 @13**	**SB4 @15**	**SB5 @7**	**SB6A @8**	**SB6A @13**	**SB8 @15.5**	**SO2**	**SO3**	
Smerdon and Beasley (1961)	3.53	3.53	3.53	3.53	3.53	3.53	3.53	3.54	3.54	τ_c (Pa)
Mitchener and Torfs (1996)	3.36	3.35	3.35	3.35	-	3.41	3.38	3.17	3.35	
Julian and Torres (2006)	7.42	5.81	7.04	7.45	6.60	6.60	7.40	6.09	6.60	
Dunn (1959)	6.67	4.97	5.34	3.55	6.83	8.70	4.74	6.85	5.39	
Smerdon and Beasley (1961)	1.06E-01	1.06E-01	1.06E-01	1.06E-01	1.06E-01	1.06E-01	1.06E-01	1.06E-01	1.06E-01	k_d (cm3/Ns)
Mitchener and Torfs (1996)	1.09E-01	1.09E-01	1.09E-01	1.09E-01	-	1.08E-01	1.09E-01	1.12E-01	1.09E-01	
Julian and Torres (2006)	7.34E-02	8.30E-02	7.54E-02	7.33E-02	7.79E-02	7.79E-02	7.35E-02	8.10E-02	7.79E-02	
Dunn (1959)	7.75E-02	8.97E-02	8.66E-02	1.06E-01	7.65E-02	6.78E-02	9.19E-02	7.64E-02	8.61E-02	
Smerdon and Beasley (1961)	1.69E-04	1.61E-04	1.53E-04	-	-	1.65E-04	-	1.86E-04	1.95E-04	C_e (m/s)
Mitchener and Torfs (1996)	1.73E-04	1.65E-04	1.57E-04	-	-	1.68E-04	-	1.97E-04	2.00E-04	
Julian and Torres (2006)	1.17E-04	1.25E-04	1.09E-04	-	-	1.21E-04	-	1.42E-04	1.42E-04	
Dunn (1959)	1.23E-04	1.35E-04	1.25E-04	-	-	1.05E-04	-	1.34E-04	1.58E-04	
Smerdon and Beasley (1961)	3.8	3.8	3.8	-	-	3.8	-	3.7	3.7	I_{HET}
Mitchener and Torfs (1996)	3.8	3.8	3.8	-	-	3.8	-	3.7	3.7	
Julian and Torres (2006)	3.9	3.9	4.0	-	-	3.9	-	3.8	3.8	
Dunn (1959)	3.9	3.9	3.9	-	-	4.0	-	3.9	3.8	
Smerdon and Beasley (1961)	MD	MD	MD	-	-	MD	-	MD	MD	Wan & Fell (2004)
Mitchener and Torfs (1996)	MD	MD	MD	-	-	MD	-	MD	MD	
Julian and Torres	MD	MD	MD	-	-	MD	-	MD	MD	

(2006)										
Dunn (1959)	MD	MD	MD	-	-	MD	-	MD	MD	
Smerdon and Beasley (1961)	MR	MR	MR	MR	MR	MR	MR	MR	MR	Hanson & Simon (2001)
Mitchener and Torfs (1996)	MR	MR	MR	MR	-	MR	MR	MR	MR	
Julian and Torres (2006)	MR	MR	MR	MR	MR	MR	MR	MR	MR	
Dunn (1959)	MR	MR	MR	MR	MR	MR	MR	MR	MR	
Smerdon and Beasley (1961)	MR	MR	MR	MR	MR	MR	MR	MR	MR	Hanson (Per. Com.)
Mitchener and Torfs (1996)	MR	MR	MR	MR	-	MR	MR	MR	MR	
Julian and Torres (2006)	MR	MR	MR	MR	MR	MR	MR	MR	MR	
Dunn (1959)	MR	MR	MR	MR	MR	MR	MR	MR	MR	

4.2 Classification of soil erodibility

Soils erodibility will be classified using the 3 previously given classification methods (Wan and Fell, 2004; Hanson and Simon 2001; Hanson personnel communication). And to do so, it is necessary to evaluate the critical shear stress and the soil erosion coefficient. The critical shear stress for each soil will be calculated using applicable methods given in (Tab. I) (Smerdon and Beasley, 1961; Mitchener and Torfs, 1996; Julian and Torres, 2006; Dunn, 1959), and the soil erosion coefficient (for both mass and volume equations) will be calculated using (Eq. 2) and (Eq. 3). The calculated values of critical shear stress and soil erosion coefficients and soil erosion quantitative classification are given in (Tab. V).

The calculated critical shear stresses using Smerdon and Beasley (1961) and Mitchener and Torfs, (1996) methods were very similar, and were smaller than those given by the 2 other methods. Julian and Torres (2006) method gave a critical shear stresses two times higher than those given by the previously mentioned methods. Dunn (1959) method predicted a critical shear stress relatively close to that predicted by Julian and Torres (2006), this result is evident, since both methods uses fine particles weight percent.

For each soil, and even with the differences observed between the calculated values of the critical shear stress, the qualitative classification of soil erosion was the same. All soils were classified as moderately rapid with Wan and Fell classification, moderately resistant with Hanson and Simon method and moderately resistance by Hanson method.

Note that soil (SB4@15) was classified as stable in the erosion susceptibility analyses, but not different from the other soils in the qualitative classification of soil erosion. This is probably due to the fact that the use of PSD only, to evaluate soil erosion parameters is poor or very limited. It was observed by Briaud et al. (2001) that the critical shear stress for soil with D_{50} greater than 0.1 mm is equal to D_{50}.

5. Conclusion

The assessment of soil susceptibility to erosion by the two empirical methods that use PSD gave similar results. This assessment can be used as a global indicator for soil

behavior to flow erosion. For a more detailed appreciation of this behavior, it is necessary to evaluate the critical shear stress and soil erosion coefficient.

To evaluate the critical shear stress for cohesive soils, many and different relations exist. These relations use other soil properties that affect soil erodibility such as plasticity index, clay weight fraction, silt-clay weight fraction, shear strength and mean particle size.

The calculated critical shear stresses using Smerdon and Beasley (1961) and Mitchener and Torfs, (1996) methods were very similar, and were smaller than those given by the 2 other methods. Julian and Torres (2006) method gave a critical shear stresses two times higher than those given by the previously mentioned methods. Dunn (1959) method predicted a critical shear stress relatively close to that by Julian and Torres (2006), this result is evident, since both methods uses fine particles weight percent.

Even with the differences observed between the calculated values of the critical shear stress, the qualitative classification of soil erosion by Wan and Fell (2004), Hanson and Simon (2001) and Hanson (personnel communication) methods was the same.

6. References

[1] Briaud J.L., Ting F.C.K., Chen H.C., Cao Y., Han S.W. and Kwak K.W., 2001. Erosion function apparatus for scour rate predictions. Journal of Geotechnical Engineering and Geoenvironmental Engineering, ASCE, Vol. 127(2), pp. 105-113.

[2] Cao S Y, Du G H. Experimental study on the erosion and deposition of cohesive soil. J Sediment Res (in Chinese), 1986, 4, pp. 73-82

[3] Dunn I.S., 1959. Tractive resistance of cohesive channels. Journal of the Soil Mechanics and Foundations division, ASCE vol. 85(SM3), pp. 1-24.

[4] Fell R. and Wan C.F., 2005. Methods for estimating the probability of failure of embankment dams by internal erosion and piping in the foundation and from embankment to foundation. Research Reppoprt, University of New South Wales, Sydney, Australia, p. 151.

[5] Hanson G.J., and Simon A., 2001. Erodibility of cohesive streambeds in the loess area of the midwestern USA. Hydrological Processes, Vol. 15, pp. 23-38.

[6] Hanson G.J. and Temple D.M., 2002. Performance of bare-earth and vegetated steep channels under long-duration flows. *Trans. ASAE* 45(3),pp. 695-701.

[7] Hanson G.J. and Cook K.R., 2004. Apparatus, test procedures, and analytical methods to measure soil erodibility in situ. Applied Engineering in Agriculture, Vol. 20(4), pp. 455-462.

[8] Istomina V.S., 1957. Filtration Stability of Soils (in Russian), Gostroizdat, Moscow, Leningrad.

[9] Julian J.P. and Torres R., 2006. Hydraulic erosion of cohesive riverbanks. *Geomorphology* 76(1-2), pp. 193-206.

[10] Kenney P.C. and Lau D., 1985. Internal stability of granular filter. Canadian Geotechnical Journal 22, pp. 215–225

[11] Leonard J. and Richard G., 2004. Estimation of runoff critical shear stress for soil érosion from soil shear stress. Catena, Vol. 57, pp. 233-249.

[12] Lyle W.M. and Smerdon E.T., 1965. Relation of Compactation and other soil properties to erosion resistance of soils. Transactions of the ASCE, pp. 419-422.

[12] Mitchener H. and Torfs H., 1996. Erosion of mud/sand mixtures. Coastal Eng, , 29, pp. 1-25

[13] Reddi L.N. and Bonala M.V.S., 1997. Critical shear stress and its relationship with cohesion for sand kaolinite mixtures. Canadian Geotechnical Journal, Vol. 34, pp. 26-33.

[14] Smerdon E.T. and Beasley R.P., 1961. Critical tractive forces in cohesive soils. *Agric. Eng*. 42(1): 26-29.
[15] Thorn M.F.C. and Parsons J.G., 1980. Erosion of cohesive sediments in estuaries: an engineering guide. Proc 3rd Int Symp on Dredging Technology. Bedford: BHRA, 1980, pp. 349-358
[16] Torri D., Sfalanga M. and Chisci G., 1987. Threshold conditions for incipient rilling. Catena. Supplement 8, pp. 97-105.
[17] Wan C.F. and Fell R., 2004. Investigation of rate of erosion of soils in embankment dams. Journal of Geotechnical Engineering and Geoenvironmental Engineering, ASCE, 130(4), pp. 373-380

Southern Romanian Black Sea Cliff Coasts

Glicherie Caraivan[1], Adrian Stanica[1], Costina Fulga[1]

***Abstract* – The Romanian coasts can be divided in two categories: erosion coasts (cliff shores) and accumulative coasts (barrier beaches). The active behavior of the cliffs is due to the action of marine abrasion and slope processes, landslides and gravitational collapses. Cliff shores between Cape Midia and Vama Veche has a complex lithological profile. Silt and clay particles are carried seaward by the rip currents system, while sand and gravel particles are conveyed along the coast. Textural and mineralogical study of these deposits provides relevant information on the source of beach detritic components. Presence of groundwater promotes the release of gravitational landslides. Therefore, complex measures are necessary to stabilize the cliff slopes by re-profiling, drains and walls.**

***Keywords* – cliff shores, coastal erosion, coastal dynamics**

1. INTRODUCTION

One of the most severe environmental problems that have affected the Romanian littoral between Cape Midia and Vama Veche is the coastal erosion, because important parts of the beaches and cliffs are eroding. Coastal protection works were performed several decades ago, but no important efficient coastal protection works have been made during the past two decades. This is why urgent, efficient and integrated coastal protection is required, according to the newest coastal defense concepts. The base of efficient coastal protection works is the knowledge of the current environmental state of the littoral, as well as of the current trends in its dynamics. This issue, between Cape Midia and Vama Veche, is focusing on the geomorphologic, sedimentological and geological description of the cliff coasts.

2. REGIONAL SETTING

The Romanian littoral is situated between the southernmost part of the Chilia Secondary Delta, in the North, and the border with Bulgaria (Vama Veche), in the South. Its length is of about 243 km. The coast can be divided into two sections both from the geological, sedimentological as well as geomorphological point of view. The limit between these two sectors is conventionally located at Cape Midia.
The coastal evolution in both sections is determined by the existing relations among the quantity of sediments available for transport, processing, accumulation and sea energy, in terms of waves and marine currents. The coastal current that redistributes the littoral

[1] National Research and Development Institute for Marine Geology and Geo-ecology (GeoEcoMar), Constanta, Romania**:** bd. Mamaia no. 304, cod 900581, Constanta, Romania, www.geoecomar.ro (gcaraivan@geoecomar.ro; astanica@geoecomar.ro; cfulga@geoecomar.ro)

ISSN-1584-5990

sediments is North-South oriented, parallel to the shore. Each section has its own specific sources of sediments and energetic influence of the sea.

The Northern Unit, with a length about 160 km, is located between the border with Ukraine and Cape Midia. This unit represents the beaches in front of the Danube Delta, consisting of sandy littoral bars that set the limit between the inner part of the delta and the sea or cuts off the former lagoons and sand bars. The main source of sediments is represented by Danube born sediments, redistributed by the littoral currents. The essential feature of the sediments is the arenite mineral fraction mainly made of quartz, with some local heavy minerals addition. The carbonates ratio, which is represented by shells and mollusks' shells fragments from the beach sediments, increases from North to South, from a few percentages (Sulina) to over 90% (Periboina). This variation is due to the increasing distance from the Danube mouths. The Northern part of the littoral is part of the Danube Delta Biosphere Reservation.

The Southern Unit has a total length of about 80 km and is located between Cape Midia and Vama Veche. This unit consists of cliffs, separated by low sandy shores (Mamaia, Eforie, Costinesti, Olimp - Mangalia).

According to Shepard's genetic classification (1967), the Southern part of the Romanian littoral is situated in the secondary shores category with two main sub-types, [2]: erosional type (with cliffs); depositional type (barrier type shores).

The geology of the coastal zone affects the amount of beach sediments and influences the entire morphology of the Southern coastal zone. Thus, in what regards the geomorphology, the main feature of the Southern littoral area is the evolution of the cliff shores. Another important feature of this area is the gradually passing from the Danubian facies to the organogenous one. This feature, together with other specific geomorphological features, allows the separation of two distinct regions:

- Cape Midia – Cape Singol, with some transitional features between the northern and the southern units; the relevant element consists of the presence of big sand littoral bars between the active cliffs.
- Cape Singol – Vama Veche, with dominant active cliff shores as specific feature, separated by sandy littoral bars.

3. DATA AND METHODS

During the years 1975-2010, GeoEcoMar performed systematic campaigns for geological and sedimentological studies along the Romanian shore. Special attention was paid to study the natural sections opened in the Black Sea cliffs. Sediment samples were collected from each cliff lithological horizon, which was subsequently analyzed in the laboratory in terms of granulometry and mineralogy. Textural parameters have been determined using sieving for arenitic and ruditic fractions, distributed on a 1 φ ranged sieve column, and dropping for silt and clay fractions. Mineralogical analysis was performed on 0.063-0.125 mm fraction, using a mineralogical microscope and binocular magnifier. Cliff configuration was determined on the field, using a portable theodolite.

4. RESULTS

The most important geomorphological element for the southern Romanian coast is the cliff. The cliff presence and evolution is the result of the interaction between the geological and tectonic-structural factors (very specific for Central and Southern Dobrogea) with other environmental factors controlling the development of the coastal processes. Formed by

waves and currents, based on a slow sea level increase, the relatively high cliff is very well developed between Cape Singol and Vama Veche. There are areas with active retreating cliffs, but also some areas where the cliff is protected by the littoral sand bars - sandy littoral accumulations at the base of the cliff (Figure 1).
The cliff's lithological and structural irregularities determine the general configuration of the coast, which is curvy, with distinguished changes of the shoreline orientation.

4.1. Shores with active cliff

Active cliffs shores are largely extended. These types of shores occur between Northern Eforie – Belona, Cape Turcului – Cape Tuzla and Cape Tuzla – Vama Veche areas. In this latter section (Vama Veche), the cliff is discontinuous due to the presence of several sandy barrier beaches in front of Costinesti, Tatlageacul Mare and Mangalia lakes, as well as in front of Mangalia and Comorova swamps.
The headlands are preferentially developed in hard rocks areas and are under the direct influence of the marine factors, offering large fronts to marine abrasion. From north to south, the main active capes are Midia, Ivan, Turcului, Tuzla and Aurora. Other capes (like Clisargic, Singol, and Constanta) were faded away in the present configuration of the shore due to the building of Midia – Navodari Harbor, Pescarie – Cape Singol sector, and Constanta Harbor. The geological contents and the structural peculiarities of the rocks outcropping along the shore have induced the formation of a vertical profile (Figure 1).
The active character of the cliff is given by the interference of two factors: marine abrasion and gravitational land slides. Active parts of the cliffs are to be found in the Cape Midia area, Cape Ivan and Cape Clisargic, as well as along the following sections: Cape Singol - Cape Constanța (Tataia beach), Constanța Sud-Agigea, Cape Agigea-Eforie Nord, Cape Turcului - Cape Tuzla.
In the coastal strip between *Cape Midia and Vama Veche* we can sometimes to observe a mixed lithological profile of the cliff. Thus, at its lower part, the cliff is represented by prequaternary formations (green schysts, Jurassic dolomites, Sarmatian limestones, clays and sands). The abbrasion process of these deposits is slower, while its final results (gravel and sand) shall be integrated to the coastal circulation.
The Quaternary cliff consists of friable deposits (clays, loess deposits) that, when eroded, become sources of detritic material for the neighboring sea. The predominant silt and clay grains are taken offshore by the currents, and are thus out of the coastal system, while the few sand and gravel are transported along the shore.
Cape Midia is the first promontory that interrupts the monotony of the low sandy beaches belonging to the Danube Delta front. It has a height of about 5 m and consists of green schysts with strata in an almost vertical position, in the base part. These are composed by an alternance of phyllitic shales with sandstones and greywacke-like microconglomerates from the *Upper Graywacke Complex* [5]. This layer is extended also several tens of metres offshore. Above the old landscape of green schysts there is a thin (20 – 30 cm) layer of residual red clays with quartz grains. The top of the cliff (2-3 m) is represented by the latest loess layer, covered by the actual soil.
Cape Ivan, with a 10-11m height, has a length of about 150 m and is subject to marine abrasion. At its base [4], Drăgănescu identified the presence of the *Oxfordian*, represented here by limestones and dolomitic calcarenites, in layers 20-40 cm thick, that dip seawards (Figure 2).
On their surface many paleocarstic formations (karrens) can be observed. Above them there lies a white-reddish dolomitic alteration crust, with a thickness of about 1.2 m.The lower part of the profile is represented by a layer with a thickness of about 50 cm, represented by

yellowish limestones with the aspect of fine sandstones. The limestones deposit consists of 3-5 cm thick strata. The *Jurassic* deposits are covered by a thin layer of residual red clay. The top of the cliff consists of the newest loess layer and the actual soil. The existence of the lower limestone part offers a certain protection to the upper cliff.

Cape Clisargic has at its base a layer with a thickness of about 1.5 m consisting of conglomerates with rounded blocks of Jurassic dolomitic limestones, [3; 4] followed by a 2-30 cm thick level of greenish clays with elements of rounded pebbles made of quartz and cherts (2-3 cm diameter). Above, there is a layer 50-70 cm thick, of green clays with elements of round pebbles (silica and cherts with oxidation iron films). The upper part of the cliff (2-3 m) is represented by the newest loess layer.

Cape Singol - Cape Constanța sector (Tataia and Modern beaches) begins at the southern end of Mamaia beach and it extends till „Trei papuci" beach, near the old center of Constanța. The cliff`s height increases from North (about 2-3 m at Cape Singol) to South

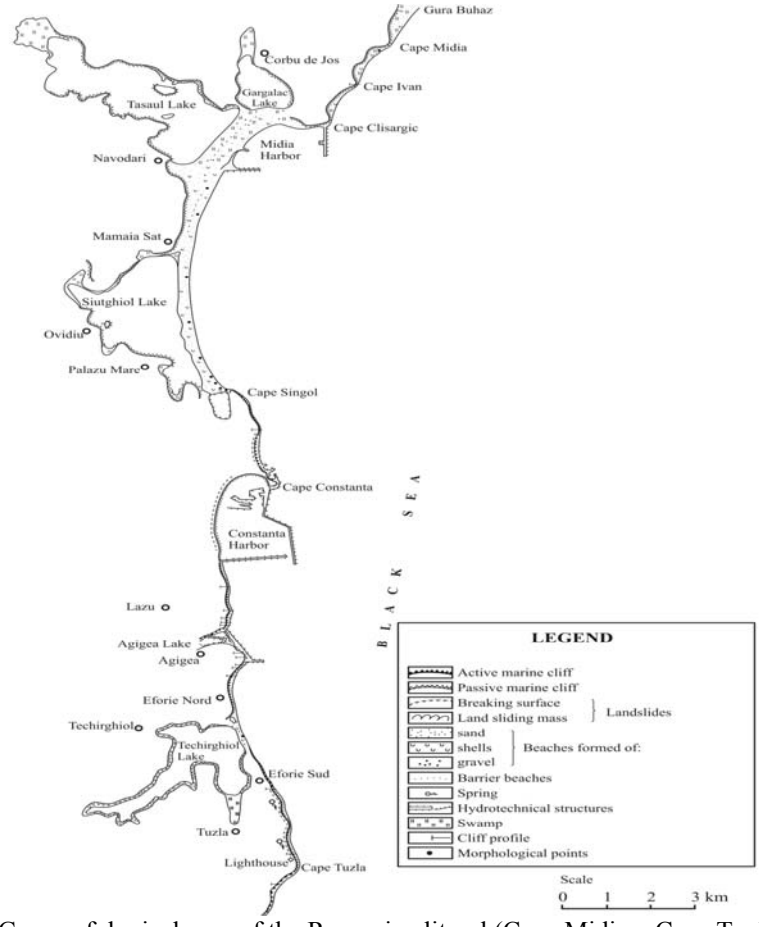

Fig.1 Geomorfological map of the Romanian litoral (Cape Midia – Cape Tuzla)

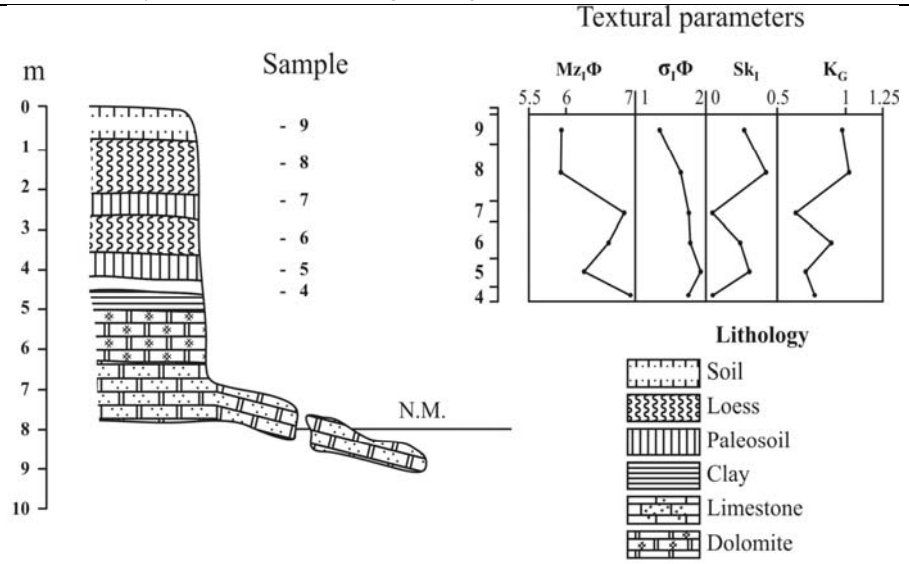

Fig. 2 Profile of the Black Sea Quaternary cliff deposits (Cape Ivan)

(about 30 m near the Military Hospital). Here the *Sarmatian* deposits dip northwards, like the rocks from above, whose thickness also decreases in the same direction (fig. 1). North of Soveja Square, the layer composed of clay and gypsum dissapears and the newest loess layer lies directly on top of the Sarmatian lumachelic limestones. From Cape Singol to Soveja Square the cliff is abrupt, almost vertical. From here southwards the cliff is made of two steps: a lower one consisting of Sarmatian limestones, sometimes covered by the landslides provenient from the upper step of the cliff, and the upper step, consisting of the Quaternary succession of paleosoils and loess levels. The surface along which slides are produced, is irregular and is situated at the contact between the red clays and paleosoil IV, where the underground water table is located.

The upper step of the cliff is actively modelled by landslides typically for loess, while the lower step is subject to marine abrasion (Figure 3).

In the loess/fossil soils succession, for the deposits between paleosoil levels II and III, a northwards increase of the erosion can be observed. On this profile, Brătescu [1] affirmed that the sediment on top of the clays and gypsum layer represents a loess accumulated in an aqueous environment.

Our personal observations make us consider that these deposits show the typical features of soil formed on aeolian loess, with frequent pores and channels. Another feature that helps us with this idea is the lack of any stratification, that would have been normal in case of underwater deposition. Here, there is a narrow beach at the base of the cliff. The beach dissapeares during storms.

Cape Agigea -Eforie Nord (Belona) section has an abrasion rate estimated, for the period 1971 to 1979 to about 5 m/year. The cliff has 10 -14 m in height and is fomred of three different lithological types: Sarmatian limestones with lens of green clays in the base; above them the red clays with gypsum; on top the loess deposits. In this section it is possible to observe in detail the abrasion mechanism with distinct peculiarities for each lithological type (fig. 4).

The Sarmatian limestones are represented by compact lumachelic limestones, followed by oolithic limestones and by friable lumachelic limestones with lens of green clays [5]. The thickness of these outcrops vary from 2 to 4 m. The top of the Sarmatian limestones is

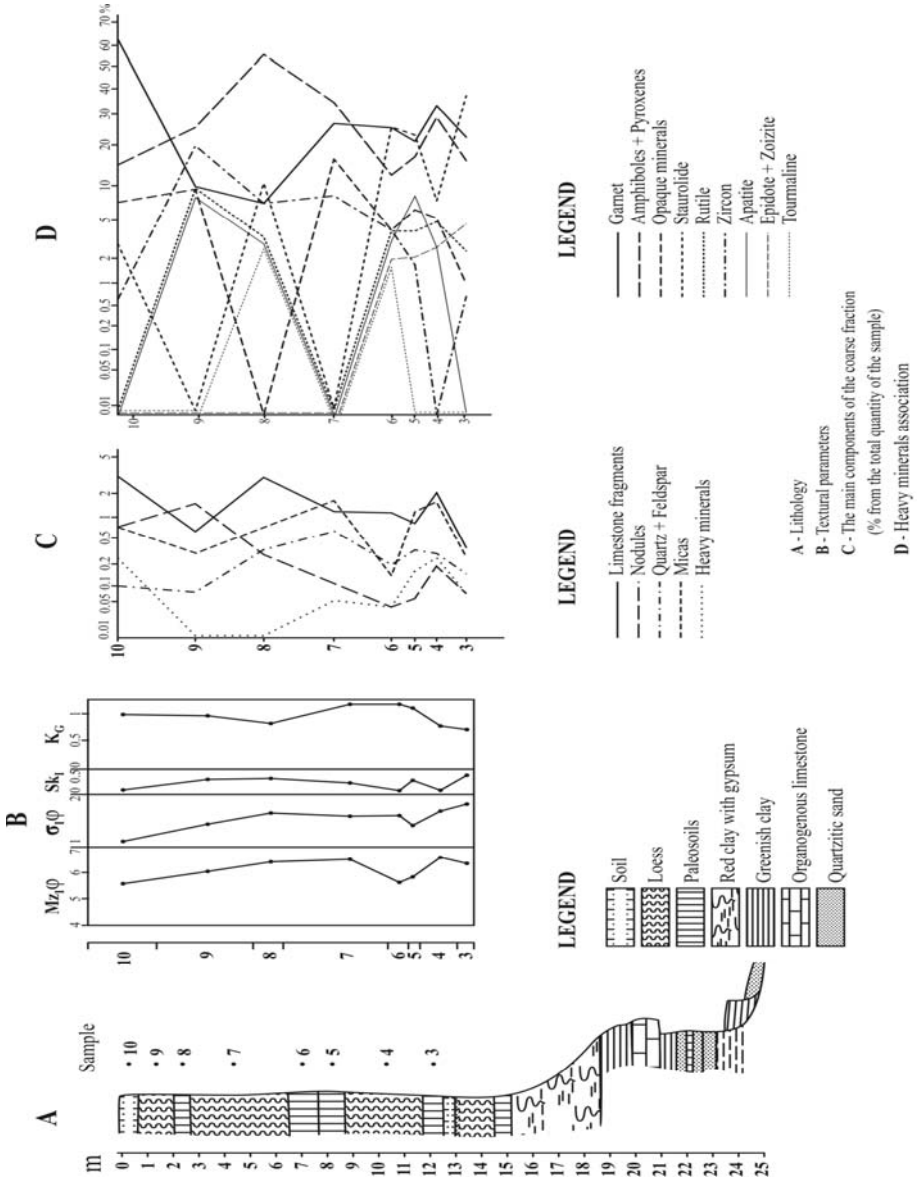

Fig. 3 Profile of the Black Sea Quaternary cliff deposits (North - East Constanta)

irregular, typical for the weathering crust, while in the holes from the upper surface residual red clays have been accumulated. The Sarmatian limestones are intensely carstified, with numerous vertical spaces filled with residues from the green clay lenses. The walls of these spaces are covered with Iron and Manganese oxides. Oftenly the abbrasion niches, cut by

the waves at the base of the limestones, intersect such palaeocarstic spaces. The residual clays consist of a reddish or green clay matrix with rolled elements of calcareous pebbles covered by black films of Iron and Manganese oxides. The pack of residual clays has irregular surfaces, both at the bottom as well as on top. The longitudinal variation of these clay strata varies along 500 m of shore from 0.60 m to 2.30 m. The Pleistocene deposits are represented by the paleosoil levels III, II and I, as well as by the latest three loess levels.
In this section the retreat rate of the upper cliff maintains the same rate with the abbrasion of the Sarmatian lower part.
Cape Turcului - Cape Tuzla section has been the least influenced by human interventions. The original active cliff is covered by numerous bodies of rocks resulted from landslides and that are now stabilised or still unstable, most of them active, while some of them have small freshwater springs at the base. At about 1 km N of Cape Tuzla there is an active rock mass provenient from landslides whose front is just at the sea level. This rock mass has a length of about 1.5 km and it consists of intercalations of loess and fossil soils that slides along the contact surface with the clays. In front of the Tuzla Cape the lumachelic limestones outcrop both on the cliff as well as on the sea bottom. The vertical profile of the cliff shows that the Quaternary consists of 5 paleosoil levels: I -V (fig. 5).
South of Cape Tuzla the morphology is directly controlled by the largely convoluted Sarmatian limestone structures. The base of the cliff is represented by intensely weathered Sarmatian limestones, with holes filled with residual clays rich in Iron oxides and hydroxides. Between Cape Tuzla and Pescărie, the erosional phenomena of the cliff have been intensified during the recent years. The protection works developed here proved inefficiency.
South of Costineşti, the cliff has a vertical profile with a height of about 20 m. Berms consisting mainly of *Mytilus* shells, with 1.5 - 2 m height are developed in front of the promontories. In front of Olimp resort, on a height of about 14 m, 5 – 7 levels of fossil soils can be identified. *Towards Tatlageac Lake* the cliff height decreases to 1 – 2 m.
At its base, there are the Sarmatian limestones, covered by a thin level of red clays and a brown-red fossil soil. The general orientation of the shore between Cape Tuzla and Cape Aurora is NNE – SSW, with large curves. South of Cape Aurora the orientation becomes N – S. For the entire section a characteristic phenomenon is the sectioning by the cliffs of large valleys, as it can be noticed North of Tatlageac Lake, South of Cape Tuzla and at Vama Veche.
Between 2 Mai - Vama Veche the cliff has an average height of about 10-12 m with the base made of the Sarmatian limestones` weathering level. A small valley can be identified in the loess level from Vama Veche, which gave birth to the existing sand beach.
The textural and mineralogic study of these deposits give relevant information about the source of several detritic compounds to be found in the beach sediments.
Villafranchian clays consist of a reddish or green clay matrix with rounded elements of calcareous pebbles, covered by black films of Iron and Manganese oxides. This formation presents some variations in lithology from North to South. Thus, in the profile from Cape Ivan (fig. 2), above the alteration surface of the Jurassic dolomitic limestones there is a thin layer (about 30 cm) of residual red clays that fill the numerous caverns existing in the limestone. Along the coast cliff between Constanța and Eforie Nord the clays become green, greenish – white or greenish – red with numerous gypsum and calcareous gravel concretions pigmented with Iron and Manganese oxides.
In the profile made at Cape Agigea (fig. 4) the red clays show textural features typical for transport under a torrential regime, the heterogenous material being very poorly sorted. The coarse fraction consists mainly of limestones, quartz and spheroidal Iron-Manganese concretions. There are also mica and heavy minerals in very small concentrations. The

heavy minerals association from the red clays is given by the formula: *garnets -opaque minerals - rutil - amphyboles and pyroxens.* Many minerals have an advanced rounding degree that prove the fact that they are provenient from elder deposits that had been eroded and then resedimentated.

From the textural point of view, the loess deposits from the Black Sea cliff belong to the following categories: silt, clayish silt, sandy silt. The constituting particles have mean dimensions that show their belonging to the siltic domain. An uniformity of the mean

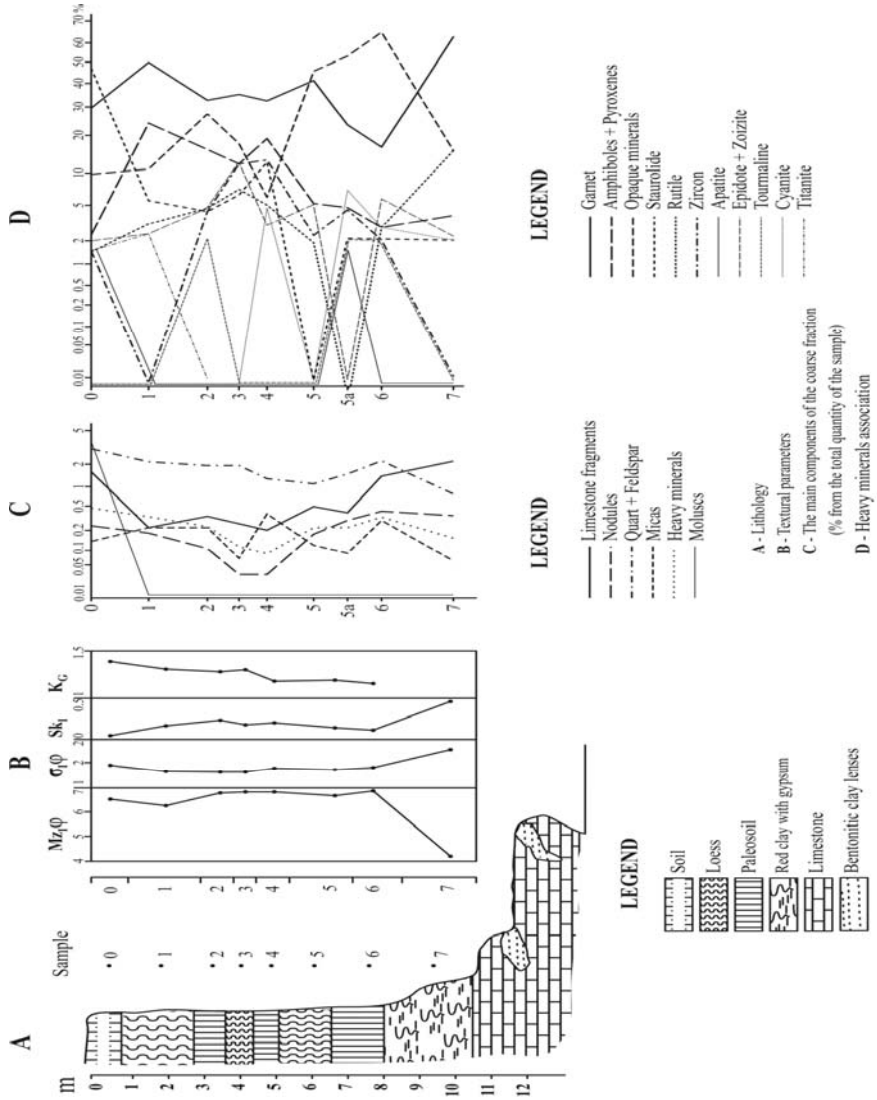

Fig. 4 Profile of the Black Sea Quaternary cliff deposits (Cape Agigea)

values along the vertical columns can be observed (fig. 2, 3, 4 and 5)**,** both in the loess and fossil soil levels. In the North East Constanța profile (fig. 3) there is an input of coarser grains towards the top of the profile. The material is poorly sorted. The coarse fraction from the fossil soils and loess of the Black Sea cliff contains the following main compounds:

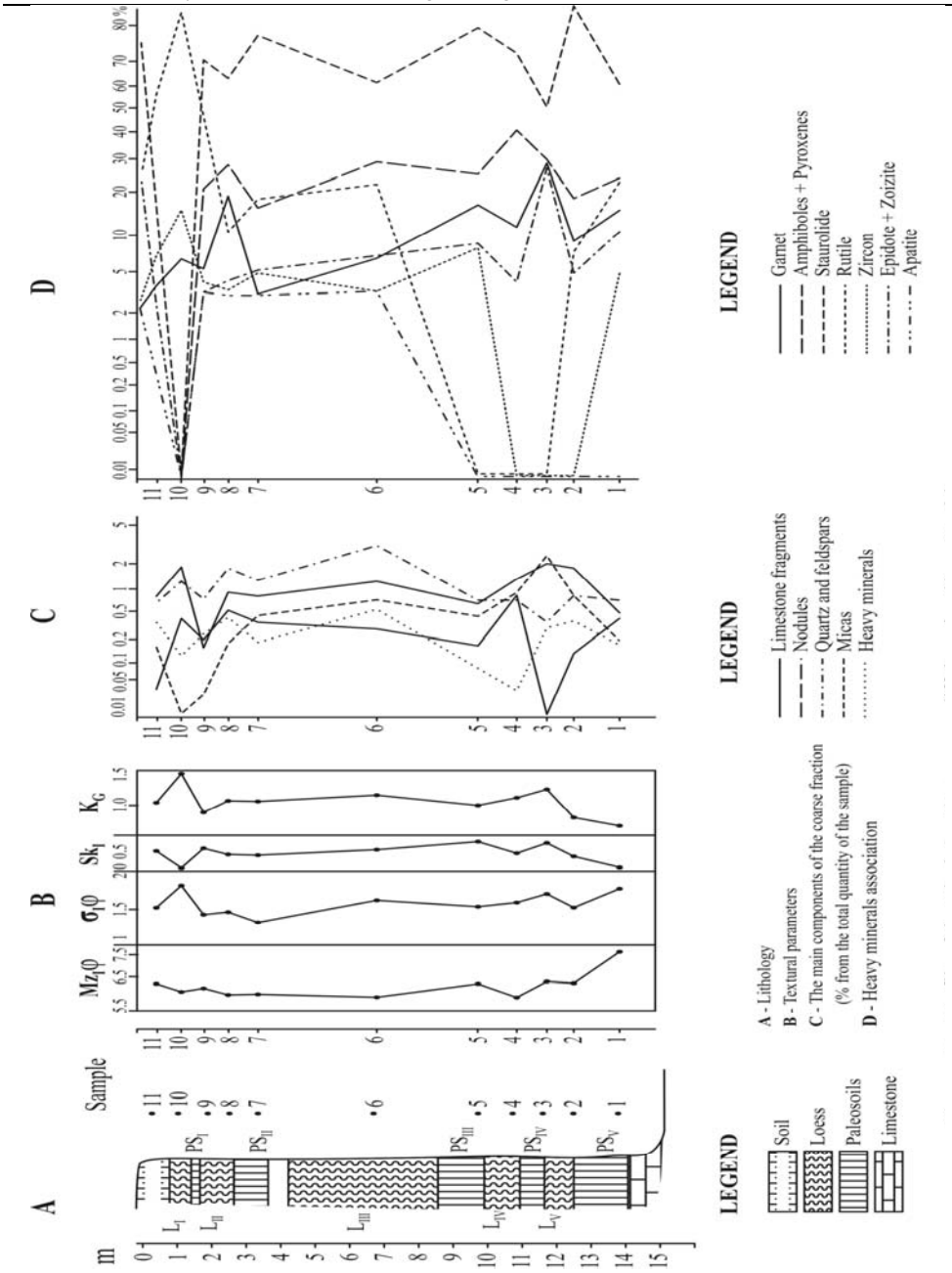

Fig. 5 Profile of the Black Sea Quaternary cliff deposits (Cape Tuzla)

quartz and feldspars, limestone fragments, small iron-manganese concretions, heavy minerals, shell fragments (fig. 3, 4 and 5).

Quartz and feldspars are found as subangular and subrounded grains, with the surface showing characteristic features for aeolian transport. *Limestone fragments* are generally of neoformation origin. The lower their frequency in samples, the newer the deposits. *Micas* are very rare, muscovite is the most representative among them. Biotite is weathered. *Iron-*

Manganese concretions are in very lowcontents. *Shell fragments* are very rare. They generally belong to pulmonatae molluscs. Thus, shells of *Helix* sp. were found in the newest loess level near Agigea. The newest level of loess in the North-eastern part of Constanța contains very rare elements of *Dreissena* shells (recogniseble after the umbonal specific configuration). Their presence may suggest as source of material the beach deposits from offshore the present shoreline.

Heavy minerals generally present superficial microstructures that are specific for wind transport.

4.2. Shores with inactive cliff

The passive cliff shores are classified in three categories, according to the fossilization:

- passive cliffs situated behind the big accumulative bodies (between Clisargic Cape and Ivan Cape);
- human influenced cliffs (the industrial platform Constanta Sud – Agigea Harbor);
- passive marine cliffs situated on the present lakes shores – former marine bays (Tasaul and Corbu Lakes, Siutghiol Lake, Agigea Lake, Techirghiol Lake, Tatlageac Lake,Comorova swamp, Mangalia Lake).

5. CONCLUSIONS

Currently, the general characteristic of the Romanian shore is an increasing erosion. The main cause is considered to be the significantly reducing of the sedimentary Danube input spilled into the sea, on the climate change background. In this regard, several parts of the coastline accuse a critical state. The sector between Singol head and Tataia beach retreats continuously because of marine abrasion and gravitational sliding of loess cliff deposits.

Slope processes are due here to the presence of an active groundwater level. Currently strong erosion of the cliff between Cape Agigea and Eforie Nord, including the Techirghiol barrier beach, required overhauling manufacturers every year. The existing hydraulic structures have been ineffective, so additional safety measures are needed. Hydro technicians have to assume that any work running on the seashore must be preceded by detailed geomorphological and sedimentological studies along the respective coastal segment, and assessed in the overall context of coastal dynamics.

6. REFERENCES

[1].Brătescu, C. "*Profile cuaternare în falezele Mării Negre*", (1934) Bul. Soc. Rom. Geogr., LII (1933), 24-58.

[2].Caraivan Gl. "*Studiul sedimentologic al depozitelor de plaja si de pe selful intern romanesc al Marii Negre intre Portita si Tuzla*", (1982) Teza de doctorat, Universitatea Bucuresti.

[3].Drăgănescu, A. "Constructional to Corpuscular Spongalgal, Algal and Coralgal Facies in the Upper Jurasic Carbonate Formation of Central Dobrogea (the Casimcea Formation)", in: "*Carbonate Rocks and Evaporites Guidebook*", D. Patrulius et al., (1976) Inst. Geol., 13-42.

[4].Mirăuță, C. "Tectonica Proterozoicului superior din Dobrogea Centrală", (1969) An. Com. Geol.,XXXVII, Buc.

[5].Chiriac, M. "Notă asupra depozitelor sarmațiene din Dobrogea", (1960) Com. Acad. R. P. R., 7, X, 613-623.

Evaluation effect of granularity on parallel Oceanography

Bahman Hashemi, Hamid Reza Qaienee, and Saeed Moghimi

***Abstract* – High resolution oceanography forecasting plays an important role in marine meteorology. But execution of these models takes so much time. Parallel processing technology speed up those models and results will be generated in reasonable amount of time. For distributing sub-domains of the forecasting domain to processes we need to evaluate granularity and effects of granularity to execution time of parallel oceanography model. In this article we will discuss about effect of granularity on two marine models i.e. a wave forecasting model and a general oceanography model.**

***Keywords*: Parallel processing, Granularity, Oceanography models, GETM, WAM.**

1. INTRODUCTION

As advances in oceanography models we need more computational resources for high resolution forecasting. Also advances in communication and computation technology make distributed memory computing more prominent in oceanography and water resource computing.

The Message Passing Interface (MPI) is a common communication standard that was used in most water resource and oceanography forecasting models. So in this paper we discuss about performance analysis of two general ocean models i.e. WAM Cycle 4.5 (WAve Model) and GETM (General Estuarine Transport Model) on a cluster of AMD Athlon processors. After description of the MPI communication language in section 2, section 3 describes the GETM model and section 4 describes the WAM model. Section 5 will describe about these parallel models. In the last section results are evaluated and compared to what theoretically predicted. This work was performed in a boundary region near Bandar Torkman harbour inside the Caspian Sea.

2. MESSAGE PASSING INTERFACE

Message passing is the most commonly used method for communication between nodes in HPC platforms. Nowadays, MPI is the best standard language paradigm for passing messages in a distributed memory system and is the common communication library is used on HPC platforms [1]. MPI is so much scalable that can be used in small

B. Hashemi is with Arak University, Markazi, 38156 -Arak, Iran (phone: +98-916-6652934; e-mail: bhashemi@ araku.ac.ir).

H. R. Qaienee is with Arak University, Markazi, 38156 -Arak, Iran (e-mail: Qaienee@gmail.com).

S. Moghimi is with Physical Oceanography and Instrumentation Section of Leibniz Institute for Baltic Sea Research, Seestraße 15, D-18119 Warnemünde, Germany (e-mail: moghimis@gmail.com).

ISSN-1584-5990

clusters to large clusters of multiprocessors. Also because of its high portability there's no need to change the parallel code to runs on different kind of HPC platforms [2].

The MPI library can be linked to an existing language such C++ or FORTRAN. Most ocean and coastal computational models was written in FORTRAN language. Hence almost every ocean or coastal computational models parallelized by using of the MPI technology.

The MPI library can be linked to an existing language such C++ or FORTRAN. Most ocean and coastal computational models was written in FORTRAN language. Hence almost every ocean or coastal computational models parallelized by using of the MPI technology.

3. GETM MODEL

The General Estuarine Transport Model is a three-dimensional free-surface ocean model that solves general ocean equations like three-dimensional momentum equations, kinematic boundary condition and surface elevation equation and so on.

In 1998, GETM has been used for current forecasting inside the Mururoa atoll in the Pacific Ocean [3]. Later, H. Burchard and K. Bolding extended many features to the GETM such as calculation of density, surface heat and momentum fluxes and so on [3,4].

4. WAM MODEL

WAM Cycle 4.5 is one of the best 3rd generation wave prediction models that recognize sea grid points to solve transport equation. The basic physics and numeric of WAM Cycle 4.5 and WAM Cycle 4 are the same. But WAM Cycle 4.5 has new technical improvements that make the model readable and simplify changing model [5,6].

The most important and time consuming part of the WAM Cycle 4.5 is program "CHIEF". This program first time, run" INITMDL" for initialization of model that read data from output files of preproc program. Then "PREPARE_WIND" and "WAMODEL" subroutines frequently called. The "PREPARE_WIND" subroutine read the wind data from input files of chief program and set the block of wind data. The "WAMODEL" subroutine integrate wave spectrum forward the time and solve the transport equation that described below:

$$\frac{dF}{dt}+\frac{\partial}{\partial\phi}\cdot\left(\phi F\right)+\frac{\partial}{\partial\lambda}\cdot\left(\lambda F\right)+\frac{\partial}{\partial\theta}\quad\left(\theta F\right)=S \tag{1}$$

Where F=spectral density; f=frequency; θ=direction; Φ=latitude; λ=longitude; λ, Φ, θ = rate of change of the position and propagation direction of a wave packet; S=source function including wind input, white capping dissipation and nonlinear transfer [5].

The "WAMODEL" subroutine consists of two important subroutines named "PROPAGS" and "IMPLSCH" that compute the transport equation. The "PROPAGS" subroutine computes propagation of a time step for grid points. Propagation of a sea point spectrum performed with data of neighbors' sea point spectrum. The "IMPLSCH" subroutine performs time integration and every sea point has no dependency to other sea points.

5. PARALLEL MODELS

The WAM model was parallelized in the Arak University HPC center in 2007. Implementing the MPI protocol on WAM Cycle 4.5.1 has two important phases ofparallelization:

- Decomposition: Data of sea points across PHYSICS loop are independent to other sea points. So sea grid points decomposed and passed to IMPLSCH subroutine**.**
- Overlapping: Every sea grid points in PROPAGS subroutine dependent to its neighbor Latitude and Longitude sea grid points. So an Overlapping subroutine that uses MPI Blocking routines to communicate between processes and collect necessary data for each process was developed**.**

The following figure describes the most important routines of the WAM model. Because of its extra routines just important routines has been described.

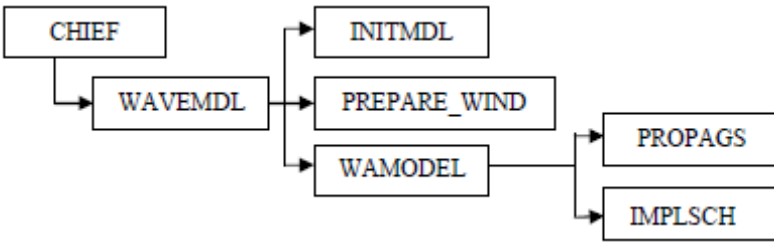

Fig. 1 Most important WAM model routines

The GETM model has been parallelized in Bolding and Burchard hydrodynamic center. This model exchange data between computation nodes by routines such as "Update_2d_halo_mpi". These routines are so flexible that GETM users can choose the communication methods such as blocking, non-blocking and so forth. Also the GETM code is so much readable and makes it easy to change the code and add optimization directives. Figure 2 shows data flow between parallel routines in the GETM application for the two dimensional equations solving.

6. RESULTS AND SIGNIFICANCES

In order to evaluate the effect of granularity on parallel models, a boundary region near Bandar Turkmen inside the Caspian Sea has been defined. In this case we assumed the model execution with low resolution forecasting as a fine-grain model that has greater communication overhead. This is true because of the ratio of computation time to communication time will be lower. On the other hand this boundary condition was defined with high resolution forecasting and assumed as coarse-grain model that has less communication time overhead [7,8].

According to Amdhal's law we have:

$$T_P \equiv T_S \cdot \left[(1-f) + \frac{f}{p} \right] \qquad (2)$$

where T_P is parallel execution time, T_S is serial execution time, P is number of processors and f is the fraction of the model that is enhanced. Table 1 to 4 shows the execution time offine-grain and coarse-grain parallel based versions of WAM model and GETM model and their speedup. In the WAM model about 75% and in the GETM model about 60% of the model code has been parallelized.

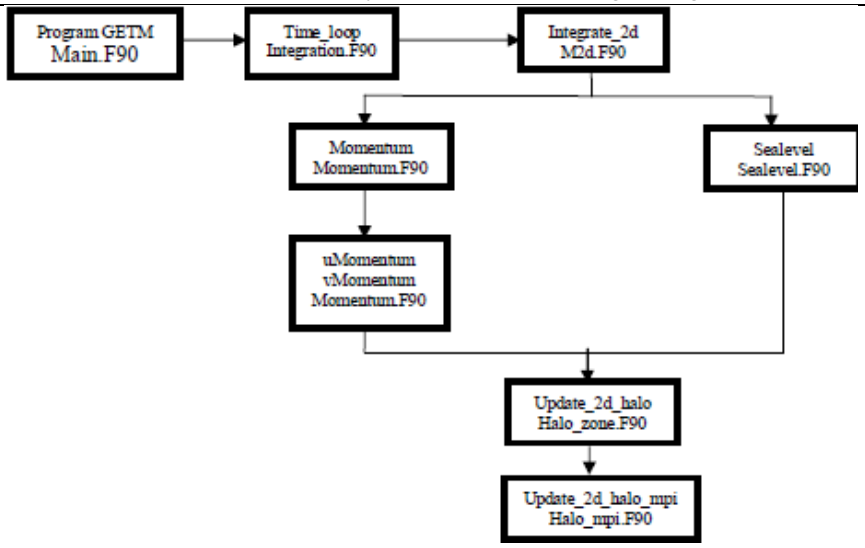

Fig. 2 Most important GETM model routines for 2D equations.

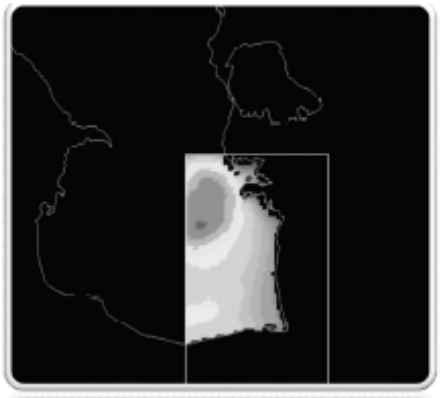

Fig. 3 Bandar Torkman and boundary region inside Caspian Sea

Table.1 Fine-grain WAM model execution results.

Number of processors	Theorethical execution time(s)	Fine-grain model execution time(s)	Fine-grain model speedup
1	413	413	----------
2	258	267	1.55
4	181	191	2.16
8	142	148	2.80

Table.2 Coarse-grain WAM model execution results.

Number of processors	Theorethical execution time(s)	Coarse-grain model execution times(s)	Coarse-grain model speedup
1	891	891	----------
2	557	571	1.56
4	390	405	2.20
8	306	290	3.07

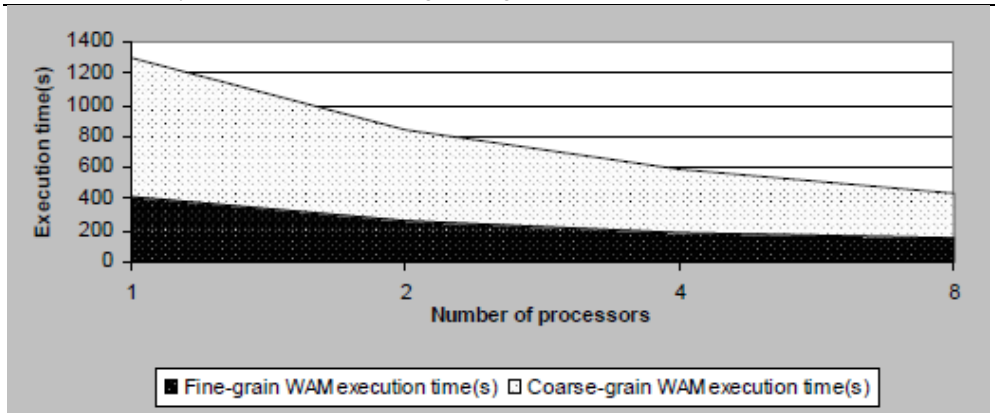

Fig. 4 Effect of granularity on WAM model execution time

Table.3 Fine-grain GETM model execution results.

Number of processors	Theorethical execution time(s)	Fine-grain model execution time(s)	Fine-grain model speedup
1	1436	1436	----------
2	1005	1043	1.38
4	790	825	1.74
8	682	713	2.01

Table.4 Coarse-grain GETM model execution results.

Number of processors	Theorethical execution time(s)	Coarse-grain model execution times(s)	Coarse-grain model speedup
1	8210	8210	----------
2	5747	5822	1.41
4	4516	4573	1.80
8	3900	4005	2.05

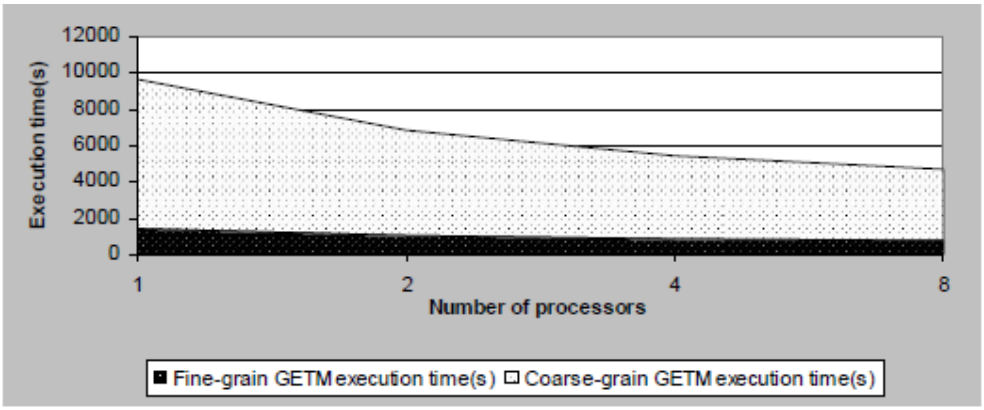

Fig. 5 Effect of granularity on GETM model execution time.

Results of these models has been drawed by th Grid Analysis and Display System (GrADS) application. Figure 3 shows the results of WAM model significant height forecasting that has been drawed by GrADS**.**

7. CONCLUSIONS

As the results shown, in a coarse-grain model we have much speedup than a final-grain model. Most of parallelization methods are based on domain decomposition. This results describe the granularity role in parallel model and so if the communication between nodes has been decreased, model parallelization will works better and dramatically will speed up the model execution [8].

Also we achieve a little difference between theoretical and experienced execution time. This little difference in execution time is because of neglected functions in theoretical calculation. One of these neglected functions is communication time in distributed memory computing.

Granularity evaluation is tailored for HPC administrators and users that require much throughput and functionality in parallel applications such as these oceanography models. So evaluation of granularity is an important phase in setuping a region in a parallel based model. If we grow number of processors without considering the granularity of model we will not have enough functionality and speedup improvement in parallel based model.

8. ACKNOWLEDGMENTS

The authors are very grateful for the support of Arak University research office. Also the authors are indebted to research department of Iran Meteorology organization for their support and cooperation. The authors would also like to thank computer and civil engineering society of Arak University for their cooperation in Arak University HPC center, Dr. Hans Burchard and Heinz Gunther for their detailed comments and constructive advice which has led to many improvements in this paper.

9. REFERENCES

[1] R. Thakur, G. William, Open Issues in MPI Implementation, Proceeding of the 12th Asia-Pacific Computer Systems Architecture Conference, Seoul, Korea, August 23-25,2007, pp. 327-338, .

[2] W. Gropp, E. Lusk, N. Doss, A. Skjellum. High-performance, portable implementation of the MPI message passing interface standard, Journal of Parallel Computing, Vol 22 pp.789–828, 1996.

[3] H. Burchard, K. Bolding, GETM, a general estuarine transport model, scientific documentation, Technical report, Ispra 2002.

[4] A. Stips, K. Bolding, T. Pohlmann, H. Burchard, Simulating the temporal and spatial dynamics of the North Sea using the new model GETM (general estuarine transport model), Springer-Verlag, Ocean Dynamics (2004) 54, pp. 266-283.

[5] H. Günther, S. Hasselmann, P.A.E.M. Janssen. The WAM model report No. 4,Hamburg, October 1992.

[6] H. Günther. The WAM cycle 4.5 model report, GKSS research center Geesthacht, February 2006.

[7] Exploitation of fine-grain parallelism, Lecture Notes in Computer Science, Volume 942/1995.

[8] K. Suzaki, D. Walsh, Scheduling on AP/Linux for Fine and Coarse Grain Parallel Processes, Job Scheduling Strategies for Parallel Processing, Springer Berlin / Heidelberg, Volume 1659/1999, pp. 111-128.

Ovidius University Annals Series: Civil Engineering Volume 1, Issue 12, June 2010

Wave conditions in the transitional zone of the romanian coast - Mamaia bay

Razvan Mateescu[*], Ichinur Omer[**], Silviu Matei[*,**]

***Abstract* – Experimental researches, multi and inter-disciplinary, related to the marine and coastal environment conservation, as well as to the socio-economic development, were become more and more important in the last decades. The study of the coastal hydrodynamic processes as affected by natural processes and human activities, in relation with littoral beaches quality/management where extended by several specialized institutions, by using the wave&currents gouging station provided by ECOH/JICA In the present work it is described the evolution of the main hydrodynamic indicators/parameters in the last 5 years, on Mamaia Bay. The measured quantities and parameters, where studied on its seasonal/annual and multi-annual variability for the extension of understanding related to protection and management of littoral touristic beaches in the transitional area of the Romanian coastal zone.**

Keywords – marine and coastal environment, wave regime, wave's parameters, extreme waves, statistic analysis

1. INTRODUCTION

Wave regime in the coastal area is a main component of all coastal engineering projects, including prediction of the shoreline/coastal bathymetry changes, design and rehabilitation of the coastal construction, setting of the navigation conditions organization and assessment of the natural bays and littoral beaches evolution for planning or facilities effectiveness monitoring. In this regard the understanding of the waves development within coastal and nearshore area is crucial a complex natural and anthropogenous environment.

As main natural factor for sediment transport, the coastal waves induce the coastal development, and determine the coastal response in case of special meteo-hydrologic events, like winter seasons storms. The variability of the wave's parameters can have the same importance as its magnitudes in several designing problems. Thus, information on

R. Mateescu is with NIMRD, National Institute for Marine and Development, "Grigore Antipa", Blvd. Mamaia nr. 300, 900581-Constanta, Romania; (e-mail: razvan_doru@yahoo.com).

I. Omer is with Ovidius University of Constanta, Bd. Mamaia nr. 124, 900527-Constanta, Romania; (e-mail: ichinur.omer@univ-ovidius.ro).

S. Matei is with the NCRW - WDDL, Water Directorate – Dobrogea Littoral, Str. Mircea cel Batran nr. 124, 900419-Constanta, Romania; (e-mail: silviu.matei@dadl.rowater.ro).

ISSN-1584-5990

marine/coastal waves, provided by moored wave gouging stations, can validate the waves forecast systems on regional or local scale, offering in the same time the grounding for an appropriate design of different coastal engineering facilities.

In this regard, since November 2005, a wave measurement device named "Multi-Functional Oceanographic Monitor" was installed in Mamaia Bay to measure the wave condition along the transitional sector of the Romanian Black Sea coast. Installation and handling methods of the device for wave monitoring and data processing procedure of the wave observation records were instructed to the counterpart officials of DADL through the JICA's technical transfer program.

2. DESCRIPTION OF THE THEORETICAL MODEL/METHODS

The sort time wave statistic considers as ground hypotheses the stationarity and ergodicity. The wave main parameters who are suitable for statistic analysis are the magnitude of the wave recording time interval (T_s), wave maximum high (H_{max}) and wave period (T).

The real sea state on short time cam be described by statistic characteristics and it is well reprezentated trough the energetic spectrum, in several representations, relating wave energy or energy density by frecvency (f) or pulsation (ω).

Thus, a mathematical expression which include several particular cases of spectral models, considers spectral density having the following structure:

$$S(\omega) = B\omega^{-p} \exp\left(-C\omega^{-q}\right) \tag{1}$$

where $S(\omega)$ is spectral density, and B, C, p, q are four spectrum parameters.

Two main parameters of several spectrums are significant wave height (H_s) and averaged period ($\overline{T}$). The concept of ssignificant wave height, scientifically represented as $\boldsymbol{H_s}$ (1947, Sverdrup and Munk), is one important level when considering the statistical distribution of marine waves, being defined as averaged high of first third of highest waves recorded. The calculation of significant wave high is:

$$H_s = H_{1/3} = \frac{3}{N}\sum_{1}^{N/3} H_i \,, \tag{2}$$

where N – total number of wave recordings in a time interval

Even the most common waves are less than that of $\mathbf{H_s}$, statistically, when two significant waves come into phase, it is possible to encounter a wave that is much larger than the significant wave **(**Fig. 1**).**

For the purpose of present work, it was selected a data set recorded in circa 5 years, in central area of Mamaia Bay, at isobaths of 11m.

Statistical analysis of the wave regime's characteristics were limited by several gaps aroused from technical reasons in the recordings, as well as from locations which not exclude

wave transforming phenomena in a complex shore situation. It includes the analysis of main wave parameters: high, direction and period. Wave measurement apparatus were composed of certain items which were transferred from JICA to DADL for further wave monitoring. Notebook type computer with software were utilized to pre-process the wave monitoring records.

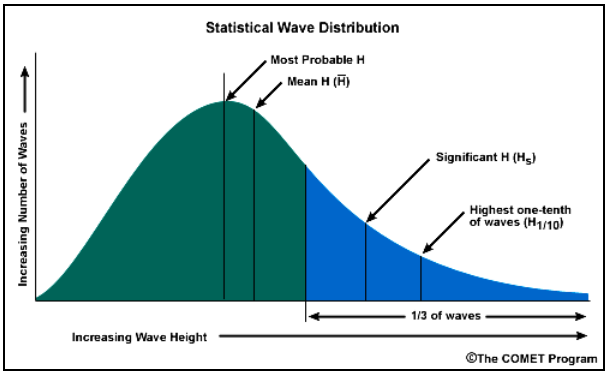

Fig. 1

Wave measurement devices named "Multi-Functional Oceanographic Monitor" were moored to measure the wave condition along the transitional Romanian Black Sea coast, which is usually named Mamaia Bay. Installation and handling methods of the device for wave monitoring and data processing procedure of the wave observation records were instructed to the counterpart officials of DADL through the JICA's technical transfer program.

The system of the wave measurement device comprises several components, as: CPU, Sensor interface, Electromagnetic current velocity sensor, Ultrasonic sensor, Semiconductor sensor, Compact flash memory(64MB), Pressure-Proof case, Accumulator, Accessories, and it is deserved by a complete soft for CSV conversion, Observation planning and Graph indicate.

Fig.2: Instruction on wave gauge operation

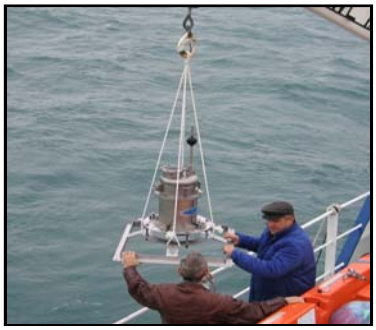

Fig. 3: Unloading of apparatus

The specifications of the wave measurement device include observation mode which was Continuous mode and long cycle wave's observation mode. Installation of the wave measurement device was done by the research ship "Marina" owned by DADL, in the median

area of -11 m water depth of Mamaia Bay. Wave monitoring interval were currently set for 120, 60 or 90 minutes, so the device is capable to record series of incoming waves for 86.3 days at 120, minute monitoring interval, and it was done since 2005, with a maintenance interval for battery replacement and memory chip at every 75-90 days, according with a Wave observation plan of DADL.

3. RESULTS AND SIGNIFICANCES

Based on the recording of more than 19500 recordings, with some discontinuities due to technical causes, were developed several statistic analyses, for the available data recorded on the time interval **03.2006-02.2010,** provided by DADL's wave gauging plan, implemented under coordination of ECOH Corporation/JICA. Generally exist a good correlation of all wave parameters, and data corresponds to a suitable quality standard.

At multiannual level, the wave data, recorded without discontinuities are showed in figure no. 4:

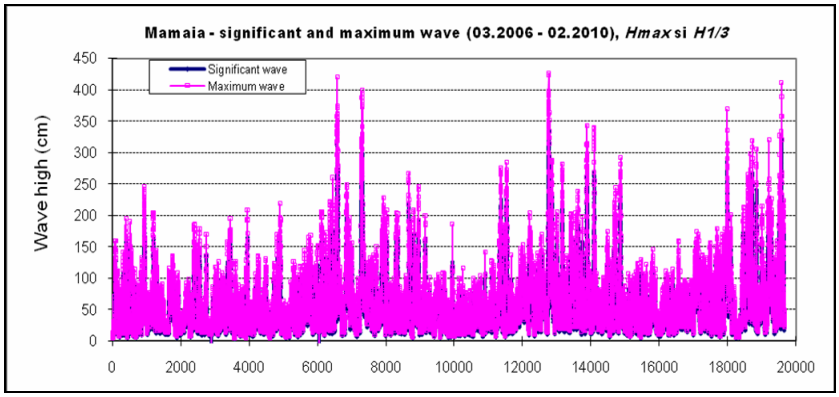

Fig. 4.a Significant and maximum wave high recorded at Mamaia gauging station

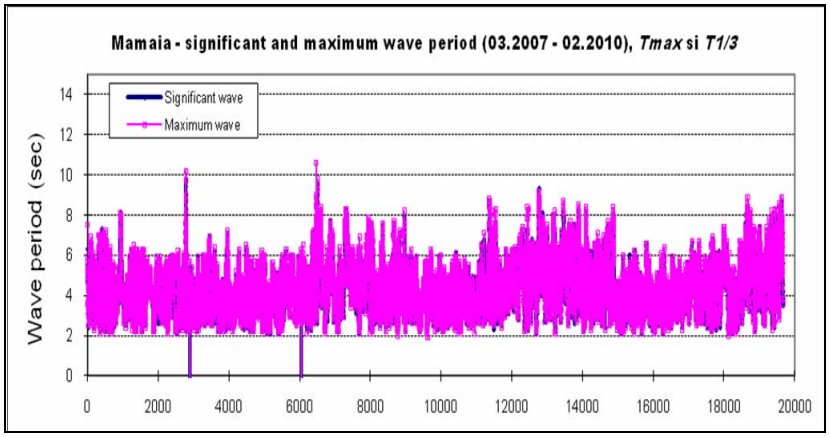

Fig. 4.b Significant and maximum wave period recorded at Mamaia gauging station

Correlation analyses between data recorded at Mamaia against available data from

Gloria platform (50m isobaths), recorded in winter season of 2007, shows that it is a good similitude for main wave parameters. It was realized a deterministic statistic correlation, double-cumulus method, for the main wave parameters recorded at two gauging coastal stations – fig.5.a, b and c. The difference between the wave height data of DADL and offshore data is small and no particular tendency of deviation is observed. Also, after graphs analysis, for directions was determinate a not linear correlations, which emphasize the influence of marine obstacles of Midia Port jetties and depth effects. Nevertheless, the overall tendency is the same, thus validating the reliability of DADL's data.

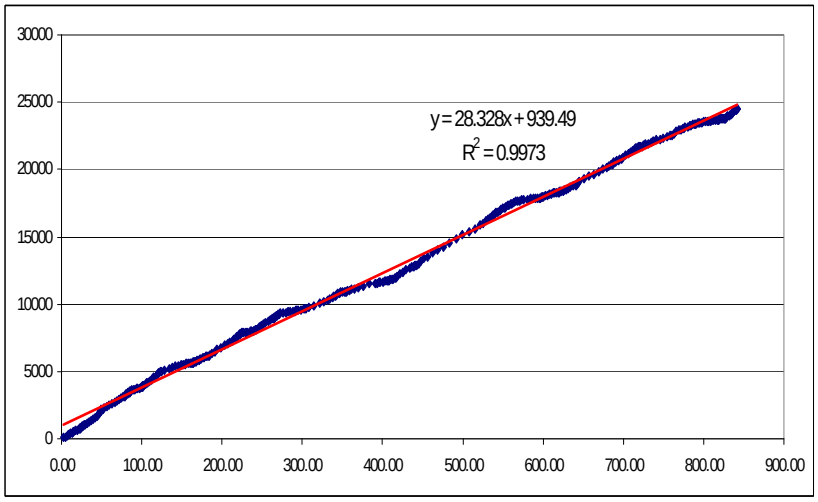

Fig. 5 a Correlation graphs between significant waves parameters recorded in winter season 2007 for height of waves

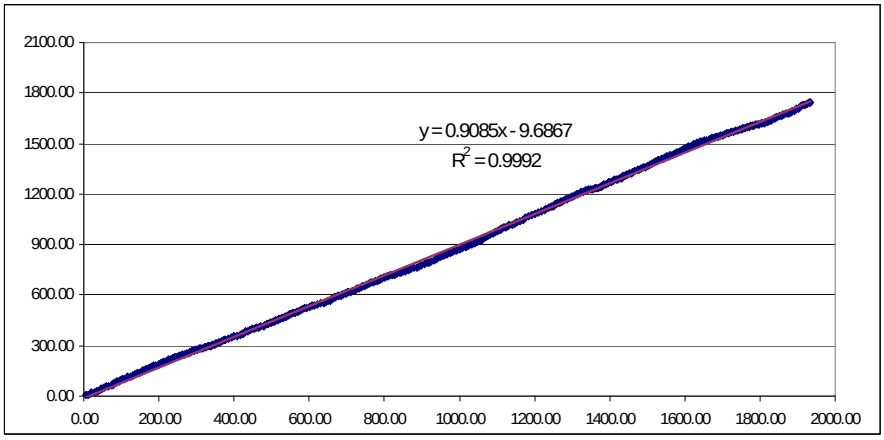

Fig. 5 b Correlation graphs between significant waves parameters recorded in winter season 2007 for the period of waves

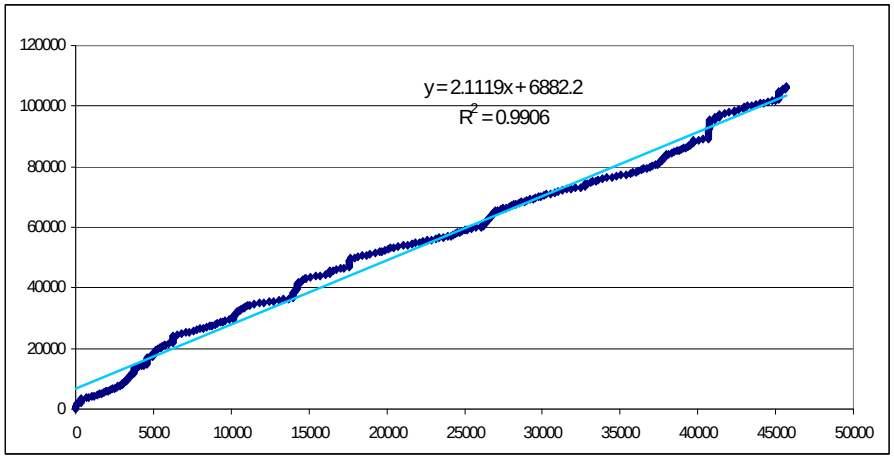

Fig. 5 c. Correlation graphs between significant waves parameters recorded in winter season 2007 for direction

It was recorded the following distribution of wave highs frequencies over main directions and to supplement the wave climate data from bellow the joint distributions of wave height, period and direction in summer and winter seasons are listed in tables. Characteristic wave heights over the space directions as listed based on monthly, seasonal, and yearly tabulation of joint frequencies of wave heights. Seasonal joint distributions of wave height, and direction were calculated. The heights and periods of the mean waves are obtained as the overall averages.

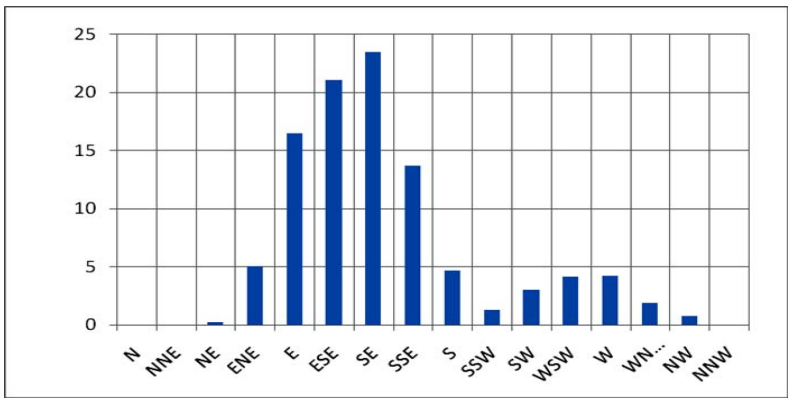

Fig.6. Frequency over directions – f(%)

3.1. Seasonal Wave Climate of Recorded Available Data

The joint distributions of wave height and period in the summer and winter seasons based on the DADL data are represented in fig. no. 7 and fig. no. 8.

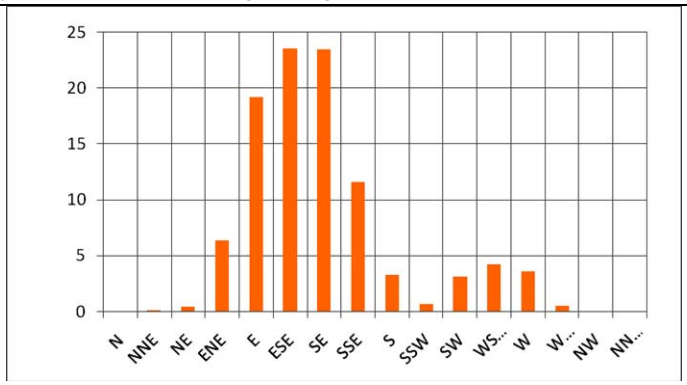

Fig.7. Frequency over directions – f(%), in summer season

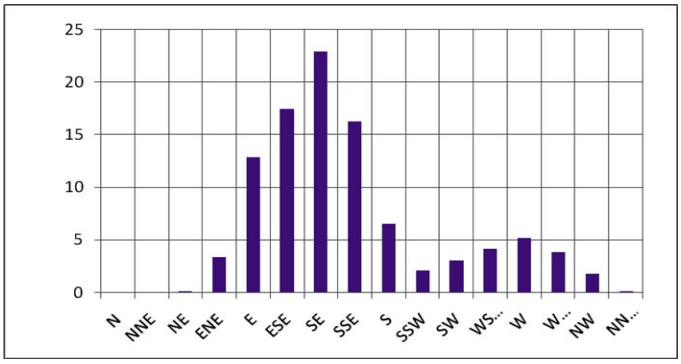

Fig.8. Frequency over directions – f(%), in winter season

Calculation based on the class-wise frequencies in Table 3 and 4 yields the mean wave height being 0.55 m and one-percent exceed height being about 3.5 m and 12.4s period, while the maximum wave recorded in the interval considered was 6.2m in height and 20.8s for the storm of 12th December 2008. It is showed that frequency with calm sea (wave high less than 0.3m – close to the limit of detection) it was under wave regime values, but in the natural variability for winter season.

4. CONCLUSIONS

Wave regime in the transitional zone of Romanian shore, outlined by present statistic analysis was included in multiannual limits for Constanta area wave regime. For Mamaia Bay it was possible an assessment of wave regime characteristics, in the conditions of a built shore, respectively existence of a port jetties on both sites of the bay, inducing certain transformation on wave field.

Correlation analysis do not provide certain conclusions with a high degree of certitude, in the present stage of monitoring program, and in described conditions of Mamaia Bay/pocket beach/unbalanced sediment situation.

For the evaluation of the cumulative multiannual impact, the study must extended for longer time interval, including for calibration studies, together with consideration of different

data sources on larger time scale.

5. REFERENCES

[1]Bondar C., 1972 – *"Marea Neagra in zona litoralului romanesc (monografie hidrologica)",* IMH Bucureşti", Bucureşti.

[2] Department Of The Army Corps Of Engineers (1984). *Shore Protection Manual*, vol I & II, Vicksburg, Mississippi.

[3] Iacob C. *Introduction mathematique a la Mecanique des Fluides*. Gauthier-Viilars. Pani-1959.

[4] Marinescu A., Puşcaşu S., Şelariu O., *Atlasul Hidrometeorologic al Bazinului de Vest al Mării Negre*, Constanța.

[5] Mateescu R. "*Experimental research regarding sediment transport – Southern area of Mamaia Beach"*, Procedings of ECOIND Seminar, Romanian Academy, 2003, Bucharest, Romania.

[6] Mateescu R, Malciu V. "*Long-term sea level and shoreline variability along the Romanian Black Sea Coast",* Proceedings of the workshop on Understanding and Modeling the Black Sea Ecosystem in support of Marine Conventions and Environmental Policies – 2006, JRC, Ispra, Italy (EUR 22176 EN).

[7] Mateescu R. *Hidrodinamica zonei marine costiere romanesti*, Ed. Academica, Bucuresti, Romania, 2009.

[8] Panin N., 1996 – "*Impact of global changes on geo-environmental and coastal zone state of the Black Sea*", GEO – ECO – MARINA, vol. 1, Bucureşti.

[9] Popescu M., Sîmbotin A. R. *Stabilitatea plajelor de pe litoralul românesc al Mării Negre*, Hidrotehnica, nr. 8, 2003.

[10] Ross D.A., 1976, "Introducere în oceanografie", Ed. Ştiinţifică şi enciclopedică, Bucureşti.

[11] Arsenie D.I., Omer, I. 2008, "Hidraulica valurilor marine", Ed. Ovidius University Press,, Constanta.

Shoreline evolution and sediment transport at Sidi-Frej Beach (Algeria)

Khoudir Mezouar , Romeo Ciortan ,Mohamed Amine Boukhemacha

***Abstract* - This study evaluated the spatial and temporal changes in beach morphology by analyzing the grain size distribution, sediment transport and the effect of the hydrodynamic conditions on the beach showing shoreline instability. Ten transects, from which morphological and hydrodynamic parameters were measured, were selected along the Sidi-Frej shoreline perpendicular to the shore. Morphological parameters such as beach orientation, beach width, and beach slopes were determined and sediment samples obtained. Wave energy was calculated from wave heights measured at the surf zone. The study showed that beach morphology was rapidly changing with time along the shoreline.**

***Keywords* – seashore, shore, sidi-frej , beach, shoreline evolution.**

1. INTRODUCTION

Recent decades have seen increasing concern in many parts of the world about the implications of future shoreline change for human communities and nature conservation interests. Predictions of accelerated sea level rise and possible increased storminess related to global warming over the next century have been linked to increased risk of coastal erosion and flooding. If such predictions prove to be accurate, present flood defences and coast protection works in many areas will become unsustainable, and important ecological habitats will be severely damaged or lost. Consequently, there is a need to review future management options and subsequently to implement strategies that allow for the uncertainties associated with possible future coastal change. In order to inform this debate, it is essential that there is an adequate understanding of past coastal change, current coastal processes, and the constraints imposed by geological and other factors on the capacity of any given section of coast to respond to changes in forcing factors.

Coastlines are dynamic in nature. Accurate mapping of the instantaneous coastline position has as a result been always associated with significant uncertainty. This situation arises because at any particular time the coastline position is influenced by the short-term effects of tide and long term relative sea level rise. It is also controlled by the actions of rip and long shore currents, which results in cross-shore and alongshore sediment movement respectively in the littoral zone. This affects the accuracy of computed historic rates of

Khoudir MEZOUAR is with Technical University of Civil Engineering of Bucharest - TUCEB B-dul LACUL TEI, NR.124, SECTOR 2, RO-72302, BUCHAREST, ROMANIA; (e-mail: mezouarkhoudir@yahoo.fr).

Romeo CIORTAN is with Ovidius University of Constanta, Bd. Mamaia nr. 124, 900356-Constanta, Romania (e-mail: ciortanromeo@yahoo.com).

Mohamed Amine BOUKHEMACHA is with Technical University of Civil Engineering of Bucharest – TUCEB B-dul LACUL TEI, NR.124, SECTOR 2, RO-72302, BUCHAREST, ROMANIA; (e-mail: boukhemacha.amine@hotmail.com

ISSN-1584-5990

change and therefore the reliability of any identified erosion. The science of coastline mapping has changed over the past 70 years due to advances in technology and the need to reduce uncertainty. Although the changes have resulted in improvement in coastal data processing and storage capabilities, the frequent change in technology has prevented the emergence of a standard method of coastline mapping [10]. The various methods have their unique capabilities and shortcomings, and therefore the use of any particular method is influenced by the data sources and resources available. The seashore of the Sidi-Frej bay, west from Alger, is characteristic to this evolution with a port extension made in 1969-1971 and several balneary infrastructures developed on the dune cord. These infrastructures contribute to the change in natural balances being translated by an increase in the withdrawal of the shore in this sector. For instance, in the central side of the coast, where the El Riad tourist complex is built there are signs of rapid decrease in the transversal profile of the beach. Actually, on one side, the dune on the edge is eroded and the sea bottoms have become increasingly deeper after the port was built. In this article we attempt to specify the sedimentary dynamics of the Sidi-Frej seashore by a diachronic analysis of the variations in the shore position between 1972 and 2008.

2. SITE PRESENTATION

The Sidi-Fredj seashore is limited to the East by the Alger massif and to the West by the Chenoua massif, Sahel and the Mitidja plain to the South and the Mediterranean Sea to the North. Our study sector lies from Moretti to the secondary jetty of the leisure port (figure1). The seashore dunes of the El-Djemila bay represent the oriental extension of a dune cord born at the Mazafran river mouth continued to the East by the Beni Messous river. The crests are not aligned parallel to the coastline, but they lie following a predominant direction of the hydrodynamic actions, generally (W.N.W –E.S.E). Following the dune cord, and toward the sea, there is mainly a sandy beach area. This beach, sustained by the southern jetty of the Sidi Fredj port, describes a wide arc of circle whose concavity is progressively attenuated toward the East.

The beach presents a maximum development of the Sidi -Fredj side (from 100 to 200 m wide), and it is considerably reduced until it disappears completely next to the Moretti tourist complex.

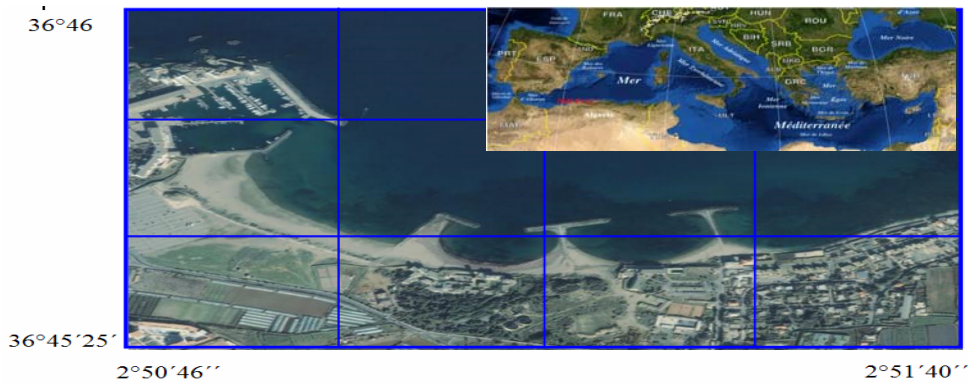

Fig.1 presentation of the Sidi-Frej seashore

Our site is not in direct relationship with the strong sea winds affecting the north of Algeria, the violent winds with a speed higher than 34 knots, are very little frequent, 2,2%. The dominant winds come from the western sectors to the south-east with a frequency of 42.65 %. The sub-sea side has sand pilings in front of the coast festooned bars, whose

morphology would rank this seashore as “rhythmic bar and beach” or as “transverse bar and rip” according to Wright and Short terminology (1984). The weak amplitude of the tide in the study area, comprised between 30 and 45 cm, is not translated by weak tide currents and divides the Sidi-Frej bay into a coast where the swell plays a major role in the morphodynamics of the beaches.
The statistical use of the records has allowed us to notice that the swells in the Western, Eastern and North-Eastern sector are most frequently seen. The sequences of occurrence are weaker for the Northern and North-Western sector.

3. EQUIPMENT AND METHODS

The dynamics of the mobile seashores are complex and very often organised on long sectors. Air pictures, with different data, allow for a global and retrospective view on the phenomena. The processing facility and the viability of the results obtained [3], [4] make that a lot of research uses the air negatives, whose diachronic analysis shows the sedimentary transfers [7], [14], [12], [14], [5], [2], [8],

The diachronic analysis of the evolution of our study seashore was determined due to the comparison of the different geographic maps with different scales and air picture missions. These documents (air missions and maps) were selected so as to cover the entire costline. To obtain more significant results concerning the evolution of the site, the interval of (32 years) for the Sidi-Frej beach was also taken into account. The results obtained by using these air missions and the maps are completed by a site survey mission. This study was conducted due to the superposition of the air pictures in 1972 and 2003 for the Sidi-Frej coast. A Global Positioning System (GPS) survey was performed in 2007 to test the shoreline position on the 2003 map. The 2003 mapped shoreline position was found to agree with HWMpoints measured in the 2007 GPS survey to within the range of the reported historic rates of change; these rates were used to estimate the 4 years of change that had occurred in the intervening years (2003–2007). The 2003 mapping was therefore deemed reliable as a reference against which the positional accuracy of the remaining maps could be checked. This was performed by manually measuring the planimetric coordinates for well-defined map features that could reasonably be assumed to be stable. By measuring the conjugate features in the earlier mapping, the root-meansquare error relative to the 2003 coordinates could then be determined. The planimetric positional error for the 1993 and 1972 maps was 0.20 and 0.32m, respectively (at the 90% confidence level). In addition to the historic map data, scans of every second photograph from the archive of near-vertical film aerial photographs used in the production of the 2002 map were also available. This was georectified to the 2002 map using conjugate points of detail within ArcGIS in order to allow subsequent analysis and to aid subsequent visualizations of the predicted change. Data on the regional hydrodynamic conditions.

3.1. SHORELINE ANALYSIS

Using the grid coordinate system, the shoreline positions were compiled in ArcGIS, and each was coded with five attribute fields: object ID (a unique number assigned to each transect), shape, shape length, date (original survey year), and accuracy. In order to calculate shoreline change rates, all shoreline features were then merged within a single line on the attribute table, which enabled the multiple shoreline files to be appended together into a single shape file with the Digital Shoreline Analysis System (DSAS) version 3.0. an extension to ESRI ArcGis V.9+ developed by the USGS in corporation with TPMC environmental services. This extension, which leads the user through the major steps of

coastline change analysis, contains three major components that define a baseline, generate orthogonal transects at a user defined spacing along the coast, and calculates rates of change (using linear regression, endpoint rate, average of rates, jack-knife and weighted linear regression). It utilises the avenue code to develop transects and rates, and the avenue programming environment to automate and customise the user interface [11]. A baseline was constructed onshore by closely digitizing the direction and shape of the outer shoreline, which was used as the starting point for all transects, set at 50 m intervals. Using linear regression, historic rates of shoreline change were then calculated at each transect. Uncertainties affecting the accuracy of the computed rates were quantified and accounted for in subsequent predictive modelling.

Various studies [1], [6], [10], [11] provided estimates of typical measurement errors associated with mapping methods and shoreline digitizing, and these were used to inform this study.

A total coastline positional error (Ex), equation 1, incorporates all the measurement errors by taking the square root of the sum of squares of field survey error (Es), digitising error (Ed) and photogrammetric error (Ep) as they apply to specific date coastline data. The root mean square error (RMSE) was calculated as a realistic assessment of combined potential error since these individual errors are considered to represent standard deviations. The maximum planetable error incorporates all of the errors associated with the mapping process including distance to rodded points, planetable position and identification of HWL [12]**.** This is applied only to the 1904 map as the more recent coastlines were derived from aerial photographs. Digitising error, which reflects the maximum digitising error estimated was applied to the 1904 and 1974 maps originally produced in hard copy format. Photogrammetric mapping error, which represents the error involved in locating relative positions of coastlines taken from aerial photographs [11], was applied to the 1974, 1996 and 2002 maps since they were all mapped using photogrammetric methods. The total coastline position error is thus expressed as:

$$E_X = \nu\left(E_S^2 + E_d^2 + E_P^2\right)^{1/2} \quad (1)$$

where Es = errors for the plane-table survey, Ep = the photogrammetric error, and Ed = the digitizing error. This
approach carries the reasonable assumption that the component errors are normally distributed.

4. RESULTS

The sandy seashore in Sidi-Frej, between the leisure port to the west and Moretti limit to the east, has an open bay beach characteristic morphology. We specify the sedimentary dynamics of the Sidi-Frej seashore by a diachronic analysis of the shore position variations in (1972 and 2008). The jetty, built in 1969-1971 plays a major role in shore evolution between 1972 and 1993, because it changes the propagation (diffraction) of the swell which determines a withdrawal of the shore in the central side of the bay and an advancement of the shore against its flank. We conclude concerning the destabilising role of developments on the dynamics of the Sidi-Frej seashore, which search for a new balance readapting the position of the shore. This seashore is a good example of the fragile imbalances of a seashore area where tourist activities are trying to be developed.

The evolution of the coastline since 1970 was retraced following the topographic surveys conducted by (L.C.H.F 1972) and those in 1993 and 1995. As well as from the air pictures taken by INCT until 2003, from the determination of the coastline position with GPS in 2006-07. Then from the satellite pictures in 2008.We distinguish four different periods:

a) The Period from 1972 to 1980

Concerning the entire coastline examined between the leisure port in Sidi-Fredj and the Eastern limit in Moretti, only the coastline of the area located between the secondary jetty of the port and the El Riad hotel has changes very little. The rest has suffered a withdrawal of -5.54m (-0.69 m.yesr^{-1}) at the level of the p11 and -44.30m (-5.54 m.an^{-1}) profile of p5. This comparison highlights at the same time the impact of human activities on the seashore. Actually, the building of the Sidi-Fredj port (1969-1971) has determined very important variations along the Eastern seashore in Sidi-Fredj. If we take as reference the coastline in 1970 we notice an advancement of 28.25 m (+3.53 m.year^{-1}) in the side adjacent to the secondary putty, but this value decreases progressively moving away to the East to reach 5.81m (+0.72 m.year^{-1}) at p12 level.

b) The Period from 1980 to 1993

The extension of the adjacent beach of the port staring with 1980 is due to the building of this port. In fact, the implementation of the port has given rise to notable changes, because this work was an obstacle for the longitudinal transport of the sediment and has changed the direction of the waves in the N.W. sector. by diffraction triggering beach erosion going to Moretti. The extension and the arched shape of the beach nearby the port are due to swell rotation around the end of this main jetty, which is translated by the change in its direction and the transfer of energy toward the protected area. This diffraction phenomenon triggers the creation of a current, which brings the sands from the Eastern beach to this area. For this reason, the western sector of the Sidi-Frej beach seashore, protected by the main port jetty, behaves like an “apple”, drawing the sands of the Eastern sector which causes an enormous erosion to this Eastern side, this value increases to reach 62m (+5.54 m.year^{-1}) m, increase whose average values decrease toward the East to reach 24m (+1.85 m.year^{-1}) at p11 profile level, the same for the seashore strip in Moretti, which was subject to -66m (-4.64m m.an^{-1}) withdrawal of its coastline for the same period**.** The decrease in the extent of the beaches was becoming alarming. Studies were conducted to protect these coasts. Protection works were implemented in 1985, the latter certainly stopping erosion, but disfiguring the landscape. Thus, the sedimentary transfers made along the seashore were stopped. The only sedimentary movements are seen in the vicinities of the port of Sidi Fredj end the beach at East from Sidi Fredj and contributed to port sanding.

c) The Period from 1993 to 2003

It should be underlined the fact that the propagation tendency continued at the level of the beach neighbouring the southern jetty of the port, an advancement of more then 22m (+2.4 m.year^{-1}) was noticed between 1993 and 2003. On the contrary, the coastline in front of Moretti continued to draw back a thus causing the almost complete disappearance of the beach in this sector in 1995 (more spectacularly, the sea front in Moretti saw its coastline drawing back from 9 to 11 m (-0.96 m.year^{-1} and -1.10 m.year^{-1}) from 1993 to 2001. When the protection works were emplaced, alveolar beaches were restored to the detriment of the coastline located in the axis of the pass which was subject to 5 m erosion at local level

d) The Period from 2003 to 2008

Starting from 2003 the shore line advancement rate is 8 m (i.e. 1.66m.year^{-1}) at the level of the left side. The advancement of the beach continued during 1972 and 2008 and the coastline continued to advance also toward the sea. On the contrary, the Moretti beach is characterised by important and continuous erosion since 1972. This erosion has triggered

a coastline withdrawal estimated at -3 m, meaning an average withdrawal rate of -0.6 m per year.

e) Synthesis

The seashore in Sidi-Frej (the right side) is characterised by important and continuous erosion since 1972. This erosion has triggered a coastline withdrawal estimated at -110 m, that is an average withdrawal rate of -3.18 m per year. Between 2003 and 2008, the erosion continues (-3 m), but only in the area going from the Moretti beach to the groyne. The amplitude of the annual average withdrawal has also diminished to reach an average of -0.22 m per year. The coastline withdrawal in this sector coincides completely to the distribution of the swell energy on the coast obtained starting form the orthogonal lines of the swells. The seashore coastline in the left side (adjacent to the secondary port jetty) registers important evolutions. In this sector there is a tendency toward propagation of almost 71.78 m (2m.year^{-1}) at the end of 2008. Its association to the eroding section located eastwards could prove the sedimentary transit westwards in this area. The sediments made available by the seashore drift currents, coming from the eroding sectors, accumulate on the left beach.

Fig.2 Shore evolution in Sidi-Frej between 1972 and 2008 and the position of the profiles.

5. LONGITUDINAL GRANULOMETRIC DISTRIBUTION

The sediment samples taken at the level of the trajectory of the beach shore in Sidi-Frej display an average grain which varies between 2.70 and 0.94 Φ, that is 0.153 and 0.52 mm. On both sides of the central part of the beach in Sidi-Frej, a spatial organisation is drawn. To the west, toward the pier, the granulometry decreases passing from 1 to 2.21 Φ (0.50 to 0.22 mm) while eastwards, the granulometry has no obvious spatial organisation varying from 1.32 to 0.97 phi (0.40 to 0.48 mm).

We have searched for a connection between granulometry and the variations in the shore position. We present a very good relation (r = 0.91) between shore evolution and beach granulometry between the secondary port jetty and Moretti. From the oriental side of the eroding seashore (Morreti), the sediment size decreases towards the increasing sector (occidental side). The granulometry would confirm the drifting direction of the seashore toward the port from the oriental side of the shore. The sample-taking performed in 2007 is compared with the evolution of the shore in different periods, but there are no previous sedimentological analyses performed during the diachronic analysis of the shore variations

that we have performed in this article. The strong correlation obtained between granulometry and shore variations is also an argument to describe a seashore transit from East to West (the leisure port in Sidi-Frej). This method confirms the previous interpretations, but it is not enough to describe the organisation of the longitudinal transit.

Tab .1. Coastline withdrawal and advancement rate of the Sidi-Frej seashore (m/year).

Profiles	***Erosion rate*** *1972-80 (m)*	***erosion speed*** *1972-80 (m/an)*	***erosion rate*** *1980-93 (m)*	***erosion speed*** *1980-93 (m/an)*	***erosion rate*** *1993-03 (m)*	***erosion speed*** *1993-03 (m/an)*	***erosion rate*** *2003-08 (m)*	***erosion speed*** *2003-08 (m/an)*	***erosion rate*** *1972-08 (m)*	***erosion speed*** *1972-08 (m/an)*
P1	-33.24	-4.15	-52.63	-4.04	-9.69	-0.96	-2.77	-0.55	-98.33	-2.73
P2	-36.01	-4.50	-54.01	-4.15	-10.24	-1.02	-3.04	-0.60	-103.30	-2.86
P3	-38.78	-4.84	-55.40	-4.26	-10.52	-1.05	-2.49	-0.49	-107.90	-2.97
P4	-40.44	-5.05	-60.94	-4.58	-11.08	-1.10	-2.21	-0.44	-114.67	-3.18
P5	-44.32	-5.54	-59.55	-4.68	3.04	0.30	-1.27	-0.25	-102.10	-2.83
P6	-43.21	-5.40	-63.70	-4.90	4.43	0.44	2.71	0.54	-99.77	-2.77
P7	-37.67	-4.70	-66.48	-5.11	5.81	0.58	3.87	0.77	-94.47	-2.62
P8	-30.47	-3.80	-54.48	-4.19	8.58	0.85	4.15	0.83	-72.22	-2.00
P9	-16.62	-2.07	-34.32	-2.64	7.47	0.74	7.75	1.55	-35.72	-0.99
P10	-24.93	-3.11	24.10	1.85	6.77	0.67	8.58	1.71	14.52	0.40
P11	-5.54	-0.69	33.24	2.55	4.15	0.41	2.77	0.55	34.62	0.96
P12	5.81	0.72	51.52	3.96	11.63	1.16	4.15	0.83	51.52	1.43
P13	8.86	1.10	56.78	4.36	18.00	1.80	5.10	1.02	88.54	2.46
P14	22.16	2.77	63.72	4.90	19.35	1.93	5.54	1.11	110.77	3.07
P15	28.25	3.53	72.02	5.54	22.16	2.40	8.30	1.66	130.73	3.63

6. LONGSHORE SEDIMENT TRANSPORT

Longshore sediment transport occurs when waves approach the coast at an angle. According to the *Shore Protection Manual* (U.S. ARMY, 1984), this transport can be calculated using the longshore energy flux, which is given by:

$$P_\ell = \left(EC_g\right)_b \sin\alpha_b \cos\alpha_b \tag{2}$$

where α_b is the angle that the wave breaking makes with the shoreline, and it depends on the coastline orientation and the wave direction. When calculating longshore transport, a convention coordinate system has to be used, in which positive values of the angles, in degrees, mean that the waves are approaching the coast from the left, and negative angles mean that the waves are approaching the coast from the. So, transport rates with positive values will indicate that the transport is to the right, and negative values will indicate that the transport is to the left. Consequently, for the calculations of the transport, the angle that the deep-water wave direction makes with the shoreline has to be converted to this system, by:

$$\alpha = \theta_n - deep - water\ angle \tag{3}$$

where θ_n is the azimuth angle of the outward normal to the shoreline [17]. However, to calculate longshore energy flux α_b is needed (Equation 2), and it can be deduced by:

$$\sin\alpha_b = \sqrt{g\frac{H_b}{K}}\frac{\sin\alpha}{C} \tag{4}$$

where

$$C = \frac{gT}{2\pi} \tag{5}$$

The energy flux method for calculating longshore sediment transport, known as the ''CERC formula'' [17] is:

$$I_\ell = KP_\ell \tag{6}$$

where I_ℓ is the immersed weight transport rate (N/s), and *K* is a dimensionless coefficient.

The *Shore Protection Manual* [18], has proposed that *K* should be 0.39. However, the simple application of this value in the formula ignores the local sediment and hydrodynamic properties. Because of this, many authors [10]have been using the BAILARD (1981) formula to calculate different values of *K,* which depend on the beach characteristics of sediment size, sediment fall velocity, and wave breaker height and angle.

$$K = 0.05 + 2.6\sin^2(2\alpha_b) + 0.007\frac{u_{mb}}{w_f} \tag{7}$$

where u_{mb} is the maximum oscillatory velocity magnitude at the breaking point [17] given by:

$$u_{mb} = \frac{K}{2}\sqrt{gKH_b} \tag{8}$$

and w_f is the sediment fall velocity (cm/s) given by the formula (BABA and KOMAR, 1981):

$$w_f = \frac{-3\mu\sqrt{9\mu^2 + gr^2\rho(\rho_s-\rho)(0.015476 + 0.19841r)}}{\rho(0.011607 + 0.14881r)} \tag{9}$$

where μ is the water viscosity, at $20^\circ C$, known to be 0.011 poise; *r* is the grain size radius (cm); ρ is the mass density of saltwater =1.027 g/cm3; and ρ_s is the mass density of quartz 2.65 g/cm3.

In order to express sediment transport rates in volumetric units (m3/s), the *Coastal Engineering Manual* [15] suggests the formula:

$$Q_\ell = \frac{I_\ell}{(\rho_s-\rho)g(1-n)} \tag{10}$$

where *n* is the sediment porosity, assumed to be 0.4.

The parameters wf, *K*, b, and *P*_ for each location, as well as the results of longshore sediment transport (*I*_ and *Q*) are calculated. Similar to wave energy, longshore sediment transport rates are different among sectors (east, center, and west) due to the different methods of data acquisition. Because of wave sheltering effects of the groins which are shown in (fig 1), the transport rate shows large variations locally. Outside the grions zone, the sediment transport varies smoothly. The eastward transport is up to about 110000 m³/year while the westward transport is up to about 50000 m³/ year. The difference is about 60000 m³/year in the eastward direction.

7. CONCLUSION

The analysis of the air pictures concerning the seashore in Sidi-Frej combined with the granulometric study has allowed us to make a first sedimentary evaluation of this bay highlighting three sectors with different behaviours. The disturbing role of the port jetty on shore variations is proved.

After a period of strong shore variations, between 1972 and 1993, during which the coastline readjusts itself following the building of the port in Sidi-Frej, the period between 1993 and 2001 does not indicate important shore changes in the central and occidental side due to the construction of three groines in the central side of our seashore On the contrary, the Moretti coast continues to erode in time. Those who develop the seashore in Sidi-Frej should therefore remain vigilant to the erosion problems which might however persist, especially as a result of the implementation of tourist complexes on the edge dunes, whose first expected consequence is a considerable decrease in the sedimentary exchanges between the seashore side temporarily covered by high tide and dunes and a blocking of the longitudinal seashore transit. These preliminary results allow us to underline the difficulties and the complexity in developing such type of beaches.

8. REFERENCES

[1] Baba, J. and Komar, P.D., 1981, „Measurements and analysis of settling velocities of natural quartz sand grains", Journal of Sedimentary Petrology, 51(2), 631–640.

[2] Courtaud, J., 2000, „Dynamiques geomorphologiques et risques littoraux, cm du tombolo de Giens (Var, France meridionale) ", These, Universit^{y} de Provence Aix-Marseille 1, 234 pp.

[3] Crowell, M., Leatherman, S.P. and Buckley, M.K., 1991, "Historical shoreline change: error analysis and mapping accuracy", Journal of Coastal Research, 7(3): 839-852.

[4]Dolan, R., Fenster, S. M. and Homes, S.J., 1991, "Temporal analysis of shoreline recession and accretion", Journal of Coastal Research, 7(3): 723-743.

[5] Durand, P., 1999, "L'evolution des plages de 1'ouest du Golfe du Lion au XXeme siecle. Cinematique du trait de cote, dynamique sedimentaire, analyse previsionnelle", Universite Lumiere Lyon II, Lyon, 460 pp.

[6] Gronier. A. et Dubois. J.M.M., „Evolution littorale récente par télédétection : synthèse méthodologique'', Photo-interprétation, N° 1990/6, pp. 3-6.

[7] Guillemot, E. and Thomas, Y.F., 1985, „Evolution de la fleche sableuse de Los Torunos (Espagne)'', Photo Interpretation, ed. Technip, 4(1985 fasc. 2): 11-16.

[8] Leatherman, S.P., 1990, „Modelling shore response to sea-level rise on sedimentary coasts", Progress in Physical Geography, 14, 447–464.

[9] Lima, S.F.; Almeida, L.E.S.B.; and Toldo, E.E., JR., 2001, „Estimate of longshore sediments transport from waves data to the Rio Grande do Sul coast", Pesquisas, 48(2), 99–107.

[10] Moore, L.J., 2000, „Shoreline mapping techniques", Journal of Coastal Research, 16(1), 111–124.

[11] Morton, R.A.; Miller, T.L., and Moore, L.J., 2004, „ National Assessment of Shoreline Change", Part 1: Historical Shoreline Changes and Associated Coastal Land Loss along the US Gulf of Mexico. U.S. Geological Survey Open File Report 2004-1043, p. 44.

[12] Sabatier. F., 2001, "Fonctionnement et dynamiques morpho-sédimentaires du littoral du delta du Rhône'', Thèse de doctorat en géosciences de l'environnement, option géographie physique. Université d'Aix-Marseille III, 272p.

[13] Suanez, S., 1997, „Dynamiques sedimentaires actuelles et recentes de la frange littorale orientate du delta du''
[14] Wang, L. and Verger, F., 1985, „Classification des paysages et cinematique de la pointe d'Arcay par traitement automatique d'images aeriennes et spatiales'', Photo-Interpretation(85-4): 1-9
[15]U.S. Army, Cecw-Ew, 2003, „Coastal Engineering Manual", Wash ington, D.C.: Corps of Engineers Internet Publishing Group, EM 1110-2-1100.
[16]U.S. Army, Coastal Engineering Research Center (CERC), 1984, „Shore Protection" Manual, Volume 1, 4th edition. Washington, D.C.: Waterways Experiment Station, Corps of Engineers, 608p.

Ovidius University Annals Series: Civil Engineering Volume 1, Issue 12, June 2010

Nearshore and beach morphological dynamics in Mamaia Coast (Romania)

Khoudir Mezouar , Romeo Ciortan , Mohamed Amine Boukhemacha

***Abstract*- Mamaia Coast has suffered from beach erosion since the extension of breakwaters and groin of Midia Harbor was completed. This is a typical example of human impact on coastal erosion in Romania. The aim of this article is to explore the erosion at Mamaia Coast using several analyses, such as shoreline revolution detected from historical maps and air photographs, planform description of depth variation, volumetric change of bathymetry, and variations in the trends of volumetric changes of the sea bottom. Beach erosion at Mamaia Coast in response to structural effects was quantitatively determined. In an attempt to improve data treatment and interpretation, Empirical Orthogonal Function statistical analysis was performed for Mamaia beach profile data. The efficiency of the method for analysing the data was evaluated and compared with previous similar works.**

***Keywords* – Mamaia, nearshore, shoreline evolution.**

1. INTRODUCTION

Coastal morphology is the result of a complex multi-scale non-linear dynamic process that involves waves, currents and sediment transport in interaction with the changing topography. These processes have medium and large-scale components with lengths of the order of hundreds to thousands of meters and storm, seasonal, yearly and decadal periods. This multi-scale variability makes the management of the coast a question that has to be faced globally in time and space, coping with the intrinsic uncertainty associated to the stochastic character of the climatic forcing. The changes induced by long-term sea level variability introduce an additional uncertainty in the prediction of morphological behaviour and in the last decades are also becoming an important issue for management purposes. Continuous sediment volume changes in beaches are a characteristic behavior of most sandy coastlines around the world. Beach profile shape responds to meteorological and oceanographic processes, especially wind waves, on time scales that range from hours to years. Several statistical techniques for describing beach changes have been used since the 70's. [8] pioneered the use of empirical orthogonal functions (EOF) to study variations in beach profiles in time and space. [1] used this technique to analyse a 10 year data set from Gorleston and Great Yarmouth beaches, Norfolk. [6] showed the EOF's ability to describe

Khoudir MEZOUAR is with Technical University of Civil Engineering of Bucharest - TUCEB B-dul LACUL TEI, NR.124, SECTOR 2, RO-72302, BUCHAREST, ROMANIA; (e-mail: mezouarkhoudir@yahoo.fr).

Romeo CIORTAN is with Ovidius University of Constanta, Bd. Mamaia nr. 124, 900356-Constanta, Romania (e-mail: ciortanromeo@yahoo.com).

Mohamed Amine BOUKHEMACHA is with Technical University of Civil Engineering of Bucharest – TUCEB B-dul LACUL TEI, NR.124, SECTOR 2, RO-72302, BUCHAREST, ROMANIA; (e-mail: boukhemacha.amine@hotmail.com

ISSN-1584-5990

the evolution in time of beach profiles located in Poland and Bulgaria. [3] proposed a beach change prediction model, based on EOF, reinforcing the statistically prediction ability of the method.

This preliminary study deals with the implementation, use and evaluation of the empirical orthogonal function statistical analysis for Mamaia seasonal and yearly beach profile data sets referent to some of the works cited above. The EOF method applied to beach profiles was used to determine their variation through time and along the beach.

2. STUDIED AREA

The studied area (Mamaia North- Navodari) beach is situated in the south eastern extremity of Romania, near Constanta city, on a narrow sand bar, 250 – 350 m wide, between the Black Sea and Siutghiol Lake. Mamaia is the largest touristic seaside resort of Romania, stretching 8 Km from north to south. It is formed by sandy material that originates from the Danube.

Mamaia beach is facing east and is a natural low sandy beach characterised by gentle sloping underwater profile down to - 6 m. The beach consists of alluvial sediments (brought into the Black Sea by the Danube and transported to the beaches by combined wave action and the north to south flowing current along the Romanian coast) and biogenic shells sediments. The sand is fine and has a grey light colour.

The site under study is located on the Southern of Mamia beach to Media harbour between the geographical coordinates 44°20‘N - 28°38‘15”E and 44°15‘N - 28°37‘30”E. Shoreline length of the region is nearly 03 km. General alignment of the shoreline is north to south.(see figure 1)

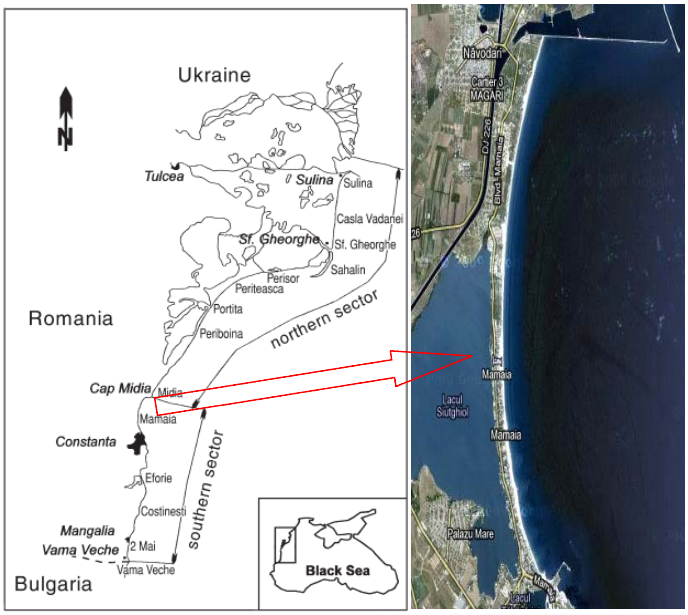

Fig. 1. Studied area (Mamaia , Romania)

3. DYNAMIC CHARACTERISTICS

The coastal zone of Mamaia is under seasonal wind regime. The hind cast wind data by the European center for medium weather forecasting (ECMWF) has been analyzed for

direction wise frequency distribution of wind speeds (figure 2). Northerly winds form NNW to NE are predominant in the Constanta area, occupying 37 percent of the total occurrences. Strong winds exceeding 10 m/sec appear frequently in the northerly direction.

The most frequent waves landing on the Mamaia coast come from the north east sector with dominating winds as well as from the north sector. Maximum wind speed is about 40 m/s. Maximum wave height during these storms is about 9.5 m and about 8 m near the shore. The North-South orientation of the Romanian shore the bathymetric contours determine the asymmetry of wave propagation. Winds from West have a confined fetch and wave crests run parallel to the shoreline because refraction in the shallow water near the shore. The highest values of the average wave parameters are recorded for waves from the East direction perpendicular to the shore: length (Lm) is about 34 m, height (Hm) about 1.2 m and the period (Tm) about 5 sec. The predominant wave direction is from NNE to E. which occupies 50% of the whole waves. Waves from S and SSW are also present with the rate of 15% because the offshore hind cast location is open to the southwest with a certain fetch, but they are small in height and short in period.

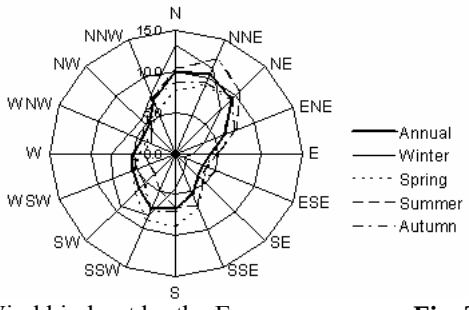

Fig. 2. Wind hindcast by the European Centre for Medium-range Weather Forecast (ECMWF) 1991-2000.

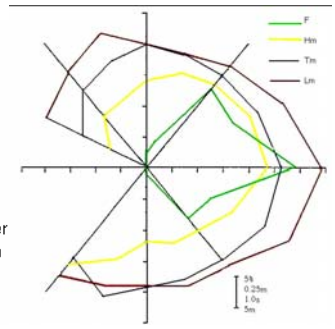

Fig. 3 Waves' parameters distribution depending on waves' direction.

4. METHODOLOGY

Beach profiles were analysed using the methodology described by [2], [4], [5] , [7] , [8]. Beach profile data was used to generate sets of empirical eigenfunctions. The data represents depth elevations (h), as a function of distance normal to the beach (x) and time (t). The concept of the method is to describe changes among different beach profiles by the smallest number possible of functions, called eigenfunctions. Each of these eigenfunctions consists of a contribution to the water depth given as a function of the distance along the profile. The first eigenfunction is selected so that it accounts for the greatest possible variance of the data (defined as the mean square of the depths). The successive eigenfunctions, which are orthogonal to the previous ones, are selected sequentially such that they represent the greatest amount of variance not yet explained.

The EOF technique may be described briefly as follows. We denote the discrete shoreline position by $y(x_l, t_k)$, where x_l is long-shore position and t_k the time of the data points, with $L \leq l \leq 1$ and $1 \leq k \leq K$. Thus, the idea of EOF analysis is to expand y as a linear combination of functions of space and time:

$$y(x_l, t_k) = \sum_{P=1}^{L} C_P(t_k) e_P(x_l) \qquad (1)$$

where e_P, often referred to as the spatial eigenfunctions, are determined directly as the eigenfunctions of the correlation matrix of the data **A**, together with their corresponding eigenvalues λ_P:

$$Ae_P = \lambda_P e_P \tag{2}$$

Hence, if **A** is real and symmetric it has L real eigenvalues, and its eigenvectors may be chosen as mutually orthonormal, that is,

$$\sum_{l=1}^{L} e_P(x_l) e_q(x_l) = \delta_{Pq} \tag{3}$$

where δ_{Pq} is the Kronecker delta. ensures that the resultant eigenfunctions form a set of statistically independent, or uncorrelated vectors, which are normalized to unity. The main factor that separates EOF analysis from other series decomposition techniques such as Fourier analysis is that rather than specifying the formof the constituent functions a priori, the data itself is used to select them. The selection is made such that the eigenfunctions best-fit the data in a least squares sense, with the first eigenfunction representing the bulk of the variability in the data set, and each subsequent eigenfunction accounting for the majority of the remaining variability. This results in the most compact representation of the data possible, ensuring that the first few eigenfunctions will describe the most significant variations.

The correlation matrix **A** is calculated from the data. It has $L \times L$ elements a_{ij} of the form:

$$a_{ij} = \frac{1}{K} \sum_{k=1}^{K} y(x_i, t_k) y(x_j, t_k) \tag{4}$$

Finally, the temporal coefficients c_P (t) called also weightings, may be calculated from equation (1) and (3):

$$c_p(t_k) = \sum_{P} y(x_l, x_k) e_P(x_l) \tag{5}$$

Several properties of real symmetric matrices may be used to aid the interpretation of some of the calculated quantities. For instance, the trace of A is equal to the mean square value (or 'energy') of the data. It is also true that the sum of the eigenvalues is equal to the mean square of the data, and so each individual eigenvalue, λ_P, represents the relative contribution of mode p to the total variability. When a real symmetric matrix is diagonalised, the diagonal elements are the eigenvalues, and the matrix rows and columns can be rearranged via elementary matrix operations so that the eigenvalues are in decreasing order, $\lambda_1 > \lambda_2 > \ldots > \lambda_L$. Then, the eigenvector e_1 is the vector that accounts for most of the mean square value and e_2 represents the maximum energy from what is left and the same with the other eigenvectors. The shape functions defined by the EOF analysis can be interpreted as various 'modes' of variation in analogy with Fourier analysis. As an example, if the data is not de-meaned, the first eigenfunction is equivalent to the time mean computed directly from the data [1]. The second eigenfunction represents the first 'mode of variation' about the time mean, and so on.

Due to the completeness of the profile data at Mamaia south, the shoreline data was decomposed into longshore and cross-shore components. This was done under the assumption that cross-shore processes result in a redistribution of sediment within the profile, while longshore processes are solely responsible for any gain or loss in sediment volume between surveys. If the further assumption is made that the observed volume changes are equally distributed over the depth of active sedimentmotion defined by (h+B), where h is the so-called depth of closure and B is the berm height, the shoreline change due to longshore processes is given by:

$$\Delta y_{ls} = \frac{\Delta V}{(h+B)} \tag{6}$$

where ΔV is the change in sediment volume between surveys. Assuming that the total shoreline change is due to a combination of cross-shore and longshore processes, the cross-shore component of shoreline change is then simply.

$$\Delta y_{cs} = \Delta y_{tot} - \Delta y_{ls} \tag{7}$$

where Δy_{tot} is the total or measured shoreline change. Prior to subjecting the Mamaia south data to EOF analysis each of the data sets was interpolated to a constant sampling interval to facilitate analysis of the results. Given the frequent and consistent sampling interval and the stable nature of the Mamaia shoreline, interpolating the data does not introduce significant error. The primary advantage of working with an interpolated data set is that the resulting temporal eigenfunctions (with constant Δt) can be subjected to spectral analysis. Peaks in the resulting spectra identify periodic variations in the temporal eigenfunctions, which can be used to help interpret the statistical modes in a physical manner.

5. RESULTS

Each of the data sets was analyzed using a systematic approach. Prior to the EOF analysis, basic statistical properties including the mean, range, and standard deviation were calculated for each data set, where the range was defined as the envelope of shoreline positions occupied at each profile location over the duration of the study. Small standard deviations and narrow ranges identify stable regions, while large standard deviations and wide envelopes are associated with regions of high variability. Empirical orthogonal function analysis was then used to identify any dominant patterns of variability within each data set. Since the original data used in this study consist of a timeseries of shoreline positions, the derived eigenfunctions, represent modes of longshore shoreline variability and an associated set of temporal coefficients.

The shorelines are projected in a common coordinate system in which the *x* axis is parallel to the longshore direction, and the *y* axis is parallel to the cross-shore direction. In order to separate the already protected part of the beach (south) and the no protected part (north), EOF analysis has been performed respectively for the North part, center part and the south part of Mamaia. For both EOF Analysis, over 92 % of the mean square of the data is contained in the first function and 97.5% of the mean square of the data is captured by the first three modes. As the data are not de-meaned, the first spatial eigenfunction corresponds to the shoreline mean position over the period. The related temporal function describes fluctuations in cross-shore position of the mean shoreline shape.

The results of the EOF analysis are summarized in Table 1, where it is shown that the first few eigenfunctions explain the majority of the shoreline variations at each site. In most

instances, the primary eigenfunction accounts for over 70% of the total variability, while the first four typically account for over 90%.

Table 1 ercentage of the total variability (pk) represented by the first four igenfunctions at each site

	Percent variance explained				
	e_1	e_2	e_3	e_4	remaining
Mamaia (south 1)	84,25%	10,21%	3,65%	0,73%	1,16%
Mamaia (south 2)	79,10%	14,15%	5,31%	0,89%	0,55%
Mamaia (south 3)	76,35%	14,76%	5,92%	1,78%	1,19%
Mamaia center	90,06%	8.89%	0.36%	0.21%	0.47%
Mamaia north	91.22%	5.34%	1.90%	0.78%	0.76%

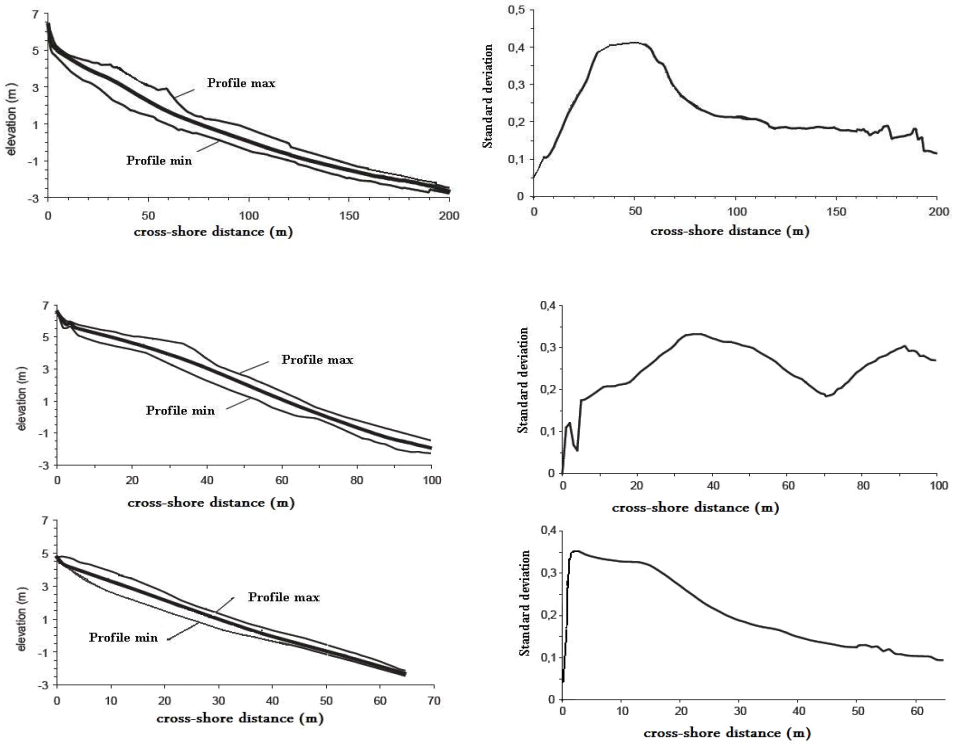

Fig. 4 Profile (min and max) and standard deviation of profiles of the three parts of Mamaia beach.

The southern beach data is decomposed into three separate data sets representing the measured shoreline change (y_{tot}), and the cross-shore (y_{cs}) and longshore (y_{ls}) components of the record. As indicated in Table 1, the first mode describes the overwhelming majority of the variability of each data set, although the variance is more evenly distributed in the component data sets. As expected, the spatial and temporal

variations become increasingly complex as the amount of variation described by each mode decreases. In the limit, these variations essentially become noise, and contain no recognizable or coherent patterns. The measured shoreline position varies by between 5 and 15 m at most locations, with the largest excursions from the mean associated with the maximum accreted condition. The dominant spatial characteristic of y_{tot} described by e_1 is a persistent linear trend which reflects the tendency for shoreline changes described by e_1 to be accentuated south of submerged breakwater. The associated temporal eigenfunction c_1 appears to contain both a linear trend as well as a long period fluctuation. In order to emphasize the interdependence of the temporal and spatial eigenfunctions, the combined mode one eigenfunction yi(x,t) is plotted. In order to emphasize both the variability within an individual mode as well as the variability between modes, the scale of the colorbar changes for each mode, while the vertical axis is held constant. The combined eigenfunction plot reinforces the three main features of mode one, including the overall accretional trend, the enhanced accretion south of the structures, and the shoreline indentation in the immediate vicinity of the structures. Compared to the complete data set, the significant variations in y_{ls} and y_{cs} are spread over a greater number of modes. The first two eigenmodes associated with y_{tot} described nearly 87% of the total variability in the data, while at least four are required to represent a similar amount of variability in the component data sets. Spatial variations similar to the consistent rhythmic features centered near the pier where not identified by the EOF analyses of the component data sets.

At the center part the first mode describes the majority of the variability (at least 90%) within each subcell, and can be considered a mean shoreline function. Most of the remaining variability is described by mode two, where together with mode one, the first two modes describe over 93% of the total variability at each site.

The statistical parameters including the mean, range, and standard deviation for Mamaia center data sets are presented. Adjacent to the boundaries, the mean shoreline is positive and advanced nearly (0,5 – 2m) with respect to the mean at the center of the site. The first spatial eigenfunction, e_1 is nearly a mirror image of the statistical mean and contains a fairly uniform interior section bounded by a region dominated by end effects. The relative importance of e_1 is reflected in its contribution of over 90% to the total variance. The dominant mode of variability about the mean beach function represented by e_2, consists of a nearly uniform shoreline advancement or recession (depending on the sign of c_2). The alternating sign of c_2 indicates that e_2 represents periods of both erosion and accretion. In the combined eigenfunction, the most obvious features are the alternating periods of erosion and accretion, and the enhanced variability near the southern boundary.

North Beach of Mamaia is also one of the most stable. End effects are typically limited to within 2 km of the boundaries, and are identified by significant increases in the mean, range, and standard deviation in these regions. Spatial eigenfunction e_1 is nearly a mirror image of the statistical mean, indicating that the primary mode of variability at the North part consists of a uniform shoreline advancement or recession with the ends experiencing similar. The shoreline changes described by mode two can also be classified as longshore uniform; however unlike mode one, the shoreline changes adjacent to the boundaries are out of phase. The combined second mode eigenfunction clearly illustrates the trends described by e_2 and c_2. The out of phase nature of the shoreline change near the

boundaries is emphasized, where accretion in the middle of the site is accompanied by erosion near the ends and vice versa.

6. CONCLUSION

Empirical Orthogonal Function analysis is an extremely useful statistical method capable of identifying the underlying patterns within noisy data sets. While EOFs have been used regularly to help identify characteristic patterns of cross-shore variability, they have been applied much less frequently to data sets which vary in the longshore direction. Longshore variability is an important concept, made even more important by the frequent and sometimes injudicious use of the assumption of longshore uniformity. The results shows that this approach allows to quantify: (1) the beach surface, (2) the natural erosion / accretion phases of the already protected shoreline, (3) the impact of beach nourishment and the trend toward the equilibrium position of the restored shoreline. Here, Empirical Orthogonal Function is used to identify the dominant modes of longshore variability within high quality shoreline data sets from three parts of Mamaia sea shore. Since EOF analysis is purely a statistical technique for identifying patterns within a data set, the results do not necessarily have an implicit physical interpretation. However, previous research has shown that given background knowledge of the environmental conditions at a site, physical interpretations of the results are often possible. As expected, shore perpendicular structures at two of the three sites are found to have a significant impact on the adjacent shorelines.

7. REFERENCES

[1] Aranuvachapun, S., Johnson, J.A., 1979, „Beach profile at Gorleston and Great Yarmouth", Coastal Engineering 2, 201–213.
[2] Dean, R. G., and Dalrymple, R. A., 2002. „Coastal Processes with Engineering Applications", Cambridge: Cambridge Univ. Press, 475p.
[3] Hsu, T.W., OU, S.H. and Wang, S.K., 1994, „On the prediction of beach changes by a new 2-D empirical eigenfunction model", Coastal Engineering, Vol. 23, p. 255-270,.
[4] Miller, J.K., Dean, R.G., 2006, „Shoreline Variability via Empirical Orthogonal Function Analysis: Part I Temporal and Spatial Characteristics", Coastal Engineering 54 (2), 111–131
[5] Miller, J.K., Dean, R.G., 2007, „Shoreline variability via empirical orthogonal function analysis: Part II relationship to nearshore conditions", Coastal Engineering 54 (2) 133–150
[6] Pruszak, Z., 1993, „The analysis of beach profile changes using Dean's Method and Empirical Orthogonal Functions", Coastal Engineering 19, 245–261.
[7] Rihouey, D., Dugor J., Dailloux D., Morichon D., 2009, „Application of remote sensing video systems to coastal defence monitoring", Journal of Coastal Research. Special Issue 56.
[8] Winant, C.D., Inman, D.L., Nordstrom, C.E., 1975, „Description of seasonal beach changes using empirical eigenfunctions", Journal of Geophysical Research 80 (15), 1979–1986.

Ways to estimate broken waves forces on vertical structures

Mirela Popa, Cosmin Filip

***Abstract* – For current design wave forces is considered as static loads because for slow oscillation due wave's period the inertial forces are negligible. Recent recorders on large scale model shows that for broken waves result high intensity pressure developed in very short time. Based on these observations, it becomes important at the beginning of the assessment of wave forces to verify meeting the criteria from breaking wave. If breaking criteria are made on can draw diagrams for hydrostatic and hydrodynamic pressure. The distribution on this pressure is related on vertical wall position from the intersection between SWL and slope. If wave breaking takes place directly on the wall and only a negligible amount of air is entrapped, resulting in a very large single peaked force followed by very small force oscillations. This load history of forces can be approximated with a triangular time-history.**

***Keywords* – breaking wave, hydrodynamic pressure, wave forces, triangular time history**

1. INTRODUCTION

Whatever form of maritime construction, the main application to which they are exposed is the horizontal force given by the waves. Changes over time depend on the wave regime and site characteristics such as structure, form and nature of the contact surface, as graphic illustrated in PROVERBS parameter map by Kortenhaus and Oumeraci 1998 [4].

For current design wave forces is considered as static loads because for slow oscillation due wave's period the inertial forces are negligible. The most formulae for estimating pressure distributions, corresponding forces and overturning moments on vertical walls due to nonbreaking and breaking waves are based on the method presented by Goda (1974) and extended by others to cover a variety of conditions. Others methods that take into account the breaking wave phenomenon, based on models tests (Wiegel 1964, Camfield 1991) are presented in [1].

In [5] and [6] Bullock and Obhrai emphasized the dynamic character by recent recorders on large scale model which shows that for broken waves result high intensity pressure developed in very short time.

An important stage of assessment of wave forces is estimated the ways of interaction waves-structure. Therefore, first reviewed the statement for breaking, responsible for

M. Popa is with Ovidius University of Constanta, Bd. Mamaia nr. 124, 900356-Constanta, Romania (corresponding author; e-mail: mpopa@univ-ovidius.ro).

C. Filip is with Ovidius University of Constanta, Bd. Mamaia nr. 124, 900356-Constanta, Romania

ISSN-1584-5990

generating high-intensity impact force with a rapid change in time, but also related phenomena such as run-up and rundown on slope.

The main objective of the paper is to provide the necessary values for modeling broken waves load in a future static and dynamic analysis.

If breaking criteria occur on can draw diagrams for hydrostatic and hydrodynamic pressure. The distribution on this pressure is related on vertical wall position from the intersection between SWL and slope, in other words, if the vertical wall is directly covered by the wave or if it is affected indirectly through the phenomenon of run up. The distributions of pressures or theirs resultants and points of application may be used for finite element static analysis.

If wave breaking takes place directly on the wall and only a negligible amount of air is entrapped, resulting in a very large single peaked force followed by very small force oscillations. This load history of forces can be approximated with a triangular time-history. Based on the load history could easily define a time curve for finite element analysis.

2. BREAKING CRITERIA AND ASSOCIATED PHENOMENA

In near-shore wavelength (L) decreases while the height (H) increases, leading to increased steepness of the wave (H/L). The phenomenon of losing their stability by breaking waves occur on reaching a limit curves is a function of relative depth and slope gradient. The process is characterized by energy dissipation and the aeration of the water mass, it depends on three parameters: the physical properties of water domain geometry, parameters associated wave.

Many studies have been developed to the discovery of relationships that allow prediction height wave at incipient breaking (H_b). Incipient breaking can be defined as the point that wave height is maximum, or the point where the front face of the wave becomes vertical.

The term breaker index is used to describe in terms of dimensionless wave height. Two factors are used frequently:

- *breaker depth index* $\gamma_b = H_b / h_b$ (h_b is depth at breaking)
- *breaker height index* $\Omega_b = H_b / H_0$ (H_0 is deepwater wave height)

From solitary wave theory, McCowan (1891) theoretically determined the breaker depth index as $\gamma_b = 0.78$. This value is commonly used in engineering practice as a first estimate of the breaker index. Munk (1949) derived the expression $\Omega_b = 0.3\left(H_0 / L_0\right)^{1/3}$ for the breaker height index of a solitary wave.

From laboratory data on monochromatic waves breaking on smooth, plane slopes, Weggel (1972) derived the following expression for the breaker depth index

$$\gamma_b = b - a\frac{H_b}{gT^2} \text{ for } \tan\beta \le 0.1,\ H_0' / L_0 \le 0.06 \quad (1)$$

T is wave period and H_0' is equivalent unrefracted deepwater wave height. The parameters a and b are empirically determined functions of beach slope, given by

$$a = 43.8\left(1 - e^{-19\tan\beta}\right); \qquad b = \frac{1.56}{1 + e^{-19.5\tan\beta}} \tag{2}$$

The breaking wave height H_b is contained on both sides of Equation II-4-5, so the equation must be solved iteratively. Fig. 1 show how the breaker depth index depends on wave steepness and bottom slope.

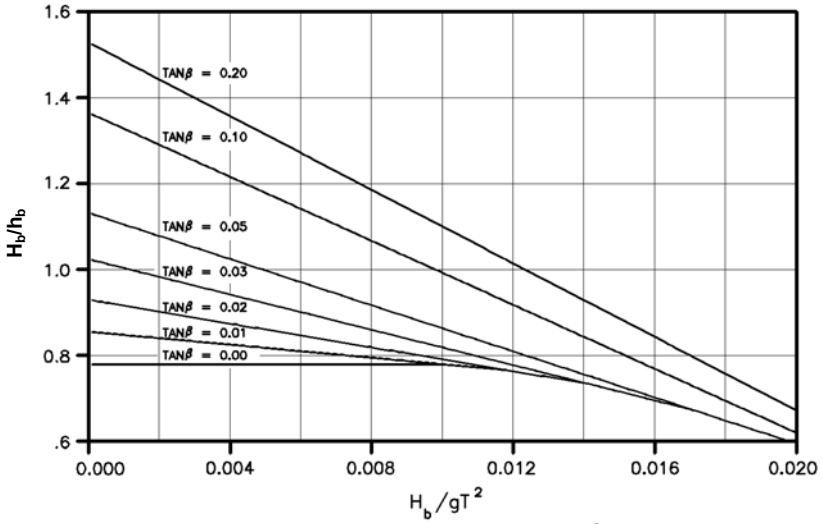

Fig. 1 Breaker depth index related on H_b/gT^2 [Weggel 1972]

Komar and Gaughan (1973) derived a semi-empirical relationship for the breaker height index from linear wave theory

$$\Omega_b = 0.56\left(H_0' / L_0\right)^{-1/5} \tag{3}$$

Experimental research (Wiegel 1964) showed that if the waves breaking on a slope located in 1:100 - 1:10, wave height located above the water level is still about 78% of broken wave height (*0.78Hb*). It is considered that the height decreases linearly, so the intersection line of the still water level with the shore line reached about 20% of broken wave height (*Hb 0.20*).

The wave breaking causes runup *Ru* and rundown *Rd*, defined as the maximum and minimum water-surface elevation measured vertically from the still water level (see Fig.2)

Runup and rundown is related by similarity parameter $\xi = \tan\beta\left(H_s / L_0\right)^{-1/2}$.

Because in the runup process incident wave crest reaches a level higher than the original crest of the wave incident, R_a (the significance of Fig. 2) is used to determine the probability that certain elements of the structure to be applied directly by waves, as crown.

R_a size corresponding to a probability of exceedance of 0.1% can be calculated based on significant wave height H_s and the surf parameter ξ

$$R_{a,0.1\%} = \begin{cases} 1.12 H_s \xi & for\ \xi \le 1.5 \\ 1.34 H_s \xi & for\ \xi > 1.5 \end{cases} \tag{3}$$

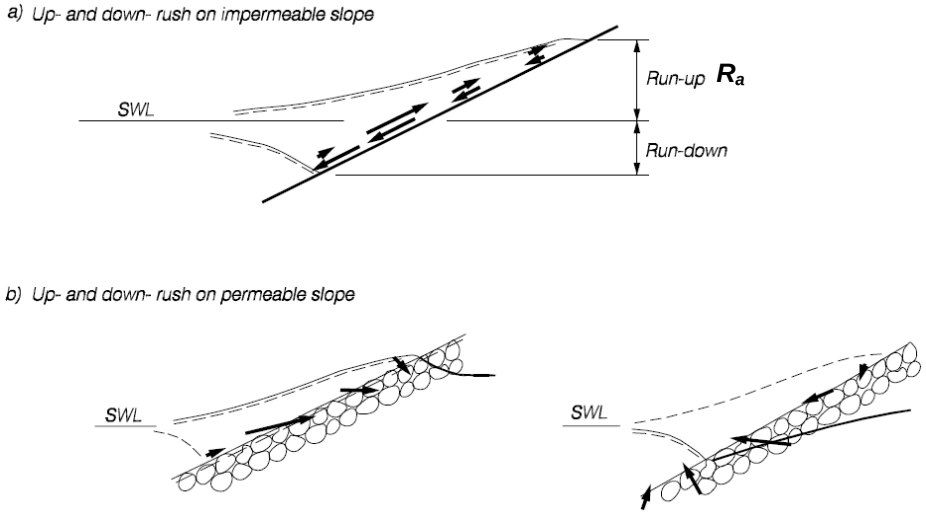

Fig. 2 Runup and rundown [Burcharth 1993]

3. WAVE PRESSURES ON VERTICAL WALLS

For vertical walls located seaward intersection between SWL and beach, is still to distinguish between dynamic pressure p_d and hydrostatic pressure p_s.

The dynamic component of pressure is a constant pressure distribution above the SWL on a wall height equal to H_w

$$p_d = \frac{1}{2}\rho C^2 = \frac{1}{2}\rho g h_b \tag{5}$$

The hydrostatic pressure has a linear variation from zero at a height H_w above the SWL to a maximum at the base of the wall

$$p_s = \rho g(h_s + H_w) \tag{6}$$

H_w is the wave height at the wall; it is determined by similar triangles

$$H_w = \left(0.2 + 0.58\frac{h_s}{h_b}\right) H_b \tag{7}$$

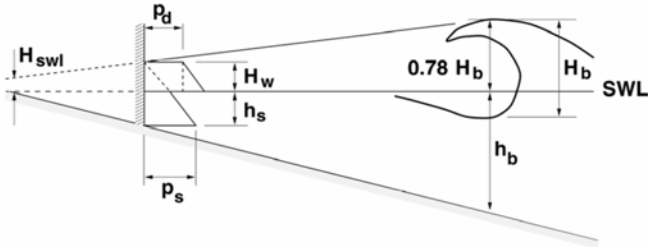

Fig. 3 Vertical wall seaward [1]

If vertical wall is located landward intersection between SWL and beach the broken wave running up slope until it reaches a maximum vertical runup height, R_a

For plane slopes in the range $0.01 \le \tan\beta \le 0.1$, if vertical wall is located in runup region, the force of per unit horizontal width of the vertical wall was approximated by Camfield (1991) is:

$$F \approx 4.5\rho g H_w^{\ 2} \tag{8}$$

where:

$$H_w = H_{SWL}\left(1-\frac{X_1}{X_2}\right) = 0.2H_b\left(1-\frac{X_1\tan\beta}{Ra}\right) \tag{9}$$

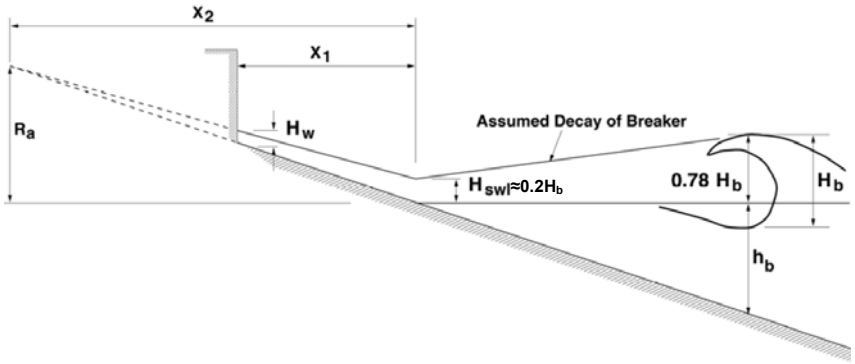

Fig. 4 Vertical wall located in the runup region [1]

4. APPROXIMATE TREATED OF SHOCK-TYPE LOAD

When waves break close to forming an vertical front just before contact with the wall and is contained only a negligible amount of air, will result a high pressure intensity and short duration. Time history of load shows a single peak, followed by very small oscillations, as is revealed by the results of large-scale models [5].

Based on investigation carried out of several large-scale models of structures with vertical walls, for the magnitude of impact horizontal forces is proposed the following relationship:

$$F_{h,\max} = 15\rho g d^2\left(\frac{H_s}{d}\right)^{3.134} \tag{10}$$

where H_s – significant wave height; d - water depth

For practical purpose the history of impact forces can be reduced to triangular load, defined by relative impact force peak (F^*_{hmax}), the rise time (t_r) and total duration of the impact t_d [4]

$$F^*_{h,\max} = {F_{h,\max}}\Big/{\rho g H_b^2} \tag{11}$$

$$t_r = k\cdot 8.94\frac{\sqrt{d_{eff}/g}}{F^*_{h,\max}};\quad t_d = t_r\left(2+8e^{-18\frac{t_r}{T}}\right) \tag{12}$$

where d_{eff} can be assumed to be identically to the breaking depth.

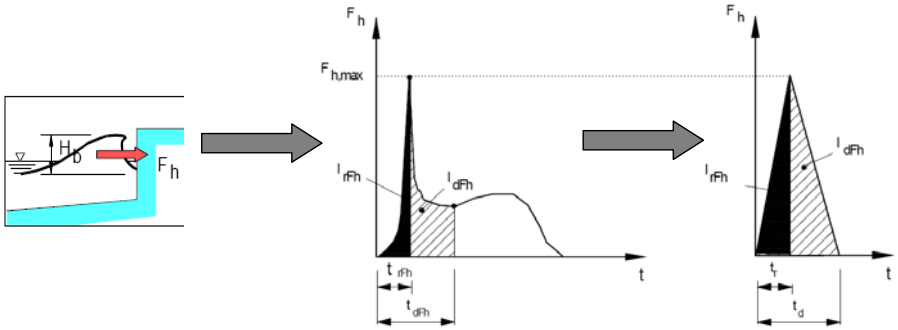

Fig. 5 Substitution history of impact load by an triangular load [4]

5. NUMERICAL APLICATIONS

In this section is present the results obtained by applying the relationships from the previous sections and it will consider the following input data:

- a regular wave with wave height *H =1.35m*, the period *T = 8s*, the water depth *d=4.5m→$L_0 \cong 100m$*
- water depth in front of wall *hs=1.5m*
- slopes on the vertical wall is located *tanβ=1:10*

These data are similar with the physical model of [5].

Identify the depth and wave height at incipient breaking

Height wave at incipient breaking (Hb) is calculated by applying the relationship proposed by Munk and 1.7m value is obtained, of which 1.326m above SWL

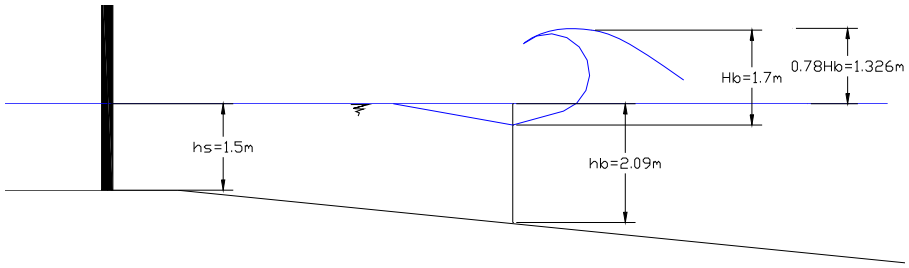

Fig. 6 Depth and height at incipient breaker

$$\Omega_b := 0.3 \cdot \left(\frac{H_0}{L_0}\right)^{\frac{-1}{3}} \quad \Omega_b = 1.259 \quad H_b := \Omega_b \cdot H_0 \quad H_b = 1.7\text{m} \quad 0.78 \cdot H_b = 1.326\text{m}$$

Breaker depth is 2.09 m (calculated by Weggel)

$$a := 43.8\left(1 - e^{-19 \cdot \tan\beta}\right) \quad a = 37.249 \quad b := \frac{1.56}{\left(1 + e^{-19.5 \cdot \tan\beta}\right)} \quad b = 1.366$$

$$\gamma_b := b - a\cdot\frac{H_b}{g\cdot T^2} \quad \gamma_b = 0.813 \quad h_b := \frac{H_b}{\gamma_b} \quad h_b = 2.09m$$

Breaking wave forces generated on a wall located in the surf zone

It was determined that the wave height is 1.048 m to the impact with the wall.

$$H_W := \left(0.2 + 0.58\cdot\frac{h_s}{h_b}\right)\cdot H_b \quad H_W = 1.048m$$

Hydrostatic pressure has a linear distribution with maximum value 25.26 kPa; its resulting (for a wall thickness of 1 m) is 32,178 kN, and applied to the foot wall at 0.849m.

$$ps := \rho\cdot g\cdot\left(h_s + H_W\right) \quad ps = 25.26kPa \quad Rs := ps\cdot\frac{\left(h_s + H_W\right)}{2} \quad Rs = 32.178\frac{1}{m}kN$$

$$\frac{h_s + H_W}{3} = 0.849m$$

Hydrodynamic pressure has a constant intensity of 10,362 kPa; its resultant 10,856 kN is applied at 2.024m from the foot wall.

$$pd := \frac{1}{2}\cdot\rho\cdot g\cdot h_b \quad pd = 10.362kPa \quad Rd := pd\cdot H_W \quad Rd = 10.856\frac{1}{m}kN \quad h_s + \frac{H_W}{2} = 2.024m$$

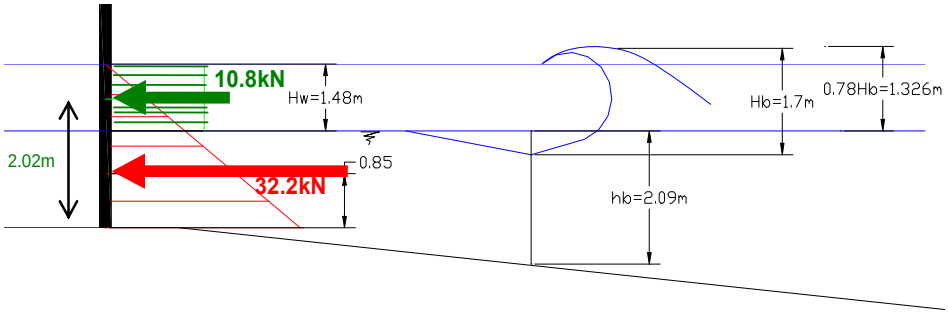

Fig. 7 Dynamic and hydrostatic pressure distribution for breaking wave

Approximating dynamic loading history due to breaking wave by triangular shock

It was determined that magnitude of horizontal impact force (for wall with a thickness of 1 m) is 240kN, about 8.4 times higher than the reference force $\rho\cdot g\cdot H_b^2$

$$Fh := 15\cdot\rho\cdot g\cdot d^2\cdot\left(\frac{Hs}{d}\right)^{3.134} \quad Fh = 240.515\frac{1}{m}kN \quad Fhr := \frac{Fh}{\rho\cdot g\cdot {H_b}^2} \quad Fhr = 8.391$$

Time rise, total duration of impact also are dependent on empirical constant k; field for this constant is quite large (0.002-0.2), leading a wide range of values for rise time (1ms – 98 ms). For the entire range, t_d results about 10-8.5 times higher than t_r.

$k := 0.002$ $d_{eff} := h_b$ $d_{eff} = 2.09m$

$tr := k \cdot 8.94 \frac{\sqrt{\frac{d_{eff}}{g}}}{Fhr}$ $tr = 0.98410^{-3} \cdot s$ $td := tr \cdot \left(2 + 8 \cdot e^{-18\frac{tr}{T}}\right)$ $td = 9.8210^{-3} \cdot s$

$k := 0.2$ $d_{eff} := h_b$ $d_{eff} = 2.09m$

$tr := k \cdot 8.94 \frac{\sqrt{\frac{d_{eff}}{g}}}{Fhr}$ $tr = 98.3710^{-3} \cdot s$ $td := tr \cdot \left(2 + 8 \cdot e^{-18\frac{tr}{T}}\right)$ $td = 827.45210^{-3} \cdot s$

6. CONCLUSIONS

The precision of the response for maritime structures, evaluated by numerical methods, depending on way the wave action is modeled. If the necessary conditions for wave breaking occurs, we can choose one of these variants

- load structure with corresponding pressures of the hydrodynamic and hydrostatic component or with their resultants, deducted as exemplified in section 5.
- replacing the impact pressure by equivalent load triangular shock type and make a dynamic analysis; a high degree of uncertainty in determining the pulse duration is introduced by empirical coefficient *k*; it is known that into a dynamic analysis the ratio of total pulse duration and the period is an important factor in the amplitude response.

In a following paper will examine the state of stress in the vertical wall related to empirical coefficient *k*.

6. REFERENCES

[1] Burchartch H. F., Hughes S. A., "Coastal Engineering Manual, Fundamentals of desingn" EM 1110-2-1100, pp II-4-1…II-4-6 VI-5-3…VI-5-18, VI-5-154…VI-5-160, VI-5-206…VI-5-209, available http://140.194.76.129/publications/eng-manuals/em1110-2-1100

[2] Camfield, F. E. "Wave Forces on Wall," Journal of Waterway, Port, Coastal, and Ocean Engineering, Vol 117, No. 1, pp 76-79.

[3] Kirkgoz M. S, Tanrikulu K., Dundar C - Dynamic analysis of a vertical plate exposed to breaking wave impact in Ocean Engineering 31(2004), ELSEVIER

[4] Kortenhaus A., s.a, "Chapter 5.1: Wave impact loads - pressures and forces" available http://www.tudelft.nl/live/binaries/ ec906edd-af0e-4ba1-bcd8-18e7e7cd73ab/doc

[5] Obhrai C., Bullock G., Woltres G., Muller G., Peregrine H., Bredmose H., Grune J. – "Violent wave impact on vertical and inclined walls: large scale model test", in Proc. 29th International Conference on Coastal Engineering ASCE Lisbon, 2004

[6] Bullock G, Obhrai C, Peregrine H, Bredmose H,– "Violent breaking wave impacts. Part1: Results from large scale regular wave test son wave impact and sloping walls", in Coastal Engineering 54 (2007) ELSEVIER

[7] Peregrine DH –Water wave impact on walls, Anual Reviews of Fluid Mechanics, Vol. 35

SECTION II

COMPUTATIONAL METHODS IN WATER RESOURCES

Composite Roughness Methods with Unsteady and Steady Flow

Angela M. Carmi-Duren, Bassam A. Younis, PhD

***Abstract* – There are several methods for determining the composite roughness value for a given channel reach and many studies have evaluated the performance of these methods in steady, uniform flow conditions. This paper evaluates the performance of five well-known composite roughness methods using steady and unsteady computation procedures. The performance between the composite roughness values were nearly the same in the cases of steady and unsteady flow. Overall, the effect of the hydraulic radius component in the applicable methods in steady flow translates to the same effects in unsteady flow.**

***Keywords* – composite roughness, Manning's roughness coefficient, steady flow, unsteady flow**

1. INTRODUCTION

A composite channel is one in which the roughness varies along the wetted perimeter. In estimating normal depth and flow behavior in channels, often a composite roughness coefficient is determined, based upon the differing roughness of one subsection with another; for example the roughness coefficient of the channel bed and the channel banks.

There are several methods for determining the composite roughness value for a given channel reach and many studies have evaluated the performance of these methods in steady, uniform flow conditions. Younis, Sousa, & Meireles [1], Yen [2], and Yang, Cao, & Liu [3] have examined well-known composite roughness coefficient methods, including five well-known methods of Pavlovskii [4], Lotter [5], Einstein & Banks [6], Cox [7], and Yen [8]. Younis, Sousa, & Meireles [1] tested these five methods assuming steady flow, with a rectangular channel and adjacent rectangular floodplains. The study found that four of the methods yielded two asymptotic water depths, depending on whether the initial depth was above or below the banks of the floodplain. The Lotter method produced a unique asymptotic water depth, regardless of the initial depth, that corresponded to the correct water depth for the given flow and channel geometry. The study found that the difference in the performance of the composite n-value methods in the steady model was attributed to the variation of $AR^{2/3}$ to two different depths; one above bankfull and one below [1].

Yang, Cao, & Liu [3] compared the resulting composite roughness values determined from several composite roughness methods in a steady flow model with laboratory data in a compound channel (trapezoidal channel with adjacent floodplains). This study concluded that the Lotter [5] method (for all channel division types) had the lowest relative error as compared to the laboratory results. Additionally, the study determined that the computed

Angela M. Carmi-Duren is with the United States Army Corps of Engineers, Engineering Division, Sacramento, California. (+1 – 916 – 557 7062. e-mail: Angela.M.Carmi@usace.army.mil).

Bassam A. Younis is with Department of Civil & Environmental Engineering, University of California, Davis (e-mail: BAYounis@ucdavis.edu).

ISSN-1584-5990

composite roughness values are closely related to the channel division (i.e. vertical, diagonal, horizontal, and bisectional channel divisions). However Yen [2] determined that the differences of the required geometry data required among the composite roughness equations had a greater impact then the division of subsections of a channel. Yen [2] evaluated the performance of seventeen different composite n-value methods with steady, uniform flow in a hypothetical trapezoidal channel, with adjacent floodplains.

Helmio [9] studied composite roughness in unsteady flow conditions, in a compound channel. The study used Nuding's method to handle the roughness and lateral shear stress between the main channel and floodplain, and divided the compound channel into vertical subsections. The Nuding's method is a computation procedure in which the contribution of the main channel and floodplains to the overall discharge is determined for a known water surface level [9]. According to Helmio [9], Nuding's method can be applied to a compound channel if the contributing width of the floodplain is less than one-fifth of the main channel width and flow is subcritical.

In general, composite roughness values are determined for a main channel with varying roughness from the channel bed and channel banks, or in compound channel with comparatively small floodplains to the main channel. In the Hydrologic Engineering Center (HEC) Riverine Analysis System (RAS) flow routing model, the method of Einstein and Banks [6] is employed exclusively in the main channel of a cross section [10].

This paper evaluates the performance of five well-known composite roughness methods using steady and unsteady computation procedures.

2. EXPERIMENT DESCRIPTION

The channel configuration for the steady and unsteady analysis involves a simple hypothetical trapezoidal channel with a base of 30 feet, side slopes of 3, and a longitudinal slope of 0.1 percent (Fig.1). The Manning's roughness coefficient for the channel bed is 0.03 and both banks are 0.01. The channel is divided vertically into three sections for estimating the composite roughness, based upon these divisions of roughness coefficient.

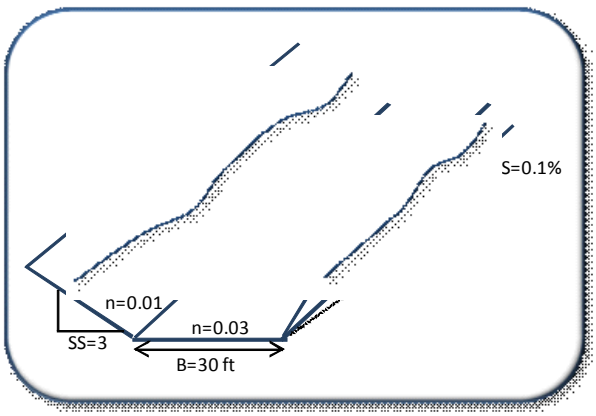

Fig. 1. Channel Configuration

The inflow hydrograph, used in the unsteady analysis is a simple wave, with a peak of 727 cubic feet per second (cfs) and a baseflow of 250 cfs. The steady analysis uses the base flow of 250 cfs.

Steady Analysis

The solution in the steady system is obtained by using numerical approximation to solve the equations for gradually varied flows:

$$\frac{dy}{dx} = \frac{S_0 - S_f}{1 - \frac{Q^2}{gA^3}\frac{dA}{dy}} \tag{1}$$

$$S_f = \left(\frac{Q}{K}\right)^2 \tag{2}$$

$$K = \frac{c_m}{n_c} AR^{\frac{2}{3}} \tag{3}$$

Where S_0 is the bed slope, S_f is the friction slope, Q is the flow, g is the acceleration due to gravity, A is the flow area, K is the channel conveyance, c_m is the unit conversion constant, n_c is the Manning's composite roughness value, and R is the hydraulic radius.

Other coefficients that can be used to represent flow resistance are the Chezy coefficient C, and the Darcy-Weisbach coefficient, f. These are correlated (in English units) as follows:

$$C = \frac{1.489R^{\frac{1}{6}}}{n} = \sqrt{\frac{8}{f}} = \frac{V}{\sqrt{RS}} \tag{4}$$

Where R is the hydraulic radius, V is the flow velocity, and S is the frictional slope. Since the Manning, Chezy, and Darcy-Weisbach coefficients can be correlated, for this study we examine composite roughness coefficient in terms of Manning's n.

The computational procedure is the standard step method to compute the water depth and surface elevation, as a function of spatial increment, x. This method is limited to apply when the change in depth with respect to the spatial increment is relatively small and is the method used in the HEC-RAS model [10]. In the iterations for the normal depth in steady flow, the iterations were set to end when the normal depths were within one ten thousands of the previous value.

The value assigned to the composite Manning's n value, n_c, is expected to represent the effective roughness of the entire cross section. Several methods for estimating n_c can be found in the literature. A comprehensive review can be found in Yen [2]. Amongst the more widely used methods, and those that are evaluated in the paper, are:

1. Pavlovskii [4]: $$n_c = \left(\frac{1}{P}\sum_{i=1}^{N} P_i n_i^2\right)^{1/2} \tag{5}$$

2. Lotter [5]: $$n_c = PR^{5/3}\left(\sum_{i=1}^{N} \frac{P_i R_i^{5/3}}{n_i}\right)^{-1} \tag{6}$$

3. Einstein and Banks [6]: $$n_c = \left(\frac{1}{P} \sum_{i=1}^{N} P_i n_i^{3/2} \right)^{2/3} \quad (7)$$

4. Cox [7]: $$n_c = \frac{1}{A} \sum_{i=1}^{N} A_i n_i \quad (8)$$

5. Yen [8]: $$n_c = \frac{1}{PR^{1/3}} \sum_{i=1}^{N} P_i R_i^{1/3} n_i \quad (9)$$

Unsteady analysis

The conventional approach to the routing of a flood wave in a river is to solve the unsteady, one-dimensional (1D) form of the equations for conservation of mass and momentum. These are the well-known St Venant equations which can be written as:

$$\frac{\partial U}{\partial t} + \frac{\partial F}{\partial x} = G \quad (10)$$

Where $$U = \begin{bmatrix} A \\ Q \end{bmatrix} \quad (11)$$

$$F = \begin{bmatrix} Q \\ \beta \frac{Q^2}{A} \end{bmatrix} \quad (12)$$

$$G = \begin{bmatrix} 0 \\ gA(S_0 - S_f) \end{bmatrix} \quad (13)$$

Where the values in the top of the vectors represent the continuity equation and the vallues in the bottom of the vector form the momentum equation. A is the flow area, Q is the flow, β is the coefficient of non-uniform flow velocity distribution, g is the acceleration due to gravity, S_0 is the bed slope, and S_f is the friction slope. The effects of surface roughness enter the equations via S_f and the river conveyance K, given respectively in equations (2) and (3).

The unsteady simulations were performed by solving the St Venant equations using finite differences. The MacCormack scheme was used and is executed in the following stages:

Stage 1-Predictor Step:

$$U_i^p = U_i^n - \frac{\Delta t}{\Delta x}(F_{i+1}^n - F_i^n) + \Delta t G_i^n \quad (14)$$

Stage 2-Corrector Step:

$$U_i^c = U_i^n - \frac{\Delta t}{\Delta x}(F_i^p - F_{i-1}^p) + \Delta t G_i^p \tag{15}$$

The new value is then the average of the predictor and corrector step:

$$U_i^{n+1} = \frac{1}{2}(U_i^p + U_i^c) \tag{16}$$

This is a second-order accurate explicit scheme with the time-step size limited by the (Courant–Friedrichs–Lewy) CFL constraint of being less then one:

$$0 < \frac{c\Delta t}{\Delta x} < 1 \tag{17}$$

The method of characteristics was employed for inlet and outlet conditions.

3. RESULTS AND SIGNIFICANCES

The composite n-values obtained at the outlet in both the steady and unsteady cases were the same (Table 1). It is important to note that in the steady flow analysis, if the starting depth was 0.7 to 1.5 times the initial normal depth calculations, each method would asymptote to its own unique normal depth (Fig.2).

Table 1. Unsteady and Steady Results

Method	Steady Outlet		Unsteady Outlet	
	Asymptotic Depth	Composite n-value[1]	Asymptotic Depth	Composite n-value[1]
Pavlovskii (1931)	2.34	0.025	2.61	0.025
Lotter (1933)	1.39	0.010	1.49	0.010
Einstein and Banks (1950)	1.86	0.017	2.07	0.017
Cox (1973)	1.58	0.013	1.73	0.013
Yen (1991)	1.68	0.014	1.86	0.015

[1] These composite n-values represents the outlet values; the point at which the asymptotic depth is obtained.

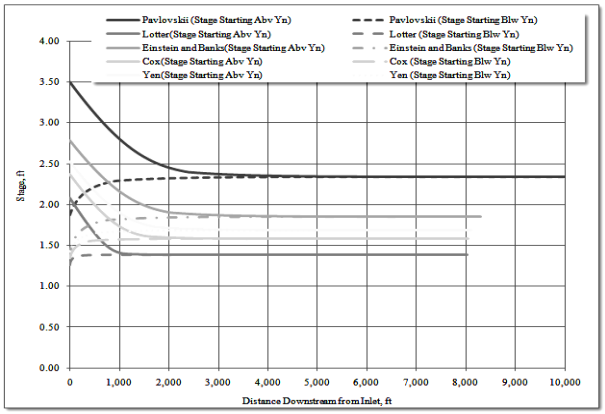

Fig. 2. Steady analysis of composite roughness methods starting above and below the normal depth

Although the composite n-value at the outlet is the same in both case of steady and unsteady flow, the asymptotic depth in the unsteady analysis was slightly larger due to the residual effect of the intermediate composite n-values obtained throughout the flood routing (Table 1).

The Lotter [5] method showed the least variation of the composite n-value from the channel bed roughness coefficient in the unsteady case, as flow is routed through the channel. This is reflected in the higher peak of the routed wave from the Lotter [5] method (Fig.3).

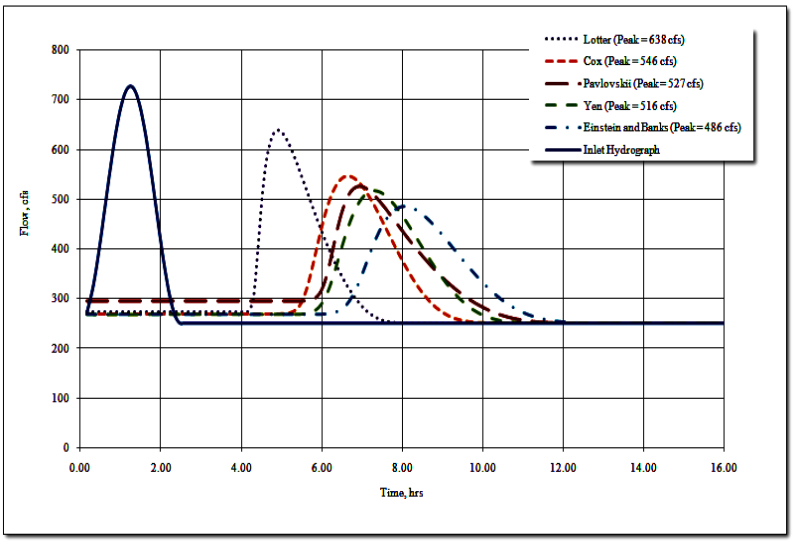

Fig. 2. Unsteady flow routing with the composite roughness methods

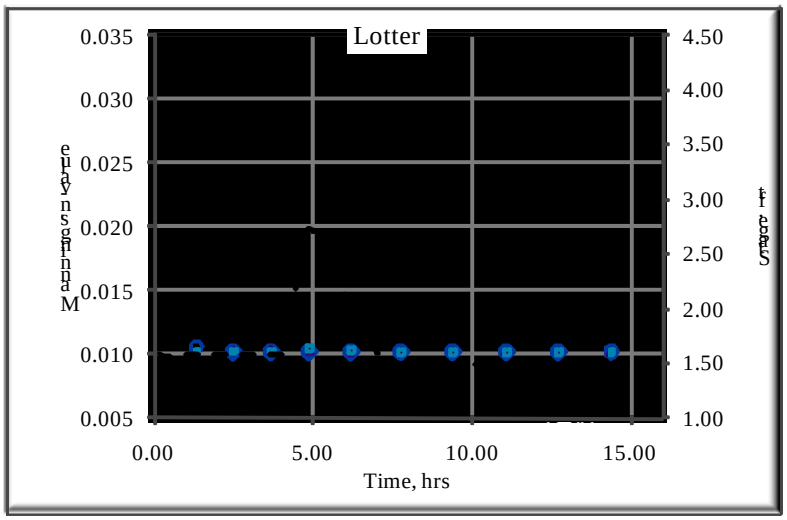

Fig. 3. Variation of the composite roughness value and stage in the unsteady flow analysis with the Lotter method.

Recall the Lotter equation (6) depends most heavily, more than the other methods, on the hydraulic radius. In calculation of the hydraulic radius for each subsection, the wetted

perimeter between the internal imaginary subsection boundaries is not counted in the overall composite *n*. This is misleading, as it discounts the momentum and energy transfer between the flow mass of each subsection [2]. Interestingly, it is this method that performed most consistently in the steady flow experiments of Younis, Sousa, & Meireles [1] study in obtaining the correct normal depth regardless of the starting depth. As explained in their paper and illustrated in Fig. 4, it is due to the fact that the Lotter [5] method obtains the greatest reduction in the composite roughness value with depth and therefore does not reach equilibrium outside of the expected correct normal depth.

The Pavlovskii method had a significantly larger asymptotic value in both methods, due to the larger composite n-values (Table 1, Fig.5). Recall from equation (5) that this method relies solely upon the wetted perimeter. The method of Einstein and Banks [6], equation (7), also relies solely upon the wetted perimeter, but does not weight the corresponding n-value to the given subsection as heavily as the Pavlovskii [4] method. The greater weight of the wetted perimeter applied to the composite n-value in the Pavlovskii method [4] results in a substantial deviation of the normal depths obtained in the other methods, for both the steady and unsteady cases.

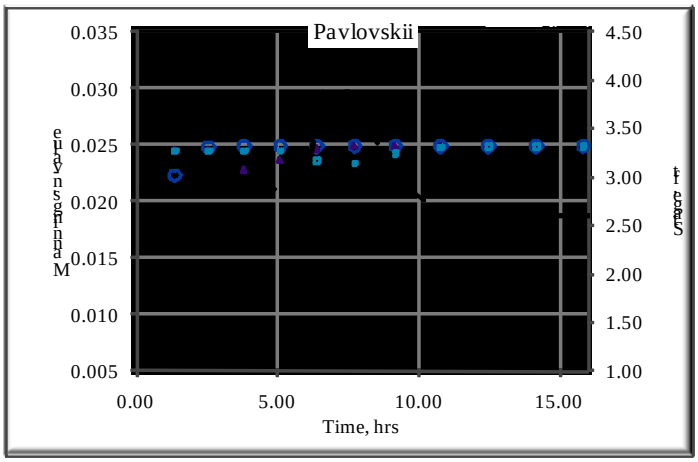

Fig. 4. Variation of the composite roughness value and stage in the unsteady flow analysis, with the Pavlovskii method.

The methods that incorporate the hydraulic radius and flow area, Lotter[5], Cox[7], and Yen [8], produced significantly lower asymptotic depths and composite roughness values. This can have a significant effect on the resulting peak of the routed flow wave (recall Fig. 3). In the case of Einstein and Banks [6] and the Lotter [5] method, this resulted in a 150 cfs peak flow difference (Fig. 3). Overall, the slope of the relationship between stage and the corresponding composite n-values for each method, in both the steady and unsteady flow cases, are nearly identical.

4. CONCLUSION

The performance between the composite roughness values were nearly the same in the cases of steady and unsteady flow. Without laboratory data to gain insight as to the performance of these methods against each other, it is helpful to look at the average composite roughness value and the deviation of each method from this. On average, the composite roughness value for the outlet of all methods is 0.016, with a standard deviation

of .006. The Pavlovlski [4] and the Lotter [5] methods dictate the extent of this standard deviation, whereas the Einstein and Banks [6], Cox [7], and the Yen [9] methods fall comfortably within this margin, in both cases of steady and unsteady flow. Overall, the effect of the hydraulic radius component in the applicable methods in steady flow translates to the same effects in unsteady flow. The Pavlovskii [4] method applies a greater weight to the wetted perimeter then in the Einstein and Banks [6] method, resulting in a substantially higher normal depth.

Without laboratory data to make substantive qualifications to each composite roughness method, it is nearly impossible to identify which equations are most universally applicable and appropriate to use. Many of the differences seen between the stages in both the unsteady and steady cases could have been attributed to inherit rounding errors in the numerical approximations.

The spatial increment in the unsteady case was relatively coarse; 50 feet, whereas the spatial increment for steady for flow was much smaller: one foot. The time increment in the unsteady flow case was variable but fluctuated between approximately 400 and 600 seconds (7-10 mins). The coarseness of the unsteady flow grid could have had an effect on the results for the composite n-values; however, due to the overall similarity between the relationship between stage and composite roughness in both steady and unsteady flow, it is unlikely.

6. REFERENCES

[1]. Younis, B. A., Sousa, V., & Meireles, I. (2009). Prediction of the asymptotic water depth in rough compound channels. *Journal of Irrigation and Drainage Engineering , 135* (2), 231-234.

[2]. Yen, B. (2002). Open channel flow resistance. Journal of Hydraulic Engineering , 128, 20-39.

[3]. Yang, K., Cao, S., & Liu, X. (2007). Flow resistance and its prediction methods in compound channels. Acta Mech.Sin. , 23, 23-31.

[4]. Pavlovskii, N. (1931). On a design formula for uniform flow in channels with non-homogenous walls. Transactions, All-Union Scientific Research Institute of Hydraulic Engineering , 3, 157-164.

[5]. Lotter, G. (1933). Considerations of hydraulic design of channels with different roughness of walls. Transactions, All-Union Scientific Research Institute of Hydraulic Engineering , 9, 238-241.

[6]. Einstein, H. A., & Banks, R. B. (1950). Fluid resistance of composite roughness. Transaction, American Geophysical Union , 31, 603-610.

[7]. Cox, R. (1973). Effective hydraulic roughness for channels having bed roughness different from bank roughness. Miscellaneous Paper .

[8]. Yen, B. (1991). Channel flow resistance: Centennial of Manning's formula. Water Resource Publications. Highlands Ranch.

[9]. Helmio, T. (2002). Unsteady 1D flow model of compound channel with vegetated floodplains. Journal of Hydrology , 269, 89-99.

[10]. Hydrologic Engineering Center (HEC). (2010). In HEC-RAS 4.1 Reference Manual (pp. 2-6 - 2-7). Davis, CA: U.S. Army Corps of Engineers, Institute of Water Resources.

Neural Network Modeling for Stable Width of Alluvial Channel Prediction

S. A. Salamatian, R. Shirkhani, and M. Mahmoodian

***Abstract* – River channel width is one of the critical parameter in the river characteristics. Estimation of river width has been studied by large numbers of Artificial neural network (ANN) is one such technique with flexible mathematical structure which is capable of identifying complex non-linear relationship between input and output data. In this study Neural Network is used for estimating the width of channels self-formed in coarse material. The performances of this network were compared with estimated results by available field data. The simulated results obtained from the proposed model are in excellent agreement with field data. Also this model compared with two available semi-theoretical models which are used widely for estimating the river width, results show that the present model gives better results than available experimental relation.**

***Keywords* – Artificial Neural Network Model, bankfull condition, Channel Morphology, Semi-Theoretical model, Stable Width.**

1. INTRODUCTION

The estimation of stable width of alluvial channel is an important topic in design of channels for irrigation and fluvial hydraulics applications. There are several approaches to analyze of this topic, namely: empirical formulas (e.g., [10], [17]), semi-theoretical methods (e.g., [7], [11]), and rational regime (e.g., [13]). However, none of these theories is widely accepted at present, due to lack of knowledge of physical processes associated with channel formation. Semi-theoretical method is one of the procedures for prediction of stable width of channels. In this procedure, some Equations derived from a combination of relationships such as flow rate, resistance to flow, and sediment load. For example, Reference [7] derived semi-theoretical hydraulic geometry relationships by combining four fundamental Equations for flow rate, resistance to flow, bed material mobility, and secondary flow in bends. These Equations were combined and solved for channel width (W), average flow depth (h), mean flow velocity (V), channels slope (S), and Shields parameter (τ^*).

S. A. Salamatian is with Amirkabir University of Technology, Department of Civil and Environmental Engineering, No. 424 Hafez Ave. Tehran, 15914, Iran; (corresponding author to provide phone:+982164543072; Fax:+982166414213; e-mail: salamatian@aut.ac.ir)

R. Shirkhani is with Amirkabir University of Technology, Department of Civil and Environmental Engineering, No. 424 Hafez Ave. Tehran, 15914, Iran; (e-mail: shirkhanireza@aut.ac.ir).

M. Mahmoodian is with Amirkabir University of Technology, Department of Industrial Engineering, No. 424 Hafez Ave. Tehran, 15914, Iran; (email: mohammad_ofu@aut.ac.ir).

ISSN-1584-5990

Artificial neural network (ANN) is one such technique with flexible mathematical structure which is capable of identifying complex non-linear relationship between input and output data without attempting to reach understanding in to the nature of the phenomena.

In this study extends the earlier contribution of reference [7] for prediction of stable width of alluvial channel with 439 field measurements. Then, we developed an ANN model by these data and finally, semi-theoretical and ANN models compare with 176 field measurements. The total data set of 655 measurements covers a wide range of flow conditions for sand-bed, gravel-bed, and cobble-bed streams with meandering to braided planform geometry. Results show that the proposed ANN model perform slightly better agreement in stable width of alluvial channel based on ±20% and ±50% error band or interval confidence.

2. CALIBRATION AND VALIDATION DATA (TRAINING AND TEST DATA)

The calibration and validation data are done with a large database including 655 measurements from [1]-[6], [8], [9], [12], [14]-[20]. In the database, 439 of total data describe field data used for model calibration in semi-theoretical model and training in ANN model. The remaining 176 field data points are used for validation or test of model. The data used for calibration and validation (training and test data) include sand-bed, gravel-bed, and cobble-bed channels with meandering to braided planform geometry. Independent variables of data points are discharge Q, mean bed particles size d_{50}, and channel slope for dominant discharge conditions. Table 1 shows the range of data used for these analyses. In this table W, Q, S, and d_{50} refer to width, discharge, slope, and mean particle size, respectively.

Table 1. Calibration and Validation data or training and test data range

Notations	Calibration data	Validation data
Number of data	439	176
W(m)	1.2-515	2-500
Q (m^3/s)	0.13-3000	2-2000
S(-)	0.00007-0.2	0.0001-0.1
d_{50} (m)	0.00012-0.45	0.001-0.3

3. MODELLING

In the topic described herein, first, earlier semi-theoretical of Julien and Wargadelam in 1995 developed for prediction of stable width with calibration data and then, ANN model developed with same data.

3.1 SEMI-THEORETICAL MODEL

Reference [7] derived semi-theoretical hydraulic geometry relationships by combining four fundamental Equations for flow rate, resistance to flow, bed material mobility, and secondary flow in bends. These Equations practical to prediction of width, depth, mean velocity, slope of channels, and Shields parameter.

Therefore, stable width of alluvial channel Equation is:

$$W = 1.33Q^{0.44}d_{50}^{-0.11}S^{-0.22} \quad (2)$$

Reference [11] developed earlier Equations from Reference [7] with larger database. They database consists of a total 1485 measurements, but the range of data were not enough to predict the reliable width stable. They proposed Equation (3) to prediction stable width of alluvial channels.

$$W = 3.004Q^{0.426}d_{50}^{-0.002}S^{-0.153} \quad (3)$$

A nonlinear analysis has been performed on the 439 field measurements of width, depth, velocity, slope, and Shields parameter as a power function of discharge Q, bed particle size d_s, and channel slope S or Shields parameter τ^*. The regression analysis has been conducted with the program SPSS. The nonlinear regression Equation that were obtained is

$$W = 2.158Q^{0.691}d_{50}^{-0.247}S^{0.264} \quad (4)$$

Figure 1 shows the calibration results for width of channel. In Fig., solid dots, solid line, and dash line refer to field measurements, perfect agreement line, and ±50% error band in the regression Equation, respectively.

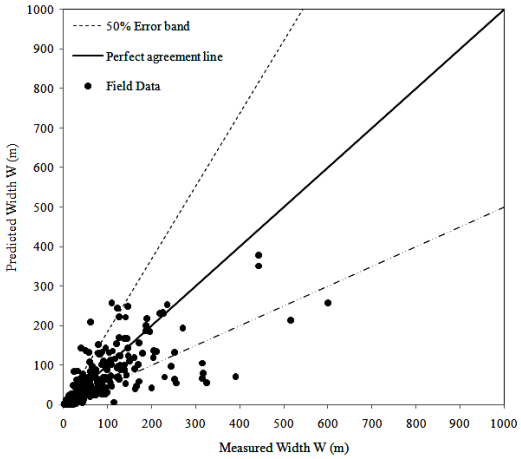

Fig. 1. Calibration of channel width

3.2 ARTIFICIAL NEURAL NETWORK

Artificial Neural Network (ANN) is a mathematical tool, which tries to represent low-level intelligence in natural organisms [6], and it is a flexible structure, capable of making a non-linear mapping between input and output spaces. If we consider the X=[x1, x2 …, xn] as input vector and W= [w1, w2 …, wn] as network parameter (weight) vector and if the goal is approximating the multi variant function f (x), the learning procedure is to find the best weight vector (W) to have the best approximation of the f (x). In this paper, Multi layer perceptron (MLP) with back propagation learning rule is used. The method of Multi layer perceptron has been described by many investigators.

In this paper, the network was designed with three parameters as input (Q, d_{50}, S) pattern and the channel width (W), as output pattern. The configuration of designed neural networks is shown in Fig. 2. It is clear that the simple network developed has a hidden layer with ten nods, which was calculated by try and error.

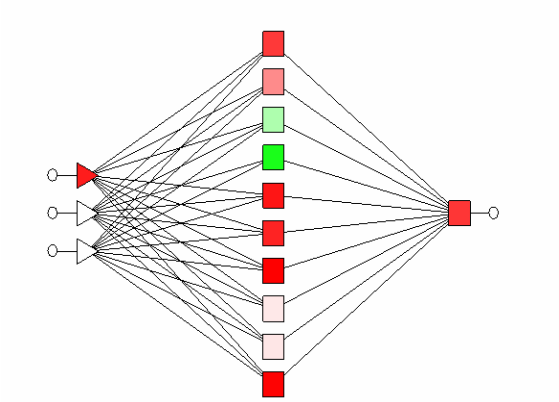

Fig. 2. Multi layer perceptron neural network learning in ANN

Figure 3 shows the variation of estimated results (W) by artificial neural networks against two input parameters (S_o, discharge). It maybe concluded that the width of scour is increased by increasing the discharge and stay constant by increasing the slop.

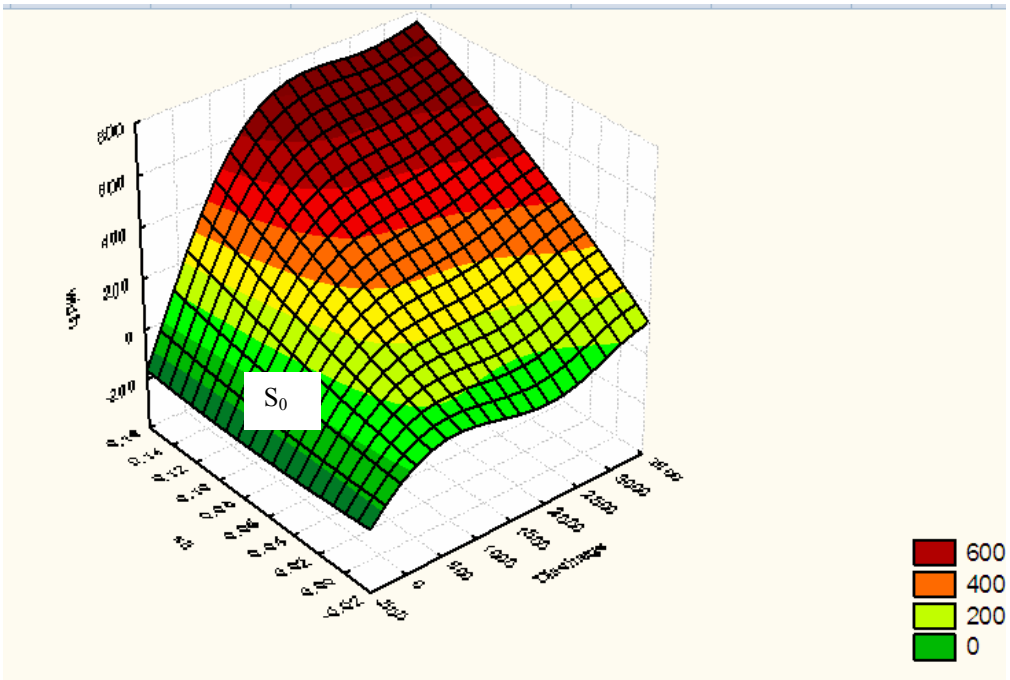

Fig. 3. The area of result by neural network

4. VALIDATION AND COMPARISON

The validation data set consists of 176 data points, these field data shown in Table 1. The field validation data classified into three bed-material types with median diameter d_{50} of sand (2.0 mm or less); gravel ($2 < d_{50} < 64$ mm); and cobble bed ($d_{50} > 64$ mm). The data set includes meandering to braiding planform geometry.

The nonlinear regression Equation that was obtained is shown in Table 2. For comparison, the J-W Equation is given in Table 2 Equation d. Also, in this table, Equation a, b, and c refer to ANN model, this study regression Equation and reference [11], respectively.

Figures 2-5 show the validation results for channel width. In these Figs., solid dots, solid line, and dash line refer to field measurements, perfect agreement line, and ±50% error band in the regression Equation, respectively. The last two columns of Table 2 show a summary of the percentage predictability scores of Equation for the validation data. The measured and predicted field channels width by ANN, S-S-G, J-W, and L-J are plotted in Figs. 2-5 and, 78.4%, 26.1%, 25%, and 26.1% of all validation field data sets fall within the ±50% error band, respectively. In sand-bed, gravel-bed and cobble-bed channels, it can be seen that from References [7, 11], and this study non-linear Equation are not well predicted in channel width (see Table 2). In terms of validation, Figs. 4-7 show channel width for field data with ANN, S-S-M, L-J, and W-J Equation, respectively. Very good agreement is obtained from ANN model.

Table 1. Comparison of Equations (models)

Author	Equation	Equation number	Calibration R^2	Error band	
				±20%	±50%
ANN	-	a	0.76	33.0	78.4
S-S-M	$W = 2.158Q^{0.691}d_{50}^{-0.247}S^{0.264}$	b	0.79	5.7	26.1
L-J	$W = 3.004Q^{0.426}d_{50}^{-0.002}S^{-0.153}$	c	-	6.8	25.0
J-W	$W = 1.33Q^{0.44}d_{50}^{-0.11}S^{-0.22}$	d	-	7.4	26.1

Note: The L-J and J-W Equations refer to from References [11] and [7], respectively. Also, the S-S-M equation refers to the regression equation presented in this analysis and ANN refers to the artificial neural network model.

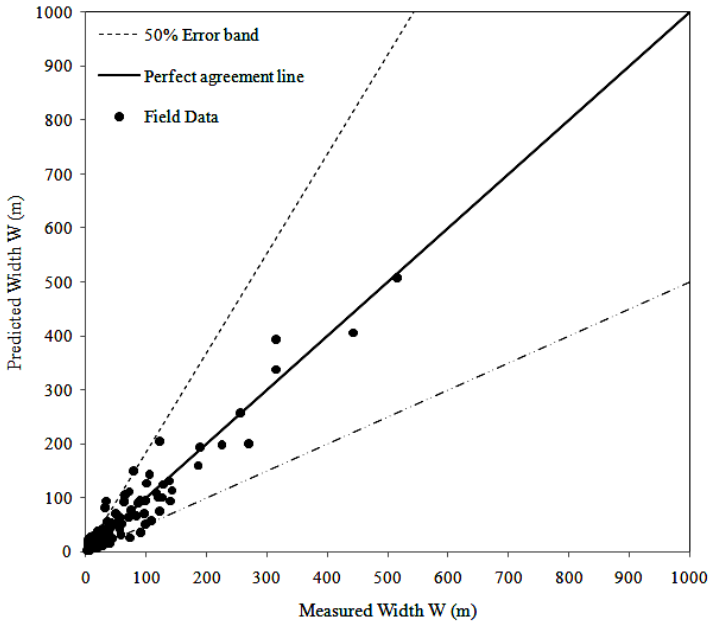

Fig. 4. Validation of channel width by ANN

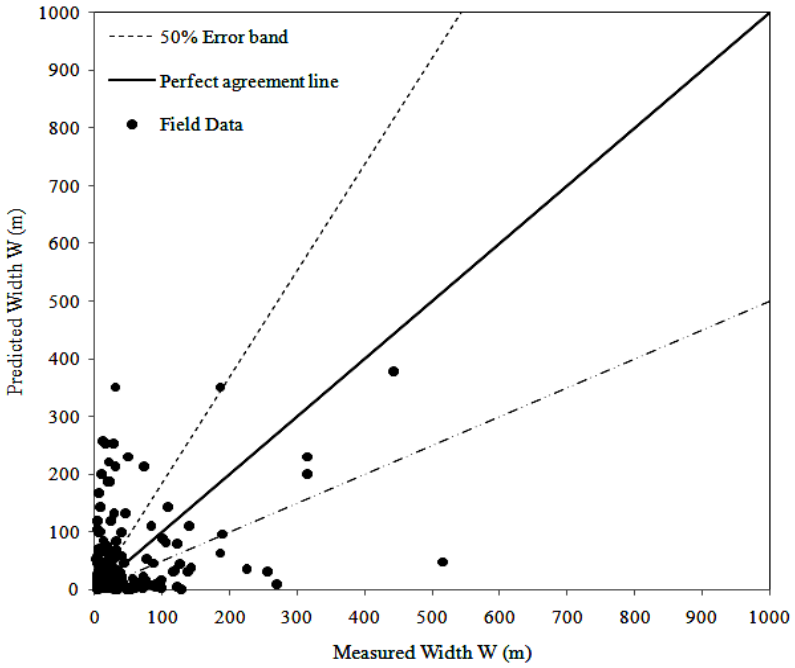

Fig. 5. Validation of channel width by S-S-M

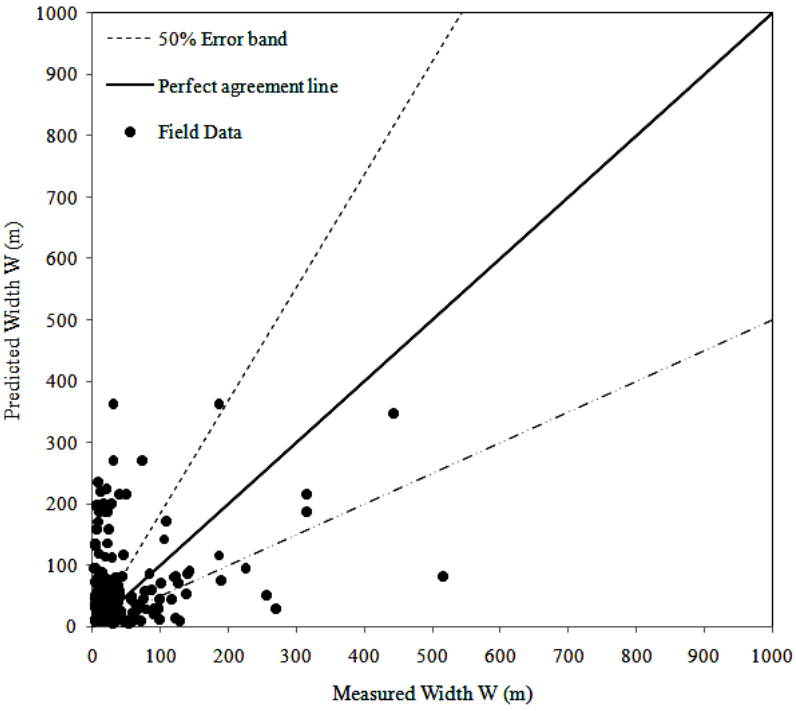

Fig. 6. Validation of channel width by L-J

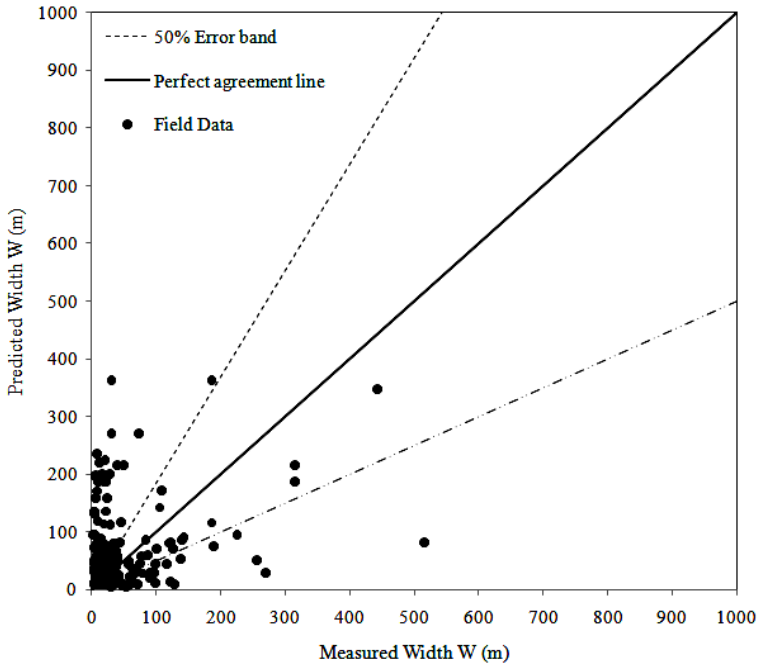

Fig. 7. Validation of channel width by J-W

5. CONCLUSION

This analysis extends the earlier contribution of reference [7]. Channel width prediction equation was obtained from a regression analysis of a large data set on downstream hydraulic geometry of alluvial rivers. This equation for channel width contains three independent variables in term of a power function of discharge, median particle size, and channel slope. The dataset used in develop this Equation consist of a total 655 data points including 439 field measurements at bankfull condition for calibration, and 176 field data for validation. Also, in this study used an ANN model to predict of channel width. Results show that the calculated value by ANN model in comparison with the J-W, L-J, and S-S-G Equation is in highly better agreement with the field measurements. The range of applicability of the proposed downstream hydraulic geometry Equation and ANN model is a channel width $1 < W < 515$ m, channels slope $0.00007 < S < 0.2$, median particle size $0.00012 < d_{50} < 0.45$ m, and bankfull discharge $0.13 < Q < 3000$ m^3/s.

6. REFERENCES

[1] Andrews, E. D., 1984, "Bed-material entrainment and hydraulic geometry of gravel-bed rivers in Colorado." Bull. Geol. Soc. Am., 95, 371–378.
[2] Bathurst, J. C., 1985, "Flow resistance estimation in mountain rivers." J.Hydraul. Eng., 111, Vol. 4, pp. 625–643.
[3] Charlton, F. G., Brown, P. M. and Benson, R. W., 1978, "The hydraulic geometry of some gravel rivers in Britain.", Report INT 180, Hydraulics Research Station, Wallingford, England, 48 p.
[4] Church, M., and Rood, R., 1983, "Catalogue of alluvial river channel regime data", Rep. Dept. of Geography, Univ. of British Columbia, Vancouver, Canada.

[5] Christiane I., Mulvihill, C.I., Filopowicz, Amy, Coleman, Arthur, and Baldigo, B P., 2007, Regionalized Equations for Bankfull Discharge and Channel Characteristics of Streams in New York State Hydrologic Regions 1 and 2 in the Adirondack Region of Northern New York: U.S. Geological Survey Scientific Investigations Report 2007-5189, 18 p.
[6] Hey, R. D., and Thorne, C. R., 1986 "Stable channels with mobile gravel beds." J. Hydraul. Eng., 112, Vol. 8, pp. 671–689.
[7] Julien, P.Y., and Wargadalam, J., 1995, "Alluvial channel geometry:Theory and applications." J. Hydraul. Eng., Vol. 121, No. 4, pp. 312–325.
[8] Kallio, S. E., 2010, "Determining the Bankfull Discharge Exceedance Potential of Agricultural Ditches in Ohio." MS.c. dissertation, Ohio State University, Ohio, USA
[9] Kellerhals, R., Neill, C. R. and Bray, D. I., 1972, "Hydraulic and geomorphic characteristics of rivers in Alberta." River Engineering and Surface Hydrology Report, Research Council of Alberta, Canada, No. 721.
[10] Lacey, G. (1930). "Stable channels in alluvium." Minutes of the Proc, Inst, of Civ. Engrs., London, England, 229, pp. 259-292.
[11] Lee, J. S. and Julien, P. Y., 2006, "Downstream Hydraulic Geometry of Alluvial Channels" Journal of Hydraulic Engineering, Vol. 132, No. 12
[12] McCandless, T. L., 2003, "Maryland stream survey: bankfull discharge and channel characteristics of streams in the Allegheny Plateau and the Valley and Ridge hydrologic regions." Report No. CBFO-S03-01, U.S. Fish and Wildlife Service Chesapeake Bay Field Office, 33 p.
[13] Parker, G., 1978a,b, "Self-formed straight rivers with equilibrium banks and mobile bed." J. Fluid Mech., Vol. 89, No. 1, pp. 109-146.
[14] Parker, G., Toro-Escobar, C. M., Ramey, M. and Beck S., 2003, "The effect of floodwater extraction on the morphology of mountain streams", Journal of Hydraulic Engineering, Vol. 129, No. 11
[15] Pitlick, J. and Cress, R., 2002, "Downstream changes in the channel of a large gravel bed river." Water Resources Research, Vol. 38, No. 10
[16] Rinaldi, M., 2003, "Recent channel adjustments in alluvial rivers of Tuscany." central Italy, Earth Surf. Process Landforms 28, pp. 587–608.
[17] Savenije, H. H. G., 2003, "The width of a bankfull channel; Lacey's formula explained", Journal of Hydrology, Vol. 276, pp. 176–183.
[18] Soar, P. J. and Thorne, C. R., 2001, "Channel restoration design for meandering rivers", Report ERDC/CHL CR-01-1, Coastal Hydraulics Laboratory, U. S. Army Corps of Engineers Engineer Research and Development Center, 416 p.
[19] Van den Berg, J. H., 1995, "Prediction of alluvial channel pattern of perennial rivers" Geomorphology 12, pp. 259-279
[20] Wohl, E., 2004, "Reach-Scale Channel Geometry of a Mountain River" Earth Surf. Process Landforms 29, pp. 969–981

Use of the Spatial Analysis Neural Network Algorithm for Regional Drought Analysis in Iran (Sann)

Saremi Ali, Arab Solghar A A, Sedghi H. and Kaveh F.

***Abstract* – Drought is one of the most serious hazards that has more effect on human societies than the others. Study an important role in drought planning and management of water resources, especially in time of crisis and predicted big event by the event that the crisis management turnover. The main objective of the research reported herein has been to develop an approach to analyze the spatial patterns of meteorological droughts based on annual precipitation data in Iran. By using a nonparametric spatial analysis neural network algorithm, the normalized and standardized precipitation data are classified into certain degrees of drought severity (extreme drought, severe drought, mild drought, and nondrought) based on a number of truncation levels corresponding to specified quantiles of the standard normal distribution. Then posterior probabilities of drought severity at any given point in the region are determined and the point is assigned a Bayesian Drought Severity Index. This index may be useful for constructing drought severity maps in iran that display the spatial variability of drought severity for the whole region on a yearly basis.**

***Keywords* – Bayesian, Drought, nonparametric spatial analysis neural network algorithm.**

1. INTRODUCTION

Reservoirs are often planned so that they will be able to supply the expected water demands during a drought of a certain magnitude, and water supply systems are often evaluated to see whether they will be able to withstand a T-year drought [3]. In any case, determining drought properties at a point and in space (or region) is an important aspect of water planning and management activities. Drought analysis may be made based on single site data [11] and multisite data [10], depending on the specific purpose of the study at hand. In this paper, we are concerned with regional droughts, so our analysis will be based on data measured at several sites in space. To analyze droughts statistically, it is necessary to specify the following factors: (1) the climatic or hydrologic variable that will be used for defining droughts; (2) the characterization of the spatial distribution of the underlying variable; (3) the truncation levels for classifying the severity of a drought at a point; and (4) the quantification of the regional drought. A number of climatic and hydrological variables, such as precipitation, stream flow, soil moisture, ground-water levels, and moisture content in the air, and similar other variables, have been widely used in the literature for characterizing regional droughts. Precipitation has been commonly used for meteorological

Saremi Ali. Lecturer and Phd Student, Islamic Azad University The Branch of Tehran Since and Research, Iran (phone: +98-912-4396772; e-mail: saremi.ptmco@gmail.com).
Arab Solghar A A Msc Student, IAU Tehran, Iran (e-mail: Ali.arabsolghar@Yahoo.com).
Sedghi H. Associate Professor, IAU Tehran, Iran (e-mail: H.sedghi@Gmail.com).
Kaveh F Fo. D Associate Professor, IAU Tehran, Iran (e-mail: Fhnkaveh@Gmail.com).

ISSN-1584-5990

drought analysis [7], while stream flow data have been widely applied for hydrologic drought analysis [3]. In this study, annual precipitation will be considered as the key variable for drought analysis.

2. EXPERIMENT DESCRIPTION

Region and Data Description

The area of Northern Iran located between 50 and 53 east longitude and 34 and 36 north latitude was used for regional drought analysis. Annual precipitation data were collected considering that (1) the observed number of years at each site be at least 30 years; (2) the number of observation points be sufficient to cover the entire area; and (3) the records be consistent both spatially and temporally. Observed yearly rainfall data from20 meteorological stations located in different parts of the Tehran province, have been selected for this study (Fig 1). The length of available records at these stations is from1979 to 2008.

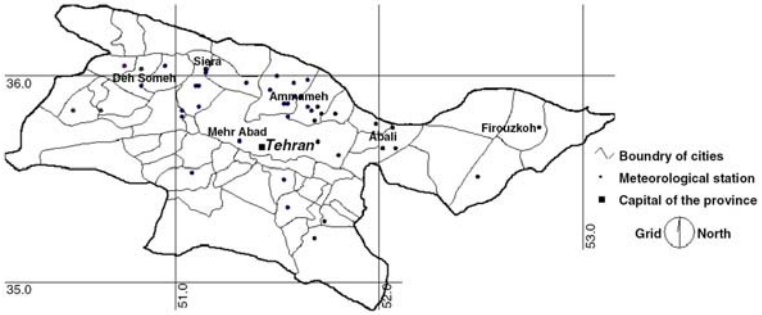

Fig. 1. A schematic map of the Tehran Province.

Normalization, Standardization, and Truncation Levels

The first step in the analysis is to normalize and standardize the historical annual precipitation data. The power and logarithmic transformations have been widely used for transforming the historical annual precipitation data into normal[4]. In the present study, the logarithmic transformation was applied. Let $Q_t(k)$ be the annual precipitation data after transformation. These data are further standardized as

$$Z_t(k) = \frac{Q_t(k) - \overline{Q(k)}}{S_Q(k)} \qquad (1)$$

where $\overline{Q_t(k)}$ and $S_Q(k)$ = mean and standard deviation of $Q_t(k)$ respectively. Hence, $Z_t(k)$ is assumed to be normally distributed, with a mean of zero and standard deviation of one. Constant truncation levels (in the standard normal domain) over the region and throughout the historical period are selected in order to identify the severity of a drought. Four degrees (classes) of drought severity are considered, namely, C^1, C^2, C^3 and C^4, representing extreme drought, severe drought, mild drought, and no drought, respectively. They are defined by the truncation levels determined by

$$\left\{\begin{array}{l} F\left[TL(1)\right]=P\left[Z\le TL(1)\right]=0.15 \\ F\left[TL(2)\right]=P\left[Z\le TL(2)\right]=0.3 \\ F\left[TL(3)\right]=P\left[Z\le TL(3)\right]=0.5 \end{array}\right\} \quad (2)$$

Where $F[.]$ represents standard normal cumulative distribution function; and $TL(.)$ =quantile for the specified probability.

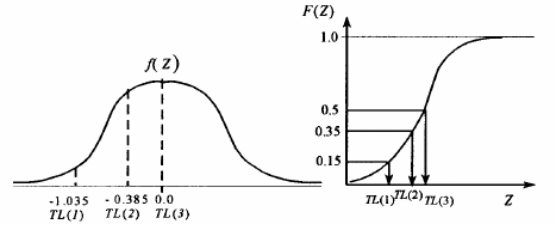

Fig. 2. Graph of Truncation Levels Based on Probability Density Function f (Z) and Cumulative Distribution Function F(Z) of Standard Normal Distribution

Thus, the truncation levels obtained from the standard normal tables are TL(1) = -1.035, TL(2) = -0.385, and TL(3) = 0.0. Fig. 2 further illustrates the definition of truncation levels. Referring to this figure, a drought at a point k occurs if Zt(k) <0. Conversely, Zt(k) > 0 signifies a no drought. Furthermore, the conditions {-0.385< Zt(k) <0},{-1.035<Zt(k)<-0.385}, and {Zt(k) < -1.035} represent mild, severe, and extreme drought severities, respectively.

Conditional Point Estimator and Classification

We want to estimate some spatial statistics at any (ungauged) point x, such as the point conditional mean estimator $\hat{Z}(x)$, the posterior probability P[Cj|x] of each drought severity at a point, and the point drought severity indicator d(x).

A nonparametric spatial analysis algorithm for point estimation and classification of spatial data.The analysis is based on Parzen's nonparametric point density estimators and the Bayesian classifier[6],[1].

Following Parzen (1962), Spetch (1991), and Bishop (1995), the conditional expectation of Z given x may be written as [6].[1],[9]

$$\hat{z}(x)=\frac{\sum_{j=1}^{4}\sum_{i=1}^{s^j}\left(\frac{1}{\sigma_x^2(i,j)}\right)Z_t(i,j)\,a_x(i,j)}{\sum_{j=1}^{4}\sum_{i=1}^{s^j}\left(\frac{1}{\sigma_x^2(i,j)}\right)a_x(i,j)} \quad (3)$$

where ax(i, j) = Gaussian kernel function (GKF) that acts as a transfer (activation) function. It is given by

$$a_x(i.j)=\exp\left[-\frac{D_x^2(i,j)}{2\sigma_x^2(i,j)}\right] \quad (4)$$

where Dx(i, j) = Euclidean distance between the input vector x and the ith center Xt(i, j) in class j

$$D_x^2(i,j)=\left[x-x_t(i,j)\right]^T\left[x-x_t(i,j)\right] \quad (5)$$

$\sigma_x(i,j)$ = width of the ith GKF in class j.

the posterior probabilities P[C|x], j = 1, . . . , 4 are determined by

$$\hat{P}\left(C^j \mid x\right) = \frac{\sum_{i=1}^{S^j}\left(\frac{1}{\sigma_x^2(i,j)}\right)a_x(i,j)}{\sum_{j=1}^{N^j}\sum_{i=1}^{S^j}\left(\frac{1}{\sigma_x^2(i,j)}\right)a_x(i,j)} \tag{6}$$

For spatial analysis of the variable z on a given region R, the Bayesian classifier provides a rule for assigning each point x to one of the four classes. The region R is regarded as being divided into subregions R1, R2, R3, R4 so that a point falling in region Rr is assigned to class Cr. The boundaries between the subregions can be determined by using the Bayesian classifier [3] as follows:

$$\begin{aligned} &If\ \max\left\{\hat{P}\left[C^1 \mid x\right],\hat{P}\left[C^2 \mid x\right],...,\hat{P}\left[C^N \mid x\right]\right\} = \hat{P}\left[C^r \mid x\right] \\ &then\ d(x) = r \\ &r = 1,...,N;\ and\ \ d(x) = class\ \text{s in}\ dicator \end{aligned} \tag{7}$$

SANN STRUCTURE

SANN is a multilayer feed forward neural network, as shown in Fig. 3. It consists of four layers, in which the neurons or nodes between layers are interconnected successively by the feed forward direction. The layers are called the input layer, GKF layer, summation layer, and estimation layer. The input layer has S nodes, each representing the x- and y-coordinates of an observation site, i.e., the vector x = [x, y]. This input coordinate vector is passed to the GKF layer with unit weights. In this layer, the observed set {Xt(k), Zt(k)|k = 1, . . . , S} is classified into four classes, becoming {Xt(i, j), Zt(i, j)|i = 1,. . . , Sj and j = 1, 2, 3, 4}.Thus, the GKF layer also consists of S nodes with Sj nodes in each class j such that S1 + S2 + S3 + S4 = S. The point Xt(i, j) is then located at the center of the ith GKF node in class j and the activation function of the GKF node, ax(i, j), is determined. Thus, each GKF node has as internal parameters the center of the GKF node Xt(i, j) and the smoothing parameter, $\sigma_x(i,j)$ .The output from each GKF node is a function of the Euclidean distance between the center Xt(i, j) and the input point x, and each GKF node only responds (or activates) when the input pattern falls within its receptive field, i.e., within the width of the GKF node $\sigma_x(i,j)$ [8].

When the input vector x is placed at the center of the GKF node Xt(i, j), ax(i, j) of (4) becomes one (the maximum value). Otherwise, it decreases exponentially as the input vector is farther from the center. The outputs of the GKF nodes are passed to the summation layer with weighted connections, as shown in Figs. 3 and 4. The summation layer estimates and gives the outputs $\sum_1$, $\sum_2$ and $\sum_{3,j}$, respectively. These outputs are passed to the estimation nodes with unit weights. Here, the conditional mean $\hat{z}(x)$ and the posterior probabilities P[Cj|x], j = 1, 2, 3, 4 are determined by:

$$\sum\nolimits_1 / \sum\nolimits_2 = \hat{z}(x) \tag{8}$$

$$\sum\nolimits_1 / \sum\nolimits_{3,j} = \hat{P}\left[C^j \mid x\right] \tag{9}$$

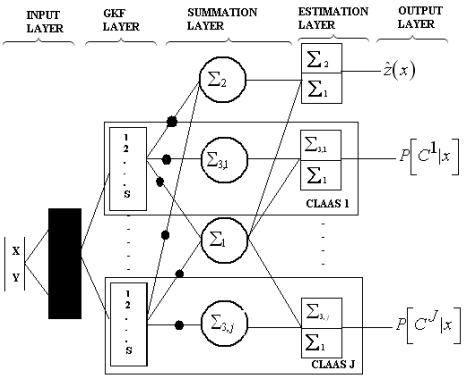

Fig. 3. Structure of SANN for Regional Drought Analysis

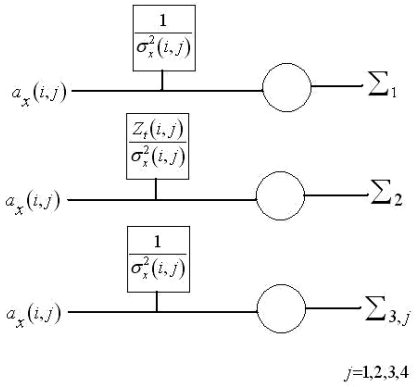

Fig. 4. Weighted Connections between GKF Nodes and Summation Nodes; Activation Function *ax*(*i*, *j*) Passes to Summation Layer Using Weights Shown in Rectangles; Index j(*j* = 1, . . . ,4) Relates to Class *Cj* and Index i (*i* = 1, . . . , *Sj*) Represents Specific Site Belonging to Class *Cj*

SANN TRAINING

The training is carried out by the so-called unsupervised training, in that the input data set Xt(i, j) alone is used to determine the parameters of the GKF. While this may not be optimal, it gives fairly good results. There is no reason why one cannot optimize the parameters in another phase of training, but one should also keep in mind that training needs to be done for each year of the record and optimizing for every year may be time consuming. The training procedure based on normalized and standardized annual precipitation data may be summarized as follows:

1. Enter the observation data set {Xt(k, Zt(k)|k = 1, . . . ,S}, where S is the total number of sites, and define the classes C^j = { C^1, C^2, C^3, C^4 } based on the truncation levels defined above. Then, classify the observation data set and get {Xt(i, j), Zt(i, j)|i = 1, . . . , Sj and j = 1,. . . , 4}.

2. Set the center of the ith GKF node in class unit j equal to Xt(i, j). Here, the class layer is arranged with four class units, as shown in Fig. 3.

3. Determine the widths $\sigma_x(i, j)$ of the GKF nodes. The *P*-nearest neighbor method is applied to determine $\sigma_x(i, j)$, where *P* is the number of the nearest neighbor points[5]. First, the root-mean-square distance (RMSD) between center Xt(i, j) and its P-nearest neighbors is determined for each GKF node as

$$RMSD(i, j) = \sqrt{\frac{1}{P}\sum_{i=1}^{P}\left[X_l - X_t(i, j)\right]^T\left[X_l - X_t(i, j)\right]} \tag{10}$$

where Xl = lth nearest neighbor point from the center Xt(i, j) (of the ith GKF node in class unit j). Then $\sigma_x(i, j)$ = RMSD(i, j)/F, where F is a control factor. Saha and Keeler (1990) stated that just one nearest neighbor, i.e., P = 1, can produce the desired performance. The biggest receptive field around a center arises when F = 1. Musavi et al. (1992) stated that a reasonable separation between two centers is to cut the distance in half (i.e., F = 2) if uniform density is desired.

Bayesian Drought Severity Index (BDSI)

Considering the four degrees of drought severity as described above, the four posterior probabilities estimated at an arbitrary point x for year t are denoted as point extreme drought probability EDPt(x), point severe drought probability SDPt(x), point mild drought probability MDPt(x), and point nondrought probability NDPt(x), respectively. They are defined as

1. Point extreme drought probability (the probability of an extreme drought given a point x)
   EDP (x) = P[C |x] = P[z (x) < TL(1)|x]
2. Point severe drought probability (the probability of a severe drought given a point x)
   SDP (x) = P[C |x] = P[TL(1) < z (x) < TL(2)|x]
3. Point mild drought probability (the probability of a mild drought given a point x)
   MDP (x) = P[C |x] = P[TL(2) < z (x) < TL(3)|x]
4. Point nondrought probability (the probability of nondrought given a point x)
   NDP (x) = P[C |x] = P[TL(3) <z (x)|x]

Table. 1. Bayesian Drought Severity at Point and Bayesian Drought Severity Index (BDSI)

Decision condition	Bayesian Drought Severity	Bayesian Drought Severity Index
$if \max[EDP_t(x), SDP_t(x), MDP_t(x), NDP_t(x)] = EDP_t(x)$	Extreme drought	1
$if \max[EDP_t(x), SDP_t(x), MDP_t(x), NDP_t(x)] = SDP_t(x)$	Severe drought	2
$if \max[EDP_t(x), SDP_t(x), MDP_t(x), NDP_t(x)] = MDP_t(x)$	Mild drought	3
$if \max[EDP_t(x), SDP_t(x), MDP_t(x), NDP_t(x)] = NDP_t(x)$	Nondrought	4

Then, any point x in the region of interest has a probability of belonging to a certain degree of drought severity, so that the Bayesian drought severity at a point x is that which has a maximum probability, as indicated in Table 1. Furthermore, the drought severity at a given point is assigned a numerical value d(x) or index. Thus, BDSIs equal to 3, 2, 1, and 0 are conveniently selected to represent extreme, severe, mild, and nondrought conditions, respectively. These indices are useful for representing the spatial pattern of drought severity at a certain point in time, as well as the time evolution of drought severity at a given point.

Regional Drought Severity

to estimating Bayesian drought severity and the drought severity index at a point, one may be interested in assessing the drought severity for the entire region. This information may be useful for many purposes, such as applying for emergency public relief funds because a region has been declared as being in an extreme drought condition during a particular year or for determining the duration and intensity of droughts over a certain period of time. First, regional drought probabilities may be determined by averaging the point drought probabilities for each drought severity as

$$\overline{EDP_t} = \frac{1}{M}\sum_{m=1}^{M} EDP_t\left(x^m\right)$$ 1. Regional extreme drought probability (11)

$$\overline{SDP_t} = \frac{1}{M}\sum_{m=1}^{M} SDP_t\left(x^m\right)$$ 2. Regional severe drought probability (12)

$$\overline{MDP_t} = \frac{1}{M}\sum_{m=1}^{M} MDP_t\left(x^m\right) \quad \text{3. Regional mild drought probability} \tag{13}$$

$$\overline{NDP_t} = \frac{1}{M}\sum_{m=1}^{M} NDP_t\left(x^m\right) \quad \text{4. Regional nondrought probability} \tag{14}$$

where M = number of points in the grid system considered.

Then, based on the regional drought probabilities, $\overline{EDP_t}$, $\overline{SDP_t}$, $\overline{MDP_t}$ and $\overline{NDP_t}$ the regional drought severity for year t, RDS_t may be determined according to the following criterion:

$$\begin{aligned}
&if\ \overline{EDP_t} > \left(\overline{SDP_t} + \overline{MDP_t} + \overline{NDP_t}\right), then \\
&RSD_t = Extreme = E \\
&if\ \ \overline{EDP_t} > 0.5 \quad then \qquad RDS_t = E \\
&or\ else\ if\ \left(\overline{EDP_t} + \overline{SDP_t}\right) > 0.5 \\
&\quad then \quad RDS_t = S \\
&or\ else\ if\ \left(\overline{EDP_t} + \overline{SDP_t} + \overline{MDP_t}\right) > 0.5 \\
&\quad then \quad RDS_t = M \\
&otherwise, RDS_t = N
\end{aligned} \tag{15}$$

3. RESULTS AND SIGNIFICANCES

The historical annual precipitation data for each station were normalized and standardized. The skewness test of normality was applied to check whether the data were normally distributed. While the data for some of the sites were approximately normal, most of the sites required the cubic root or the logarithmic transformations.

The SANN algorithm as described above was applied on a yearly basis using the 30 precipitation sites. The summary of the estimated parameters obtained after training SANN for year 1986 is shown in Table 2. It gives the centers Xt(i, j) and widths $\sigma_x(i, j)$ of the GKF nodes. the Zt(k) values have been arranged into four classes, with one, 8, 20, and one sites belonging to the extreme drought, severe drought, mild drought, and nondrought categories, respectively. the posterior probabilities defining various degrees of drought severity, such as extreme, severe, mild, and nondrought, were obtained. Figs. 5, 6, and 7 show the spatial distribution of drought severity based on the BDSI for the entire region. They may be useful for making a probabilistic statement of drought occurrence and severity at any arbitrary point or area. Successive columns of Table 3 give the sum of the probabilities, $\overline{EDP_t} + \overline{SDP_t}$, $\overline{MDP_t} + \overline{NDP_t}$, $\overline{EDP_t} + \overline{SDP_t} + \overline{MDP_t}$ and $\overline{SDP_t} + \overline{MDP_t} + \overline{NDP_t}$.

They are useful for identifying the degrees of regional drought severity, as indicated by (10) and (11). They are useful for visualizing the pattern of regional drought severity through time. The last column of Table 3 gives the regional drought severity indices determined by (11) for the years 1979–2008.

Table. 2. Summary of Estimated Parameters Obtained after Training SANN Based on 1986 Precipitation

i	Station Number	$Z_{1986}(i,j)$	Center $Z_{1986}(i,j)$		Width $\sigma_x(i,j)$	S^j
			Longitude (Degrees)	Latitude (Degrees)		
1	46	-1.28	51.66	35.215	0.22	1
1	82	-1.02	52.048	35.758	0.23	-
2	62	-1.01	51.188	35.666	0.33	-
3	8	-0.95	51.722	35.307	0.09	-
4	57	-0.95	51.088	35.957	0.13	-
5	55	-0.82	51.091	35.956	0.19	-
6	65	-0.77	51.042	35.681	0.42	-
7	69	-0.64	50.984	35.681	0.46	-
8	66	-0.44	50.764	36.179	0.18	8
1	72	-0.38	52.767	35.759	0.44	-
2	50	-0.38	52.063	35.717	0.12	-
3	77	-0.38	52.17	35.566	0.25	-
4	2	-0.38	52.512	35.807	0.47	-
5	24	-0.38	51.353	35.701	0.19	-
6	13	-0.375	51.397	35.647	0.12	-
7	5	-0.375	51.857	35.732	0.09	-
8	21	-0.375	51.385	35.739	0.34	-
9	10	-0.375	51.407	35.762	0.37	-
10	14	-0.375	51.397	35.726	0.18	-
11	9	-0.375	51.427	35.592	0.21	-
12	20	-0.37	51.45	35.844	0.07	-
13	12	-0.37	51.466	35.827	0.46	-
14	17	-0.37	51.506	35.669	0.2	-
15	1	-0.37	50.598	35.591	0.34	-
16	18	-0.36	51.367	35.741	0.19	-
17	64	-0.36	50.971	35.471	0.27	-
18	81	-0.3	50.852	35.726	0.32	-
19	25	-0.25	51.411	35.683	0.31	-
20	75	-0.2	50.958	35.831	0.18	20
1	61	0.53	52.323	35.626	0.21	1

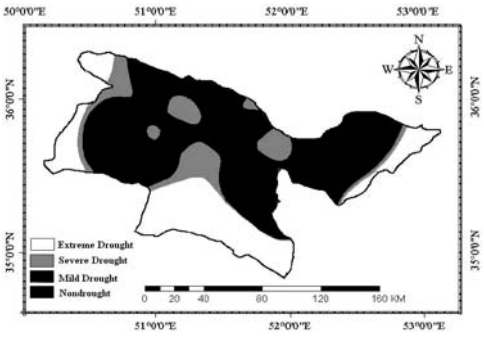

Fig. 5. Spatial Distribution of Drought Severity Based on Bayesian Drought Severity Index (BDSI) IN 1986

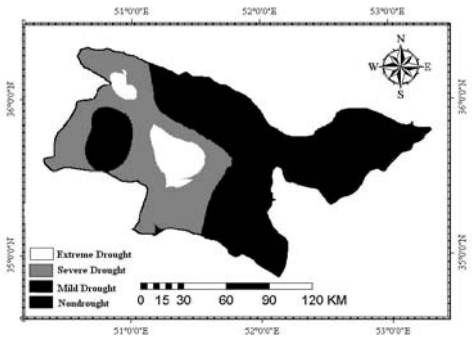

Fig. 6. Spatial Distribution of Drought Severity Based on Bayesian Drought Severity Index (BDSI) IN 1993

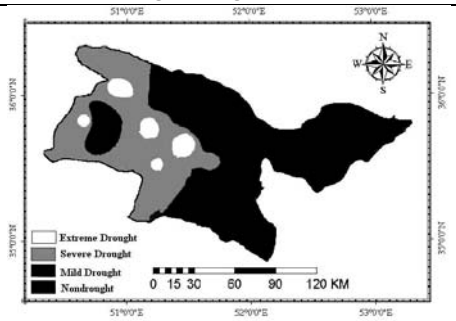

Fig. 7. Spatial Distribution of Drought Severity Based on Bayesian Drought Severity Index (BDSI) IN 2005

Table. 3. Regional Drought Severity Probabilities and Regional Drought Severity for Period 1970–2008

year	$\overline{EDP_t}$	$\overline{SDP_t}$	$\overline{MDP_t}$	$\overline{NDP_t}$	$\overline{EDP_t} + \overline{SDP_t}$	$\overline{MDP_t} + \overline{NDP_t}$	$\overline{EDP_t} + \overline{SDP_t} + \overline{MDP_t}$	$\overline{SDP_t} + \overline{NDP_t} + \overline{EDP_t}$	Regional Drought Severity
1979	0.105	0	0.012	0.883	0.105	0.896	0.117	0.896	N
1980	0.874	0.092	0	0.034	0.966	0.034	0.966	0.127	E
1981	0.077	0.087	0.423	0.413	0.164	0.836	0.587	0.923	M
1982	0.018	0.104	0	0.877	0.123	0.877	0.123	0.982	N
1983	0.207	0.384	0.182	0.227	0.591	0.409	0.773	0.793	S
1984	0.125	0.051	0.352	0.472	0.176	0.824	0.528	0.875	M
1985	0.18	0.147	0.104	0.569	0.327	0.673	0.431	0.82	N
1986	0.211	0.337	0.123	0.329	0.548	0.452	0.671	0.789	S
1987	0.078	0.279	0.068	0.576	0.357	0.643	0.425	0.922	N
1988	0.041	0.042	0.047	0.87	0.082	0.918	0.13	0.959	N
1989	0.146	0.205	0.22	0.429	0.351	0.649	0.571	0.854	M
1990	0.171	0.116	0.134	0.579	0.287	0.713	0.421	0.829	N
1991	0.585	0.285	0.07	0.06	0.87	0.13	0.94	0.415	E
1992	0.225	0.239	0.098	0.437	0.464	0.536	0.562	0.775	M
1993	0.151	0.184	0.204	0.462	0.334	0.666	0.538	0.849	M
1994	0.014	0.286	0.192	0.508	0.3	0.7	0.492	0.986	N
1995	0.112	0.482	0.334	0.072	0.594	0.406	0.928	0.888	S
1996	0.207	0.423	0.122	0.248	0.63	0.37	0.752	0.794	S
1997	0.644	0.257	0.047	0.051	0.901	0.099	0.949	0.356	E
1998	0	0	0.008	0.992	0	1	0.008	1	N
1999	0.225	0.663	0.1	0.011	0.889	0.112	0.989	0.775	S
2000	0.013	0.108	0.378	0.501	0.121	0.879	0.499	0.987	N
2001	0.136	0.555	0.173	0.136	0.69	0.31	0.864	0.864	S
2002	0	0.083	0.115	0.802	0.083	0.917	0.198	1	N
2003	0.375	0.398	0.14	0.086	0.774	0.227	0.914	0.625	S
2004	0.255	0.312	0.216	0.217	0.433	0.433	0.783	0.745	S
2005	0.035	0.299	0.343	0.323	0.334	0.666	0.377	0.964	M
2006	0	0	0.019	0.981	0	1	0.019	1	N
2007	0.186	0.471	0.191	0.151	0.342	0.342	0.849	0.814	S
2008	0.031	0.117	0.266	0.586	0.148	0.852	0.414	0.969	N

4. CONCLUSIONS

The statistical analysis of regional droughts has been the main subject of this paper. The main objective of the research has been to develop an approach to analyze and quantify regional droughts so that the spatial and temporal patterns of droughts of various degrees of severity can be described and characterized. The study has been limited to meteorological droughts based on annual precipitation data as the underlying forcing function of water supply in a region. The approach developed is based on normalized and standardized precipitation data that are further analyzed and classified based on a nonparametric SANN algorithm. It involves training SANN, estimating or interpolating data, classifying the data, determining the drought severity at a point, and determining the regional drought severity. The proposed regional drought analysis approach was applied to analyze and quantify the regional meteorological droughts for the southwestern region of Colorado. Annual precipitation data at 30 sites available for the period 1979–2008 were utilized. Cubic-root and logarithmic transformations were required to transform most of the data into normal. After normalization and standardization, SANN was applied to estimate the precipitation field at an equally spaced grid, to classify the data into various degrees of drought severity, and to estimate posterior probabilities of drought severity, Bayesian drought severity indices, and regional drought severity. The results were useful for deriving maps of precipitation fields for the entire region, maps of posterior probability of drought severity, and maps of drought severity indices. They were quite useful for visualizing the spatial pattern of droughts and for deriving other drought properties such as duration. The results obtained suggest that the proposed approach is a viable tool for analyzing and synthesizing droughts on a regional basis.

5. REFERENCES

[1] Bishop, C. M. (1995). Neural networks for pattern recognition. Clarendon, Oxford, U.K.
[2] Cain, J. B. (1990). ‘‘An improved probabilistic neural network and its performance relative to other models.’’ Application of Artifical Neural Networks, SPIE 1294.
[3] Dracup, J. A., Lee, K. S., and Paulson, E. N. Jr. (1980). ‘‘On the statistical characteristics of drought events.’’ Water Resour. Res., 16(2), 289–296.
[4] Kottegoda, N. T., and Rosso, R. (1997). Probability, statistics, and reliability for civil and environmental engineers. McGraw-Hill, New York.
[5] Moody, J. E., and Darken, D. J. (1989). ‘‘Fast learning in networks of locally-tuned processing units.’’ Neural Computation, 1, 281–294.
[6] Parzen, E. (1962). ‘‘On the estimation of a probability density function and mode.’’ Annals of Math. Statistics, 33, 1065–1076.
[7] Pinkayan, S. (1966). ‘‘Conditional probabilities of occurrence of wet and dry years over a large continental area.’’ Hydrol. Paper 12, Colorado State University, Fort Collins, Colo.
[8] Poggio, T., and Girosi, F. (1990). ‘‘Regularization algorithms for learning that are equivalent to multilayer networks.’’ Sci., 247, 978–982.
[9] Tase, N. (1976). ‘‘Area-deficit-intensity characteristics of drought,’’ PhD dissertation, Colorado State University, Fort Collins, Colo.
[10] Yevjevich, V. (1967). ‘‘An objective approach to definitions and investigations of continental hydrologic droughts.’’ Hydro. Paper 23, Colorado State University, Fort Collins, Colo.
[11] Zelenhasic, E., and Salvai, A. (1987). ‘‘A method of streamflow drought analysis.’’ Water Resour. Res., 23(1), 156–168.

"Time Domain Analysis" Models and Their Application in Prediction of Dam Reservoir Inflows

Soheil Ghareaghaji Zare[1], Mohammad Hossein Karimi Pashaki[2] and Hosein Sedghi[3]

***Abstract* – Understanding the relation between elements of hydrology, climate, geology and morphology of a hydrologic system, is a clue to find future out put of the system which is an ambitious aim. All attempts to this goal, classify in stochastic hydrology which uses probability, mathematical and statistical methods for this goal In this paper, we use a method called "Time Domain Analysis". This method uses "Auto Correlation Function" and "Partial Auto Correlation Function" to analyze the process. Method established according to auto-covariance parameter in "K" delay and mentioned functions utilized to simulate the parameter's trend. This Method, checked on "Sephidrood-Gilan-Iran" to simulate studies. Finally, According to time series ARIMA models and assisting to "Over Fitting" strategy, one model selected to simulate and predict inflow to Dam reservoir of mentioned river.**

Keywords – Time Domain Analysis, Time series, ARIMA Models, Dam Reservoir.

1. INTRODUCTION

A time series is a collection of numerical observations arranged in a natural order. Usually each observation is associated with a particular instant or interval of time, and it is this that provide the ordering. The observations could equally be associated with points along a line, but whenever they are ordered by a single variable it is referred to conventionally as "time". It will be generally assumed that the time values are equally spaced [3].

Classic auto regressive-Moving average models introduced by Box and Jenkins in 60 decade and improved by Davis and Brackwell (1978). According to Yevjevich (1972), hydrologic time series can be modeled by a deterministic component and a stationary stochastic process. The deterministic component is composed of trends, jumps, and periodicities, while the stochastic component consists of the random deviations of the seasonal values (Haan 1982). This type of analysis has been applied to many kinds of hydrologic time series including water-use time series and groundwater table time series (Law 1974; Rao et al. 1975; Knotters and van Walsum 1997)[5]. "Sedghi"(1999) used integrated auto regressive moving average models to study and modeling of Karoon river discharge data and their future variations. "Zare"(2009) fitted an integrated auto regressive

Zare S.G is with Dept. of Water Science and Engineering, IAU, Science and Research branch of Tehran, Tehran, IRAN,Tel:+98-914-3450321; e-mail:soheil.zare@gmail.com

Pashaki is with Dept. of Water Science and Engineering, IAU, Science and Research branch of Tehran, Tehran, IRAN;Tel:+98-911-1436073; e-mail: m20karimi@yahoo.com

Sedghi H is with Dept. of Water Science and Engineering, IAU, Science and Research branch of Tehran, Tehran, IRAN, hsedgh@yahoo.com

ISSN-1584-5990

moving average model to "shahar-chaii" river and predict the future amount of this river's discharge data ."Zare and Sedghi" (2009) analyzed "Shahar-chaii" river discharge data in frequency domain and fitted a fourier model to time series of discharge data and optimized the method with "Genethic Algorithm".

1-1. SIMULATION STUDY

River basin of sephid-rood divided to 4 sub-basins include: 1." Kizil-ozan" Basin 2. "Shah-rood" Basin 3.Intrmediate basin of "Kizil-ozan" and "Shah-rood" rivers combination 4. "Sephid-rood" basin at the dam site.

"Sephid-rood" is the second longest river in Iran which sometimes mentioned as it's ancient name: "Amard". "Amard" is the name of ancient nation who lived beside the river.The dam of "Sephid-rood" river located in north of Iran, with 110 Km distance to "Caspian sea" at the position of two"Kizil-ozan" and "Shah-rood" rivers jointing place near "Manjil" city in "Gilan" state. Dam bulding started at 1955 and finished at 1961. Reservoir operation started at 1962.This concerete leggy weight dam has 106 meter height and it's crest has 425 meter. Initial reservoir volume was 1760 million cubic meter includes an area about 53.92 Km^2. The basin has semi-arid climate and uncovered land with poor vegetable coating and soil with considerable erosion.The whole area of this river's basin is about 56200 Km^2 wich includes sub basin's area about 49300 Km^2 for "Kizil-ozan" and 5070 Km^2 for "Shah-rood". "Kizil-ozan" joins to dam lake after passing about 500 Km from mountains of "kordistan" state and "hamadan" state at "Gilvan". River regime approximately includes both rain and snow regimes, but almost has snow regime with floods in spring. Average inflow to dam reservoir is 4838 million cubic meter per year with maximum of 14000 million cubic meters and minimum of 2300 million cubic meters pear year. 58 million cubic meters sediments move to reservoir each year that 84 percent carry by "kizil-ozan" and 16 percent by "shah-rood".Maximum sedimantation intrance to resvoire is 218 million ton and minimum amount of that is 14 million ton. Variation of average density of suspended load is between 5 to 80 grams for 500 and 1000 cubic meters discharges respectively. Graph of river discharge shown in figure (1). As the graph shows data has variance un-stationarity and trend. So, first we need to make them stationary first because stationarity is the first step in time series analysis.

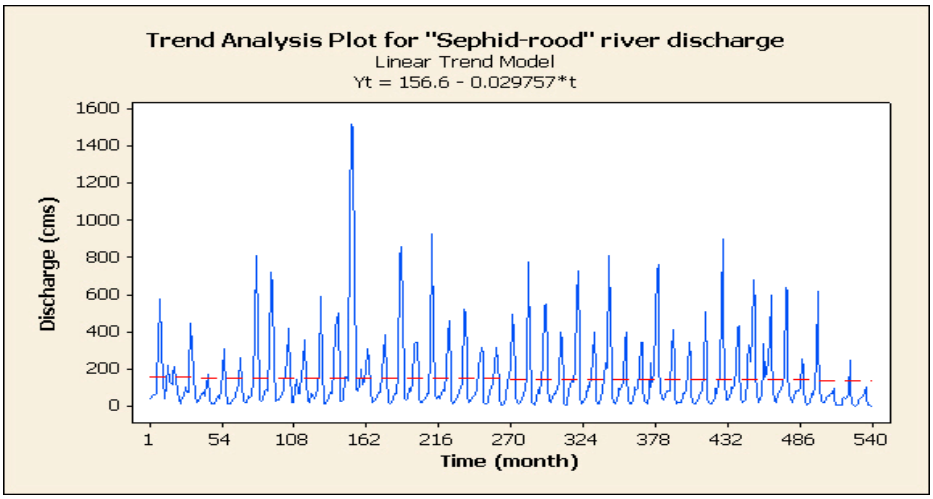

Fig. 1. River discharge and Trend analysis plot for "Sephid-rood" river.

2. DESCRIPTION OF THE METHOD

2.1 TIME SERIES ANALYSIS

There are two main methods for analyzing time series, these methods analyze time series in different time and frequency domain and nominated as their working space. So, time series analyzing methods divided to two methods: "Time domain" and "Frequency domain". "Time Domain" method is based on autocorrelation coefficient. In this method, autocorrelation, partial autocorrelation and autocovariance functions are used to study gradual time series evolution according to parametric patterns. In "Frequency Domain", we try to explain time series characteristics by sinusoid behavior in different frequencies and use spectral density function.

A key idea in time series is that of stationarity. Roughly speaking, a time series is stationary if its behavior does not change over time. This means, for example, that the values always tend to vary about the same level and that their variability is constant over time. Stationary series have a rich theory and their behavior is well understood. This means that they play a fundamental role in the study of time series. Obviously, not all time series that we encounter are stationary. Indeed, non stationary series tend to be the rule rather than the exception. However, many time series are related in simple ways to series which are stationary. Two important examples of this are:

Trend models: The series we observe is the sum of a deterministic trend series and a stationary noise series. A simple example is the linear:

$$Y_t=\beta_0+\beta_1 t+\varepsilon_t \tag{1}$$

Another common trend model assumes that the series is the sum of a periodic "seasonal" effect and stationary noise. There are many other variations.

Integrated models: The time series we observe satisfies.

$$Y_{t+1}-Y_t=\varepsilon_{t+1} \tag{2}$$

where ε_t is a stationary series. A particularly important model of this kind is the random walk. In that case, the ε_t values are independent "shocks" which perturb the current state Y_t by an amount ε_{t+1} to produce a new state Y_{t+1}.

2.2 TIME DOMAIN ANALYSIS

It will assumed that the time series values we observe are the realisations of random variables $Y_1, \ldots, Y_T$, which are in turn part of a larger stochastic process $\{Y_t : t \in Z\}$. It is this underlying process that will be the focus for our theoretical development.

Although it is best to distinguish the observed time series from the underlying stochastic process, the distinction is usually blurred and the term time series is used to refer to both the observations and the underlying process which generates them. The mean and the variance of random variables have a special place in the theory of statistics. In time series analysis, the analogs of these are the "mean function" and the "autocovariance function". The "mean function" of a time series is defined to be $\mu(t) = EY_t$ and the "autocovariance function" is defined to be $\gamma(s, t) = \mathrm{cov}(Y_s, Y_t)$. The mean and the autocovariance functions are fundamental parameters and it would be useful to obtain

sample estimates of them. For general time series there are 2T + T(T − 1)/2 parameters associated with $Y_1, \ldots, Y_T$ and it is not possible to estimate all these parameters from T data values. To make any progress at all we must impose constraints on the time series we are investigating. The most common constraint is that of stationarity. There are two common definitions of stationarity:

- Strict stationarity
- Weak stationarity

When time series are stationary it is possible to simplify the parameterization of the mean and autocovariance functions. In this case we can define the mean of the series to be $\mu = E(Y_t)$ and the autocovariance function to be $\gamma(u) = cov(Y_{t+u}, Y_t)$. We will also have occasion to examine the autocorrelation function.

$$\rho(u) = \frac{\gamma(u)}{\gamma(0)} = cor(Y_{t+u}, Y_t) \tag{3}$$

2.2.1 AUTO CORRELATION FUNCTION (ACF)

Given a stretch of data $Y_1, \ldots, Y_T$, the usual estimate of the autocovariance function is

$$\hat{\gamma}(u) = \frac{1}{T}\sum_{t=1}^{T-u}\left(Y_{t+u} - \bar{Y}\right)\left(Y_T - \bar{Y}\right) \tag{4}$$

Note that this estimator is biased — an unbiased estimator would have a divisor of T − u in place of T. There are two reasons for using this estimator. The first of these reasons is that it produces a $\hat{\gamma}(u)$ which is positive definite.

This means that for any constants $c_1, \ldots, c_k$,

$$\sum_{u=1}^{k}\sum_{\upsilon=1}^{k} c_u c_\upsilon \hat{\gamma}(u-\upsilon) \geq 0 \tag{5}$$

This ensures that our estimate of the variance of

$$\sum_{u=1}^{k} c_u X_{t-u} \tag{6}$$

will be non-negative, something which might not be the case for the unbiased estimate. The second reason is that for many time series $\gamma_{u\to 0}$ as $u \to \infty$. For such time series, the biased estimate can have lower mean-squared error.

The estimate of ρ(u) based on $\hat{\gamma}$(u) is

$$r(u) = \frac{\hat{\gamma}(u)}{\hat{\gamma}(0)} = \frac{\sum_t (Y_{t+u} - \hat{Y})(Y_t - \bar{Y})}{\sum_t (Y_t - \bar{Y})^2} \tag{7}$$

Again, this can have better mean-squared error properties than the estimate based on the unbiased estimate of γ(u). In order to say whether an observed correlation is significantly different from zero, we need some distribution theory. Like most time series results, the theory here is asymptotic (as T→∞). The original results in this area were obtained by Bartlett in 1947. We will look at results due to (T. W. Anderson in 1971).

Suppose that

$$Y_t = \mu + \sum_{u=0}^{\infty} \psi_u \varepsilon_{t-u} \tag{8}$$

with the ε_t independent and identically distributed with zero mean and non-zero variance. Suppose that

$$\sum_{u=0}^{\infty} |\psi_u| < \infty \text{ and } \sum_{u=0}^{\infty} u|\psi_u|^2 < \infty \tag{9}$$

2.2.2 PARTIAL AUTO CORRELATION FUNCTION (PACF)

Given a stretch of time series values

$$\ldots, Y_{t-u}, Y_{t-u+1}, \ldots, Y_{t-1}, Y_t, \ldots \tag{10}$$

the partial correlation of Y_t and Y_{t-u} is the correlation between these random variables which is not conveyed through the intervening values. If the Y values are normally distributed, the partial autocorrelation between Y_t and Y_{t-u} can be defined as

$$\varphi(u) = \text{cor}(Y_t, Y_{t-u}|Y_{t-1}, \ldots, Y_{t-u+1}) \tag{11}$$

A more general approach is based on regression theory. Consider predicting Y_t based on $Y_{t-1}, \ldots, Y_{t-u+1}$. The prediction is

$$\hat{Y}_t = \beta_1 Y_{t-1} + \beta_2 Y_{t-2} \cdots, \beta_{u-1} Yt_{-u+1} \tag{12}$$

with the _s chosen to minimize

$$E(Y_t - \hat{Y}_t)^2 \tag{13}$$

It is also possible to "think backwards in time" and consider predicting Y_{t-u} with the same set of predictors. The best predictor will be

$$\hat{Y}_{i-u} = \beta_1 Y_{t-u+1} + \beta_2 Y_{t-u+2} + \ldots + \beta_{u-1} Y_{t-1} \tag{14}$$

The coefficients are the same because the correlation structure is the same whether the series is run forwards or backwards in time. The partial correlation function at lag u is the correlation between the prediction errors.

$$\phi(u) = cor(Y_t - \hat{Y}_t, Y_{t-u} - \hat{Y}_{t-u}) \tag{15}$$

By convention we take $\varphi(1) = \rho(1)$.

2.2.2 AUTOREGRESSIVE SERIES

If Y_t satisfies

$$Y_t = \varphi_1 Y_{t-1} + \cdots + \_\varphi_p Y_{t-p} + \varepsilon_t \tag{16}$$

where ε_t is white-noise and the φ_u are constants, then Y_t is called an autoregressive series of order p, denoted by AR(p). Autoregressive series are important because:

1. They have a natural interpretation - the next value observed is a slight perturbation of a simple function of the most recent observations.

2. It is easy to estimate their parameters. It can be done with standard regression software.
3. They are easy to forecast. Again standard regression software will do the job[3].

2.2.3 "ARIMA" MODELS

If $W_t = \nabla^d Y_t$ is an ARMA(p,q) series then Y_t is said to be an integrated autoregressive moving-average (p, d, q) series, denoted ARIMA(p,d,q). If we write

$$\varphi(L) = 1 - \varphi_1 L - \cdots - \varphi_p L^p \tag{17}$$

and

$$\theta(L) = 1 + \theta_1 L + \cdots + \theta_q L^q \tag{18}$$

Then we can write down the operator formulation

$$\varphi(L)\nabla^d Y_t = \theta(L)\varepsilon_t \tag{19}$$

3. RESULTS AND THEIR SIGNIFICANCE

We use Box-Cox transformation to study variance stationarity, results shown in fig (2). According to the results, Box-Cox transformation shows that data need to change before analyzing to be stationary. As the fig. (3)(b) shows, Box-Cox transformation makes data better in distribution.

Study of Autocorrelation and Partial Autocorrelation functions –after trend analysis– shows non-stationarity and seasonal cycle in data, so we need differences operators and seasonal differencing to make them stable. ACF and PACF of data are shown in fig. (4).

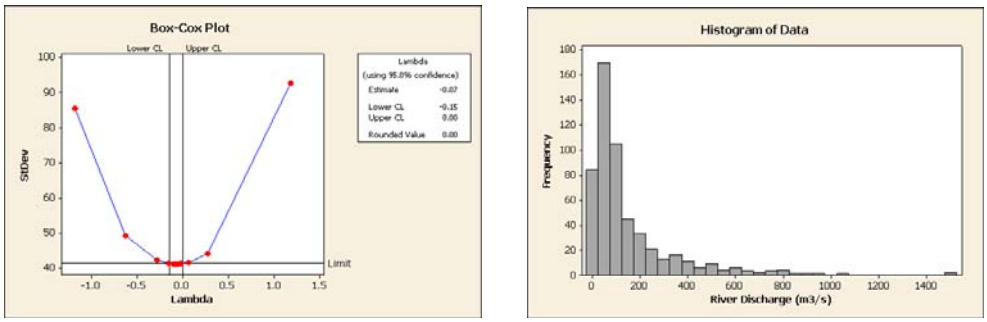

Fig. 2. (a). Box-Cox plot of data (b). Histogram and distibution of discharge data.

According to ACF and PACF functions, we fitted 17 common autoregressive models (ARIMA models) to data and modified box-pierce (Ljung-Box) Chi-Square statistic has calculated for each model in 12-24-36-48 lags. Finally, ARIMA(1,0,0)(1,1,1)*12 chosen based on AIC index which defines as:

$$AIC = n \ln(MSE) + 2(p+q) \tag{20}$$

Results of model estimation are shown in Table 1.

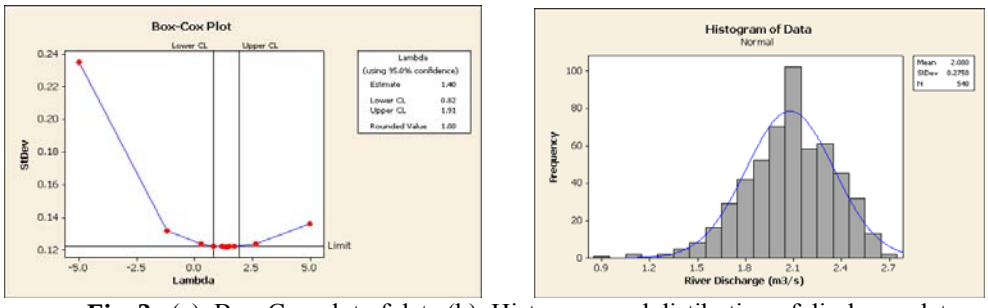

Fig. 3. (a). Box-Cox plot of data (b). Histogram and distibution of discharge data. (After Box-Cox Transformation)

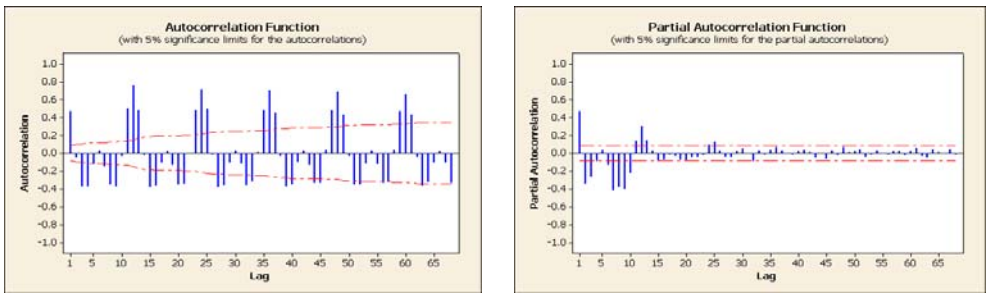

Fig. 4. (a). ACF of data (b). PACF of data

Table. 1. Fitted ARIMA models and their statistics

	Model	BOX-PIERCE P value Lag : 12-24-36-48	AIC		Model	BOX-PIERCE P value Lag : 12-24-36-48	AIC
1	ARIMA(1,1,1)(1,1,1)12	0.16-0.67-0.5-0.66	-1144	9	ARIMA(1,1,0)(1,1,0)12	0-0-0-0	_
2	ARIMA(1,1,1)(0,0,0)12	0-0-0-0	_	10	ARIMA(2,0,0)(0,1,1)12	0.008-0.1-0.06-0.01	-1111
3	ARIMA(1,1,1)(1,1,0)12	Without answer	_	11	ARIMA(2,0,0)(1,1,1)12	0.08-0.37-0.24-0.41	-1142
4	ARIMA(1,1,1)(0,1,0)12	Without answer	_	12	ARIMA(2,0,0)(2,1,1)12	0.05-0.33-0.18-0.35	-1139
5	ARIMA(0,1,1)(1,1,1)12	0.001-0.05-0.04-0.09	-1128	13	ARIMA(1,0,0)(1,1,1)12	0.1-0.31-0.25-0.41	-1145
6	ARIMA(1,1,0)(1,1,1)12	0-0.009-0.006-0.02	-1122	14	ARIMA(1,0,1)(2,1,1)12	0.06-0.35-0.19-0.36	-1141
7	ARIMA(0,1,1)(1,1,0)12	0-0-0-0	_	15	ARIMA(1,0,0)(2,1,0)12	0.07-0.006-0-0.002	-1106
8	ARIMA(1,1,0)(0,1,1)12	0-0.002-0.002-0.006	-1126	16	ARIMA(1,0,1)(1,1,1)12	0.09-0.39-0.25-0.42	-1143
				17	ARIMA(1,0,1)(2,1,2)12	0.03-0.27-0.16-0.3	-1137

4. CONCLUSION

Results shows ARIMA(1,0,0)(1,1,1)*12 is the best one with minimum AIC index. Additionally, residual analysis results confirm goodness fitting of this model. To test the residuals, we evaluate normal probability, residual versus fitted values plus observation orders and residual histogram plots in figure 5.b.Comparing observed and forecasted data in figure 5a, illustrates acceptable difference and appropriate model prediction potency.

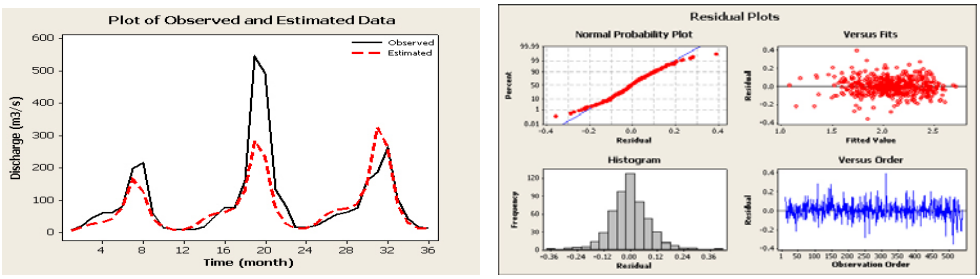

Fig. 5. (a). Plot of Observed and estimated discharge data for sephid-rood river
(b). Residual Analysis for goodness-fitting of ARIMA(1,0,0)(1,1,1)*12

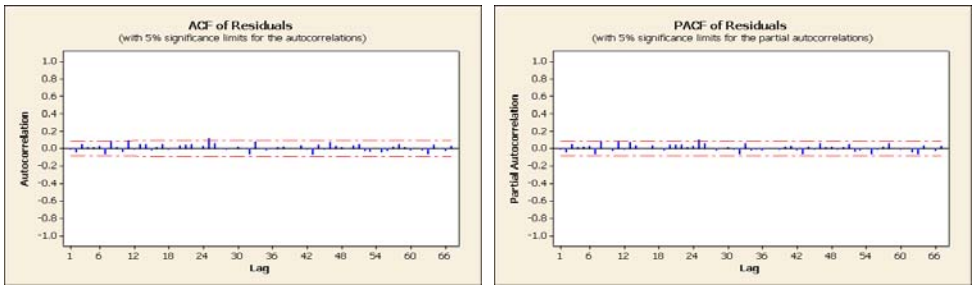

Fig. 6. (a). ACF of Residuals (b). PACF of Residuals

Figure (6) shows Auto Correlation Function and Partial Auto Correlation Function of residuals. As depicted in fig.6 (a) and (b), there is no correlation between residuals in different lags. So it could be defined as good model fitting to data because the model could simulate all correlations in the series as we aimed already. Residual analysis shows normal distribution of data which is the important article to model validating. ARIMA models commonly have the same limitations in long range predictions based on constant values of data, it means that this kind of models have acceptable accuracy in limited future predictions (maximum as mid time of time series), in the other hand, they could not be able to updated with new series of data, so it is necessary to fitting a new model according to new time series and this is the one of the intrinsic defects of this kind of models.

5. REFERENCES

[1]Box, G. E. P. and Jenkins G. M. (1976). Time Series Analysis: Forecasting and Control, Holden-Day, Oakland, California, revised edition.

[2]Box, G. E. P., Pierce, D. A. and Newbold, P. (1987). "Distribution of the Residual Autocorrelations in Autoregressive Integrated Moving Average Models," Journal of the American Statistical Association, 65:1509-1526.

[3]Ihaka, R . (2005). Time Series Analysis: lecture notes for 475.726, Statistic Department, University of Auckland.

[4]Salas, J. D, Delleur, J.W, Yevjevich, V and Lane, W.L. (1998) Applied Modeling of Hydrological Time Series, Water Resource publication.

[5]Vazquez-Amabile, G. G. and Engel, B. A. (2008). "Fitting of Time Series to Forecast Steamflow and Ground water Using Simulated Data from SWAT," Journal of Hydrologic Engineering, ASCE, vol. 13, No.7: 554-562.

[6]Wei, W. S. (1981) . Effect of Systematic Sampling on ARIMA models, Theor & Math.

[7]Ghareaghaji Zare, S. "Time Domain Analysis" Based Modeling of Time Series and Their Application to Prediction of River Discharge, January 21th-23th (2010), Ahwaz, IRAN http://www.8irec.ir

SECTION III

ENVIRONMENT AND HUMAN ACTIVITIES

Modern Solutions used in Maritime Pollution Prevention

Şerban Berescu, Alexandra Niţă, Gabriel Raicu

***Abstract* – This paper presents a comparative analysis regarding modern solutions used to prevent the marine pollution, using protective booming made from polymeric materials. A major oil spill has potentially devastating effects on nearby coastal states irrespective of their status regarding the Conventions. Some developments in last year's permit very efficient actions to reduce long term pollution effect on sea. Composite materials are used throughout the marine industry for numerous applications including primary and secondary structure, superstructures, piping, shafts, foundations, ducts, and gratings.**

Keywords – **multicriterial analysis, oil pollution, polymeric material, water booming**.

1. INTRODUCTION. GENERALITIES ABOUT MARITIME POLLUTION

The MARPOL Convention is the main international convention covering prevention of pollution of the marine environment by ships from operational or accidental causes. The International Convention for the Prevention of Pollution from Ships (MARPOL) was adopted on 2 November 1973 at IMO and covered pollution by oil, chemicals, and harmful substances in packaged form, sewage and garbage.

The Oil Pollution Act of 1990 (OPA) established liabilities for polluters and recovery methods for areas affected by oil spills. It was preceded by the Oil Pollution Act of 1924 and the Oil Pollution Act of 1961. The 1924 act prohibited the discharge of oil into U.S. coastal waters and was regulated by the U.S. Coast Guard. The 1961 act forbade the discharge of oil in any waters within fifty miles of the U.S. coast, extending the area regulated by the previous legislation.

Pollution occurs when concentrations of various chemical or biological constituents exceed a level at which a negative impact on ecosystem or human health can occur. Pollution results primarily from human activities. More specifically, in the marine context "Pollution of marine environment means the introduction by man, directly or indirectly, of substances or energy into the marine environment, including estuaries, which results or is likely to result in such a deleterious effect as to harm living resources and marine life, hazardous to human health, hindrance to marine activities, including fishing and other legitimate uses of the sea, impairment of quality for use of seawater and reduction of amenities". Among all land based activities that cause marine pollution, dredging of ports

Şerban Berescu with Romanian Naval Authority, Constanta Port, no.1, 900900-Constanta, Romania (corresponding author to provide phone: +40-722 605508)

Alexandra Niţă is with Constanta Maritime University, Str. Mircea cel Batran, no.104, 900663-Constanta, Romania (corresponding author to provide phone: +40-722 605508; e-mail: alexandranita@imc.ro).

Gabriel Raicu is with Constanta Maritime University, Str. Mircea cel Batran, no.104, 900663-Constanta, Romania (corresponding author to provide phone: +40-723 614043; e-mail: graicu@imc.ro).

ISSN-1584-5990

and harbours is probably the most significant in terms of propagation of pollutants. The process of dredging causes the disruption of bottom sediments. More often than not, bottom sediments of ports and harbours, are contaminated by chemicals, minerals, hydrocarbons and domestic wastes.

Discharges and spills from ships and shore based facilities result in the environmental degradation of marine life. In ports, the situation is even more critical due to the fact that most ports have relatively poor exchanges with the open sea. This results in the pollutants having long residence times in the port area.

Using sorbents in oil spill remediation has proven to be effective. Since the performance is quick and the amount of oil collected is very high compared to the weight of sorbent and normally the oil. However, the method is not suitable for dealing with large oil spills at open sea due to the fact that under such conditions, the oil spill will be spread quickly by wind, waves and currents so that it is difficult for removing the oil from water by using this method. For that, another method using polymeric materials to prevent the marine pollution is the protective booming. Booms are employed to prevent oil from spreading on the water's surface and surround the spill close to the source. Booms are also used to prevent oil from entering harbours, docks or any sensitive areas and to divert the oil spill to an area where operation can be made. The majority of the booms are made of strength synthetic fabric covered with heavy duty neoprene rubber. The boom is oil resistant, wear resistant, seawater resistant, and UV-resistant. Boom characteristics important for fast-water booming include shallow skirt depth to minimize entrainment, bottom tension member to prevent boom planning, curtain versus fence design for vertical flexibility, high buoyancy to weight ratio to prevent submersion, and sufficient tensile strength to prevent structural failure [1].

To collect oil slicks plastic it is used also, polymeric materials such as polyurethane foam. The use of plastic or other polymeric materials offers and excellent solution to the problem, since no residues are left on the ocean bottom and large quantities of oil can be reclaimed for subsequent use.

2. LOGISTICAL SYSTEMS USING PROTECTIVE BOOMING FROM POLYMERIC MATERIALS

Boom mooring systems with the high holding power necessary for deflection booming across a high current are not readily available from booming contractors. Suitable mooring system components can be assembled with adequate advance planning. Traditional containment booms can be positioned at sharp angles to the current (with great difficulty) to divert oil in up to two or three knots. With developing technologies, a current of six knots is considered the upper limit for controlling floating oil in the foreseeable future.

When the current exceeds the critical velocity and entrainment prevents effective oil containment, boom can be angled across the current to divert or deflect oil away from sensitive areas or toward lower current areas for recovery. Deflection may be effective in up to three knots of current, if a very sharp boom angle can be maintained across the current (about 15° from the direction of current flow, for a 3 knot current). Newer boom designs and refinements in technique may extend this capability [3]. Boom characteristics important for fast-water booming include shallow skirt depth (draft of 6 inches or less) to minimize entrainment, bottom tension member to prevent boom planning, curtain versus fence design for vertical flexibility, high buoyancy to weight ratio to prevent submersion, and sufficient tensile strength to prevent structural failure. Some manufacturers offer specially designed High Current Booms incorporating the above features. Shallow draft deflection boom must transition to traditional deeper draft containment boom to hold diverted oil for recovery in the low-current oil collection area. For the purposes of this

paper, the term "fast water" is applied to any water body with currents of one to six knots [2]. Logistic support to install the more complex cascade system may be of longer duration, but less demanding in terms of the installation of smaller mooring systems and lighter rigging. Smaller, less powerful towboats may be adequate for deployment and recovery of the lighter weight cascade system moorings.

An oil absorbing boom to be deployed across the effluent stream from a separator or settling basin on the downstream side of oil transfer operations at a seaport for the purposes of collecting and removing from the water thin films of oil such as those which sometimes escape from oil spill booms surrounding a tanker at a loading dock, and comprising an elongated flat tubular sleeve of polymer netting enclosing within itself a plurality of flat elongated slabs or bats of "picker-lap" fibrous polymer material such as blown polypropylene film arrayed end to end within the tubular sleeve and sufficiently spaced apart to permit accordion folding of the sleeve at fold lines between adjacent bats, with a tension-bearing rope or cable being positioned within the tubular sleeve alongside the successive plurality of absorbent bats to reinforce the structure for carrying its own weight or impact loads placing it in tension between its ends. Alternatively, a continuous, wide, flat sheet of extremely porous hydrophobic foam material such as fully reticulated polyurethane foam, suspended from overlying buoyant flotation material, is formed into a similar elongated boom deployed across a floating oil film or into a continuous endless belt repeatedly cycled through the floating oil. After trapping oil within the porosities or interstices of the boom or belt material, it is squeezed between pinch rolls to force out and recover the trapped oil, and the device is thus capable of successive repeated deployment cycles of oil recovery operation.

3. MARITIME POLLUTIONS TESTING FACILITY

OHMSETT - The National Oil Spill Response Research and Renewable Energy Test Facility is the only facility where full-scale oil spill response equipment testing, research, and training can be conducted in a marine environment with oil under controlled environmental conditions (waves, temperature, oil types). The facility provides an environmentally safe place to conduct objective testing and to develop devices and techniques for the control of oil and hazardous material spills, as you can see in figure 1 [9].

Fig. 1. OHMSETT testing facility

Standard test protocols are used at OHMSETT to evaluate oil spill containment booms and skimmers. OHMSETT provides the intermediate step between small scale and open water testing of equipment. It is estimated that 95% of the performance data on mechanical equipment was obtained at OHMSETT. In 1998, in situ burning was added. An air-injected underwater propane burner system simulates the temperatures associated with burning oil at sea. The system is used to evaluate the performance and survivability of fire

resistant booms. In 1999, the capability to measure dispersant effectiveness over a wide range of conditions was added. In 2009, MMS added Spanish language response classes, dispersant training classes, and renewable wave energy testing capabilities.

OHMSETT provides oil spill response testing, training, and research opportunities to government, industry, academia, and private organizations on a reimbursable basis. OHMSETT is the only facility that can test full sized oil spill response equipment with a variety of crude oils and refined petroleum products under reproducible marine conditions.

OHMSETT aims are to fulfil oil spill regulatory responsibilities under the Oil Pollution Act of 1990 (OPA 90). Responsibility to manage OHMSETT came from OPA 90. Funding for operation and maintenance costs of OHMSETT are covered by the Oil Spill Liability Trust Fund (OSTLF). The OSTLF derives its funds from a tax on companies that produce or transport oil [5, 6].

4. MULTICRITERIAL COMPARISONS BETWEEN TWO CLASSES OF HIGH CURRENT BOOMS

Canadyne offers the widest range of containment booms available on the market today. Booms are available in a variety of sizes, styles, and fabrics to meet any conceivable response requirements.

Canadyne RubberBoom, as you can see in figure 2 is made of double strength synthetic fabric covered with heavy duty neoprene rubber. The boom is oil resistant, wear resistant, seawater resistant, and UV-resistant.

Booms can be inflated using handheld or backpack inflation blowers, or with integrated hydraulic blowers (stand alone or mounted on a boom storage and deployment reel).

Fig. 2. Floating Rubber Boom

The features of this rubber boom are: rapid inflation, airtight buoyancy chambers, fully symmetric boom, either side can be used to combat spills, independent, segmented buoyancy chambers, fibreglass rod vertical stiffeners between chambers, stainless steel end fittings, external ballast chain, lies flat in storage for easy recovery, cleaning, maintenance [7]. Regarding harbour and coastal oil containment booms are the NOFI EP-series of solid flotation booms you will find the NOFI BoomBag: The fastest available response systems with unique operating characteristics in mobilization and operating speed. – The NOFI Current Buster (figure 3) is the world's most advanced oil containment system efficiently containing and controlling oil in up to 3 to 4 knots towing speed.

Instead for the offshore oil containment booms the NOFI 1000-series is recognized as a very reliable boom, especially designed for optimal performance in demanding conditions. The product range includes manual- and automatic inflatable booms and the

advanced NOFI Ocean Buster which in addition to its high oil containment speed of up to 3 to 4 knots also may be supplied with a NorMar Integrated Skimme Skimmer.

Fig. 3. Long range Booms

Fig. 4. Pipe Booms

The figure 4 present the NOFI 1000-series [8]. The NOFI Spill Raider 800 Offshore Rapid Response Boom represents a significant step forward for customers requiring rapid deployment and retrieval, involving a minimum of personnel. This new concept, presently available in 800mm freeboard, requires only one person during deployment/retrieval. For a length of 300m both deployment and retrieval time is approximately 15 minutes. The inflation and deflation is performed from the reel end of the boom. The boom has a heavy duty PU/PVC fabric with excellent abrasion resistance. NOFI's experience in designing and developing oil booms with excellent wave following characteristics and improved oil containment ensure a high quality product. To select a protective booming is very difficult and a comprehensive multicriterial analysis proved to be extremely useful [4]. Figure 5 presents the features for two current booms made from polymeric materials, the comparative analysis between these classes of High Current Booms. We made a comprehensive multicriterial analysis. We choose two types of protective booms made from polymeric materials and for them characteristics we give qualifications from three to five. Each booms characteristic has an importance in percent, as you can see in figure 5. In the end, from the booms qualifications and from the importance of criteria results the final score for each protective boom: for the AllMaritim NOFI VEE-SWEEP and for the Canadyne PermaBoom. We can observe that from our requirements the second preventive booming, Canadyne PermaBoom is most suitable for our application. This boom made from Heavy duty PVC coated polyester fabric is optimal from our point of qualifications. The final results are presented in a graphic shown in fig. 5.

4. CONCLUSIONS

A major oil spill has potentially devastating effects on nearby coastal states irrespective of their status regarding the Conventions. In each case, information provided by a comprehensive multicriterial analysis proved extremely useful. There is ample justification for all coastal states to participate in this information gathering process. Thus, a complete and accurate list for use by both the stricken vessel and affected coastal states can expedite response and minimize damage. Adequate mooring systems for fast-water booming are not readily available. Deployment and especially recovery of heavy anchors requires specially equipped workboats and experienced crews. Prespill installation of permanent boom mooring buoys and anchor points ashore, to protect sensitive areas, is highly recommended.

Multicriterial BOOM comparisons

	AllMaritim NOFI VEE-SWEEP (1)	Canadyne PermaBoom (2)
Freeboard (mm)	600	500
Boom Height (mm)	1600	1500
Draft (mm)	1000	750
Length (m)	19	30
Weight (kg)	670	435
Volume (m^3)	3	3,2
Buoyancy/Weight Ratio	16	11
Skirt material	Heavy duty PVC coated polyester fabric, 1100 g/m2 (32,6 oz/sq.yd) The heavy	Heavy duty Double EP-200 with synethetic rubber The heavy duty
Wave height (m)	4	3
Towing speed (knots)	1,6	3
Buoyancy (kg)	12	10

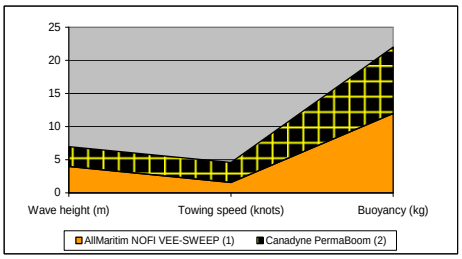

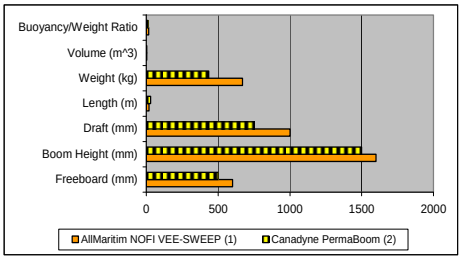

Mullticriterial BOOM comparisons

	AllMaritim NOFI VEE-SWEEP (1)	Canadyne PermaBoom (2)	Importance of criteria (%)	Final score (points)
Freeboard (mm)	5	3	5	0.25
Boom Height (mm)	5	4	2.5	0.125
Draft (mm)	5	3	10	0.5
Length (m)	2	5	10	0.2
Weight (kg)	4	5	10	0.4
Volume (m^3)	4	5	5	0.2
Buoyancy/Weight	5	3	5	0.25
Skirt material	4	5	2.5	0.1
Wave height (m)	5	4	10	0.5
Towing speed (knots)	3	5	20	0.6
Buoyancy (kg)	5	4	20	1
	47	46	100	4.125

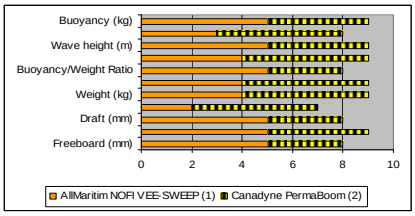

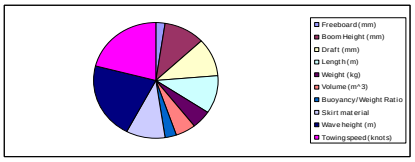

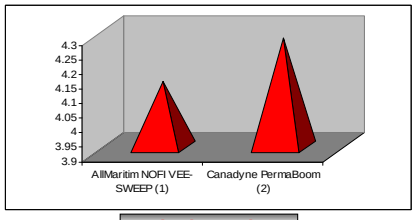

Fig. 5. Multicriterial Analysis with results and graphical representations

5. REFERENCES

[1] USCG, Selection Guide for Oil Spill Applied Technologies, Vol. 1 Decision making.
[2] Walker, A.H., J. Michel, G. Canevari, J. Kucklick, D. Scholz, C.A. Benson, E. Overton, and B. Shane, Chemical Oil Spill Treating Agents. Marine Spill Response Corporation,Washington DC., MSRC Technical Report Series 93-015. 328 p., 1993.
[3] Al-Muzaini, S., The use of air flotation for the treatment of industrial wastes discharged into coastal waters. Journal of Environmental Science and Health, Part A: Environmental Science and Engineering. 1994; A29(7):1367-1382; ISSN: 0360- 1226.
[4] Niță Alexandra, Raicu Gabriel, Tehnologii si materiale avansate utilizate in constructiile navale destinate combaterii poluarii, 10th Scientific Conference with International Participation – SIGPROT 2007, Academia de Poliție "Alexandru Ioan Cuza", București, România, 25 Mai 2007, Pag. 247 - 252, vol. „SIGPROT 2007", Editura Printech, București, CNCSIS - cod 54, ISBN 978-606-521-031-8.
[5] *** International Convention for the Prevention of Pollution from Ships 1973, MARPOL, and Later Amendments.
[6] *** OIL Pollution Act 1990, OPA, and Later Amendments.
[7] *** [Online]. Available: http://www.canatec.com.
[8] *** [Online]. Available: http://www.allmaritim.com.
[9] *** [Online]. Available: http://www.mms.gov/tarprojectcategories/ohmsett.htm.

MARPOL and OPA conventions regarding oil pollution

Şerban Berescu

Abstract – **This paper presents the MARPOL and OPA conventions regarding oil pollution and legislation to prevent the marine pollution. Accordingly MARPOL and OPA in case of oil pollution emergencies, information flow is very useful in finding appropriate contact points and, in particular, allowing IMO to act as a "Clearing House" for offers of assistance from donor States and co-ordinate these services with receiving States. There is ample justification for all coastal states to participate in this information gathering process. A major oil spill has potentially devastating effects on nearby coastal states irrespective of their status regarding the Conventions. Relevant informations about efficiently of different oil pollution methods may increase the quality of maritime pollution prevention.**

Keywords – **MARPOL, oil pollution, OPA.**

1. INTRODUCTION. HISTORY AND PRESENT FOR MARITIME POLLUTION CONVENTION

Oil pollution of the seas was recognized as a problem in the first half of the 20th century and various countries introduced national regulations to control discharges of oil within their territorial waters. In 1954, the United Kingdom organized a conference on oil pollution which resulted in the adoption of the International Convention for the Prevention of Pollution of the Sea by Oil (OILPOL). Following entry into force of the IMO Convention in 1958, the depository and Secretariat functions in relation to the Convention were transferred from the United Kingdom Government to IMO.

The 1954 OILPOL Convention, which entered into force on 26 July 1958, attempted to tackle the problem of pollution of the seas by oil - defined as crude oil, fuel oil, heavy diesel oil and lubricating oil - in two main ways: it established "prohibited zones" extending at least 50 miles from the nearest land in which the discharge of oil or of mixtures containing more than 100 parts of oil per million was forbidden; it required Contracting Parties to take all appropriate steps to promote the provision of facilities for the reception of oily water and residues. The 1954 Convention, was amended in 1962, 1969 and 1971, primarily addressed pollution resulting from routine tanker operations and from the discharge of oily wastes from machinery spaces - regarded as the major causes of oil pollution from ships.

In 1962, IMO adopted amendments to the Convention which extended its application to ships of a lower tonnage and also extended the "prohibited zones". Amendments adopted in 1969 contained regulations to further restrict operational discharge of oil from oil tankers and from machinery spaces of all ships. Although the 1954 OILPOL Convention went some way in dealing with oil pollution, growth in oil trade and developments in industrial practices were beginning to make it clear that further action, was required. Nonetheless, pollution control was at the time still a minor concern for IMO, and indeed the world was only beginning to wake up to the environmental consequences of an increasingly industrialised society.

Şerban Berescu with Romanian Naval Authority, Constanta Port, no.1, 900900-Constanta, Romania (corresponding author to provide phone: +40-722 605508 e-mail: alexandranita@imc.ro).

ISSN-1584-5990

The MARPOL Convention is the main international convention covering prevention of pollution of the marine environment by ships from operational or accidental causes. It is a combination of two treaties adopted in 1973 and 1978 respectively and updated by amendments through the years. The International Convention for the Prevention of Pollution from Ships (MARPOL) was adopted on 2 November 1973 at IMO and covered pollution by oil, chemicals, and harmful substances in packaged form, sewage and garbage. The Protocol of 1978 relating to the 1973 International Convention for the Prevention of Pollution from Ships (1978 MARPOL Protocol) was adopted at a Conference on Tanker Safety and Pollution Prevention in February 1978 held in response to a spate of tanker accidents in 1976-1977 (Measures relating to tanker design and operation were also incorporated into a Protocol of 1978 relating to the 1974 Convention on the Safety of Life at Sea, 1974) [1]. As the 1973 MARPOL Convention had not yet entered into force, the 1978 MARPOL Protocol absorbed the parent Convention. The combined instrument is referred to as the International Convention for the Prevention of Marine Pollution from Ships, 1973, as modified by the Protocol of 1978 relating thereto (MARPOL 73/78), and it entered into force on 2 October 1983.

2. OPA 90 VERSUS MARPOL

The first mandatory phase out of any type of vessel was not dictated by OPA ‘90 as many people in the United States might believe, but rather by the MARPOL Regulations of 1977/78. The world was set to phase out single hull tankers long before the ink on OPA ‘90 was dry. OPA ‘90 was, in a way, necessary because the U.S. was not a signatory party to the MARPOL Regulations of 1977/78. At the time, OPA ‘90 did pose a somewhat though not significant accelerated phase out of single hull tankers. The significance of OPA ‘90 was not its mandatory phase out provisions for vessels trading to the United States, but the potential oil spill liability. This liability was met in part by the creation of marine insurance that could satisfy OPA ‘90 requirements and provide risk coverage for tanker owners. One risk management tool was to ensure that quality tankers both in construction and operations called on U.S. ports. For many charterers and owners, quality took the form of having newer tonnage call on U.S. ports and older tonnage for the rest of the world. The belief that age and quality are related can be disputed; nevertheless the trend toward using younger tankers calling on U.S. ports is clear. For example, Aframax tankers (between 80,000 and 120,000 dwt) that called at U.S. ports in 2001 had an average age of about 9; this was considerably younger than the world fleet’s average age of 12.

Sending younger ships to the United States is a risk management tool that can be used in response to perceived public reactions to an oil spill. Older tankers were employed in other parts of the world where MARPOL requirements held sway. Thus, longevity of single hull tankers was not affected by the mandatory phase out provisions of OPA ‘90.

2.1. SINGLE HULLS WERE ON THEIR WAY OUT

However, the MARPOL Regulations did affect the longevity of single hull tankers in worldwide trading. With some degree of simplification, tankers were to be phased out at their 25th year of age without segregated ballast tanks or at their 30th year of age without segregated ballast tanks (SBTs). Moreover, tankers were free to operate to their 30th year of operation with hydrostatic ballast loading. What this meant in practical terms was that light-loading a tanker by about 15-20% could extend the life of single hull tankers to 30 years subject to a “drop-dead” year of 2025, after which there would be no more single hull tankers.

The chief provisions of the New MARPOL Regulations are that single hull tankers without SBT are to be phased out at 30 years of age which is stepped down to 24 years by 2004. (for the past three years, the average age of VLCCs that have been scrapped has been around 25). For single hull tankers with SBT the step down to 24 years occurs in 2011. This narrows the difference between MARPOL and OPA '90 phase-out schedules. But the major change in the New MARPOL regulation is that the drop-dead year for nearly all large single hull tankers is 2015.

2.2. IMPACT ON VLCCS

A fairly substantial portion of the current VLCC fleet will have their phase-out date advanced. From between now and 2007, a total of 122 VLCCs will have to be phased out. However, there are an estimated 100 VLCCs on order for delivery between now and 2004. This excludes the number that will be ordered and built between 2004 and 2007. Worldwide maximum shipyard capacity for VLCCs has been variously estimated at between 60 to 80 vessels per year. In other words, the entire fleet of 430 VLCCs could conceivably be replaced in six years.

Moreover VLCC owners have been aggressively ordering tonnage throughout the 1990s in anticipation of the mandatory phase out of single hull tankers. One of the remarkable aspects about our business is that most of these orders were placed without firm employment and at a moment in time when spot rates did not justify the new building costs.

The risk-free return is 10-year Treasuries. The owner's actual return does not take into consideration operating risks such as engine breakdowns or the risks associated with oil spills. Orders placed during the 1990s were eventually well-rewarded when rates reached their recent peak levels. Interestingly orders placed during the 1990s have now created a fleet that is relatively young.

2.3. THE NET RESULT

The world economic slowdown has adversely affected oil trade. This slowdown in the growth of tanker demand coupled with an aggressive shipbuilding program means that there is a possibility of supply getting ahead of demand even with the implementation of the new MARPOL phase out requirements. In other words, we see no capacity crunch.

The true impact of the New MARPOL phase-out requirements could occur from 2010 to 2015 when a large number of VLCOs and Suezmaxes are forcibly retired. If there is a crunch, it will occur during 2010 and 2015. At the other end of the scale a large number of Panamax tankers will be phased out before 2010. The recent surge in orders for Panamax tankers suggest that this supply crunch will also be avoided [2].

One important note is that mandatory phase out applies not just to single hull tankers carrying persistent oils such as crude oil and fuel oil, but to product carriers carrying clean cargoes as well. Whereas the older mandatory phase-out schedule covered crude carriers of 20,000 dwt (deadweight tonnage) and above and product carriers of 30,000 dwt and above, the new Category 3 oil tanker now applies MARPOL phase-out requirements to single hull crude and product carriers over 5,000 dwt.

In summary, we see no immediate tanker supply problems with regard to crude carriers. Owners have already ordered sufficient tonnage to take care of mandatory phase out until 2010. We anticipate that sufficient numbers of vessels will be ordered to take care of the accelerated phase out between 2010 and 2015.

3. EUROPEAN UNION POLITICS

The EU oil trade is the largest in the world - crude oil imports represent 27% of total world trade (US 25%)

Oil demand in the EU is around 640 million tons p.a., but approx. 800 million tons p.a. is transported to, from and between EU ports. Also 90% of the total oil trade with the EU is seaborne. The world oil tanker fleet on 1 January 1999 comprised 7,030 ships totalling 289 million dwt. This represented 38.5% of world merchant tonnage. The average age of the world tanker fleet in 1999 was 18 years (compared to 16,7 years in1995).

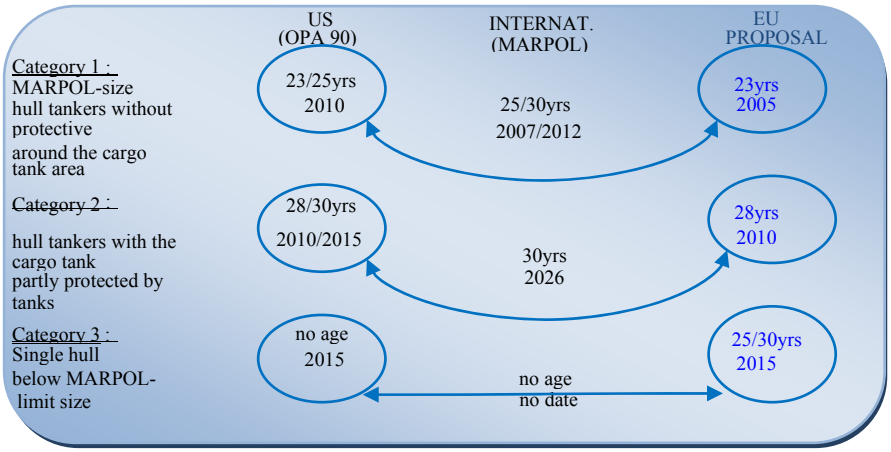

Fig. 1. Comparison OPA 90 vs. MARPOL

Table. 1. Comparison OPA 90 vs. MARPOL

	USA (OPA 90)	**International (MARPOL)**
Category 1: Single hull oil tankers, MARPOL size, without **tanks in protective locations**	23/25yrs 2010	25/30yrs 2007/2012
Category 2: Single hull oil tankers; MARPOL size, **with partial protection** of the cargo tank area	28/30yrs 2010/2015	30yrs 2026
Category 3: Single hull oil tankers **below the MARPOL size limit**	2015	No deadline

Of the total 1999 fleet, 41% (2,939 ships) were built before 1979, i.e. are now over 20 years old. In tonnage terms these represent 36% of the total tanker tonnage. The EU registered oil tanker fleet of 855 tankers 9 totalling 43,2 million dwt represents14.9% of the world total, but it is estimated that companies established within the EU control about 35% of the world's oil tanker fleet [3]. Regarding, *phase-out of single hull tankers in the EU*, the idea underlying this proposal is twofold: build upon the assessment already made internationally, those double hull tankers and equivalent designs are safer than single hull tankers but also to reduce the gap between the phasing out schemes in the US and in Europe. As you can see, in the Table 1 we made a Comparison OPA 90 vs. MARPOL regarding key point of single hull oil tankers and the figure 1 presents this important aspects.

3.1. Preventing Black Tides In The Black Sea

The European Maritime Safety Agency (EMSA) is participating in an oil pollution response exercise organised off the port of Varna by the Bulgarian Maritime Administration. Two EMSA-contracted oil spill recovery vessels are taking part: the GSP

Orion and Santa Maria. This is the first time this type of exercise has been conducted in Bulgaria, with the aim of testing the coordination and cooperation between EMSA's contracted vessels and Bulgarian oil spill response resources.

How can Europe protect the coasts of Black Sea from oil spills, in the face of rising oil exports from the Caspian Sea region? "We need to better protect the Black Sea", says Willem de Ruiter, Executive Director of the Lisbon-based European Maritime Safety Agency. This is a sea area known for its fragile marine environment, and it plays a vital role in enabling waterborne trade across Central Europe and beyond, linking to the Danube River, major oil ports and high-density marine traffic chokepoints such as the Bosporus and Kerch Strait. The Black Sea is surrounded by countries that either export oil or facilitate the transit of oil, and so a risk of a major oil spill exists, most recently illustrated by a major oil pollution incident in the Kerch Strait in November 2007.

As in other European waters, EMSA has contracted an oil spill response vessel in the Black Sea to "top-up" the resources already in place at Member State level to respond to potential oil spills. The GSP Orion is an EMSA-contracted vessel based in Constanta. Should an oil spill occur, it is available to help protect the coastlines of Bulgaria and Romania within 24 hours. Furthermore, the vessel can also be made available within 48 hours to recover oil across the entire Western Black Sea, roughly half of the Black Sea's surface area. Two EMSA-contracted vessels are taking part in the exercise, which is being held in the vicinity of the Bulgarian port of Varna. Santa Maria, a bunker vessel with tank capacity of 2,420 m³ is usually stationed in Malta. The GSP Orion, a supply vessel with a capacity of 1,330 m³ has her home port nearby in Constanta, Romania. This marks the very first exercise between EMSA and the Bulgarian Maritime Administration. In the afternoon, an "open ship" event at the passenger terminal in Varna enables interested members of the public and media to visit the vessels and receive more detailed information about the vessels, and demonstrations of the oil spill response equipment onboard. In accordance with Regulation 724/2004/EC, EMSA has established a network of stand-by oil spill response vessels across Europe. This network covers all the regional seas in Europe, and the recovery vessels are strategically distributed along the European coastline to boost national capabilities, to plug perceived gaps, and to provide effective and efficient assistance to Member States when requested. The EMSA pollution response vessels thus provide a "European tier" to provide assistance to coastal States if an oil spill incident exceeds a Member [4].

3.2. STATE'S OWN CAPABILITY TO RESPOND

The Action Plan for Oil Pollution Preparedness and Response of 2004 as developed by the Agency provided the initial framework and identified activities to strengthen preparedness and response structures in co-operation with Member States. In the figure 2 you can see Network of EMSA contracted oil recovery vessels and equipment depots.

These activities, updated annually through the EMSA Work Programme, fall into three main categories: operational support services, cooperation. More recently, in mid 2007 the Action Plan for Pollution Preparedness and Response was developed to address incidents involving Hazardous and Noxious Substances, so called "chemical" spills. To ensure an appropriate level of service, EMSA's contracted vessels participate in regular training activities and drills. These are designed to verify and improve the operation of the onboard equipment, including the testing of equipment such as booms, skimmers and oil slick detection radars. Together with national maritime authorities – national coast guards, port administrations, search-and-rescue organisations etc. – EMSA's vessels also participate in wider exercises involving larger-scale marine disaster preparedness activities.

The result is to improve cooperation among all actors who, when an accident happens, will be better prepared to respond to, and limit the damage of, an oil spill at sea.

Fig. 2. State capability for oil spill response

4. CONCLUSIONS

In addition to its other tasks, the European Maritime Safety Agency (EMSA) has been active, in the field of marine pollution preparedness and response since mid-2004. The role of EMSA as a European Agency is to provide added value support to EU Member States and the European Commission. This Agency carries out its range of spill response activities with regard to information, co-operation and co-ordination as well as operational support.

The performance of "specialised" vessels would have been more effective if information on slick locations had been more precise and timely. Consequently, improving this aspect through by aerial surveillance guidance or onboard slick detection systems would facilitate large scale operations.

Implementing its legal obligations in the field of pollution preparedness and response has posed a number of technical, scientific, operational and financial challenges to the Agency. A particularly difficult activity has been to define and phase-in an at-sea oil recovery service available to coastal States potentially affected by a major spill. Key to the success of the service was the co-operation from Member States when reviewing their approaches to this type of operation.

5. REFERENCES

[1] ***International Convention for the Prevention of Pollution from Ships, 1973, as modified by the Protocol of 1978 relating thereto (MARPOL 73/78) [Online].
Available:
http://www.imo.org/Conventions/contents.asp?doc_id=678&topic_id=258#intro.
[2] Nersesian, Roy L., "MARPOL's new phase out: what's its impact? (Tankers)", Marine Log , January 2002.
[3] Willem De Ruiter, „EU Initiatives In The Aftermath Of The Erika Casualty, IUMI Workshop on Liability" 12 September, London, 2005.
[4] EMSA Press Releases, 10 03 2010 – "Preventing black tides in the Black Sea: first EMSA oil spill preparedness exercise off the Bulgarian coast" [Online] Available: http://www.emsa.europa.eu/ennews20100310115932.html, February 2010.

The impact of a storage reservoir harnessing on the environment by intending the reduction of human activities

Donciu (TIMOFTI) Diana Andreea, Mihai Dima, Gheorghita Oana

Abstract: **The pollution of the environment appeared at the same time with the human species and developed as the human society continued to evolve, becoming today one of the most important concerns of scientists. The evaluation of all the impact elements represents a solution in which regards the measures that need to be adopted for the minimizing of the negative effects of the anthropogenic actions on the environment.**

In this paper the authors present a study regarding the impact of a storage reservoir facility on the environment, as a result of the anthropogenic activities from the referred zone.

***Keywords*: environmental pollution, human activities, storage reservoir**

1. Introduction

Globally, the first hydrotechnical works date since ancient times, when humans started to practice agriculture and livestock. Interesting to observe is the fact that many mutations, which gradually interfered in the life of humans, were induced by the permanent necessity of water or by protection measures against the negative effects of water. Thus, humans had to entrap sources of water, to dig fountains for water resources and to protect their homes with the help of dikes and channels for water evacuation.

Because of the development, water necessity met a continuous increasing and humans had to find a solution which could resolve the non-existing correlation between the possibilities of the natural resources and the necessary of water. Dams have been constructed in order to prevent floods, to supply drinking and domestic water, to generate energy and for irrigation purposes since the old-times. They have a great deal of positive and negative effects on the environment.

It is estimated that there are now more than 40,000 large dams throughout the world, with an aggregate storage capacity of about 6,000 km^3. This represents a seven-fold increase in the standing supply of natural river water. However, for most of the world's existing stock of large dams, environmental issues have played a small part in their design. Most dams have been constructed to maximize the economic use of water, with no understanding of the long-term consequences of alterations to flow volume, flow patterns and water quality.

Donciu (Timofti) Diana Andreea is with Technical University of Iasi, Faculty of Hydrotechnics, Bd. D.Mangeron 65, 700050, Iasi, Romania, e-mail: diana_timofti@yahoo.com).

Dima Mihai is with Technical University of Iasi, Faculty of Hydrotechnics, Bd. D.Mangeron 65, 700050, Iasi, Romania (e-mail: mdima_2003@yahoo.com).

Gheorghita Oana is with Technical University of Iasi, Faculty of Hydrotechnics, Bd. D.Mangeron 65, 700050, Iasi, Romania (e-mail: oanaluciana2002@yahoo.com)

ISSN-1584-5990

A lot of studies have investigated the impact of the dams on specific components of ecosystems and were focused on the abiotic primarily first order impact. For studies of second and third order impact a long time frame is required before new equilibrium states are attained and total change becomes apparent (fig 1).

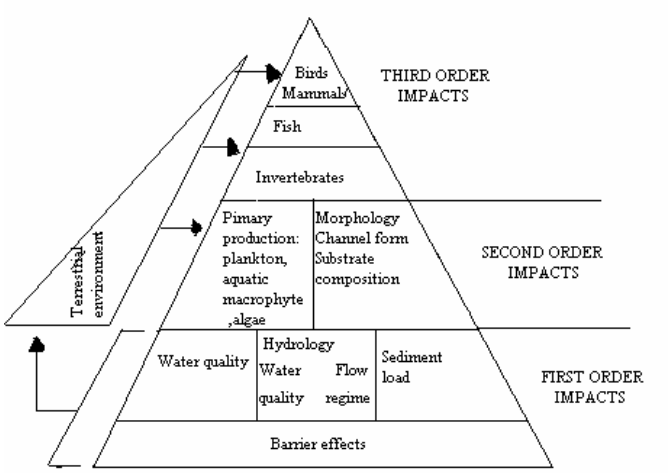

Fig. 1 – A framework for assessing the impact of dams on river ecosystem

2. Effects on the environment

It is important to take into account the interconnected nature of ecosystems concerned and the consequences of change in individual ecosystems components when considering the impact of dams on river ecosystem.

First order impacts are the immediate abiotic effects that occur simultaneously with dam closure and influence the transfer of energy and material into the downstream river and connected ecosystems.

Second order impacts are the abiotic and the biotic changes in upstream and downstream ecosystem structure. These depend upon the characteristics of the river prior to dam closure and may take place over many years.

Third order impacts are the long term biotic changes resulting from the integrated effect of all the first and second order changes, including the impact on species [table 1].

2.1. Morphology and flow regime

The hydrotechnical works modify in a significant way the surface morphology and the flow regime of water. The dam construction influences the water level and also the volume and the surface of the storage reservoir. The flow regime is sensibly changed and the velocity of water in lake decreases to zero.

2.2. The physical and chemical quality of water

The water stored in storage reservoir has different physical and chemical qualities in relation to the water from the existing river before the harnessing of the storage reservoir. From qualitative point of view, new processes occur in storage reservoirs. One of these processes is represented by water stratification, produced due to the pressure differences that are determined by the differences in density.

In storage reservoirs with low depths, the wind action harmonizes the water and the stratification becomes non-existent. At great depths, stratification represents an important factor. During hot periods, the epilimnion get warmer under the sun action, while the hipolimnion has a temperature adjacent to 4° C. These 2 zones are separated by

metalimnion, which represents a zone with an increased thermal gradient. In this way, the thermal variations occur in the epilimnion due to the wind and the differences in external temperatures. During cold periods, low temperatures, wind action and the gain of water from the river balance the temperature in the epilimnion and hipolimnion. Thus, the water in storage reservoir is uniform because the metalimnion is non-existent due to the vertical drafts. During the harnessing period, temporary pollution is produced downstream due to the oils, combustible, residues discharge and wastewater evacuation.

Table 1 – Upstream and downstream impacts according to first, second and third order

Location in relation to the dam	Category of impact	Impact
Upstream	Firs order impact	Modification of the thermal regime
		Accumulation of sediment in the reservoir
		Changes in water quality
		Groundwater along reservoir
	Second order impact	Plankton and Periphyton
		Growth of aquatic macrophytes
		Riparian vegetation
	Third order impact	Invertebrates, fish, birds and mammals
Downstream	First order impact	Daily, seasonal and annual flows
		Water quality
		Reduced sediment flows
		Changes to the channel, floodplain and coastal delta morphology
		Groundwater in riparian zone
		Water temperature-thermal pollution
		Ice formation
	Second order impact	Plankton and Periphyton
		Growth of aquatic macrophytes
		Riparian vegetation
		Carbon flows and cycle distortions
	Third order impact	Invertebrates, fish, birds and mammals
		Estuarine and marine impacts

2.3. The change in vegetation

The most obvious change in landscape is produced at the vegetal level, its repartition and qualitative and qualitative constitution being modified. The chopping of resinous trees (fig.2) for constructions use leads to the limitations of the surfaces covered by this type of tree or even to their disappearance. From ecological point of view, the local climate also contributed to the appearance of benefic conditions for beech and this permitted their regeneration and intensive development.

2.4. The biological quality of water

The eutrophication represents a process that affects the biological quality of water. It consists in great concentrations of nutrients that overpass the limits and lead to the deterioration in water quality (fig. 3). The two major causes of eutrophication are excess nitrates and excess phosphates in water. It is important to study these nutrients because oftentimes, human activity is responsible for their negative effect on the environment. Depending on the trophic states, the storage reservoirs can be: (i) oligotrophic, being

characterized by the predominance of physical and chemical factors, low concentrations of nutrients and a minor biological production; (ii) mezotrophic, consisting in big concentrations of nutrients that lead to a great biological production and a minor oxygen deficiency; (iii) eutrophic, being very affluent in nutrients that lead to an excessive biological development and a minor oxygen deficiency

Fig. 2 – The deforestation

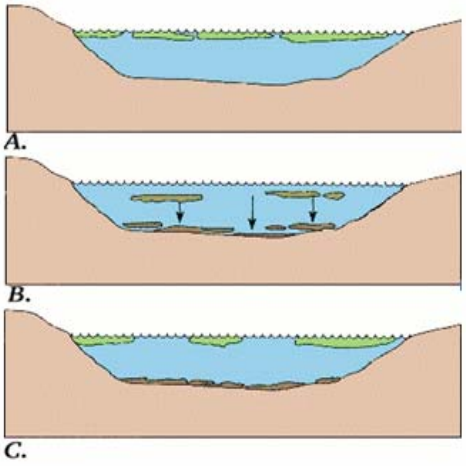

Fig. 3 – The effects of algal bloom on water quality. (A) Abundant growth of algae in sunlit shallow water when nutrients are abundant. (B) During cold periods, algae die and sink to the lake bottom. (C) The next growing season, more algae thrive at the surface while older materials decay at the bottom, increasing BOD and releasing more nutrients to supply new growth

The eutrophication process is accelerated by the pollution with detergents, hydrocarbons, domestic and industrial wastewater. The effects of eutrophication are represented by: (i) overproduction of macrophytes, algae on the shores and phytoplankton; (ii) change of balance between fish species and the storage reservoir economy due to the oxygen deficiency (iii) low transparency and changes in water color; (iii) oxygen deficiency in hipolimnion (iv) great quantities of degraded materials settled at the bottom of the storage reservoir; (v) gas bubbles

The consequences of eutrophication are represented by: (i) the difficulty for industrial and domestic water use; (ii) the important diminution of biological potential; (iii) the diminution or even disappearance of recreation activities and fishery

2.4. The impact on fauna

Terrestrial fauna. Big mammals are chased away by the noises of explosions that are necessary in the quarry and for the construction of roads. They are affected by the disappearance of some areas reach in nourishment, the absence of usual passes and by the abrupt shores that block the access to water. Normally, after the construction period, the animals come back and try to adapt to the new biotope. The existing birds are not so disturbed by the appearance of the storage reservoir. Water birds find ideal conditions for food, life and reproduction. For the preservation of species, studies are necessary to be made and protection measures need to be taken.

Aquatic fauna. At the same time with the storage reservoir appearance, the conditions in the life of fish and amphibians, the flow regime, the volume and surface of water, the concentrations of oxygen and flora are totally changed. During construction period, workers practice a wild poaching of fish fauna.

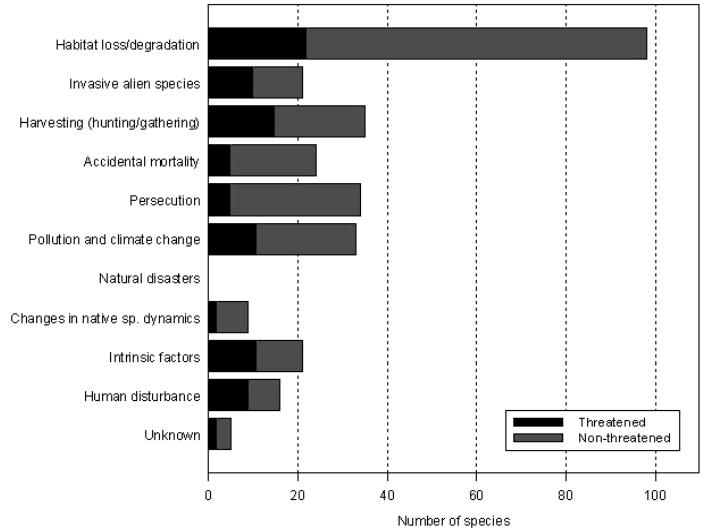

Figure 4 – Major threats on species

The effect of sluicing on the aquatic fauna in the case of a storage reservoir with water discharge must be studied in four special ecosystems: (i) the upstream ecosystem; (ii) the new ecosystem from the storage reservoir; (iii) the ecosystem between the interception zone and the zone with the turbines and returned debits; (iv) the downstream ecosystem.

There are many forms of impact on the environment and it is impossible to make a complete identification. The effects of superior order are hard to predict because the unknown effect existent in the design phase. Therefore, it is recommended that the identification of effects and protection measures on the environment need to be continued in exploitation.

3. Measures for diminishing the impact of a storage reservoir harnessing on the environment

Social and environmental impacts of dams and reservoirs built today must be avoided, or mitigated. Every effort is made to have the dam and reservoir more related with the environment. The following are taken into account when developing modern water projects:

- **Concern for the environment is highlighted:** This concern is part of all phases of engineering, construction and operation of the project. Alternative solutions should be identified to provide the required water at the lowest long-term cost to society with a small or no impact to the environment.
- **ICOLD engineers include environmental protection among their responsibilities:** Today, they use their collective knowledge and experience to design environmentally responsible water projects.
- **Dam and reservoir projects require system planning which recognizes the impact on an entire river basin and its ecosystems:** The great potential effects will be on the natural

and social environment when the project is large. The project size is determined based on regional and local needs.

- **Many countries now require the formal identification of environmental impacts during the conceptual phase of a project:** In the designing projects, ample environmental impact assessments are taken into account to reduce the costs to society and the environment.
- **Rigorous economic analyses of the benefits and costs of large projects provide critical information to decision-makers:** Benefits and costs as well as social and environmental considerations form a common basis for decision making. Realistic project costs, including impacts on the natural and social environment, must be weighed against project benefits.
- **Public consultation and input to obtain a consensus is necessary for the most effective project planning, implementation and operation:** This consent is often driven by the environmental compatibility of the project. A free exchange of information among the various interest groups, technical experts and decision makers is critical for this consent and must be implemented at the earliest possible stage of the project.
- **Monitoring of the environmental impacts of existing projects provides a better understanding of the true impacts rather than projected impacts**: Monitoring must begin during the planning and design of the project and continue through construction. As soon as the project becomes operational, its impact and the effectiveness of mitigation measures must be monitored at regular intervals. The results are evaluated and implemented to continually improve the project operations.
- **Research on the ecological aspects of the many existing dams and reservoirs can provide important lessons for future projects:** The results obtained from the monitoring of existing dams must be compared with the current environmental standards. Research on the ecological behavior of many existing dams and reservoirs provides important lessons for future projects and improves environmental technology.

4. Conclusions

In this study, the authors present a large amount of information in order to highlight the impact of a storage reservoir harnessing on the environment and the resulting necessary measures in order to create a harmonious link between the dam, reservoir and the environment.

The diminishing of these impacts can be improved by embracing some of the measures that are taken into account by experts, engineers and international commissions.

5. References

[1] Peter Coles, *LARGE DAMS—THE END OF AN ERA*, 2004, published on www.unesco.org

[2] Lori Pottinger, *Environmental Impacts of Large Dams: African examples*, 1996, published on **www.internationalrivers.org**

[3] Andrew S. Goudie, The Human Impact on the Natural Environment: Past, Present, and Future, 2006, Blackwell Publishing, sixth edition

M. Sait Tahmiscioglu, Nermin Anul, Fatih Ekmekci, Nurcan Durmus, *Positive and negative impacts of dams on the environment*, International Congress on River Basin Management

[4] Don E. McAllister, John F. Craig, Nick Davidson, Simon Delany, Mary Seddon, *Biodiversity impacts of large dams*, Background paper no. 1 prepared for IUCN/UNEP/WCD

[5] Nistreanu Valeriu, Nistreanu Viorica, *Amenajarea resurselor de apa si impactul asupra mediului*, published on www.hydrop.pub.ro

Ensuring Environmental Quality in the Context of Sustainable Development of Human Activities

Oana Gheorghita, Teodora Manuela Cornea, Mihai Dima

Abstract: **Following the general economic growth and progress in all areas of life, achieved without control over its actions, the man favored the triggering of ecological imbalances with negative effects on the quality of life and the environment. Quality assurance and environmental protection is a necessity for survival and progress and is a matter of current concern for planet evolution. In the current global environmental crisis and the limited degree of supportability of the environment, the authors of this paper, highlights the importance of promoting environmental protection as a component of sustainable development of human society in a clean environment free from environmental risks.**

Keywords **– environment, human activities, pollution, sustainable development**

1. INTRODUCTION

In today's world it is a must to have an ecologist behavior in the conduct of all economic and social activities as climate change presents a disturbing dynamic. It is known that the lately storms and the most devastating rains are alternating with terrible droughts, and in less than 50 years we will have desert areas in Europe, because forests will disappear and water resources will dry up. The exploitation of nature and ignorance of its alteration, human activities that have led to technological progress, economic development and not least demographic explosion caused imbalance of the planetary ecosystem and led to the environmental crisis facing the world. Manifestations of the current environmental crisis are the depletion of nature resources, the increase of extinction rate of plants and animals (loss biocenosis spaces), and the pollution that warms the planet and destroy the ozone layer. Ensuring environmental quality in the current context of climate change and economic globalization is possible only through sustainable development and through control of human activities that have an environmental risk.

2. ENVIRONMENTAL QUALITY

The environment is an essential element of human existence and represents the result of interference of natural elements - earth, air, water, climate, biosphere and man and the elements created by human activities. All these interact and affect the existential conditions and the possibilities for society's future development. The ensemble and the exchange of relations established between man and nature, and their interdependence influence the ecological balance, the living conditions and thus determine the working conditions for

Georghita Oana, Technical University of Iassy, Faculty of Hydrotechnical Geodesy and Environmental Engineering, Bd. D. Mangeron 65, Iassy 700050, Romania; email: oanaluciana2002@yahoo.com

Cornea Teodora Manuela, Technical University of Iassy, Faculty of Hydrotechnical Geodesy and Environmental Engineering, Bd. D. Mangeron 65, Iassy 700050, Romania; phone:0740665798; e-mail: corneateodoramanuela@yahoo.com

Dima Mihai, Technical University of Iassy, Faculty of Hydrotechnical Geodesy and Environmental Engineering, Bd. D. Mangeron 65, Iassy 700050, Romania; phone: 0742311888, mdima_2003@yahoo.com

ISSN-1584-5990

human and social development. The 20th is the period of the greatest discoveries and transformations of human civilization that brought also the most complex environmental effects due to the development of human activities. With demographic growth, industrial development, transport, economy based on consumption of energy resources with recovery rates that exceed their potential occurred the altering of the quality of natural environmental factors, global pollution and disrupting planetary ecosystem.

Any human activity and the existence of the man is inconceivable outside environment. Therefore, its quality as a whole marks the level of existence and development of individuals. The environment must be adapted and organized to meet the needs of individuals, which means taking the nature's resources and processing them to serve the needs of the population. This dependence has a highly degree of reciprocity, because human needs are adapted more or less to the environment. Ensure adequate quality of environment protection - as a need for survival and progress - is a matter of concern and great actuality for social development. In this context, it is necessary to maintain environmental quality and to reduce the negative effects and its implications of human activity. Environmental protection is a major issue discussed worldwide in the last decade, which had raised numerous disputes between developed countries and those undergoing development. This called for the establishment of international organizations which have as main objectives the adoption of solutions to mitigate pollution and improving environmental quality in general.

3. MAINSTREAMING ENVIRONMENTAL SUSTAINABILITY INTO THE CONCEPT OF SUSTAINABLE DEVELOPMENT

Sustainable development concept was born in response to the emergence of environmental and natural resources crisis, especially those related to energy. The Conference on Environment held in Stockholm in 1972 was the first time when it was recognized that human activities contribute to environmental damage, endangering the future of our planet.

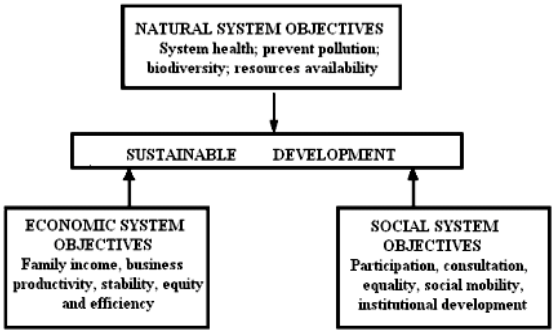

Fig. 1. Main areas that are characterizing sustainable development

The term of sustainable development has started to become, however, well known only after the Conference on Environment and Development organized by the United Nations in Rio de Janeiro in the summer of 1992 known as the "Earth Summit". It resulted in the development of several conventions on climate change (emissions of methane and carbon dioxide), on biological diversity (species conservation, on stopping deforestation and foundation of Agenda 21 which states that environmental protection and quality assurance is fundamental to ensuring sustainable development. The figure below presents

the fundamental of sustainable development whose foundation principle is to ensure a balance between socio-economic systems and elements of natural capital.

The main objectives of sustainable development are: resizing and reshaping economic and social structure to transform it into a sustainable system by stopping the deterioration of natural capital, ensuring the health of the population and ongoing monitoring and evaluation of economic performance and social protection environment and developing of a coherent legislative and institutional system. Environmental protection is an issue of social development, of recovery, conservation and environmental protection. Environmental actions are defined in conjunction with economic development policy, with social and economic forecasts on medium and long term. Sustainable development integrates environmental protection and environmental protection condition sustainable development, environmental protection strategy is therefore found by its essential coordinates in the strategy for sustainable development.

4. HUMAN ACTIVITIES WITH NEGATIVE ENVIRONMENTAL IMPACTS

Entire human activity taking place in the environment interacting with it, is causing a number of changes and impacts (pollution) that have accumulated over time and reached a critical mass that gives them explosive and irreversible potential.

Brundtland Report identifies the most important environmental issues that have emerged due to human activities and population explosion and are listed below:

1. Industry development, burning fossil fuels that enhance the greenhouse effect and disrupts the climate of the entire planet. Intensive usage of fossil fuels contributes with 80-85% in carbon emissions, and reached higher values than environments fixing capacity. As a result, in 1959, when such records began systematically to date, the concentration of carbon dioxide in the atmosphere increased from 316 ppm (parts per million) to 369 ppm (in 2000). Direct consequence is the emergence of the greenhouse effect, leading to gradual warming (and also the acceleration) of the planet.

2. Exploitation of natural reserves, deforestation (rainforest destruction). Another type of human aggression on the environment is the reducing of forestry fund by massive deforestation, therefore losing the benefits trees provided for millions of years (soil fixation, regulation of hydrological regime, the regime temperature, carbon dioxide fixation, harboring and protecting biodiversity, and wind and the intensity of it control, etc.). Changes in land, forestry and land clearing for agriculture contributes with 15 - 20% of current carbon dioxide emissions. Most of the net carbon dioxide emissions resulting from deforestation are occurring in tropical regions.

3. Agriculture development and overgrazing that leads to desertification; agricultural activities have a significant impact on environment, particularly on soil salinization and desertification of land in irrigated areas, soil compaction due to heavy machinery use and pollution by excessive use of pesticides (used against pests)and fertilizers (used for soil fertilization). Soil erosion takes the second place in terms of land degradation due to intensive grazing by irrational exploitation of the funciar fund. The irrational and uncontrolled usage of chemical fertilizers causes soil acidification, pollution of groundwater and surface water. Emissions to air water and soil resulted from agriculture consist of methane gas and ammonia gas from fermentation processes and animal droppings.

4. Enormous amounts of waste and residues; methane is the second most important greenhouse by amount released criteria, 8 times more polluted than carbon dioxide that results from human activities. It is produced by rice cultivation, cattle and sheep and not least after wastes fermentation. Human activities have increased the concentration of

methane in the atmosphere by about 145%, produced largely by waste decomposing and agricultural practices.

5. Thinning of atmospheric ozone layer; the ozone of the troposphere, in the lower atmosphere, is another important greenhouse gas arising from industrial activities. It is created naturally and also by reactions involving gases resulting from human activities, including nitrogen oxides from cars and power plants. More frequent the occurrence of major storms and destructive hurricanes, prolonged periods of drought followed by rains and catastrophic floods, every year more pronounced changes in climate, with emphasis of extreme temperatures (summers increasingly arid, cold winters with no precipitation) raised the first questions related to long term effects that would be irreversible of human activities impact on nature.

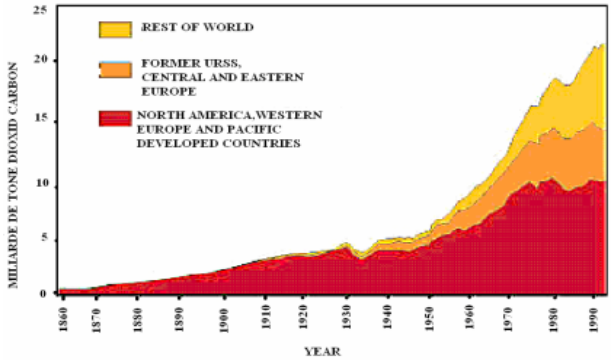

Fig. 2. Carbon dioxide emissions from burning coal, oil and natural gas are presented for the period 1860 - 1992 for three groups of countries

5. REDUCING ENVIRONMENTAL IMPACT OF ENERGY SECTOR BY USING ALTERNATIVE ENERGY

To produce electricity and/or heat by burning fossil fuels (coal, oil, gas, etc..) thermoelectric and electric power plants determine the energy sector to have a decisive contribution to air pollution by quantitatively significant emissions of carbon dioxide, sulfur dioxide, nitrogen oxides, aerosols, carbon monoxide, methane.

Figure below (fig. 3) shows the share in the energy sector, particularly electricity generation sector that contributes to emissions of greenhouse gases (an average of 48% of total pollutant emissions comes from the energy sector).

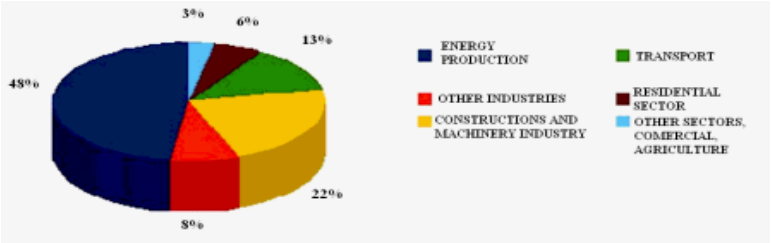

Fig. 3. Percentage in which major activity sectors contribute to human emissions of greenhouse gases

The most important emissions and simultaneously most harmful are those from burning coal, especially inferior coal. Burning fuel oil is an important source of emissions, mainly atmospheric acids (sulphur oxides, nitrogen oxides). Burning natural gas, although a major source of carbon dioxide and nitrogen oxides, is the most complete combustion,

resulting in reduced emissions of carbon monoxide, sulphur oxides and aerosols. The volving of the energy sector resulted in a significant increase of emissions of greenhouse gases responsible for global warming, acidifying gases - cause of acid rain, and other harmful emissions for environment and human health. The energy sector plays a decisive role in implementing the concept of sustainable development.

The control of energy consumption and the increased use of energy from renewable sources, together with energy savings and increased energy efficiency, constitute important parts of the package of measures needed to reduce greenhouse gas emissions and comply with the Kyoto Protocol to the United Nations Framework Convention on Climate Change, and with further Community and international greenhouse gas emission reduction commitments beyond 2012.

Tab. 1. National overall targets for the share of energy from renewable sources in gross final consumption of energy in some European countries in 2020

Country	Share of energy from renewable sources in gross final consumption of energy in present	Target for share of energy from renewable sources in gross final consumption of energy, 2020
France	10,3 %	23 %
Italy	5,2 %	17 %
Luxembourg	0,9 %	11 %
Hungary	4,3 %	13 %
Austria	23,3 %	34 %
Portugal	20,5 %	31 %
Romania	17,8 %	24 %
Finland	28,5 %	38 %
Sweden	39,8 %	49 %
United Kingdom	1,3 %	15 %

Conservation, efficient and ecological capitalization and sustainable usage of these resources, represents a major concern worldwide.

The mitigating of the negative impact of energy sector is reachable by the use of renewable energy: biomass and bio fuels, solar, wind, and hydropower. Using renewable energy sources ensures improving in security of energy supply and limits the import of energy resources in terms of sustainable development.

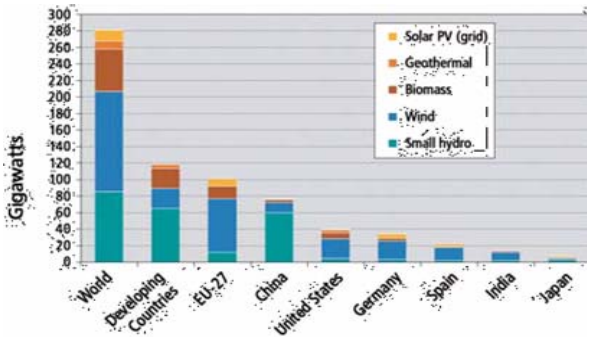

Fig. 4 . Renewable power capacities in 2008 for developing world, EU and top six countries

Those factors also have an important part to play in promoting the security of energy supply, promoting technological development and innovation and providing opportunities for employment and regional development, especially in rural and isolated areas and can reduce the dependence on imported oil in the transport sector, in which the security of

energy supply problem is most acute, and influence the fuel market for transport.When favouring the development of the market for renewable energy sources, it is necessary to take into account the positive impact on regional and local development opportunities, export prospects, social cohesion and employment opportunities, In order to reduce greenhouse gas emissions within the Community and reduce its dependence on energy imports, the development of energy from renewable sources should be closely linked to increased energy efficiency.

The use of agricultural material such as manure, slurry and other animal and organic waste for biogas production has, in view of the high greenhouse gas emission saving potential, significant environmental advantages in terms of heat and power production and its use as biofuel.

Harnessing renewable energy is based on three important premises conferred by them, namely: accessibility, affordability and acceptability.

Exploiting alternative energy gives the guarantee of increasing security of energy supply by diversification and reduction on import share of energetic resources and it is one of the easiest ways to obtain conservation and sustainable development of energy sector. It demonstrated that such a method used in an organized manner, can produce large amounts of renewable clean energy and at the same time can bring a huge economic incentive because they were effective in the long term costs. The main solution to limit environmental pollution is to reduce dependence on oil by replacing it with renewable energy sources - green energy.

6. CONCLUSION

Ensuring appropriate environmental quality and protection - as a need for survival and progress - is a matter of current concern and social evolution. In this regard, it is necessary to maintain environmental quality and reduce the negative effects of human activity with its implications. In this context the objective is not only rational use of resources, but also linking human activities with measures to protect natural factors by adopting cleaner technology to prevent and minimize the negative effects on the environment.

In this paper, the authors will highlight the main aspects of environmental protection through a reconsideration of human activities with high pollution and negative environmental impacts considering giving security to promote green energy sustainable development.

7. REFERENCES

[1] Michael B. McElroy, *"The Atmospheric Environment: Effects of Human Activity (Hardcover)"* 2008

[2] Banu Alexandra, Radovici Octavian Mircea , *"Elemente de ingineria si protectia mediului"* Editura Tehnica, 2008

[3] Dumitru Porojan, Cristian Iftimoaie, *„Dezvoltare locala durabila in contextul globalizarii"* Editura Irecson 2008

[4] Lupoi. E, "*Dreptul mediului*" Editura Lumina Lex, Bucuresti 1993

[5] *Raport privind starea mediului in judetul Suceava* , ch 12 Energia

[6] *DIRECTIVE 2009/28/EC OF THE EUROPEAN PARLIAMENT AND OF THE COUNCIL of 23 April 2009* (L 140/16 ,L 140/17 L 140/46)

[7] Renewable status report 2009 [Online]. Available: http://www.ren21.net/pdf/RE_GSR_2009_Update.pdf

Considerations on landscape degradation by landslides

Florin Mărăcineanu, Elena Constantin, Şerban Roşulescu, Marian Sbarcea

Abstract - **The paper addresses the issue of sliding-caused land degradation in the southern Carpathians area, in the Buzau-Arges sector which is known for itshigh environmental degradation due to the large sliding potential. It highlights the diverse anthropogenic factors that favour landslide production, in association with other forms of soil degradation, as well as their environmental and economic impacts.**

Landslides determine the classification of the affected areas as unfavourable areas whose ecological reconstruction is the special concern of Romanian and European organisations and institutions.

The paper also presents the strategy and technique principles to be applied for landslide stabilization and capitalization purposes.

Kaywords: **landslide, environmental degradation, sustainable rural area, unfavourable areas, ecological reconstruction**

1. INTRODUCTION

The socio-economic development of a territory depends on the natural resources it provides for use according to the needs imposed by development, evidenced by policies and strategies. The latter is based on the assessment of the natural resources that should be capitalized in a sustainable manner, depending upon the different categories of resources and operating limits to achieve maximum effect with a minimum consumption of resources.

The natural resources of a territory, defined by complex environmental resources can be analyzed by the magnitude and specificity of each constituent, expressed by the current state of natural landscape [2].

Landscape is a defined area in a given space, formed in time by the interaction between the physical and biotic environment, and human activity whose condition reflects the organization and development of society.

The European Landscape Convention (20.X, 2000, Florence) defined landscape as part of the territory as it is perceived by the population, whose characteristics result from the action and interaction of natural and/or anthropogenic factors.

Florin Mărăcineanu is with The Faculty of Land Improvement and Environmental Engineering, Bucharest, Romania (corresponding author to provide phone: +40-21-318-3075; e-mail: florin_maracineanu@yahoo.com);

Elena Constantin is with The Faculty of Land Improvement and Environmental Engineering, Bucharest, Romania (phone: +40-21-318-3075; e-mail: elenaema_constantin@yahoo.com);

Serban Rosulescu is with The Faculty of Land Improvement and Environmental Engineering, Bucharest, Romania (phone: +40-248-224191; fax: +40-248-213270; e-mail: serban.rosulescu@roconstructcenter.ro).

Marian Zbarcea is with The Faculty of Land Improvement and Environmental Engineering, Bucharest, Romania (phone: +40-748-238182; fax: +40-248-213270; e-mail: serban.rosulescu@roconstructcenter.ro).

ISSN-1584-5990

Towards the end of the last century, community awareness was raised following the occurrence of serious imbalance caused by the overexploitation of the environment. The solution proposed by the UN and adopted by Heads of State and Government participating in the Rio Summit Conference (1992) was to apply the concept of sustainable development as a key strategic element in the socio-economic field.

For the European countries that signed the European Convention on Landscape, the protection of this basic component of the environment is governed by the definition according to which "landscape protection and conservation measures include maintaining significant aspects or characteristics of a landscape, justified by its net asset value given by natural configuration and/or human intervention. "

The purpose of the European Convention is to include specific prospective actions aimed at highlighting, rebuilding or creating landscapes.

2. MATERIAL AND METHOD

The physical state of a landscape is subject to various degradations in scope and intensity, culminating with natural disasters. These are destructive natural phenomena, generating damage and casualties (floods, landslides, etc.) that are anthropogenically influenced by chance and whose size is likely to overcome the typical size of a complex phenomenon within a certain time length.

The areas exposed to landslide hazard are those in which the probability of sliding is high and it affects goods and population.

The typical size of a destructive landslide depends on the slide type: slow sliding is characterized by differential field trips whereas retrogressive sliding is marrked by the displacement of the sliding speed, and the kinetic energy of the moving mass.

Landslide iss the displacement of an earth mass on slopes; it occurs under favorable conditions created by the action of gravity, the combined effect of several factors that determine land mass imbalance and create a new balance of the sliding slope.

Fig.1. Tectonic diagram of the area under study

Among the causes that lead to landslides there are: changes in slope geometry, the loading volume of the slope, the production of vibration/shock, deep erosion processes, etc.

The sub-Carpathian foothills between the Buzau and Olt Rivers have similar natural characteristics which give favorable conditions for landslide production.

From the tectonic point of view, the area is distinguished by large folds, recumbent folds and diapirs edged on the external South by a non-folded area lying on the Moesian platform (Fig. 1).

The quaternary period identified deposits of Cândeşti and Pleşcoi, clay, yellow-spotted grey shale, coal and sandy shale at a depth of 200-500 m, which influences the instability of the superficial covering deposits. Therefore, the hills in the area are covered with a varied superficial deposit of low stability, except for the depression areas [2].

The superficial deposits (Fig.2) consist of deluvio-colluvial sandy-clayey and proluvial glacis deposits, associated with terrace deposits (7), aluvio-deluvial deposits on tertiary molasses, hones and sands (12), as well as piedmont deposits and a thin layer of loess deposits together with eluvio-colluvial deposits, formed on flysch (13) or coarse sandy-clayey deposits resulting from crystalline rock weathering (14).

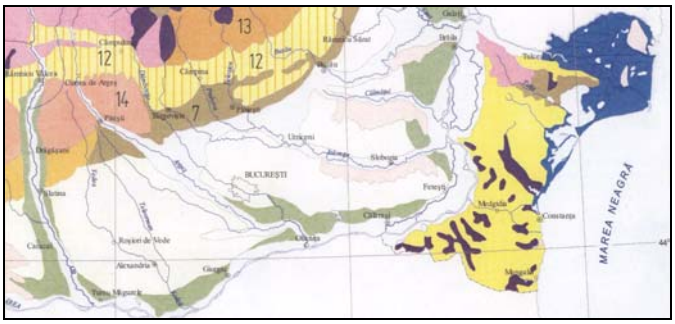

Fig.2. Superficial deposits in the area under study [3]

Limitary to these deposits are large quaternary riverine-lacustrine deposits covered with a thick loess layer (5) and even aeolian sands.

Relief energy varies between 450 – 600 m, characteristic of mediium-high mountains, and 175 – 250, characteristic of high hills, and creates favourable conditions for landslides by pronounced fragmentation resulting from the increasing erosion of the water basins (Fig.3) [3].

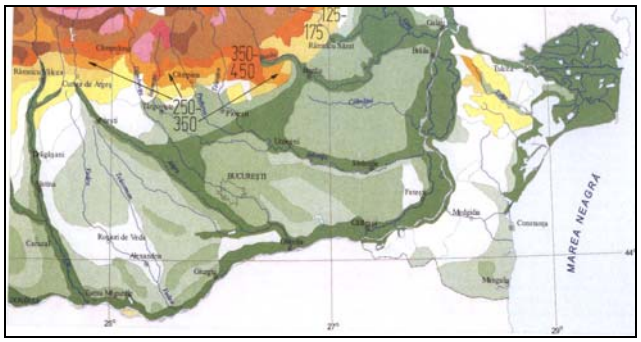

Fig.3. Relief energy of the area under study[3])

Mass transport (Fig.4) is characterized by: intense and moderate superficial landslides and surface erosion (8), deep landslides on slopes (9) and ravine formation in torrential basins (10).

Mass transport include the whole matter movement on the slopes by sliding, flowing or falling under the action of gravity [3].

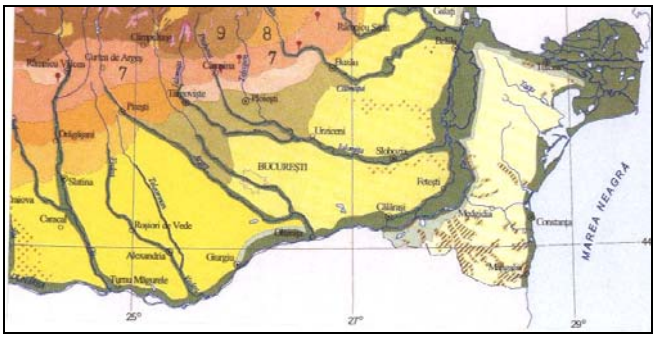

Fig.4. Mass transport processes[3]

Land stability, assessed by the effect on human settlements and various other facilities (forms of communication, aerial power lines, etc.), show that the land areas under study are inclined, rugged slopes of 8 to 30%. Land stability is reduced or relatively stable at the risk of activation in rainy years, with active ravine formation and landslides. Between them there are many relatively unstable areas with slopes exceeding 15%, exposed to a high risk of landsliding, weathering and collapse (10) Fig.5.

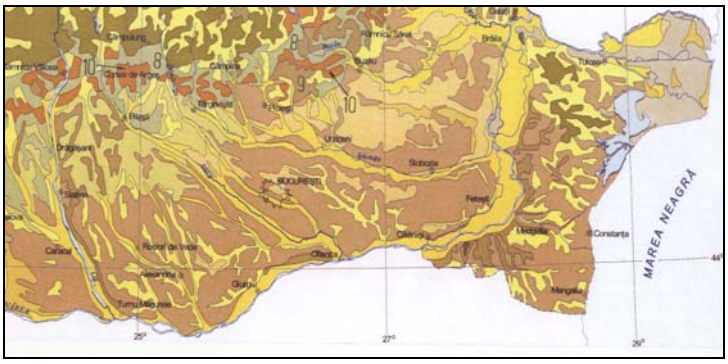

Fig.5. Land stability[3]

Geological hazards (Fig. 6) have a direct impact on the landscape and its anthropic improvement. Geological structure, relief configuration, weather, earthquakes and human activity are the main factors leading to these hazards [3].

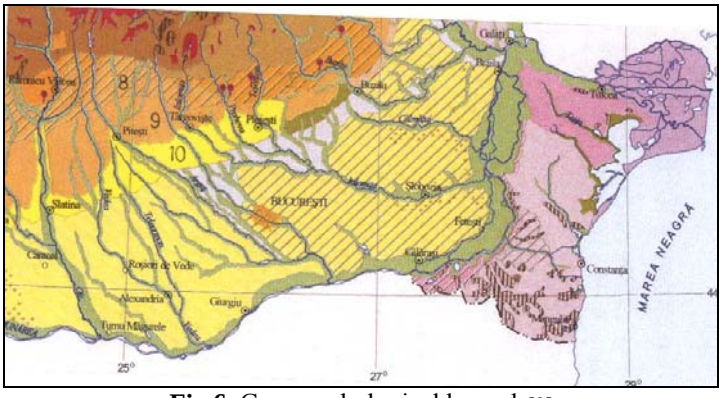

Fig.6. Geomorphological hazards[3]

In the hilly area between the Buzău and the Olt there are lands susceptible to mass displacement associated with surface erosion and intense ravine formation (8), mass displacement and moderate ravine formation (9) and torrent erosion in the valley limits (10).

3. RESULTS AND SIGNIFICANCES

Environmental degradation through erosion is particularly intense in the area under study due to the conditions of soil formation and evolution, as we mentioned before in our brief presentation. Under these circumstances, in-depth erosion records its highest intensity in the following counties: Buzău (24.4 t/ha x year), Prahova (14.4 t/ha x year) and Vâlcea (8.5 t/ha x year).

The variety and intensity of the erosion forms and intensity are favored by such human activities as overexploitation of subsoil resources, abusive forest use, irrational farming, overgrazing, etc.. If we consider that environmental favorability of a particular natural factor for a particular use or plant is expressed by the evaluation coefficient, it follows that the different types of active landslides record a minimum value: 0.5 for arable lands, 0.2 to 0.3 for vineyards, from 0.3 to 0.5 for fruit-tree plantations [1]. The evaluation coefficient indicates the favourability degree of a feature for land use.

In their natural state, such lands have no longer production resources to provide them with an economic value and, thus, turns them into disadvantaged areas of specific natural conditions. These areas consists of teritorial administrative units forming continuous surfaces with an evaluation certification under 28 and do not include individual evaluation scores beyond 30. The evaluation note illustrates the land quality for certain use, and results from the outcome of the evaluation coefficients of the indicators involved in determining it. Such lands can de found predominantly in the extreme curve of the sub-Carpathians and the Getic sub-Carpathians; these lands have high slopes and brittle rocks that favour erosion and landslides, resulting in decreased production potential and land use.

4. CONCLUSIONS

The paper leads to the following important conclusions:

- Landslides are natural processes caused by the manner in which relief was formed during the geological ages, indicating that they will also occur in the future;
- The potential areas subjected to landslide are currently changing through human intervention on lands or abusive exploitation of natural resources, either underground or above ground;
- Environmental degradation, resulting in disasters caused by landslides, should be stopped by prevention measures;
- The main measures to prevent landslides is based on mapping the potential risk areas and ceasing the activities that may destabilize the slope;
- For active landslides, it is important to collect and dispose of still waters found in the sliding surface soil mass, and to stop leakage from the adjacent areas by modelling, collecting and discharging;
- Hydraulic management of the soil mass is recommended for the use of stabilized landslides;
- The ecological reconstruction of the sliding areas should be included in sustainable development programs for the unfavoured natural areas.

5. REFERENCES

[1]. Florea N.,Balaceanu V., et al. - Soil study methods (in Romanian: Metodica elaborării studiilor pedologice). CMDPA, Bucharest,1986.
[2]. Mărăcineanu Florin et al. - Sustainable development in rural areas of Prahova county (in Romanian: Dezvoltare durabilă în spațiul rural al județului Prahova), Ceres Publishing, Bucharest, 2006.
[3]. Popescu I.D., Constantinescu S., Balteanu D., Dumitru M. – coord. – Romania. Soil quality and the electric transport network (in Romanian: Romania. Calitatea solurior şi rețeaua electrică de transport). Romanian Academy Publishing, Bucharest, 2004.

Influence on a uranium mine on macrozoobenthic communities in Luda River, Bulgaria

Teodora Stoyanova, Ivan Traykov, Ivanka Yaneva, Valentin Bogoev

***Abstract* – The aim of the study is to determine the influence of uranium mine Senokos (Pirin Mountain, Bulgaria) on Luda River, a left tributary to the Struma River. The predominant substrate on the river bed is sand and gravel. The uranium mining in the region started in 1988 and continued until 1991 as an open mine ore extraction in the upper reaches of the river. The mine was rehabilitated in the beginning of the 90's, but the lack of maintenance has led to intense surface erosion of the protective layer and washout of radioactive material. In the lower reaches, waters are diverted for irrigation, thus enhancing the negative effect of the uranium mine on the benthic invertebrates and posing a health risk for the local community. During the low water-level period, the over exploitation of the river leads to almost complete dry off of the river. The small tributaries and the hyporeal of the river act as refuge for the benthic communities at low water flows. Macrozoobenthic communities make a quick recovery with the beginning of the autumnal precipitations. The influence on the uranium mine on the water quality is assessed by the use of structural and biotic indices of the benthic communities'.**

***Keywords* – macrozoobenthos, structural and biotic indices, uranium mine, water quality**

1. INTRODUCTION

Streams and rivers are under various changes due to anthropogenic activities in their catchment areas [15]. The effects of human activities have resulted in degradation of stream and riverine ecosystem [18] which ultimately alter the structure and function of stream biota [21]. A major environmental problem relating to mining in many parts of the world is uncontrolled discharge of contaminated acid water from mines [2], [14]. Acidic drainage water contains high concentrations of heavy metals. European uranium mining and milling was mainly carried out in Bulgaria, Romania, Czech Republic,Hungary, Germany, France and Spain. Uranium minerals are always associated with more radioactive elements such as

The study was partly supported by the National Science Fund of the Ministry of Education and Science of Bulgaria within the Project DO12-131/2008 and Project BG051PO001-3.3.04/41.

Teodora Stoyanova is with University of Sofia, Faculty of Biology, Ecology and Environmental Protection, 8 Dragan Tzankov Boulevard, 1164-Sofia, Bulgaria (e-mail: stoyanova.t.l@gmail.com).

Ivan Traykov is with University of Sofia, Faculty of Biology, Ecology and Environmental Protection, 8 Dragan Tzankov Boulevard, 1164-Sofia, Bulgaria (e-mail: itraykov@biofac.uni-sofia.bg).

Ivanka Yaneva is with University of Sofia, Faculty of Biology, General and Applied Hydrobiology, 8 Dragan Tzankov Boulevard, 1164-Sofia, Bulgaria (e-mail: vanianeva@yahoo.com).

V. Bogoev is with University of Sofia, Faculty of Biology, Ecology and Environmental Protection, 8 Dragan Tzankov Boulevard, 1164-Sofia, Bulgaria (e-mail: bogoev@biofac.uni-sofia.bg).

ISSN-1584-5990

radium and radon in the ore. During the decay processes, the parent uranium-238, its decay products, and their subsequent decay products release a series of new elements and radiation, including radium and radon, alpha and beta particles, and gamma radiation. Uranium is also toxic element, being comparable with lead.

As water erodes waste rock material, those radioactively contaminated sediments can be held in suspension within the water and can enter the river or stream ecosystems. Uranium mines lead to many changes in aquatic ecosystems.

The biological response and sensitivity of different organisms to physical and chemical changes of aquatic system can be used as an indicator for the assessment of habitat quality [9]. Biological indicators may reflect the intensity of anthropogenic stress and have been used as a tool in risk assessment and evaluation of human induced changes in freshwater ecosystem [23]. Benthic macroinvertebrates have been widely used as biological indicators of river health because they play an important role in food webs [3] and they are known to be sensitive to changes in their environment and habitat characteristics [5], [10], [14], [16].

Diverse biotic indices have been used to assess the water quality in rivers [7], [8], [11]. The most widely used are those based on the benthic invertebrates [4], [13]. The qualitative and quantitative changes in the benthic communities have also been used as a tool for checking pollution.

The aim of the study is to determine the influence of uranium mine Senokos (Pirin Mountain, Bulgaria) on Luda River, a left tributary to the Struma River.

2. EXPERIMENT DESCRIPTION

Uranium mine Senokos is located in Pirin Mountain, Bulgaria in the upper reaches of Luda River. The mining started in 1988 and continued until 1991 as an open mine ore extraction. In the beginning of the 90's the mine was rehabilitated, but the lack of maintenance has led to intense surface erosion of the protective layer and washout of radioactive material toward Luda River. The river is a left tributary to the Struma River – one of the biggest rivers in Bulgaria. The predominant substrate on the river bed is sand and gravel. In the lower reaches, waters are diverted for irrigation, thus enhancing the negative effect of the uranium mine on the benthic invertebrates and posing a health risk for the local community. During the low water-level period, the over exploitation of the river leads to almost complete dry off of the river. The small tributaries and the hyporeal of the river act as refuge for the benthic communities at low water flows. Macrozoobenthic communities make a quick recovery with the beginning of the autumnal precipitation. Macrozoobenthic samples were collected from seven stations during spring and autumn of 2009 (**Fig. 1**).

Margalefs' diversity index (d) [12], Simpson dominance index (c) [19] and Shannon-Weaver diversity index (H) [20] were used to assess the influence of the uranium mine on the water quality. These indices reflect the changes in the community structure with pollution, and are used to measure stress in the environment. The richness of the community is reduced with pollution.

Biotic indices which were used in this study are Biological Monitoring Working Party (BMWP), Average Score Per Taxon (ASPT) [1] and Irish Biotic Index (IBI) [6], adapted by [22] for Bulgaria. BMWP assigns scores to different families of aquatic organisms based on their sensitivity to pollution. The greater their sensitivity towards pollution, the higher the BMWP score. This scoring system provides an excellent early warning of deteriorating water quality. ASPT represents the average tolerance score of all taxa within the community, and was calculated by dividing the BMWP by the number of families represented in the sample. From this value, the water quality was assessed. IBI places

groups of animals into five broad classes A-E, of which group A includes the most tolerant forms. Using combinations of the relative abundance of these groups the water quality is expressed as a Q value where Q1 is bad and Q5 is excellent quality.

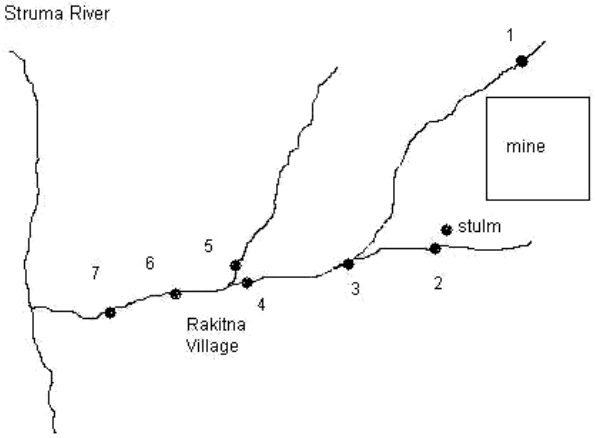

Fig. 1 Scheme of the Luda River basin with relative position of the mine and the sampling stations

3. RESULTS AND SIGNIFICANCES

Margalefs' diversity index (d) is in the range 5.8 – 12.6 (**Table 1)**. According to [17] when the water quality is good the values of this index are above 8. The low values of Simpson index (c) (0.1 – 0.6) show a lack of dominance among the groups of the benthic communities in Luda River. Shannon-Weaver diversity index (H) is in the range 1.3-3.7. At most of the stations the benthic communities are characterized with rich species diversity.

Table 1 Values of structural indices at different stations along Luda River

Sampling stations	Indices					
	d		c		H	
	spring	autumn	spring	autumn	spring	autumn
1	9.2	9.9	0.2	0.2	3.2	3.4
2	5.8	-	0.3	-	2.3	-
3	7.4	7.6	0.2	0.1	2.9	3.6
4	8.8	-	0.1	-	3.5	-
5	12.6	-	0.1	-	3.7	-
6	3.5	9.1	0.6	0.2	1.3	3.3
7	5.4	6.3	0.2	0.3	2.6	2.4

The confluence to the main river of a number of small unimpacted tributaries determines the quick recovery of the benthic communities below the mine (from station

thee to station five) (**Fig. 1**). The influence of the Rakitna Village leads to deterioration in water quality at station six. The low values of the BMWP, ASPT and IBI at station two marks the direct inflow of seepage waters from the stulm to the river (**Table 2**). The highest values of BMWP are at station one (88 during the spring and 103 during the autumn) and the lowest one at station seven (25 during the spring and 53 during the autumn). The steeper slope of the upper reaches leads to transportation and accumulation of eroded materials downstream bellow the Rakitna Village. The observed deterioration of the water quality at stations six and seven are due to the synergetic effect of the mine and the diversion of river waters for irrigation on the benthic invertebrates. During the late summer, the over exploitation of the river waters leads to almost complete dry off of the river.

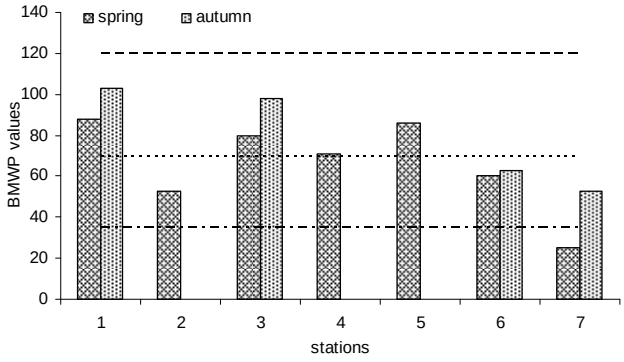

Fig. 1. BMWP values at different stations along Luda River during the spring and autumn of 2009. Horizontal lines mark the border value between water quality classes (---- between excellent to good; ····· good to moderate; -·-·- moderate to bad).

Table 2. ASPT and IBI values at different stations along Luda River.

Sampling stations	Biotic indices			
	ASPT		IBI	
	spring	autumn	spring	autumn
1	6.8	6.6	3-4	3-4
2	5.3	-	3	-
3	7.3	7	3-4	3-4
4	6.5	-	3-4	-
5	6.1	-	3-4	-
6	6.7	5.7	3-4	3-4
7	6.3	5.9	3	3

The highest values of ASPT is at station thee (7.3 during the spring and 7 during the autumn). According to IBI the water quality at stations two and seven is moderate to bad. The water quality at all other stations along the river are good to moderate.

4. CONCLUSIONS

The abandoned uranium mine Senokos continues to affect the benthic communities of Luda River. The negative negative effect of the mine is enhancined by the diversion of river waters. During the low water-level period, the over exploitation of the river leads to almost complete dry off of the river. Downstream the benthic invertebrates make a quick recovery.

5. ACKNOWLEDGMENTS

T.S. Author aknowledgees Associate Professor, PhD Ivanca Yaneva (University of Sofia, Faculty of Biology, General and Applied Hydrobiology, Bulgaria), Associate Professor, PhD Yordan Uzunov (Central Laboratory of General Ecology, Department Bio-Indication and Environmental Assessments, BASc, Bulgaria), MSc Yanca Vidinova (Institute of Zoology, Department of Hydrobiology, Bulgarian Academy of Sciences), MSc Violeta Tyufekchieva (Institute of Zoology, Department of Hydrobiology, Bulgarian Academy of Sciences), PhD Dimitar Parvanov (University of Sofia, Faculty of Biology, General and Applied Hydrobiology, Bulgaria) and MSc Lubomir Kenderov (University of Sofia, Faculty of Biology, General and Applied Hydrobiology, Bulgaria) for their help with the species determination of the macrozoobenthos.

6. REFERENCES

[1] Armitage, P. D., Moss, D., Wright, J. F. and Furse, M. T., *The performance of a new biological water quality score system based on macroinvertebrates over a wide range of unpolluted running-water sites*. 1983, Water Research vol. 17, pag 333-347.

[2] Banks, D., Younger, P.L., Arnesen, R-T., Iversen, E.R. and Banks, S.B., *Mine-water chemistry: the good, the bad and the ugly*. 1997, Environmental Geology Nr 3, vol. 32, pag 157-174.

[3] Balcombe, S. R., Bunn, S. E., McKenzie-Smith, F. J. and Davies, P. M., *Variability of fish diets between dry and flood periods in an arid zone floodplain river*. 2005, Journal of Fish Biology vol. 67, pag 1552–1567.

[4] J. Jr. Cairns and J. R. Pratt, A history of biological monitoring using benthic macroinvertebrates. New York-London: Chapman and Hall, 1993, pag 10-27.

[5] Chakona, A., Phiri, C., Magadza, C.H.D. and Brendonck, L., *The influence of habitat structure and flow permanence on macroinvertebrate assemblages in temporary rivers in northwestern Zimbabwe*. 2008, Hydrobiologia vol. 607, pag 199-209.

[6] Clabby, K. J., Bowman, J. J. Report of Irish Participants. Third Technical Seminar on Biological Water Assessment Methods, Parma, 1978.

[7] N. De Pauw and H. A. Hawkes, Biological monitoring of river water quality. UK: Aston University Publishers, 1993, pag 87-111.

[8] J. M. Hellawell, Biological indicators of freshwater pollution and environmental management. London and New York: Elsevier Applied Science, 1986, pag 546.

[9] Karr, J. R., *Biological integrity: a long-neglected aspect of water resource management*. 1991, Ecological Applications vol. 1, pag 66-84.

[10] King, J. M., Day, J. A., Hurly, P. R., Henshall-Howard, M. P. and Daives, B. R., *Macroinvertebrate communities and environment in a southern African mountain stream*. 1988, Canadian Journal of Fisheries and Aquatic Sciences vol. 45, pag 2168-2181.

[11] Knoben, R. A. E., C. Roos and M. C. M. Van Oirschot, *Biological Assessment Methods for Watercourses*. 1995, UN/ ECE Task Force on Monitoring & Assessment vol. 3, pag 86-70.

[12] Margalef, R., *Information theory in ecology*. 1958, General Systems vol. 3, pag 36-71.

[13] Metcalfe, J. L., *Biological water quality assessment of running waters based on macroinvertebrates communities: history and present status in Europe*. 1989, Environmental Pollution vol. 60, pag 101–139.

[14] Palmer, C., Palmer, A., O'Keeffe, J. and Palmer, R., *Macroinvertebrate community structure and altitudinal changes in the upper reaches of a warm temperate southern African river*.1994, Freshwater Biology vol. 32, pag 337-347.

[14] W. Pulles, S. Banister and M. Van Biljon, The development of appropriate procedures towards and after closure of underground gold mines from a water management perspective. Report No. 1215/1/05. Water Research Commission, Pretoria, 2005.

[15] Qadir, A. and Malik, A. R., *Assessment of an index of biological integrity (IBI) to quantify the quality of two tributaries of river Chenab, Sialkot, Pakistan*. 2009, Hydrobiologia vol. 62, pag 127–153.

[16] D. M. Rosenberg, and V. H. Resh, Freshwater monitoring and benthic macroinvertebrates. New York: Chapman and Hall Publishers, 1993.

[17] B. Russev, Fundamentals of saprobiology. Sofia: University Publisher "Kliment Ochridski, 1993, pag 1-161.

[18] Schleiger, S. L., *Use of an index of biotic integrity to detect effects of land uses on stream fish communities in west-central Georgia*. 2000, Transactions of the American Fisheries Society vol. 129, pag 1118–1133.

[19] Simpson, E. H., *Measurement of diversity*. 1949, Nature 163:688.

[20] C. E. Shannon and W. Weaver, The mathematical theory of communication. Urbana: University Illinois Press, 1963.

[21] J. L., Stoddard, D. P., Larsen, C. P., Hawkins, R. K., Johnson and R. H., Norris. (4 April 2007). Setting Expectations for the Ecological Condition of Streams: The Concept of Reference Condition. [Online]. Available: http://watersheds.montana.edu/mwcc/workgroups/docs/Stoddard%20et%20al%20reference%20 condition%20final.pdf].

[22] Uzunov, Y., Penev, L., Kovachev, S. and Baev, P., *Bulgarian Biotic Index (BGBI) - An express method for bioassessment of the quality of running waters.* 1998, Comptes Rendus de Bulgarian Academy of Sciences Nr. 11/12, vol. 51, pag 117-120.

[23] Toham, A. K. G. and Teugels, G., *First data on an index of biotic integrity (IBI) based on fish assemblages for the assessment of the impact of deforestation in a tropical west African river system*. 1999, Hydrobiologia vol. 397, pag 29-38.

Modelling Traffic-Induced Air Pollution in Cluj-Napoca

Cristian TOSA, Mihai ILIESCU

Abstract – **Urban traffic pollution represents a potential risk factor for everyone because of the negative influence on human health and the environment. The quantity of pollutants released in the urban atmosphere because of the traffic can be quantified with classical methods or using mathematical models for dispersion of pollutants. This is possible by taking into consideration geographical conformation of the area, pollution sources, meteorological conditions as well as possible obstacles on the pollutant's plume propagation path. We conducted a traffic study in which we modelled the emissions from traffic during rush hours in a high traffic location in Cluj Napoca City using Caline4 atmospheric pollutant dispersion model. We obtained CO concentrations in different spots with considerable pedestrian concentration and compared them with the limit values admitted by the regulations.**

Keywords – **atmospheric pollution modelling, Caline4, dispersion model, pollutant limit values, traffic study.**

1. INTRODUCTION

Activities due to urban traffic are the main source of pollution that causes serious damages to human health [1]. The activities in the urban environmental represent sources of pollution to all natural and anthropic factors, so they must be measured and controlled in a way that environmental impact and effects on human health are within the limits admitted by the legislation [2]. Natural factors like air, water, soil, flora, fauna, still suffer important qualitative and quantitative changes under the impact of human activity.

Traffic-related emissions are a complex mix of pollutants consisting of nitrogen oxides (including nitrogen dioxide), particulate matter, carbon monoxide, sulphur dioxide, volatile organic compounds, ozone, and many other chemicals such as trace toxics and greenhouse gases [3]. The concentration of pollutants varies both spatially and temporally. Studies conducted during recent years concluded that road transport is the main cause for releasing into the atmosphere of 6% of SO2 emissions, 69% of NOx emissions, 64% of the CO, 49% of the VOC (volatile organic compounds) and 33% of total emissions of particulate matter [2].

In Cluj-Napoca the pollution problem is of growing importance given the escalating number of vehicle dynamics, but also increased levels of emissions due to the large number of old cars. For instance in 2008 in Cluj Napoca City there were 104,200 vehicles, while county's total number of cars exceeds 190,000.

Cristian TOSA. Author is with Civil Engineering Faculty, Technical University of Cluj-Napoca, Memorandumului 28, 400114, Cluj-Napoca, Romania (e-mail: cristitosa@gmail.com). Financial support from SIDOC Project within AMPOSDRU Program is gratefully ackowledged.

Mihai ILIESCU. Author is with Civil Engineering Faculty, Technical University of Cluj-Napoca, Memorandumului 28, 400114, Cluj-Napoca, Romania; e-mail: Mihai.Iliescu@cfdp.utcluj.ro).

ISSN-1584-5990

In this paper, we present a model of street pollution at the intersection of main traffic arteries in the city of Cluj Napoca. The reason we chose this area is related to outstanding traffic intensity. The presence of the monitoring station of the National Environmental Agency CLJ-1 in the modelled area is important as we can calibrate the results of the calculations against hourly measured values of the pollutant. Moreover, Caline4 model that we used to estimate pollution is adapted to the configuration of the area.

The structure of this paper is the following: Section 2 presents evidence of transport and dispersion of pollutants in the atmosphere as well as some of the mathematical models used for assessing the phenomena, in particular Caline4, which is devoted to the evaluation of carbon monoxide impact and human exposure. Section 3 describes the modelling over the traffic area in which we conducted the pollution study as well as the results, and last section presents conclusions on the study and some considerations on the feasibility of extending the model for larger areas in Cluj-Napoca.

2. TRANSPORT AND DISPERSION OF POLLUTANTS

The phenomena of transport and dispersion of pollutants includes four stages: accumulation, convection (advection), diffusion, physical changes (including dry and wet deposition), chemical and biochemical transformation (between pollutants and between pollutants and the environment). Substances emitted because of urban traffic are carried out by wind, mixed in the atmosphere by the turbulences phenomena and deposed on Earth's surface due to gravitational sedimentation or by heavy rainfall. Emission parameters such as geographical position and altitude of the emitting source, the output speed of the pollutant, its temperature and output flow, all enter the final calculation, regardless the dispersion model used.

In the process of atmospheric diffusion, the meteorological factors taken into consideration are the wind, vertical structure of temperature, moisture and precipitation. Turbulence is actually responsible for the dispersion of pollutants in space around average directions of propagation. All factors that generate a good turbulence in the air contribute to the decreasing of impacts on the environment, mixing the pollutants into the atmosphere. Recently, special attention is devoted to the study of dispersion of pollutants emitted into the atmosphere, because of their effects on the human health and the environment.

One of the cheapest ways to assess the air pollution is mathematical modeling. Mathematical modeling of dispersion of pollutants in the atmosphere is used to estimate concentrations of pollutants at ground level and at certain height depending on the characteristics of pollution sources, meteorological and topographical conditions, the physical and chemical transformation processes that may be pollutants in the atmosphere and their behaviour at interaction with soil.

Dispersion models require a large amount of input data, such as:

- Weather conditions: wind speed and direction, atmospheric stability class, ambient temperature and its vertical variation;
- Emission parameters: the height and location of emission source, size and shape of the source, temperature, flow rate and exhaust emissions;
- Field emission configuration and receptor position;
- Physical obstacles location and configuration downwind pollution source.

The models for the assessment of pollution from transport activities use mostly as sources of pollution linear segments. They must also take into account traffic volume and structure, speed and composition of emissions, and meteorologic conditions. It is often

recommended to consider worst case weather conditions when computing concentrations of air pollutants [6].

In the category of most affected traffic areas with high concentration of air pollutants we can mention: nodal points near major intersections, traffic delay zones around pedestrian crossings or urban transport stations, urban highways and street canyons.

There are several comercial pollution dispersion modelling software on the market. These are ADMS3, developed by Cambridge Environmental Research Consultants of the UK, AERMOD, developed by the American Meteorological Society and the United States Environmental Protection Agency [15], OSPM, developed by the National Environmental Research Institute in Denmark [16].

The software we used in this study is CALINE4, which stands for CAlifornia LINE Source Dispersion Model, version 4. This is the standard modeling program used by Caltrans to assess carbon monoxide impacts near transportation facilities. The purpose of this program is to prevent human exposure to excessive concentrations of CO. Caline4 uses a Gaussian type computational model and requires a linear source of pollution emission. The user defines the street geometry, weather conditions, anticipated traffic volume and position of receptor where the pollution concentration is calculated [6]. The user can also specify the type of roads as intersections, parking spaces, low or elevated (compared to a reference level), or street canyons. Caline4 is based on a graphical user interface, designed to facilitate data entry. The output is displayed in a text file and can be used for interpretation using other applications.

3. TRAFFIC STUDY AND MODELLING

In the following we will describe the street configuration where we conducted the evaluation of traffic emitted carbon monoxide. The giratory lane is located at the intersection of main traffic arteries that cross the city of Cluj Napoca from the west to the east side. The mean number of vehicles per day that cross this area exceeds 10.000. For this reason, traffic related emissions, such as PM_{10} reaches attention values [5]. The National Environmental Agency placed 4 different monitoring stations in different hot spots of the city, for measuring urban polutants resulting from human activities. In this study we used the data measured and registered by one of these stations, CLJ-1, placed nearby the traffic study area. CLJ-1 is a traffic-type measurement station located at street level, at the altitude of 349 meters above sea-level. It measures the mean hourly concentration of several pollutants every hour, at the height of three meters above ground level. The population around the measuring station's area is between 1500 and 2000 persons [5].

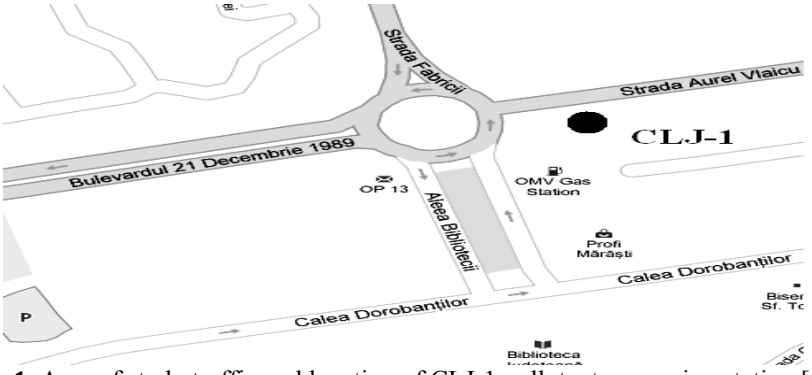

Fig. 1. Area of study traffic and location of CLJ-1 pollutant measuring station [13]

We conducted a traffic study on the streets that intersect the giatory lane in the Piața Mărăști Square, as seen in Fig. 1. The measurement were performed on March 25, 2010, between 7^{30} and 9^{30} a.m., when we considered the maximum number of vehicles, The total number of vehicles passing on the streets surrounding the measuring station during one-hour survey were transformed into passenger car equivalents, using [7]. The reason for which we choose this time interval is beacause of the high concentrations of carbon monoxide emissions from traffic registered by the measuring station, as seen in Fig. 2 [5].

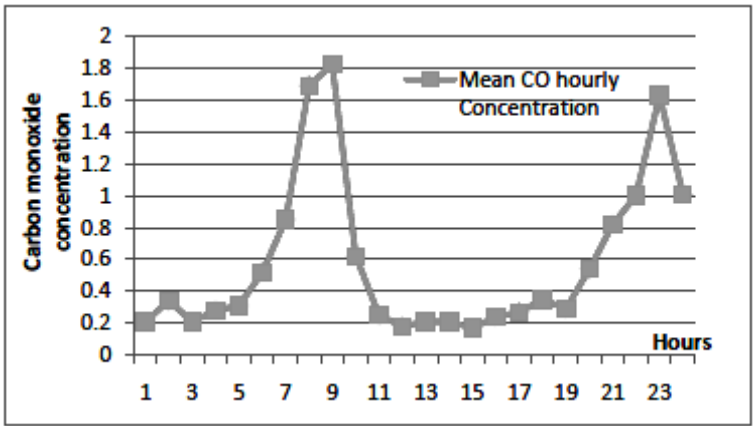

Fig. 2. CO hourly mean concentration (ppm) as measured by CLJ-1 monitoring station on March 25th, 2010

Figure 3 shows the symplified scheme of the streets intersecting the giratory lane and was introduced with cartesian coodinates in the Caline4 pollution modelling programme. The position of the receptor where we obtain the pollutant concentration is also characterized by chartesian coordinates and height, with respect to the surface of the streets where the traffic is carried on. Having the links geometry, the next step in realizing complete input data was link activity, which consists of the characteristic traffic volume and emission factors for each link. Emission factors represent total amount of pollutants emitted by the passenger vehicle over a distance of one kilometer. The mean emission value of carbon monoxide taken into consideration was 7.5 g/km [10].

The Caline4 software requires run conditions in order to return the correct results of the modelling. Run conditions refer to wind speed, wind direction and its standard deviation, atmospheric stability class, mixing height, ambient temperature and ambient pollutant concentration, often reffered as background pollutant concentration.

According to [8], the weather conditions on the 25th of March 2010, between 7^{30} and 9^{30} a.m. were as it follows:

- Wind direction: SW;
- Wind speed: approx. 0.55 m/s;
- Air temperature on site: 13° C.

Pasquill & Gifford (1961) atmospheric stability classes are used for calculating the dispersion parameters. Taking into consideration the small wind speed, atmospheric stability class 2 is used in the calculation of dispersion parameters [12].

The mixing height, the depth of the surface mixed layer is the height of the atmosphere above the ground, which is well mixed due either to mechanical turbulence or

convective turbulence [11]. We considered the value of the mixing height 100 meters, given the stable atmospheric conditions.

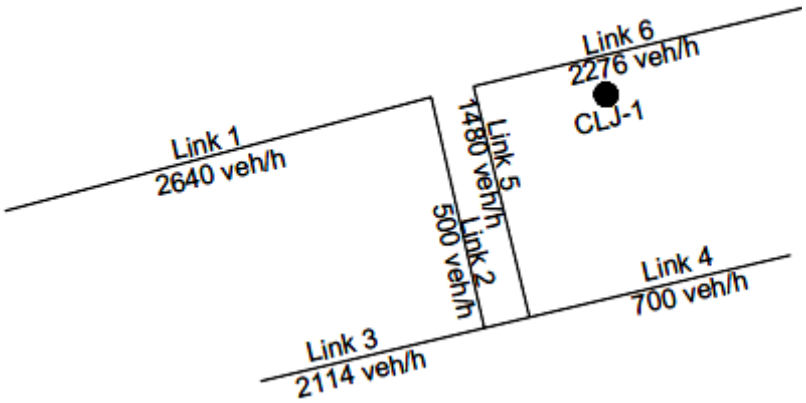

Fig. 3. Symplified scheme of main roads nearby monitoring station CLJ-1. The measured traffic activity transformed in passenger car equivalents is also shown.

Background ambient air pollutant concentration represents the concentration of the carbon monoxide in the air brought by the wind from other polluted areas of the city. In this study we considered the background air pollution with carbon monoxide, the concentration of the pollutant at early hour in the morning, before the beginning of the big traffic activity. The value of the ambient air pollutant concentration, according to [5], estimated value was arond 0.3ppm.

Caline4 gives the user an option for defining the aerodynamic roughness coefficient, that represents an uneven flow of air caused by irregularities in the surface over which the flow takes place, which is different depending on the urban topography. The value used for input was around 400 cm, which corresponds to central bussiness district, according to Caline4 predefined aerodynamic roughness coefficients.

Taking into consideration the stability class of the atmosphere and the small wind speed, we used an option of Caline4 that computes the data taking into consideration the worst-case wind angle with respect to the street geometry, in order to obtain maximum concentration from all possible variations of wind direction.

4. RESULTS AND CONCLUSIONS

Using the input data as described in the previous section, we obtained the carbon monoxide concentration at the receptor position, corresponding to the measurement station sensor. The concentration value of CO at 8_{00} a.m., as reported by CLJ-1 monitoring station was 1.69 mg/m_3. One can observe that this value is below limit values admitted by the regulations, which is 10 mg/m_3 [14]. The measured value is an average over one hour time interval. Caline4 returned a computed concentration of carbon monoxide of 1.30 ppm. We can transform this value into mg/m_3, by taking in consideration air temperature, atmospheric pressure and mollecular mass of the air, yielding 1.56 mg/m_3. One can notice a good agreement between the observed (measured) and predicted (calculated) values of the concentration of carbon monoxide resulted from traffic. The reason for the smaller value

obtained by calculation may be attributed both to cumulative effects and to the presesnce of additional sources of pollution due to human activity.

By modelling various configurations, we observed the dependence of the calculated CO concentration not only on known or measured parameters like wind speed, air temperature and pressure or traffic volume, but also on less determined parameters like vehicle composition, vehicle emission rates, atmospheric stability class or aerodynamic roughness coefficient. Given the result obtained, we conclude that the present modeling can be improved and extended to larger areas. A realistic modelling is possible and the amount of different air pollutants resulting from urban traffic activity might be predicted using well developed software and reliable field data. Obviously, having information about the terrain and buildings configuration, as well as a better knowledge on fleet composition may improve the quality of the prediction in order to estimate the impact of the pollutants in different hypothetical future scenarios.

Predicting pollutant concentrations in the urban environment can, and must be used further for estimating the human exposure. Values of the pollutant concentrations can be obtained after an appropriate traffic study and prediction in different locations of the city, where measuring or monitoruing of air quality might be quite expensive and difficult for the local authorities. Therefore, modelling of air quality is a valuable future instrument in urban and territorial planning.

5. REFERENCES

[1] Faiz, A., 1993. Automotive emissions in developing countries—relative implications for global warming, acidification and urban air quality. Transportation Research A 27, 167–186.

[2] Ardelean F., Poluarea atmosferei in mediul urban, Teză de doctorat, Universitatea Tehnică de Construcţii Bucureşti (2005).

[3] M. Campbell, K. Bassil, C. Morgan, M. Lalani, R. Macfarlane and M. Bienefeld, Air Pollution Burden of Illness from Traffic in Toronto – Problems and Solutions, Toronto Public Health Canada (2007).

4] Program Integrat de Gestionare a Calităţii Aerului în Judeţul Cluj pentru indicatorii PM_{10} şi NO_2 (2008);

[5] Agenţia Naţională pentru Protecţia Mediului - Reţeaua naţională de monitorizare a calităţii aerului.

[6] Coe L. D., Eisinger S. D., Prouty D. J., Kear T., User's Guide for CL4: a user-friendly Interface for the Caline 4 Model for Transportation project Impact Assessments, Sacramento, CA, 1998;Michael D. Meyer, Eric J. Miller, Urban Transportation Planning, Second Edition, McGrawHill (2001).

[7] SR 7348/2001 Lucrări de drumuri - Echivalarea vehiculelor pentru determinarea capacităţii de circulaţie.

[8] http://www.wundergorund.com.

[9] http://www.openstreetmap.com.

[10] A. Ghenu, J.-M. Rosant, J.-F. Sini, Dispersion of pollutant and estimation in a street canyon in Rouen, France, Environmental Modelling and Software 23 (2008), 314-321.

[12] Anjaneyulu M.V.L.R., Harikrishna M., Chenchuobulu S., Modeling Ambient Carbon Monoxide Pollutant Due to Road Traffic, World Academy of Science, Engineering and Technology 17 2006.

[13] www.maps.google.com.

[14] Agenţia Pentru Protecţia Mediului, Raport privind starea factorilor de mediu din judeţul Cluj, 2009.

[15] http://en.wikipedia.org/wiki/Atmospheric_dispersion_modeling.

[16] http://www.dmu.dk/International/Air/Models/OSPM.

SECTION IV

HYDRAULIC: THEORY AND APPLICATIONS

Post Darcy filtration through rigid permeable media and real situations in engineering practice

Bartha Iosif, Marcoie Nicolae

Abstract – **The paper presents post-Darcy's flow corresponding weak and strong inertia, transition and turbulent flow of the movement in permeable media.**

There are pointed out practical situation where these flow happened and their solving possibilities.

There are analised flows under pressure and with free surface.

***Keywords* – flow through permeable media, flow parameters, post-Darcy law.**

1. INTRODUCTION

In 1856, Ph. Darcy discovered that, for a monophasic flow through a porous media at small Reynolds numbers, the apparent velocity V_0 is directly proportional to the pressure gradient $\nabla p = \frac{dp}{dl}$ and inversely proportional with dynamic viscosity coefficient, the factor of proportionality being the permeability coefficient k_p.

$$\nabla p = \frac{-k_p}{\mu} \cdot V_0 \tag{1}$$

After the relevant experiments of Reynolds over flow's nature (1883) and its nonlinear effects on the flow have shown that also in filtrations the major parameter is not the apparent velocity of filtration, but Reynolds number, which this depends of it. The Reynolds number is the relative measure of viscous and inertial forces.

In the year of 1901, the determined deviation of superficial velocity of filtration from Darcy's law, at larger Reynolds numbers at filters (lower velocity than the ones defined by Darcy) leaded to redefinition of superficial velocity of filtration by Forchheimer [1, 2], in power form,

$$\nabla p = -c_1 \cdot V_0^{c_2} \tag{2}$$

or approximated by a polynomial of 2nd or 3rd order:

$$\nabla p = aV_0 + bV_0^2 \tag{3}$$

and

$$\nabla p = aV_0 + bV_0^2 + cV_0^3 \tag{4}$$

The filtration at upper velocities than Darcy's domain has theoretically and practice importance to fuel extraction (fluids or gases), to hydraulics of rivers with different

Bartha I. is with Technical University "Gheorghe Asachi" of Iasi, Bd. D. Mangeron nr. 67, 700050-Iasi, Romania (corresponding author to provide phone/fax: +40-232-270690; e-mail: ibartha@tuiasi.ro).

Marcoie N. is with Technical University "Gheorghe Asachi" of Iasi, Bd. D. Mangeron nr. 67, 700050-Iasi, Romania (corresponding author to provide phone: 0721572995; e-mail: nmarcoie@yahoo.com).

ISSN-1584-5990 ©

permeability beds, flow on permeable surfaces (could be considered such as surfaces: dense urban areas, dense vegetative areas). The results of these studies are useful to pollution dispersion in urban areas, oxygen exchange and carbon dioxide in forests and crop lands, forest firestorm propagation [14]. The theory of permeable walls is applicable to snow layers, and by analogy, to heat exchangers. This theory is successfully applied to medicine at circulatory and breathing systems.

Many inadvertences have explanation by study of post-Darcy filtration at underground water capture near wells and drains and in filters itself [3, 5, 7, 8]. By post-Darcy filtration it could be found an answer to flow through drain mattres, river side rock fill mattres, water flow in gravels, permeable rock fill embankments, rock fill culverts, rock fill dams etc. [12, 13, 17, 18, 21].

The study of post-Darcy filtration flow in porous material without forced fixed laying has application in solid fluidisation in hydro transport.

2. DARCY AND POST-DARCY FLOW

The isotherm flow through porous media of incompressible fluids is governed by Navier-Stokes and mass equations:

$$\frac{\partial V}{\partial t}+(V\nabla)V=-\frac{1}{\rho}\nabla p+\nu\nabla^2 V+g+\frac{1}{\rho}F \tag{5}$$

$$\nabla\cdot V=0 \tag{6}$$

where: $X=[x,y,z]^T$ is position, t – time, $V(x,t)=[V_x(x,t),V_y(y,t),V_z(z,t)]$ - velocity, $p(x,t)$ - pressure, ρ – density, g – gravity acceleration, μ – dynamic viscosity coefficient, $\upsilon=\mu/\rho$ - kinematic viscosity coefficient.

The above equations describes temporal changing of velocity fields due to inertia, pressure, viscous and gravity forces, also, other external forces could contribute to movement (in gravity field $F = 0$). Equations (5) and (6) together with boundary conditions forms the four partial differential nonlinear equations with four unknowns: $V(x,t)$ and $p(x,t)$.

The dimensionless parameters are (with zero indexes in specific flow scale):

$$\mathrm{Re}=\frac{V_0 L_0}{\upsilon} \tag{7}$$

and Froude number:

$$Fr=\frac{V_0^2}{L_0 g} \tag{8}$$

These parameters are the relative measure of inertia and viscous forces, inertia and gravity, respectively. These forces it highlights in (5) and (6) through introduction of dimensionless parameters: $\overline{V}=\frac{V}{V_0}$; $\overline{x}=\frac{x}{x_0}$; $\overline{t}=\frac{tV_0}{L_0}$; $\overline{p}=\frac{p}{\rho V_0^2}$, so

$$\frac{\partial\overline{V}}{\partial t}+(\overline{V}\cdot\nabla)\overline{V}=-\overline{\nabla}\overline{P}+\frac{1}{\mathrm{Re}}\overline{\nabla}^2\overline{V}+\frac{1}{Fr} \tag{5'}$$

$$\overline{\nabla}\cdot\overline{V}=0 \tag{6'}$$

The decrease of Reynolds number, imply the growth in movement of a viscous forces effects. The growth of Froude number, imply the decrease of gravity forces effects.

Usually, the flow through porous media occurs under difference in pressure on macroscopic length $\Delta p / L$, L being macroscopic scale of the length and corresponds to the porous material thickness. The analyse of the Stokes equation which govern the liquid flow through free spaces of granular material defines the velocity scale: $V = \frac{d^2 \Delta p}{\mu L}$, where d is measure of solid particles, of the cavity between these respectively, and is the microscopic scale of the length, μ being the dynamic viscosity.

The microscopic Reynolds number (or local) is defining by:

$$\mathrm{Re}_d = \frac{\Delta p \cdot d_p^3 \cdot \rho}{L \mu^2} \tag{7'}$$

and by this number and by the geometric parameters of the porous media depends the hydraulic gradient. The deviation of the hydraulic gradient by the Darcy's law, determined by Fochheimer, leads to zone of the flow on domains, but even now there are no an adequate answer unanimous accepted.

By principal of experimental measurements, the flow is zoned in representation of the pressure gradients relative to the local velocity averaged function of Reynolds number, thus: 1. Darcy domain - $\mathrm{Re}_d \in (0,1)$; 2. weak inertia domain - $\mathrm{Re}_d \in (1,4.3)$; 3. Forchheimer domain (strong inertia) - $\mathrm{Re}_d \in (4.3,180)$; 4. transition to turbulence - $\mathrm{Re}_d \in (180,900)$; 5. fully developement turbulence - $\mathrm{Re}_d \in (900,10000)$. Sometimes the domains 1 and 2 are considered to be the creeping flow domain, the domains 1, 2 and 3 the domain of laminar regime, the 3rd domain laminar nonlinear regime, **Fig. 1.**

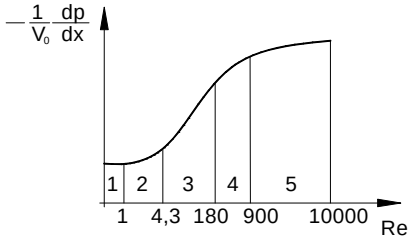

Fig. 1. The domains of flow through porous media

3. FLOW MODELS THROUGH POROUS PERMEABLE MEDIA

The dissipation of mechanical energy of the fluids into the flow through porous permeable media has technical significant importance in many engineering fields. Along over 150 years by study of filtration, there are developed flow models which could be grouped in five categories: phenomenological models, geometrical (based on the flow into the pipes) models, statistical models, models based on Navier-Stokes equations, flow around solid objects models. The purpose of these studies is to establish the flow parameters. All the models contain the unknown parameters which must be determined experimentally. The majority of the experiments measure the decrease of pressure function by the fluid velocity which flows through different materials with known thickness [3, 4, 5, 6, 9, 10, 11, 14, 15]. For a relatively large range of the Reynolds numbers, which includes all flow domain, it is frequently utilised transformed form of (3):

$$\frac{\Delta p}{LV_0} = M^* V_0 + N^* \tag{9}$$

where $\frac{\Delta p}{L}$ is pressure gradient, V_0 – superficial velocity of filtration, L – thickness of permeable material (experimentally measured), M^* and N^* - coefficients of the line regression statistically calculated. The pressure loss depends, besides these factors, by fluids physical properties: by density - ρ, viscosity - μ, geometric properties of porous media, particles diameter – d_p and by the porosity – n. For uniform spherical particles, d_p is even itself diameter, and for non-spherical particles:

$$d_p = \frac{6}{A_s} \tag{10}$$

where A_s is the static specific surface of particles.

The pressure loss at flow through porous media depends by the solid-liquid contact area which could be at most static, but usually is lower than static and it is named active or dynamic specific area - A_d. Also the pressure loss depends by the contact surface roughness and by the flow regime. The flow regime through pores is characterised by microscopic Reynolds number, by the form:

$$\mathrm{Re}_{dp} = \frac{\rho V_0 d_p}{\mu} \tag{7"}$$

At experiments it must be controlled the water temperature which influences the viscosity and density, also the velocity and pressure loss measurement's errors, as well as the porosity. The geometric stability of the porous materials is also an imposed condition of the experiments.

4. THE GEOMETRIC MODEL OF FLOW INTO THIN TUBES

It is supposed that the permeable material pores are forms by a bundle of m tortuous tubes with diameter - d and length – L' having the totally surface – A. The filter column has the total apparent volume – W, with diameter – D and total length – L [10, 11, 14, 15]. The pathline of current are upper than the column length with permeable material, its describe curves trajectory between solid particles.

It is define the tortuosity τ such as the ratio:

$$\tau = \frac{L'}{L} \tag{11}$$

The fictive diameter of the model tubes results from equality between pores volume and tubes volume:

$$d = \frac{4W_p}{A} = \frac{4n}{A_d(1-n)} \tag{12}$$

where $A_d = \frac{\text{average surface of the particle}}{\text{particle volume}} = \frac{\text{totaly surface of the particle}}{\text{solid totaly volume}}$.

Considering that the geometric (static) surface of the particles could be partially overlapped,

$$\frac{A_d}{A_s} = AB \le 1 \tag{13}$$

(in case of spherical particles $AB \to 1$).

The velocity in fictive tubular pores thus becomes:

$$V = \frac{V_0 L'}{nL} = \frac{V_0 \tau}{n} \tag{14}$$

Tortuosity's value of homogenous spherical particles rhombohedral layout is theoretically in range of τ =1.02 (for n = 0.46) to τ = 1.22 (for n= 0.26), but as porosity and tortuosity could vary in larger limits.

The head loss at small Reynolds numbers which includes creeping flow (Darcy type) and weak and strong inertia (Forchheimer zone) could be considered as a sum of two terms:

- first term, proportionally to the velocity, due to viscous resistance at solid walls;
- the second one, proportionally with the square velocity, due to inertial resistances, kinematic energy loses at direction changes of the current lines.

$$h_r = \frac{\Delta p}{\gamma} = \left(\frac{64}{\mathrm{Re}_p} + \lambda_t \right) \frac{L'}{d} \frac{V^2}{2g} \tag{15}$$

where Re_p is number Reynolds of the fictive tortuous tubes with length L', calculated at diameter d, λ_t – turbulent Darcy-Weisbach's coefficient.

The general form accepted for λ is:

$$\lambda = \frac{\alpha}{\mathrm{Re}} + \beta \tag{16}$$

with α = 64 and β = 0.7743 (in literature often are utilised notion of friction factor $f = \lambda/4$).

The viscous resistance's term it is calculated from Poiseuille equation:

$$\frac{(\Delta p')}{L'} = \frac{8\mu}{r_0^2} V \tag{17}$$

which, for macroscopic permeable material's thickness – L, with porosity – n, tortuosity - τ, specific surface exposed to friction A_d, related to apparent velocity, becomes:

$$\frac{(\Delta p)'}{L} = \frac{2\mu\tau^2 (1-n)^2 A_d^2}{n^3} V_0 \tag{18}$$

The terms corresponding to loss of kinematic energy (inertia) it could be calculate as for very rough pipes due to many direction's changes of the current lines.

$$\frac{\Delta p}{\gamma} = \lambda \frac{l'}{d} \frac{V^2}{2g} \tag{19}$$

After Himbert (1965), Peach (1984), Comiti (1988), the fictive tortuous tubes it is assumed such as very roughness tubes, for which the equivalent roughness is $k_e = d$, and the λ coefficient is calculated after Nikuradze:

$$\frac{1}{\sqrt{\lambda}} = 2 \lg \frac{3.7d}{k_e} \tag{20}$$

λ = 0.7743 or f = 0.0968.

Replacing in (19) it is obtain

$$\frac{(\Delta p)''}{L} = 0.0968 \frac{\rho \tau^3 (1-n) A_d}{n^3} V_0^2 \tag{21}$$

Combining (18) and (19), taking into account by (15) results:

$$\frac{(\Delta p)}{L} = \frac{(\Delta p)' + (\Delta p)''}{L} = \frac{2\mu \tau^2 (1-n)^2 A_d^2}{n^3} V_0 + 0.0968 \frac{\rho \tau^3 (1-n) A_d}{n^3} V_0^2 \tag{22}$$

which has the Forchheimer equation's form (3).

These above presented does not solute the Darcy and post-Darcy's type flow, but combined with experiments permits a unification of the study. The experimental studies at macroscopic scale aims the determination of pressure loss Δp on the thickness permeable material L at different superficial velocities V_0 of the flow. Equation (22) under form:

$$\frac{(\Delta p)}{L V_0} = \frac{2\mu \tau^2 (1-n)^2 A_d^2}{n^3} + 0.0968 \frac{\rho \tau^3 (1-n) A_d}{n^3} V_0 \tag{23}$$

is by form (9) for which, by statistical methods has been calculate M^* and N^*, having relations:

$$M^* = 0.0968 \frac{\rho \tau^3 (1-n) A_d}{n^3} \tag{24}$$

and

$$N^* = \frac{2\mu \tau^2 (1-n)^2 A_d^2}{n^3} \tag{25}$$

From (24) and (25), having established n and μ, results the characteristics of porous media after this model: tortuosity - τ and dynamic specific surface – A_d.

The generalisation is done by possibility's calculus of λ coefficient function of pore's Reynolds number Re_p.

$$\lambda = \frac{(\Delta p)}{L} \frac{n^3}{2\rho \tau^3 (1-n) A_d V_0^2} \tag{26}$$

$$\mathrm{Re}_p = \frac{\rho \tau V_0}{\mu (1-n) A_d} \tag{27}$$

The pressure gradient it could be written as:

$$\frac{(\Delta p)}{L} = \frac{\mu^2 (1-n)^2 A_d^3 \tau}{2\rho n^3} \left(\mathrm{Re}_p + 0.0121 \mathrm{Re}_p^2 \right) \tag{28}$$

When the experiments are done in infiltrometers with diameter D, for roughness it could consider the wall effect of the infiltrometers. The layout of the first layer of the particles, differ by the rest of the core and the infiltrometer's wall must be added to surface of contact between solid and liquid. At infiltrometer's wall the curvature of current lines is lower than the rest and it could be considered the equivalent roughness $k_e = d/2$. The factor $\lambda_{wall} = 0.1652$ resulted for the wall's infiltrometer together with the model's tubes is averaged at surface for kinematic energy loss, resulting:

$$M = \left\{ \left[1 - 0.00413 \left(1 - \frac{d_p}{D} \right)^2 \right] + 0.0968 \left(1 - \frac{d_p}{D} \right)^2 \right\} \frac{\rho \tau^3 (1-n) A_d}{n^3} \tag{29}$$

$$N = \left[1 + \frac{4}{A_d D(1-n)}\right]^2 \frac{2\mu\tau^2(1-n)^2 A_d^2}{n^3} \tag{30}$$

The proportion of inertial contribution of viscous friction q and of inertia P to energy losses relative to flow through impermeable materials, function of pore's Reynolds number correspond to **Fig. 2.**

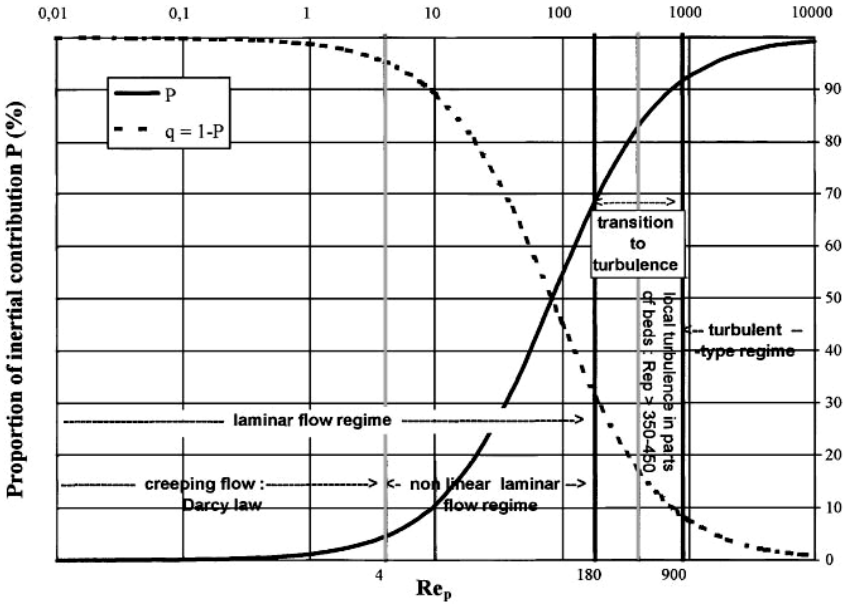

Fig. 2. Newtonian fluid flow regime transitions in packed beds [10]

The limit of Darcy's flow in engineering purpose is accepted $\lim \mathrm{Re}_{\mathrm{p}\,5\%}^{\mathrm{Darcy}} = 4.3$ with inertial losses P = 5 %, and, more accurate, for P = 1 % - $\lim \mathrm{Re}_{\mathrm{p}\,1\%}^{\mathrm{Darcy}} = 0.89$. The upper limit of strong inertia domain (Forchheimer) is $\lim \mathrm{Re}_{\mathrm{p}}^{\mathrm{Forch}} = 180$ with inertial losses P~67%.

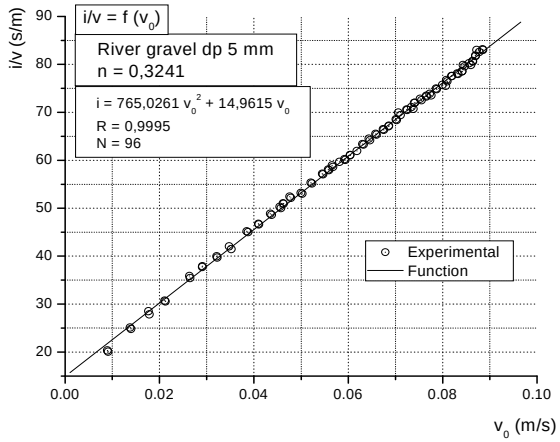

Fig. 3. Example of experimental results eq. (23) [20]

The experiments on the microscopic scale aims to establish the velocity field in pores using different technics: microtransducers with frequency 6000 Hz, velocimetry based on particle incurge velocimetry (PTV), particle tracking velocimetry (PVT), tracer velocimetry [21].

In **Fig. 3. 4**. and **5**. is exemplified the calibration way in base of experimental macroscopic measurements (in infiltrometer) of the equations belonging to flow in tortuos tubes model, and the linear form of Forchheimer's equation (23), hydraulic gradient (3), the coefficient $\lambda/4 = f(Re_p)$ (16) respectively [20].

The presented model it could be extrapolated to pressure flow (pipe's hydraulic) or with free surface (channels) under condition of use the coefficient λ corresponding to (16).

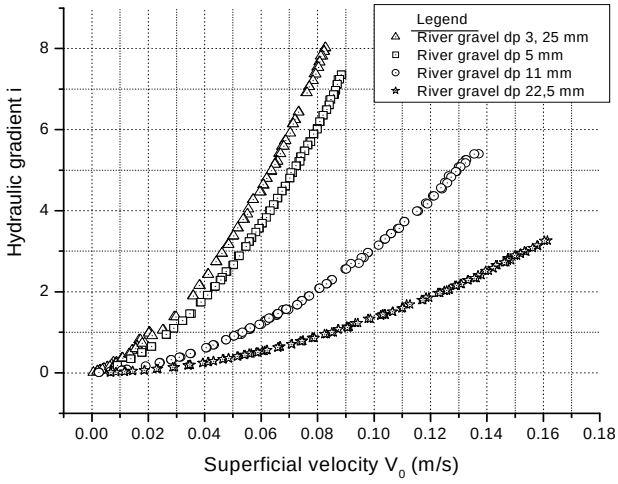

Fig. 4. Results of hydraulic gradient's measurements for river gravel [20]

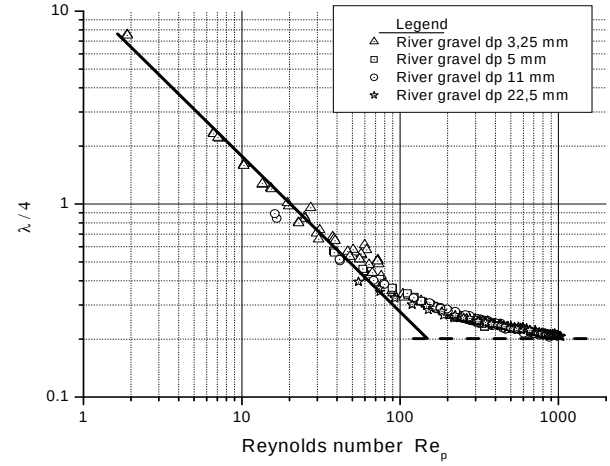

Fig. 5. Unified experimental results for gravel, eq. (16) [20]

5. CONCLUSIONS

In many practical cases, fluid flow through porous media is in post-Darcy law. The flow model through thin tubes approximates the flow phenomena sufficiently good from engineering point of view. Good calculation's might be done for filters, flow near wells, in fractured media, in large cavity, in packed material from textile and chemical industry etc.

In frame of post-Darcy's study, there are elaborated new theories concerning flow over permeable walls, such as flow in river with permeable bed **Fig. 6.,** air pollution diffusion in urban areas, air movements in vegetation.

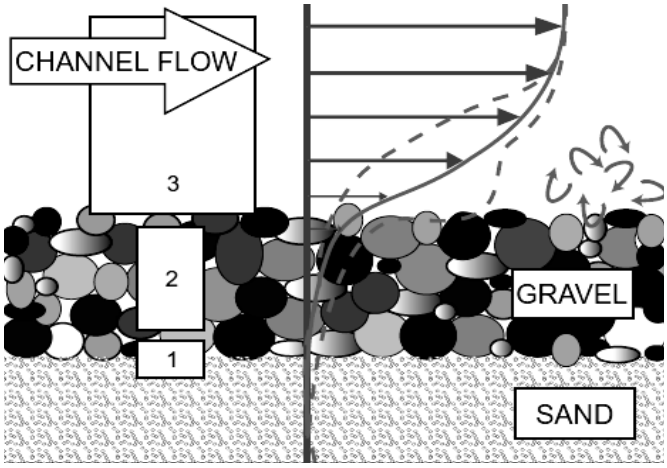

Fig. 6. Flow in rivers with permeable bed [21]

APPENDIX

a – coefficient, $Pa \cdot m^{-1} \cdot s^{1}$;
b – coefficient, $Pa \cdot m^{-2} \cdot s^{2}$;
c – coefficient, $Pa \cdot m^{-3} \cdot s^{3}$;
c_1– coefficient, $Pa^{-1} \cdot s^{\beta} \cdot m^{\beta-1}$;
c_2 – coefficient, dimensionless;
d – fictive cylindrical pore diameters, m;
dl – length difference, m;
d_p- particle diameter, m;
dp, Δp – pressure difference, Pa;
f – friction coefficient $(4f - \lambda)$, dimensionless;
g – gravity acceleration, $m \cdot s^{-2}$;
i – hydraulic gradient, dimensionless;
k_e – equivalent absolute roughness, m;
k_p – permeability coefficient, m^2;
n – porosity, dimensionless;
p, $\overline{p}$ - pressure, Pa;
∇p – pressure gradient, $Pa \cdot m^{-1}$;
q – the proportion of viscous frictions, dimensionless;
r_0 – equivalent cylinders radius of the pores, m;
t – time, s;
V_0 – superficial velocity, m/s;
V_x, V_y, V_2, V_0, V – velocity, m/s;
X– distance, m;
A – average cross section of pores, m^2;
A_d, A_s – specific dynamic and static area, m^{-1};
AB – relative deviation, dimensionless;
D – cylindrical infiltrometer diameter, m;
F – specific force, N/m^3;
Fr – Froude number, dimensionless;
L, L_0, L' - distance, m;
M^*, M – the inertial coefficient of the model, $P \cdot s^2 \cdot m^{-3}$;
N^*, N - the viscous coefficient of the model, $Pa \cdot s \cdot m^{-2}$;
P – the proportion of inertia contribution, dimensionless;
Re – Reynolds number, dimensionless;
W_p – volum of pores, m^3;

Greek letters

α, β – coefficients, dimensionless;
γ – specific weight, $N \cdot m^{-3}$;
λ – Darcy-Weisbach coefficient, dimensionless;
ν – kinematic viscosity, $m^2 \cdot s^{-1}$;
μ – dynamic viscosity, Pa·s;
ρ – density, $kg \cdot m^{-3}$;
τ – tortuosity; dimensionless;

6. ACKNOWLEDGMENTS

Research has been financed by CNCSIS, grant ID_2298/2009.

7. REFERENCES

[1] Forchheimer, P. "Wasserbewegungdurch boden", Zeitschrift das Vereines deutscher Ingenieure 45(50), p. 1781-1788, 1982.
[2] Forchheimer, P. "Hydraulic" Leipzig und Berlin Druck und Verlag von B.G. Teubner, 1914.

[3] Ergun, S., "Fluid flow through packed columns", Chemical Engineering Progress, vol. 48, nr. 2, p. 89-94, 1952
[4] Costa, U. M. S., Andrade, J. S., Makse, H. A. and Stanley, H. E. "Inertial effects on fluid flow through disordered porous media" Physica, A., 1998.
[5] Plesis, J. P. "Analytical qualification of coefficients in the Ergun equation for fluid friction in a packed bed", Transport in Porous Media 16, p. 189-207, 1994.
[6] Rasoloarijaona, M. and Auriault, J. L. "Nonlinear seepage flow through a rigid porous medium", European Journal of Mechanics. B/Fluids 13(2) p. 177-195, 1994.
[7] Skjetne, E. "High-velocity flow in porous media", Phd thesis, Norvegian University of Science and Technology, 1995.
[8] Venkataraman P. and Rao, P. R. M. "$\lambda = \lambda$ = Darcian, Transitional and Turbulent Flow through Porous Media", Journal of Hydraulic Engineering, ASCE, vol. 124, no. 8, p. 840-846, 1998.
[9] Wahyudi, I., Montillet, A., Khalifa, A. O. A. "Darcy and post-Darcy flows within different sands", Journal of Hydraulic Research, vol. 40, no. 4, 2002.
[10] Comity, J., Sabiri, N. E., Montillet, A. "Experimental characterization of flow regimes in various porous media - III: limit of Darcy's creeping flow regime for Newtonian and purely non-Newtonian fluids" Chem. Eng. Sci. 55, p. 3057-3061, 2000.
[11] Comiti, J., Renaud, M. "A new model for determinating mean structure parameters of fixed beds from pressure drops measurements: application to beds packed with parallelipipedical particles", Chem. Eng. Sci., 44, p. 1539-1545, 1989.
[12] Martin, R. "Turbulent seepage flow through rock-fill structures", Int. Water Power nad Dam Construction, 03, p. 41-45, 1990.
[13] Bogomolov, A. I., Konstantinov, N. M. "Primeri ghidravliceskih rascetov", Naucino tehnicescoe izdatelstvo, Moskva, 1962.
[14] Seguin, D., Montillet, A., Comiti, J. "Experimental characterization of flow regimes in various porous media - I: Limit of laminar flow regime", Chem. Eng. Sci. vo. 53, no. 21, p. 3751-3761, 1998.
[15] Seguin, D., Montillet, A., Comiti, J., Huet, F. "Experimental characterization of flow regimes in various porous media - II: Transition to turbulent flow regime", Chem. Eng. Sci. vo. 53, no. 22, p. 3897-3909, 1998.
[16] Abbood, D., W. "An analytical model study for flow through porous media", 17th International Water Technology Conference, IWTC, Egypt, 2009.
[17] Firdaouss, M., Guermond, J., L, Quere, P. "Nonlinear corrections to Darcy's law at low Reynolds numbers", J. Fluid Mech. Vo. 343, 1997.
[18] Malinovska, E., Sas, W., Szymanski, A. "Nonlinear water flow characteristics describing organic soil conservation", Electronic Journal of Polish Agricultural Universities, http://www. ejpau.media.pl.
[19] Aulisa, E., Bleshanskaya, L., Hoang, L., Ibragimov, A. "Analysis of generalized Forchheimer flows of compressible fluids in porous media", 2009, Inst. For Math. And its Appl., University of Minessota, www.ima.umn.edu.
[20] Contract CNCSIS, Grant ID 2298, 589/2009. "Cercetări asupra curgerilor turbulente în medii poroase permeabile rigide", www.hidromed.ro
[21] Klar, M. "Design of an endoscopic 3-D Particle Tracking Velocimetry System and its Application in Flow Measurements within Gravel Layer", PhD Thesis, Ruperto-Carola University, Heidelberg, Germany, 2005.

Research of filtration through uniform geometry permeable material – glass spheres

Bartha I., Marcoie N., Toma D., Gabor V., Toacă D.[1]

***Abstract* – Experimental results of fluid flow through homogeneous permeable media – uniform glass spheres of diameter 20, 10, 5 and 2,5 mm – the paper presents.**

Experiments for hydraulic gradients corresponding to Darcy's law up to 7,5 (post Darcy's movement) has been undertaken.

Using a capillary tube model of filtration, parameters of the movement has been determined: porosity, pores diameter, tortuosity, Forchheimer type quadratic relationship of hydraulic gradient, the dynamic and static specific area and friction factor law in function of pore diameter Reynolds number.

***Keywords* – Newtonian fluid, post Darcy's filtration, uniform geometry of solid phase.**

1. INTRODUCTION

At the beginning of the last century, Forchheimer [1], Slichter and others the incongruity of movement of water within filters with respect Darcy's linear law observed, the obtained discharge of filters being lower than that computed by relationship

$$Q = A \cdot k \cdot i \tag{1}$$

The head loss of filters has been greater than that obtained by (1). Closed to viscous friction contribution, the head loss has to contain part of kinetic energy losses too. The new assumption considered, and based on them three new empirical relationships for the hydraulic gradient have been proposed:

a) power type:

$$i = \alpha \cdot V_0^{\beta} \tag{2}$$

b) quadratic polynomial:

$$i = a \cdot V_0 + b \cdot V_0^2 \tag{3}$$

c) cubic polynomial

$$i = a \cdot V_0 + b \cdot V_0^2 + c \cdot V_0^3 \tag{4}$$

Within pores of permeable materials liquids flow in a curve path lines, their curvature being of the same order like grains size, so the way of liquid is longer than that the bed height, the elementary liquid currents having tortuosities and variable geometry on their length, so local loss of head occurs due to velocity modification. The head loss developing two terms have contribution: the first proportional the superficial velocity by viscous resistance at the pores wall (computed after Poiseuille), and the second proportional the kinetic head, due to inertial resistance.

Post Darcy's filtration has many technical applications for: fluid raw material extraction, flows within permeable hydraulic structures, movement over permeable walls, atmospheric

[1] Bartha I. is with Technical University "Gheorghe Asachi" of Iasi, Bd. D. Mangeron nr. 67, 700050-Iasi, Romania (corresponding author to provide phone/fax: +40-232-270690; e-mail: ibartha@tuiasi.ro).

Marcoie N. is with Technical University "Gheorghe Asachi" of Iasi, Bd. D. Mangeron nr. 67, 700050-Iasi, Romania (corresponding author to provide phone: 0721572995; e-mail: nmarcoie@yahoo.com).

ISSN-1584-5990 ©

pollution dispersion on dense built up areas, oxygen-carbon dioxide changing in vegetation zones, fire propagation in forests, in permeable bed channels hydraulic, rapid filters, in medicine etc.

2. DESCRIPTION OF POST-DARCY'S FILTRATION

Description of fluid movement through permeable media different types of models, from simple to complex, are used [2] as follows:

a) *Darcy model* of filtration considers the movement takes place on the whole cross section (solids and pores), defining the average superficial velocity $V_0=Q/A$, length of the movement L as the bed height on the flow direction, hydraulic gradient $\Delta p/\gamma L$, mean velocity in the pores $V=V_0/n$ (n being the porosity) for nonpermanent flows.

b) *Permeable media of spherical solid grains model* assume that fluids flow through spherical solid particles having the same or different diameters, laid-dawn on the most stable position, having minimum porosity or porosity experimentally determined. The criticizable part of this model refers definition discord of equivalent spheres diameter. Results by different authors difficult are comparable.

c) *Capillary tube model of the permeable media* consider that bed void is formed in a set of cylindrical small diameter equivalent curve tubes within that the loss of head occurs like in circular pipes, having equivalent roughness equal the fictive tubes diameter (**Fig. 1.**) [1, 2, 3, 4, 5].

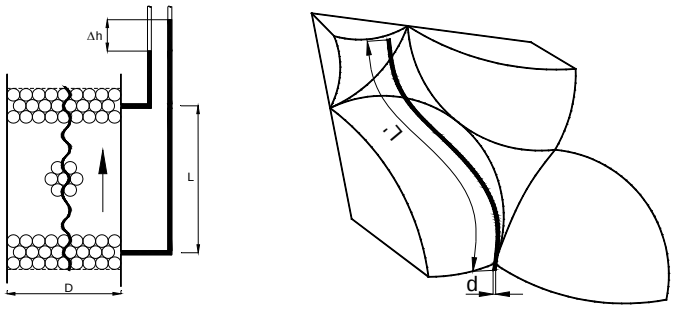

Fig. 1. Scheme of the capillary tub model of permeable mediathe paper uses this model presented in [2, 3, 4, 5]

Presume the permeable granular material, firmly fixed by upstream and downstream permeable walls, is formed in a set of m tubes of diameter d, tortuous length L', total surface S. The total surface of the set of tubes is considered the solid granular material surface exposed to fluid current (for homogeneous spheres all their surface, reciprocal contacts being punctual).

The total volume of the column of diameter D and length L is W. Tortuosity of the permeable media is:

$$\tau = \frac{L'}{L} \tag{5}$$

Static specific surface As is considered the ratio:

$$A_s = \frac{\text{mean surface area of the particles}}{\text{mean volume of solid}}$$

and dynamic specific surface A_d:

$$A_d = \frac{\text{surface area presented by the particles to the flow}}{\text{volume of solid}}$$

resulting:

$$X = A_d / A_s \leq 1 \tag{6}$$

Maximum for X=1 happen for punctually reciprocal contact of solid particles (ex. spheres).

Fictive tubes diameter for granular permeable material, with porosity *n* is:

$$d = \frac{4 \cdot n}{A_d \cdot (1-n)} \tag{7}$$

The mean velocity in tubes as a function of superficial velocity is:

$$V = V_0 \cdot \frac{\tau}{n} \tag{8}$$

The pressure drop for a range of pores Reynolds number over passing the limit of creeping flow, including week and strong inertia and transition zones, where:

$$\mathrm{Re}_d = \frac{V \cdot d \cdot \rho}{\mu} \tag{9}$$

could be considered as sum of two terms:

- the first, proportional to the flow velocity, is due to viscous resistance at the walls of the pores, expressed by Poiseuille equation:

$$\left(\frac{\Delta p}{L}\right)_{viscous} = \frac{2 \cdot \mu \cdot \tau^2 \cdot (1-n)^2 \cdot A_d^2}{n^3} \cdot V_0 \tag{10}$$

- and the second, due to inertial resistance, loss of energy caused by direction changing and roughness. Pores with very rough pipes are assimilate, the equivalent roughness k_e having the same range of magnitude as the diameter *d* of pores. Accepting, by analogy from circular pipes, for Darcy-Weisbach coefficient, Nikuradze relationship the inertial pressure drop:

$$\left(\frac{\Delta p}{L}\right)_{inertial} = 0{,}0968 \cdot \frac{\rho \cdot \tau^3 \cdot (1-n) \cdot A_d}{n^3} \cdot V_0^2 \tag{11}$$

will be obtained.

The total relative pressure drop becomes:

$$\left(\frac{\Delta p}{L}\right)_{total} = \left(\frac{\Delta p}{L}\right)_{viscous} + \left(\frac{\Delta p}{L}\right)_{inertial} \tag{12}$$

In form of general accepted linear head loss in pipes:

$$h_r = \lambda \cdot \frac{L}{D} \cdot \frac{V_0^2}{2 \cdot g} \tag{13}$$

results:

$$\lambda = \frac{64}{\mathrm{Re}} + 0{,}7743 \tag{14}$$

or the friction factor:

$$f = \frac{\lambda}{4} = \frac{16}{\mathrm{Re}} + 0{,}194 \tag{15}$$

Instead of relationship (12) customary is the form:

$$\frac{\Delta p}{L \cdot V_0} = M \cdot V_0 + N \tag{16}$$

with

$$M = 0{,}0968 \cdot \tau^3 \cdot \rho \cdot A_d \cdot \frac{1-n}{n^3} \tag{17}$$

$$N = 2 \cdot \tau^2 \cdot \mu \cdot A_d^2 \cdot \frac{(1-n)^2}{n^3} \tag{18}$$

Tortuosity τ and dynamic specific surface A_d being micro scale amounts of the permeable media their determination by direct measurements present some difficulties.

Experimental and statistical drawing of (16) by macroscopic averaged pressure drop measurements Δp on length L, as the superficial velocity function V_0, obtained by flow Q measurement on the whole cross section A and porosity n practical measurements permit computation of tortuosity τ and dynamic specific surface A_d. During experimentation liquid temperature has to be measured, it influences viscosity and density of the liquid. Using method of least squares M and N parameters of (16) results, then:

$$A_d = \left[\frac{N^3 \cdot (0{,}0968 \cdot \rho)^2}{M^2 \cdot (2 \cdot \mu)^3} \cdot \frac{n^3}{(1-n)^4} \right]^{\frac{1}{4}} \tag{19}$$

$$\tau = \left[\frac{M^2 \cdot 2 \cdot \mu \cdot n^3}{N \cdot (0{,}0968 \cdot \rho)^2} \right]^{\frac{1}{4}} \tag{20}$$

are computed. Relationship (16), experimentally calibrated permits computation of the friction factor:

$$f = \frac{2 \cdot \Delta p \cdot n^3}{L \cdot \tau^3 \cdot \rho \cdot A_d \cdot (1-n) \cdot V_0^2} \tag{21}$$

3. EXPERIMENTAL EQUIPMENT

The experimental equipment contains a vertical cylindrical infiltrometer, with upstream and downstream fixing permeable walls, with upwards water circulation for continuous air evacuation (**Fig. 2.**, **Photo 1., 2.**) [9].

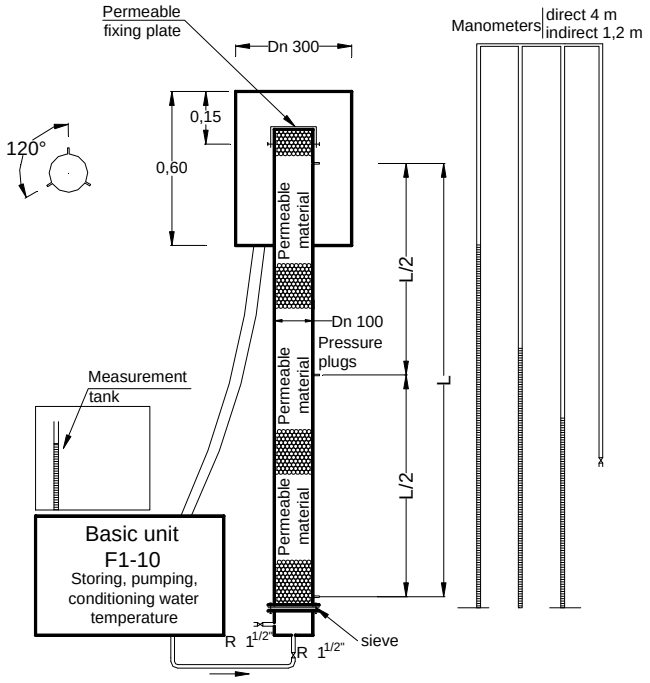

Fig. 2. Vertical infiltrometer under pressure

Infiltrometer diameter is D=100 mm, its total length 2,50 m, length between extreme pressure intake port (PIR) L=2,00 m. On its upstream part there is a demountable inlet

section, bordered by the upstream permeable wall. On its downstream end the experimented porous material is fixed by other permeable wall that compress it.

Photo 1. General view of the equipment with direct manometers

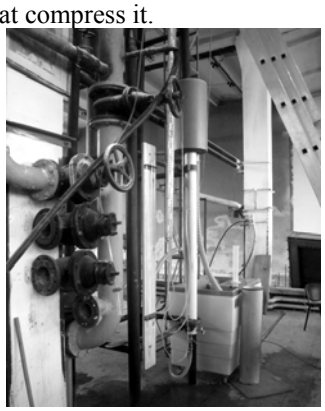

Photo 2. General view of the equipment with indirect manometers

Loading the experimental granular material is done under vibrations, the compact lying being assured. The infiltrometer by a flexible 1 1/2" hose is supplied and the flow regulation by two 1 1/2" check valves assured. Water storage and pumping is realized by F1-10 ARMFIELD bench, with characteristics H_{pump}=18 m water column and flow Q=1,5 l/s, modified for experimental water temperature automatic regulation by a contact thermometer.

The infiltrometer with three pressure intake port at equidistant ΔL=1 m is provided. Each PIR consist in three d_{PIR}=0,8 mm orifices at 120°. Flow measurement is volumetrically, maximum relative flow errors being $\delta Q \leq 0{,}001$. Pressure drop by inclined tube micro manometers (for $\Delta h \leq 0{,}1$ m water column), direct differential manometers ($0{,}1 \leq \Delta h \leq 4$ m water column) and indirect differential manometers with mercury ($4 \leq \Delta h \leq 15$ m water column) are measured. Pressure pulsations at pump by air chamber on pumping pipe are damped. On pressure transmission to manometers capillary sections are used for the same purpose. The demountable section of the infiltrometer is provided by an inlet/outlet tap (1/2") for porosity measurements.

4. RESULTS

Experiences with uniform diameter glass spheres, as permeable solid material, and drinking water, as liquid phase, on the described installation has been undertaken [9]. Four diameter glass spheres has been used, from each set 200 balls diameters has been measured. During experiments the stable lay of the spheres has been assured.

First, porosity measurements, by minimum five repetitions, then theoretic values in tetrahedron, pyramidal and cubic lying has been determined. Results are presented in **Table 1**.

Table 1. Geometric characteristics of the permeable material used

d_{nb} (mm)	d_b (mm)	n_{exp}	$n_{effective}$	$n_{tetrahedron}$	n_{pyr}	n_{cubic}
2,5	$2{,}5^{+0{,}02}_{-0{,}10}$	0,3326	0,3163	0,2384	0,2595	0,4764
5,0	$5^{+0{,}02}_{-0{,}12}$	0,3615	0,3550			
10,0	$10^{+0{,}02}_{-0{,}10}$	0,5598	0,3543			

20,0	$20^{+0,00}_{-0,12}$	0,4137	0,4079			

Differences of theoretic and experimental porosity due to spheres laying inside the infiltrometer, the first spheres layer porosity at the wall is higher, due to rigidity of the infiltrometer and glass spheres wall and. This rigidity does not permit tetrahedron or pyramidal lying of the experimental material (**Photo 3-4.**).

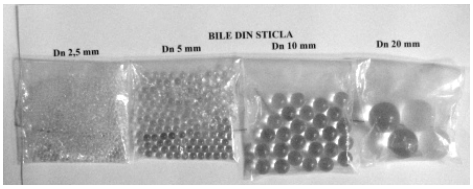

Photo 3. Glass spheres used in experiments

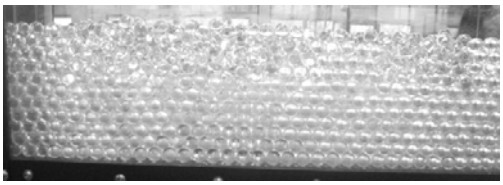

Photo 4. Glass spheres laying in a transparent canal (down-part tetrahedron, up-disorderly laying)

Loss of head measurements in a function the superficial velocity, expressed in relative hydraulic gradient - $i/V_0 = f(V_0)$ are presented in **Fig. 3-6**.

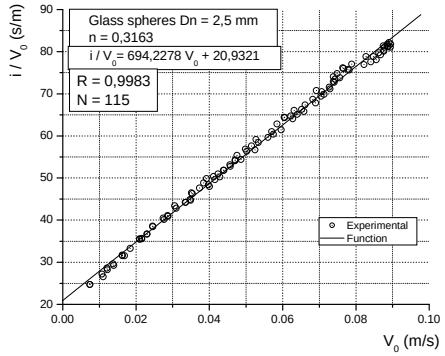

Fig. 3. Experimental relative hydraulic gradient for Dn=2,5 mm spheres

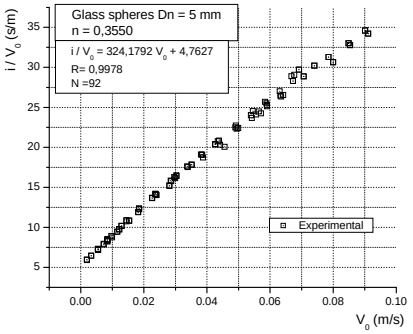

Fig. 4. Experimental relative hydraulic gradient for Dn=5 mm spheres

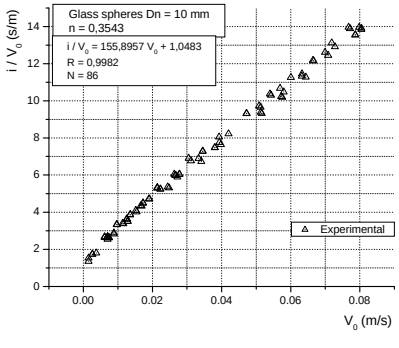

Fig. 5. Experimental relative hydraulic

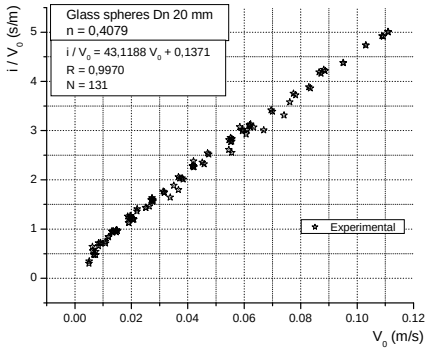

Fig. 6. Experimental relative hydraulic gradient for Dn=10 mm spheres gradient for Dn=20 mm spheres

The hydraulic gradient i for the experimented permeable material with respect superficial velocity V_0 corresponds to **Fig. 7**.

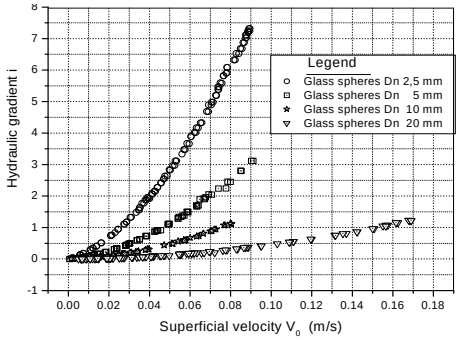

Fig. 7. Hydraulic gradient in the superficial velocity function for glass spheres

Other computed hydraulic characteristics refer: M and N parameters of (16) with determinating coefficient R, specific static and dynamic surfaces A_s, A_d, tortuosity τ, (20), diameter of fictive tubes d, (7), mean velocity in the pore v, (8), pores Reynolds number Re_d, (9), and friction factor f, (21). Experimental conditions and part of determined hydraulic characteristics are presented in **Table 2**.

Table 2. Filtration parameters through homogenous glass spheres

Dn (mm)	M (s^2m^{-2})	N (s^1m^{-1})	R	n	θ (^oC)	NME	τ	A_d (m^{-1})	A_s (m^{-1})	X	10^3d (mm)
2,5	694,2278	20,9321	0,998	0,3163	10,3	115	1,119	2322	2400	0,9675	0,797
5,0	324,1792	4,7627	0,998	0,3550	18,4	92	1,214	1173	1200	0,9775	1,877
10,0	155,8957	1,0483	0,998	0,3543	18,3	86	1,228	587	600	0,9783	3,739
20,0	43,1188	0,1371	0,997	0,4079	18,2	131	1,194	294	300	0,9800	9,373

Friction factor $f = \lambda / 4$, (21), in a pore Reynolds number function, Re_d, for all experimental diameters is draw in **Fig. 8**.

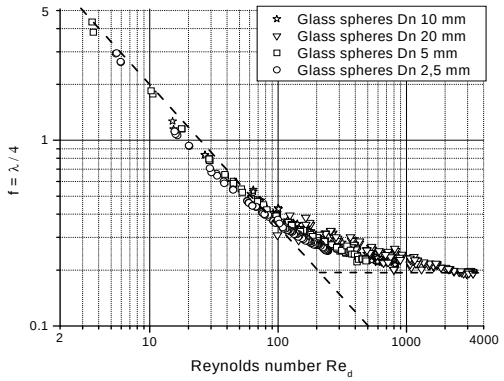

Fig. 8. Pore friction versus pore Reynolds number

5. CONCLUSIONS

Relationship (15) exact enough describes friction factor $f = \lambda / 4$ in the wide field of studied pore Reynolds number (Re_d=2-3000) for glass spheres. The studied Reynolds number field joins week and strong inertia and transition to turbulence of the movement.

In engineering practice Darcy's law could be accepted for $\mathrm{Re} \leq 4{,}3$, errors due to kinetic losses being up to 5%. More pretentious works claim higher precision, for errors up to 1% the limit pore Reynold's number is $\mathrm{Re}_d \leq 0{,}8$.

Figures 3-6 show an easy curvature of experimental data, and the quadratic relationship (2), (16) are approximations of the phenomena. Corrections of Darcy's law for inertial and transition zones have to be polynomial [1, 6, 7, 8], at least cubic.

APPENDIX

a – coefficient, $m^{-1} \cdot s^{1}$;
b – coefficient, $m^{-2} \cdot s^{2}$;
c – coefficient, $m^{-3} \cdot s^{3}$;
d – pore tub equivalent diameter, m;
d_b – sphere diameter, m;
dn_b – sphere nominal diameter, m;
f – friction factor, dimensionless;
g – gravity acceleration, $m \cdot s^{-2}$;
Δh – loss of head, m water column;
i – hydraulic gradient, dimensionless;
k – filtration coefficient, $m \cdot s^{-1}$;
k_e – equivalent roughness, m;
m – number of fictive pores, dimensionless;
n – porosity, dimensionless;
Δp – pressure drop, Pa;
A – cross section area, m^2;
A_d, A_s –dynamic and static specific area, m^{-1};
D – infiltrometer diameter, m;
M – coefficient, $Pa \cdot s^2 \cdot m^{-3}$;
N – coefficient, $Pa \cdot s \cdot m^{-2}$;
NME – number of experiments in a set, dimensionless;
Q – flow, $m^3 \cdot s^{-1}$;
Re_d – pore diameter Reynold's number, dimensionless;
S – total surface of solid particles, m^2;
V – mean pore velocity, $m \cdot s^{-1}$;
V_0 – superficial velocity, $m \cdot s^{-1}$;
W – total volume of the infiltrometer, m^3;
X – coefficient, dimensionless;

Greek Letters

α – coefficient, $m^{-\beta} \cdot s^{\beta}$;
β – coefficient, dimensionless;
γ – unit weight, $N \cdot m^{-3}$;
λ – Darcy-Weisbach coefficient, dimensionless;
ν – kinematic viscosity, $m^2 \cdot s^{-1}$;
μ – dynamic viscosity, Pa·s;
ρ – density, $kg \cdot m^{-3}$;
τ – tortuosity, dimensionless;

6. ACKNOWLEDGMENTS

The paper on results of grant PN2, ID_2298, financed by CNCSIS, contract 589/2009 CNCSIS-UTI are based.

7. REFERENCES

[1] Forchheimer, P., 1914, "Hydraulik. Druck und Verlag von B.G. Teubner", Leipzig und Berlin
[2] Comiti, J., Renaud, M., 1988, "A new model for determining mean structure parameters of fixed beds from pressure drop measurements: application to bed packed with parallelepipedal particles", Chem. Eng. Sci., vol. 44, No. 7
[3] Seguin, D., Montillet, A., Comiti, J., 1998, "Experimental characterization of flow regimes in various porous media – I: Limit of laminar flow regime", Chem. Eng. Sci., vol. 53, No. 21
[4] Seguin, D., Montillet, A., Comiti, J., Huet, F., 1998, "Experimental characterization of flow regimes in various porous media – II: Transition to turbulent regime", Chem. Eng. Sci., vol. 53, No. 22
[5] Comiti, J., Sabiri, N.E., Montillet, A., 2000, "Experimental characterization of flow regimes in various porous media – III: Limit of Darcy's or creeping flow regime for Newtonian and purely viscous non-Newtonian fluids", Chem. Eng. Sci., vol. 55
[6] Wahyudi, I., Khalifa, A.O.A., 2002, "Darcy and post-Darcy flows within different sands", Journal of Hydraulic Research, vol. 40, No.4
[7] Firdaouss, M., Guermond, J.L., Le Quéré, P., 1997, "Nonlinear corrections to Darcy's law at low Reynolds numbers", Journal of Fluid Mechanics, vol. 343
[8] Balhoff, M., Mikelic, A., Wheeler, M.F., 2009, "Polynomial filtration laws for low Reynolds number flows through porous media", The University of Texas at Austin
[9] xxx, 2009, "Cercetări asupra curgerilor turbulente în medii poroase permeabile rigide", Proiect ID_2298, www.hidromed.ro

Ovidius University Annals Series: Civil Engineering Volume 1, Issue12, June 2010

Piping Erosion Mathematical Modeling and Applications

Mohamed Amine Boukhemacha, Ioan Bica, Koudir Mezouar

***Abstract* – Internal erosion is one of the major causes of failure of hydraulic works (embankment dams and dikes). It manifests by the migration of soil particles by suffusion or piping. Piping is induced by regressive erosion of particles from downstream and along the upstream line towards an outside environment until forming a continuous pipe. In this paper, a mathematical model for piping erosion will be presented; this model is derived from pipe flow equations, soil detachment and mass conservation laws. Then, a comparison with experimental data from an existent physical model (hole erosion test) will be used as validation. Finally, as application, it will be presented how such a model can predict the evolution of the geometry of a truncated cone crack and a cylindrical hole near an existent conduit under some simplifying hypotheses.**

***Keywords* –Crack, internal erosion, hole erosion test, piping.**

1. INTRODUCTION

Nowadays, embankment dams represent the majority (70-80%) of the world population in dams [1]. According to [2] statistics, most failed dams are earth made with a failure frequency 2 times higher then concrete dams. However, since 1985, the probability of failure became similar to that of concrete dams [3]. One of the main causes of failure of this majority of dams' population is internal erosion [2], [4]-[5]. Internal erosion involves the removal of solid material, usually in suspension, from within an embankment or its foundation by the flow of water. Internal erosion mechanisms are complex and involve many parameters. Previous experimental studies [6]-[7] identify the mechanisms responsible for the migration of the particles as either suffusion or piping. Suffusion is the migration of soil particles within soil matrix causing modifications in its physical and mechanical properties. Piping is a process that starts at the exit point of seepage and in which a continuous passage or pipe is developed in the soil by backward erosion.

Piping can occur through the embankment, through the foundation or from the embankment into the foundation. The first mode is the more frequent [4]-[5]. Further, it was noticed in [5] that about half of all piping failures through the embankment are associated with the presence of conduits. The different modes of piping associated with conduits are: piping into the conduit, along the conduit or out of the conduit [3].

M. A. BOUKHEMACHA is with the Technical University of Civil Engineering of Bucharest, Bd. Lacul Tei nr. 124, Sector 2 RO-020396-Bucuresti, Romania (phone: +40-762 911 999; e-mail: boukhemacha-amine@hotmail.com).

I. BICA is with the Technical University of Civil Engineering of Bucharest, Bd. Lacul Tei nr. 124, Sector 2 RO-020396-Bucuresti, Romania (e-mail: bica@utcb.ro).

K. MEZOUAR is with the Technical University of Civil Engineering of Bucharest, Bd. Lacul Tei nr. 124, Sector 2 RO-020396-Bucuresti, Romania (e-mail: mezouarkhoudir@yahoo.fr).

ISSN-1584-5990

In this paper, a mathematical model for piping erosion will be presented. In the first part, the formulas used to derive this model are presented (soil detachment and pipe flow equations). Then, a comparison with experimental data from an existent physical model (hole erosion test) will be used as validation. Finally, supplementary applications for this model will be exposed.

2. SOIL DETACHMENT QUANTIFICATION

The erodibility of a soil can be quantified in terms of the rate of erosion when a given hydraulic shear stress is applied to the soil, and the ease of initiating erosion in the soil. This can be expressed as [8]:

$$\dot{\varepsilon} = C_e(\tau_t - \tau_c) \tag{1}$$

Where: $\dot{\varepsilon}$ (kg/s/m^2) is the rate of erosion per unit surface area of the hole at time t, C_e (s/m) is a constant named the coefficient of soil erosion, τ_t (Pa) is the hydraulic shear stress along the hole at time t and τ_c (Pa) is the minimum hydraulic shear stress for initiation of erosion, also referred to as the critical shear stress by a number of authors.

The precedent equation is applicable when ($\tau_t > \tau_c$) only, otherwise the erosion rate is equal to zero. The hydraulic shear stress for a horizontal cylindrical hole can be calculated by:

$$\tau_t = \frac{\gamma_w D_t H}{4L} \tag{2}$$

Where: γ_w (kg.s^2/m^2) is the specific weight of water, D_t (m) is the hole diameter at time t, L (m) is the hole length and H (m) is the head loss along the hole due to friction.

Equation 2 is made under the following assumptions:

- Linear head loss from upstream to downstream,
- Steady uniform flow along the cylindrical hole (**Figure 1**),
- Zero pressure head at the downstream end,
- Uniform frictional resistance along the surface of the crack or cylindrical pipe,
- Driving force = frictional resistance.

Figure 1 describes the parameters and the effects of a fluid flow through a cylindrical horizontal hole in the soil.

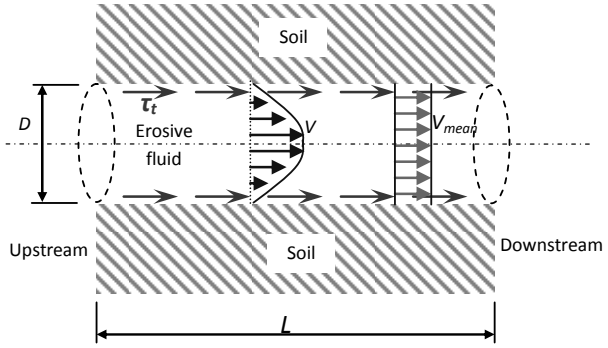

Fig. 1. Schematic description of flow parameters through a cylindrical hole in soil

3. PIPE FLOW EQUATIONS

Considering that the flow through the soil matrix is negligibly small compared to the flow through the hole, the flow rate through the hole can be evaluated using pipe flow

equations. And to do so, we need to evaluate two parameters: Reynolds number and the Fanning friction factor. The used equations to estimate the flow rate are the following:

$$f = \frac{HD_t g}{2L\overline{V}^2} \tag{3}$$

$$R_e = \frac{\rho_w \overline{V} D_t}{\mu} \tag{4}$$

Where : f is the friction loss factor for pipe flow ; $\overline{V}$ is the mean velocity of flow along the pipe ; R_e is the Reynolds number ; μ is the dynamic coefficient of viscosity of water (10^{-3} kg/m.s at 20˚C).

To estimate the flow rate through the pipe, we need a third equation relating the friction factor to the Reynolds's number. For laminar flow (R_e<2000), this relation is well known. But for turbulent flow, this relation has still stirred the interest of many studies. A simple relation was proposed by [9]; this relation gives good results for our purpose [10]. For fully turbulent pipe flows we have [9]:

$$\frac{1}{\sqrt{f}} = 2\log_{10}\left(R_e\sqrt{f}\right) - 0.8 \tag{5}$$

4. PIPING EROSION MATHEMATICAL MODEL DEVELOPMENT

The model consists of an analytical equation that gives the temporal variation of the internal diameter of the hole by erosion and another equation to estimate the flow rate.

4.1. Estimation of the variation of the hole diameter in time

The mathematical development of the model is based on the assumptions that:

- The shape of the concentrated leak/pipe remains circular throughout the course of the erosion process ;
- The assumptions used to evaluate the hydraulic shear stress.

Considering the general case where the hydraulic head can change in time, quantifying the change in the diameter of the hole (pipe) during a time step Δt, transition from the diameter D_t to the diameter $D_{t+\Delta t}$, can be done by calculating the change in mass by the equation of detachment and equalizing with the variation obtained from volume change. The integration of system by the trapezium rule under the previous assumptions gives:

$$D_{t+\Delta t} = \frac{D_t\left[C_e\Delta t\gamma_w\left(H_{t+\Delta t}+H_t\right)+8L\rho_d\right]-16LC_e\Delta t\tau_c}{8L\rho_d - C_e\Delta t\gamma_w\left(H_{t+\Delta t}+H_t\right)} \tag{6}$$

Where: H_t and ($H_{t+\Delta t}$) the hydraulic head a time t and ($t+\Delta t$) respectively, ρ_d (kg/m^3) is the soil dry density.

Equation 6 gives more accurate results the smaller is the time step. The estimation of the temporal variation of the diameter of the hole must be done in an iterative way using a time step Δt of 1 to 10 s.

In the case of a constant hydraulic head, this model can be written as [10]:

$$D_t = D_0 + \left(\frac{8L\rho_d - C_eD_0\gamma_w}{2C_eH\gamma_w}\right)\left[\left(1+\frac{4C_eH\gamma_w}{8L\rho_d - C_eD_0\gamma_w}\right)^t - 1\right]\left(\frac{2C_eH\gamma_wD_0}{8L\rho_d - C_eD_0\gamma_w} + \frac{4C_eL\tau_c}{C_eH\gamma_w - 4L\rho_d}\right) \tag{7}$$

4.2. Flow Rate Calculation

Since for most hole erosion tests, the flow is turbulent [11], our interest is to estimate the flow rate for this case. This can be done using pipe flow equations. From the numerical

resolution of (5) and knowing the hole diameter at any time from (6) or (7), the flow rate at any time can be calculated by:

$$Q_t = 0.482381\frac{D_t^2}{\sqrt{L}}\sqrt{D_t gH\left(1.26761 - 0.5\ln\left[\frac{D_t^3 gH\rho_w^2}{L\mu^2}\right]\right)^2} \tag{8}$$

5. VALIDATION

The validation of the proposed mathematical model is made by the comparison of the results of the simulations with experimental data from 14 Hole Erosion Test (HET) records from [12] as shown in **figure 2**. The comparison is in term of the flow rate. The HET is a physical model for piping erosion developed by [12], this test simulate internal erosion by flow (under a controlled water head) through a predrilled horizontal cylindrical hole in a compacted cylindrical soil sample.

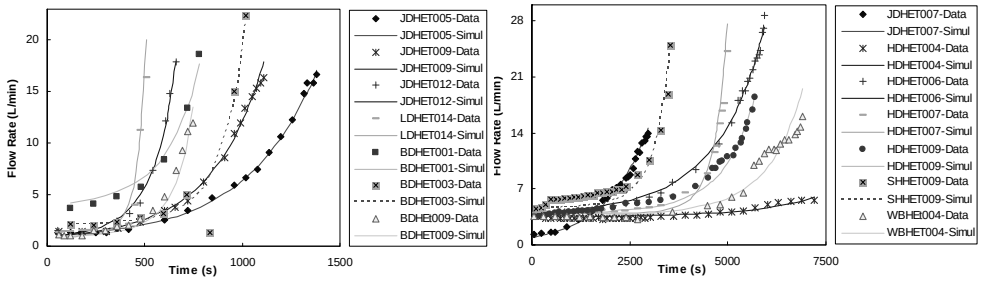

Fig. 2. Flow rate based comparison between constant head hole erosion test data (symbols) with the results of the simulations with the proposed mathematical model (lines) (HET data from [12])

The comparison between the measured and the calculated values of the flow rate shows, with a high correlation (R^2= 0.975), that the mathematical model gives results very close to those from the physical model (**Figure 3**).

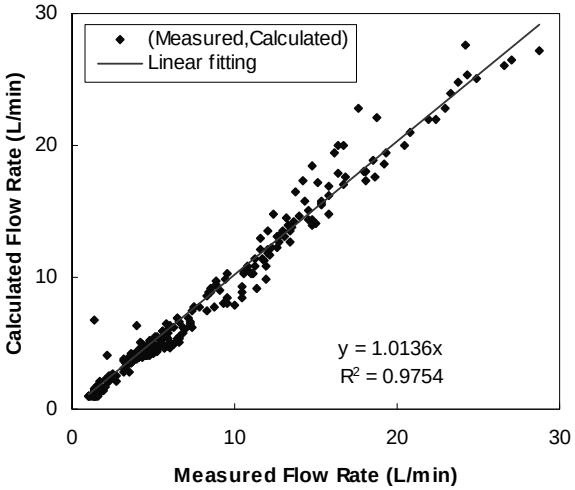

Fig. 3. Correlation between the measured values and the values calculated using the mathematical model for the 14 HET record (Measured data from [12])

6. APPLICATIONS

As applications for the mathematical model, the adaptation of this model for two problems will be presented under some simplifying assumptions.

6.1. A truncated cone crack geometry evolution by internal erosion

This application is an attempt to model backward erosion; this is why the position of the crack must be on the downstream face of the impervious zone of the embankment. And since the simplest and most representative geometry for a crack is the truncated cone, the crack is assumed to have a tapered geometry of length L, maximum diameters D_{out} (downstream) and minimum diameter D_{in} (**Figure 4**).

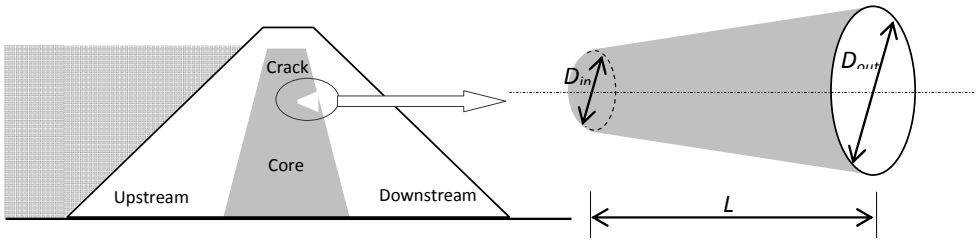

Fig. 4. Description of the position and the chosen geometrical form of the crack

To adapt equation 6 to the case of a crack, the truncated cone geometry will be discretized into N cylinders (see **Figure 5**).

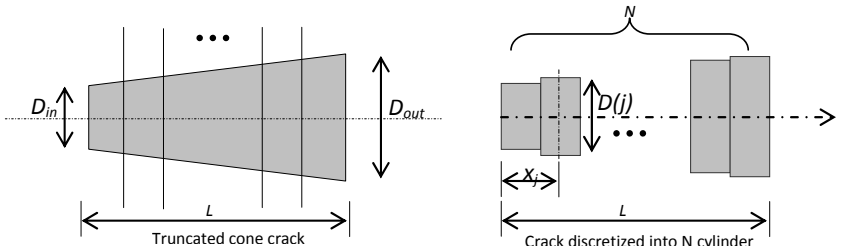

Fig. 5. Discretization of the truncated cone crack into N cylinders

Assuming the dimensions of the crack, and choosing a value for N that ensures the convergence of iterations, it is possible to determine the dimensions of each cylindrical element of the discretization. The soil properties are the same for all elements. It remains to estimate the loss of hydraulic head for each element.

Considering that the head loss across each element is constant in time, and by taking the value of the head equal to h_{in} at the minimum diameter D_{in} and equal to h_{out} at the maximum diameter D_{out}, 3 possible types of distributions can be considered for hydraulic head along the axis of a cylinder hole, 2 nonlinear and 1 linear (**Figure 6**). The nonlinear distributions are obtained using the Newton polynomials (9).

$$h(x_j) = H - \frac{H}{L}x_j \pm \frac{H}{L^2}x_j(x_j - L) \tag{9}$$

Where: $H = h_{in} - h_{out}$ is the head loss across the crack and $h(x_j)$ is the water head at the distance x_j (**Figure 5**).

As a numerical application, the analysis of changes in the geometry of a tapered crack by internal erosion at different moments (t = 45 min, t = 90 min and t = 180 min) is considered. The crack was discretized with N = 1000 and with a time step Δt = 10 s. The soil properties, water head and geometry of the crack are given in **Table 1**.

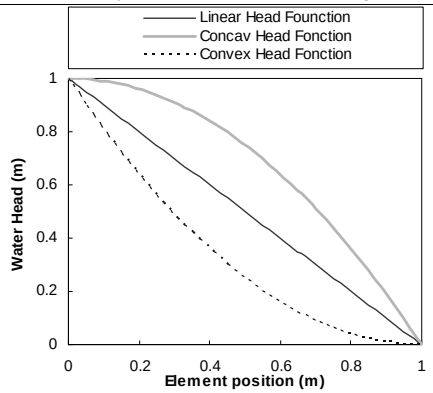

Fig. 6. Possible variations for the water head along the truncated cone crack

Tab. 1. Input parameters for the numerical application of the analysis of the erosion of a tapered crack

Geometry	Value (mm)	Soil	Value	Head	Value
D_{out}	5	τ_c	0 (Pa)	h_{out}	0 (m)
D_{in}	10	C_e	10^{-4} (s/m)	h_{in}	5 (m)
L	100	ρ_d	1.7×10^3 (kg/m^3)	γ_w	9.8×10^{-3}

The Changes in the geometry of the crack in terms of the variation in diameter along its axis is given in **Figure 7** for the 3 head functions.

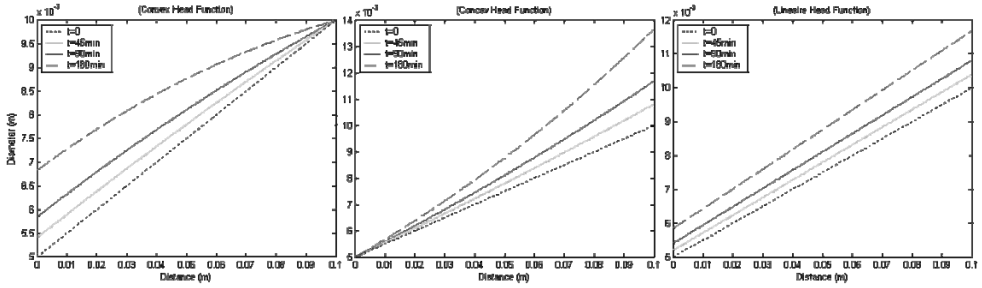

Fig. 7. Geometry variation of the truncated cone crack using the different head functions

6.2. Piping erosion of a cylindrical hole near an existent conduit

The internal erosion may take place if a concentrated leak near a conduit that goes through the hydraulic work is present. This phenomenon can occur for different reasons:

- Presence of weak zone near the conduit from poor compaction or inefficient design considerations creating local concentration of flow lines;
- Presence of rupture in the conduit itself, which will generate a concentration of flow lines, and/or creates an exit point of the soil particles.

The study of initiation and continuation of such a phenomenon is very complex since everything happens within the embankment. This is why it is necessary to introduce the following simplifying assumptions that will allow the application of the model (**Figure 8**):

- The initial geometry of the hole is cylindrical. This geometry remains cylindrical during the erosion process;
- The hole is initially and remains tangent to the conduit.

The assumptions described in **Figure 3** can be written mathematically by a variation of the water head as well as a variation of the hole length during the erosion process (10).

$$\begin{cases} H_{i+1} = H_i - \left(\dfrac{D_i + D_{i+1}}{2}\right)\sin\beta \\ L_{i+1} = L_i - \left(\dfrac{D_i + D_{i+1}}{2}\right)(\cot\alpha_1 + \cot\alpha_2)\sin\beta \end{cases} \tag{10}$$

Where: H_{i+1} (H_i) is the head loss at time step i+1 (i) respectively, D_{i+1} (D_i) is the hole diameter at time step i+1 (i) respectively, L_{i+1} (L_i) is the hole length at time step i+1 (i) respectively, α_1 (α_2) are respectively the slope of the upstream (downstream) face of the core of the dams and β is the slope of the path of evolution of the hole (**Figure 8**).

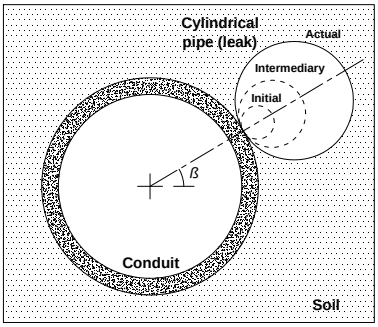

Fig. 8. Schematic description of the assumptions on the evolution path of the leak cylindrical near a conduit by piping erosion

A numerical application has been made with the conditions presented in **Table 2**. The application consists of 4 analyses with different values of β, with an external diameter of the conduit of 1 m. the hydraulic head at the axis of the conduit is 5m and it length is 10 m.

Tab. 2. Input parameters for the numerical application of the analysis of the internal erosion of a cylindrical hole near a conduit

ρ_d	1500 (kg/m^3)	D_0	5 (mm)
τ_c	5 (Pa)	α_1 , α_1	30˚
C_e	0.001 (s/m)	β	90˚, 45˚, -45˚, -90˚

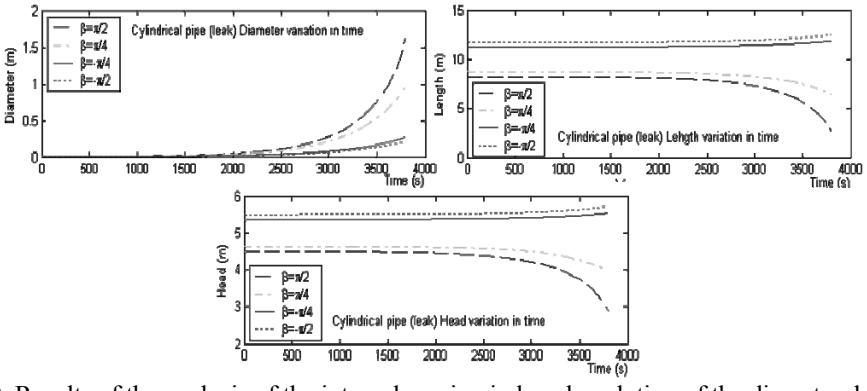

Fig. 9. Results of the analysis of the internal erosion induced evolution of the diameter, length and the head in a initially cylindrical hole tangent to a conduit with different values for β

7. CONCLUSION

The obtained results are shown in **Figure 9**. The extreme values of β are ± 90˚. Analysis with these two values would cover all possible cases. These analyses show clearly that the case in which erosion is most rapid is the case $\beta = 90˚$, and it is the most slow when $\beta = -90˚$.

Using soil detachment quantification law, pipe flow equations and under some simplifying assumptions, a mathematical model for piping erosion is obtained. This model can be written into an analytical radius-time equation in the case of a constant pressure drop. A comparison with some experimental data from a physical model for piping erosion (hole erosion test) was made. This comparison has confirmed the validity of the model.

The theoretical adaptations of the model to study the evolution of a crack or a leak near a conduit by piping erosion, as it was presented, expose some potential applications of such a model. Also, it can be used for the interpretation of the hole erosion test.

9. REFERENCES

[1] ICOLD, 2003. *World register of dams*. International Commission on Large Dams.
[2] ICOLD, 1995. *Dam failures statistical analysis*. International Commission on Large Dams, Bulletin 99.
[3] Fell, R., MacGregor, P., Stapledon, D. & Bell, G. 2005, *Geotechnical engineering of dams*. Balkema, Leiden, 912 p.
[4] Foster, M., Fell, R. & Spannagle, M., 2000. *The statistics of embankment dam failures and accidents*. Canadian Geotechnical Journal, 37(5), pp. 1000-1024.
[5] U.S. Bureau of Reclamation, November 4-6, 2003, Safety Evaluation of Existing Dams Seminar, Technical Service Center.
[6] Monnet, A., 1998. *Boulance, érosion interne, renard. Les instabilités sous écoulement*. Revue Française de Géotechnique 82, pp. 3-10.
[7] Skempton, A.W., and Brogan, J.M., 1994. *Experiments on piping in sandy gravels*. Géotechnique, 44(3), pp. 440-460.
[8] Duboys, M. P., 1879. *Le Rhône et les rivières à lit affouillable*. Annales des Ponts et Chaussées, Séries 5, Vol 18, pp. 141-195.
[9] Nikuradse J., 1933. Stromungsgesetz in rauhren rohren, vDI Forschungshefte 361. (En. translation: *Laws of flow in rough pipes*). Technical report, NACA Technical Memorandum 1292. National Advisory Commission for Aeronautics (1950), Washington, DC.
[10] Boukhemacha M.A., 2009. *A hole erosion test model- A step on internal erosion modeling*. Scientific Journal-Mathematical Modelling in Civil Engineering, 5(3), pp. 17-24.
[11] Wan C.F. and Fell R., 2004. *Laboratory tests on the rate of piping erosion of soils in embankment dams*. Geotechnical Testing Journal, 27(3), pp. 295-303.
[12] Wan, C.F. & Fell, R., 2002. *Investigation of internal erosion and piping of soils in embankment dams by the slot erosion test and the hole erosion test*, UNICIV Report No R-412, The University of New South Wales, Sydney. 325 p.

Ovidius University Annals Series: Civil Engineering Volume 1, Issue12, June 2010

Hydraulic of Free Overfall in Δ-Shaped Channels

Seyed Vahid Nabavi, Syamak Davoudi Nezhad

Abstract **– To measure flow discharge and study the erosion at the brink of free overfalls, the computation of the end depth ratio (EDR) is required in civil engineering practices. This paper presents a theoretical model to predict the pressure head distribution at the brink of free overfalls, in a smooth in Δ-shaped (equilateral triangle-shaped) channel. Based on the momentum equation, the flow upstream of a free overfall is theoretically analyzed to calculate the end-depth-ratio. In sub-critical flows, the EDR related to the critical depth is found to be 0.695 for critical depth-channel height ratio up to 0.6. In super-critical flows, the Manning equation is used to express the end-depth as a function of the upstream Froude number and relative bottom slope (S_0/S_c).of the channel. In super-critical flows, applying the momentum equation based on the Boussinesq approximation another method used to analyze the free overfall in Δ-shaped channel. Methods to estimate discharge from the end-depth in sub-critical and super-critical flows are presented. The discharge is also related to the end-depth and a characteristic parameter of the channel. The computed and experimental results of Dey are in satisfactory agreement in sub-critical flow.**

Keywords **– Brink depth, free overfall, steady flow, sub-critical, super-critical.**

1. INTRODUCTION

Flow at an abrupt end of a long channel is known as free overfall. At the brink or end of a channel, the pressure at the upper and lower of the flow is atmospheric; within the flow at the end section the pressure is no atmospheric. At distance well upstream of the overfall, vertical accelerations are negligible and a hydrostatic pressure distribution can be safely assumed as shown in figure 1. In Fig. 1, a section with critical depth forms the upstream boundary of the control volume for the momentum equation analysis. At the brink section, a unique relationship exists between the end-depth and the critical-depth. The ratio of end depth to the critical depth (EDR) offers a possibility to measure flow discharge. The method based on critical-depth for the computation of flow discharge has a disadvantage, owing to variable location of the critical depth in open channels. In order to overcome the problem associated with locating the position where the flow becomes critical, attempts have been made to relate the end-depth to the critical-depth (EDR), since the end-depth never changes its location and being easy to measure.

Fundamental experimental research was carried out by Rouse to determine the End Depth Ratio (EDR), which was found 0.715 in mildly sloping rectangular channels [1]. In 2002, Dey has written a review of these investigations [2]. Diskin derived an equation of end-depth for a rectangular, triangular, exponential and trapezoidal free overfall using the

Seyed Vahid Nabavi, Faculty member, Islamic Azad University –Khomein Branch, Iran (Corresponding author phone: +98-918-8631769; fax: +98-861-2230230; e-mail: nabavi@cv.iut.ac.ir

Syamak Davoudi Nezhad, Faculty member, Islamic Azad University –Farahan Branch, Iran. e-mail: Syamak_dav@yahoo.com

ISSN-1584-5990

momentum approach with zero end pressure [3]. Smith gave a simple solution of the momentum equation with zero end pressure for a horizontal circular free overfall [4]. He conducted experiments on a horizontal circular free overfall. Rajaratnam and Muralidhar also derived theoretical equations of EDR for exponential channels using the momentum approach. They conducted a large number of experiments to verify the theoretical results [5]. Rajaratnam and Muralidhar applying the momentum approach with zero end pressure have developed generalized theoretical equations for EDR in horizontal and sloping circular channels [6]. Rajaratnam and Muralidhar reexamined the rectangular and trapezoidal free overfall [7, 8]. Ali and Sykes applied the free-vortex approach to calculate the end-depth in rectangular, parabolic, triangular and trapezoidal channels and estimated the EDR value of 0.678 in horizontal rectangular channels [9]. Hager treated two-dimensional free overfall by using the extended energy and momentum equations taking account of the streamline inclination and curvature [10]. Murty Bhallamudi theoretically analyzed free overfall in mildly and steeply sloping exponential channels, using the momentum equation based on the Boussinesq approximation [11]. Dey theoretically analyzed circular free overfall to calculate the EDR, applying the momentum equation based on the Boussinesq approximation [12]. Ferro assumed flow in a rectangular, triangular and trapezoidal overfall to be similar to that over a sharp-crested weir having a crest height equaling zero. The EDR and discharge estimated by Ferro had a good agreement with the experimental observations [13]. Sterling and Knight experimentally studied circular free overfall and estimated EDR equal to 0.743 in horizontal circular channels [14]. Dey presented a simplified approach to estimate the end-depth of a free overfall in horizontal circular channels, where that simulates the flow of a free overfall over a sharp-crested weir [15]. Ahmad applied the theoretical procedure to compute the discharge over a weir, to get EDR in triangular channels [16]. Dey used momentum equation based on the Boussinesq approximation and studied free overfalls in elliptic [17], Δ-shaped [18], circular with flat base [19], inverted semicircular [20], and U-shaped channels [21], respectively. Beirami et al. based on the free vortex theorem and the momentum equation a theoretical model presented to predict the pressure head distribution, the pressure coefficient, the end depth ratio (EDR), and flow discharge at the brink of free overfalls in channels of different cross sections with sub-critical flow [22]. This paper presents an analytical model for a free overfall in smooth Δ-Shaped channel applying a momentum approach. The model yields the EDR and flow discharge in Δ-Shaped channels for sub and super approaching flow. Also based on the Boussinesq approximation and applying momentum equation, another model used to analyze free overfall in super-critical approaching flow, which applied by Dey [18] in sub-critical approaching flow.

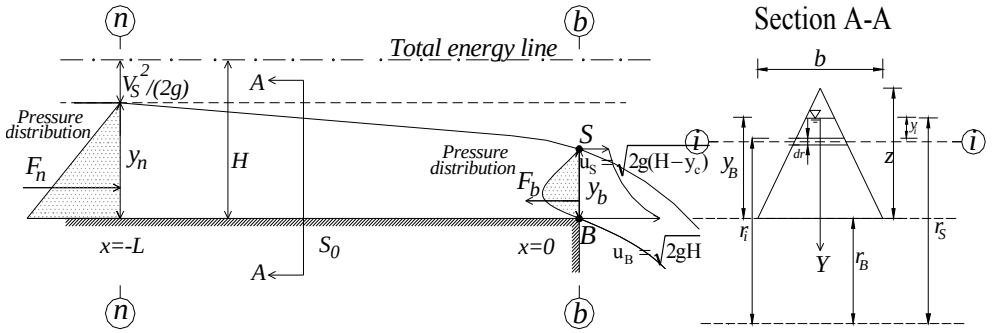

Figure 1: Definition sketch

2. PROPOSED MODEL

Figure 1 shows a free overfall in a prismatic channel of constant bottom slope S_0. A control Volume is considered between the end section (section b-b) and the upstream section (section n-n) where the pressure distribution is hydrostatic. At the end section, the pressure is non-hydrostatic and, the pressure head (h) at any stream tube can be found [24] as

$$h_i=y_i[1-u_i^2/(r_ig)] \quad (1)$$

where g= acceleration of gravity; y_i, u_i and r_i are flow depth, flow velocity and radius of curvature of stream tube i, respectively. Pressure head at the channel bottom of b-b section is

$$h_B=y_B[1-u_B^2/(r_Bg)] \quad (2)$$

where u_B and r_B are the flow velocity and the radius of curvature at the channel bottom of the end-depth. Since h_B is equal to zero, the radius of streamline curvature at the channel bottom (r_B) can be obtained as u_B^2/g.

Same as Ali and Sykes [9], applying the Bernoulli's theorem to the top (index S) and bottom (index B) streamlines in the brink section, the boundary velocities can be estimated as

$$u_S=\sqrt{2g(H-y_n)} \quad (3)$$

$$u_B=\sqrt{2gH} \quad (4)$$

where y_n= upstream depth at section n-n, $H=y_n+\alpha V_n^2/(2g)$ is specified energy at section n-n, and α= energy correction coefficient which is assumed to be unity. Using equation (4), $r_B=2H$ is obtained. Using free-vortex theorem as $u_ir_i=u_Br_B=C$, the radius of curvature at any point of section b-b can be estimated as

$$r_i=\frac{2H\sqrt{2gH}}{\sqrt{2g[H-y_u+(y_i/y_b)y_u]}} \quad (5)$$

If y_b is divided into n parallel streamlines, then for each streamline equation (1) gives the pressure head as

$$h_i=y_i-\frac{y_i[H-y_n+(y_i/y_b)]^{3/2}}{H^{3/2}} \quad (6)$$

In a general case, if $y=y_i$, as shown in Fig. 1, the pressure force at the end section is equal to

$$F_b=\gamma\int_0^{y_b}\left\{y-\frac{y[H-y_n+(y/y_b)y_n]^{3/2}}{H^{3/2}}\right\}dy \quad (7)$$

The above procedure gives the coefficient of pressure distribution as

$$K=F_b/(0.5\gamma y_b^2) \quad (8)$$

At the end section, the pressure is non-hydrostatic (zero pressure at the channel wall) owing to the accelerated down flow and the inclined streamline pattern. A control section is considered between the end section and the far upstream section where the pressure distribution is hydrostatic. Applying the one-dimensional momentum equation between the sections at (n-n) (far upstream section having hydrostatic pressure) and (b-b) for the free overfall having a stream wise bed slope S (Fig. 1), one obtains

$$F_n - F_b - \int \tau dx + W \sin\theta = \rho Q(\beta_b V_b - \beta_n V_n) \quad (9)$$

where γ= specific weight of fluid ($\gamma=\rho g$), F= hydrostatic load, τ= wall and bed frictional stress, W= gravity force of fluid in the control volume, ρ= mass density of fluid, Q= flow discharge, V= mean flow velocity, and β= Boussinesq coefficient, and subscripts n and b refer to sections n-n and b-b, respectively. For simplicity, in this analysis, β is assumed to be unity because it varies from 1.01 to 1.12 in straight channels [23].

For analytical simplicity, a state of pseudo-uniform flow is assumed within the control section, where the wall frictional resistance is compensated by the stream-wise component of gravity force of fluid. Therefore, the difference of pressure force is equal to the rate of change of momentum between the end section and the far upstream section. However, the case of adversely sloping channels, where the wall frictional resistance and the stream wise component of gravity force add to a substantial effect, is beyond this study. In Sub-critical flows, an error of around 1% in estimation of the EDR is obtained due to exclusion of the wall frictional resistance [24].

$$F_n\text{-}F_b=\rho Q(V_b\text{-}V_n) \quad (10)$$

Introducing $F_n=\gamma(A\hat{y})_n$ and $F_b=\gamma(A\hat{y})_b$ in equation (10), one gets

$$\gamma(A\hat{y})_n\text{-}\gamma k(A\hat{y})_b=\rho Q(V_b\text{-}V_n) \quad (11)$$

Where $\hat{y}$= center of area of a cross section below the flow surface. Using V=Q/A and $\gamma=\rho g$, the Eq. (11) can be simplified,

$$(A\hat{y})_n\text{-}K(A\hat{y})_b=(Q^2/g)(1/A_b\text{-}1/A_n) \quad (12)$$

In the critical section, the flow discharge can be computed as

$$Q^2=Fr_0^2 g A_n^3/T_n=g A_c^3/T_c \quad (13)$$

Substituting Q from Eq. (13) into Eq. (12), one gets

$$(A\hat{y})_n\text{-}K(A\hat{y})_b=(Fr_0^2 A_n^3/T_n)(1/A_b\text{-}1/A_n) \quad (14)$$

In which Fr_0=upstream Froude number and A, $\hat{y}$ and T define as below,

$$A=z^2(2\text{-}\lambda)\lambda/3^{0.5} \quad (15)$$

$$\hat{y}=(3\lambda\text{–}\lambda 2)z/(6\text{-}3\lambda) \quad (16)$$

$$T=2z(1-\lambda)/3^{0.5} \quad (17)$$

where $\lambda=y/z$, b= wide of the channel and z= height of the channel, which is given by

$$z=(3^{0.5}/2)b \quad (18)$$

Inserting equation (15), (16) and (17) into Eq. (14) yields,

$$\frac{(3-\lambda_n)^2}{2-\lambda_n}-k\left(\frac{\lambda_b}{\lambda_n}\right)^2\frac{(3-\lambda_b)^2}{2-\lambda_b}=\frac{3F_0(2-\lambda_n)^2}{2(1-\lambda_n)}\left[\frac{\lambda_n(2-\lambda_n)}{\lambda_b(2-\lambda_b)}-1\right] \quad (19)$$

3. THE EDR

The EDR, which is the ratio of end depth (y_b) to critical depth (y_c), is computed for a Δ-shaped channel using the preceding equations.

3.1 Sub-critical Flow

When the stream wise slope of the channel is horizontal or mild, critical flow ($Fr_0=1$ and $y_n=y_c$) results upstream of the control section. Introducing $Fr_0=1$ and $\lambda_n=\lambda_c$ in Eq. (19), one gets

$$\frac{(3-\lambda_c)^2}{2-\lambda_c}-k\left(\frac{\lambda_b}{\lambda_c}\right)^2\frac{(3-\lambda_b)^2}{2-\lambda_b}=\frac{3}{2}\frac{(2-\lambda_c)^2}{1-\lambda_c}\left[\frac{\lambda_c(2-\lambda_c)}{\lambda_b(2-\lambda_b)}-1\right] \quad (20)$$

where index c refers to the critical state of flow. Equation (20) is an implicit equation being solved numerically. The EDR is calculated from the following equation:

$$EDR=y_b/y_c \quad (21)$$

The variation of EDR with $\lambda_c=y_c/z$ is shown in Fig. 2(a). Eq. (21) produces a singular condition at $\lambda_c=0$. The curve obtained from the present study has a satisfactory agreement with the experimental data. The value of EDR is around 0.695 up to $\lambda_c=0.6$, and then rises sharply from $\lambda_c=0.8$ to EDR=1 as λ_c approaches one.

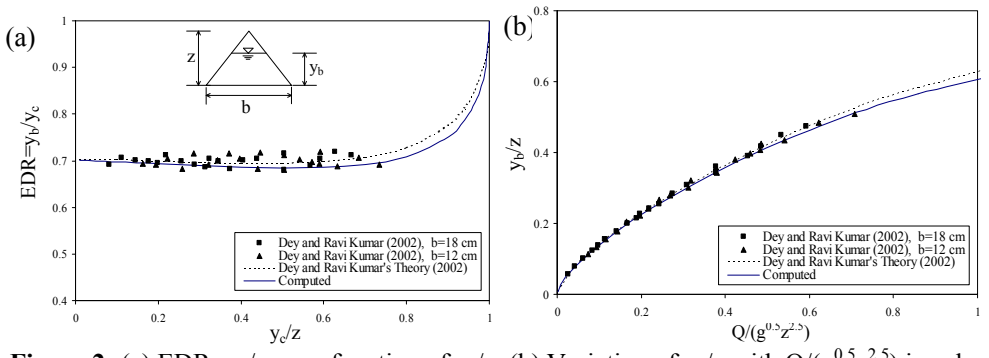

Figure 2: (a) EDR=y_b/y_c as a function of y_c/z; (b) Variation of y_b/z with $Q/(g^{0.5}z^{2.5})$ in sub-critical flow

3.2 Super-critical Flow

In super-critical flows, y_b depends on Fr_0, which is a function of channel slope S. The functional relationship of y_b is

$$y_b=y_b\,(y_c, S) \tag{22}$$

The upstream Froude number Fr_0 in Eq. (13) is divided by the critical Froude number to obtain

$$Fr_0 = \left[\frac{2-\lambda_c}{2-\lambda_n}\right]^{3/2}\left[\frac{\lambda_c}{\lambda_n}\right]^{3/2}\left[\frac{1-\lambda_n}{1-\lambda_C}\right]^{1/2} \tag{23}$$

The Manning equation of uniform flow is divided by that of critical flow resulting in

$$Fr_0 = (S_0/S_c)^{1/2}(T_n/T_c)^{1/2}(A_n/A_c)^{1/6}(P_c/P_n)^{2/3} \tag{24}$$

Equating Eqs. (23) and (24), one gets

$$(S_0/S_c)^{1/2} = [(2-\lambda_c)/(Y(2-\lambda_n))]^{5/3}[(1+2\lambda_n)/(1+2\lambda_c)]^{2/3} \tag{25}$$

Where $Y=y_n/y_c$. Eq. (25) is solved numerically to evaluate λ_n for given values of λ_c and S_0/S_c. Subsequently, Fr_0 is evaluated from Eq. (24). Again, numerical technique is adopted to solve Eq. (19) for λ_b. The EDR is, therefore, predicted from Eq. (21). Fig. 3(a) shows the dependency of EDR on S_0/S_c for different λ_c.

4. DISCHARGE

A free overfall in an inverted triangular channel may be utilized to estimate discharge using the end-depth. The generalized equation of discharge obtained from Eq. (13) is

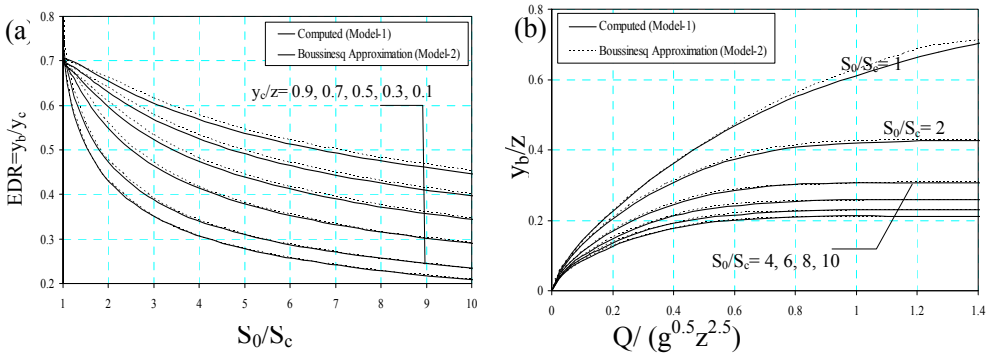

Figure 3: (a) dependency of $EDR=y_b/y_c$ on S_0/S_c for different y_c/z and (b) Variation of y_b/z with $Q/(g^{0.5}z^{2.5})$ for different S_0/S_c in super-critical flow

$$\frac{Q}{g^{1/2}z^{5/2}} = \frac{Fr_0}{\sqrt{6}}\frac{[\lambda_n(2-\lambda_n)]^{3/2}}{(1-\lambda_n)^{1/2}} \tag{26}$$

4.1. Sub-critical Flow

Introducing $Fr_0=1$ and $\lambda_n=\lambda_c$ in Eq. (26), the equation of discharge for sub-critical flows is

$$\frac{Q}{g^{1/2}z^{5/2}}=\frac{1}{\sqrt{6}}\frac{[\lambda_c(2-\lambda_c)]^{3/2}}{(1-\lambda_c)^{1/2}} \tag{27}$$

Eq. (20) is solved and subsequently $Q/(g^{0.5}z^{2.5})$ is computed from Eq. (27). The relationship between λ_b and $Q/(g^{0.5}z^{2.5})$ is shown in Fig. 2(b). The computed curve agrees well with the experimental data.

4.2. Super-critical Flow

In super-critical flows, Q depends on y_b and Fr_0. As Fr_0 is a function of S, the functional relationship of Q can be written as

$$Q=Q(y_b, S) \tag{28}$$

Equations (19), (21), (24), and (25) are solved numerically for Fr_0 and λ_n for given values of λ_b and S_0/S_c. Subsequently, Eq. (26) is used to compute $Q/(g^{0.5}z^{2.5})$. The variation of $Q/(g^{0.5}z^{2.5})$ with λ_b for different S_0/S_c is shown in Fig. 3(b).

5. SUPER-CRITICAL FLOW (MODEL 2- BOUSSINESQ APPROXIMATION)

According to momentum equation based on the Boussinesq approximation, Dey [18] presents the following equation and solved it for sub critical approaching flow ($Fr_0=1$ and $\lambda_n=\lambda_c$). In order to compare proposed method (Model-1) for super critical flow, equation (29) solved.

$$\lambda_n^2\left[1-\frac{\lambda_n}{3}\right]-\lambda_b^2\left[1-\frac{\lambda_b}{3}\right]+\frac{\lambda_b^2}{2}\left[\frac{4}{3}-\frac{\lambda_b}{2}\right]=\frac{F_0^2}{2}\frac{(2-\lambda_n)^3\lambda_n^3}{1-\lambda_n}\left[\frac{1}{\lambda_b(2-\lambda_b)}-\frac{1}{\lambda_n(2-\lambda_n)}\right] \tag{29}$$

In super critical approaching flow, the equations that obtained based on Boussinesq approximation was similar to Model-1; the only different between these two models is usage of equation (29) in Model-2 instead of equation (19) in Model-1. This model (Model-2) eliminates the need of coefficient of pressure distribution (K).

6. RESULTS

6.1 Sub-critical flow:

The dependence of EDR on $\lambda_c=y_c/z$ is shown in figure 2(a). The EDR varies almost linearly from 0.701 to 0.686 up to $y_c/z=0.60$ and the curve rises sharply from $y_c/z=0.80$. The curve obtained from this model corresponds closely to the experimental data of Dey and Ravi Kumar [18] with an accuracy of ±5%. Also, the computed curve agrees well with Dey and Ravi Kumar's theory. The variations of EDR with $Q/(g^{0.5}z^{2.5})$ presented in figure

2(b). The experimental data of Dey and Ravi Kumar are agreeable with the curve obtained from the present model with an accuracy of ±5%.

In addition, the computed curve agrees well with Dey and Ravi Kumar's theory. Figure 2(b) can be used to estimate the flow discharge from measured end-depth.

6.2. Super-critical flow:

Nobody has studied, in Δ-shaped channel and for super critical approaching flow yet, so in order to compare the proposed method, the momentum equation based on the Boussinesq approximation (Model-2, which used by Dey [18] in sub critical flow) used and obtained the curves.

Figure 3(a) show the variation of EDR with S_0/S_c for different $\lambda_c=y_c/z$ and the variation of $\lambda_b=y_b/z$ with $Q/(g^{0.5}z^{2.5})$ for different S_0/S_c shown in figure 3(b). According to figures when S_0/S_c increases the amount of EDR decrease, also between the curves obtained from the proposed model (Model-1) and momentum equation based on the Boussinesq approximation (Model-2) has a good agreement. So that obtained curves for both the models are to some extent conformity.

In order to estimate flow discharge in super critical flow the dependency of y_b/y_n on y_n/y_c obtained and show in fig. 4, in Δ-shaped channel when y_b & y_n are known and with uses the curve in fig. 4, critical depth (y_c) obtained and with replacing this value in equation (13) flow discharge determine. It must be noted that this curve use when $y_c/z<0.6$.

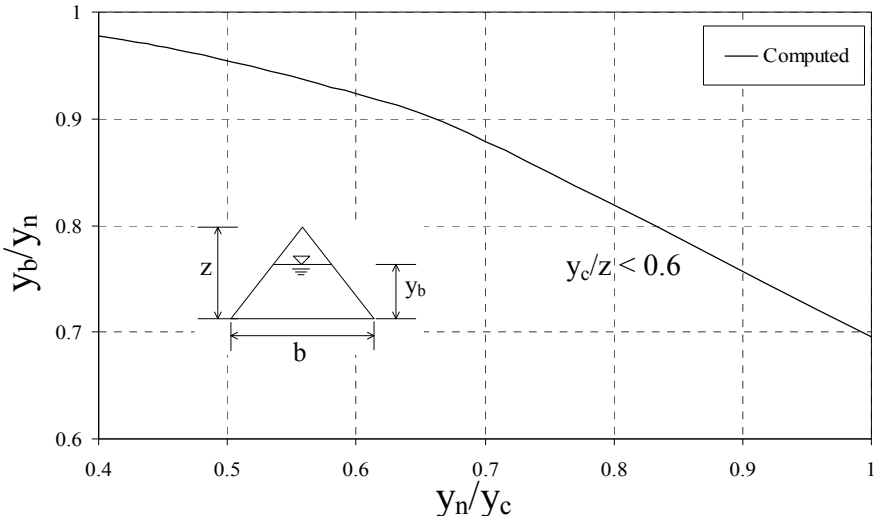

Figure 4: Variation of y_b/y_n with y_n/y_c in super-critical flow

7. CONCLUSIONS

Based on the free vortex theorem the pressure distributions at the brink depth and end-pressure coefficient (K) of the free overfall in sub-critical and super-critical approaching flow have been theoretically estimated. Using the momentum equation, the end depth ratio (EDR) is obtained. For design purposes, charts have been constructed to facilitate the prediction of flow discharge when end-depth is known. In sub-critical approaching flows, The EDR is varying almost linearly from 0.701 to 0.686 for a critical

depth-channel height ratio up to 0.6, whereas in super-critical flows, the end-depth has been expressed as a function of the stream wise bed slope using the Manning equation. In super-critical flows, applying the momentum equation based on the Boussinesq approximation another method used, to analyze the free overfall and compare with first model. The proposed method has been verified with experimental and theoretical results of Dey and Ravi Kumar [18]. The results showed that the experimental and theoretical results are satisfactory for sub and super-critical flows.

8. REFERENCES

[1] Rouse H. "Discharge characteristics of the free overfall", Civ. Eng., ASCE, Vol. 6, No. 4, 1936, pp. 257–260.
[2] Dey S. "Free overfall in open channels: State-of-the-art review", Flow Meas. and Instrum., Vol. 13, 2002, pp. 247–264.
[3] Diskin M.H. "The end depth at a drop in trapezoidal channels", J. Hydraul. Div., ASCE, Vol. 87, No. 4, 1961, pp. 11–32.
[4] Smith C.D. "Brink depth for a circular channel", J. Hydraul. Div., ASCE, Vol. 88, No.6, 1962, pp. 125–134.
[5] Rajaratnam N., Muralidhar D. "End depth for exponential channels", J. Irrig. Hydral. Div., ASCE, Vol. 90, No. 1, 1964, pp. 17–36.
[6] Rajaratnam N., Muralidhar D. "End depth for circular channels", J. Hydraul. Div., ASCE, Vol. 90, No. 2, 1964, pp. 99–119.
[7] Rajaratnam N., and Muralidhar D. "Characteristics of rectangular free overfall", J. Hydraul. Res., Vol. 6, No. 3, 1968, pp. 233–258.
[8] Rajaratnam N., and Muralidhar D. "The trapezoidal free overfall", J. Hydraul. Res., Vol. 8, No. 4, 1970, pp. 419–447.
[9] Ali K.H.M., and Sykes A. "Free-vortex theory applied to free overfall", J. Hydraul. Div., ASCE, Vol. 98, No. 5, 1972, pp. 973–979.
[10] Hager W.H. "Hydraulics of the plane overfall", J. Hydraul. Eng., ASCE, Vol. 109, No. 2, 1983, pp. 1683–1697.
[11] Murty Bhallamudi S. "End depth in trapezoidal and exponential channels", J. Hydraul. Res., Vol.32, No. 2, 1994, pp. 219–232.
[12] Dey S. "End depth in circular channels", J. Hydraul. Eng., ASCE, Vol. 124, No. 8, 1998, pp. 856–863.
[13] Ferro V. "Theoretical end-depth-discharge relationships for free overfall", J. Irrig. Drain. Eng., ASCE, Vol. 125, No. 1, 1999, pp. 40–44.
[14] Sterling M., Knight. D.W. "The free overfall as a flow measuring device in a circular channel", Proc. Inst. Civ. Eng., Waters Maritime Energ., Vol. 148, No. Dec., 2001, pp. 235–243.
[15] Dey S. "EDR in circular channels", J. Irrig. Drain. Eng., ASCE, Vol. 127, No. 2, 2001, pp. 110–112.
[16] Ahmad Z. "Free overfall as measuring device in triangular channels", Conf. of hydr.,Water resources and ocean engineering, 2002, pp. 115–119.
[17] Dey. S. "Flow metering by end-depth method in elliptic channels", Dam Eng., Vol. 12, No. 1, 2001, pp. 5–19.
[18] Dey S., Ravi Kumar B. "Hydraulics of free overfall in Δ-shaped channels", Sadhana Proc. Indian Acad. Sci., Vol. 27(June), 2002, pp. 353-363.
[19] Dey S. "Free overfall in circular channels with flat base: A method of open channel flow measurement", Flow Meas. and Instrum., Vol. 13, 2002, pp. 209-221.

[20] Dey S. "Free overfall in inverted semicircular channels", J. Hydraul. Eng., ASCE, Vol. 129, No. 6, 2003, pp. 438–447.
[21] Dey S. "Overfall in U-Shaped Channels", J. Eng. Mech., ASCE, Vol. 129, No. 3, 2003, pp. 358–362.
[22] Beirami M.K., Nabavi S.V., and Chamani M.R. "Free overfall in channels with different cross sections and sub-critical flow", Iranian Journal of Science and Technology, Vol. 30, No. B1, 2006, pp. 97–105.
[23] Chow V.T. "Open Channel Hydraulics", Mc Graw Hill, New York, 1959.
[24] Henderson F.M. "Open Channel Flow", Macmillan Book Company, 1966

Ovidius University Annals Series: Civil Engineering Volume 1, Issue12, June 2010

Free Overfall in Inverted Semicircular Channels

Syamak Davoudi Nezhad, Seyed Vahid Nabavi

***Abstract* – A free overfall at the end of an open channel provides a simple means for measuring flow discharge. This paper presents a theoretical model to predict the pressure head distribution at the brink of free overfalls, in horizontal or mildly sloping inverted semicircular channels. Based on the momentum equation, the flow upstream of a free overfall is theoretically analyzed to calculate the End-Depth-Ratio (EDR). The EDR, related to the critical depth, is around 0.7 for a critical depth–diameter ratio up to 0.4. Methods to estimate discharge from the end-depth in sub-critical approaching flows are presented. The computed results agree satisfactorily with the computed and experimental results of Dey.**

***Keywords* – Brink depth, free overfall, sub-critical, semicircular channels.**

1. INTRODUCTION

If the flow at an abrupt end of a long channel is not submerged by the tailwater, it can be referred to as a free overfall. In channels with mild slopes, the approaching flow is sub-critical (Fig. 1). At the upstream control section with a critical depth y_c, vertical accelerations are negligible and a hydrostatic pressure distribution can be safely assumed. At the brink section with depth y_b, the pressure distribution is no longer hydrostatic, both due to the curvature of the flow and the aeration of the under nappe. Since there is a unique relationship between the critical depth and flow discharge, the ratio of the end-depth to the critical depth (EDR) offers a possibility to predict the flow discharge and study erosion at the brink of a free overfall. For steep slopes, where the approaching flow is super-critical, flow discharge is a function of end-depth, channel slope, and channel roughness.

Especially, it is useful to measure flow discharge in channels having covers (sewer, duct, tunnel etc.), where the commonly used weir method is not so effective due to their shapes. Rouse [1], being the first to investigate the problem experimentally, put forward a relationship termed end-depth-ratio (EDR = end depth/ critical depth), which was found to be 0.715 in mildly sloping rectangular channels. Since then numerous studies on free overfall in various channels were reported. Dey put forward a comprehensive state-of-the-art review of researches on free overfall [2]. Other researchers have conducted a large number of experiments and given different theoretical approaches for a single or a few number of channels [3] to [24].

Smith gave a simple solution of the momentum equation with zero end pressure for a horizontal circular free overfall [3]. He conducted experiments on a horizontal circular free overfall. Rajaratnam and Muralidhar explored circular overfalls by developing a theoretical model based on the momentum equation and conducting experiments [4]. Numerical

Syamak Davoudi Nezhad, Faculty member, Islamic Azad University –Farahan Branch. (E-mail: Sdavodinejad@iau-farahan.ac.ir).

Seyed Vahid Nabavi, Faculty member, Islamic Azad University –Khomain Branch, Iran (Corresponding author phone: +98-918-8631769; fax: +98-861-2230230; E-mail: nabavi@cv.iut.ac.ir).

ISSN-1584-5990

solutions using potential flow theory were presented by Montes [5], whereas analytical solutions for circular overfalls were given by Dey based on the momentum equation and the simulation of a free overfall with a sharp-crested weir, respectively [6, 7]. The modified energy equation based on the Boussinesq approximation was used by Anderson to determine the EDR for the rectangular overfall [8]. Ali and Sykes applied the free-vortex approach to calculate the end-depth in rectangular, parabolic, triangular and trapezoidal channels and estimated the EDR value of 0.678 in horizontal rectangular channels [9]. Considering the streamline inclination and curvature, the solutions of momentum and extended energy equations were put forward by Hager [10]. The theory of direct fluid sheet was applied by Naghdi and Rubin to develop an exact solution of the associated nonlinear equations [11]. Another analytical approach, termed cnoidal wave theory, was reported by Marchi to solve the two-dimensional free overfall [12]. Also, the end-depths in trapezoidal and exponential channels were analytically determined by Murty Bhallamudi using the momentum approach based on the Boussinesq approximation [13]. Sterling and Knight experimentally studied circular free overfall and estimated EDR equal to 0.742 in horizontal circular channels [14]. Ahmad applied the theoretical procedure to compute the discharge over a weir, to get EDR in triangular channels [15]. Dey used momentum equation based on the Boussinesq approximation and studied free overfalls in elliptic [16], Δ-shaped [17], circular with flat base [18], inverted semicircular [19], and U-shaped channels [20], respectively. Beirami et al. based on the free vortex theorem and the momentum equation a theoretical model presented to predict the pressure head distribution, the pressure coefficient, the end depth ratio (EDR), and flow discharge at the brink of free overfalls in channels of different cross sections with sub-critical flow [21].

In this paper, a general theoretical model to predict the EDR and flow discharge in inverted semicircular channels with approaching sub-critical flow is presented, which are verified experimentally.

However, little attempt has so far been made to analyze the free overfall in inverted semicircular channels. Though that section is not common, inverted semicircular tunnels or sewers are found in some places of India. Furthermore, the horseshoe shaped sewers that are common in practice, have an almost similar shape of inverted semicircular channels. This analysis is done for the sub-critical approaching flow condition. Since the supercritical approaching flow is not so common in practice, it is beyond this study.

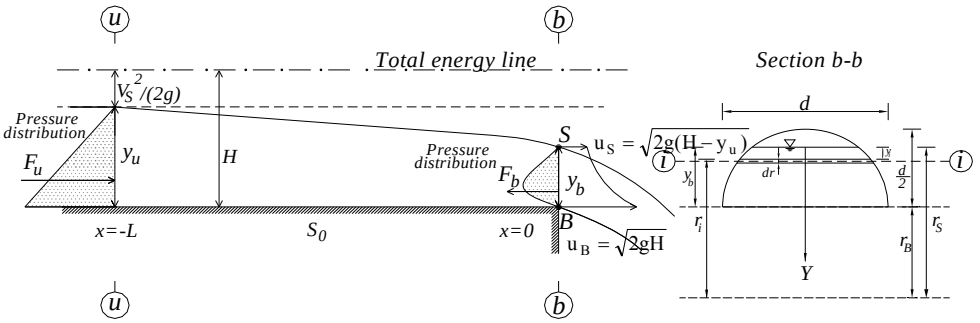

Figure 1: Definition sketch

2. PROPOSED MODEL

Figure 1 shows a free overfall in a prismatic channel of constant bottom slope S_0. At the end section, the approximate centrifugal pressure head at any streamtube can be

computed by Newton's law of acceleration as $y_i u_i^2/(r_i g)$ [22]. Therefore, the pressure head at any streamtube (h_i) can be estimated as

$$h_i=y_i[1-u_i^2/(r_i g)] \quad (1)$$

where g= acceleration of gravity; y_i, u_i and r_i are flow depth, flow velocity and radius of curvature of stream tube i, respectively. The pressure head at the channel bottom of b-b section is

$$h_B=y_B[1-u_B^2/(r_B g)] \quad (2)$$

where u_B and r_B are the flow velocity and the radius of curvature at the channel bottom of the end-depth. Since h_B is equal to zero, the radius of streamline curvature at the channel bottom (r_B) can be obtained as u_B^2/g.

The same as Ali and Sykes [9], applying the Bernoulli's theorem to the top (index S) and bottom (index B) streamlines in the brink section, the boundary velocities can be estimated as

$$u_S = \sqrt{2g(H - y_u)} \quad (3)$$

$$u_B = \sqrt{2gH} \quad (4)$$

where y_u= upstream depth at section u-u, $H = y_u+\alpha V_u^2/(2g)$ is specified energy at section u-u, α= energy correction coefficient which is assumed to be unity. Equation (4) gives $r_B=2H$.

Using free-vortex theorem as $u_i r_i=u_B r_B=C$, the radius of curvature at any point of section b-b can be founds as

$$r_i = \frac{2H\sqrt{2gH}}{\sqrt{2g[H - y_u + (y_i / y_b)y_u]}} \quad (5)$$

If y_b is divided into n parallel streamlines, then for each streamline Eq. (1) gives the pressure head as

$$h_i = y_i - \frac{y_i[H - y_u + (y_i/y_b)]^{3/2}}{H^{3/2}} \quad (6)$$

In a general case, if $y=y_i$, as shown in Fig. 1, the pressure force at the end section is equal to

$$F_b = \gamma \int_0^{y_b} \left\{ y - \frac{y[H - y_u + (y/y_b)y_u]^{3/2}}{H^{3/2}} \right\} dy \quad (7)$$

The above procedure gives the coefficient of pressure distribution as

$$K = F_b /(0.5\gamma y_b^2) \quad (8)$$

In which, based on the computer program the coefficient of pressure distribution (K) are between 0.3033 and zero in the range of $0<y_c/d<0.5$ from the above procedure, for sub-critical flow.

Applying the momentum equation to the control volume between sections u-u and b-b in Fig. 1, yields

$$F_u - F_b - \int \tau dx + W\sin\theta = \rho Q(\beta_b V_b - \beta_u V_u) \tag{9}$$

where γ= specific weight of fluid, F= hydrostatic load, τ= wall and bed shear stress, W= gravity force of fluid in the control volume, ρ= mass density of fluid, Q= flow discharge, V= mean flow velocity, and β= Boussinesq coefficient, and subscripts u and b refer to sections u-u and b-b, respectively. For simplicity, in this analysis, β is assumed to be unity.

For analytical simplicity, a state of pseudo-uniform flow is assumed within the control volume, where wall and shear stresses are compensated by the stream-wise component of gravity force of fluid. In sub-critical flows, an error of about 1% in estimation of the EDR due to the exclusion of wall and bed shear stresses is obtained [23]. Rajaratnam and Muralidhar [24] have shown that this error is about 3% in horizontal and mildly sloping channels. However, in sub-critical flow for low flow rates, the distance between sections u-u and b-b is of the order of (3~4) y_c [22, 23], and as such is sufficiently small for this assumption to be accurate for a first order approximation. Using the above assumptions, Eq. (9) can be simplified as

$$F_u-F_b=\rho Q(V_b-V_u) \tag{10}$$

Introducing $F_n=\gamma(A\,\bar{y})_u$ and $F_b=\gamma(A\,\bar{y})_b$ in equation (10), one gets

$$\gamma(A\,\bar{y})_u-\gamma K(A\,\bar{y})_b=\rho Q(V_b-V_u) \tag{11}$$

Where $\bar{y}$ = center of area of a cross section below the flow surface. Using V=Q/A and $\gamma=\rho g$, the equation (11) can be simplified as

$$(A\,\bar{y})_n-K(A\,\bar{y})_b=(Q^2/g)(1/A_b-1/A_u) \tag{12}$$

In the critical section, the flow discharge can be computed as

$$Q^2=F_0^2 g A_u^3/T_u \tag{13}$$

Substituting Q from Eq. (13) into Eq. (12), one gets

$$(A\,\bar{y})_u-K(A\,\bar{y})_b=(F_0^2 A_u^3/T_u)(1/A_b-1/A_u) \tag{14}$$

In which F_0=upstream Froude number and A, $\bar{y}$ and T define as below,

$$A=0.25d^2\psi(\hat{y}) \tag{15}$$

$$\bar{y}=\left[\hat{y}-\frac{1-(1-4\hat{y}^2)^{1.5}}{3\psi(\hat{y})}\right]d \tag{16}$$

$$T=d(1-4\hat{y}^2)^{0.5} \tag{17}$$

where $\hat{y}=y/d$, and

$$\psi(\hat{y})=\arcsin(2\hat{y})+2\hat{y}(1-4\hat{y}^2)^{0.5} \quad (18)$$

Inserting equation (15), (16), (17) and (18) into Eq. (14) yields,

$$3\hat{y}_u\psi(\hat{y}_u)-[1-(1-4\hat{y}_u^2)^{1.5}]-3K\hat{y}_b\psi(\hat{y}_b)-K[1-(1-4\hat{y}_b^2)^{1.5}]=\frac{3F_0^2\psi^2(\hat{y}_u)}{4(1-\hat{y}_u^2)^{1.5}}\left[\frac{\psi(\hat{y}_u)}{\psi(\hat{y}_b)}-1\right] \quad (19)$$

Where

$$F_0=8Q^*(1-4\hat{y}^2_u)^{0.25}/\psi^{1.5}(\hat{y}_u) \quad (20\text{-a})$$

$$Q^*=Q/(g^{0.5}d^{2.5}) \quad (20\text{-b})$$

3. THE EDR

When the stream wise slope of the channel is horizontal or mild, critical flow (F_0=1 and y_u=y_c) results upstream of the control section. Introducing F_0=1 and $\hat{y}_u$= $\hat{y}_c$ in Eq. (19), one gets

$$3\hat{y}_c\psi(\hat{y}_c)-[1-(1-4\hat{y}_c^2)^{1.5}]-3K\hat{y}_b\psi(\hat{y}_b)-K[1-(1-4\hat{y}_b^2)^{1.5}]=\frac{3\psi^2(\hat{y}_c)}{4(1-\hat{y}_c^2)^{1.5}}\left[\frac{\psi(\hat{y}_c)}{\psi(\hat{y}_b)}-1\right] \quad (21)$$

where index c refers to the critical state of flow. Eq. (21) is an implicit equation being solved numerically. The EDR is calculated from the following equation:

$$EDR=y_b/y_c \quad (22)$$

The variation of EDR with $\hat{y}_c$ is shown in Fig. 2. The value of EDR is around 0.7 up to $\hat{y}_c$=0.4, and then rises sharply from $\hat{y}_c$=0.45 and EDR approaches 1 as $\hat{y}_c$ approaches one. The curve obtained from the present study has a satisfactory agreement with the theoretical results and experimental data of Dey [19]. The value of EDR base on the Sterling and Knight's work [13] is about 0.742, which slightly overestimates the EDR from the proposed model.

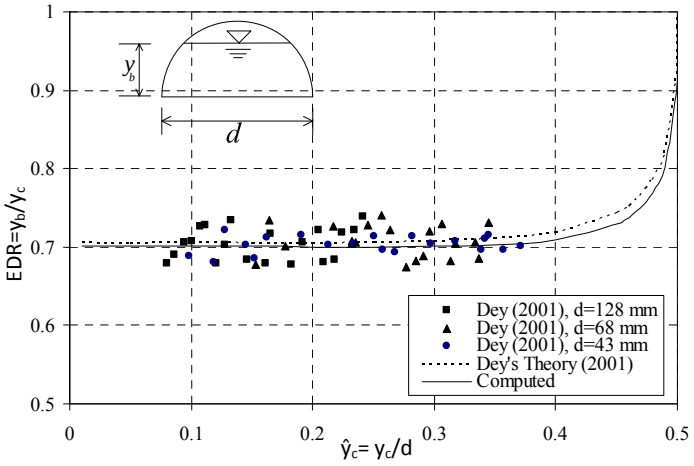

Figure 2: Variation of EDR=y_b/y_c with $\hat{y}_c$= y_c/d

4. DISCHARGE

The concept of free overfall from inverted semicircular channels is utilized to estimate the discharge using a known end depth. The generalized equation of discharge obtained from Eq. (20-a). Introducing $F_0=1$ and $\hat{y}_u=\hat{y}_c$ in Eq. (20-a), one gets

$$Q^*=\psi^{1.5}(\hat{y}_c)/[8(1-4\hat{y}^2_c)^{0.25}] \quad (23)$$

Eq. (21) is solved and subsequently non-dimensional discharge Q^* is computed from Eq. (23).

The variation between $\hat{y}_b$ and Q^* is shown in Fig. 3, which are useful to estimate the flow discharge from measured end-depth.

The experimental data and theoretical result of Dey [19] are agreeable with the curve obtained from the present model with an accuracy of ±5%.

The presented model can be used for the super-critical flow. In this case, using Manning's equation and a control volume between the brink and uniform flow sections, flow discharges as a function of the end-depth and channel slope can be estimated.

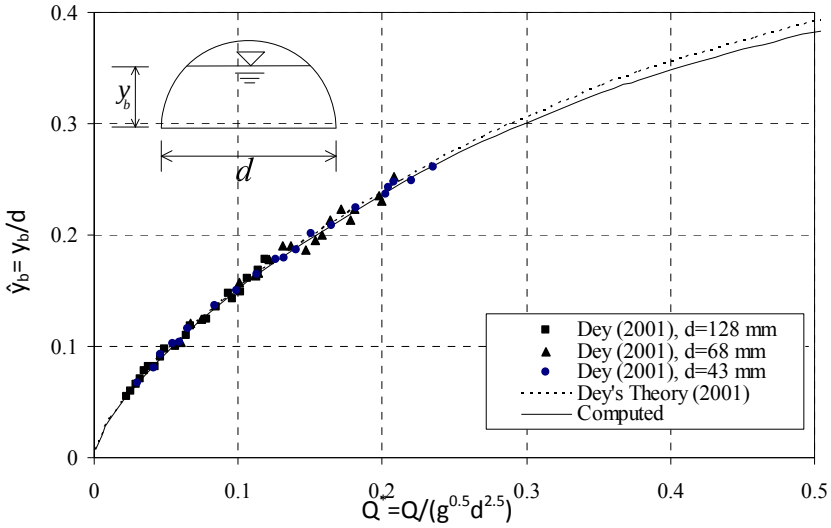

Figure 3: Variation of $\hat{y}_b= y_b/d$ with $Q^*=Q/(g^{0.5}d^{2.5})$

5. APPLICATIONS

The interest of investigators lies in the free overfall owing to a simple means of the flow discharge measurements in open channels. Especially, the end-depth method is very effective to measure flow discharge in channels having covers (sewer, duct, tunnel, etc.), where the most commonly used weir method is not so effective due to their shapes. Therefore an easy to use model like this is attractive. As the computational results are presented in normalized form, their direct application is possible in prototype. For example, Fig. 2 can be utilized to obtain end-depth, and the discharge can be estimated from Fig. 3 using the known end-depth.

6. CONCLUSIONS

Based on the free vortex theorem the pressure distributions at the brink depth and end-pressure coefficient (K) of the free overfall in sub-critical approaching flow have been theoretically estimated. Using the momentum equation, the end depth ratio (EDR) is obtained. For design purposes, charts have been constructed to facilitate the prediction of flow discharge when end-depth is known. In sub-critical approaching flows, The EDR related to the critical depth found to be around 0.7 up to $\hat{y}_c$=0.4. The proposed model has been verified with experimental and theoretical results of Dey [19]. The results showed that the experimental and theoretical results are satisfactory for sub-critical flows. This model is not applicable to an adversely sloping or rough channel.

7. REFERENCES

[1] Rouse H. "Discharge characteristics of the free overfall", Civ. Eng., ASCE, Vol. 6, No. 4, 1936, pp. 257–260.
[2] Dey S. "Free overfall in open channels: State-of-the-art review", Flow Meas. and Instrum., Vol. 13, 2002, pp. 247–264.
[3] Smith C.D. "Brink depth for a circular channel", J. Hydraul. Div., ASCE, Vol. 88, No.6, 1962, pp. 125–134.
[4] Rajaratnam N., Muralidhar D. "End depth for circular channels", J. Hydraul. Div., ASCE, Vol. 90, No. 2, 1964, pp. 99–119.
[5] Montes J.S. "A potential flow solution for the free overfall", Proc. Inst. Civ. Eng., Wates, Maritime Eng, Vol. 92(Dec.), 1992, pp. 259–266.
[6] Dey S. "End depth in circular channels", J. Hydraul. Eng., ASCE, Vol. 124, No. 8, 1998, pp. 856–863.
[7] Dey S. "EDR in circular channels", J. Irrig. Drain. Eng., ASCE, Vol. 127, No. 2, 2001, pp. 110–112.
[8] Anderson M.V. "Non-uniform flow in front of a free overfall", Acta Polytech. Scand., Civ. Eng. Constr. Ser., Vol. 42, 1967, pp. 1–24.
[9] Ali K.H.M., and Sykes A. "Free-vortex theory applied to free overfall", J. Hydraul. Div., ASCE, Vol. 98, No. 5, 1972, pp. 973–979.
[10] Hager W.H. "Hydraulics of the plane overfall", J. Hydraul. Eng., ASCE, Vol. 109, No. 2, 1983, pp. 1683–1697.
[11] Naghdi P.M., and Rubin, M.B. "On inviscid flow in a waterfall", J. Fluid Mech, Vol. 103, 1981, pp. 375–387.
[12] Marchi E. "On the free overfall", J. Hydraul. Res., ASCE, Vol. 31, No. 6, 1993, pp. 777–790.
[13] Murty Bhallamudi S. "End depth in trapezoidal and exponential channels", J. Hydraul. Res., Vol.32, No. 2, 1994, pp. 219–232.
[14] Sterling M., Knight. D.W. "The free overfall as a flow measuring device in a circular channel", Proc. Inst. Civ. Eng., Waters Maritime Energ., Vol. 148, No. Dec., 2001, pp. 235–243.
[15] Ahmad Z. "Free overfall as measuring device in triangular channels", Conf. of hydr., Water resources and ocean engineering, 2002, pp. 115–119.
[16] Dey. S. "Flow metering by end-depth method in elliptic channels", Dam Eng., Vol. 12, No. 1, 2001, pp. 5–19.
[17] Dey S., Ravi Kumar B. "Hydraulics of free overfall in Δ-shaped channels", Sadhana Proc. Indian Acad. Sci., Vol. 27, No. June, 2002, pp. 353-363.

[18] Dey S. "Free overfall in circular channels with flat base: A method of open channel flow measurement", Flow Meas. and Instrum., Vol. 13, 2002, pp. 209-221.
[19] Dey S. "Free overfall in inverted semicircular channels", J. Hydraul. Eng., ASCE, Vol. 129, No. 6, 2003, pp. 438–447.
[20] Dey S. "Overfall in U-Shaped Channels", J. Eng. Mech., ASCE, Vol. 129, No. 3, 2003, pp. 358–362.
[21] Beirami M.K., Nabavi S.V., and Chamani M.R. "Free overfall in channels with different cross sections and sub-critical flow", Iranian Journal of Science and Technology, Vol. 30, No. B1, 2006, pp. 97–105.
[22] Chow V.T. "Open Channel Hydraulics", Mc Graw Hill, New York, 1959.
[23] Henderson F.M. "Open Channel Flow", Macmillan Book Company, 1966.
[24] Rajaratnam N., and Muralidhar D. "Characteristics of rectangular free overfall", J. Hydraul. Res., Vol. 6, No. 3, 1968, pp. 233–258.

CFD Validation of Slug Two-Phase Flows in a Horizontal Channel

Y.Razavi, M M.Namin

***Abstract* – The article presents a CFD (Computational Fluid Dynamics) model to simulate two-phase slug flows that can predict the slug initiation, growth and subsequent development in horizontal channels. The two-dimensional simulation results for slug characteristics are validated by experimental optical observations captured at the horizontal Channel. In this study, (volume of fraction) VOF approach is applied to capture the interface between two incompressible phases. In addition, the model is simulated by the Realizable K-ε model as a viscosity model. The commercial CFD package, FLUENT, is used for this study. Comparison between FLUENT code and experimental data shows the satisfactory agreement. As a result, presented model seems to be appropriate to predict the formation and development of slug flow in horizontal channel.**

***Keywords* – CFD package, Horizontal channel, Numerical simulation, Slug flow**

1. INTRODUCTION

Two-phase flow of water –air occurs due to sudden increase of water level in tunnel or sudden drop in water level of upstream reservoir in the entrance of a channel. It conforms to all governing rules of fluid mechanics. Interaction between air and water and generation of two-phase flow is observed in some hydraulic structures such as culverts that are prone to form two-phase flow and also pressure tunnels and different kinds of conduit with different geometric conditions. Sometimes, it leads to special regime such as slug flow that its final consequence can result in severe failure and irreparable damage of structures.

Two-phase flow systems are extremely complex and contain many variables that it is hard to analyze, and their application requires specific initiatives and assumptions. In order to simplify these complexities, many researchers have intended to accomplish modelling tests that they can obtain simple equations in order to analyze the scientific problems and practical issues by means of experimental results. In addition, the researchers have also provided some techniques to determine flow patterns and pressure drop during two-phase which are reasonable for specific regimes and certain conditions.

The most important characteristic of two-phase flow is interface between liquid and gas phases that consist of various forms. Using classification of various interface distribution of two phases that so-called fluid flow patterns, this type of flow can be expounded. Generally, seven types of flow patterns in horizontal gravity pipe can be described as follow: Bubble flow, Plug flow, stratified smooth flow, Stratified wavy flow, Slug flow, annular flow and Spray flow [1].

Y.Razavi, University of Tehran, Faculty of Civil Engineering, Student of M.SC, Tehran, Iran, e-mail: yrazavi@ut.ac.ir.

M. M. Namin, University of Tehran, Faculty of civil eng, Associate Professor, Tehran, Iran,e-mail: mnamin@ut.ac.ir.

ISSN-1584-5990

Slug flow regimes have been found in horizontal conduit for high liquid flow rates. As the airflow rate is increased, surface wave amplitudes become larger to seal the conduit, and wave forms frothy slug where it touches the roof of the conduit. Slugs that travel with a higher velocity than average liquid velocity can cause severe vibration and extremely hazard in equipment that located in the direction and assemblage centers. The significant factors of slug flow are regular fluctuations in pressure and amount of fluid accumulation that can be maintained as appropriate criteria for recognition of this type of flow regime. Since slug flow is the most possible flow in horizontal and near horizontal conduits and closed channels, this paper attend to numerical modelling of slug flow and studying major parameters of this kind of two-phase flow in horizontal channels.

2 GOVERNING EQUATIONS

The basis of the two-fluid model is the formulation of conservation equations for the balance of mass, momentum for each of the phases. Furthermore, transport equation of volume fraction is solved for an isothermal flow. In addition, the realizable model of K-ε is a two-equation model in which two separate transport equations are solved for turbulence kinetic energy and rate of dissipation independently For one-dimensional stratified and slug flow they are[2]

$$\nabla \cdot \mathbf{u} = 0 \tag{1}$$

$$\frac{\partial \rho \mathbf{u}}{\partial t} + \nabla \cdot (\rho \mathbf{u}\mathbf{u}) + \nabla \cdot P = \rho \mathbf{g} + \mathbf{F_s} + \nabla \cdot \left[\mu \left(\nabla \cdot \mathbf{u} + \nabla \cdot \mathbf{u}^{\mathrm{T}} \right) \right] \tag{2}$$

$$\frac{\partial C}{\partial t} + \nabla \cdot (\mathbf{u}\ C) = 0 \tag{3}$$

Equations (1), (2) are conservation equations of mass and momentum those are named Navier–Stokes equations. Where ρ is density, μ shows viscosity P represents pressure and g is gravity vector. Term of F_s is the identity interaction between phases across the interfaces. Equation (3) is transport equation of volume fraction that is pointed by C. this formula demonstrates the transport of interfaces by means of velocity vectors u_i and u_j.

In case of two-phase flow, since density and viscosity variations are just affected by phase changes in domain, these variables are determined base on percent of volume that each phase occupies in any given cell as follows[2].

$$\rho = C \cdot \rho_1 + (1 - C) \cdot \rho_2 \tag{4}$$

$$\mu = C \cdot \mu_1 + (1 - C) \cdot \mu_2 \tag{5}$$

The modelled transport equations for turbulence kinetic energy, k and its rate of dissipation, ε in the realizable k-ε model are[5]

$$\frac{\partial}{\partial t}(\rho k) + \frac{\partial}{\partial x_i}(\rho k u_i) = \frac{\partial}{\partial x_j}\left(\left(\mu + \frac{\mu_t}{\sigma_k} \right) \frac{\partial k}{\partial x_j} \right) + G_k + G_b - \rho\varepsilon - Y_M + S_k \tag{6}$$

$$\frac{\partial}{\partial t}(\rho\varepsilon)+\frac{\partial}{\partial x_i}(\rho\varepsilon u_i)=\frac{\partial}{\partial x_j}\left(\left(\mu+\frac{\mu_t}{\sigma_\varepsilon}\right)\frac{\partial\varepsilon}{\partial x_j}\right)+\rho C_1 S_\varepsilon-\rho C_2\frac{\varepsilon^2}{k+\sqrt{\upsilon\varepsilon}} \quad (7)$$

$$+C_{1\varepsilon}\frac{\varepsilon}{k}C_{3\varepsilon}G_b+S_\varepsilon$$

In these equations, k is G_k represents the generation of turbulence kinetic energy due to the mean velocity gradients, G_b is the generation of turbulence kinetic energy due to buoyancy, Y_M represents the contribution of the fluctuating dilatation in compressible turbulence to the overall dissipation rate,. C_2 and C_1 are constants. σ_k and σ_ε are the turbulent Prandtl numbers for k and ε, respectively. S_k and S_ε are user-defined source terms.

3. NUMERICAL METHOD

3.1 Finite volume technique

This study employ finite volume method as a numerical technique in which, values are calculated at discrete places on a meshed geometry. Generally, "Finite volume" refers to the small volume surrounding each node point on a mesh. In the finite volume method, volume integrals in a partial differential equation that contain a divergence term are converted to surface integrals, using the divergence theorem. These terms are then evaluated as fluxes at the surfaces of each finite volume. Because the flux entering a given volume is identical to that leaving the adjacent volume, these methods are conservative. The method is used in many computational fluid dynamics packages.

3.2 VOF Model Theory

The VOF (Volume of Fluid) model is not only simple model but also efficient method that used in order to track the liquid-gas interface. Generally, the VOF model can model two or more immiscible fluids by solving a single set of momentum equations and tracking the volume fraction of each of the fluids throughout the domain. In case of water flow in a channel with a region of air on top and a separate air inlet, VOF method is appropriate technique for prediction of .Interface between phases .The employed formulation relies on the fact that two or more fluids (or phases) are not interpenetrating. For each additional phase that is added to the model, a variable is introduced: the volume fraction of the phase in the computational cell. In each control volume, the volume fractions of all phases sum to unity. The fields for all variables and properties are shared by the phases and represent volume-averaged values, as long as the volume fraction of each of the phases is known at each location. Thus the variables and properties in any given cell are either purely representative of one of the phases, or representative of a mixture of the phases, depending upon the volume fraction values. In other words, if the qth fluid's volume fraction in the cell is denoted as α_q, then the following three conditions are possible [5]:

$\alpha_q = 0$: The cell is empty (of the q_{th} fluid).
$\alpha_q = 1$: The cell is full (of the q_{th} fluid).
$0 < \alpha_q < 1$: The cell contains the interface between the qth fluid and one or more other fluids.

3.2.1 Volume Fraction Equation

The tracking of the interfaces between the phases is accomplished by the solution of a continuity equation for the volume fraction of one (or more) of the phases. For the q_{th} phase, this equation has the following form[5]

$$\frac{1}{\rho_q}\left[\frac{\partial}{\partial t}\left(\alpha_q\rho_q\right)+\nabla\bullet\left(\alpha_q\rho_q\vec{u_q}\right)=S_{\alpha_q}+\sum_{p=1}^{n}\left(\dot{m}_{pq}-\dot{m}_{qp}\right)\right] \tag{8}$$

where m_{qp} is the mass transfer from phase q to phase p and m_{pq} is the mass transfer from phase p to phase q.

3.2.2 The Geometric Reconstruction Scheme

Control-volume formulation requires that convection and diffusion fluxes through the control volume faces be computed and balanced with source terms within the control volume itself [3].
Geometric reconstruction applies a special interpolation treatment to the cells that lie near the interface between two phases. It assumes that the interface between two fluids has a linear slope within each cell, and uses this linear shape for calculation of the advection of fluid through the cell faces [5]. The first step in this reconstruction scheme is calculating the position of the linear interface relative to the center of each partially-filled cell, based on information about the volume fraction and its derivatives in the cell. The second step is calculating the advecting amount of fluid through each face using the computed linear interface representation and information about the normal and tangential velocity distribution on the face. The third step is calculating the volume fraction in each cell using the balance of fluxes calculated during the previous step [8]. Figures 1-a and 1-b show an actual interface shape along with the interfaces assumed during computation by this method.

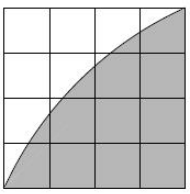

Figure 1.a: actual interface shape

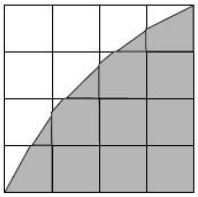

Figure 1.b: interface shape represented by geometric reconstruction scheme

4. SETUP AND SOLUTION

Based on the experimental study that has been undertaken by Vallee and Hohne [4], the channel with rectangular cross-section was modelled using a commercial CFD package, FLUENT [5]. Dimensions of the model are 4000 x 100 x 30 mm³ (length x height x width). Simulation was performed by a grid consists of 4 x 10^4 hexahedral elements which is displayed in figure 2 and 82086 nodes using specific technique that can consider the wall effect of channel in a 2Dmodel. Since two-dimensional geometry only able to show upper and lower Walls as boundary, the lateral walls and their effect, which play important role in generation of slugs, are neglected in 2D models. In order to avoid this issue, width of any elements is fitted into the width of channel. Using this technique, it can be possible to decline number of elements in comparison of a 3D model, also take advantage of reduction of computation in a 2D model.

Two-phase flow with a superficial water velocity of 1.0 m/s and a superficial air velocity of 5.0 m/s was chosen for the CFD calculations. The model inlet was divided into

two parts: in the lower 50% of the inlet cross-section, water was injected and in the upper 50% air. An initial water level of 50 mm was assumed for the entire model length. In addition, initial velocity 1.0 m/s was considered for liquid and air phases, and the velocity of air phase was increased gradually until it archived its final amount that was 5.0 m/s. During the simulation, reference pressure was 1 bar., Surface tension was supposed to be 0.0073 n/m. A hydrostatic pressure was assumed for the liquid phase.

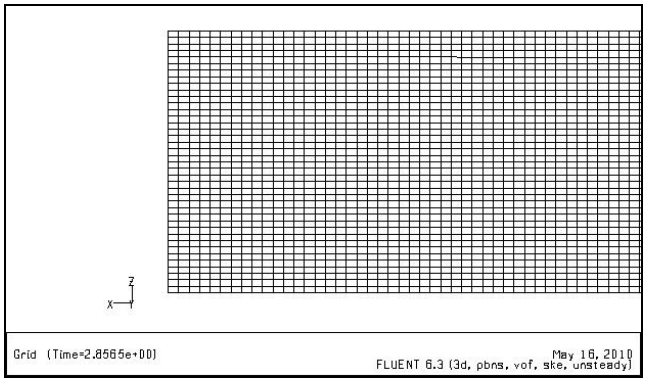

Figure2: grid display

As it was the goal of the CFD calculation to induce surface instabilities, which are r generating waves and slugs sequentially, the interfacial momentum exchange and also the turbulence parameters had to be modelled correctly[5]. To this end (Finally), turbulent model of Realizable K-ε model was selected as a viscosity model that is able to model instabilities and turbulence of slug flow. Solution time for calculating 5.0 s of simulation time on the 6 processor lasted about 20 hours using parallel processing method. Selected discretization schemes were presto for pressure, Geo Reconstruction for volume fraction, and first order upwind for other cases. Variable time step between $10^{-6}$and 10^{-3} was appropriate step for simulation of this instable phenomena. Using amounts of 10^{-3} for residuals, the acceptable convergence has been achieved based on courant number 0.1 for VOF method.

5. RESULTS AND DISCUSSION

Considering the calculated void fraction sequences, expected phenomena that leads to formation of slug flow are observed in simulated model (Figure 3-a and 3-b). These phenomena are small waves and superficial instabilities that have been generated by interfacial momentum transfer, appear on the interfaces of two-phase. These waves can move in different velocity, combined together, create larger waves that can roll over and block the channel completely.

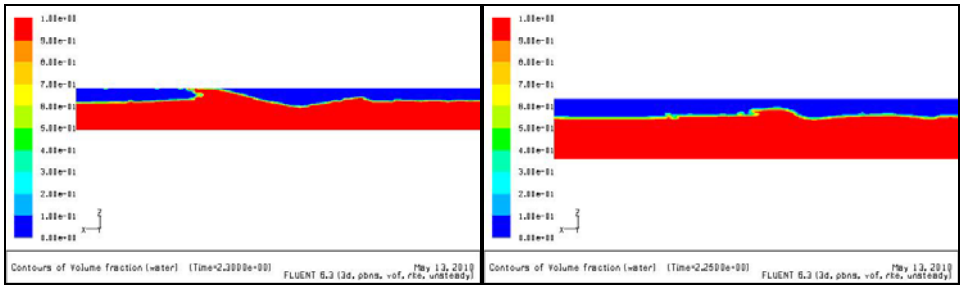

Figure 3.a **Figure 3.b**

According to flow pattern map in horizontal channel (Figure 4) presented by Taitel and Dukler (1976), for superficial water velocity of 1.0 m/s and superficial air velocity of 5.0 m/s expected flow pattern is slug flow that results of 2Dmodel can predict the generation and development of slug flow based on maintained map.

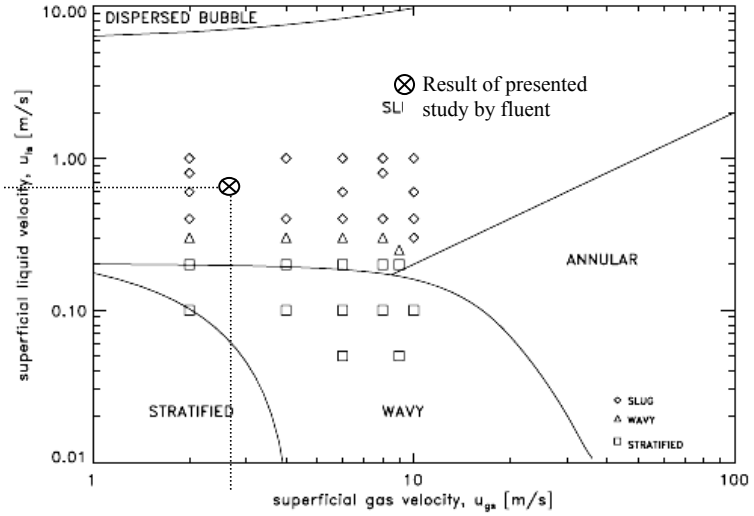

Figure 4: Generalized flow regime map for horizontal two-phase flow[7]

Figure 5-a and 5-b Display velocity vector and contour of pressure. Sudden changes in these figure are result of generation of slug because of turbulent and oscillating nature of slug flow.

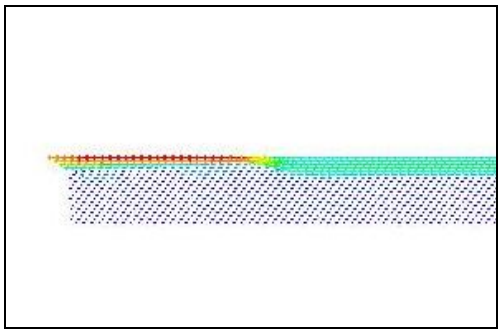

Figure 5.a: velocity vectors near the position of slug

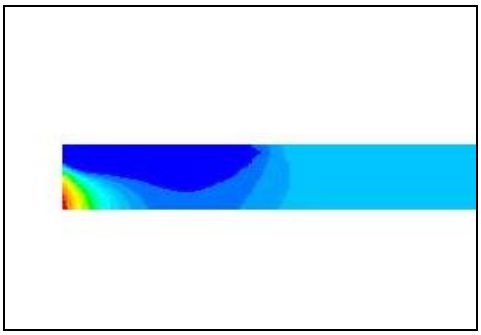

Figure 5.b: pressure counters near the position of slug

Figure 4-a shows calculated sequence of void fraction of 2D model, and figure 4-b shows the optical measurements of HAWAC channel was performed by Vallee and Hohne [3].Qualitative comparison between CFD model and experimental model shows that a slug is generated. The sequences show that the behavior of the creation and propagation of the slug is similar in both cases. In addition, numerical model confirms that stratified flow is generated after exit of slug. Since the slug is cleared an important amount of water from the channel, the next slug appears after the channel is slowly filled up again by the transport of liquid from the inlet [3]. Therefore, providing the possibility of next slug formation, it is required to maintain stratified flow in the channel. Furthermore, experimental sample shows frothy zone in slug flow that can grow with development of slug, these frothy slugs cannot be found in CFD model. In

spite of VOF capability to model of multi-phase flow, this method is unable to simulate frothy area in slug flow, and there is little difference in the form of slugs between experimental and CFD model.

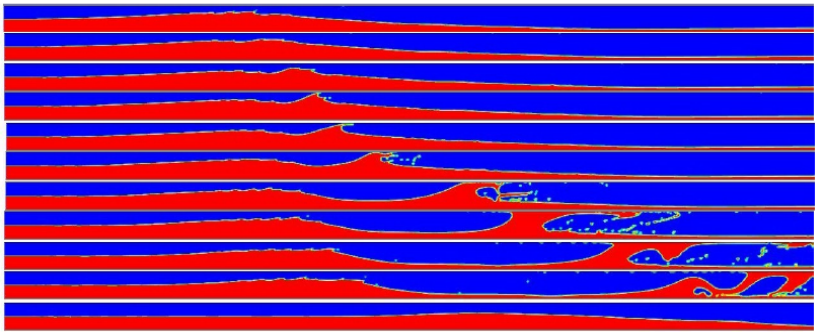

Figure 6.a: Sequence of void fraction at for superficial water U_{ls} =1.0 m/s and U_{gs}=5.0 m/s calculated by numerical model

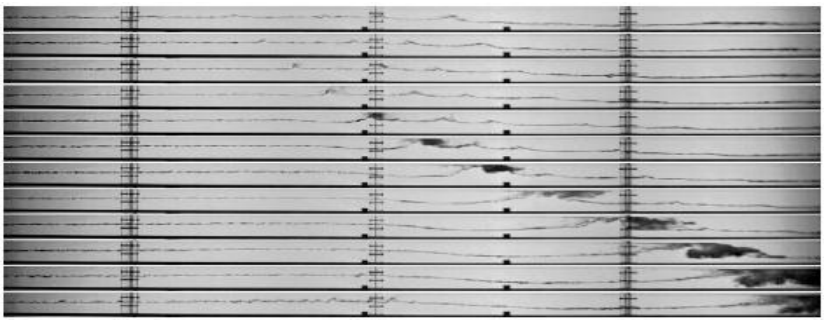

Figure 6.b:result of experimental study done by Vallee and Hohne [3]

5. Conclusion

In this paper a numerical model for qualitative study on slug two-phase flows in a horizontal channel is presented. The FLUENT software (computational fluid dynamics (CFD) package) is utilized. Considering the volume of computational operations, three-dimensional simulation is too expensive, so the sufficient two-dimensional model is generated for the simulation of formation and development of slug flow. The model is simulated based on solution of RANS equations with the help of finite volume method and also solution of transfer equation for the volume fraction term. Moreover, the VOF method is used for tracking the joint level of two phase flows. Furthermore, using Realizable K-ε turbulence model, transport equations was solved separately for both terms of k and ε. based on the capabilities of FLUENT package to simulate such flows, the results shows all expected phenomena of slug flow in the tow dimensional model. Finally, the results were compared with the experimental model, that the acceptable compatibility and similarity between numerical and experimental results are observed. It is worth noting that the assessment of hydraulic characteristics and also quantitative study of slug flow in a horizontal channel can be possible by more study and accurate simulation.

6. REFERENCES

[1] Lauchlan,C.S., Scaramela,M., (2005), "Air in pipeline", A literature review, Report SR 349.
[2] A. Bohluly , S.M. Borghei and M.H. Saidi, (2009), "A New Method in Two Phase Flow Modeling of a Non-Uniform Grid", Journal of Scientia Iranica, Sharif University of Technology, Vol. 16, No. 5.
[3]Hirt, C. W. and Nichols, B. D., (1981), "Volume Of Fluid (VOF) Method for the dynamic of free boundaries", Journal of Computational Physics 39, 201-225.
[4] Vallee, C. and Hahne,T., (2007), "CFD Validation of stratified two-phase flows in a horizontal channel", Forschungzentrum Dresden-Rossendorf, Germany.
[5] ANSYS.Inc., (2006),ANSYS CFX-10.0 , User Manual.
[6] Taitel,Y. and Dukler,A.E., (1976), "A model for predicting flow transition in horizontal and near horizontal liquid flow", AIChE, Journal, Vol.22, No.1, pp47-55.
[7] FLUENT.Inc., (2006),Version 6.3.2, User Manual.
[8] R.I. Issa and M.H.W. Kempf (2003), "Simulation of slug flow in horizontal and nearly horizontal pipes with the two-fluid model," International Journal of Multiphase Flow, 29, 69–95.

Ovidius University Annals Series: Civil Engineering Volume 1, Issue12, June 2010

The Respiratory Circuit of the Diving Equipment for Interventions in Contaminated Waters

Tamara Stanciu

***Abstract* – The Research Laboratory of the Diving Center has homologated an experimental model of the Diving equipment for interventions in contaminated waters, to assure the total protection of the diver in these interventions. This paper presents the respiratory circuit of the Diving equipment for interventions in contaminated waters:**

1. **The first pressure regulator of the main reservoir**
2. **The distributor**
3. **The first pressure regulator of the second reservoir**
4. **The helmet valve**
5. **The second regulator with extra pressure**

***Keywords* – contaminated waters, pneumatic pressure regulators, pneumatic circuit for diving equipment, surface air supply**

1. INTRODUCTION

The contaminated water is defined as water, which contains any chemical, biological, or radioactive substance, which poses a chronic or acute health risk to exposed personnel. The contamination may be naturally occurring or come from a variety of sources including terrorist acts, leaking vessels, industrial discharges and/or sewer effluent.

As a result of this potential health risk to Navy divers and additional impact to mission and operational readiness, it's imposed to design a specific equipment which allows the speedy diving in contaminated water after the evaluation of the causes. This equipment has a respiratory apparatus (the second regulator) with open circuit and surface supply.

In this paper it is presented the pneumatic respiratory circuit of the equipment.

2. DESCRIPTION OF THE RESPIRATORY CIRCUIT

The respiratory circuit of the equipment consists from:

- The first pressure regulator of the main reservoir
- The distributor
- The first pressure regulator of the second reservoir
- The helmet valve
- The second regulator with extra pressure, part of the tight helmet

Tamara Stanciu is with Diving Center, Bd. 1 May nr. 19, Constanta, Romania, (phone: +40241586600/137; e-mail: tamarastanciu@yahoo.com)

ISSN-1584-5990

2.1. THE FIRST PRESSURE REGULATOR OF THE MAIN RESERVOIR

The diving equipment is supplied from the surface, from a large reservoir, where the air is stocked at 150-200bar. Before the diving, the tanks pressure is reduced at a medium pressure, to a preordained value, by the adjustment screw 1.

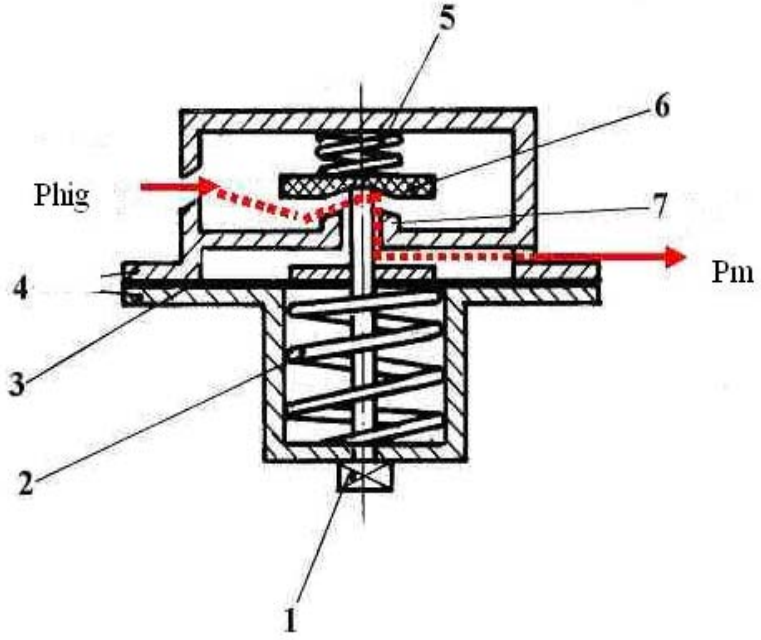

Fig. 1 The first pressure regulator of the main reservoir

1. Adjusting screw
2. Adjusting spring
3. Diaphragm
4. Body
5. Keeping spring
6. Piston
7. Seat

2.2. THE DISTRIBUTOR FOR THE AIR SUPPLY

A medium pressure hose assures the junction with the distributor in "T". The distributor is designed to blockade the main access to the helmet valve (ball tightness) and to open the access from the second reservoir hose, when the air supply from the surface is brusquely interrupted. To the second reservoir is installed a first pressure regulator which supplies the air at the same medium pressure like the first pressure regulator of the surface, manifold by the water pressure. Thus it's avoiding the danger to pervade the second pressure regulator water and the diver receives enough air from the second reservoir, to be in self.

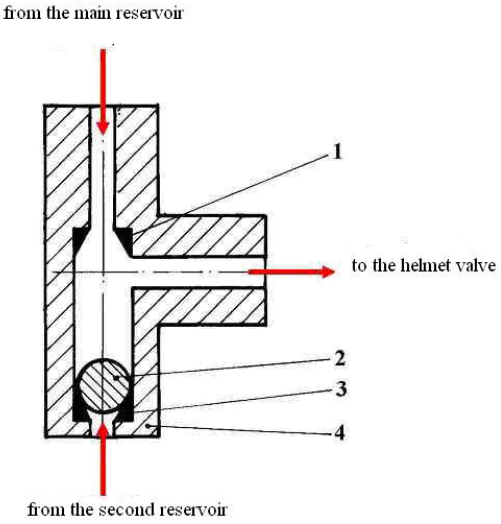

Fig. 2 The distributor for the air supply

1. Teflon seat
2. Ball
3. Teflon seat
4. Body

2.3. THE FIRST PRESSURE REGULATOR OF THE SECOND RESERVOIR

This is a regulator piloted by the water pressure; it is in permanently contact with the water. The regulator is balanced, with piston. The high pressure (150 bar) from the second reservoir is reduced to the medium value of the pressure, like the pressure supplied from the surface and directed it to the distributor.

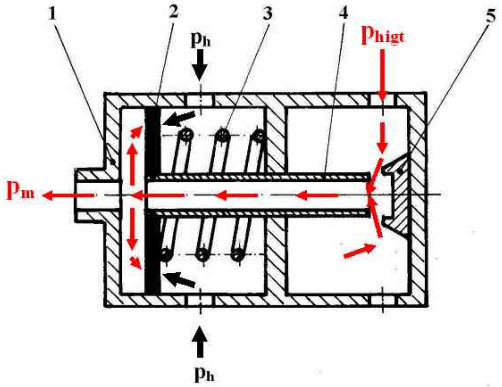

Fig. 5 The first pressure regulator of the second reservoir

1. Body
2. Diaphragm
3. Adjusting screw
4. Plug
5. Seat

2.4. THE HELMET VALVE

The valve was designed to supply respiratory gas to the second pressure regulator from the helmet and to orientate an air spray to the helmet glass against steaming.

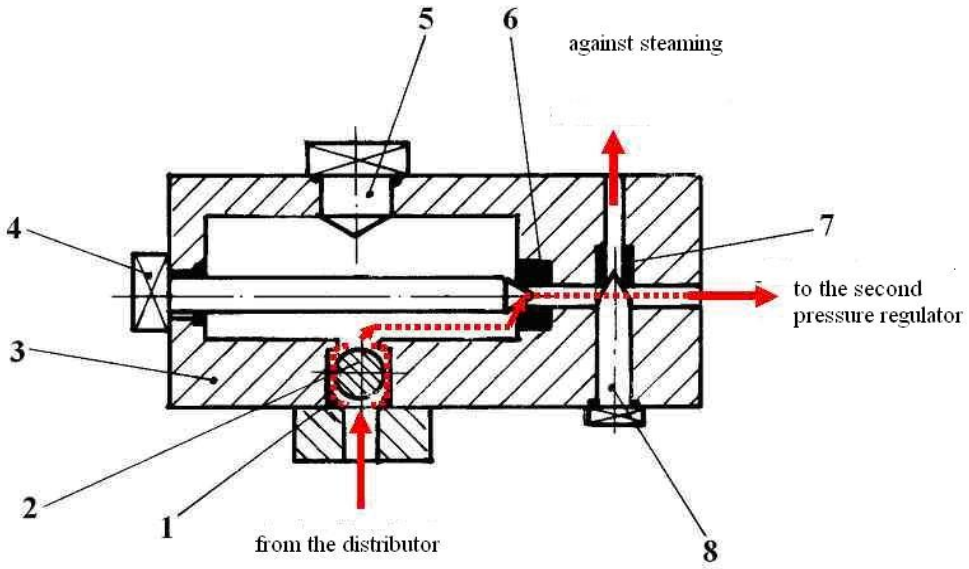

Fig. 4 The helmet valve

1. Teflon seat
2. Ball
3. Body
4. Faucet
5. Stopper
6. Gasket
7. Gasket
8. Against steaming faucet

2.5. THE SECOND REGULATOR WITH EXTRA PRESSURE

The regulator receives medium pressure air and delivers gas, to a pressure over 5 cmH_2O the hydrostatic pressure, to the diver. This extra pressure into the helmet is an extra safely operation for the diver, because the contaminated water can't penetrate the helmet.

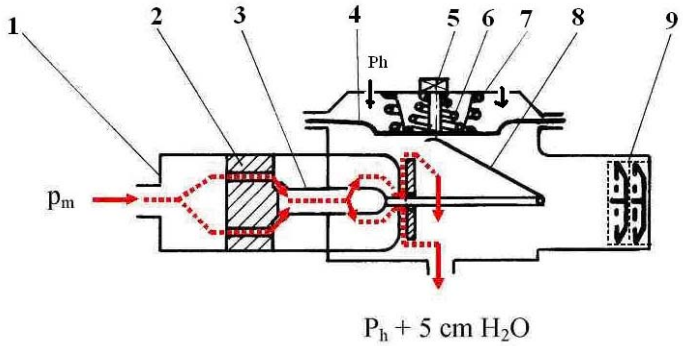

Fig. 5 The second regulator with extra pressure

1. Body
2. Seat
3. Downstream plug
4. Diaphragm
5. Adjusting screw
6. Keeping spring
7. Extra-pressure spring
8. Lever
9. Valves block

3. RESULTS AND SIGNIFICANCES

3.1. THE FIRST PRESSURE REGULATOR OF THE MAIN RESERVOIR

It's coupled to the surface gas tank and receives respiratory air at the stocked pressure p_a . This pressure is reduced to a medium value, p_m:

$$p_m = p_h + 10bar \tag{1}$$

where p_h – the surrounding pressure on the deep h;
p_m- medium pressure from hose;
Because the pressure regulator isn't in contact to the water, at the work depth, it settles the profounder for every level and implied:

$$p_h = 1bar + h \tag{2}$$

P_h– pressure at the deep h
h - pressure of the water column

3.2. THE DISTRIBUTOR FOR AIR SUPPLY

It has a simple construction in T form. The medium pressure which comes from the main first pressure regulator keeps the ball pressed on the Teflon seat 3 and blocks the access from and to the second reservoir. If it is accidentally interrupted the air supply from the surface, because strangulation or breakage of the medium pressure hose, or other loss of

the pressure from the main reservoir, it opens the valve of the second reservoir. The first pressure regulator piloted by the water pressure supplies air at medium pressure, which upends the ball 2 on the Teflon seat 4 and admits the air supply of the helmet valve, simultaneous closing the access to and from the main supply hose.

3.3. THE FIRST PRESSURE REGULATOR OF THE SECOND RESERVOIR

When is balanced, the piston closes the air input on the Teflon seat. The pressure descents into the medium pressure room on the diver inspiration, the piston is pushed by the greater water pressure and by unbalance it opens the air access from the tank. The dragged spring is adjusted to admitting the respiratory gas into the seat and the piston on a pressure up to 10 bar over the surrounding pressure, in fact the medium pressure p_m assured by the main first pressure regulator.

3.4. THE HELMET VALVE

The air admission from the distributor it makes from the system ball – Teflon seat too, the air pressure upends the ball 2 from the seat 1 and the air pervades into the valve room. The open of the helmet valve it makes with the faucet 4, by detaching it from the seat 6. If it is necessary, the faucet 8 opens the air access into the helmet against steaming.

3.5. THE SECOND REGULATOR WITH EXTRA PRESSURE

This represents a simple design solution by attaching the extra – pressure spring into the cover of the apparatus. Without this spring, the mechanism is type downstream plug and it closes on balancing. By inspiration the lever 8 is acted from diaphragm 7, opens the plug 3 and it permits to the air to pervade into the dry room, until at the balancing of the pressures from the upstream and the downstream. In this moment, the downstream plug returns on the seal seat and closes the circuit. The spring 7 keeps pushed the diaphragm, with a force which generates the pressure of $5cmH_2O$ and this it adds to the admission pressure p_h. In this mod the diver receives to the mask the pressure $p_h + p_s$. The little pressure difference ps $=5cmH_2O$, prevents the accidental penetration of the contaminated water into the helmet and assures the easiness in respiration, to the person.

The evacuation of the air it makes by the valves block, position 9 and represents a supplementary measure to hinder the penetration of the contaminated water into the helmet.

3.6. SIGNIFICANCES

The circulation of the air from the main reservoir to the lungs of the diver is started by inspire, when is surmounted the resistance of the spring 5 to permit the gas input between the downstream plug 3 and the seat 2. The hydrostatic pressure p_h and the spring 7 pressure p_s action to the diaphragm. The relaxation of the air is made by means of the two restrictors: restrictor 1 from the main first pressure regulator and restrictor 2 between the downstream plug and the seat from the second regulator. The medium pressure is variable and the air movement is critical for a long value range of the pressure into the restrictor of the second regulator. In the minimum cross section the gas parameters take critical values.

Therefore the air passes out of the restrictor by supersonic velocity and shortly downstream the movement becomes subsonic due to the shock waves. The mass flow rates are equal in the two restrictors.

$$\dot{m}_1 = \dot{m}_2 \tag{3}$$

$$\dot{m}_1 = E(\alpha, k)\frac{\sigma_{c1} p_a}{\sqrt{RT_m}} \tag{4}$$

$$\dot{m}_2 = E(\alpha, k)\frac{\sigma_{c2} p_m}{\sqrt{RT_m}} \tag{5}$$

$$\Rightarrow \frac{\sigma_{c1}}{\sigma_{c2}} = \frac{p_m}{p_a} \tag{6}$$

α = the discharge coefficient

k = the adiabatic coefficient of the air

$\dot{m}_1$ = the mass flow rate from the restrictor 1 of the main first regulator

$\dot{m}_2$ = the mass flow rate from the restrictor 2 of the second regulator

$\sigma_{c1,c2}$ = the restrictor's sections surfaces from the two regulators

p_m = the medium pressure from the hose

p_a = the supply pressure

R = the gas constant

T_m = the temperature at the medium pressure

p_s = the extra pressure = 5cmH_2O

The second regulator sets the value of the mass flow rate. For a constant temperature during the diving, the mass flow rate depends alone the downstream medium pressure from the second regulator p_m and the value of the restrictor section surface too. This variable section depends by the diver's inspire, which means Δp, the differential pressure from the second regulator body and by the extra pressure p_s = 5cmH_2O.

4. CONCLUSIONS

The equipment for interventions in contaminated water, experimental model, was tested both in simulation conditions, in Hiperbaric Laboratory and in real conditions in the Black Sea.

The experimental diving was made with different subjects, at diverse depths: 3 m; 6 m; 9 m; 18 m, either into the Simulator or into the marine polygon.

There were tested:

- The air supply, by the main pressure regulator – distributor – helmet valve – second pressure regulator.
- The extra pressure p_s at the second pressure regulator.
- The accuracy of the distributor operation.
- The opening pressure of the first pressure regulator of the second reservoir.

The equipment passed all the tests and proved that the conceiving manner and engineering design of the respiratory circuit were appropriate, according to the requirements for such an equipment. It was a success.

A few moments during the testes were intercepted in the following images, Fig.6.

Technical team

The entrance into the Simulator

Technical team

Probes at the Black See

Fig. 6 Images taken during the homologating tests

5. ACKNOWLEDGMENTS

Author thanks to the projecting assistant Radita IOAN for her contribution in finalize of the schedules.

6. REFERENCES

[1] B. Broussolle, "Physiologie et medicine de la Plongee ", Editure Ellipses, Paris, 1992;
[2] E. Carafoli, and V.N. Constantinescu, "Dinamica fluidelor compresibile", Editura Academiei, Bucureşti, 1984;
[3] A. Constantin, "Aparate de respirat în circuit deschis. Elemente de calcul" , Tehnica militară, nr. 4, Ed. M.Ap.N., Bucuresti, 1997;
[4] M. Degeratu, A. Petru and S. Ionita, "Manualul scafandrului", Editura Per Omnes Artes, Bucuresti, 1999.

Comparative studies regarding the infiltration through an earth dam profile

Ioan Şumălan

Abstract – **Infiltration evaluation through water structures like earth dams or dikes consisting in water levels, flow rates is useful in design and maintenance processes but also in the management of accidental events like flooding. The topic is dedicated the water structures as permanent or temporary earth dams, river regulation works containing earth dikes but also in the irrigation or drainage engineering. The study of infiltration through homogeneousness porous media by analytical methods is well represented in the literature by several authors and their methods grace of the Russian hydraulic school, also others. In the last years, grace especially of the huge development of computer sciences numerical methods gained important positions because of their significant advantages offered to users. For many traditional hydrologists handling such models is quite a challenge and the analytical methods are considered more trusted but more difficult to apply and therefore the question is which method is most rapid and accurate. The paper presents a comparative study by using two different categories methods (analytical and numerical) for water infiltration through an earth profile for multiple variants.**

Keywords – **analytical methods, earth dam profile, infiltration, numerical methods.**

1. INTRODUCTION

Infiltration evaluation through water structures like earth dams or dikes is useful in design and maintenance processes but also in the management of accidental events like flooding. The present paper refers especially to earth dams of average height.

From a permanent reservoir built by an homogeneousness earth dam profile infiltrations can occur through earth dam body or under the dam through dam foundation terrain. Knowing the exact evolution of this infiltration phenomena has a high importance because alowws to evaluate the water losses by infiltration, the path of the water and its effects on the dam body material behavoir. Also it is verry important to locate the areas where the water spring on the backward slope or in the case of accident like flooding tyo take the technical measures in order to reduce this infiltartions effects or damages.

1.1 ASSUMPTIONS

A large space in the literature is dedicated to analytical methods for water infiltration through homogeneousness earth dam[2]-[4].Traditionally the infiltration is considered in steady state flow regime variable time parameter is missing, that occurs in the natural very rare operating conditions because of the climate and hydrology. In the most of the practical cases the

Politehnica University of Timisoara, G. Enescu Street, No.1/A, 300022, Romania,phone: +40-256-404086; fax: +40-256-404113; e-mail: ioan.sumalan@hidro.upt.ro.

ISSN-1584-5990

earth dam foundation is considered as impervious, which is not always true, the dam body material having almost the same hydraulic proprieties like permeability as its foundation.

At least but the last, the horizontally plane flow is considered in the most used models which covers the majority of practice (Dupuit, [8]).

2. ANALYTICAL SOLUTION

For an established earth dam profile as it is shown in the Fig. 1 the given parameters are as following:

-H_b- the height of the earth dam, [L];
-H_o –the constant water level on reservoir, [L];
-b - the crown width, [L];
-h_o- the constant water level donstream of the earth dam, [L];0
-n – upstream slope, dimensionless;
-m – downstream slope, dimensionless;
-k – earth dam permeability, [LT^{-1}];.

The requested parameters are:

-h- water level into earth dam profile located close to the its entrance [L];
-a_o the water level on downstream slope of the dam where it appears, [L];
-q- flow rate, [L^2T^{-1}];
-L – the length from earth crest vertical line to water appearance on downstream slope(the distance between R and P points on Fig.1);

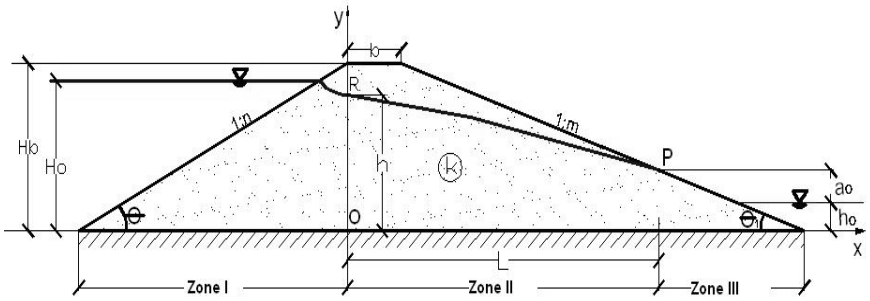

Fig. 1. Steady state infiltration through homogeneousness dam

Several authors, from which Pavlovski is the most cited and known in the literature, but also others (Cozeny-Casagrande, Numerov, Dachler [2], [3], [4]), consider as necessary to split the earth dam profile into three different zones (Fig.1) where the infiltration curve and flow rate are given by the following equations:

$$\frac{q^I}{k} = \frac{H_o - h}{n} \ln \frac{H_b}{H_b - h} \tag{1}$$

$$\frac{q^{II}}{k} = \frac{h^2 - (a_o + h_o)^2}{2L} \tag{2}$$

$$\frac{q^{III}}{k} = \frac{a_o}{m}\left[1 + \ln \frac{a_o + h_o}{a_o}\right] \tag{3}$$

$$L = b + m\left[H_b - (a_o + h_o)\right] \tag{4}$$

Notice: The last equation was obtained by geometrical consideration.

The specific literature contents several methods to solve obove equations by different analytical methods whits more or less considerations and simplifications.

In the present paper an iterative algorim based on Newton-Raphson equation solving method [5] is presented. It must be mentioned than equations (1)-(4) contain four unknown parameters, the equations are not linears and supplimentary the natural logaritm function is present in two of them.

Based on Newton-Raphson method, for a given function *f(x)* in terms of *x* variable the searched solution x_f is given from innitrially value x_i by using an iterative relationship:

$$x_f = x_i - \frac{f(x_i)}{f'(x_i)} \tag{5}$$

where *f'(x)* is the derivative of the function *f*.

The process being iterative, ends after a prescribed maximum number of iteration or when the admited criteria of a maximum relative percent error is achieved [6]:

$$\left| x_f - x_i \right| < \varepsilon_a \tag{6}$$

The goal of the iterative algoritm is that to combine equations (1)-(3), to substitute the variables *h* and *q* resulting by this procedure only a single function *f* in terms of remaining parameter a_0 which will be found by Newton-Raphson method. This can be realised based on the fact that the phisical unit flow discharge *q* (considered along of unit length of the dam crest) is the same into three different infiltration zones on earth dam profile. Once the parameter a_0 is found the rest of parameters like *h*, *q* and *L* can be calculated based on (1)-(4).

2.1 STEPS OF THE METHOD

In (1)-(3) several constants and functions in terms of parameters a_0 and *h* can be identified as follows:

$$C_1 = b + m(H_b - h_o) \tag{7}$$

$$C_2 = \frac{2h_0 m + 2C_1}{m} \tag{8}$$

$$g_1 = h_o^2 - a_o^2 \tag{9}$$

$$g_2 = \frac{2C_1 a_o - 2ma_o^2}{m} \tag{10}$$

$$g_3 = \ln \frac{a_o + h_o}{a_0} \tag{11}$$

$$g_4 = \ln \frac{H_b}{H_b - h} \tag{12}$$

$$g_5 = \frac{H_o - h}{n} \tag{13}$$

the basic equations (1)-(3) become:

$$\begin{cases} \dfrac{q^I}{k} = g_5 \cdot g_4 \\ \dfrac{q^{II}}{k} = \dfrac{h^2 - (a_o + h_o)^2}{2(C_1 - m a_o)} \\ \dfrac{q^{III}}{k} = \dfrac{a_o}{m}(1 + g_3) \end{cases} \tag{15}$$

By combining (2) and (3)and eliminating q variable, the h parameter in terms only of variable a_0 is identified as:

$$h = \sqrt{g_1 + a_o C_2 + g_2 \cdot g_3} \tag{16}$$

The next step is to combine (1) and (3) and considering defined functions g_4 and g_5 the new general function f is obtained as:

$$f(a_o) = g_4 \cdot g_5 - \frac{a_o}{m}(1 + g_3) \tag{17}$$

containing only parameter h and variable a_0. Finally, the derivative of the function f must be obtained as folows:

$$f'(a_0) = g_8 g_5 - \frac{h'}{n} g_4 - g_6 + \frac{a_0}{m} g_9 \tag{18}$$

Where the new functions f', g_6 ,g_7, g_8 and g_9 are defined by the expresions:

$$h' = \frac{-2a_0 + C_2 + g_7 g_3 - g_2 g_9}{2h} \tag{19}$$

$$g_6 = \frac{1 + g_3}{m} \tag{20}$$

$$g_7 = \frac{2C_1 - 4m a_o}{m} \tag{21}$$

$$g_8 = \frac{h'}{(H_b - h)} \tag{22}$$

$$g_9 = \frac{h_o}{a_o(a_o + h_o)} \tag{23}$$

The last step is to apply the Newton-Raphson algoritm by using (5) and to find final value for a_0 and after that the last parameters q,h and L. Like a general review of the above presented steps the calculus for a case study based on given parameters follows the

estimation sequence for the constant and functions in the following order: C_1, C_2, a_0 input, g_1, g_2, g_3, g_6, h, g_7, g_9, h' g_4, g_5, f, g_8, f", ε_a (3-4%), final a_0, h, q and L. The entire calculul can be easy performed by using an appropriate workbook designed and developed by user.

2. NUMERICAL SOLUTION

For the numerical solution the popular and useful Modflow model was used [1], [7]. It is based on the two-dimensional Finite Difference Method. By considering the fact than the model is using multiple different layers it can be considered the model working in 3D.

The first problem was about the orientation of the earth dam into horizontal plane of the model. Along the vertical axis the top and bottom of the model was established to obtain a unit meter length of the dam like in the analytical solution. Prior to construct the model, a couple of DXF files were created in order to respect the geometry of the dam and to set correctly the boundary conditions. Different values for downstream and upstream slopes of the dam in the range of 2-3.5 were considered [3]. For the variant 2-2 (values of upstream and downstream slopes, n and m) the contour lines plot obtained with Modflow model is presented in the Fig.3.

It is known the fact that the Modflow model does not run for the case of phreatic aquifer type with respecting specific conditions of the present problem. By using the Water Budget module of the model it was possible to obtain the flow discharge through the dam profile. Generally, the obtained values in the numerical solution are in the same range like in the analytical solution (about units of 10^{-5} m^3/sm) but with significant errors.

4. CASE STUDY, RESULTS AND CONCLUSIONS

A common homogeneousness earth dam profile was considered by using the followind input data: -Hb= 50 m; Ho =40 m; b =6 m;ho=2.5 m, n and m parameters in the range 2-3.5, and the permeability k =1m/day.

The results in the analytical solution are presented in the Fig2. and the comparison between analytical solution and numerical solution for the flow discharge are presented in the Fig.4

The obtained results with relevant errors suggest than in this problem the use of the Modflow model is not properly. The analytical solution of Pavlovski in the variant of iterative algorithm appears to be the adequate solution for the infiltration through earth dam profile.

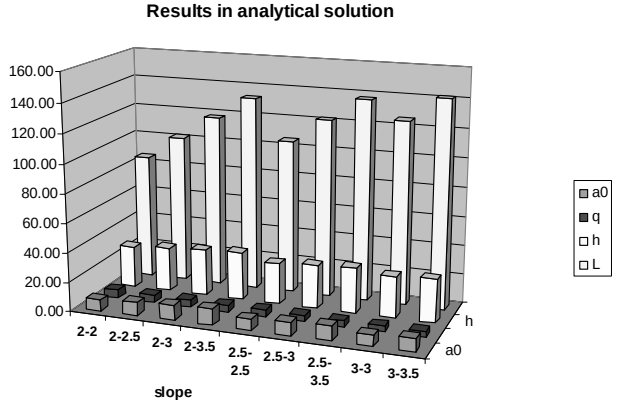

Fig.2 Results in analytical solution

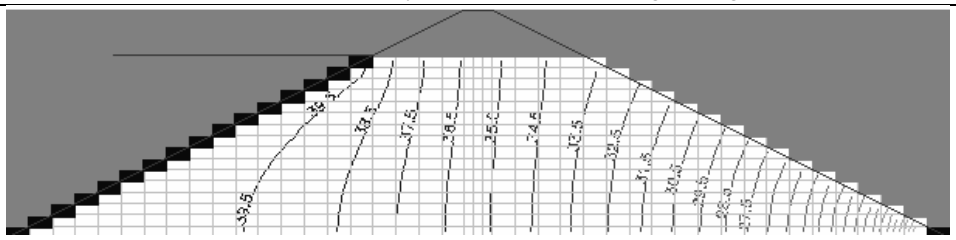

Fig.3 Contour lines plot and boundary conditions in the variant n=2, m=2

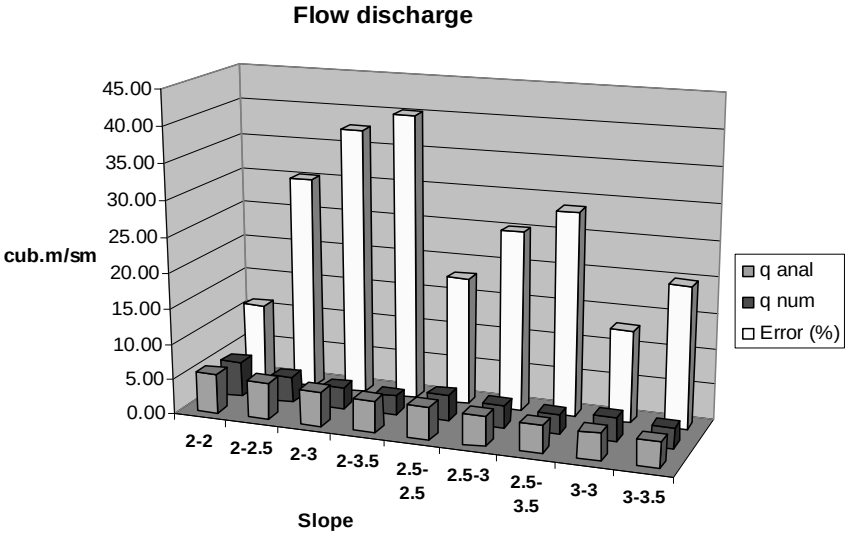

Fig.4 Comparison between analytical and numerical solution

6. REFERENCES

[1] C. Wen-Hsing, W. Kinzelbach, 3D-Groundwater Modeling with PMWIN, Springer-Verlag Berlin Heidelberg New York

[2] V. Pietraru, Calculul infiltratiilor, 1970, Ceres, Bucuresti

[3] R. Priscu, Constructii Hidrotehnice, 1974, E.D.P. Bucuresti, vol.I

[4] M.D. Certousov, Hidraulica, 1966, E.T. Bucuresti

[5] Gh. Coman, Analiza numerica, 1995, Libris, Cluj

[6] I. David, I. Sumalan, Metode numerice cu aplicatii in hidrotehnica, 1998, Mirton Timisoara

[7] Waterloo Hydrogeologic Inc., Visual MODFLOW User's Manual, 1999b

[8] I. David, Grundwasserhydraulic, Stromungs und Transportvorgange, 1998, Braunschweig; Wiesbaden: Vieweg

SECTION V

HYDRAULIC CONSTRUCTIONS

The Influence of Sudden Decrease of Water Level in the Lake on the State of Stress and Strain of Embankment Dams

Gelmambet Sunai

***Abstract* – The paper presents some calculation aspects of the embankment dams at the action of the sudden decrease a water level in lake and highlighted the importance of nonlinear models in analyzing the response of the embankment dams. To analyze the state of stress and strain was used numerical simulations on the Săcele dam. Numerical analysis was realized in nonlinear behaviour hypothesis of materials in the body of the dam, using the finite element program, Cosmos 2.6, and for analysis was used Drucker-Prager model. Fitting Săcele is located on the river Tarlung tributary of Black River in turn flows into the Olt River. The dam is located at 3 km upstream of the city Săcele. Accumulation is achieved by a filling of earth dam with clay core. The end of the paper from the analysis results is presented conclusions and recommendations on the design of dams from local materials.**

***Keywords* – embankment dams, nonlinear analysis, stress, strain.**

1. INTRODUCTION

Earth dams represent the most common and oldest category of all dams. With all the spread and the age of earth dams, with all the remarkable scientific and technologic progresses realised in this domain, especially in the last five decades, the knowledge of the behaviour of the earth dams at sudden variations of the water level in the reservoir is not totally understood.

Because of these reasons, in this work is represented and studied with the help of numeric methods based on MEF, the nonlinear behaviour of earth dams and the sudden variations of levels in the reservoir, adding to a better knowledge of the studied phenomena, the rise in performance and safety in the use of earth dams.

For the analysis of the state of stress and strains is important to take in consideration the hypothesis of sudden variation of water level in the reservoir. This sudden variation can appear in the situation in which is necessary of a rapid empting or the case of a flood wave [3]. The rapid empting of the dam may appear necessary for reasons of safety of the dam, urgent needs of the use of the water in the reservoir or other special situations.

Therefore, a series of numerical simulations were made, using Cosmos 2.5 finite element program, in order to show how the earth dams react in case of sudden emptying water in the lake. These simulations were done at the Sacele Dam, located on the Tarlung river, affluent of Negru river which is an affluent of Olt River. The dam is located approx. 3 km upstream of Sacele town.

Gelmambet Sunai is with Ovidius University of Constanta, Bd. Mamaia nr. 124, 900356-Constanta, Romania (e-mail: gelmambets@univ-ovidius.ro).

ISSN-1584-5990

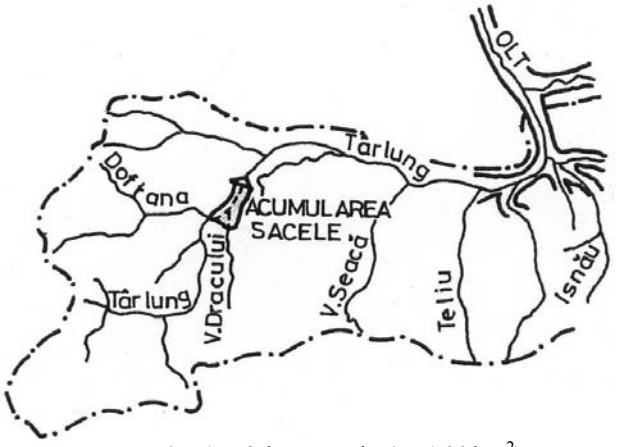

Fig. 1. Târlung Basin (F=166 km^2)

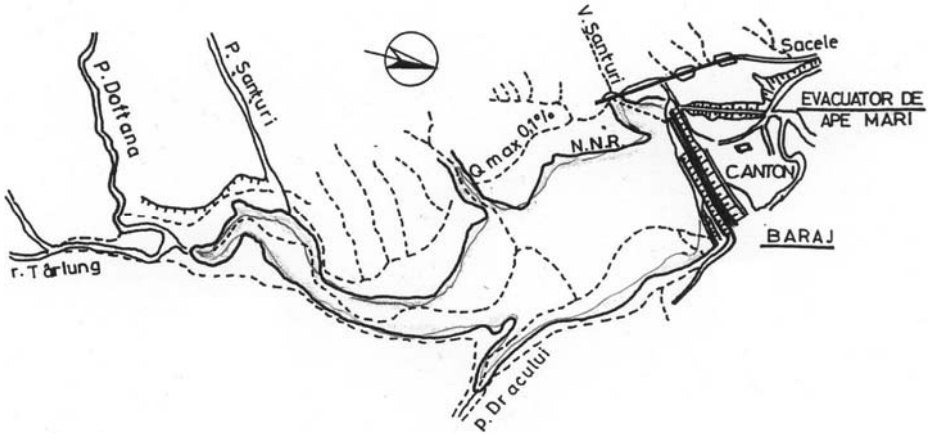

Fig. 2. The situation plan of the Săcele lake

Accumulation is achieved by an earth dam with a clay core. Other objects of the facility are: the overflow of large water, situated on the left bank and the intakes tower which controls the access to the bottom drain and supply gallery, both located on the right side. Section dam's is shown in Fig. 3.

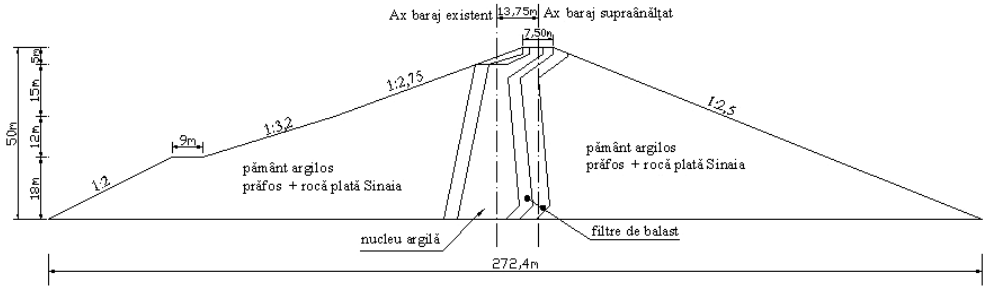

Fig. 3. The section of Sacele dam

2. NUMERICAL SIMULATION

This simulation was performed for a sudden descending of the water level from 745 mdM to 618 mdM (a sudden descending of the water level on 27 m difference of level). The descending speed of water level was assumed to be 4.2 m/day, so the sudden descending would occur in 6.42 days. This value was chosen based on studies of water level variations in time. Fig. 4 presents the section of the dam and the water level variation. A nonlinear analysis, using the Drucker-Prager plastic flow criteria, was used to simulate the action of Sacele dam.

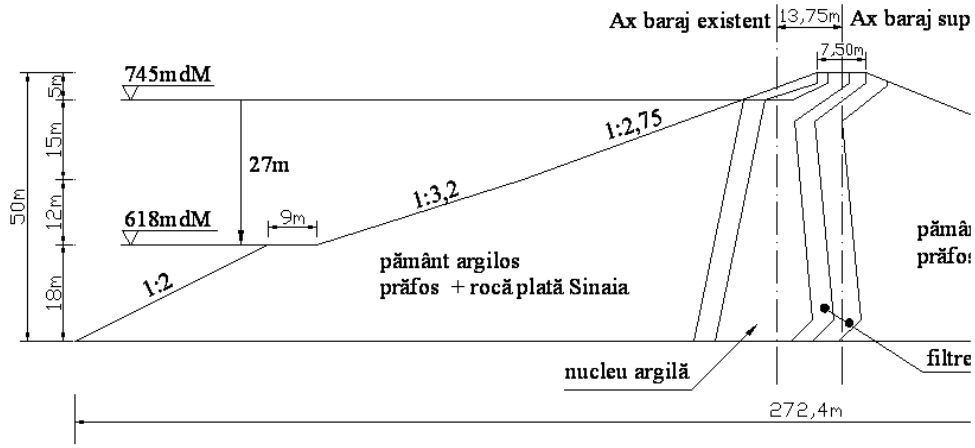

Fig. 4. The section of Sacele dam, with the difference of the water level

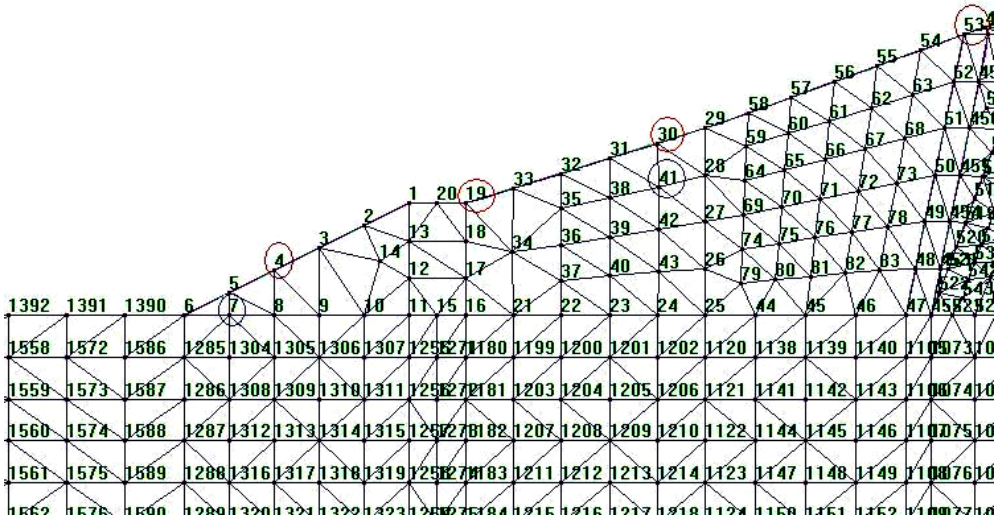

Fig. 5. The numbering of nodes

In 4, 19, 30 and 53 nodes are represented the diagrams of displacement variations, and in 7 and 41 nodes are represented the diagrams of tension variations. The results obtained are presented in the following figures.

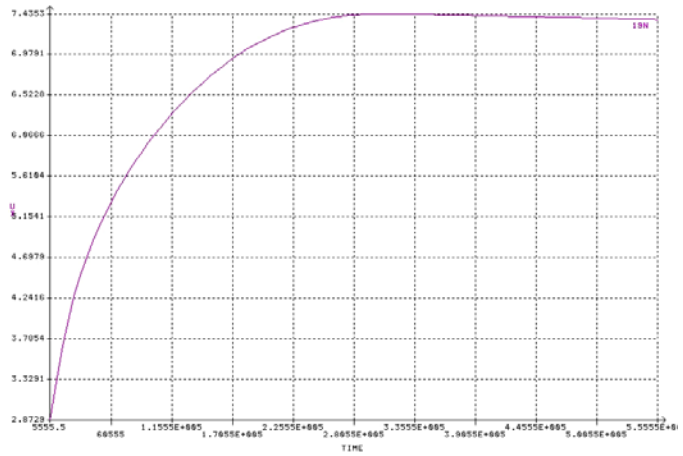

Fig. 6. The variation of the displacement in the x direction in node 19 (cm)

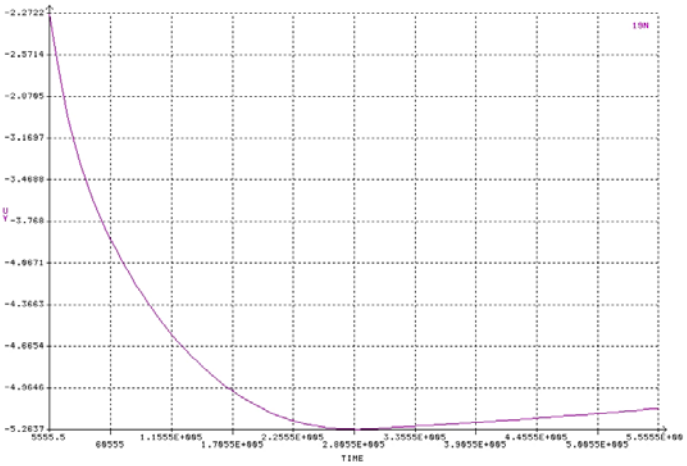

Fig. 7. The variation of the displacement in the y direction in node 19 (cm)

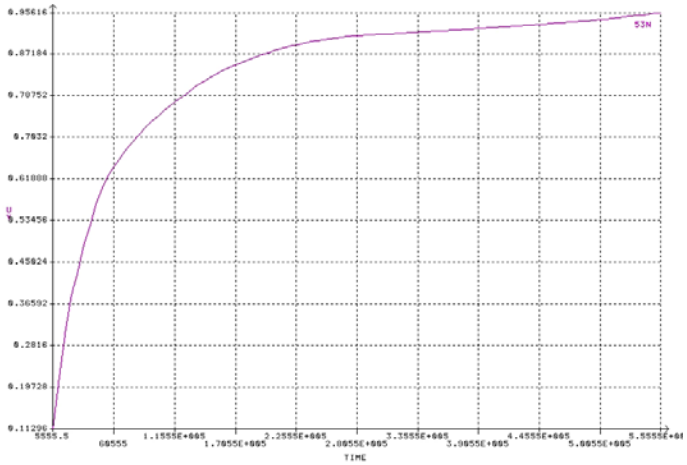

Fig. 8. The variation of the displacement in the y direction in node 53 (cm)

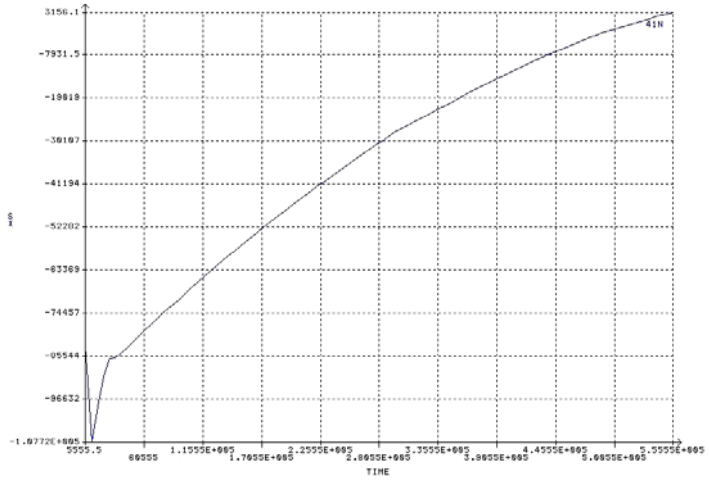

Fig. 9. The variation of the stress σ_x in node 41 (Pa)

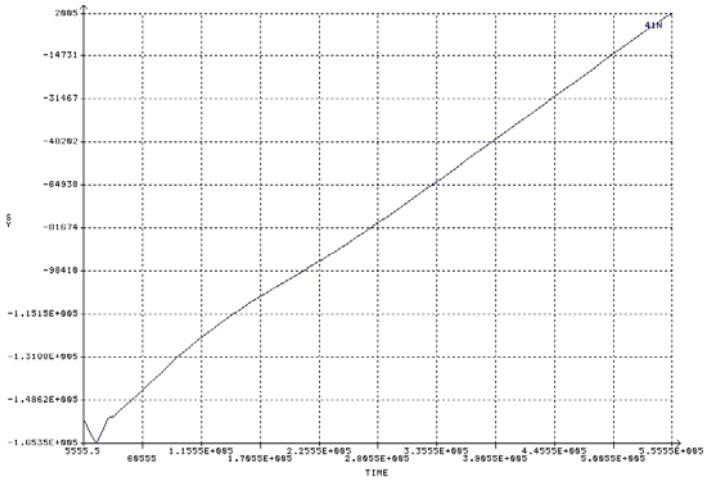

Fig. 10. The variation of the stress σ_y in node 41 (Pa)

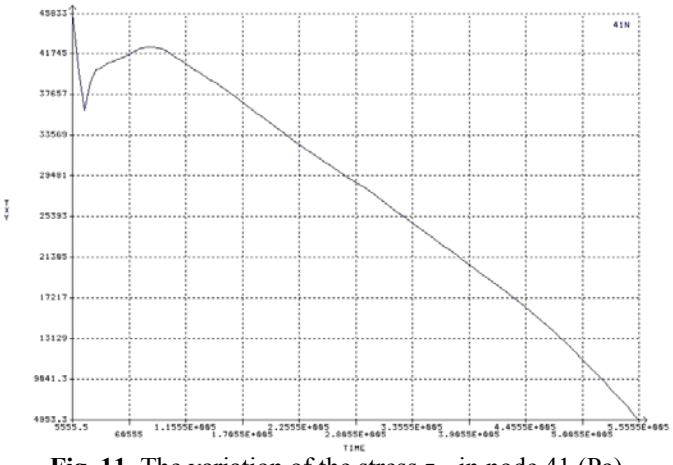

Fig. 11. The variation of the stress τ_{xy} in node 41 (Pa)

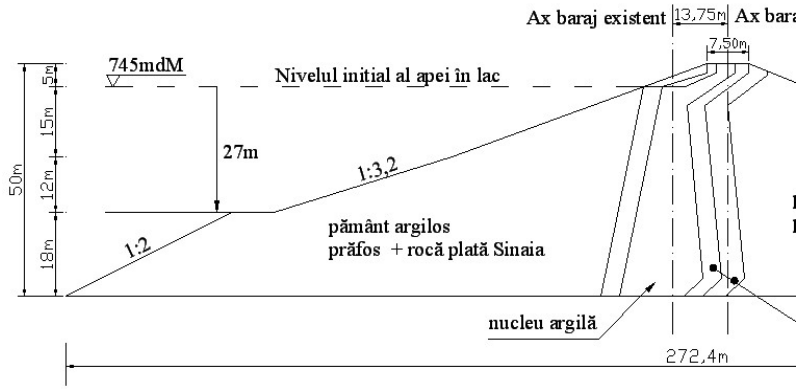

Fig. 12. The section with the water level after going down 27m equivalent to 100 integration step from t = 555,552 seconds is 6.42 days

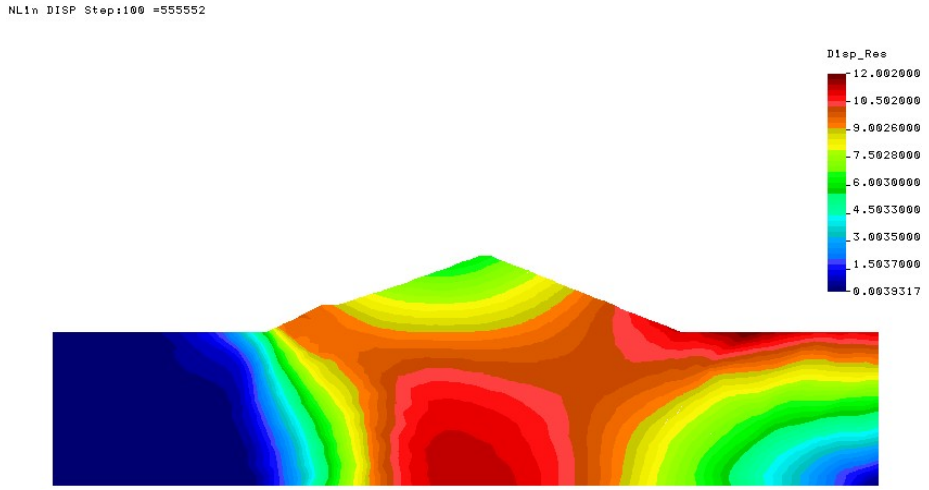

Fig. 13. The displacement diagram when the water level in reservoir going down 27m. (cm)

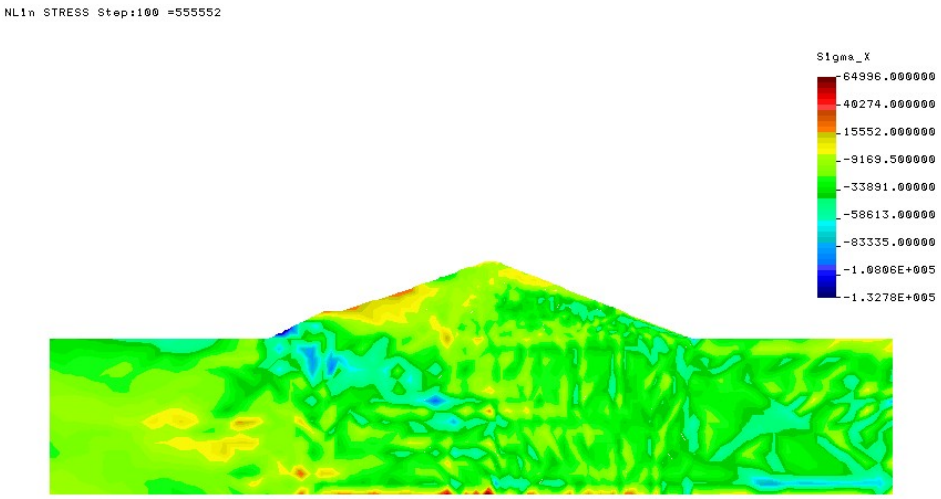

Fig. 14. The stress diagram σ_x when the water level in reservoir going down 27m. (Pa)

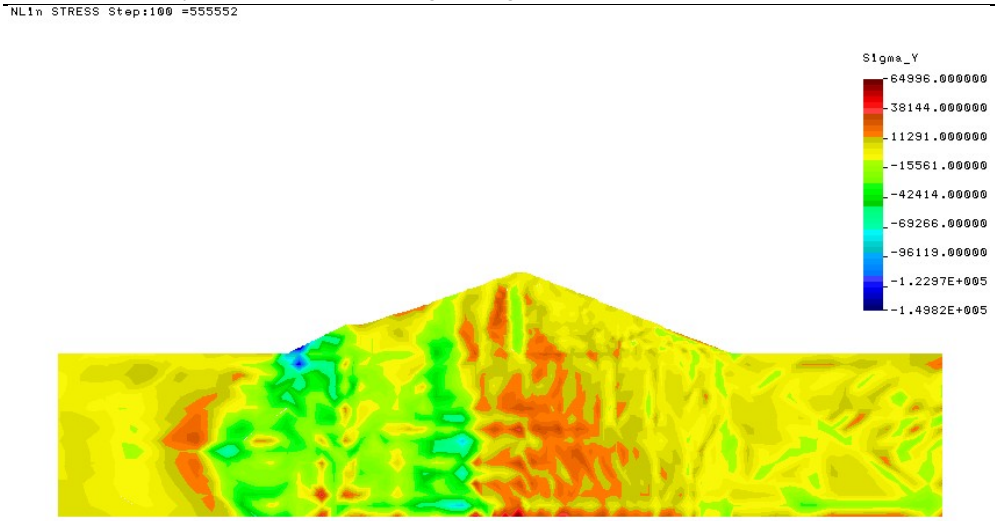

Fig. 15. The stress diagram σ_y when the water level in reservoir going down 27m. (Pa)

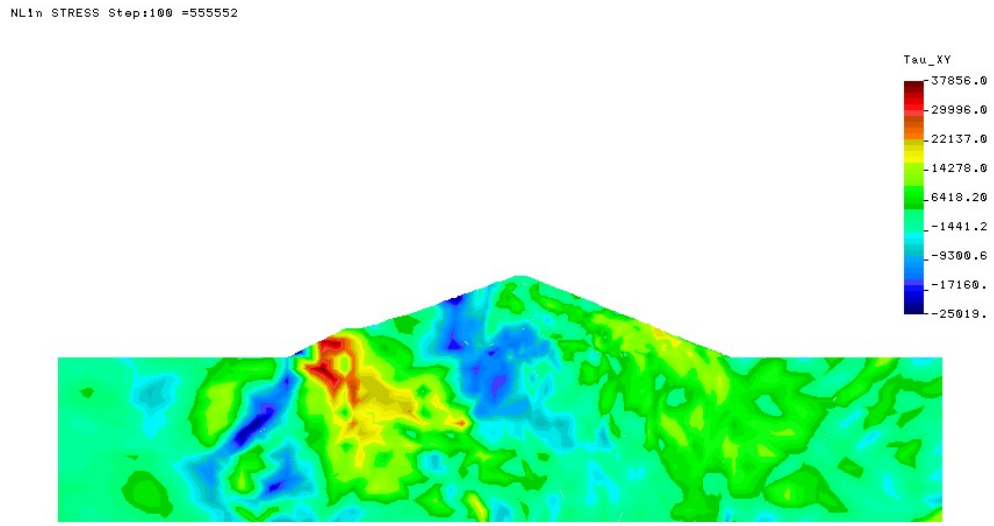

Fig. 16. The stress diagram τ_{xy} when the water level in reservoir going down 27m. (Pa)

3. CONCLUSIONS

Analyzing the results obtained, note that, if the water level sudden drops, the stress values decrease as the water level drops. Because the deformations of the dam are plastic deformations, the displacement values remain the same and don't decrease considering the water level. The horizontal movement at the upper part of the dam still has an elastic behaviour and doesn't essentially effect the deformations. The hydrostatic pressure to a fast decrease in the upstream area of the dam because fast emptying.

A cause of failure of earth dams can be the slipping of the upstream billow due to sudden emptying of water level of the lake. From this reason, the design must pay attention to the stability of upstream billow in case of sudden emptying.

The complex nature of action of the embankment dam at the fast emptying of the lake requires a careful monitoring through their entire emptying. Comparing data obtained from measurements with predictions of design calculations, making post analyze is the most direct way of understand the phenomena and to prevent the incidents or accidents. Based on the studies in this essay and studies in technical literature, the following recommendations for calculations can be done:

- it is appropriate to use nonlinear analysis for calculations and to avoid, as possible, linear analysis for calculations, because nonlinear analysis leads to results much closer to reality.
- it is appropriate to use tensions- deformations correlations obtained from laboratory tests that reflect more realistic nonlinear material action.
- use of plasticity theory concepts leads to good results.
- to obtain results close to reality, it is important to consider the interaction with foundation soil, the liquid in lake and pore water pressure.
- to establish data entry for nonlinear analysis must pay attention to material characteristics.

4. REFERENCES

[1] Dibaj,M., Penzien, J., Nonlinear seismic response of earth structures, Report No. EERC 69-2 , Univ. of California, Berkeley, 1974.

[2] Popovici, A., Dynamic analysis by numerical methods, 1978, I.C.Bucuresti..

[3] Popovici, A., Dams for water accumulation, Vol.II, 2002, Editura Tehnică Bucuresti.

[4] Gelmambet, S., Dam-foundation seismic interaction analysis, Simpozionul Concepții Moderne în ingineria Amenajărilor Hidrotehnice, 13 mai 2005, Timişoara, Buletinul Ştiințific al Universității „POLITEHNICA" din Timişoara, Seria Hidrotehnică, Tomul 49 (63), Fascicola 1, pag.46-53, Editura Politehnica, România 2005;

[5] Gelmambet, S., Dam-reservoir seismic interaction analysis, The XXXth National Conference of Solid Mechanics Mecsol 2006 , 15-16 septembrie 2006, Constanta, Vol.9 pag.251-258.

[6] Zienkiewicz, O.C. The finite element method in engineering science, McGraw-Hill, London, 1971.

[7] Zienkiewicz,O.C., Bettess,P. Fluid-structure Dynamic interaction and wave forces; an introduction to numerical treatment, Int.J.Num.Meth.in Engng., Vol.13, 1978.

Studies and Research to Realize Water Intakes Located in the Suction Basin of the Draining Station Baciu 1

Gelmambet Sunai

Abstract – **The draining station - SPD Baciu 1 - is located at 8 km from the village Rasova - Constanta County, on the right bank of the Danube River. The draining station - SPD Baciu 1 is part of the draining system Rasova - Vederoasa. The station serves an area of 1053 hectares and over waters drainage channel Baciu 1, length 2270m, discharging in Danube River. For rehabilitation and modernization Baciu1 draining station for restoring it to the parameters of the project was realized water intakes for placement of two submersible electro pumps. The paper presents studies and research stresses and strains analysis of the hydro construction and execution details necessary for achieving it.**

Keywords – **draining station, stress analysis, strain analysis, water intakes.**

1. INTRODUCTION

Climate change from the last years, who led to repeated flooding to our country, drew attention to the importance of the draining systems. Baciu draining pumping station, from the Rasova Vederoasa draining system, was designed and built to drain the excess of water from an area of approximately 1053 ha. This area is bounded by Ostrovul Lung on the North and by Vederoasa Lake and by the national road Rasova- Ion Corvin on East, South and West.

The station was put into operation in 1981. It is equipped with two axial horizontal pumps, type AR-7-85. Theoretical efficiency of pumps at the operating point H= 4,2 m and Q= 1 mc/s is 55%. So, since the entry into service, the station had a low efficiency, corresponding to the technological level of the eighties. Over the time, the efficiency decreased due to long wear of the aggregates and installation, lead to significant energy consumption.

Station operation takes place at geodesic heights that varies in a wide range because of level variation of the Danube. So, the operating point moves on a considerable range. The contract of research under the theme „Energy efficiency optimization of the draining station Baciu, Constanta" says that the contractor undertakes to develop a study to determine modernization measures of the draining pumping station to increase energetic efficiency, considering the level variation of the Danube.

Gelmambet Sunai is with Ovidius University of Constanta, Bd. Mamaia nr. 124, 900356-Constanta, Romania (e-mail: gelmambets@univ-ovidius.ro).

ISSN-1584-5990

For the rehabilitation and modernization of draining station Baciu1, in order to restore its projected parameters, a water intakes was made for two submersible pumps, pumps how will replace the two axial, horizontal pumps, type AR-7-85.

2. NUMERICAL SIMULATION

In order to design the water intake, a series of numerical simulations was made, using the finite element program – Cosmos 2.6., for the analysis of the tension and deformation of the reinforced concrete structure.

Simulations were performed for two situations: full vacuum tank and empty vacuum tank. Figure 1 presents the situation plan with the location of the draining pumping station. Figure 2 presents the section and the plan view of the pumping station Baciu.

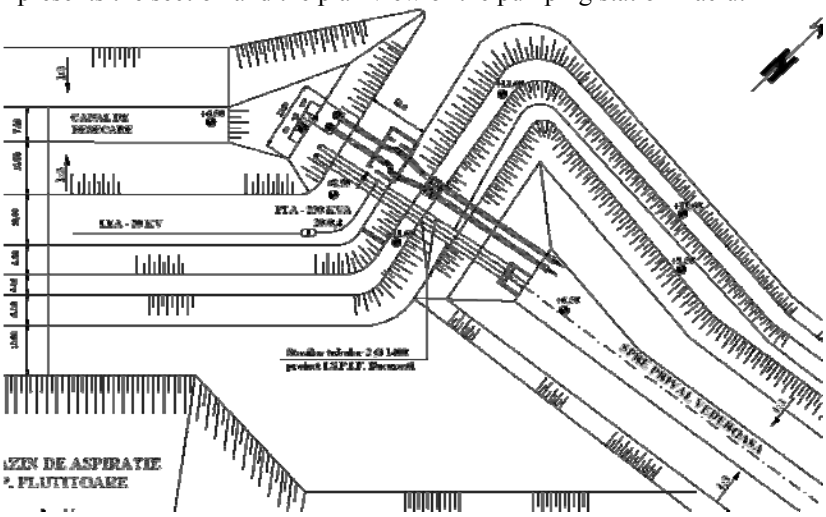

Fig. 1. Situation plan

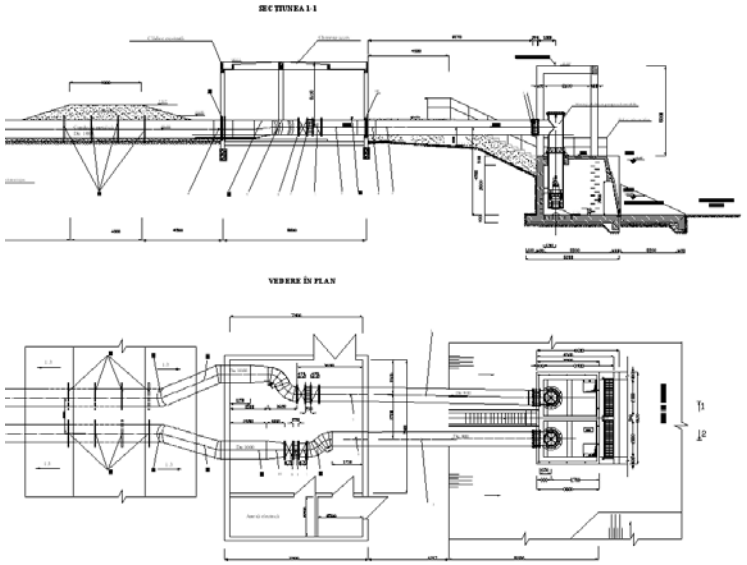

Fig. 2. Plan view and the section of the draining station Baciu

Following numerical simulations performed using the program is presented diagrams of stresses and strains obtained.

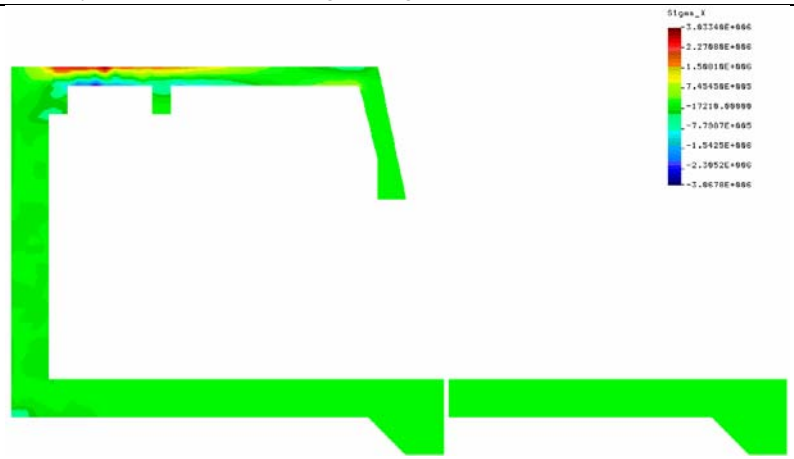

Fig. 3. The stress diagram σ_x (Pa)

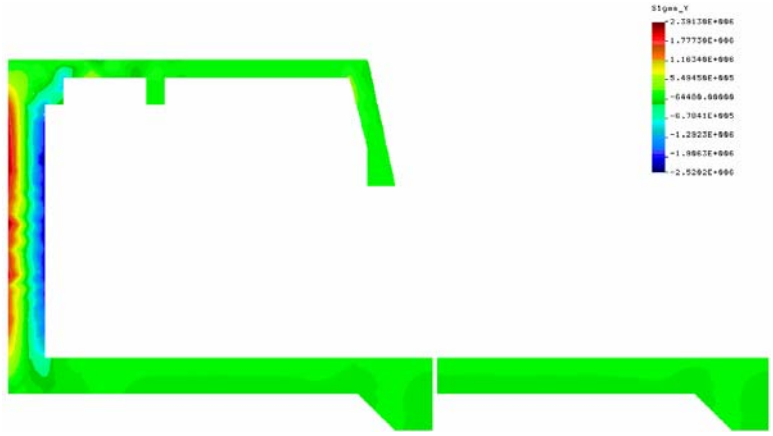

Fig. 4. The stress diagram σ_y (Pa)

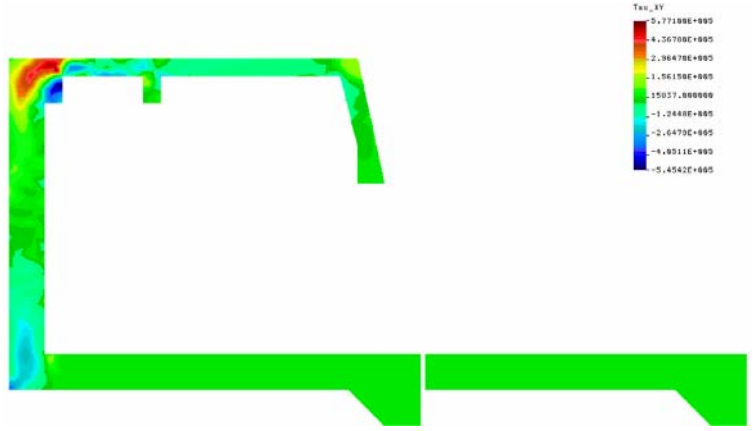

Fig. 5. The stress diagram τ_{xy} (Pa)

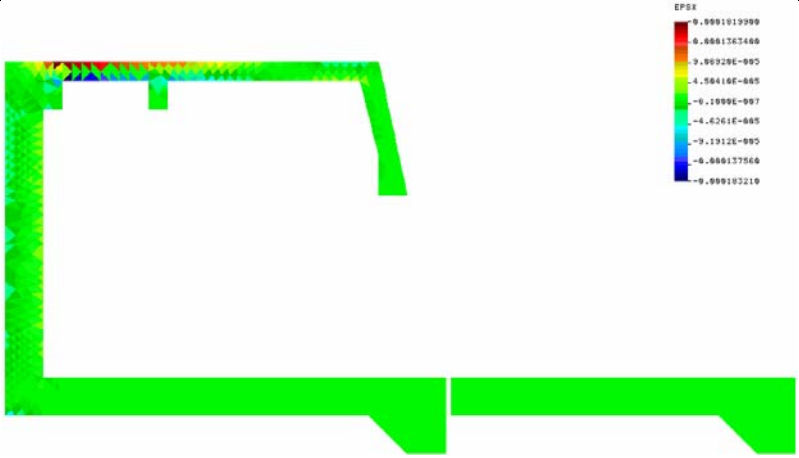

Fig. 6. The strain diagram ε_x

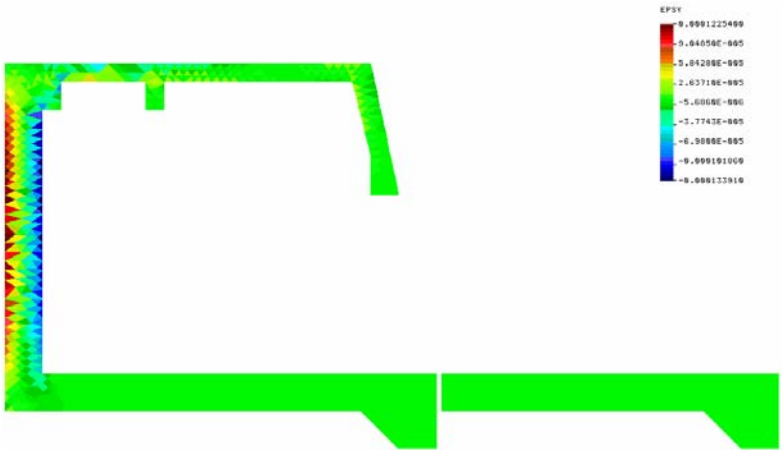

Fig. 7. The strain diagram ε_y

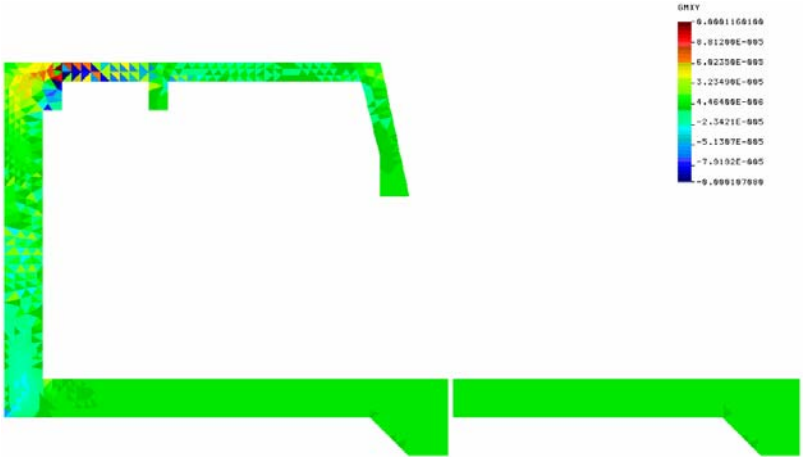

Fig. 8. The strain diagram γ_{xy}

3. CONCLUSIONS

The analysis of the stresses and strains diagrams shows that most stressed area is the goal of placing submersible pumps. We can observe in that area there is a stress concentration and it was necessary an additional reinforcement (see fig.9). Another area in which there are higher values of stresses and strains is the back wall of the tank, especially the connection area between plate and this wall. Reinforcing this area is presented in fig. 10. Excepting these areas of tensions concentration, the tensions values in structure are small.

The reinforcement plans, presented in the figures below, are made considering the analysis and calculations made.

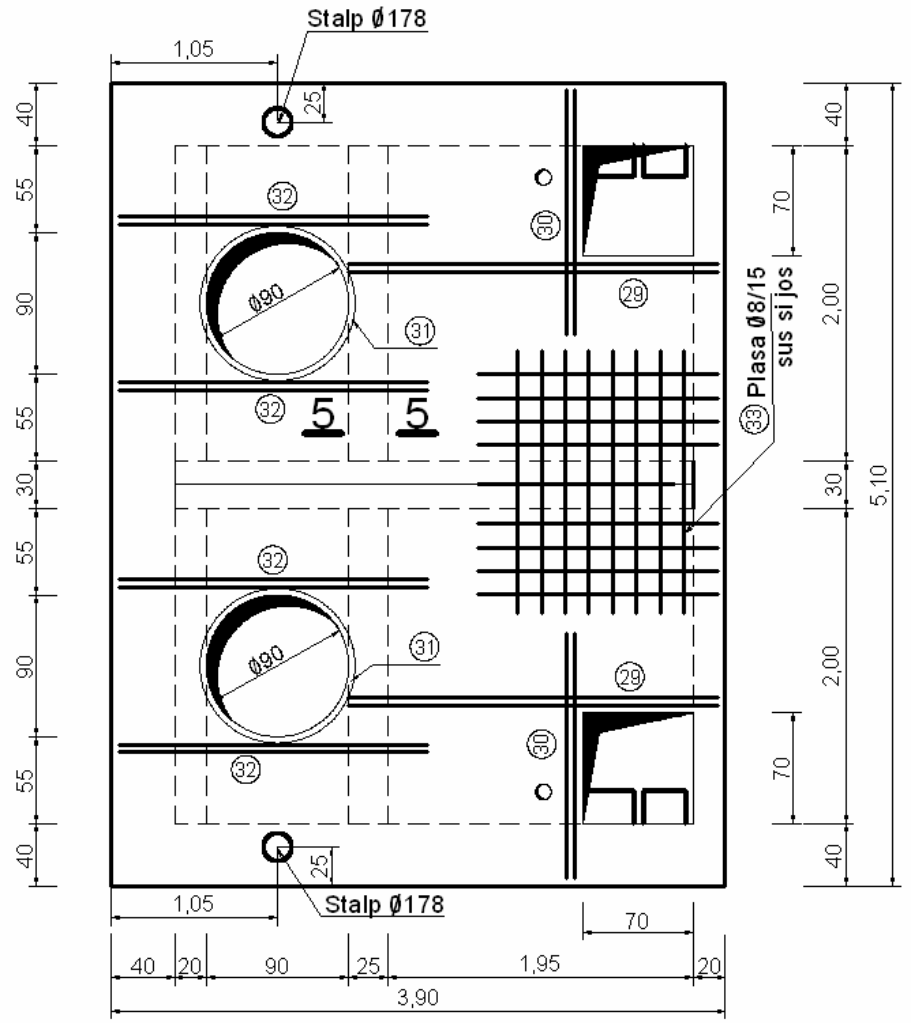

Fig. 9. Reinforcement plate plan

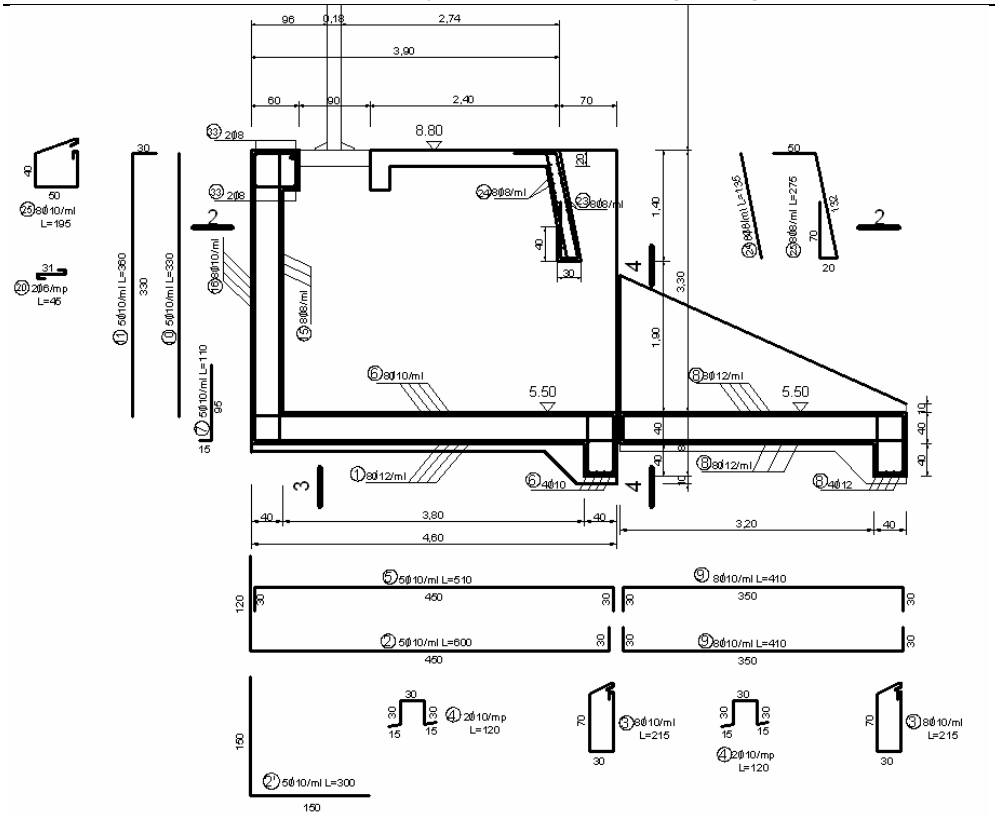

Fig. 10. Reinforcement plan section 1-1

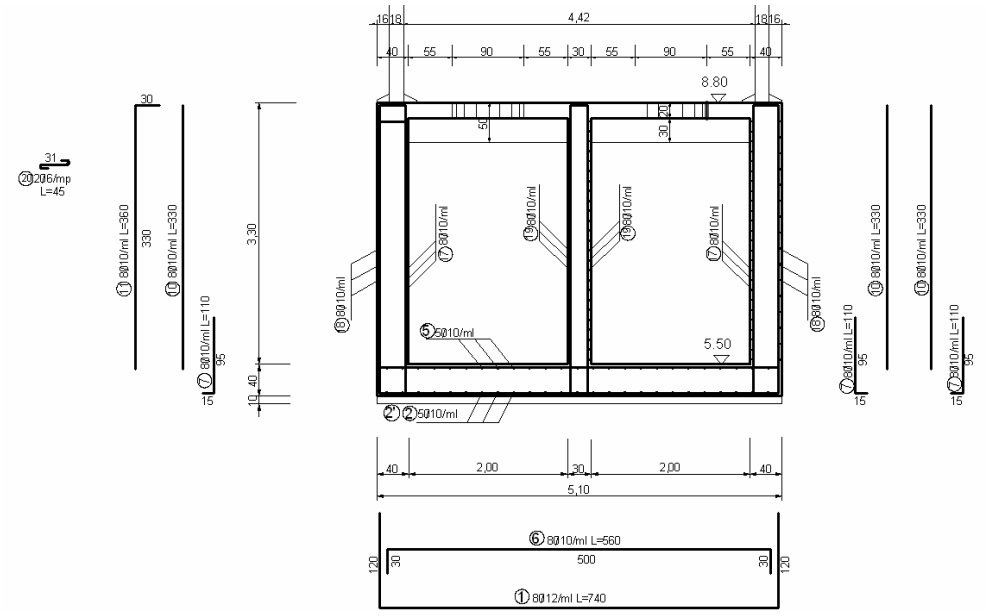

Fig. 11. Reinforcement plan section 3-3

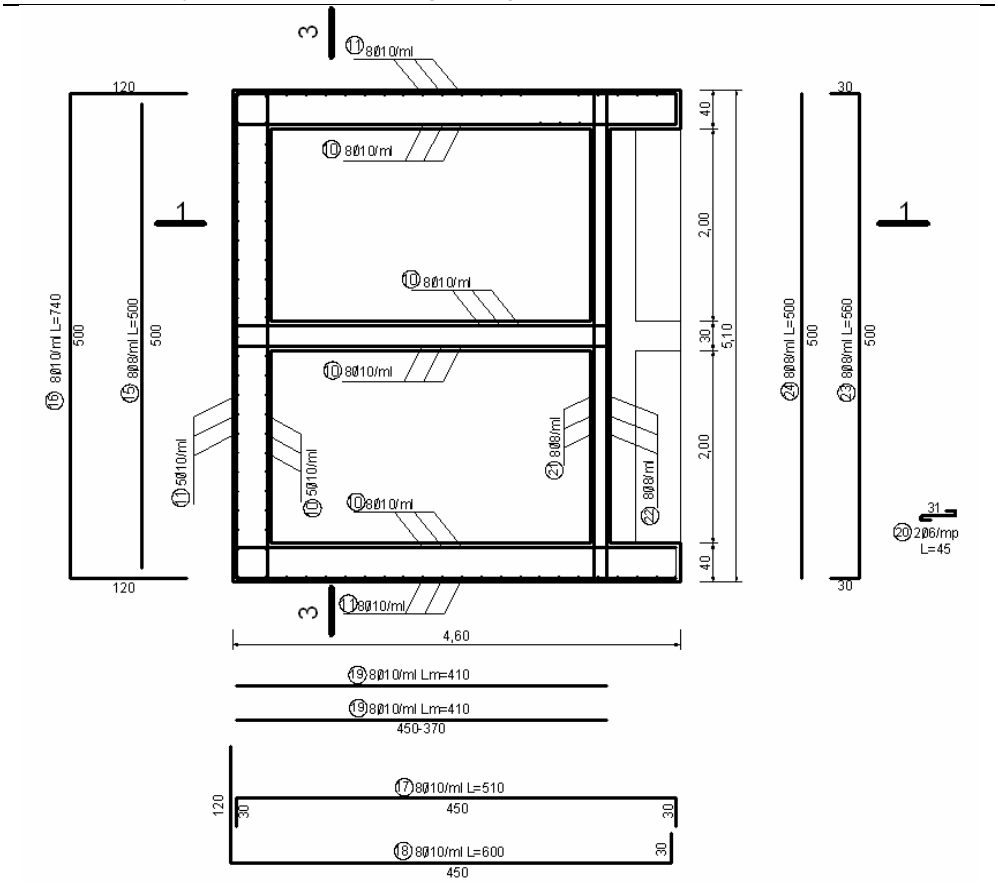

Fig. 12. Reinforcement plan section 2-2

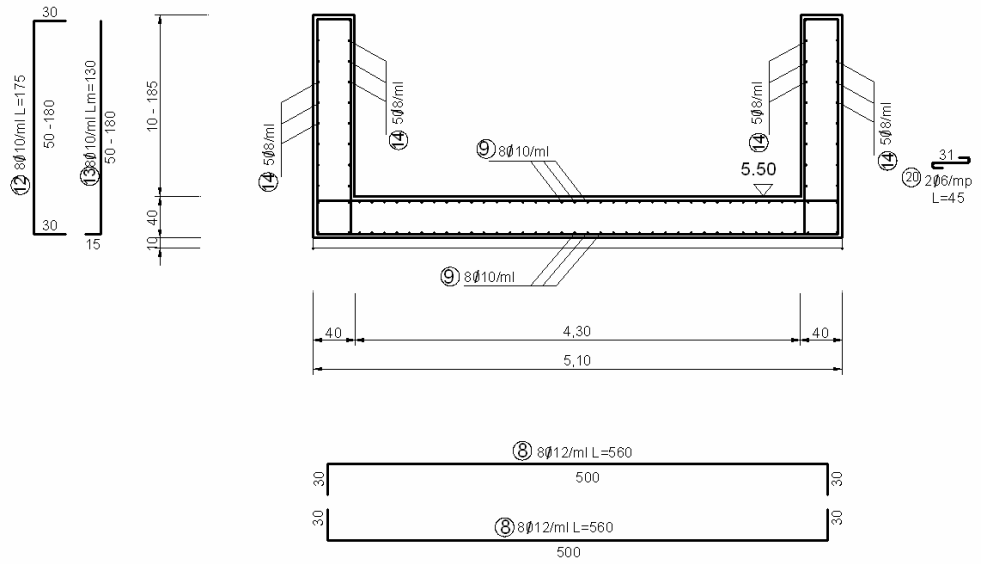

Fig. 13. Reinforcement plan section 4-4

4. REFERENCES

[1] *** Cosmos/M Manual Teoretic, Structural Research Corporation, Santa Monica USA, 1996.
[2] Breaban V., Gelmambet S., The influence of the water level variation in reservoirs upon the earth dams strain state, Ovidius University Annals – CONSTANTZA year IX (2007) series: Civil Engineering, Volume 1, Proceedings of The Symposium CIVIL ENGINEERING 2007 - the 30-th anniversary of higher education in civil engineering in Constantza 2007, May, 3 - 5 ISSN 1584-5990.
[3] Dibaj,M., Penzien, J., Nonlinear seismic response of earth structures, Report No. EERC 69- Univ. of California, Berkeley, 1974.
[4] Gelmambet S., The analysis of the embankment dams strains caused bay sudden variations of the reservoir water level – Teza de doctorat, Universitatea Ovidius Constanta, decembrie 2006.
[5] Gelmambet, S., - Dam-reservoir seismic interaction analysis, The XXXth National Conference of Solid Mechanics Mecsol 2006, 15-16 septembrie 2006, Constanta, Vol.9 pag.251-258.
[6] Gelmambet, S., Dam-foundation seismic interaction analysis, Simpozionul Concepţii Moderne în ingineria Amenajărilor Hidrotehnice, 13 mai 2005, Timişoara, Buletinul Ştiinţific al Universităţii „POLITEHNICA" din Timişoara, Seria Hidrotehnică, Tomul 49 (63), Fascicola 1, pag.46-53, Editura Politehnica, România 2005;
[7] Popovici, A., Dams for water accumulation, Vol.II, 2002, Editura Tehnică Bucuresti.
[8] Popovici, A., Dynamic analysis by numerical methods, 1978, I.C.Bucuresti..
[9] Zienkiewicz, O.C. The finite element method in engineering science, McGraw-Hill, London, 1971.
[10] Zienkiewicz,O.C., Bettess,P. Fluid-structure Dynamic interaction and wave forces; an introduction to numerical treatment, Int. J. Num. Meth in Engng., Vol.13, 1978.

An Investigation of Energy Dissipation in Various Types of Stepped Spillways including Inclined Steps and Steps with End Sills by Numerical Model

Naderi Rad

***Abstract* – the aim of this research is to evaluate energy dissipation in various types of stepped spillways; inclined steps and steps with end sills by taking into accounts parameters such as; characteristic height of step(m), flow discharge per unit width (q) and overall slope of steps stepped spillway(θ) by numerical method. In this research the governing equations are solved by finite volume discretization method and the standard $k-\varepsilon$ model is used for estimating the turbulence flow. In this research the structured grid is used to accommodated the well-defined boundaries and the volume of fluid (VOF) method is introduced to solve the complex free-surface problem. Results of the numerical method compare well with the experimental results of other researchers.**

***Keywords* –Stepped Spillways, Inclined Steps, Steps with End Sills, Standard $k-\varepsilon$ Model, Volume of Fluid (VOF)**

1. INTRODUCTION

The implication of stepped spillway started 3500 years ago .The first stepped spillway used in a dam in ancient Greece a bout 1000 B.C. This kind of spillway can be used in different types of dam such as Roller compacted concrete . During the recent decades the advent of modern technology and roller compacted concrete have brought the usage of stepped spillways to attention . That is because stepped spillway construction is compatible with the RCC technique (chanson & Gonzalez 2005).

2. TYPES OF STEPPED SPILLWAYS

Stepped spillways can be classified into 3 groups:

1- stepped spillway with simple steps
2- stepped spillway with end sills
3- Stepped spillway with inclined steps

Fig.1 depicts all these types. In Fig.3 different parameters such as height of steps(s). Length of steps (L) and the increment in step's height due to end sills or inclined steps were showed.

Department of Civil Engineering, Malayer Branch of Azad University, Malayer, Iran, Naderi@iau-malayer.ac.ir

ISSN-1584-5990

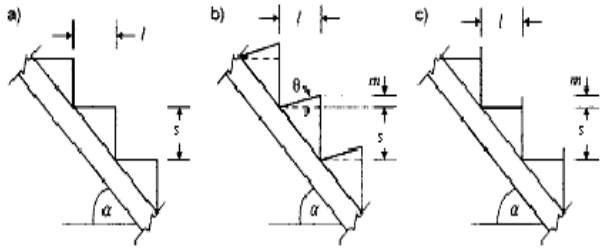

Fig.1- Different types of stepped spillways (Chinnarasi and Wongwisess, 2006)

3. LITERATURE REVIEW

3.1. Dimensional analysis of parameters affect Energy dissipation in stepped spillways:

The main parameters influence on energy dissipation in stepped spillways are the number of steps (N) steps height (S) length of steps (L) width of steps (b) initial flow energy of upstream (E1) discharge per unit width (q) and the increment of steps height due to steps inclination or end sills. Therefore we have eq. 1:

$$E_L = E_L(E_1, q, l, s, g, m) \tag{1}$$

By dimensional analysis we then have :

$$\frac{E_L}{E_1} = \frac{E_L}{E_1}\left(\frac{y_c}{s}, \frac{s}{l}, \frac{m}{s}, N\right) \tag{2}$$

Which is none dimensional.

As shown In Eq. (2), critical flow depth (yc) in a rectangular conduit, $y_c = \left(\frac{q^2}{g}\right)^{\frac{1}{3}}, N, s, l, q, m, g, E$ are the main parameters (Chinnarasi & Wongwisess 2006).

3.2. How to determine the type of flow over stepped spillways:

In this section we refer to the equations proposed by researchers to determine the types of flow over stepped spillways:Chinnarasi & wongwisess in 2006 proposed equations 3 and 4 for inclined stepped spillways.

The Minimum critical depth for having skimming flow obtained from Eq. 3, and the maximum yc for nappe flow in simple and inclined spillway got from Eq.4.

$$\frac{y_c}{s} = (0.844 + 0.003\theta)\left(\frac{s}{l}\right)^{-0.153+0.004\theta} \tag{3}$$

$$\frac{y_c}{s} = (0.927 - 0.005\theta - 0.388\left(\frac{s}{l}\right) \tag{4}$$

in Equations 3 & 4 θ the slope of steps and s is steps height which can be replaced by eq . 5 for spillways with End sills (chinnarasi end Wongwisess 2006).

$$\theta = \tan^{-1}\frac{m}{l} \tag{5}$$

3.3. Laboratory equations for calculating Energy dissipation in stepped spillways:

Chinnarasi and wongwisess in 2006 found equation 6 for inclined spillways and spillways with end sills.

$$\frac{E_L}{E_1} = \eta\left(\frac{y_c}{s}\right)^{\xi} \tag{6}$$

η, ξ can be calculated from eq.7 for inclined spillways and for stepped spillways end sill from eq. 8 (Chinnarasi and Wongwisess, 2006).

$$\eta = -0.034\ln\left(\frac{s}{m}\cdot\frac{s}{l}\right) + 0.767$$
$$\xi = -0.015\ln\left(\frac{l}{m}\right) - 0.216 \tag{7}$$

$$\eta = -0.028\ln\left(\frac{s}{m}\cdot\frac{s}{l}\right) + 0.812$$
$$\xi = -0.030\ln\left(\frac{l}{m}\right) - 0.149 \tag{8}$$

3.5. Numerical model study of spillways by other researchers:

Tabbora et. al., in 2005 conducted studies on stepped spillway by using finite element analysis. They applied k-ε model to account for turbulence (Tabbara et al., 2005). Chatial & Tabbara in 2004 studied ogee spillways numerically. They used finite element method and k-ε model for this purpose (chatila & Tabbara 2004). Chatila & Tabbara in 2004, and Tabbara et. al., in 2005 took velocity boundary condition to study energy dissipation over stepped spillway and ogee spillway for initial boundary condition they applied a flow profile assuming that the profile reduced the solution time. To achieve their studies they used ADINA software which used finite element to solve the problems (Chatila & Tabbara, 2004 Tabbara et. al., 2007).

The aim of this research is to evaluate energy dissipation in stepped spillways by taking into accounts parameters such as; characteristic height of step(m), flow discharge per unit width (q) and overall slope of steps stepped spillway(θ)by numerical method. In this research the governing equations are solved by finite volume discretization method and the standard $k-\varepsilon$ model is used for estimating the turbulence flow. In this research the structured grid is used to accommodated the well-defined boundaries and the volume of fluid (VOF) method is introduced to solve the complex free-surface problem.

4. GOVERNING EQUATION OF FLOW FIELD

The governing equations of incompressible, viscous fluid are a continuity equation and three momentum equations in three directions. There equations are known as Navior- stokes Equations. In fact, these equations express conservation of mass and momentum from mathematical points of view. Based on Eulearan points of view, if a particle of a fluid is considered as a fixed volume in computational space, the exerted forces on this particle and the principle of conservation of mass are expressed with partial differential equations. In this paper

the authors present a new configuration, simple stepped spillway, and numerically simulate this new configuration with using a finite volume code with the $k-\varepsilon$ closure to model the turbulence unsteady flow. The volume of fluid (VOF) method is an interface capturing scheme that has been used to model the free surface flow (Nikseresht et. al., 2008).

The momentum equation for the j direction of the turbulence flow reads:

$$\frac{\partial}{\partial t}\left(\rho u_j\right)+\frac{\partial}{\partial x_i}\left(\rho u_i u_j\right)= -\frac{\partial P}{\partial x_j}+\frac{\partial}{\partial x_i}\left[(\mu+\mu_t)\left(\frac{\partial u_i}{\partial x_j}+\frac{\partial u_j}{\partial x_i}\right)\right]+\rho g_j+F_j \tag{9}$$

where ρ is the density, P is the pressure, μ is the molecular viscosity, μ_t is the eddy viscosity which is determined by $k-\varepsilon$ closure model and *F* is any external forces.

Let $\vec{U}$ be the velocity vector field, then the incompressible continuity equation is:

$$\nabla\cdot\vec{U}=0.0 \tag{10}$$

Note that the dynamic condition, i.e., continuity of pressure at the interface is automatically implemented. The kinematic condition, which states that the interface is convicted with the fluid, can be expressed in terms of volume fraction *C* as follows (Nikseresht et. al., 2008):

$$\partial_t C+\vec{U}\cdot\nabla C=0 \tag{11}$$

In the VOF method, the interface is described implicitly(Nikseresht et. Al., 2008), the data structure that represents the interface is the fraction C of each cell that is filled with a reference phase, say phase 1. The scalar field C is often referred to as the color function. The magnitude of C in the cells cut by the free surface is between 0 and 1 (0<C<1) and away from it is either zero or one.

μ and ρ at any cell (denoted by ij) can be computed using a simple volume average over the cell :

$$\rho_{ij}=C_{ij}\rho_L+(1-C_{ij})\rho_a \tag{12}$$

$$\mu_{ij}=C_{ij}\mu_L+(1-C_{ij})\mu_a \tag{13}$$

where the subscripts *L* and *a* denote Liquid and air respectively.

4.1. Calibration Model:

At first a classical test which is the flow over a step is solved. The geometry, dimensions, flow field and the reattachment length of the circulation zone downstream of the step is depicted in Fig. 2. Fig. 3 shows the boundary conditions of this problem. To check the accuracy of this numerical analysis, the numerical velocity at x position of .05 meter from the step, versus y (depth of the flow) are compared with the laboratory data in Fig. 4, and shows a good agreement. In table (1) the numerical reattachment length (X_r) is compared with laboratory reattachment length (Ruck, &Makiola, 1998). The percentage of error between these two methods is 6.97% which shows a good agreement.. Fig. 5 depicts the stream lines of flow field downstream of the step.

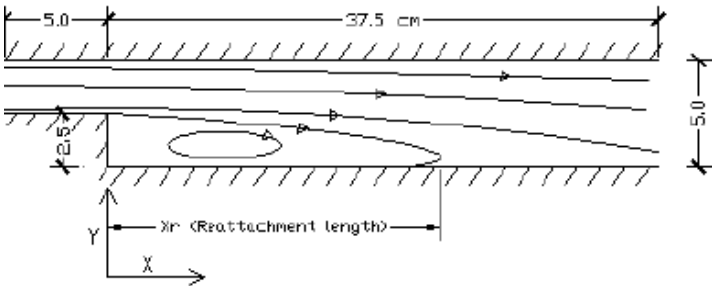

Fig.2- Flow over a step and eddies that appear down stream of step

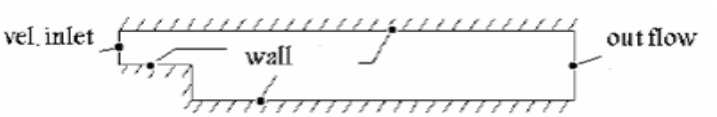

Fig. 3 - Flow field & boundary conditions

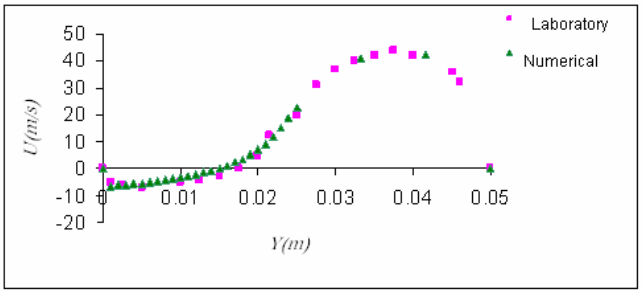

Fig. 4-Changes of velocity along depth (y) in standard $k-\varepsilon$ model by

Table.1-Results of X_r ***for laboratory and numerical tests***

X_r $(Reattachment\ \ length)$	***Method***
20.1	***Numerical***
21.5	***Laboratory***
6.97	***Percentage of Error***

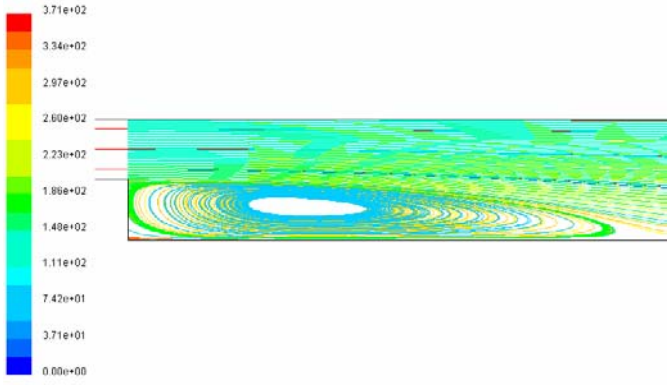

Fig .5- Streamline of flow over step

5. MESH GENERATION BOUNDARY CONDITIONS AND DISCRIMINATION OF EQUATRIONS

To generate meshes for the models m structured meshes were used, The size of meshes was chosen 5mm after several trial and Errors. The main reason for choosing this size was keeping y^+ in the range 30< y^+ <300 in boundary layers of walls. A commercially available computational fluid dynamics (CFD) program, which solves the flow filed. That basically uses finite volume method to accomplish numerical study of flow over stepped spillway .The power law method was applied to discretize the parameters.

Finally, the so-called SIMPLE algorithm was used to couple the velocity and pressure. Flow field calculation continues so that the residuals are less than 10^{-6}. In this research, unsteady Flow was initially modeled and calculations go on to reach steady state condition. Boundary conditions that were used were depicted in Fig.6, A is Velocity inlet boundary condition, B is air inlet boundary condition in terms of zero pressure m C is similar to B, D is wall boundary condition, F is out –let boundary condition in terms of zero relative pressure, and E is the initial free surface condition.

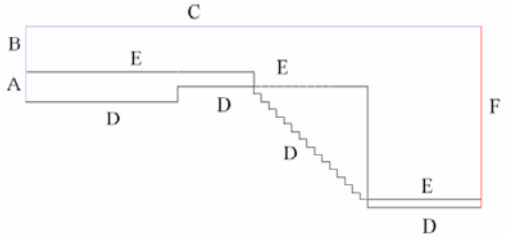

Fig. 6- Boundary conditions and numerical model of a stepped spillway

In the considered models, the length of reservoir is 1m, downstream is 1m, the height of reservoir is 10cm and total height of A and B is 50cm.

6. NUMERICAL MODELS

In this research 6 series of stepped spillways were studied each of which was examined for three different discharge .

Table (2) ,(3) includes the geometric charactistics, flow type, and the energy dissipation in inclined and with end sills stepped spillway. In tables, TR stands for transition, SK and NA represent for skimming and nappe, respectively.

Table . 2 - Geometric characteristics flow type and energy dissipation of inclined stepped spillway with numerical modeling solution

Group	$H_d(m)$	$q(\frac{m^3}{s.m})$	$y_c(m)$	$S(m)$	$L(m)$	H_{dam}	N	*Type Flow*	$\frac{E_L}{E_1}\%$	θ *(degree)*	α *(degree)*
1	**0.05**	**0.019**	**0334.0**	**05.0**	**05.0**	**8.0**	**16**	**TR**	**16.88**	**3.11**	**45**
	0.1	**.0537**	**0667.0**	**05.0**	**05.0**	**8.0**	**16**	**SK**	**96.80**	**3.11**	**45**
	0.15	**.09870**	**1.0**	**05.0**	**05.0**	**8.0**	**16**	**SK**	**72.73**	**3.11**	**45**
2	**0.05**	**0.019**	**0334.0**	**05.0**	**05.0**	**8.0**	**16**	**TR**	**94.87**	**8.21**	**45**
	0.1	**.0537**	**0667.0**	**05.0**	**05.0**	**8.0**	**16**	**SK**	**94.81**	**8.21**	**45**
	0.15	**.09870**	**1.0**	**05.0**	**05.0**	**.80**	**16**	**SK**	**51.75**	**8.21**	**45**
3	**0.05**	**0.019**	**0334.0**	**05.0**	**05.0**	**8.0**	**16**	**TR**	**94.87**	**96.30**	**45**
	0.1	**.0537**	**0667.0**	**05.0**	**05.0**	**8.0**	**16**	**SK**	**79.82**	**96.30**	**45**
	0.15	**.09870**	**1.0**	**05.0**	**05.0**	**8.0**	**16**	**SK**	**10.77**	**96.30**	**45**

Table. 3- Geometric characteristics, flow type, and energy dissipation of inclined stepped spillway with end sills by numerical solution

Group	$H_d\,(m)$	$q\,(\frac{m^3}{s.m})$	$y_c\,(m)$	$S(m)$	$L(m)$	H_{dam}	N	*Type Flow*	$\frac{E_L}{E_1}\%$	$m(m)$	α *degree)*
4	**0.05**	**0.019**	**0334.0**	**05.0**	**05.0**	**8.0**	**16**	**TR**	**28.83**	**01.0**	**45**
	0.1	**.0537**	**0667.0**	**05.0**	**05.0**	**8.0**	**16**	**SK**	**6.78**	**01.0**	**45**
	0.15	**.0987**	**1.0**	**05.0**	**05.0**	**8.0**	**16**	**SK**	**8.71**	**01.0**	**45**
5	**0.05**	**0.019**	**0334.0**	**05.0**	**05.0**	**8.0**	**16**	**TR**	**87.84**	**02.0**	**45**
	0.1	**.0537**	**0667.0**	**05.0**	**05.0**	**8.0**	**16**	**SK**	**72.81**	**02.0**	**45**
	0.15	**.0987**	**1.0**	**05.0**	**05.0**	**.80**	**16**	**SK**	**31.73**	**02.0**	**45**
6	**0.05**	**0.019**	**0334.0**	**05.0**	**05.0**	**8.0**	**16**	**TR**	**32.89**	**03.0**	**45**
	0.1	**.0537**	**0667.0**	**05.0**	**05.0**	**8.0**	**16**	**SK**	**2.82**	**03.0**	**45**
	0.15	**.0987**	**1.0**	**05.0**	**05.0**	**8.0**	**16**	**SK**	**79.74**	**03.0**	**45**

For with q equaled to 0.014, 0.0537, 0.0987 $m^3/(\sec.m)$. The designed height of spillway (H_d) was 0.05, 0.1, 0.15m and y_c (critical depth) were 0.0334, 0.0667, 0.1m. In group 1, 2 and 3 the slope of steps stepped spillway(θ) were 11.3, 21.8, 30.96 degree, respectively. In group 4, 5 and 6, the height increment of steps (m) were 0.01,0.02,0.03m, respectively.

In Figures (7) and (9) the profile of velocity in models were presented. The results of Numerical study of flow over stepped spillway with end sills were depicted in depicted in fig. 9. It states that with fixed number of steps and spillway slope increasing the sills height increases energy dissipation of spillway.

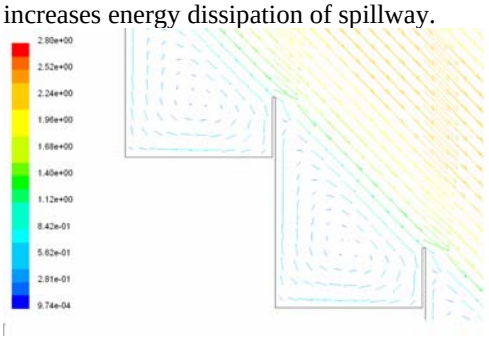

Fig. 7- Velocity vectors skimming flow over stepped spillways with end sills group10

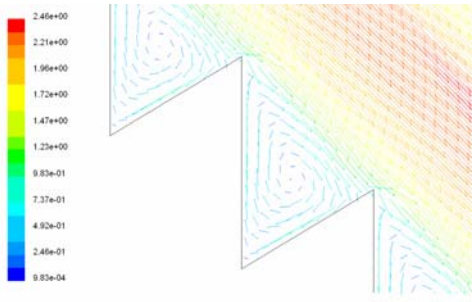

Fig. 8 - Velocity vectors skimming flow over simple inclined spillways group 7

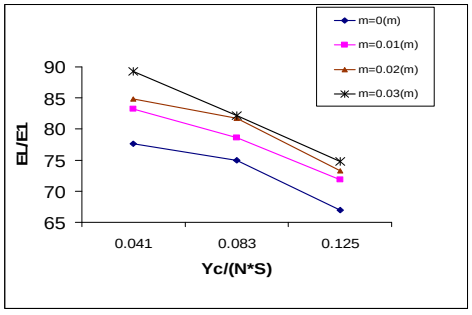

Fig. 9 – Variation of steps inclination in inclined spillways with end sills

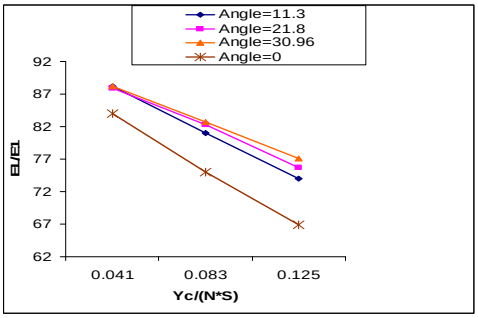

Fig. 10 – Variation of end sills height in stepped spillways with end sills

The results of numerical study of from over incline stepped spillway were presented in fig.10. According to the Fig.10, with fixed number of steps and spillway steps, increasing

the inclination of steps increases the efficiency of spillway in dissipating Energy. In two type of stepped spillway discharge plays the main role in energy dissipation and the type of flow that is existing over steps is not influential. In fact it can be stated that as discharge increases the amount of energy which dissipated along stepped spillway decreases.

8. COMPARISON BETWEEN THE RESULTS OF NUMERICAL STUDY AND THOSE OBTAINED FROM EXPERIMENTAL EQUATIONS

In tables (4) (5) and (6) the results of numerical-analysis of flow were compared with results obtained from Experiment equations proposed by Rajaratnam (1990) chanson (1994) and Christodoulou, (1993).

The results are in terms of the amount of energy dissipated. For calculating the error between the results the following relationship was used:

$$Error = \frac{\left| (\frac{E_L}{E_1})_{Experiment\ al} - (\frac{E_L}{E_1})_{Numerical} \right|}{(\frac{E_L}{E_1})_{Experiment\ al}} \quad (33)$$

In tables (4) and (5), the comparison between the results of numerical study and those experimental equations proposed by chinnarasi & wongwisess in 2006 for inclined stepped spillways and stepped spillways with end sills were shown. comparing the numerical results of current study with the results obtained from inclined steps and steps with end sills reveals that for discharge per unit width of 0.019, error was about 8 percent while for discharge per unit width of 0.0537 and 0.0987, errors were within 17 ~ 20 percent.

Table. 4- comparison of numerical results with those from Chinnarasi and Wongwisess (2006) for inclined stepped spillways group 7

$q(\frac{m^3}{s.m})$	$H_d(m)$	$\frac{E_L}{E_1}\%$ ***Numerical Method***	$\frac{E_L}{E_1}\%$ ***Chinnarasi and Wongwisess (2006)***	% ***Error***
0.019	**0.05**	**94.87**	**7.80**	**8.8**
.0537	**0.1**	**94.81**	**88.68**	**9.18**
.0987	**0.15**	**51.75**	**7.62**	**20.3**

Table. 5- Comparison of numerical results with those from Chinnarasi, and Wongwisess (2006) for stepped spillways with end sills group 9

$q(\frac{m^3}{s.m})$	$H_d(m)$	$\frac{E_L}{E_1}\%$ ***Numerical Method***	$\frac{E_L}{E_1}\%$ ***Chinnarasi and Wongwisess (2006)***	% ***Error***
0.019	**0.05**	**28.83**	**96.82**	**0.37**
.0537	**0.1**	**6.78**	**37.72**	**59.8**
.0987	**0.15**	**8.71**	**8.66**	**2.7**

For inclined stepped spillways, the comparison of numerical results with hose of chinnarsi and wongwisess from experimental studied showed 1-9 percent errors for different discharges.

9. COMPARISON OF NUMERICAL DETERMINATION OF FLOW TYPE WITH EXPERIMENTAL RELATIONSHIPS

Tables 6 include the comparison of numerical results with experimental way of chinnarsi and wongwisess (2006) for determination of flow type over stepped spillways with end sills and inclined stepped spillways .In tables, TR stands for Transition, SK and NA represent for skimming and nappe, respectively.

Table. 6 - Comparison of numerical results with experimental outcomes of Chinnarsi and wongwisess(2006) for determining flow type in inclined spillways and end sills spillways

$H_d\,(m)$	Numerical Method	Chinnarsi and Wongwisess (2006)
0.05	TR	TR
0.1	SK	SK
0.15	SK	SK

Figures 11 and 12 show the changing of different parameters and comparison of their results with experimental outcomes .

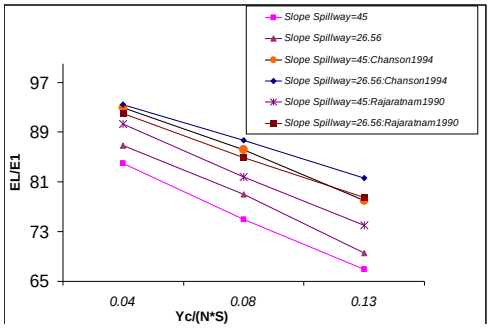

Fig 11- Rate of change of spillway's in numerical and experimental study for simple stepped spillways

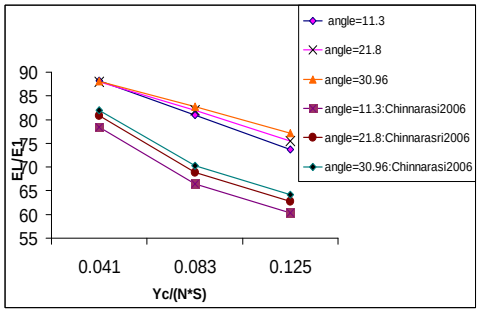

Fig 12- Rate of change of steps inclination for numerical experimental models

10. CONCLUSION

1- In spillways with end sills and fixed dam height number of steps length of steps steps height and spillway's slope, increasing the sills height increase the efficiency of spillway in dissipating energy . finally, in inclined stepped spillways and variable steps inclination, increasing the inclination increases the amount of dissipated energy .

2- By conducting this numerical study we can conclude that numerical method is a robust way of determining flow field over stepped spillway and can rival experimental and laboratory study . while experimental studies are highly affected by laboratory conditions in numerical study different conditions. Can be modeled and consider each condition's effect promptly .

3- In the case that stepped spillway is inclined stepped spillway and the slope is fixed increasing the sills height or inclining the steps are highly efficient in energy dissipation . In addition stepped spillways with end sills provide better situation from aeration points of view . when the spillway is constructed out of dam body the minimum slope is preferred . It is important to take the minimum steps' height if simple stepped spillway is taken . If the energy dissipation doesn't satisfy design criteria stepped spillway with end sills can be replaced .

4 - VOF, flow surface model, and the $k-\varepsilon$ turbulent model are suitable for modeling flow over stepped spillways. VOF model can be used for all flow type modeling and, hence, it obviates the determine flow type . The discrepancy between numerical and experimental approaches are very close; error is within 1-28 percent. Therefore, numerical method is suitable for studying flow over stepped spillway .

5- Due to the employment of VOF model to determine free-surface it takes relatively large amount of time to reach a stable flow situation over steps . The existence of eddy and turbidity on steps cause the run-time to increase. To help the convergence, an internal boundary condition was assumed (refer to fig 6) when the dimensions and number of computational cells increase, these is sues would intensify.

11. REFERENCES

[1] Chen, Q., Dai, G., and Liu, H. (2002). "Volume of fluid model for turbulence numerical simulation of stepped spillway overflow." Journal of Hydraulic Engineering. ASCE, Vol.128, No.7, 683-688.

[2] Chinnarasi, C., and Wongwisess, S. (2006). "Flow patterns and energy dissipation over various stepped chutes." Journal of Irrigation and Drainage Engineering. ASCE, Vol.132, No.1, 70-76.

Nikseresht, A.H., Alishahi, M.M., and Emdad, A.,"Complete flow field computation around an ACV (Air Cushion Vehicle) using 3-D VOF with Lagrangian propagation in computational domain", Computer and Structures Journal, 2008..

[3] Tabbara, M., Chatila, J., and Awwad, R. (2005). "Computational simulation of flow over stepped spillways." Journal of Computers and Structures. No.83, 2215-2224.

[4] Vischer, D.L., and Hager, H.W. (1999). Dam Hydraulics. John Wiley and Sons.

SECTION VI

IMPACT OF CLIMATE CHANGE IN WATER RESOURCES AVAILABILITY AND CROP PRODUCTIVITY

Climate change and its influence on water resources and on agricultural productivity

Cornea Teodora Manuela, Gheorghita Oana, Dima Mihai

Abstract – **The peril of ecological disturbances manifested globally due to climate change is the most current and serious problem facing the XXI century.**

The negative effects of climate change are felt in all areas of life and they are endangering the sustainability of environmental sectors, health and safety of population and the global economy.

In this context, based on extensive studies, the authors of this paper highlight the environmental risks caused by climate anomalies on water resources and on soil in terms of agricultural productivity.

Keywords – **Climate Change, Environmental Risks, Water Resources, Agricultural Productivity**

1. INTRODUCTION

The last century climate data shows a gradual warming of the atmosphere and a significant reduction in precipitation amounts, items considered limiting for crop growth and productivity, and water resources. These changes can have significant consequences for growth and development of crops during the growing season, depending on the degree of intensity of disturbance factors, the method and duration of action and the vulnerability of plant species at extreme weather events. In the following decades, the implications of global warming on industrial economy, water supply, agriculture, biodiversity will be very obvious.

Global warming effect has therefore, increased frequency and intensity of extreme events, particularly drought and floods. Causes which give rise to these phenomena are linked so obviously to climate and human interventions like irrational use of land and water resources, inappropriate agricultural practices, deforestation, overgrazing and, last but not least, air and soil pollution.

2. CLIMATE CHANGE. CAUSES AND EFFECTS

Since 1750, once with the Industrial Revolution, among other environmental changes, human activities have increased concentrations of CO_2 and greenhouse gases (GHG), the

Cornea Teodora- Manuela, Technical University of Iassy, Faculty of Hydrotechnical Engineering, Geodesy and Environmental Engineering, Bd. D. Mangeron 65, Iassy 700050, Romania; phone:0740665798; e-mail: corneateodoramanuela@yahoo.com

Georghita Oana, Technical University of Iassy, Faculty of Hydrotechnical Engineering, Geodesy and Environmental Engineering, Bd. D. Mangeron 65, Iassy 700050, Romania; email: oanaluciana2002@yahoo.com

Dima Mihai, Technical University of Iassy, Faculty of Hydrotechnical Engineering, Geodesy and Environmental Engineering, Bd. D. Mangeron 65, Iassy 700050, Romania; phone: 0742311888, email: mdima_2003@yahoo.com)

ISSN-1584-5990

main reason for the manifestation of global warming. The global average temperatures increased in the last century by 0.74°C. Scientists admit that this is the upward trend in world history. Current forecasts shows that trend will continue and even accelerate. Most optimistic forecasts indicate that the Earth could warm during the XXI century with 3°C Researchers now recognize that most changes produced by greenhouse gases are the result of anthropic factor.

The average concentration of carbon dioxide in the atmosphere before the industrial age was around 280 ppm, as shown below in Table 1. Today, it has exceeded 380 ppm, which means an increase of at least 100 ppm, of which only 2.6 ppm in 2005. Recent analysis, showed that this increase is due almost entirely to fossil fuels combustion for energy production and the rest comes largely from deforestration and natural processes. Under the reference scenario of the International Energy Agency (IEA), global energy demand will increase by 60% by 2030.

Tab. 1. Concentration levels of GHG before and after The Industrial Revolution

No	GHG	Pre-industrial level (pmm)	Curent level (pmm)
1	Carbon dioxide	280	387
2	Methane	700	1745
3	Nitrogen	270	314
4	CFC-12	0	533

Global warming has profound effects in the various fields. It causes raising sea levels, extreme climate, melting glaciers, extinction of many species and changes on human health, changes that occur globally. Climate does not respond immediately to reduce emissions of greenhouse gases. Some of GHG remain in the atmosphere for decades or even centuries. A possible result would be an increased climate change that can last hundreds of years after stabilization of atmospheric concentrations.

Climate scenarios are associated with degrees of impact including sea level rise, changes in seasons and an increase in frequency and intensity of extreme events such as storms, floods and droughts. The impact of these climate changes will vary by region, the most significant effect in ascertaining the Arctic, the Asian deltas, in the developing small countries, islands and in sub-Saharan Africa. Climate change restricts water resources, already overburdened by demand from agriculture, industry and cities.

Rising temperatures reduces the layers of snow on mountain peaks and will increase evaporation, thus altering the seasonal availability of water. Fauna and biodiversity are threatened by habitat destruction and other anthropogenic pressure factor, and face a strong risk of extinction. The most vulnerable ecosystems include coral reefs, boreal forests (sub-arctic), mountain habitat and dependent areas of Mediterranean climate. Oceans also support higher temperatures and, as it absorb more carbon dioxide; marine life will be negatively affected by increasing acidity.

Reduction of arable land, widespread shortage of water, diminishing food and fish stocks, floods and prolonged droughts are already happening in many parts of the world. Climate change affects agriculture, fauna and flora, water and energy reserves.

Global climate changes manifested by increasing average temperature, precipitation amounts and regime change, have led in recent decades, an increase of drought affected areas worldwide. Climate change will alter rainfall conditions and will further reduce available freshwater resources up to 20 to 30% in some regions.

Decreased agricultural productivity will lead to food insecurity in less developed countries and a general increase in food prices. Crops - affected by temperature and water

regime, the length of the harvest season and the extent and intensity of extreme weather events - will drop by up to 10-25% and will be less predictable as key regions will pass printed.

Rainfall will register tendencies of increase / decrease between 5-20% globally; significant differentiation will be mainly regional. It will also increase, extreme weather events (winter-summer temperature extremes, droughts, floods, tornadoes, hurricanes, etc.), with major consequences on the entire planetary ecosystem. Long term measures required for prevention and mitigation of climate change include reforestation programs, reducing pollution, restoring and upgrading anti-erosion works and enhancing the development and improvement of sandy soils, etc.. Also, educating people and raising awareness on environmental protection are major requirements in developing adaptation strategies to climate change.

Climate changes can lead to robust growth in poverty and undermine sustainable development, especially in less developed countries. Efforts to mitigate the effects of global climate change can strengthen the prospects for global development partly by reducing the risk of negative impact of climate change.

3. SCENARIOS OF GLOBAL CLIMATE CHANGE

After the century in which modern civilization has experienced the fastest period of global warming, the first 10 years of XXI century are witnessing an acceleration of atmospheric warming, as global average temperatures raises by 2 to 5^{o} F per decade.

The climate change scenarios for the next decades are presented in Fig .1.

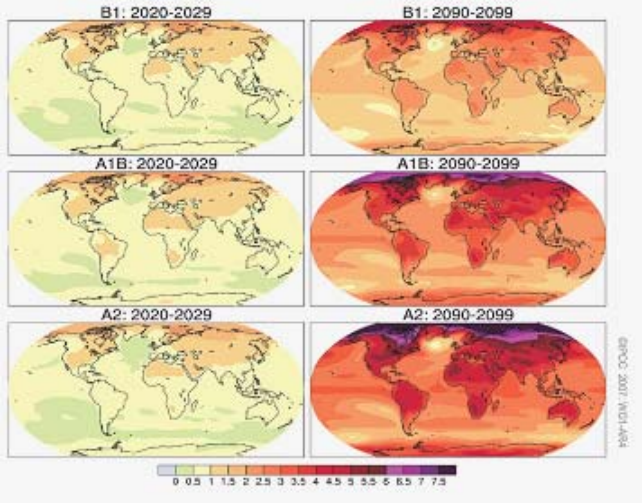

Fig. 1. Climate scenarios on global temperatures [8]

In most of North America, Europe and other parts of South America will register 30% more days with peak temperatures above 90^{o} F, unlike the end of the last century, and fewer days with temperatures below freezing.

Besides heat, there are some weather patterns: more floods, especially in mountain regions, and prolonged drought in agricultural areas of the coast and grain. Generally, THE threat of climate change affect economically various regions by phenomena such as storms, droughts and heat waves that have impact on agriculture and other activities dependent on

weather conditions. It is expected that in the 21st century the land in high northern latitudes will experience the most pronounced warming.

The average of global warming at the end of the 21st century (2090-2099) over the period 1980-1990 is currently projected to be between 1.8 ° C and 4.0 ° C depending on the scenario of greenhouse gas emissions gases considered. Rainfall case for the period 2090-2099 (compared to 1980-1990) are estimated increases of 5-10% during the winter season and for the same period, decreases of 10-30% in summer, as shown in Fig. 2. Decrease in resources, especially in poor areas will exacerbate the consequences of lack of water, both globally and regionally, the effects being exacerbated by pollution and inappropriate technologies.

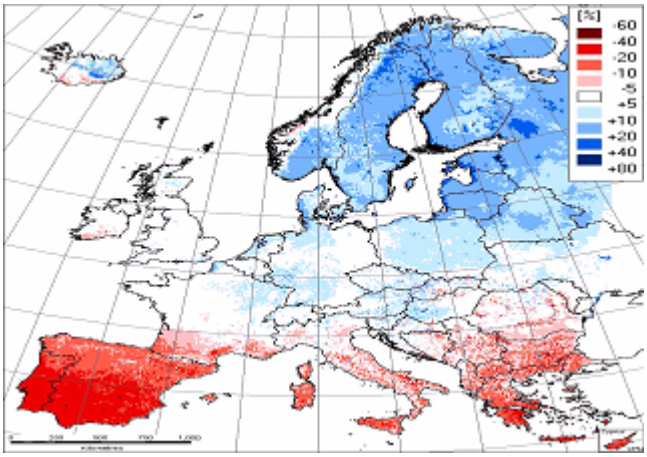

Fig. 2 . Precipitation: Changes in annual amounts [%]. [8]

Europe will be affected most by climate change; annual average temperatures will drop to 60^{o} F in a period less than a decade, more dramatic changes being recorded along the northwestern coast. The climate of NW Europe will be cooler, more arid, with strong winds, similar to that of Siberia.

Southern part of Europe will feel these changes less, but everything will go through intermittent periods of abrupt cooling and rapid temperature changes. Reduced rainfall will cause losses of landslides that will become a problem across the continent, thus contributing to depletion of food. [7]

United State of America's cold, more arid weather with strong winds will lead to shorter seasons and lower productivity in the NE of U.S. and its extension, along with drought in the south-west part. Desert areas will be faced with snow. Agricultural areas will suffer after land loss due to increasing wind speeds and reduced soil moisture. Switching to a dry climate will be particularly pronounced in the SE states. Coastal areas that were at risk during the heating period will be still in danger becouse of higher sea levels.

Asia has increased food need and will be heavily hit by monsoon rains decrease. Occasional monsoon during periods of summer rainfall will be a blessing through which they will bring, but will have devastating effects - such as flooding deforested lands.

Africa, especially *Kenya, Tasmania* and *Mozambique* will face slightly milder weather, but will be challenged by persistent drought. Accustomed to drought, these countries will be least affected by weather changes, but their food reserve will be affected as the grain-producing regions will face the effects of drought.

Australia as the largest exporter of food will struggle to provide food for regions across the globe, because agriculture will not be seriously affected by climate change. But

the great uncertainty in what climate changes pertaining to the southern hemisphere, will call into question this assertion. [4]

In the *Arctic* region rapid melting of ice caps is opening new waterways and international trade routes. In addition, increased accessibility of the enormous hydrocarbon resources of the Arctic changes geo-strategic dynamics of the region can have consequences on the stability of international and EU interests in security.

A simplified view of the affected regions by meteorological patters is presented below in Fig. 3.

Fig. 3. Affected regions for 2010-2020.Simplified view of meteorological patter portrayed in the scenario above. [5]

For *Romania*, the projections of global scenarios, namely the period 1991-2099 compared to 1961-1990, outlines the growth of average air temperature by approximately 2° C in winter and 3.5 ... 4.3° C in summer season (3.5° C in the northern and 4.3° C in the southern region)

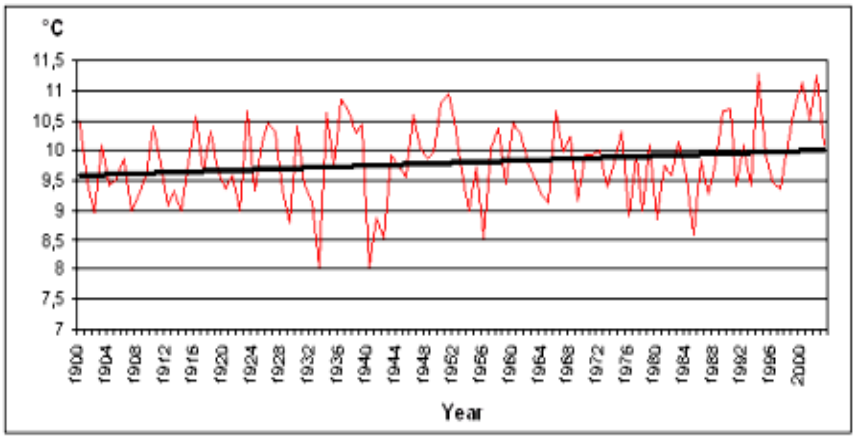

Fig. 4. Changes observed in the evolution of annual temperature in Romania (1961-2000)

Regarding precipitation changes are insignificant; summer will be deficits, and in winter, light surpluses in the northwestern part and deficits in the southwestern regions of our country. As a result of global warming can be added following changes in production meteorological phenomena of hot weather or cold season of the year: increasing frequency of tropical days, decrease the frequency of winter days, increasing the average maximum

temperature in winter and summer (up to 2.0º C in south and south-east), a significant decrease in the thickness of snow cover in north-east and west, increased annual production in the frequency of winter weather phenomena (frost, ice).

4. THE INFLUENCE OF CLIMATE CHANGE ON WATER RESOURCES. WATER CRISIS

Ironically, on a planet 70% covered in water, one billion people suffer from water scarcity and the other four billion (about 65% of total population) have limited access to fresh water. Only 15% of the total population lives in areas where water is abundant. 2.6 billion people, almost half of the total population, has lack access to adequate sanitary conditions.

As a result of rising temperatures, the world's water reserves are diminishing, and increasing water temperatures and low river rate affects in turn water quality. According to UN statistics, world population will increase from 6 billion people in 2000 to nearly 9 billion by 2030. One person from a developed country can consume up to 3,000 m^3 of water in a single year, but due to population growth and to assure the demand for water will need to find sources for at least 2000 cubic kilometers of water. Water consumption has increased six times in the last century, and will double by 2050. Results of studies show that Earth's fresh water reserves are insufficient to supply the entire population.

Beyond all the current problems that contribute to global water crisis, factors such as global warming, population growth, the need to ensure food, high water consumption in domestic sector, rising temperatures will accelerate the negative effects of the crisis. If, nowadays one billion people have a lack access to water, the Intergovernmental Panel on Climate Change data show that global-scale climate change will bring water scarcity to 1,1-3,2 billion people, if the temperatures would rise by 2-3 degrees C. [1] Specialists are already on alert and said the measures to improve water crisis must be taken immediately. The list of proposed measures and they include the collection of rainwater in huge tanks, water will be used for irrigation of agricultural fields and greenhouses.

Water crisis in Europe

In spring of 2008 water level in water tanks of Barcelona were so low that the authorities have taken steps to import water by ship through the acquisition of six loads of water, each containing enough water to fill ten Olympic swimming pools.

Cyprus is facing a drought of catastrophic proportions. Water demand has been an upward trend over the past 17 years, and now is more than 100 million m^3 of water per year. In the last three years, the country had available only 24, 39 and 19 million m^3 of water. To improve the water crisis last summer they brought water from Greece. By September 2008 there were imported from Greece 29 vessels with water. Shipments were delayed by the fact that Greece is facing water shortages. Cypriot government had to implement emergency measures that included reducing the water supply by 30%.

In Turkey, last summer, the water level has dropped steadily, according to the relevant competent authorities.

Mediterranean countries increasingly rely on desalination for obtaining drinking water. Currently, Spain has 700 desalination plants which produce daily sufficient drinking water for 8 million people.

In Spain, is expected to double the quantity of desalinated water in the next 50 years. Lack of water is not confined only to southern Europe.

In turn, the UK is also building the first desalination station in eastern part of London.

An EEA report, which will appear soon, is about the Alps, often called "water tower of Europe" because 40% of Europe's drinking water comes from this mountain range. In the last century, the Alpine region has increased in temperature by 1.48° C - twice the global average value. According to the report, melting glaciers, snow limit climbs higher and the whole mountain range is changing the water collection and storage during the winter and its distribution during the summer months. [2]

5. INFLUENCE ON AGRICULTURAL PRODUCTIVITY

Climate change affects many sectors; agriculture is one of the most exposed, since agricultural activities are directly dependent on climatic factors. This is important for the European area as 90% of this area consists of agricultural land and forests.

The negative effects on agricultural production will be affected by extreme weather events, and this will cause increased risk of famine. The greatest impact of change climate on agriculture will come via water. Climate change may cause a decrease in annual water availability in many parts of Europe as a result of reduced precipitation during summer - mainly in southern areas and in some parts of Central Europe.

The consequences of increasing frequency of extreme weather events, such as hail, heavy rain of winter, heat waves and drought will be felt all across Europe. Succession of floods, droughts and storms in recent years has demonstrated the extreme vulnerability of Europe. Their frequency could increase the short and medium term (until 2020). Also, the risk of drought in southern EU and the risk of flooding in Central and Northern Europe will increase.

Consequences of climate change will affect the agricultural production and variability, livestock management and production site for the agro-climatic zone. These effects can threaten food supplies in certain parts of Europe, causing also an increase in price volatility and increased risk for farmers' incomes.

Likelihood of reduced production in some EU regions, variability in production, seasonal changes in production structure, increased costs for farmers are possible consequences of climate change that adversely affect consumers. Particularly vulnerable are mountainous areas, in particular the Alps, where temperature increases rapidly causing widespread melting of snow and ice, and changes in river flows. Densely populated areas will be flooded more at risk of increased storms, floods and heavy rains, leading to widespread damage to agricultural land, built-up areas and infrastructure.

Addressing the impact on climate change requires, however, scientific data and expert analysis, risk management in agriculture including mainly actions on environmental management and conservation, and making correct decisions in perspective. Solutions and recommendations for the development of actions and procedures to prevent and reduce the effects of climate variability in agriculture should include all the whole complex of measures known (agro-technical, cultural, irrigation, etc.) intervention and rapid action to locate and limit expansion of extreme events in order to avoid increasing the consequences.[6]

In dry years, farming practices recommend: setting the range of varieties and hybrids at the beginning of each crop year and the appropriate technology according to soil water reserve on planting moment; cultivating a larger number of varieties / genotypes with different vegetation period for better use of climate conditions, to prevent such significant crop losses; and phasing agricultural work; respect the time of planting; seeding trend toward more "early stage" of maize, especially in dry springs, is more obvious due to the seed quality for sowing and their treatment. Thus ensuring the development of a deeper root system and during periods of drought plants can use water from the sub soil layer, and offer

more favorable conditions for pollination, fertilization, grain formation and maturation with early effects on production, on land with a high level of water in the soil; applying a minimum system of ground work (minimum-tillage) for water conservation and preservation. [3]

6. CONCLUSION

The earth's climate is predicted to change because human activities are altering the chemical composition of the atmosphere through the build up of greenhouse gases. It is accepted that one of the most important environmental problems of the present century will be climate change. This will give rise to changes in weather patterns and an increase in the frequency and severity of extreme events such as floods and droughts.

Available water amount is 1500m^3 per capita. It is expected to decline to 1000 m^3 in 2050 as a result of population growth and impact of climate change. As the largest user of water, the agricultural sector is expected to be affected by global climate change more than the other sectors.

In this study the authors evaluate global climate change and its impact on world's agriculture and water resources.

6. REFERENCES

[1] Contribution of Working Group for Natural Sciences at the 4th IPCC Assessment Report, Nairobi, 6th February, 2007(source: Climate Change 2007)
[2] Raport AEM, 2009 "Adaptarea la crizele de apă din Alpi" (în curs de publicare)
Fişă informativă " Climate change - the challenges for agriculture"
[3] Mihaela Zăvoianu - Materialul documentar al CE: "The role of European agriculture in climate change mitigation" 2009
[4] Document al Înaltului Reprezentant si al Comisiei Europene adresat Consiliului European "Schimbările climatice si securitatea internatională"
[5] Un scenariu al "SCHIMBARILOR CLIMATICE ABRUPTE-EPISODUL II. UN SCENARIU AL SCHIMBARILOR CLIMATICE IN VIITOR 16 aprilie 2005
[6] Corneliu Cismaru, Victor Gabor, Iosif Bartha, Daniel Scripcariu " Gestiunea secetelor" Editura Performantica, 2004
[7] Raport AEM nr. 4/2008 AEM "Impacturi ale schimbărilor climatice în Europa" — 2008 evaluare pe bază de indicatori.
[8] Regimul temp si prep pe glob: http://ec.europa.eu/environment/climat/adaptation

Ovidius University Annals Series: Civil Engineering Volume 1, Issue12, June 2010

Danger of floods in a changing climate

Cristina Doltu

***Abstract* – The climate changes are one of the major challenges of our century. They are caused, directly or indirectly by human activities that cause global atmospheric composition changes. The climate change increases the water flow at the soil surface and in its depth, making droughts and floods to be more frequent, more severe and developed on large surfaces. In recent years, the severity and frequency of flooding have increased significantly, constituting a main cause of the climate changes as they start to make their appearance and in Romania. In this paper the author presents a study on the evolution of floods in Romania, which is a consequence of climate changes.**

***Keywords* – climate change, vulnerability, weather scenarios, heavy precipitation.**

1. INTRODUCTION

The climate changes is one of the major challenges of our century. The observations and measurements made worldwide and in Romania on climatic parameters and the climate effects on water resources indicate certain signs that support the hypothesis of climate changes.

Lately we hear more and more about global warming, about the decrease of the ozone layer, the greenhouse effect and about their catastrophic consequences. The Climate change increases the water flow to the soil surface as well as to the deep soil, making the droughts and the floods to be more frequent, more severe and expanded on larger surfaces.

The weather on Earth is like a spider network in which weather systems, in different regions, are connected and are sensitive to weather variations. For example, due to the increase of the temperature the glaciers in the polar regions are melting and this will determine the average sea level to rise. This, in turn, can cause disasters in several coast regions in the form of famine, floods, tornadoes etc. with disastrous consequences for human civilization and for the economy.

The international scientific community organizes congresses, conventions and mediations between the world states to reduce these effects, just that for the moment the economic interests are stronger than the awareness of a long-term environmental distruction.

In this paper the author presents a study on the evolution of floods in Romania, this being a consequence of the climate changes.

Doltu Cristina is with Technical University of Iasi, Faculty of Hydrotechnics, Bd. D. Mangeron 65, 700050, Iasi, Romania, e-mail: cristinadoltu@yahoo.com.

ISSN-1584-5990 ©

2. IMPACT, VULNERABILITY AND ADAPTATION OF THE CLIMATE CHANGES

The global warming is an phenomenon well recognized by the international scientific community, already revealed by analysis of observational data on long periods of time. The Simulations made with global climate models have indicated that the main factors that cause this phenomenon are both natural (variations in solar radiation and volcanic activity) and anthropogenic (atmospheric composition changes due to human activities). The increase in concentration of greenhouse gases in the atmosphere, especially of carbon dioxide, has been the main cause of warming in the last years of the century (Fig. 3).

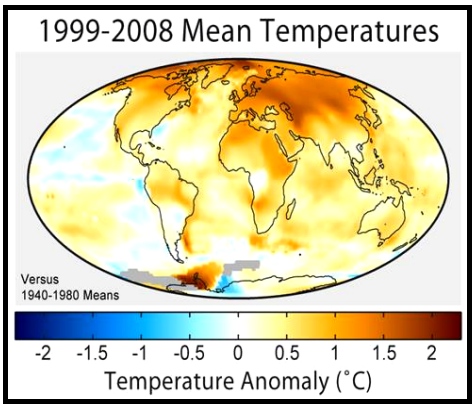

Fig.3. The Anomalies of Temperature recorded between 1999 and 2008 all around the globe.

The Meteorological Office of the United Kingdom has elaborate a weather scenario according to which the planet-wide temperatures are expected to increase by 1.5 degrees in 2100 and the oceans level to rise by 35 cm. Also, in the simulations performed, it is expected that the sea level will rise to four centimeters (Fig. 4), partly due to increased global warming, thermal expansion of sea water and melting of continental ice sheets. [9]

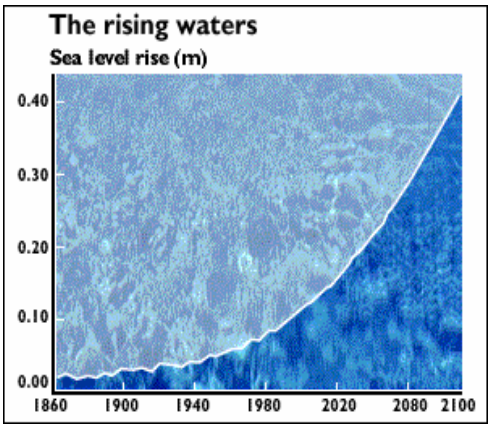

Fig.4 The rise of the sea level up to 4 cm

To understand the complexity of Earth's climate, scientists have drawn scenarios of the impact of the climate change by computer simulations.In these simulations, the

equations used represent the physical processes of climate, such as seasonal changes in sunlight, water evaporation and condensation, atmospheric warming determined by the ocean water and so on. Each simulation begins with a different hypothesis regarding the future possibilities of global warming.

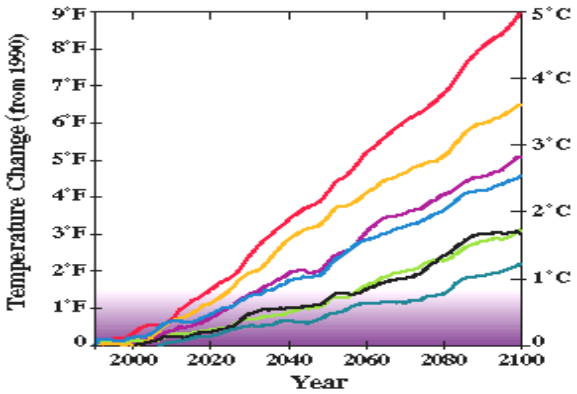

Fig.5. The temperature variations determined by simulations in reference to year 1990

In the making of the graphic (Fig. 5), researchers have assumed that there would be no action in fighting to stop the emissions of greenhouse gases in the future . Each line represents a different set of assumptions about future economic development and the fundamental climate processes. The trends concerning the frequency and intensity of flooding will be closely connected to the changes in rainfalls and river discharge and therefore to the long-term changes in climate.

Extreme rainfalls occur more often in tropical areas and in continental areas there is a drying tendency indicating a high risk of drought in these regions. [6]

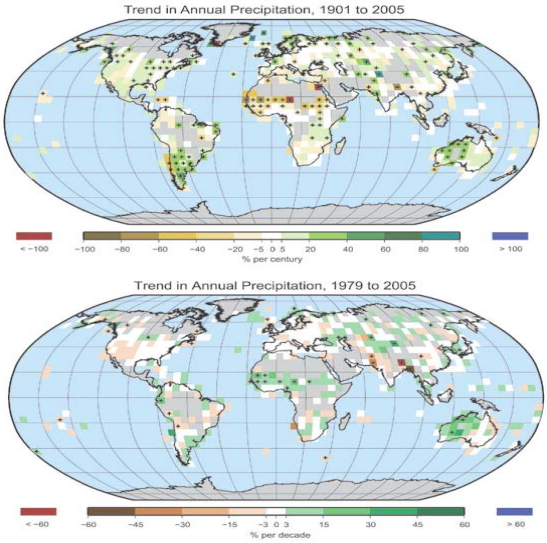

Fig. 6 The anual rainfall recorded between 1901 and 2005 (% per century) and between 1979 and 2005 (% per decade) on the globe surface.

Although there are many unknown variables when it comes to such predictions, there is a growing confidence amongst the scientists in the ability of the climate models to estimate future conditions.

3.THE SIGNS OF CLIMATE CHANGES IN ROMANIA

The Climate change in Romania fits into the global warming trend, but with regional particularities related to its global position, in south-eastern part of Central Europe, and the existence of the Carpathian mountains. These changes include the evolution of the main climatic parameters (temperature, rainfall, humidity, the wind, lake levels, the flow of the rivers), the sequence of seasons and the existence of extreme events and trends of desertification [1]. For the last century it has been highlighted an increase in the annual average temperature in Romania with 0.3 ° C [2], increase intensificated after 1960. The increases are differentiated, being more pronounced in the south and southeast with values of 0.8 ° C and lower in the central and northern part of the country. [4]

The estimation of the impact of climate changes on Romania has been realised through a study conducted by the Romanian Academy, who has selected different atmospheric general circulation models that best reflect the conditions of our country. According to the results generated by these models, in terms of doubling carbon dioxide concentration in the atmosphere, it is expected that in the next decades an increase of the average global temperature between 2.4 and 7.4 ˚ C. [5]

The observations and measurements made upon several climatic parameters and the effects of climate on the water resources show some signals produced in Romanian territory that sustain the hypothesis of the climate change.

From the signs worth taken into consideration we mention the following:

- the emergence of non-specific weather climate in Romania (on 12.08.2002 at Făcăieni a tornado occurred which destroyed 420 houses and cut trees in the near forest) (Fig.7);

Fig.7 Forest destroyed by the tornado in Facaieni – 12.08.2002

- the drying of the climate and the increase in frequency of producing extreme temperature and rainfall values (extreme temperatures - July 5, 2000 on station Bucharest (43.5 ° C) and Giurgiu (42.4 ° C);

- heavy rain fell on very small areas that produced catastrophical effects - 285 mm rain had fallen in 30 hour, 21-22 September Bucharest in 2005 which represents 60% of the annual rainfall value);

- increased duration of dry periods and so the increase of the variability of hydrological conditions from one year to another;

- the largest flood produced on the Danube river in April-May 2006 with the disastrous nature when there was a flow of 14,240 cubic meters / s also the disastrous floods of 2005 which were spread over a very long time period (from February to September) affecting almost all areas of the country (Fig. 8);

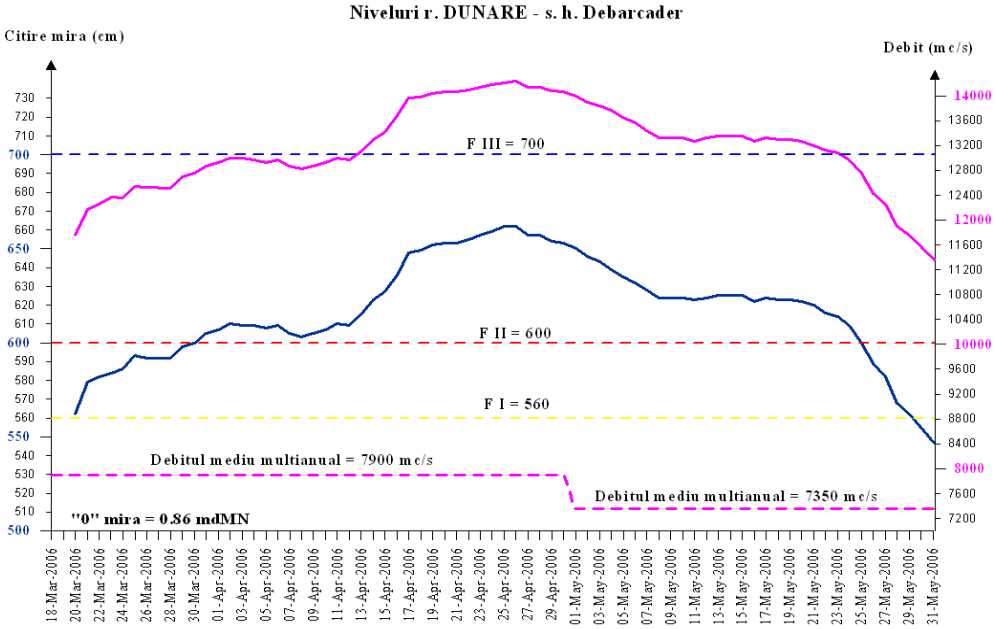

Fig.8 The maximum flow level recorded on the Danube river at s.h. Debarcader in 25.04.2006 – a flow of 14240 mc/s

- the Scărişoara glacier decrease in thickness with 150 cm in the last 100 years;
- the rise of the Black Sea level causing advanced coast erosion;
- faster alternation of rainy periods with droughts.[4]

The Climate changes affects all of us, both globally and nationally. Recently, the romanians could see that Romania was not spared and extreme meteorological phenomenons mentioned above are only the first alarm signal. Even if they are or not the direct result of climate changes, they still give us a clue of how it can possibly affect our country.

4. CONCLUSION

The Climate changes represent a reality and are studied through methods that can be tested and whose results are validated in the worldwide scientific community. The climate changes lead to the increase of land and sea temperatures, to changes in the rainfall amounts, and generate global average sea level rise, risk of coastal erosion and to expected increase in the severity of natural disasters caused by weather phenomenons.

The predictions based on global climate models show that we can expect a more frequent occurrence of weather events (storms, floods, droughts, etc.). The change of the local and regional climate conditions will influence the ecosystems, human settlements and infrastructure.

Although these events may seem insignificant at first glance, their effects on daily life can become extremely serious. For Romania, the effects of climate change on agriculture, forestry, water management and human settlements are an increasingly important concern.

5. REFERENCES

[1] Balteanu D., Serban M (2005), -„ Modificarile globale ale mediului. O evaluare interdisciplinara a
incertitudinilor", 2005, Editura CNI Coresi.
[2] Busuioc A, V. Cuculeanu, P. Tuinea, A. Geicu, C. Simota, Adriana Marica, A. Alexandrescu, N.
Patrascanu, V.Al. Stanescu, P. Serban, I. Tecuci, Marinela Simota, C. Corbus „Impactul potential al schimbarilor climatice in Romania", 2003, Ed. ARS DOCENDI, National Comity for Environmental Global Change of the Romanian Academy, ISBN 973-558-125-6 Bucuresti.
[3] Viorel Al.Stanescu, Ciprian C, Marinela S. „ Modelarea impactului schimbarilor climatice asupra resurselor de apa", 1999, Editura H*G*A.
[4] Ioana Cofrescu „Utilizarea scenariilor de schimbari climatice pentru Romania pentru orizontul temporal 2050", Scoala Nationala de Meteorologie [Online]. Available: http://snm.inmh.ro.
[5] Ministerul Mediului si Gospodaririi Apelor „Strategia nationala pe termen mediu si lung de management al riscului la inundatii. Aspecte cantitative si schimbari climatice".[Online].Availabel: www.mmediu.ro.
[6] United Nations Framework Convention on Climate Changes „Climate change: impacts, vulnerabilities and adaptation in developing countries" 2007, [Online]. Available: http://unfccc.int.
[7] Bakos Mihaela Violeta, Crisan Mihaela-Monica-„The effects of the climatic changes upon the quality of environmentand life", 27-31 May 2008, Ohrid, Republic of Macedonia.
[8] Bronstert A. „Floods and Climate Change: Interactions and Impacts", 2003, Risk Analysis, Vol. 23, No. 3.
[9] Zbigniew W. Kundzewicz "Flood risk and vulnerability in the changing climate".- Annals of Warsaw University of Life Sciences , SGGW, No 39, 2008.
[10] Teodoro Estrela, Manuel Menéndez, Mirta Dimas s.a „Sustainable water use in Europe Part 3: Extreme hydrological events: floods and droughts", ISBN Copenhagen, 2001 (European Environment Agency).
[11] Juan-Carlos Ciscar „Climate change impacts in Europe". Final report of the PESETA research project ,2009
[12] Evan Vlachos „Socio-economic impacts and consequences of extreme floods", U.S.-Italy Research Workshop on the Hydrometeorology, Impacts and Management of Extreme Floods Perugia (Italy), November 1995, Sociology Department Colorado State University Fort Collins, Colorado, USA
[13] Elaine Collins, Lucy Simpson „The impact of climate change on insuring flood risk" Presented to the Institute of Actuaries of Australia, Biennial Convention 23-26 September 2007 Christchurch, New Zealand.
[14] J. Hansen, R. Ruedy, M. Sato "Global Temperature Trends: 2005 Summation" Goddard Institute for Space Studiesand Columbia University Earth Institute New York, NY 10025, USA.Online]. Available: http://data.giss.nasa.gov.
[15] * * * http://ro.wikipedia.org/wiki/Global-warming.

Ovidius University Annals Series: Civil Engineering Volume 1, Issue12, June 2010

Extreme weather – the new trend that farmers must face

Claudiu Adrian Purdescu, Cristian Niculescu, Florin Danalache

Abstract – **Climate change is and probably will be for the next years a delicate issue. Even if many people and scientifics believe and are aware about climate change, still there are and will be some voices denying that. But the real story and the truth is what we're living, facing, feeling and observing.These are the realities that nobody can deny and the ones that affect us a lot. Drought, floods, heat waves, severe blizzards and even tornados do not affect only people but also animals and plants.**

In this way due to the extreme weather, the crop productivity can strongly fluctuate generating a bad economic situation for producers. In Romania unfortunately, the state of irrigation systems worsened year by year after 1990 and now excepting little areas are almost inexistent, leaving the crops exposed to weather hazard more than ever. The paper tries to identify and analyze what cause extreme weather especially in Europe and Romania and to evaluate the impact of the weather hazard over the people, environment, water resources and crops productivity.

Keywords – **Environment management, extreme weather, global warming, water quality**.

1. INTRODUCTION

Water is the the essential element for live, was and will be always. But, once with the evolution of the society, many things have changed. People have changed together with their needs, wishes, mentalities, habits, lifestyle and of course their alimentation. Industrial activities also have changed. But all of these changes do not have any implications for the surrounding environment?

The answer at that question is fore sure yes, it does and it does a lot. The planet has a very fragile balance and if that balance is disrupted then we can expect at changes. And if more human activities will disrupt the earth balance, more violent will be the changes. In this context, a big and important change that we all can observe taking place is the climate change.

Of course, weather has been always characterized by a word: variability. But even that variability has some limits and if that limits are overcome, then we can say that a change has produced. The climate is defined as an average weather conditions varying from years to million of years. This mediation is realized for some relevant variables such as: wind, temperature and precipitation. Currently, normal conditions are being considered the data captured in the 1961 – 1990 period and these average values are taken into account as

Claudiu Adrian Purdescu is with the University "Politehnica" of Bucharest, Str. Splaiul Independentei, nr. 313 , 060042 - Bucuresti, Romania (e-mail: claudiuapurdescu@yahoo.com).

Cristian Niculescu is with the University "Politehnica" of Bucharest, Str. Splaiul Independentei, nr. 313, 060042 - Bucuresti, Romania (e-mail: cristian@niculescu.ro).

Florin Danalache is with the University "Politehnica" of Bucharest, Str. Splaiul Independentei, nr. 313, 060042 - Bucuresti, Romania (e-mail: florin.danalache@gmail.com).

ISSN-1584-5990

the base for all the future comparisons.

Climate change is associated with variability on long term and means a change in state of clime that can be identify by using different statistical tests.

A lot of factors can contribute to the climate change but two of them are the most significant and these are the depletion of the Ozone layer and the greenhouse gases.

The UV rays from the sun are filtered by the Ozone layer. Part of them are reflected by the land and seas of the world back towards space, but, with a damaged portion of the Ozone layer, UV rays penetrate the Earth's atmosphere unfiltered. Then, the excessive heat is trapped by large concentrations of carbon dioxide in the Earth's atmosphere. This causes abnormal climate changes within various areas of the world.

Because the society, people and activities have changed it's not realistic to believe that now we can change again and no longer harm the planet but it's very possible to achieve with a strongly cooperation and goodwill a minimization of our impact.

2. RESEARCH STUDY

The world if full by articles, research studies or senzational news about climate changes, but still there are some voices among scientifics or business people denying or minimizing this fact according to their convictions or interest. Our work do not want to take part in this „battle". The goal of our research is to identify, compute and show based on real numbers, what have really changed in the last years in Romania geographic area and nearby (meaning between 40 and 50 degrees North latitude) regarding the repartition and the amount of the precipitation.

Firstly, in the research that was made, we tried to find best suitable locations in order to be able to make the research results relevant, knowing the fact that a lot of factors can influence heavily the data. Once the data being obtained, the numbers were compared to the actual situation to show the relevant changes. As mentioned earlier, Romanian agriculture unfortunately, depends a lot on the amount of precipitation that fall over it's territory.

The study tries to show how, where and why things changed regarding the amount of precipitation quantity and location in the past six years.

For the begining, we have to explain some factors that influence the amount of precipitation that falls in a particular period of time.

It's very well known that the evaporation has a lot to do with the amount of precipitation. For that reason, at the equator falls the most heavily precipitations and the amount decrease toward the polls. So, for middle-latitudes, where the climate is considered to be temperate (of course with the typically local influences), the maximum evaporation occur in the warm season, which is why, in Romania, normally the maximum amount of precipitation should occur in the summers times. The statistics do not contradict us and show the same thing, as illustrated in fig. 1 for Bucharest area [1].

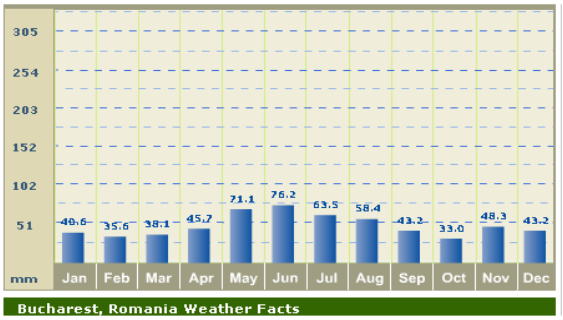

Fig. 1 – Bucharest average month precipitation

The amount of precipitation is presented in mm. If were in inches (1 inch = 25 mm), than we can say that in the wettest month of the year, whish is July, the average amount of precipitation is above 3 inches.

The altitude it's another factor that heavily influence the precipitation, that's why if in Bucharest at 90 m high the yearly average quantity of precipitation is 597 mm, at VF. Omu located in Meridional Carpatians at 2507 m above ground sea level, the yearly average rich 1050 mm, as showed in fig 2 [1].

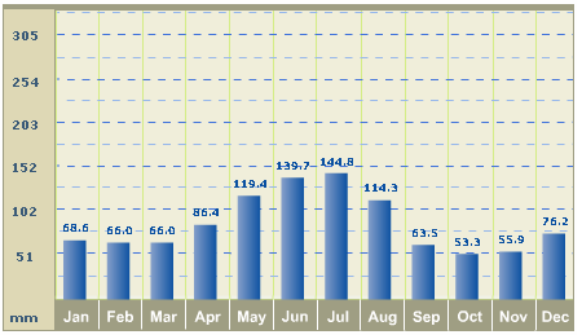

Fig. 2 – Varful Omu average month precipitation

Latitude and longitude together with local specific conditions have a lot to do with precipitation repartition. A simple but eloquent comparison reveals that Cairo located at 30.13 degree North and 31.4 degree East, 64 meters above sea has only a 23 mm yearly average of precipitation compared with Bucharest located at 44.26 degree. More interesting things can be identify with longitude, where compared with Cairo, at almost the same latitude 30.66 North but much more to the east at 104.01 degree in China, at Chengdu (508 m above sea) we find an yearly average precipitation of 922 mm as showed in figure 3 [1].

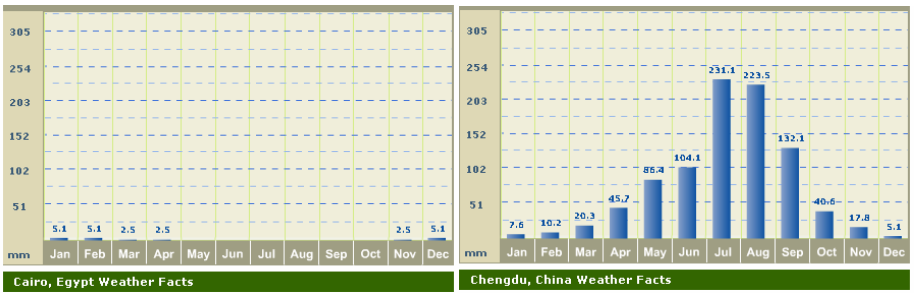

Fig. 3 – Avarage precipitation comparison at the same latitude

Finally but fore sure not the last factors: deserts or forests, sea, oceans, lakes or maybe huge urban metropolis also affect the amount of precipitations in different proportions.

We've showed all these exemples to illustrate how much latitude, longitude and altitude individually or together can influence the amount of precipitation that fall over a region at a time.

Now, back to Europe and Romania in the last decade a very important and unpleasant phenomenon in the summer was the heat wave. This phenomenon also have huge impact on the precipitations. Of course, it's not exist an unique definition of the heat wave and also it

couldn't be a single one because of the multiple factors that must be taken into account like the size of an area, humidity, latitude etc.

The World Meteorological Organization specifies that a heat wave occurs when in five consecutives days the maximum temperatures are 5 Celsius degree or more above the normal averages as we said before, calculated for the 1961-1990 period.

For Romania a hot summer day is when the max temperature rich 35 degrees and a tropical night is considered when the min temperature is equal or above 20 degrees.

For Bucharest if we take into account the fact that in July, the warmest month of the year , the average max temperature is 29 degree, this means that from these two affirmation results that if at least for five consecutive days the max temperature reaches 34 degrees than we can speak about a heat wave. For others countries and zones, in Egypt at Cairo for example, the normal maxim average temperature in July is 34 degrees so, in that region would be considered a normal period.

The heat wave is very unpleasant for every one but especially for the agriculture and farmers. Heat wave means not only high temperature but also the lack of precipitation. If the period is prolonged, that exist the risk that the crops will be very affected and the productivity will seriously decrease. For crops, also very important is the month or months in which heat wave appear because regarding this, it can be affected different stages of crops life (grow or maturity for example) with different consequences.

But why heat waves do happens in Romania?

The synoptic experience for the heat waves indicates that the "Key" for their appearance is the position of the Subtropical Jet Stream (STJ) in the upper troposphere. When the meteorological conditions during the summer over the Mediterranean and especially over the Greek area are normal, the main position of the STJ is observed over the following areas: SW Spain, Sicily, South of the Greek peninsula, Central Aegean Sea and SW Turkey (Prezerakos, 1978) [2].

Jet streams are fast flowing, narrow air currents found in the atmospheres of some planets. The major jet streams on earth are westerly winds (flowing west to east). The strongest jet streams are the polar jets, at around 7–12 km (23,000–39,000 ft) above sea level, and the higher and somewhat weaker subtropical jets at around 10–16 km (33,000–52,000 ft). Jet streams are caused by a combination of atmospheric heating (by solar radiation and, on some planets other than earth, internal heat) and the planet's rotation on its axis. They form near boundaries of adjacent air masses with significant differences in temperature, such as the polar region and the warmer air towards the equator. The subtropical jet forms at the poleward limit of the tropical Hadley cell and to first order this circulation is symmetric with respect to longitude [3].

Moreover the physical process that takes place under these synoptic conditions is the large-scale subsidence within the tropospheric air down and south of the STJ which leads to the following results:

- raise of the air temperature due to the adiabatic compression,
- surface horizontal divergence of the vertical flux,
- increase of the Sea Level Pressure enchasing the anticyclonic circulation and hot weather.

In other words, this procedure of the large scale subsidence in relation to the horizontal movements from South sectors are responsible for the Heat Wave phenomenon. In this point it is reminded that the STJ commonly is located at the northern edge of the Hadley Cell (Chandler, 1979) where, as it is well known, the large scale subsidence of the air is observed. This subsidence contributes also to the formation of the Subtropical High Pressure Systems. The northwards shift of the STJ contributes to the simultaneous movement of the Hadley Cell to the same direction. This means that the axis of the

descending movements in the tropospheric air , is now observed over geographical areas with latitudes 35 – 40 degrees N, instead of the usual position located over the parallel of 30 degrees N [2].

Thus, heat wave are not so uncommon. They do occur in the summer time and have their on variability. But the uncommon is the increasing in number and strength of the heat wave.

Statistically, if prior to 1990 period, in Romania were in average only 30 days per year in which the max temperature was above 30 degree, now in the last decade that number increased to almost 60 days.

If in a year the heat waves are very prolonged and the rains are completely missing, then the severe droughts appear. A relevant example for Bucharest area is the heat wave from 17 to 25 July 2007, in which the max temperature was above 37 degrees in each day with a maximum of 40.7 degree on 22 July and that month the amount of precipitation was only by 22 mm meaning only 29 % of the month average.

To be able to correlate all of these changes and to formulate the best possible realistic conclusions and having in mind the wider range of factors that influence the amount of precipitations that falls in a region we choose to compare the average monthly precipitation from no less that 10 locations with almost the same characteristics: relief form, longitude (max two degrees difference) and climate type which in this case is considered to be temperate).

The only slightly variation is the latitude (no more that 1 degree between locations) because the objective of the study was to investigate how latitude influenced the precipitation repartition in normal times (1961-1990 period) and what happened in the last 6 years for 3 of these locations during the winter and the summer season. As can be observed in table 1, the anual amount of precipitation increases with latitude and decreases with longitude in normal situation.

In table 1 are represented the locations and their characteristics [1]-[4].

Table. 1. Locations and characteristics

Location	Latitude (^{o}N)	Longitude (^{o}E)	Altitude (m)	Year average precipitation (mm)
Alexandroupolis	40,85	25,91	7	552
Edirne	41,66	26,56	51	548
Bourgas	42,48	27,48	16	523
Varna	43,2	27,91	41	473
Constanta	44,21	28,63	14	400
Bucharest	44,48	26,13	90	597
Galati	45,48	28,01	72	481
Chisinau	47,01	28,86	180	552
Iasi	47,16	27,63	102	591
Vinnytsia	49,23	28,46	298	627

3. RESULTS AND SIGNIFICANCES

After acquiring all the statistic data, we choose to compare three of these locations situated at the at the lowest, middle an higher latitude from these 10 considered locations meaning Alexandroupolis, Bucharest and Vinnytsia. From the results we only took into account the precipitations occurred during the cold and the warm season considering enough arguments to make a conclusion. In figure 4 are presented Alexandroupolis and Vinnytsia monthly average precipitations and in table 2, 3 and 4 are presented some calculations that we've made.

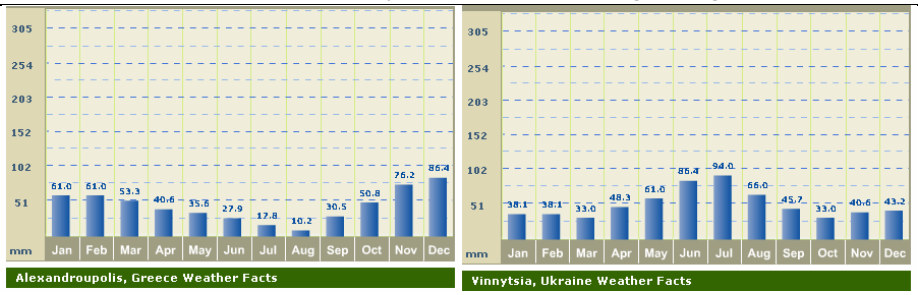

Fig. 4 - Alexandroupolis and Vinnytsia monthly average precipitations

Table. 2.Calculations for Bucharest

Year	Jan	Feb	Dec	Jun	Jul	Aug	Winter	Dif.from winter av	Summer	Dif from summer av
2003			59							
2004	59	21	53	79	87	73	139	19	239	41
2005	61	59	27	82	126	146	173	53	354	156
2006	39	33	10	29	63	69,4	99	-21	161	-36,65
2007	28	16	86	28	22	87	54	-66	137	-61
2008	29	8	21	42	59	8,63	123	3	110	-88,37
2009	56	29	58	87	112	40,1	103	-14	239	41,13
Ave rage	120			198			Bucharest			

Note that the calculations for winter season is made by summing precipitation occurred in December last year and January plus February actual year.

Table. 3.Calculations for Alexandroupolis

Year	Jan	Feb	Dec	Jun	Jul	Aug	Winter	Dif.from winter av	Summer	Dif from summer av
2003			57							
2004	93	5	92	50	9	14	155	-53	73	17
2005	182	163	123	42	17	12	437	229	71	15
2006	163	51	19	42	100	28	337	129	170	114
2007	4	57	47	31	0	2	80	-128	33	-23
2008	37	6	31	19	27	5	90	-118	51	-5
2009	90	82	117	19	3	0	203	-5	22	-34
Ave rage	208			56			Alexandroupolis			

Table. 4.Calculations for Vinnytsia

Year	Jan	Feb	Dec	Jun	Jul	Aug	Winter	Dif.from winter av	Summer	Dif from summer av
2003			25							
2004	40	37	21	29	91	247	102	-17	367	121
2005	34	42	48	40	35	76	97	-22	151	-95
2006	14	20	7	184	45	96	82	-37	325	79
2007	28	37	27	39	83	112	72	-47	234	-12
2008	29	15	54	43	92	47	71	-48	182	-64
2009	19	45	56	111	47	7	118	-1	165	-81
Ave rage	119			246			Vinnytsia			

The results shows that once with the increasing of latitude, also the annual amount of precipitation is increasing. But instead the repartition of precipitations between the two seasons it's totally opposed at 40 degrees N compared to at 45 and 50 degrees.

The explanation is simple. The Mediterranean sea is a great generator of humidity and in winter season is strongly influences latitudes between 30 to 40 degrees and that is why at Alexandroupolis we find the biggest value of precipitations in average in December. In the summer, because of the influences of the Subtropical Jet Stream that brings a lot of hot air from north of Africa, these latitudes see very little precipitations.

At 45 and 50 degrees N, the Mediterranean influence should be less significant in the winter season and very significant in the summer season, once with it's shifting to north influence in the hot season.

These things were observed in the 1961-1990 period but as we can see in the last years, things are quite different unfortunately [5]. The hot air from north of Africa is now more strong, and has a lot more spreading area. Together with high temperature in the summer season, it's also blocks possible cold air from north-west of Europe also due to high pressure that builds and Mediterranean sea becomes practically death from the point of view of precipitation generator.

In 2007, In Bucharest had fall in june and july only one-third compared to average precipitation and in 2008 in august, the amount of precipitation that had fall was even smaller than the average from Alexandroupolis for that month with only 8.6 mm compared to 10 – the average for Alexandroupolis.

For agriculture instead, the news are not so good because if in Alexandroupolis in the winter season the humidity reserve of the soil can be remade, at 45 and 50 degrees N we do not observe the reverse effect that occur in summer. Thus the amount of precipitations is still low, and for Vinnytsia in every of the last 6 winters the amount of precipitations were below the average.

For Bucharest it's almost the same situation in winter with last 3-4 years precipitations being below the average.

4. CONCLUSIONS

According to the study and according to the numbers, in the last years, we can say that in the hot season and especially in August, we find that the amount of precipitation that normally falls at 40 degree N appears now at 45 degree N.

If in 1961 – 1990 period, for Bucharest area, August were the fourth wettes month of the year, now unfortunatelly it's the dryies month of the year. Also, according to the numbers, with little exceptions, after a relatively dry winter with less precipitation than normal, it follows a summer with less precipitation than normal, while at 50 degree N, in the last years, excepting 2006, in every summer the total amount of precipitation was below the averages.

From the farmer's point of view this situation means trouble in two major aspects: fistly the crops that must be collected in september or october may not reach the complete ripeness due to the acute lack of water from August and secondly the preparation of the lands for autumn cultures may be very difficult and in the worst case even impossible is the lack of water is to deep in the ground.

Regarding the facts that were presented, with the actual trend, more and more water deficit in the soil will appear. In this situation, some important actions should be taken by farmers in order to avoid a disastrous situation. From a logistic point of view, more investments should be done for irrigation systems especially in the south and east of the country. The water supplies should be wised administrated because in a worse scenario

even the river flows can be affected, like was couple years ago, when due to low level of the Danube, the nuclear power plant from Cernavoda was shut down. Making activities more efficient and using new technologies available, we can reduce water consumption to have enough water for all our needs and of course keeping the same course of the society meaning evolution and development.

5. REFERENCES

[1] www.weather.com
[2] Ch.J.Balafoutis, T.J. Makrogiannis, Analysis of a heat wave phenomenon over Greece and it's implications for tourism and recreation, 2001
[3] http://en.wikipedia.org/wiki/Jet_stream#Subtropical_jet
[4] http://www.tutiempo.net/en/Climate/europe.html
[5] S. Ciulache, N. Ionac, Esential in meteorologie si climatologie, Ed. Universitara, 2007

Ovidius University Annals Series: Civil Engineering Volume 1, Issue12, June 2010

Tornadoes – Natural local and global hazards

Slave Camelia

Abstract – **Natural and technological hazard make every year human victims and damages that affects the economical and social development. The size of this phenomenon is directly proportional with increase of population and big environment misbalance. Humans influenced a lot the environment and made changes that through their amplitude became global phenomenon. In Romania due to damage of environment, forest massive destruction and irrigation systems the impact of natural hazards increased.**

Keywords – **global changes, natural hazards, tornadoes.**

1. INTRODUCTION

The word "tornado" comes from Latin "tonare" which means "thunder". Tornadoes are violent atmospheric disturbances, on small size, with rotator character, with the aspect of a narrow column that spins very quickly or of a reversed funnel that touches the ground. Still the meteorologists think that is not so simple to define a tornado. For example the difference between a strong meso-cyclone (a circular storm) on the ground level and a big tornado that is not very strong is not very clear. There are misunderstandings also in case of two vertigos (multi vortex tornados and multiple vortexes) formed during the same storm as being two separate tornados or not. It is well-known the fact that a tornado might not have a visible column shaped as a funnel.

There are more than 1000 tornados in USA each year. No matter the place they are born tornados can destroy farms, cities or even metropolis. In 2002 only, 52 people perished during tornados and hundreds have been wounded. The eye witnesses that were close to these raging vertigos tell that at the beginning of the storm they could hear a noise similar to an airplane. Tornados wipe out everything in their way usually with speed of hundred kilometers per hour. Most of the houses are built to resist speeds of 112 km per hour, but the maximum speed of a tornado is 117 km per hour.

For vertigo - a rotator wind funnel shaped – to be considered a tornado it must touch the ground and the cloud that produces the storm, figure 1, types of tornados. When this funnel touches the ground a concentrated destruction zone is created. Vertigo's surface is usually not bigger than 250 meters but can be 2 km tall.

The scientists study the tornados to understand better the way they appear, their behavior and structure, with few specific instruments. The advanced technology made possible simulation of storms that generate tornados using computer models.

Slave Camelia, FIFIM, USAMV, Bucharest, Romania (e-mail: camelia_slave@yahoo.com).

ISSN-1584-5990

Fig. 1 Types of tornados

2. EXPERIMENT DESCRIPTION

It is very difficult and dangerous to measure directly a tornado. In 1971, Theodore Fujita- professor of meteorology at Chicago University, tornado specialist, made a classification system that was named after him based on the destructions of man-made structures. Fujita scale or F- Scale ranks the damages made by tornados as being weak (F0 and F1), strong (F2 and F3) and violent (F4 and F5). It is important to mention that this scale applies only in the areas where man-made structures are, and vertigos are not measured according to their size but the damage they make. The size of a tornado doesn't necessarily show its violence, big tornados can have small intensity while small ones can be violent. Scientists can correlate the values of Fujita Scale only with the speed of winds. For example, the winds with speed of 145 km per hour can produce only little damage to a structure that was built correctly (F0), while a structure that have been built superficially will have important damage (F2). The speed of winds ranked on this scale has never been tested or proven scientifically, a lot of attention being necessary when used.

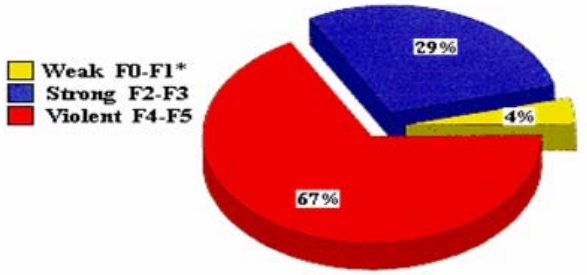

Fig. 2 Percent of tornado related deaths 1950 -1994 by Fujita Scale Class

F0 – wind speed between 64 and 116 km/h.

Doesn't make important damage, but even these tornados can rip the roof tiles and fling cars from the road. Mobile houses can be turned over and the warehouses crush. It could break trees branches and road signs.

F1 – wind speed between 117 and 181 km/h.

It is a moderate tornado that can lead to medium damage. It represents the equivalent of the weakest hurricane. The roofs fall down and mobile houses from the most affected area collapse. This type of tornado could displace the train from railways.

F2 - wind speed between 182 and 253 km/h.

This is a strong tornado. Big trees are ripped from the roots and big buildings crush like matches.F3 - wind speed between 254 and 332 km/h.This tornado produces damages on a large scale. The roofs and walls of big buildings collapse. Locomotives and trucks of 400 tones fly in the air like toys, while an entire forest brakes down.

F4 - wind speed between 333 and 419 km/h.

A tornado of such intensity destroys everything in the way. Solid houses are lift up in the air, and the structures with weak foundation are thrown far away.

F5 - wind speed between 420 and 512 km/h.

It is an incredible tornado with the force of an atomic bomb. Everything in its way is moved on big distance.

3. RESULTS AND SIGNIFICANCES

The term "tornado" was recently accepted in our country more used being pseudo-tornado or mini-tornado. Most of the meteorologists in Romania say that in Europe could be similar phenomenon but not tornados and in Romanian storms and small vertigos could appear. But what happened in August 2002 in Facaieni, figure 1, 2 and 3, and in May 2005 in Movilita prove that this is more complex phenomenon. It is possible that this kind of phenomenon existed in the past but until now there were no strong data and proofs, there were no recordings and buildings have not been affected. Nowadays these phenomenons happen due to major climatic changes and are highly probable to have this kind of phenomenon again in Romania.

In the last 3-4 years, tornado-type storms were registered in Danube Delta, in Jurilovca in 2001, near Baisoara Mountain also in 2001, and in 2002 in Facaieni. The tornado from 2002 in Facaieni - Ialomita had a devastating effect. The meteorological event from 12 of August, affected near 1.500 people, 33 houses were completely destroyed and 440 partially. Two people died crushed by the roof of their house. The storm spread on 1, 5 km, it's devastating character was the result of the fact that it happened in a populated area.

The Făcăieni event belongs to a long series of events that happened in the evening of 12 of August 2002 on an extended area near Feteşti (Ialomiţa) all the way to Ghindăreşti (Constanţa).

The deputy of the Scientific Director of National Meteorology, Hydrology and Water Management Vladimir Ivanovici said at the time that the Facaieni event is not a tornado, because in Romania and usually at the latitude of 45 degrees this kind of meteorological events are not possible. Ivanovici said that the "pseudo-tornado" was produced under a cloud with a big vertical development who's tips were situated at 14-15 km, The air currents were extremely powerful generating rotations, vertigos and storms with devastating effects The deputy of the Scientific Director of INMH explained that the Facaieni meteorological event happened in an unstable atmosphere, heavy rains and hail at the beginning of August 2002. This type of phenomenon happen every year in Romania but on concentrated areas said Ivanovici.

But for the second time in Ialomita County another tornado appeared in May this year. After Facaieni this time it happened in Movilita. Meteorologists say that they cannot predict this phenomenon. The tornado from Movilita, destroyed the roofs of 15 houses in the afternoon of 7th of May 2005, at 14.30, „It was a storm tornado type, the intensity of wind was 90-100 km/h. It did not have the strength of an American tornado, that can lift a car and the intensity of wind is 180-200 km/h, but it was a damaging phenomenon.

Fig 1. Facaieni tornado

Fig 2. Facaieni after tornado

Fig 2. Facaieni house after tornado

In the last years, tornados have happened in Jurilovca and Razem Lake in 2002, in Facaieni and Viisoara in 2003“, said Ion Sandu, director of National Meteorology Administration (ANM). While the director of ANM says that in Movilita it was a tornado, the members of Ministerial Comity for emergencies from Water Ministry qualify the phenomenon as “storm of high intensity”.

The damages produced by the tornado from Movilita on Saturday, 6th of May, were of three billion lei and the Commission for Emergencies detected that 24 houses were affected. One house was completely ruined, three roofs were destroyed and the rest had 80% damage on the roofs.

Now Movilita, few years ago Facaieni – these are two incredible moment, impossible in theory in Romania, in reality devastating. Why did it happen? The specialists say that it happened because of important climatic changes. The meteorologists warn us that, only in the last years, the average temperature increased with almost one degree. The spring nearly doesn’t exist anymore and this is the main cause. People should know that this kind of tragedies might happen anytime the same way an earthquake might take place.

4. CONCLUSIONS

The tornados are the result of many different types of climatic conditions. Most of the meteorologists think that the tornados start when the hot air and cold air currents meet and form a circular surface of low pressure, but this a general answer. Tornados form at the bottom of cumulonimbus clouds, where the dry cold air meets the hot wet one and they are always associated with strong storms.

The air with low atmospheric front tends to rise and create a strong vertical current. This current attracts the hot air from ground level that spins faster and faster and sucks the surrounding air like a vacuum cleaner. In extreme cases these strong currents can reach 500 km per hour or even 800 km per hour. The strongest tornados happen during storms called ‘super-cell’. Storm’s circular clouds can be detected by meteorological radars to have a well-defined circulation which meteorologists call meso-cyclone. Huge ‘super-cell’ clouds can be even higher than the Everest, have a diameter between 10 and 16 km, last a long time, as long as few hours and travel on thousands of kilometers starting few tornados.

But even if there are good conditions for a storm to form vertigos this thing doesn’t always happen. This process is not completely understood. Recent theories suggest that as soon as the meso-cyclone is formed the development of the tornado is strictly associated with temperature differences.

Funnel-shaped air column becomes visible due to condensed water vapors from exterior layers, when the humidity is high enough, but even if air-circulation is oriented towards center and tends to rise, the cloud inside the low pressure vertigo extends descending from the bottom.

The Frame Convention of United Nations for Climatic Changes and Kyoto Protocol provides the international institutional frame for approaching climatic changes, defines efforts objective and key principles for its. Within Kyoto Protocol, the highly developed countries are being asked to reduce the green-house effect emissions (carbon dioxide, methane, and azoth protoxide) with around 5% comparing to 1990, during the first cycle of engagement from 2008 to 2012. An engagement cycle of five years have been adopted instead of one target year to compensate the annual emissions fluctuations due to factors that cannot be managed like meteorological conditions.

As a result of technological development and increase of fuel and energy need an out-of-control increase of emissions took place. This led to a maximum pollution factor in the last years, pollution being the main factor of global warming.

In Romania the effects of climatic changes are more and more present. The change from summer to winter is very sudden with big difference of temperature. In the last years we witnessed strange meteorological events. The warming and the prolonging of the vegetation season will allow the use of new types of cultures.

The agriculture will be especially affected by this climatic changes and temperature variations. The changes of atmospheric circulation regime, rainfalls and evapo-transpiration will influence the zonal placement of vegetation and soil. This way the plants will grow better due to the increase of carbon dioxide concentration in air.

The increase of carbon dioxide concentration in air is considered the main cause of climatic changes but it is not the most dangerous.

The table 1 below presents few of the most important tornados that damaged the Earth between 1975 and 2000.

On national level the Government must take action to promote the management and good preservation of forests that act like real traps against green-house effect gases.

Tabel 1 History of Recent Tornadoes

Worst tornadoes from 1975 - 2000				
Location	**Country**	**Date**	**Killed**	**Affected**
Manikgani, Dhaka	Bangladesh	April 26, 1989	800	102,000
Colorado	USA	June 13, 1984	800	-
Orissa	India	April 16, 1978	500	1400
North-east Moscow	Soviet Union	June 1984	400	-
West Bengal, Orissa	India	March 24, 1998	250	450,500
Casamance	Senegal	August 21, 1999	165	-
Ghorasal, Tungi>	Bangladesh	May 7, 1991	121	300
Orissa	India	April 17, 1981	120	10,000
Pennsylvania, Ohio and Missouri	USA	May 31, 1985	104	500
West Bengal	India	April, 1978	100	100

6. REFERENCES

[1] D Bălteanu, M Şerban.,– Modificările globale ale mediului – o evaluare interdisciplinară a incertitudinilor – Editura CNI Coresi, Bucureşti, 2005;

[2] Al.,Gore. - Un adevar incomod – pericolul planetar prezentat de incalzirea globala si posibilele masuri care pot fi luate,Ed.Rao International publishing company, Bucharest 2007;

[3] http://terra.nasa.gov

[4] http://earthobservtory.nasa.gov

SECTION VII

INTEGRATED MANAGEMENT

OF WATER AND LAND RESOURCES

Drawing bathymetric map of Siutghiol Lake, basic step in carrying out projects of tourism development of the area

Geanina Cosmina ADAM, Ramona Daniela DOSPINESCU, Gabriel Iulian MIHAI

Abstract – **To attract investments aimed at the Romanian seaside resorts, tourist development projects should be prepared. These projects are used to create, develop and upgrade tourism infrastructure, to maximize the natural resources and to increase the quality of tourism services.**

The paper presents data obtained by specialized measurements necessary for the drawing of the bathymetric map of Siutghiol Lake, from Constanta and the manner of fitting it in order to organize here a phase of Class One Romanian Grand Prix competition.

Keywords **– Bathymetric, bathymetric rates, regional tourism development project.**

1. INTRODUCTION

The city of Constanta is located in Constanta county in the extreme south-east of Romania,by the Black Sea coast. Mamaia resort is situated at the northern boundary of the city . What characterizes this resort is the beach that is stretching over a distance of 8 km, with a width of about 100 m, and also the fact that hotels are very close to the beach.

Located in the western side of Mamaia resort, Siutghiol Lake occupies an area of 1900 hectares, with a length of 7.5 kilometers and 2.5 kilometers wide (Fig. 1).

The tourism potential of the resort is very high due to the fact that, geographically, Mamaia offers what no other resort can offer: the lake and the sea in just one location. To develop the tourism sector of the area and in particular to increase the attractiveness of interest in Mamaia resort, have been proposed a number of projects including:

Development and modernization of leisure amenities:

- pedestrian bridge and Mamaia marina
- Pescărie marina;
- Tomis marina;
- Tomis Riviera - modern access road between Mamaia resort and the historic center of Constanta;

- Rehabilitation of the hydrotechnical system to protect beaches and combating erosion process:

Geanina Cosmina Adam is with Ovidius University of Constanta, Bd. Mamaia nr. 124, 900356-Constanta, Romania (e-mail: adam_geanina@yahoo.com).

Ramona Daniela Dospinescu is with the Constantza Town Hall, România, (e-mail: ramona.dospinescu@yahoo.com).

Gabriel Iulian Mihai is with S.C. Velacost S.R.L., Constanta, Romania (e-mail: mihaigabriel79@yahoo.com).

ISSN-1584-5990

- arranging seven artificial leisure islands (three in the Constanta area, along the Black Sea and four in Mamaia resort area);
- rehabilitation of the peninsular area;

- Increasing tourist activity for Siutghiol and Tabacarie Lakes:
  - greening and dredging of Tabacarie Lake;
  - planning a navigable link between Tabacarie Lake and Siutghiol Lake;
  - planning a navigable link between the Black Sea and Tabacarie Lake
  - planning a "town lake" on Siutghiol Lake;
  - lift water on Siutghiol Lake
  - planning of new leisure and sports on the Siutghiol and Tabacarie Lakes;
  - Siutghiol Lake fitting in order to organize Class One Romanian Grand Prix competition.

Fig. 1. Siutghiol Lake, Constanța (Google Earth, 2009)

2. BATHYMETRY. MEASUREMENT TECHNIQUES AND EQUIPMENT

Bathymetry can be considered the equivalent of aquatic altimetry. Representing a branch of hidrometry, bathymetry is concerned with measuring the depth of water in seas, lakes and rivers, so that underwater relief maps could be drown. Corroborating the depth measurements technique, using the sonar, with the,precise position using GPS technology, maps of depth or relief maps of the foundation of lakes or rivers and bathymetric profiles on areas of interest could be drown.

The accuracy of the bathymetric maps is directly dependent on the method and on the equipments used in making the measurements, since on just one point two independent determinations are beeing executed: geographical position and depth.

Bathymetric mapping work is currently carried out and based on traditional methodologies. The measured depths are reported in a local reference level, corresponding to the level of 1.40 m compared to the average level of the Black Sea. A main disadvantage of the classical methodology of bathymetric mapping is the low attention given to the mapping of the bank areas and to the connecting of the bathymetric data with the existing datasets of levelling or acquired separately on/from the adjacent land.to ensure the hydrographic determination in the same accuracy class of planimetric precision with the topographic determination, it has been developed a system which is taking over simultaniously the GPS signals from the equipment installed on the sonar and the GPS receiver for post-processing storage. Thus is beeing cancelled the need for calibration after each stop of the equipments from the measuring boat. In order to make available to seafareres the set of continuously updated information which should coincide with the reality on site, it has been designed and implemented an automated system for collecting field data and graphic transposition of the results derived from their processing. Field data

collection is done using a set of sensors (sensors of GPS - DGPS positioning, a radar which captures images, ecosonda for determining the depth), each of these beeing necessary for the acquisition of certain characteristics between points within the lake shores.

3. BATHYMETRIC MAPPING OF SIUTGHIOL LAKE

The first Edition of Class One Romanian Grand Prix was held in 2007, on Siutghiol Lake in Mamaia, and it was a success from every perspective, this beeing possible due to the positive changes that the Romanian seaside has undergone within the last years.

For such competition to be organized and take place under optimum conditions it is necessary to comply with a number of technical conditions, such as: the lake depth, length, width and its surface.

To this end, bathymetric measurements made in 2007, enabled the development of bathymetric map of Siutghiol Lake (Fig. 2).

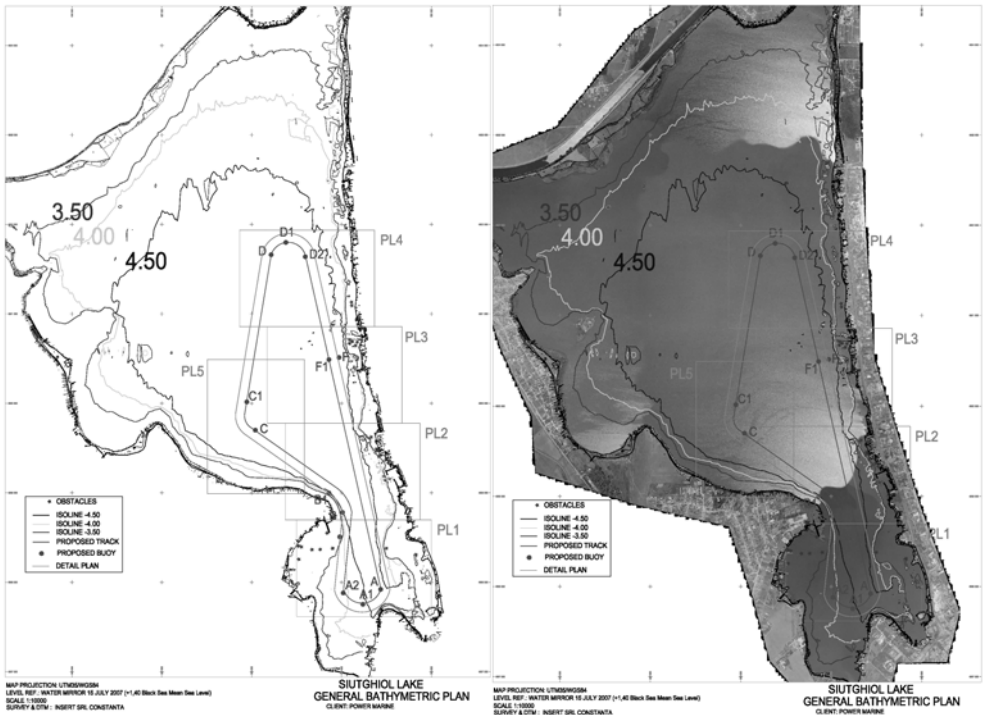

Fig. 2 Siutghiol Lake general bathymetric plan (scale 1:10 000)

These measurements were made on the WGS 84 ellipsoidal reference, using the Universal Transverse Mercator projection system (UTM 35).

The final result is presented as a hydrographic plan, drawn to scale 1:10 000, and the level curves of the riverbed have been reported in the "+1.40" to the average of the Black Sea level.

Following the measurements, were established the positions of some obstacles usually indicated on the bathymetric plan and on the local bathymetric plans made for areas where they have been identified: Sunquest area (Fig. 3 (a)), Mioritza area (Fig. 3 (b)), Scandinavia area (Fig. 4).

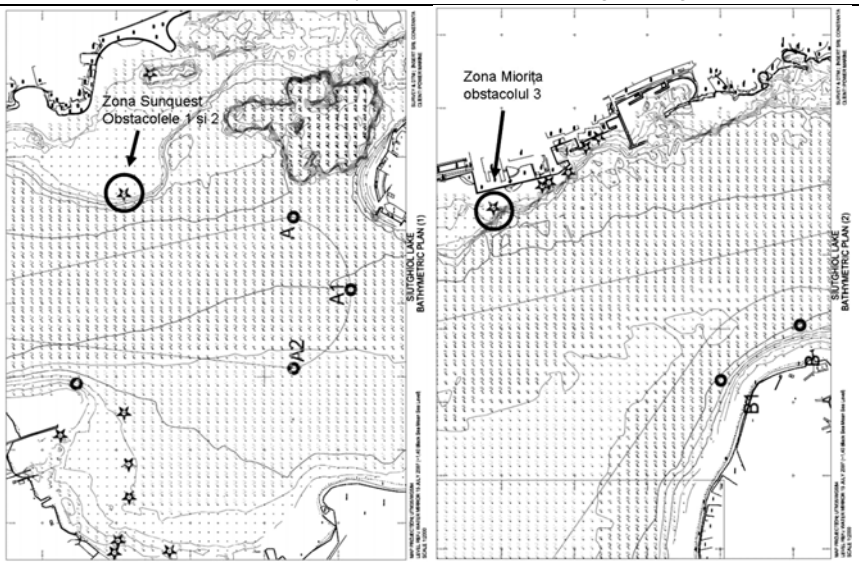

Fig.3 Local bathymetric plan (1:2 000)
(a) Plan Sunquest area (b) Plan Mioriţa area

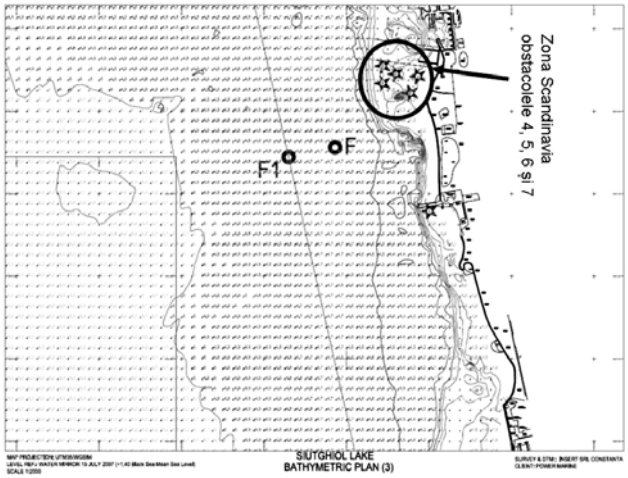

Fig. 4 Local bathymetric Plan Scandinavia area (1:2 000)

Fig. 5 Removal of the obstacles from the water by crane

So that the boats could be admired by the spectators located along tha shore of Mamaia resort and so that the boats could be launched at water, the obstacles from these areas have been removed and those situated in close proximity to the shore were removed by crane (Fig. 5). Other obstacles have been removed by dredging (Fig. 6).

Fig. 6 Dredging

To carry out dredging, cross profiles were drawn in order to conduct excavations required to reach the appropriate rate of the project, which was fixed so as to meet the technical and safety standards required for such contests. After dredging, measurements were made in order to verify the rates.

For each area bathymetric plans were drawn to different scales (Fig. 7 (a), (b)).

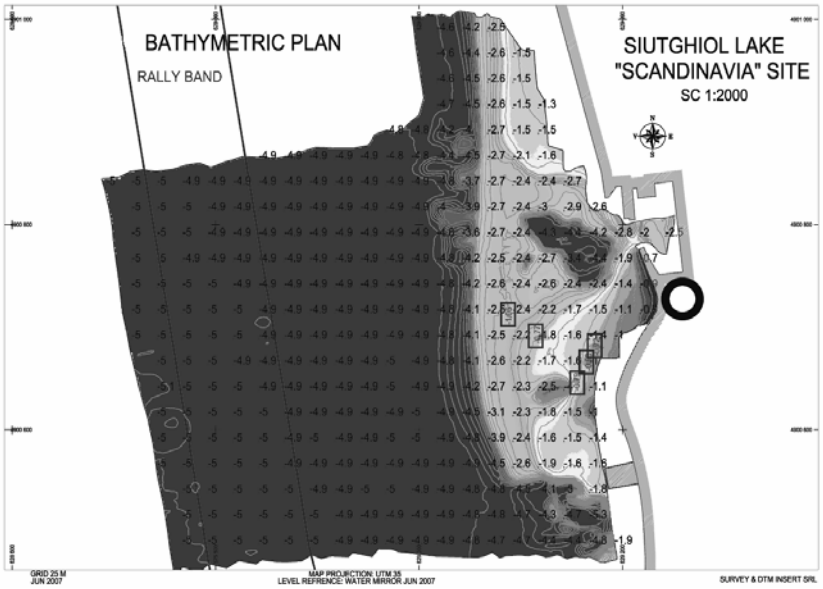

Fig. 7 (a) Local bathymetric Plan Scandinavia area (1:2 000)

Fig. 7 (b) Local bathymetric Plan Scandinavia area (1:500)

Measurements made in the Scandinavia area, data were obtained, which were processed resulting in the following coordinates for the obstacles:

PROGRAM UTMS			**NATIONAL GEODETIC SURVEY** **UTMs TO GP PROGRAM** GRS80/WGS84 ELLIPSOID			**VERSION 2.1**
Name	**North(Y)**	**East(X)**	**Latitude**	**Longitude**	**Zone**	**Convergence Scale Factor**
1	4900710	629087	44 14 53.47058	031 22 59.40337	25	1 07 41.98 0.99980493
2	4900690	629120	44 14 52.80156	331 22 57.93373	35	1 07 43.00 0.99980504
3	4900646	629154	44 14 51.35433	331 22 56.44034	35	1 07 44.01 0.99980515
4	4900666	629168	44 14 51.99335	331 22 55.79156	35	1 07 44.48 0.99980519
5	4900681	629173	44 14 52.47614	331 22 55.55288	35	1 07 44.65 0.99980521

After studying the plans it was decided that the race track to look like in Figure 8.

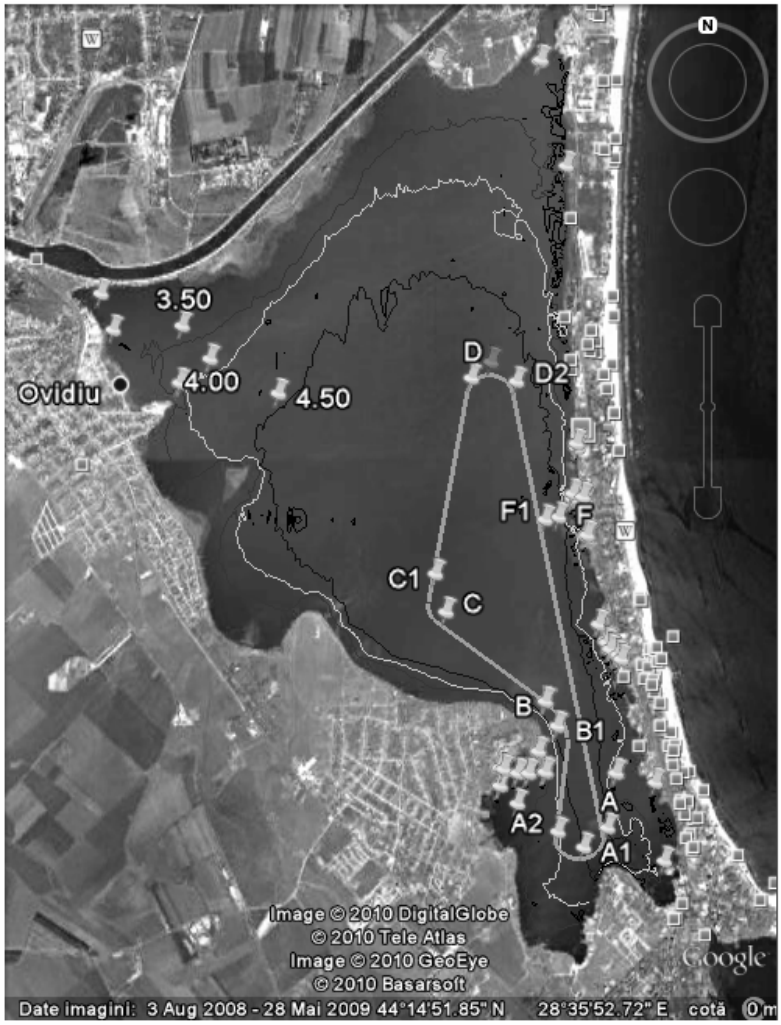

Fig. 8 The Class One Romanian Grand Prix race track

On this race track signs were placed for navigation (buoys A, B, C, D and F).

3. CONCLUSIONS

The representatives of the International Offshore Team Association (IOTA) declared themselves to be very pleased with the way that the organizers were prepared for hosting the race.

Organizing Class One Romanian Grand Prix is representing a big plus for tourism on the coast, extending the season due to this event till the end of August.

4. ACKNOWLEDGMENTS

The authors thank Company S.C. Insert S.R.L., Constantza for their kindness to provide the necessary data for this paper.

5. REFERENCES

[1] Constantinescu A.G., Constantinescu D.C., *Tehnici de măsurare a adâncimii apei*, Buletinul tehnico-ştiinţific al Icemenerg, Editura Icemenerg, 2006;
[2] Breier, A. *Lacurile de pe litoralul românesc al Mării Negre*, Studiu hidrogeografic, Ed. Academiei României, Bucuresti, 1976
[3] Leick ,A. *GPS Satellite Surveyiling*, John Wiley & Sons, inc.New York, 1998
[4] http://www.altimetry.info/html/appli/geodesy/bathymetry_en.html
[5] http://www.geoecomar.ro/website/publicatii/supliment2009/7.pdf
[6] http://www.geoecomar.ro/website/publicatii/supliment2009/5.pdf

The evaluation of the quantities of mineral aggregates extracted from ballast- pits by using the GIS technique: Case study.

Biali Gabriela, Pavel Dan

Abstract: **The evaluation of mineral aggregates quantities from the watercourses beds, and the monitoring of activities from ballast-pits represents actions of great importance, since the exploitation of alluviums sources from the river beds, much over the power of natural regeneration, has determined high decalibrations of beds and of the transit regime of alluviums. They estimated that in our country, at the end of this century, only 65% of the reserves of bed alluviums would be available for explorations.**

As regards the things presented, the current paper exposes an own methodology, based on a SIG/GIS technique, for the quantification of the extraction rate of mineral aggregates from a quarry/gravel pit for the duration of 4 years, making also some references regarding the impact of this exploitation on the bed morphology.

Keywords**: ballast-pit, river bed, GIS technique**

1. INTRODUCTION

It is generally a known fact that the ballast exploitations from the river beds can sometimes determine significant modifications of their morphology and of the liquid and solid courses dynamics, representing "aggressive" actions.

In the current conditions, in which we discover in Romania a significant increase of the number of ballast-pits and quantities of extracted mineral aggregates, the modifications that are produced in the beds obviously affect a series of riparian economic-social objectives, both regarding their safety and the possibilities of exploiting the water resources [3].

The Informational Spatial /Geoinformational systems were created with the purpose of computed acquisition and processing of data and of analyzing the information concerning the terrestrial space (Geo suggesting the ides of Earth and georeferential data).

The geographic Informational Systems (SIG) were created from the necessity of knowledge, monitoring and arrangement of the territory based on the digital maps.

They are capable to ensure the automatic map plotting, the inventory of resources, management of human activities etc., being the only which have the capacity to accomplish complex functions, carry out spatial analyses and data modelling/georefential information [2].

In the present paper, for emphasizing the placement taken in the study, we used the AutoCAd Map software and for the GIS modelling and the evaluation of the extracted mineral aggregates volumes, we used the Surfer software.

Biali Gabriela is with Conf. Technical University "Ghe. Asachi" of Iasi , Bd. D. Mangeron nr.65, 700050, Iasi,, Romania (gbiali@yahoo.com)

Pavel Dan is with ECOERG, str. Oituz, nr. 11, Suceava, Romania (dan@ecoerg.ro)

ISSN-1584-5990

2. THE LOCALIZATION OF RESEARCHES: THE BALLAST-PIT TIMIŞEŞTI – CRISTEŞTI

The ballast-pit Timişeşti – Cristeşti is situated in the middle sector in the minor bed of Moldova river, on the territory of Cristeşti commune, Iaşi county, downstream at about 700 m from the concrete road bridge from DN 15 B (km 60 + 800), figure 1. Hydrographically, in this area, the Moldova river (right affluent of Siret) is characterized through the elements presented in table no. 1.

In the sector studied, the Moldova river has a very unstable minor bed, divided in 2-3 main branches whose positions and depths change during the out rushes and the major bed has a large opening, reaching up to 1 ... 2 km.

Table 1 – Morphometric data of Moldova river at Timişeşti (outrush confluence Neamț ,Ozana), [8])

Data regarding the watercourse					**Data regarding the hydrographical basin**		
Length (m)	Amplitude (m)		Average descent (‰)	Sinuosity coefficient	Surface b.h. (km^2)	Average altitude (m)	Wooded surface (%)
	Upstream	Downhill					
156	1116	276	5	1,31	3057	762	59,8

Under the hydrological aspect, the river Moldova is characterized through a permanent flow regime, but with high variations of the debits during a year of longer periods. For the section Timişeşti we can notice a few more important data [9]:

- multi-annual average debit: 30.4 m^3/s;
- monthly average debits: 57.9 m^3/s (June); 58.3 m^3/s (July); 46.2 m^3/s (August); 38.2 m^3/s (September) 22.4 m^3/s (October);
- maximum debit with the probability 1%: 1530 m^3/s; maximum debit with the probability 5%: 1310 m^3/s;
- average debit of alluviums in suspension: R=18 kg/s;
- minimum daily average debit with the probability of 95 %: 1.35 m^3/s.

In Moldova Valley, the accumulation of alluvium deposits along the lowland, under the form of successions of dejection cones, interrupted by the expansion of outfall fans of the right affluents (Râşca, Ozana, Topoliţa) and even of the left ones, is characteristic (Moţca, Boureni etc.),[1].

Through the extremely close granulometry through sorts of the mineral aggregates requested by the constructors, the alluvial of Moldova bent, represents the largest exploitable perimeter from Molvoda, a permanently renewable richness because of the lack of hydrotechnical barrier arrangement.

In the analyzed area, Moldova river flows in a large bed formed of its own alluviums producing erosions on the right bank. The most important transformations are produced during the large waters, when the flow in the major bed has a normal direction of the meanders direction, some branches disappearing by sand-up while other branches may appear further on with a completely different route.

The relatively accentuated descent of the river makes the volume of solid harsh alluviums transported through traction become significant.

The exploration method used in the ballast-pit is imposed by the Company Romanian Water, through the annual exploitation authorization, outlining the directions and the sense of exploitation, the width of the exploited layer, the quantities and restrictions applied in view of protecting the rived bed against the erosion and abatement, corrosion of banks in the periods Starting from these issues, the extraction method used is the following the mechanized exploitation with DRAGLINĂ, IFRON, VOLA on parallel, successive lines, longitudinally oriented from the downstream to the upstream and from the water course to the bank, on a width of 1.0 m, according to the characteristics of the alluvium deposit, the positions and the prognosis of the solid and liquid debits dynamics of the river.

3. THE WORK MANNER AND THE RESULTS OBTAINED

In order to determine the influence of the ballast exploitation on the surface flow and the river bed (thalweg) dynamics, we delimited an extended polygonal area, mainly represented by the major river bed in the analyzed area, delimited by the points P1, P2, P3, P4 (table 2). These points delimit an area of : S = 706841 mp ~ 70,7 ha, on a length of watercourse of 1400 m. On this distance, the altitude (Z) varies between: 270 ÷ 280 m.

Table 2 – The coordinates of the points in the system STEREO ’70 (to limit of studies perimeter)

Point	X - NORTH (m)	Y - EAST (m)
P1	639471	616961
P2	639823	617213
P3	639119	618480
P4	638707	618011

In order to establish the modifications occurred on the major bed during time, especially in the years 2001 ÷ 2004 we used the calculation of the volume of the body delimited by the horizontal plan, passing through the Z area = 269 k and the surface generated by the topographic measurements.

At the same time, we established 5 routes for the transversal profiles delimited by the point’s 1A-1B ÷ 5A-5B. It is recommended that these points be marked in the land for the subsequent monitoring of the bed modification, the river bed (thalweg) and for the control of exploitation works.

Their report of Z axis (altitude) was carried out having as reference the road bridge near the position whose quota, in the south corner, towards the ballast-pit, was considered **:** $Z_{bridge} = 280{,}00$ m

In order to monitor in time the modifications that occurred in the area delimited by P1÷P4 we used the land surveys achieved for the documentations of existent authorization.

Thus, we used surveys achieved in the years 2001 (T1), 2002 (T3), 2003 (T5) and for 2004 (T7) we achieved our own measurements with the total station GEODIMETER 444, with a precision of 1 sec. ($\pm$ 2 mm/km).

The old plans were digitized and processed in software applications of CAD type in order to achieve the profiles through the points established and their superposition. At the same time, we used a GPS system, model GARMIN eMAP in order to place as correctly as possible in the coordinates STEREO ‘70 the analyzed area. Thus, we can claim that the

placement precision was determined with an error of 0,5 ÷ 1,0 m. At the same time, because of the presence of the bridge on DN 15B we could achieve a correlation of these plans with the cadastral ones.

The work stages have been:

3.1. Processing and centralizing data:

- We used previous topographic plans (2001, 2002)
- We achieved topographic measurements
- Z was correlated based on the common elements (fix points) existent in the available plans
- The analyzed perimeter was established (figure 1)

3.2. Creating the database based on the topographic measurements

- The introduction of data in a table containing the coordinates of the points from the measurements (figure 2)
- Data processing; obtaining the files *.grd (figure 3)
- Choosing the interpolation method (figure 4)
- Generating the M.N.T. (figure 5)

3.3. Calculating the volume

- Generating the surfaces
- Establishing the secant plan (apron) (fig 6)
- Calculating the volumes (fig. 7)

3.4. Achieving MNT thrpugh the RTN combined method (triangular irregular network) with interpolation in RD (rectangular network)

- Representing the perimeter in the 4 years taken in the study (figs 8,9,10,11)

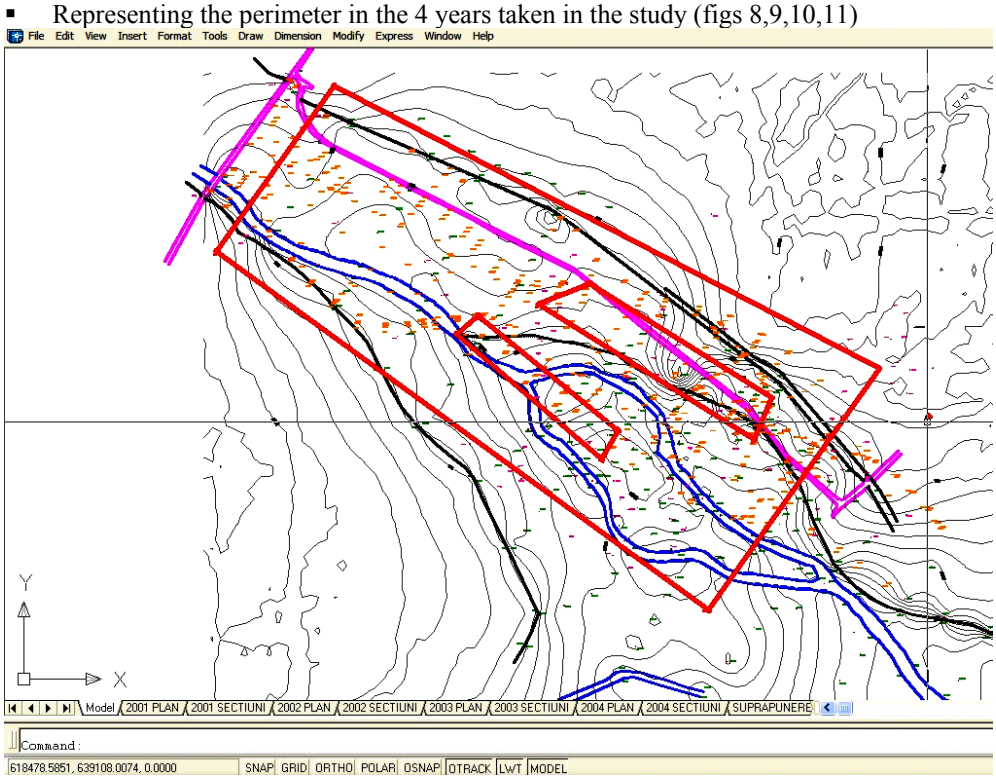

Fig 1. The placement of the perimeter studied within the ballast pit Timişeşti – Cristeşti

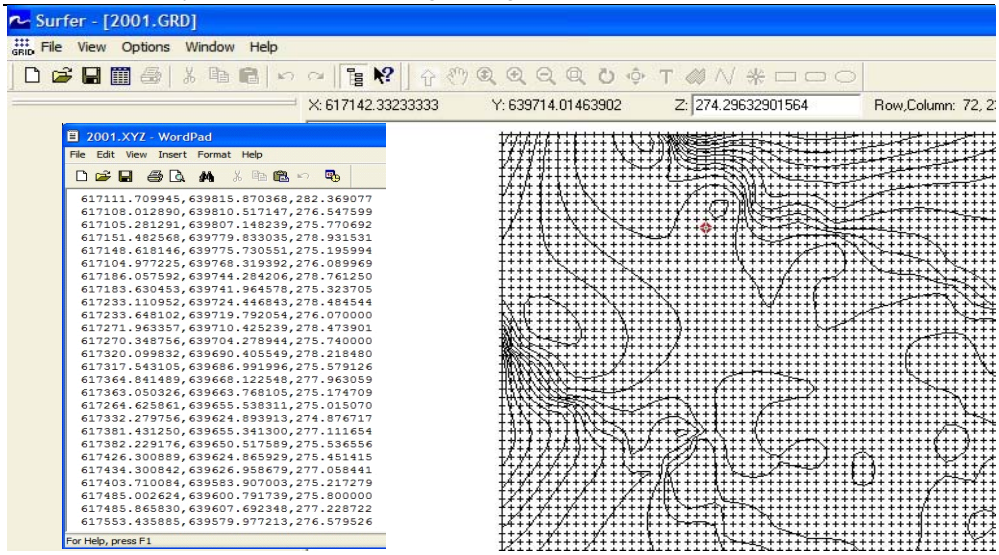

Fig. 2 Data introduction (coordinates from the measurements)

Fig. 3 Data processing obtaining the files *.grd

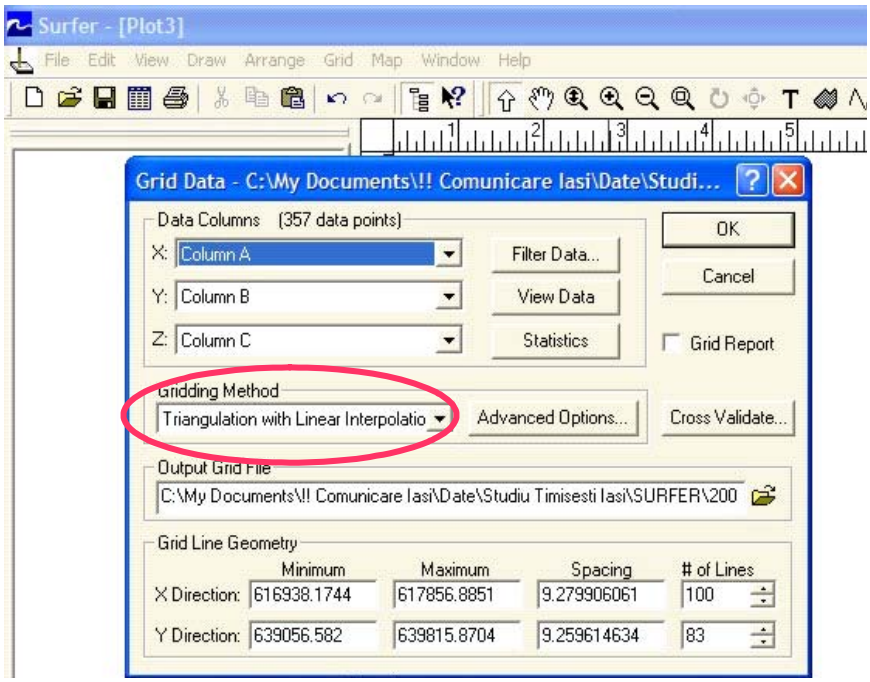

Fig. 4 Data interpolation through TIN method (with Surfer Software)

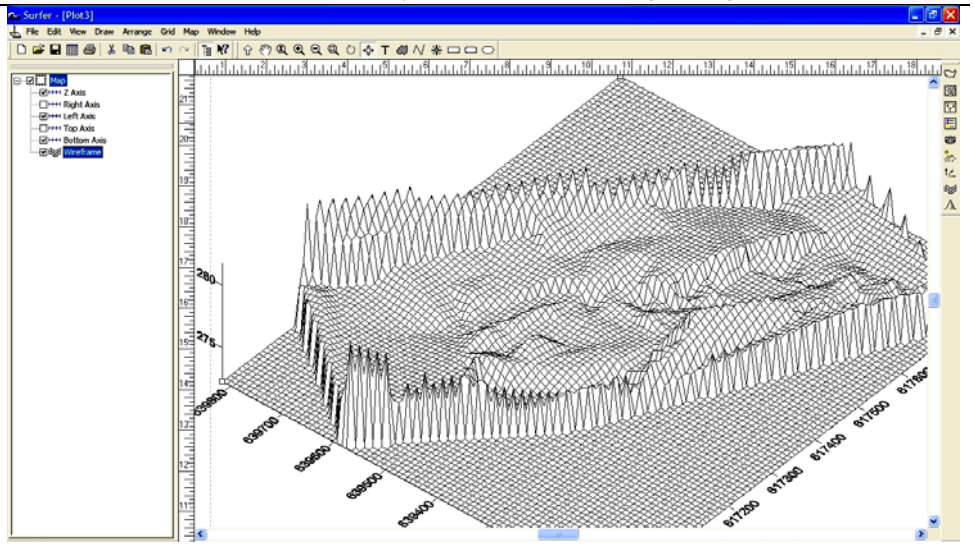

Fig. 5 – 3D representation in wire - frame of the Land Numerical Model (MNT) of the studied perimeter

3.3. Calculating the volumes of the ballast

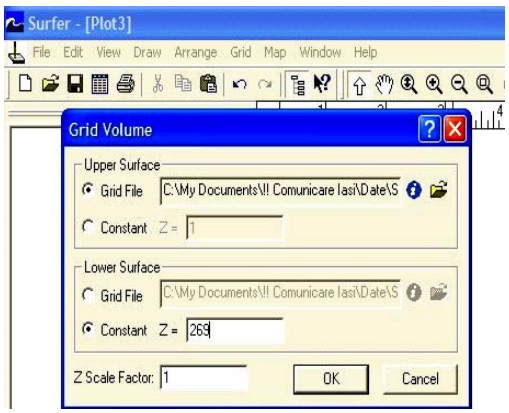

Fig. 6 Establishing the secant plan (apron) for calculating volumes

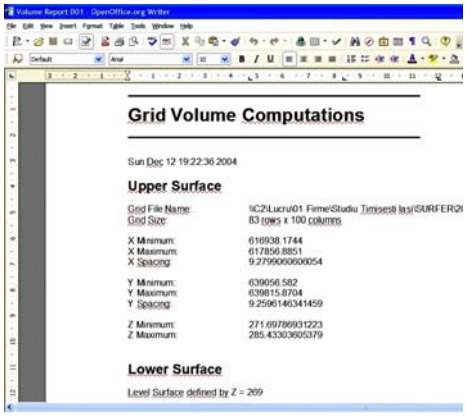

Fig. 7 The sequence for the automatic calculation of volumes with Surfer software

After establishing the limits of the ballast-pit and the secant plan, we continued with the calculation of the evaluated volumes (through extraction and alluvium transport) in each year and for which the topographic plans were available.

Without Ballast Exploitation	**With Ballast Exploitation**
Volume Input	Volume Input
$\mathbf{V_{IN}}$	$\mathbf{V_{IN}}$

Area / perimeter analyzed

$$V_{ANALYZED} = V_{OUTPUT} - V_{INPUT}$$

$V_{ANALYZED} > 0$ → Regeneration

Area / perimeter analyzed

$$V_{ANALYZED} = V_{OUTPUT} - V_{INPUT} - V_{EXPL.}$$

$V_{ANALYZED} < 0$ → Erosion

3.3. Making MNT combined method (RTN with interpolation DR) software Surfer

Year analysis: **2001**
Share the plan: Z = 269 m
Volume calculated: **5.511.299 mc**

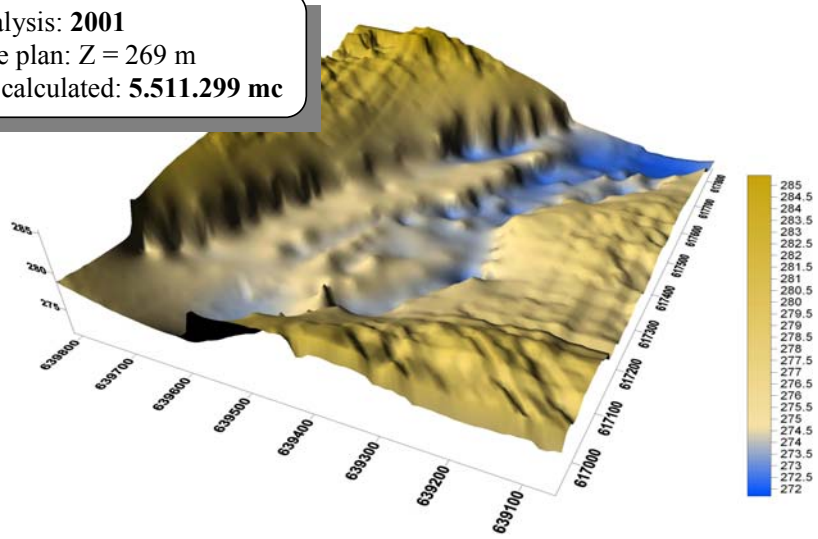

Fig. 8 Digital Model of Terrain (MNT) of the studies perimeter – Year 2001

Year analysis: **2002**
Share the plan: Z = 269 m
Volume calculated: **8.689.231 mc**

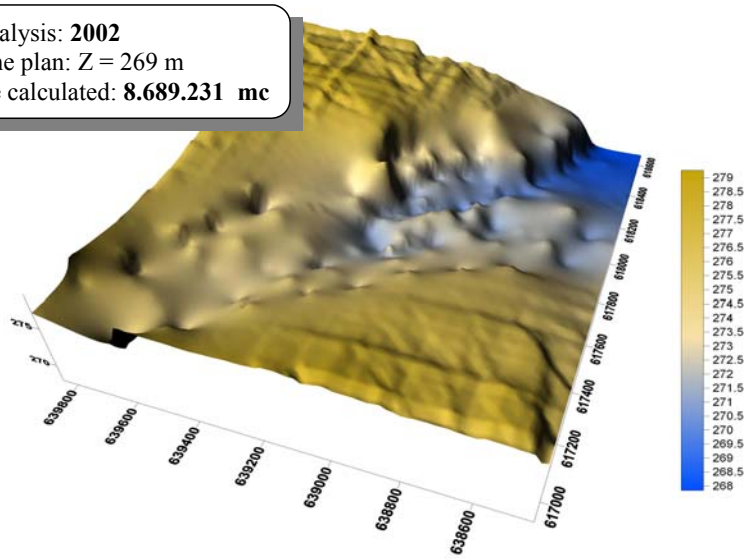

Fig. 9 Digital Model of Terrain (MNT) of studies perimeter – Year 2002

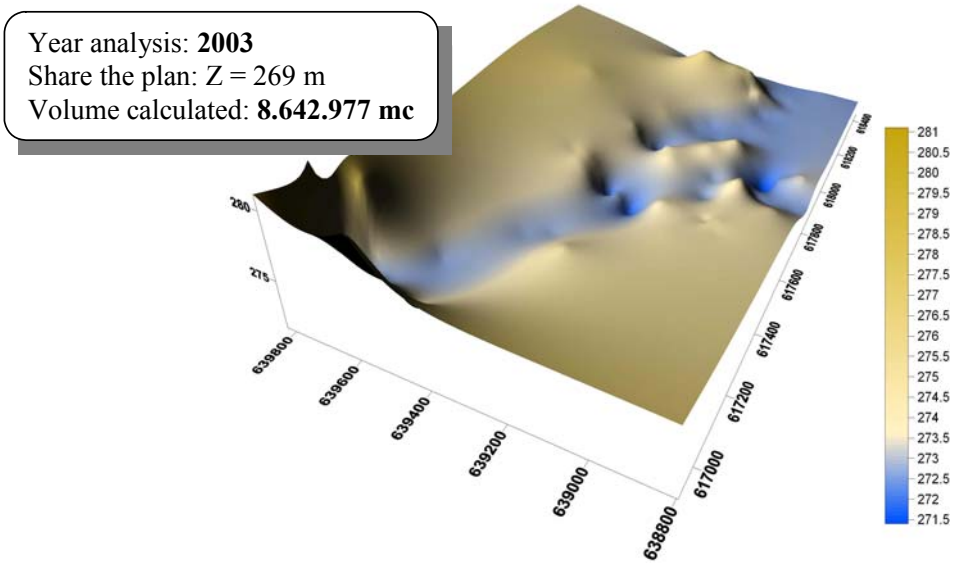

Fig 10 Digital Model of Terrain (MNT) of studies perimeter – Year 2003

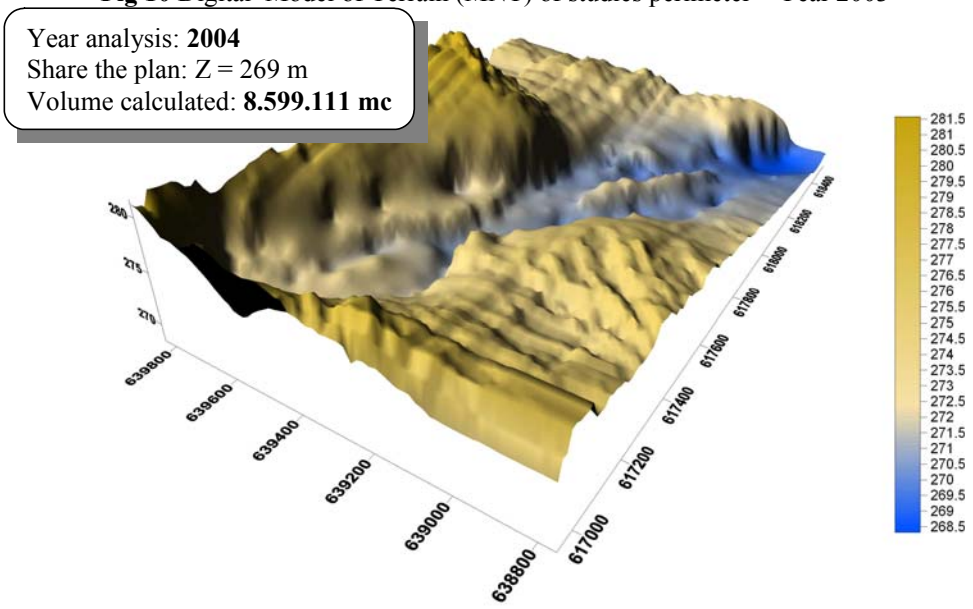

Fig. 11 Digital Model of Terrain (MNT) of studies perimeter – Year 2004

4. INTERPRETING THE RESULTS FROM THE CALCULATION OF VOLUMES

Since the topographic measurements from 2001 did not comprise the entire analyzed area, this year will not be taken into the calculation of regenerations.

Analyzing the things presented in the paper, we ascertain in general a decrease of the thalweg quota, more emphasised in the years 2002, 2003 and more reduced in 2004.

We notice that in general, the thalweg quota decreased to values between 0,2 and 1,3 m. This fact is confirmed also by the previous calculation of volumes.

Table 7. Results obtained and interpretation

Year	Calculated volume (m^3)	Difference from the previous year (m^3)	Quantity exploited in the area according to the authorization (m^3)	Quantity resulted from regeneration (m^3)
2001	-	-	-	-
2002	8.689.231	-	-	-
2003	8.642.977	-46.254	75.000	28.746
2004	8.599.111	-43.866	75.000	31.134

We ascertained that there are also areas in which the thalweg increased with 0,2 ÷ 1,1 m, especially in the area in the downstream.

Table 8. Changes in thalweg of the years studied

Year	Maximum value	Minimum value	Average
2001			
2002	-1,000	0,600	-0,397
2003	-1,320	-0,065	-0,416
2004	-1,86	-0,017	-0,899

5. CONCLUSIONS

a.) By using a MNT / MNA we can determine with high precision the ballast exploitation rate in an exploitation perimeter of the ballast in an exploitation perimeter, in comparison with the currently used topographic methods.

b.) Having at the disposal a MNT / MNA in the exploitation perimeter (ballast-pit) we can achieve profiles on any direction, which facilitates the detailed knowledge of the bed processes in the area, including the evolutions of quotas on the river bed (thalweg).

c.) The exploitation depth must not be equal with the depth of the thalweg and the exploitation must focus on the holms that appear in the area and decrease the transversal section through which the water passes, increasing the speed. Through the exploitation of holms, the surface for the water passage is increased in transversal section, which implicitly leads to the speed reduction and the increase of deposits in the affected area.

6. REFERENCE

[1]. Amăriucăi M., *Sesul Moldovei extracarpatice între Păltinoasa şi Roman*. Ed.CORSON, 2000, Iaşi.

[2]. Burrough P.A. (1998) – Principles of geographical Information systems for land resources assessment. Calderon Press. Oxford University Press, 1998.

[3]. Ichim I. şi colab. (1998) – Dinamica sedimentelor. Aplicaţie la râul Putna – Vrancea. Ed. Tehnică, Bucureşti.

[4]. Haidu I., Haidu C. (1998) – S.I.G. Analiză spaţială. Ed. H.G.A. Bucureşti.

[5]. Popovici N., Biali G. (2000) – Sisteme geoinformaționale. Ed. „Gh.Asachi" Iași.
[6] Popovici N., Cojocaru I., Biali Gabriela, - *The study of ballast-pit influence on the dynamics of river bed*. Analele Univ. Oradea, Fasc. Construcții şi Instalații hidroedilitare. Vol. IX,2006. Ed. Univ. Oradea.
[7]. Olariu P (1997) – Gospodărirea resurselor de aluviuni în spațiul hidrografic Siret. Măsuri non-structurale în gospodărirea apelor. Ed. H.G.A. Bucureşti.
[8]. * * * *Atlasul Cadrastrului apelor din România*. Partea 1. Date morfo hidrografice asupra rețelei hidrografice. Ministerul Mediului, Bucureşti, 1992.
[9]. * * * *Studiul influenței balastierei Timişeşti asupra curgerii de suprafață şi dinamicii pânzei subterane*. Inst. de Cercetări şi Ingineria Mediului. Secția de Hidraulică, 1990, Bucureşti.Inst.

The assessment of deformations in the decantation pool Valea Tărnicioara, through the signal analysis method

Biali Gabriela, Iftode Gabriela

Abstract: **The appropriate design and execution of the decantation pools ensure the increase of the stability reserve of this type of construction.**

In the present paper, we partially approach the study of deformations, decisional element in the analysis of taluses and versants.

Thus, in the following paper we will present the evolution of the deformations in Valea Tărnicioara decantation pool from Suceava county, deformations that were measured topographically, on scale marks situated on the berms of the decantation pools. There are horizontal and settlement deformations, towards the downstream, of the decantation pool body, measured in 2004 and 2005.

Keywords **– decantation pools, stability, horizontal and settlement deformations**

1. INTRODUCTION

The deformations that appear in the interior of earth rocks, on taluses or in versants, having a very varied range of forms, from hardly visible cracks, to morphological forms specific to the relief affected by landslides, represents the best indication regarding the incipient landslide process or in course of occurrence. Therefore, the study of deformations represents the main source of information for the practical prognosis of the landslides.

The decantation pools are special hydrotechnical retention constructions, of permeable type having as objective the safety depositing of the sump mine and the evacuation of all the water debits from the sites.

The stability of decantation pools, barrages and dams for their formation, of banks and bordering areas is analyzed under the aspect of the general stability of the dump talus, of the initial barrage (dam) and foundation land.

The factors that can cause the instability of a dump deposit are:

- exceeding due to the bending of the talus or its height of the limits that ensure the stability in the real conditions of the geomechanical characteristics of the deposited dump, dam or initial barrage and foundation land;
- the action of water flowing in the dump mass.

The analysis of stability is achieved for certain breakage hypotheses (in the mass of the foundation land, through the body of the initial dam or only in the dump mass). The study of deformations must be considered as a main process for the prognosis of the landslides and taluses. For the practical efficacy increase of this work process, it is necessary that the deformations measurement have a preventive character, for the discovery of the sliding process in its incipient stage. That is why it is necessary to extend the

Biali Gabriela is with Technical University "Ghe. Asachi" of Iasi , Bd. D. Mangeron nr.65, 700050, Iasi, Romania (gbiali@yahoo.com)

Iftode Gabriela is with S.C. TOP CONSTRUCT, str. Cernauti, nr.112B, Suceava, Romania (domus_96@yahoo.com)

ISSN-1584-5990

geodesic measurements for all the taluses, without exception, on all the versants susceptible of landslides.

The discovery of a landslide, in its incipient stage, means a great economy of money and technical means for stabilizing or reducing the intensity of the sliding process. It is unanimously recognized that the technical measures taken for the prevention of landslides are much more economic and practically easier to achieve than those necessary for stabilizing the landslides when the sliding process is already in course of evolution.

2. LOCALIZATION OF RESEARCHES

Valea Tărnicioara decantation pool is situated in the hydrographic basin of Brăteasa course, affluent of Moldova river.

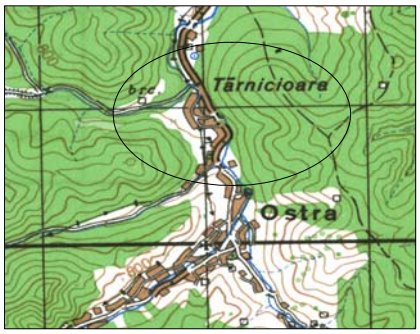

Fig. 1 – The localization of the decantation pool Valea Tărnicioara

Leşu Ursului mine exploitation, the Preparation factory Tarnița and Servicing Base Frasin are positioned on a very large territory, in Stânişoarei Mountains. The distance on the road between the extreme points exceeds 60 km, and as altitude, from 555 mm (Baza Frasin), at over 1000 m. The road Frasin – Holda, crosses Stânişoarei peak through Puzdra clough, at the altitude of 1160 m.

From the upstream of Ostra begins the area with the highest density of improvements and installations, with the two decantation pools no longer functioning, overgrown with grass and almost completely remade. Then come the two affluents of Brăteasa, Tărnicioara and Străjii river, from the left and respectively right of Brăteasa valley.

In the area of brooks, two active decantation pools were created, ***Tărnicioara*** and Straja. Then follows the complex of buildings and installations of Tarnița preparation Factory with the two sections, nonferrous and barite, continued at around 500 m upstream from a group of buildings with administrative purposes of E,M, Leşu Ursului, near them being the mine Aluniș, the Ostra quarry and Ostra dump.

The density of the hydrographic network grows from 0.53 kg/km^2 in Moldova basin and the inferior and middle basin of Suhăi, at 0.68 kg/km^2 in the hydrographic basins Brăteasa and Bistrița.

The pool Valea Tărnicioara was destined to exploitation in 1975. The decantation pool reached presently a height of over 80 m (the main closing barrage) and the average slope of the general talus being under 18˚ (1:3).

As "valley pool" it has the priming dam situated on Valea Tărnicioara. The dam is founded on old, Cretaceous deposits, known under the name of "Sinaia layers", made up of marl chalks and sandstone, resistant rocks that ensure both the stabilization of foundation land, and of the pool bed. The rocks are bended towards the upstream, at around 40 – 50˚, which represents an important condition in favour of stability.

The pool has two ramifications, one on Valea Tărnicioara and the other on Scăldători brook- left affluent of Valea Tărnicioara. The watercourse of Valea Tărnicioara was deviated and moved into a gallery dug in the right versant of the valley, and the watercourse of Scăldători brook goes under the pool in a visitable under-crossing gallery (with a diameter of 1.8 m) and is continued to Valea Tărnicioara existing the pool in the downstream from the primer dam.

The decantation pool Valea Tărniciora is a valley pool that is founded on a priming dam and was built through the elevation process "towards the upstream".

The pool has in the upstream two tail barrages, one on Valea Tărnicioara which is barring the watercourse in order to take it to the gallery and another on Scăldători brook.

3. CHECKING THE STABILITY OF VALEA TĂRNICIOARA DECANTATION POOL. THE RESEARCH METHOD

Valea Tărnicioara decantation pool belongs to the importance category "special importance barrage" from:"The Emergency Ordinance regarding the safety of barrages from November 28th 2000".

In this context, through "barrage" we understand "any hydrotechnical work with an existent structure or proposed which is capable to ensure the accumulation, permanent or non-permanent of water, liquid industrial waste deposited under the water (from the chemical industry, energetic industry, and the decantation pools from the mine industry) whose breakage could produce the uncontrolled loss of the accumulated contests, with extremely important negative effects on the social, economic and/or natural environment (Emergency ordinance regarding the barrages' safety from November 28th 2000).

The two serious events occurred in the decantation pools in our country in the last three decades integrally motivate the fact that the pools belong to the II importance class.

The two events are:

The breakdown, in 1971, of the decantation pool Certej – Săcărâmb – Deva mining area, where about 100 people lost their life;

The accident from the decantation pool "Aurul" (The Gold) – Baia Mare mining area, from January 2000.

For estimating the stability of the decantation pool, the settlement deformations and the horizontal deformations, topographically measured, were analyzed.

In the first stage we analyzed the information registered until March 2004 and in the second stage, the results obtained until March 2005.

For evacuating the purified water, presently, only one inverted probe is functioning, positioned near the last dam from Valea Tărnicioara, which ensures the normal functioning of the pool. By lifting up the pool, the rest of the inverted probes were abandoned, respectively deteriorated and taken out of service.

Figure 2 – The water screen from the beach of the decantation pool Valea Tărnicioara

Figure 3 – The inverted probe from the beach of the decantation pool Valea Tărnicioara

The purified water was initially evacuated through two systems; one on Scăldători brook formed from inverted probe which discharged the water in the undercrossing gallery and another one on Valea Tărnicioara formed of inverted probes which discharged the water in the undercrossing gallery and another one on Valea Tărnicioara formed of inverted probes as well connected to a pipe posted on the pool bed. As a result of the elevation of the pool some inverted probes were taken out of service. In the inverted probe, the smallest width possible of the water screen is maintained, of about 0.5 m.

The natural stability of the versants of the decantation pool, both on Valea Tărnicioara and on Scăldători brook is very good. In the future, the versants of these valleys will not endanger the pool stability either.

The decantation pool stability is monitored with topographic guiding marks for measuring the taluses deformations, and with piezometric forages for measuring the depth of the underground water from the pool bed.

The estimation of the taluses stability starts from the deformations measured in the interval of the last 5 years (2002-2007) processed through the method of signal analysis, the only method for evaluating stability based on real deformations, measured "in situ".

Taking into account the time intervals between the measurements, for the signal of the horizontal movement we used the formula:

$$\eta_d = \left(\frac{d_0}{\alpha \cdot d} - 1 \right) \cdot 100$$

In which:

d_0 – is the non-cumulated "current deformation" corresponding to the last time interval measured t_0 (current time) – expressed in millimetres;

d – "previous deformation" non cumulated, corresponding to the previous time interval t – expressed in millimeters;

α – deformation proportioning coefficient depending on the time interval in which it was made – dimensionless

η_d – horizontal displacement signal – expressed in percentage (%).

Recording periods:

22.07.2002 – 16.07.2003 t = 359 days

16.07.2003 – 03.07.2004 t_0 = 352 days

In this case the previous time interval being greater than the current time interval ($t > t_0$), the proportioning coefficient is expressed like this:

$$\alpha = \frac{t_0}{t} = \frac{352}{359} = 0{,}98$$

Fig. 5 – Topographic marks on the bank of Valea Tărnicioara decantation pool

Considering the size of time intervals t_0 and t we calculated the correction coefficient for which we obtained the correction value $\alpha = 0.98$, which gives the displacement signal a high degree of confidence in the calculation results.

4. RESULTS OBTAINED AND THEIR INTERPRETATION

4.1. Assessment of Horizontal Displacements: Expertise of 2004

Concerning the calculation results, the negative values of the horizontal displacement signal, they point out a normal evolution of the pool stability, a tendency of attenuation of the deformations. The positive values and the null values show, on the contrary, an increase of the deformations, which requires a very careful supervision of stability, by reducing the time interval between measurements and even of application of some measures for increasing stability.

Using the deformations measured on the profiles 1 and 2 at the basis of the pool there were calculated the signal analyses 1 and 2, Analysis 1 including the topographic marks no. 11, 12, and 13, and Analysis 2 the topographic marks no. 15 – 28. Both analyses are calculated in table 1 and illustrated in the charts of figures 6 and 7.

Table 1 – Signal Analyses 1 and 2 – marks of the profiles at the basis of the pool

No. topographic marks	$\eta_d = \left(\frac{d_0}{\alpha \cdot d} - 1\right) \cdot 100$			
	d_0 (mm)	**d (mm)**	**η_d (%)**	
11	5,4	11,2	-51	
12	22,3	8,6	165	
13	8,9	15,5	-42	Profile no. 1
15	9,8	25,5	-61	Profile no. 2
17	3	12,5	-75	
18	14	25	-43	
19	2	25	-92	
20	20,2	18,8	7	
21	31	31,5	0	
22	13,6	11,3	23	
24	29,1	19	57	
25	8	10,4	-22	
26	12,1	34,4	-64	
27	6,7	26	-74	
28	13,6	31,8	-56	

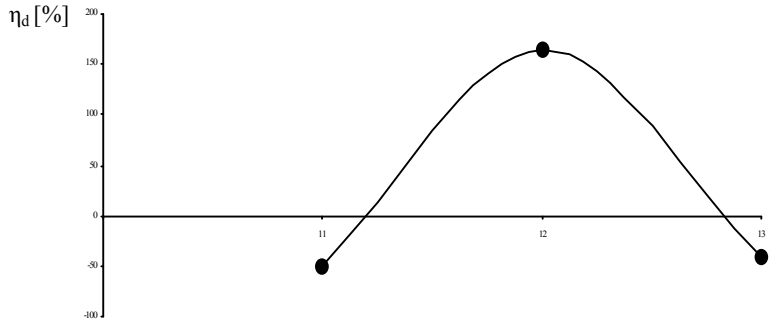

Fig 6 – Signal Analysis 1 – Tărnicioara Decantation Pool

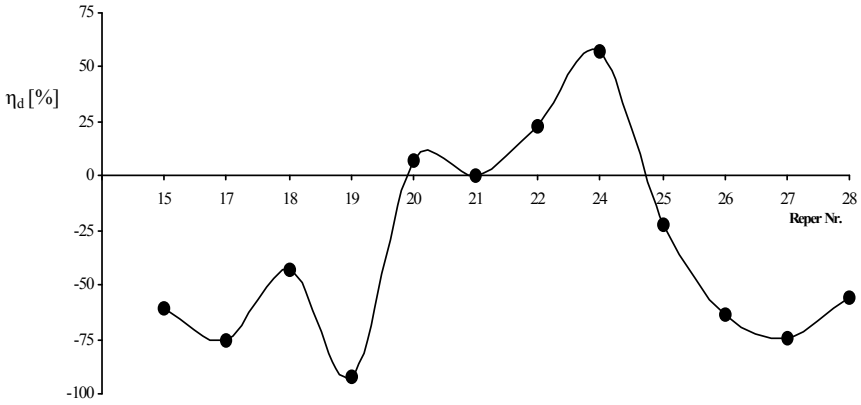

Fig. 7 – Signal Analysis 2 – Tărnicioara Decantation Pool

Studying the results of table 1, of the 15 values of the displacement signal, 10 of them are negative, which indicates a tendency of attenuation of the deformations, whereas 4 values are positive and one value is null, they emphasizing, locally, deformations still active within the lake body.

4.2. Assessment of Horizontal Displacements: Expertise of 2005

Expertise periods: 25.07.2002 – 15.07.2003 t = 300 days and 15.07.2003 – 22.03.2005 t_0 = 614 days. In this case the previous time interval being smaller than the current time interval ($t < t_0$), the proportioning coefficient is expressed like this:

$$\alpha = \frac{t}{t_0} = \frac{300}{614} = 0{,}5$$

Table 2 – Signal Analyses 4 and 5 – marks of the profiles at the basis of the pool

No. topographic marks	$\eta_d = \left(\frac{d_0}{\alpha \cdot d} - 1\right) \cdot 100$			
	d_0 (cm)	d (cm)	η_d (%)	
11	10,8	1,58	240	
12	14,5	1,5	380	
13	39,4	1,27	1450	Profile no. 1
15	5,8	1,2	140	Profile no. 2
17	8,8	1,1	300	
18	9	1,3	250	
19	6,7	1,22	170	
20	5,6	0,86	220	
21	4,5	0,9	150	
26	2,3	1,48	- 22	
27	4,7	1,03	130	
28	5,7	1,42	100	

Considering the size of time intervals t_0 and t we calculated the correction coefficient for which we obtained the value $\alpha = 0.5$, which gives the displacement signal a high degree of confidence in the calculation results.

Concerning the calculation results, the negative values point out active deformations within the body of the decantation pool. As physical sizes, there are a few centimeters per year, values that are within the admissible deformations for the stability of the decantation pools.

The Tărnicioara pool being at rest from the end of 2004, the underground water descended, in most piezometres, at over 10 m deep, which represents an important factor in favour of stability.

Using the information measured on the profiles 1 and 2 at the basis of the pool there were calculated the signal analyses 4 and 5, Analysis 4 including the topographic marks no. 11, 12, and 13, and Analysis 5 the topographic marks no. 15 – 28. Both analyses are calculated in table no. 2 and illustrated in charts in figures 8 and 9.

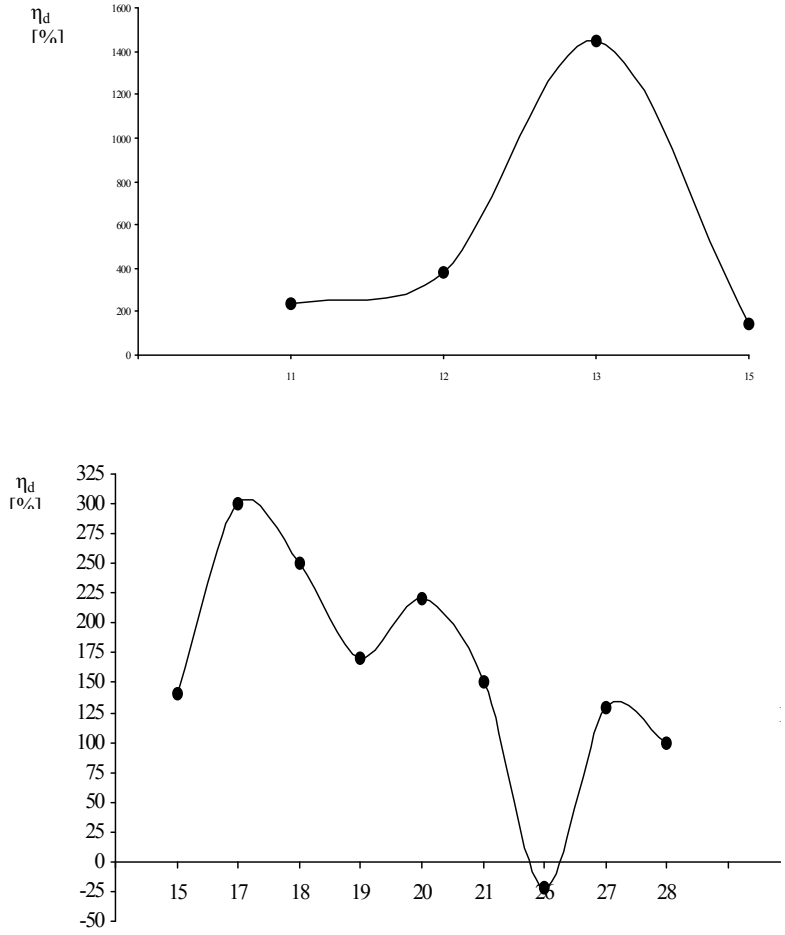

Fig. 8 and **Fig. 9** – Signal Analysis 4 Horizontal Displacements – Profile 2 and Signal Analysis 5, Horizontal Displacements – Profile 2 –Tărnicioara Decantation Pool

3. RESULTS AND SIGNIFICANCES

4.3. Assessment of Vertical Displacements (settlements): Expertise of 2004

For the vertical information we used the vertical displacement signal expressed as follows:

$$\eta_s = \left(\frac{s_0}{\alpha \cdot s} - 1 \right) \cdot 100$$

where:

s_0 – is the "current deformation" related to the last time interval measured t_0 (current time) – expressed in millimeters;

s – "previous deformation" related to the previous time interval t - expressed in millimeters;

α – proportioning coefficient of the deformation depending on the time interval in which it was made - dimensionless;

η_s – vertical displacement signal – expressed in percentage.

Expertise periods:

22.07.2002 –16.07.2003 t = 359 days; 16.07.2003 – 03.07.2004 t_0 = 352 days

In this case the previous time interval being smaller than the current time interval ($t > t_0$), the proportioning coefficient is expressed like this:

$$\alpha = \frac{t_0}{t} = \frac{352}{359} = 0{,}98$$

Concerning the significance of the calculation results, the negative values of the vertical displacement signal point out a normal evolution of the pool stability, a tendency of attenuation of the deformations. The positive or null values, on the contrary, show an increase of the deformations, which requires a very careful supervision of stability, by reducing the time interval between measurements and even by applying some measures for increasing stability.

The vertical displacement signal is showed in table no. 3 and represented in the charts of figure 10.

Table 3 – Signal Analyses 6 – marks of the profiles at the basis of the pool

No. topographic marks	$\eta_s = \left(\frac{s_0}{\alpha \cdot s} - 1 \right) \cdot 100$		
	s_0 (mm)	**s (mm)**	**η_s (%)**
13	7	8	-10
22	7	2	250

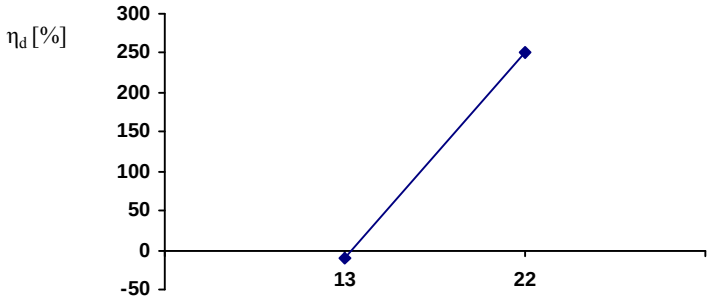

Figure 10 – Signal Analysis 6, Vertical Displacements – Tărnicioara Decantation Pool

This signal also confirms, by its results, both the tendency of attenuation of the deformations, and the existence of active deformations.

4.4. Assessment of Vertical Displacements (Settlements): Expertise of 2005

For the vertical deformations we used the vertical displacement signal which is calculated with the same formula.

Expertise periods: 15.07.2003 – 30.10.2004 t = 472 days and 30.10.2004 – 22.03.2005 t_0 = 149 days

In this case the previous time interval being greater than the current time interval ($t > t_0$), the proportioning coefficient is expressed like this:

$$\alpha = \frac{t_0}{t} = \frac{149}{472} = 0{,}31$$

Concerning the significance of the calculation results, the negative values of the vertical displacement signal point out a normal evolution of the pool stability, a tendency of attenuation of the deformations. The positive or null values, on the contrary, show an increase of the deformations, which obliges to a very careful supervision of stability, by reducing the time interval between measurements and even by applying some measures for increasing stability.

The vertical displacement signal is showed in table no. 4 and represented in the charts of figure 11.

Table 4 – Signal Analyses 7 – marks of the profiles at the basis of the pool

No. topographic marks	$\eta_s = \left(\frac{s_0}{\alpha \cdot s} - 1\right) \cdot 100$		
	s_0 (cm)	s (cm)	η_s (%)
13	10	3	900
15	11	1	3400
20	3	6	60
28	5	7	130

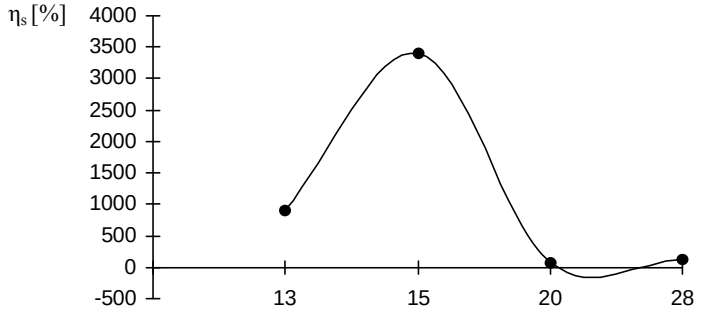

Fig. 11 – Signal Analysis 7, Vertical Displacements – Tărnicioara Decantation Pool

This signal also confirms the existence of active deformations.

5. CONCLUSIONS

a.) Following the results of tables 1-4, we may notice a tendency of attenuation of the deformations, but locally, there are deformations still active within the pool body.

We notice that the bank deformations are within the admissible limits for the stability of the decantation pool. According to the provisions of the joint Order of the Ministry of Waters, Forests and Environmental Protection of May 7th 1996 and Ministry of Public Works and Territory Management of May 13th 1996 concerning the "Methodology Approval and Contents of Expertise of Safety Status of Related Dams and Accumulation Lakes" and its adaptation to decantation pools.

b.) Concerning the second pool monitoring system, represented by the variations of the level of the underground water and its effects on stability, the situation is under control. At present there are activated 7 piezometric drillings, the level measurements being systematically made. Valea Tărnicioara pool being at rest from the end of 2004, the underground water descended, in most piezometres, which represents an important factor in favour of stability.

The underground water remaining at 8 – 10 m deep, in all piezometres, it doesn't produce negative effects on pool stability, this depth representing even a factor in favour of pool stability.

We mention that along the Tărnicioara Valley there are created strong air currents which blow the sand from the beach but especially from the main bank of the pool, which leads to the reduction of steps height and covering the berms, forming in the lower part of the pool, a bank with a continuous slope. Sand removal by the wind reduces the cap dyke height, by several centimeters every year, leaving without support the transport line pipe of dirty water, which requires the periodical restoration of the cap dyke.

c.) Tarnicioara decantation pool is a valley pool, built on two valleys: one of the Tarnicioara creek which is deviated through a gallery that turns round the deposit and one of the Scaldatori creek which is directed, under the deposit, through an undercrossing gallery.

This leads to the need to make more ample works to increase pool stability. Of which we mention the most important ones: deformations measurement, during the operation period only, twice a year, in spring and in autumn; weekly measurement, of the piezometric level in the observation drillings;maintaining a low water level, from 0. 5 m thick, at the inverted probe, to attenuate the suffusion in the pool body; maintaining the valve of the damaged water discharge pipe from the right slope in the "on" position, as long as there are not entrainments of sand in the water stream; periodic examination of concrete condition from the undercrossing ditch and elimination of water infiltrations appearing in the ditch; accelerated consolidation of dump by eliminating the water through the pores by installing vertical drains, following a pre-established distribution network; executing enrokments with gross stone to protect the banks and the hydraulic structures in case there are large water inrushes on the streams of the Scaldatori and Tarnicioara creeks; preventing the entrainment by the water inrush of the dump from the pool and the banks erosion; controlled collection and direction outside the pool perimeter of rain waters by making drains at the basis of the slopes, impermeabilization of the ditches foundation plate with geomembrane;

6. REFERENCES

1. Lăzărescu Mihaela (2000) – Influenţa iazurilor de decantare din industria minereurilor neferoase asupra mediului înconhurător, Revista Hidrotehnica, nr. 11-12.
2. Florea M. N., Iaru (1977) – Studiul deformaţiilor, element de decizie în analiza stabilităţii iazurilor de decantare. Revista Mine, Petrol şi Gaze, vol. 28, Bucureşti.
3. Stematiu D. (2001) – Utilizarea evaluării riscului în analiza siguranţei iazurilor de decantare din industria minieră, Revista Hidrotehnica, nr. 5.
4. Stamatiu D. (2002) – Date statistice privind cauzele accidentelor tehnice de la iazurile de decantare din industria minieră, Revista Hidrotehnica, nr. 2.
5. Sofonie V. (2002) – S.F. "Stabilizarea şi conservarea ecologică a iazului de steril de flotaţie D_1, localitatea Borşa, jud. Maramureş, A. N. V., Baia Mare" de decizie.
6. * * * (1988) – Studiu de impact E. M. Leşu Ursului, Stabilizarea taluzului – Iaz de decantare Tărnicioara. Institutul de Cercetări şi Proiectări miniere pentru Substanţe Nemetalifere, Cluj – Napoca.
7. * * * (1988) – Instrucţiuni tehnice departamentale privind proiectarea, executarea, întreţinerea, exploatarea iazurilor de decantare din industria minieră. Indicativ I. D. – 88. Institutul de cercetări, Inginerie tehnologică şi Proiectarea alunecărilor de Construcţii şi Instalaţii pentru Minereuri.
8. * * * (1993) – Ghid privind iazurile de decantare din industria minieră I. P. R. O. M. I. N., Bucureşti.
9. * * * (2000) – Metodologia privind evaluarea stării de siguranţă în exploatare a barajelor şi digurilor care realizează depozite de deşeuri industriale – T. L. H. – 023. M. O. partea I, Anul XII, Nr. 167.
10. * * * (1996) – P. T. Obiect 1. 3. 5. " Lucrări pentru protecţia mediului la iazul de decantare Tărnicioara şi hălzile de steril inactive". I. C. I. T. P. M. N. S.A. Baia Mare.

Advanced Software Application for Digital Terrain Models Used in Infrastructure Projects

S. Cazanescu,. P. M. García and Paulina Iancu

Abstract – **In our days, the activities related to digital survey and data acquisition become standard procedures accepted all over the world, including Romania, for IT based topographic practices.**

The paper presents a software application which helps designer to create, view and edit Digital Terrain Models (D.T.M) from all over the world. The application creates DTMs based on Delaunay triangulation algorithm and has the possibility to include break-lines and to draw contour lines with a reliable smoothing algorithm, adding labels whenever necessary. The application uses a system as the WMS, Web Map Service, to access the data of the digital terrain models on internet.

All the necessary tools are included for engineers working with DTMs. On the other hand, the application can edit dynamically the drawn triangulation in the CAD, (AutoCAD or BricsCAD) and display the changes in real time.

Keywords **– digital survey, digital terrain models, LanDTM**

1. INTRODUCTION

Digital terrain model (DTM) is a digital representation of ground surface topography or terrain. It is also known as a digital elevation model (DEM). A DTM can be represented as a raster (a regular grid of squares) or as a triangulated irregular network (TIN). TIN models are most commonly used in engineering applications because they always keep the original data points. Coordinate points are assembled from a variety of sources (digitized, imported from files, entered from field notes etc). The DTMs are commonly built using land surveying.

The quality of a DTM is a measure of how accurate the elevation is at each pixel (absolute accuracy) and how accurately is the morphology presented (relative accuracy). Several factors play an important role for quality of DEM-derived products:

- terrain roughness;
- sampling density (elevation data collection method);
- grid resolution or pixel size;
- interpolation algorithm;
- vertical resolution;
- terrain analysis algorithm;

Severin Cazanescu is with Land Reclamation and Environmental Engineering Faculty, USAMV Bucharest, 59 Marasti Boulevard, Sector 1, Bucharest, Romania, (corresponding author to provide phone: +40-722-567877; fax: +40-21-6242994; e-mail: cazanescu@gmail.com).

Pedro Maciá García is with Aplicaciones Topográficas S.L., Spain

Paulina Iancu is with Land Reclamation and Environmental Engineering Faculty, USAMV Bucharest, 59 Marasti Boulevard, Sector 1, Bucharest, Romania, .

ISSN-1584-5990

Common uses of DTMs include: extracting terrain parameters, modelling water flow or mass movement, creation of relief maps, creation of physical models, terrain analyses, Geographical Information Systems (GIS), engineering and infrastructure design, precision farming and forestry, surface analysis. DTM is also a valuable component in analyses involving various terrain characteristics such as profile, cross-section, line-of-sight, aspect and slope.

The paper presents a software application which helps designer to create, view and edit Digital Terrain Models (D.T.M) from all over the world. The software application name is LanDTM, the last release being made available for the public on 26th of March 2010 [1]. The only similar program is developed by the well-known Autodesk Inc. company and is still under testing (beta release). Thus, experts' opinions on the usefulness and performance of the LanDTM software are still expected.

It is significant that the software application is the result of cooperation between a Romanian institution (Land Reclamation and Environmental Engineering Faculty - Bucharest) and Aplicaciones Topográficas S.L. from Spain. The application was tested with good results in the frame of the project "Water excess removing in Ghelința-Brates area, Covasna County, Romania".

2. MATERIAL AND METHOD

This software application creates triangulations and contours using the newest computation techniques. It can make triangulations for 100000 points very fast, based on Delaunay triangulation algorithm (a collection of edges satisfying an "empty circle" property: for each edge we can find a circle containing the edge's endpoints but not containing any other points) and its dual – Voronoi diagrams (a partition of space into cells, each of which consists of the points closer to one particular object than to any others).

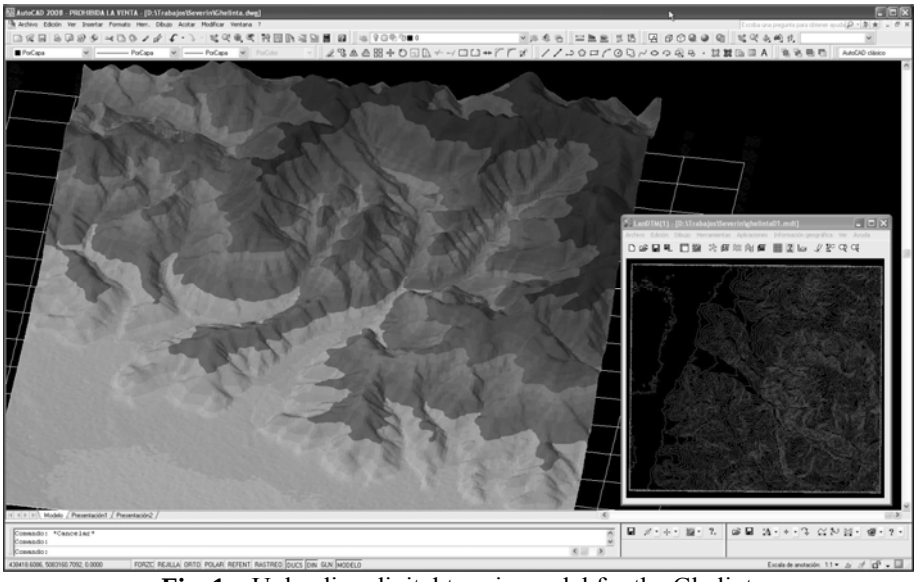

Fig. 1 – Uploading digital terrain model for the Ghelinta area

There is included the possibility to have access to the digital terrain model of all the world, each 30 meters for USA and 90 meters for the rest of the world. It has prepared a data server, where are saved all the files containing the digital terrain models of all the world, separated in files of 1 grade, and it is possible to get the corresponding data by selecting with a window the interested zone to view. In this last version it is included the possibility to add topographical data from digital terrain models files created by „Shuttle Radar Topography Mission"- SRTM, (providing the elevations of the earth in 1 second interval - 30 meters for USA and 3 second interval for the rest of the world). There are other formats, such as MDT25 of Instituto Geografico Nacional - IGN, which are also compatible with the program having a point at every 25 meters, as appropriate, extracted from, National Topographic Map - MTN, 1:25000, instead of satellite image. And any other format could be included in the program, in the future [2].

The program runs on AutoCAD 2007/2008/2009, AutoCAD 2010 and BricsCAD v10, and uses "Protopo" libraries, (a famous Spanish engineering civil and surveying program) [3].

Other specific features, besides the DTM generation with a reliable Delaunay triangulation algorithm, are: the possibility to include break-lines and to draw the contours without smoothing or with a reliable smoothing algorithm and to add labels on the contour lines (Fig. 2).

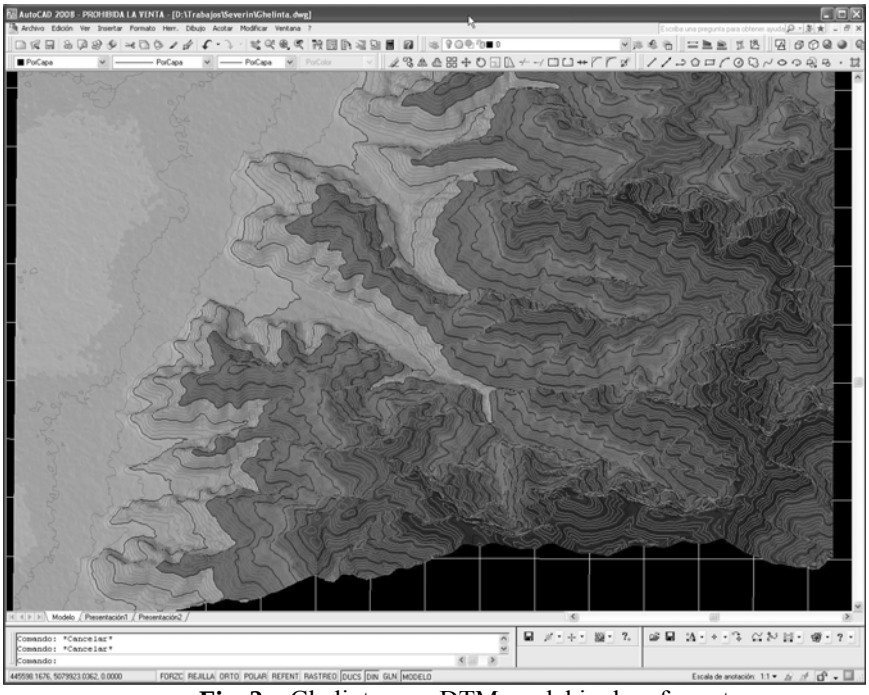

Fig. 2 – Ghelinta area DTM model in dwg format

The best feature of the software application is that it allows to edit and draw triangulation lines, as "LINE" entity in the CAD, and after, to import to the program that triangulation quickly. Thus, the program will keep the DTM points, lines, break-lines, boundary lines and contours like it is shown in Figure 3.

The software application has a main dialog box, where all these data can be accessed and view in graphical form. The data are separated in two windows, one as table and the other

as drawing [1]. Thus, by clicking on a point in the data table, the point is identified in the drawing and the properties can be changed easier.

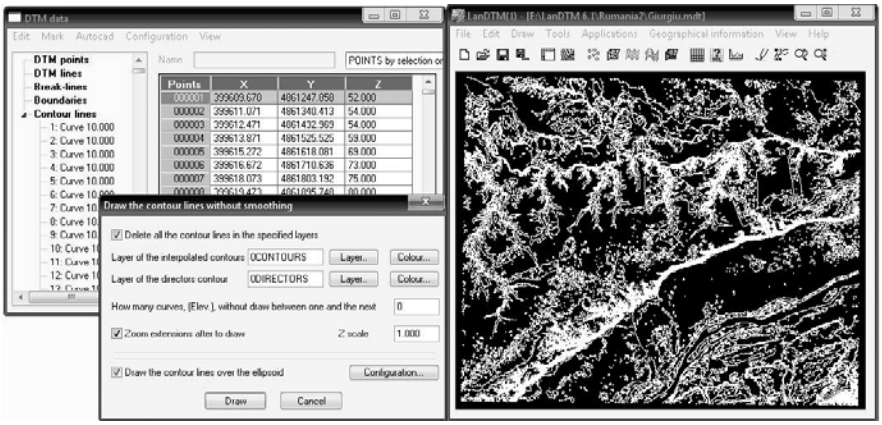

Fig. 3 –DTM data in tables

In order to facilitate the triangulation and contours computation, a set of performant editing tools has been created, which allows that any change in AutoCAD drawing to update immediately the data stored in the DTM file.

The input data for triangulation and contouring computation are data regarding lines and polylines and can be grouped in five categories [1]:

- DTM points – these set of data includes all the points belonging to the final triangulation; these points can be selected from an image or a file, but can be also end points of break-lines further selected. If we deal with polylines, it is necessary to insert the polylines vertices;
- DTM lines - to see the computed triangulation lines and identify them in the drawing or to choose a triangulation created with other application or changed with AutoCAD tools ;
- breaklines – data referring to the breaklines of the design, meaning selection of breaklines or selection of the breaklines existent layer. There is a variable called "the boundary" which has to be observed when o group of breaklines form a polyline.
- contours to be excluded, meaning all the contours which don't need to be curved, like buildings, walls, generally speaking – planimetry.
- contours – meaning the contours which are going to be computed or contours created in other applications which need to be uploaded

Among the details, generally are taken into account the following:
- doubling of points – the application checks the duplicity of points and lines prior to any computation and erases the duplicates;

- color of the ranks - in the group of "DTM Points", the points belonging to a break-line appear green. During triangulation processing, the points which are not taken into consideration, due to any problem to the correspondent breakline, are colored in red.
- dimensions of the contours – it is possible to change the elevation of any contour line, simply, by changing the value displayed in the edit box of the benchmark.

- identification of points – by clicking on a point or line data table, immediately appears a circle or line, in yellow, in the graphic window indicating the position of point or line (always and when the viewport is configured to display the points and breaklines).
- display in the graphic window – during entering data into the data window, the viewport is updated, presenting these data points and lines. The viewport need to be configured to view these data.

Triangulation and contours computation

After all data are inserted, the following step is to create the triangulation and contours, using "Create DTM" or "Create contour" commands.

The software application uses "The maximum distance search" as method to compute the triangulation. This method means that a maximum value is inserted for the length of the triangle side, value which is not exceeded. The maximum distance of search can be also indicated by clicking it with the mouse on the drawing. There is also tool called "Contour inclusion" helping to define a boundary beyond which any contour is created [1].

The points which are not part of any associated contour are deleted if this option is activated.

The contour lines can be created just after the DTM computation or later, using "Edit / Create contour" command. The application asks for the distance between contours and the number of contour lines wanted between the master contours. Once the triangulation and contours are computed, the next step is to draw the contours (Figure 4), being two options;

- to draw without smoothing – meaning simple AutoCAD polylines with elevation,
- to draw with smoothing – meaning to create new entities "contours" of Protopo, for subsequent presentation.

Fig. 4 – Drawing contours for Ghelinta area

Usually the drawing is made without smoothing, because the regeneration is faster, and the contouring is clear. Once the contours are finished, with the appropriate changes done, the smoothed curves are drawn for presentation. Both type of contours (with or without smoothing) can be edited using the toolbar PProtopo, but it is necessary to change the labels in order to include elevation contours in.

There are two tabs for the drawing settings, the first for the basic configuration of the drawing, like: layers, colors, zoom, etc, and the second for a more detailed configuration of

the smoothed contours, where the number of vertices by corner and the level of smoothing are decided (Figure 5).

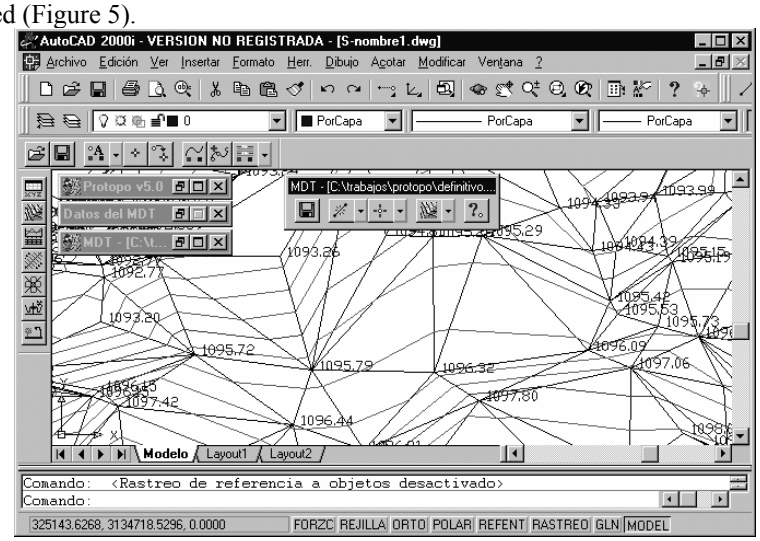

Fig. 5 – Contours smoothing

If all options are set by default, there will be a smoothing quite appropriate to any designer needs. Once the drawing is made using PProtopo tools, labels on the contour lines and for distances should be inserted manually.

The program has a series of options to export points, DTM lines and contours (Figure 6) in KML / KMZ format files for Google Earth.

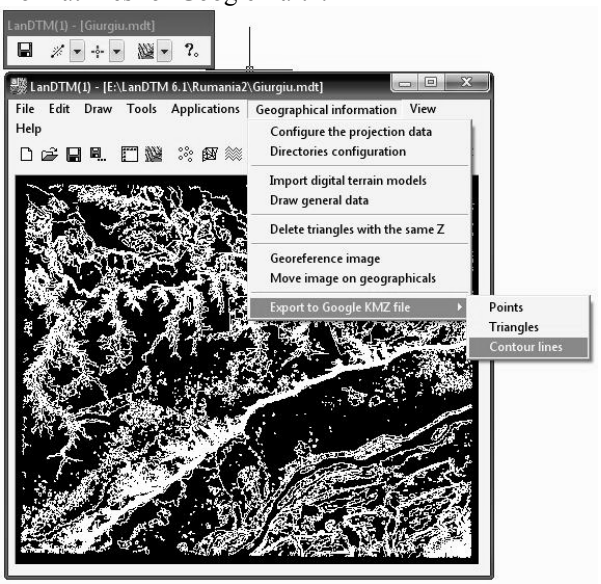

Fig 6 – Points, lines and contours export in KMZ format file

3. RESULTS AND SIGNIFICANCES

LanDTM is a multitasking software application because it allows opening until five sessions and works with a different DTM in each of them.

The application uses Delaunay triangulation in order to represent the real terrain in a CAD environment and has professional approach and design. It is reliable and runs fast with unlimited number of points and can use a large number of breaklines (more than 20000). Breaklines are an important part of DTM. They prevent triangles from crossing over a linear feature such as a road edge or ditch line. Breaklines can include curved segments. However, such a great number of breaklines should be avoided on a slow computer because it can slow down the designing process.

The program has advanced tools which can modify the computed triangulation and allow the user to see the changes during the design process. Smoothed and labeled contours can be generated at any interval from the triangulated model. Different colors, linetypes, symbols and labeling can be applied to major and minor contours. After the contours have been automatically generated they can be edited on the screen. It also sets the elevation to the contour lines by the aid of a special tool in a CAD floating window where an elevation value is inserted, adding or subtracting an interval to the previous value. Thus, all the selected polylines are created, again, with the new elevation.

The software application is also able to "insert line", "change edge", "insert point", "delete triangle", which are very easy to handle. When all the changes in LanDTM are done, one can close the application and continue editing the file using standard CAD tools.

When the edition is completed, the lines have to be imported and the program will re-create the new triangulation easily.

On the other hand, LanDTM has advanced features for detecting and repairing errors.

It has also a smoothing test for the contour lines, highlighting the intersection between curves and allowing the user to decide if the contour lines need to be corrected or smoothed with different parameters.

The software application export data in KML / KMZ format. Thus, all images can be displayed easily with Google Earth (Figure 7).

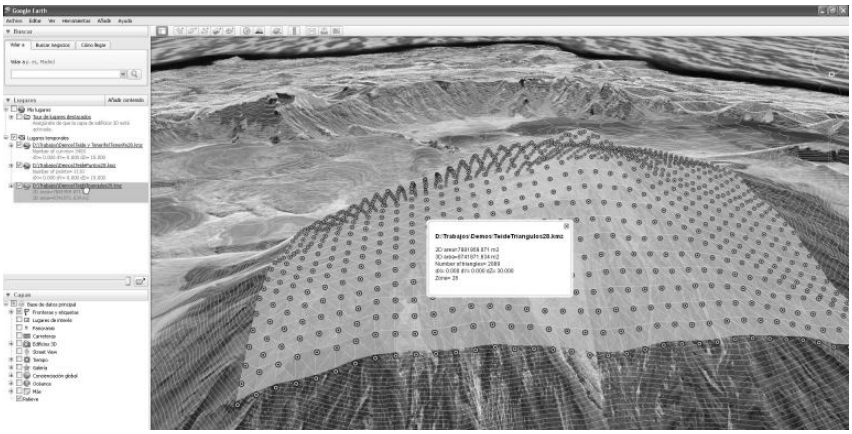

Fig. 7 – DTM surface draped in Google Earth

4. CONCLUSIONS

LanDTM is a new software application created using many new computation techniques. It is useful bout for general surveying, as well as for civil and environmental engineering, due to the following features:

a) generation of cut and fill volumes between two surface.

b) performance of dynamic longitudinal profiles on DTM. According to a drawn polyline in the CAD on a DTM, the "Applications/Dynamic profile on DTM" option allows to see the longitudinal profile as a graphic, which is changing in real time while that polyline is edited.
c) drawing slopes according to a polygon and levelling the land if necessary. The levelling process, needs slopes in the limits of the flat area. With the tool "Slopes according a polygon" the application allows to draw the lines of the resulting slope of cut and/or fill.
d) importing and exporting files to Protopo - '.CRD' file format or to AutoCAD - '.DXF' file, by means of another software application called ProLink, included in LanDTM.
e) exporting points, triangulations and contours in KML / KMZ format files to Google Earth or Google Maps, allowing to view them as images.

LanDTM has been tested for the first time in Romania, for Ghelinta area, the obtained results being compared with the data gathered in the survey activities during the project development. Given the accuracy of the results, we consider that the software application is very useful especially for educational projects in this development stage.

5. REFERENCES

[1] P.M.Garcia, LanDTM version 6.1 – User Manual, 2010, Available: http://www.landtm.com.
[2] NASA, the National Geospatial-Intelligence Agency, and the German and Italian Space Agencies, „The Shuttle Radar Topography Mission" Project, February 2000
[3] P.M.Garcia, Protopo version 6.0 – User Manual, 2009, Available: http://www.aptop.com.

Ovidius University Annals Series: Civil Engineering Volume 1, Issue 12, June 2010

The threat of natural hazards to people and economies in south east european countries

C. Filip, M. Popa, G. Drăghici and G. Păduraru

***Abstract* – In 11 countries from South East European region, 2-4 million people are exposed to natural disaster events, which represent 7 percent of the region's population. About 8 million people are susceptible to natural disasters that have a likelihood of occurrence of once every 20 years. First of all, the geographic concentration of natural hazards is presented (earthquakes, floods and landslides), then a hazard profile by subregion. The quantitative risk assessment performed for this study confirms that natural disasters can have significant consequences for the economic performance of the South East European countries and present some aspects of countries' hazard and vulnerability to disasters.**

***Keywords* – disaster, EM-DAT, flood vulnerability, hazard, risk assessment**

1. INTRODUCTION

The South East European (SEE) countries are exposed to a wide range of natural hazards. These nations have a history of devastating earthquakes, floods, landslides, drought, extreme temperature, wildfires and windstorms that have caused economic and human losses across the region. Often these disasters, which transcend borders, overwhelm the management capacity of a single country. Also, the level of preparedness and prevention varies from country to country, and regional cooperation does not exist to the extent necessary. Because of this high vulnerability, and the relatively small size of the countries in the SEE region, as well as the historical links between them, it will be more efficient and economically prudent for the region's countries to cooperate in the areas of civil protection and disaster preparedness and prevention [1].

Bearing in mind all these challenges, the Europe region is systematically promoting the implementation of a comprehensive framework that integrates risk assessment, emergency preparedness, disaster prevention, and catastrophe risk financing with the objective of reducing client countries' economic and social exposure to natural hazards on an *ex ante* basis. Special emphasis is given to the need to strengthen the institutional capacity to prevent and better manage emergencies.

C. Filip is with Ovidius University of Constanta, Bd. Mamaia nr. 124, 900356-Constanta, Romania, e-mail: cosminfilip@univ-ovidius.ro

M. Popa is with Ovidius University of Constanta, Bd. Mamaia nr. 124, 900356-Constanta, Romania, e-mail: mpopa@univ-ovidius.ro

G Paduraru is with Ovidius University of Constanta, Bd. Mamaia nr. 124, 900356-Constanta, Romania, e-mail: gpad@univ-ovidius.ro

G. Draghici is with Ovidius University of Constanta, Bd. Mamaia nr. 124, 900356-Constanta, Romania, e-mail: g_draghici_univ@yahoo.com

ISSN-1584-5990

This kind of strategic framework serves as the conceptional basis for the design of a new generation of hazard risk mitigation operations currently under preparation or implementation in the Kyrgyz Republic, Poland, Romania, the Russian Federation, and Turkey. The willingness to borrow about $1 billion for these projects demonstrates the importance the countries in the region place on protecting their populations and economies, and reflects the increased demand for hazard risk management initiatives. Economic losses, human suffering, and loss of life from natural catastrophes can be reduced by a systematic approach to planning and preparing for disasters and mitigating their impact. The need to improve hazard management is now recognized worldwide and incorporated as one of the Millennium Development Goals [2].

2. GETTING PREPARED: THE IMPORTANCE OF HAZARD ASSESSMENT

2.1 Risk Assessment: An Overview

Disasters (due to natural and technological hazards) can have catastrophic impacts on nations and regions. These events can lead to economic, social and environmental damages affecting overall economic activity, lifestyles, the emotional and physical well-being of humans and animals, social unrest and homelessness; and can cause disruption of communities and natural resources. The extent of damage caused by disasters depends on the vulnerability of affected areas. Harmful impacts of disasters result from the severity of hazard events and from the high vulnerability of the areas concerned. Therefore, prior hazard forecasting and improving the resilience of people and property can help to reduce hazard impacts.

International initiatives in the South Eastern Europe (SEE) region have proclaimed that all countries should, as part of their plans to achieve sustainable development through prevention, preparedness, building codes and enforcement of legislation, develop and have access to local, national, regional and global warning systems. However, this effort is only in the early stages of development in many SEE countries, and SEE countries have yet to inculcate disaster risk management into their development plans [3].

Vulnerability and risk factors coalesce around the concept of risk reduction, or disaster risk management. Appreciating and implementing this concept requires proper understanding of these factors, including the history of disasters and the nature of impacts, trends, the severity of different disasters, and the vulnerability of population and property. Severity is sometimes assessed against a country's gross domestic product (GDP) based on its particular development front (e.g. agriculture or service sector). The UN/ISDR secretariat and UNDP are working to develop a core set of indicators and a methodology to guide and monitor disaster risk reduction for hazards like earthquake, flood, cyclone and drought [4].

2.2 Evolving global trends

It finds that there has been an increase in the number of disaster events, particularly due to hydro-meteorological hazards, in most of the countries in the South East European Region. Disasters due to technological hazards are also on the rise in many countries. Overall, it shows a pattern of growing levels of economic loss, rather than growing mortality, due to disasters in this region. The region has experienced damaging and catastrophic earthquakes in the recent past, and seismological studies show that there is a high probability of future occurrence.

The focus of the international development community is shifting from emergency response and postdisaster reconstruction to disaster prevention and risk reduction. This focus is highlighted in the Millennium Declaration, which includes intensifying "collective efforts to reduce the number and effects of natural and man-made disasters" as a Millennium Development Goal (MDG) [2]. The inclusion of hazard assessment in risk management as part of the MDG's will further facilitate the inclusion of hazard assessment as an essential part of the economic development process.

3. DATA SOURCES IN ANALYSING HAZARDS AND VULNERABILITIES TO ASSESS RISK

Disasters (due to natural and technological hazards) are time and space reference events, but disasters don't follow political boundaries. For this reason, regional cooperation is very important in disaster preparedness and mitigation. The vulnerability of a nation or region to disaster events is often measured in terms of the total numbers of events, people killed, people affected and the economic losses. The impact diffusion of an event extends far beyond the visible physical damage. Vulnerability assessment is a means to develop appropriate mitigation measures and strategies at national, regional and international levels. Vulnerability assessment will help in prioritization of planning areas for disaster preparedness and prevention, and ultimately will assist with both sustainable development and poverty reduction.

Historic data plays a crucial role in hazard and vulnerability assessments of a country or region. Analyzing the historic events and losses helps to identify the risks in a country or region. Harmonizing data and setting criteria are important parts of a quality risk assessment. Limits on the availability of standardized risk data often constrain quantitative assessments of countries and regions. Planners, policymakers, field agencies and others engaged in disaster preparedness have often expressed the need for good-quality data. When countries report an event, there may be a bias factor, as the reporting authority may provide higher figures to get attention and international support or may suppress or exaggerate critical information. Reinsurance companies also maintain loss data, but it is not accessible to public. Moreover, these companies focus on certain geographies and often won't give global or regional pictures [5].

4. THE USE OF EM-DAT DATABASE IN REGIONAL RISK ASSESSMENT

This study present data from EM-DAT database [1], [6] for the last 33 years. The report provides hazard risk assessments for 11 SEE countries: Albania, Bosnia and Herzegovina, Bulgaria, Croatia, Macedonia, Moldova, Montenegro, Romania, Serbia, Slovenia and Turkey. EM-DAT, developed by the Office of U.S. Foreign Disaster Assistance (OFDA) and the Centre for Research on the Epidemiology of Disasters (CRED) is widely used for macro-level risk assessment [5]. The main objective of this database is to serve the purposes of humanitarian action at national and international levels. It is an initiative aimed to rationalise decision making for disaster preparedness, as well as providing an objective base for vulnerability assessment and priority setting. EM-DAT contains essential core data on the occurrence and effects of over 18,000 mass disasters in the world from 1900 to present. The database is compiled from various sources, including UN agencies, non-governmental organisations, insurance companies, research institutes and press agencies.

EM-DAT has been constantly improved over the last 30 years. EM-DAT was used as the main data source for risk assessment, because it provides standardized data, which is important when analysing the risks for individual countries and regions. The events and impacts in country-level reports and other published documents are also presented for the

country-level assessments, while EM-DAT was used for analysing the hazards and vulnerabilities of the countries and the region. As economic loss data for many countries is scanty in EM-DAT, other sources, like the UNEP (United Nations Environment Programme) Disaster Risk Index analysis tool [7], the World Bank Global Natural Disaster Hotspots project [8], the National Geophysical Data Center [9] and other published research papers on hazards and vulnerability in the region were also used as a supplementary information, because EM-DAT cannot be treated as complete.

In the regional assessment using EM-DAT, only major hazards like earthquake, flood, drought, windstorm and technological hazards were considered. Disaster and disaster impact indicators were ranked separately, and a cumulative rank was also calculated. The disaster rank shows disaster risk of each country, while disaster impact ranking gives a picture of its relative vulnerability. For disaster impact, the number of deaths, the total affected population, and the amount of economic loss all were used, along with total population, population density, population density in the affected area, urban population growth, percentage of arable land, the Human Development Index and GDP. The cumulative ranking was calculated from these variables to assess the risks faced and relative vulnerability of countries in the region [1].

5. SOUTH EASTERN EUROPE REGIONAL DISASTERS ANALYSIS

5.1 Regional setting

A regional risk assessment of SEE needs to be examined against the background of the existing, transboundary nature of the region's physical and social contiguity (**Fig.1**).

The Transboundary Rivers, the regional climatic conditions, the geological contiguity, the socio-economic and cultural settings, and the past political situation are important factors contributing to the complexity of the region. The small size of the countries also contributes to the region's homogeneous physiographic and climatic characterization, and leads to common and shared hazards. The relatively small size of the countries often makes it difficult to respond to hazards at a country level.

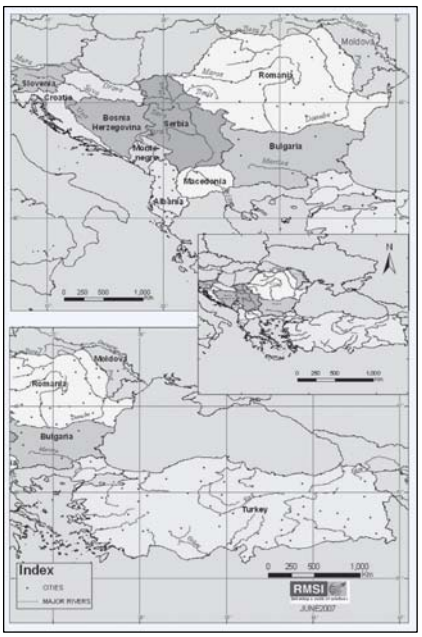

Fig.1 SSE countries [10]

In addition to the geophysical, social and political settings of the region, other reasons exist for the aggravated transboundary disaster risk. They include: the transition from centrally planned to market economics; historic national and regional conflicts; the creation of new nations; political tensions and war; rapid and unplanned land-use changes;

5.2 Risk Assessment

Aggregate country-level data from EM-DAT was used for the regional analysis. First, the occurrence of different hazards in each country was examined (**Table 1**). This gives an understanding of the common risks in the region. The disaster and disaster impact

indicators were ranked and a cumulative ranking computed, to understand the relative vulnerability of countries in the region. The country-wise hazard matrix shows that flood is a common hazard in all the countries in the region. Except for Moldova and Slovenia, all the countries in the region have recorded seven or more hazards. The country-wise hazard matrix shows that flood is a common hazard in all the countries in the region. Except for Moldova and Slovenia, all the countries in the region have recorded seven or more hazards.

Tabel 1 Country-wise hazard matrix, [1]

Country	Hazards								
	Earth-quake	Flood	Land Slides	Drought	Extreme Tempe-rature	Wind-storm	Wild-fire	Epi-demic	Tehno-logical
Albania	●	●	●	●	●	●		●	●
Bosnia-Hertegovina		●	●	●		●	●	●	●
Bulgaria	●	●		●	●	●	●		●
Croatia	●	●		●	●	●	●	●	●
Republic of Macedonia		●		●	●	●	●	●	●
Moldova		●		●	●	●		●	●
Romania	●	●	●	●	●	●		●	●
Serbia	●	●			●	●	●	●	●
Montenegro	●	●			●	●	●	●	●
Slovenia	●	●			●			●	●
Turkey	●	●	●		●	●	●	●	●

This matrix doesn't capture the severity of events in each country. For this, both annual average disaster events and the annual average of disaster impact variables (number of deaths, number of victims and economic loss) were calculated [1]. To assess the relative vulnerability and risks in the region, these variables were ranked, and a cumulative ranking was used to assess the vulnerability levels of the countries. For disaster ranking, hazards were grouped into earthquake, flood-related, drought-related, windstorm and technological hazards (**Table 2**).

Table 2 Disaster and disaster impact ranking, [1]

Country	Disaster ranking	Diasaster impact ranking	Cumulative rank
Albania	10	5	9
Bosnia-Hertegovina	3	6	5
Bulgaria	5	8	7
Croatia	9	5	8
Republic of Macedonia	4	4	4
Moldova	8	3	6
Romania	2	2	2
Serbia	7	5	3
Montenegro	7	5	3
Slovenia	6	7	10
Turkey	1	1	1

Turkey has the highest risk, both in terms of hazards and vulnerability, and Romania is in the second position. In geographic area, Turkey is almost as large as all the other countries put together. The large size of the nation contributes to the fact that Turkey had the highest number of hazards.

Annual average events show that almost one earthquake event occurs every year in Turkey, and one event occurs every eight years in Romania and Bulgaria. An average of one flood and related hazard occurs every year in Romania, while in Turkey, Serbia and Montenegro, one flood occurs every two years. Except Slovenia, all the countries experience a flood almost every six years. Highest economic losses are reported in Turkey and Albania. Average annual economic losses from all disasters in Romania are USD 150 million [11].

Earthquake

The SEE region is one of the major seismically active zones in Europe. Both the Mediterranean-Transasian seismic belt in the Balkan region and the Vrancea seismic belt extend beyond any one single country.

Turkey is one of the most seismically active regions in the world, suffering from frequent and devastating earthquakes, such as the 1999 Marmara earthquake. Seventy percent of the country's population lives in areas that are highly vulnerable to earthquake. Bucharest, Romania is one of the world's 10 most vulnerable cities to earthquakes [11]. Descriptions of some of the major damaging earthquake events recorded in the region are provided in **Fig 2.**

Flood and related hazards

90% of the area of SEE countries falls within transboundary river basins, including the Danube, Drin, Martisa/Evros, Neretva, Nestos, Sava, Struma/Strimon, Vardar/Axios and other river basins. These transboundary rivers flow into the Adriatic, the Aegean, the Ionian and the Black Seas. More than half of the transboundary basins are shared by three or more riparian states. Shared lake basins include Doiran, Ohrid, Prespa and Shkoder.

The Mediterranean-Transasian fault zone passes through the Balkans, and the mountainous terrain, poor land-use and river basin management practices, and deteriorating infrastructure have all increased vulnerability to floods and landslides [2].

All countries except Slovenia face high risk due to flood (**Table 3**). Flood has severely impacted Romania, Moldova, Bulgaria, Serbia and Montenegro. Romania is one of the most flood-prone countries in the region. In Bosnia and Herzegovina, the flood protection structures were destroyed during the war. The country used to have sufficient flood protection structure to protect 50 per cent of its flood prone area.

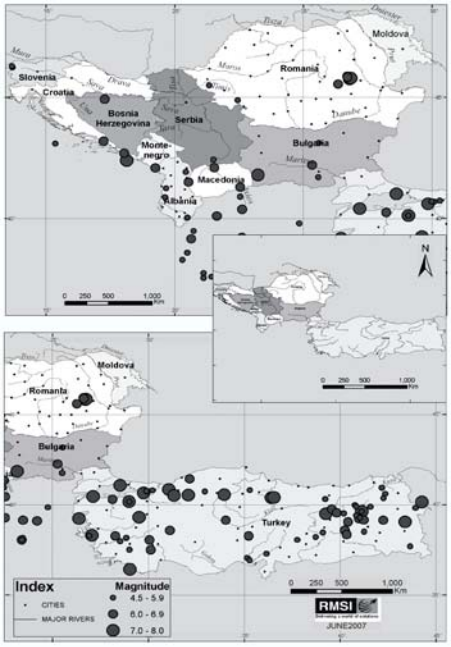

Fig 2. Some damaging earthquake reported in SEE region (1667-2006), [9]

According to [11], in Croatia, floods endanger more than 15% of the national inland territory. Flood protection systems are extremely complex and comprise a large number of structures that regulate and protect water.

The only city adequately defended from flooding is Zagreb, estimated to be safe from a 1,000-year flood event [11] Albania, Bosnia and Herzegovina, and Montenegro are highly

vulnerable to landslide. Landslide events have considerably increased in these countries lately due to unplanned land use, forest and mineral resource exploitation, heavy rains, and change of water and land regimes. In countries like Albania and Romania, landslides are often reported as associated hazards of flood and earthquake.

Table 3 Some Major floods in SEE countries, [1]

Country/Countries	Date	Number of deaths	Number of victims	Economic loss (mill USD)
Albania	Nov-1992	11	35.000	7
	Sept-1995	4		
	Dec-1997		8.000	
	Dec-2004		2.500	0.1
	Sept-2002		66884	17.5
	Nov-2005	3		
Bosnia-Hertegovina	April-2004		275.000	
	Jun-2001		9.000	
	Dec-2005		3.100	
	Mar-2004		3.000	
Bulgaria	Jul-2005	17		247
	Aug-2005	7	12.000	3.23
Romania	1926	1.000		
	May-1970	215	238.755	
	Jul-1975	60		1.000
	Jun-2006	30		
	Apr-2000		60.341	
	Jul-1991			
	Sept-2005		30.800	
	Mar-2006		16.477	
Serbia and Montenegro	Jul-1999	11	70.678	
	Nov-1992	1	6.000	
	Dec-2000		2.000	
	Jun-2002		2.400	
	Apr-2005	2	3.790	
	Feb-2006		1.200	
Turkey	May-1998		1.240.047	1,00
	Nov-1995		306.617	1,00

Drought and drought-related hazards are severe in many countries in SEE. Drought events are most frequent in Bosnia and Herzegovina. No deaths have been recorded due to drought in EM-DAT. But economic loss due to drought has been recorded in Albania, Bosnia and Herzegovina, Croatia, Macedonia and Romania. Albania, Croatia, Moldova and Serbia and Montenegro are highly vulnerable to extreme temperature. The number of deaths reported in these countries is relatively higher. Almost all countries in the region are prone to fire-related hazards, even though fire-related hazards are not recorded in EM-DAT in Albania and Slovenia [8].

Albania, Bosnia and Herzegovina, Bulgaria, Croatia and Moldova are highly vulnerable to *windstorm*. The 2000 windstorm in Croatia incurred a loss of USD 177.5 million, and the 2003 event caused a loss of USD 20 million. The November 2000 windstorm and frost in Moldova caused an economic loss of USD 20.8 million [12].

Technological hazards are highest among Serbia, Montenegro, Slovenia and Turkey. Turkey experiences the highest number, with an average of three events every year.

Technological hazards, including industrial accidents and transport accidents, are common in many countries in the region. With rapid industrial and economic expansion, many countries have experienced fast growth in industry and infrastructure development, contributing to an increase in technological hazards in the region. The region is vulnerable to risk from hazards related to handling hazardous materials and to chemical and nuclear plants. Deaths due to technological hazards have been recorded in Albania, Bosnia and Herzegovina, Bulgaria, Croatia, Romania, Serbia, Montenegro and Turkey. Transport-related hazards are in general higher than industrial accidents in these countries. Among all the countries, Romania has recorded the highest number of deaths. Even though the number of events is high in Turkey, the number of deaths recorded is relatively lower.

5.3 Vulnerability assessment

The vulnerability assessment of the SEE countries is based on the incidence rate of hazards, the annual average number of deaths and the exposed population. There is a dearth of data for hazard-specific exposed populations in all the countries, due to the unavailability of sub-national level data in organized formats. Some countries have statistics departments with sub-national level data, but it could not be accessed during this study. Therefore, regional vulnerability is analysed using data from the EM-DAT database, the National Geophysical Data Center website, and hazard/country-specific research papers [13].

Table 4 shows that, on average, one flood strikes Romania and Turkey every year, and the combined data on Serbia and Montenegro shows that one flood event occurs every two years in those two countries.

Table 4 Average annual incidence of major hazards and vulnerability of SEE countries, [1]

Country	**Annual average incidence of major hazards**					**Annual average number of deaths due to all hazards**	**Exposed population**		
	Drou-ght	Earth-quake	Flood	Wind-storm	Tehno-logy		Drou-ght	Earth-quake	Flood
Albania	0.12	0.09	0.24	0.06	0.06	7.82	NA	155,688	131,704
Bosnia-Hertegovina	0.17	x	0.28	0.11	0.17	3.72	71397	NA	NA
Bulgaria	0.21	0.15	0.27	0.15	0.15	6.64	325,406	NA	275,537
Croatia	0.28	0.06	0.22	0.06	0.17	8.61	NA	30,928	108,929
Macedonia	0.17	X	0.22	X	0.11	13.39	NA	NA	17,784
Moldova	0.09	0.09	0.22	0.09	X	1.83	279,603	18,909	193,262
Romania	0.45	0.12	1.03	0.24	0.48	82.42	347,229	1,007,506	1,174,894
Serbia and Montenegro	0.17	0.06	0.50	0.06	0.56	10.00	NA	NA	321,934
Slovenia	0.04	0.09	0.04	X	X	0.04	NA	30,984	NA
Turkey	0.30	0.97	1.06	0.21	3.00	941.36	NA	2,745,757	1,883,782

x – data not available for computation, NA – data not available in the website

Substantially large populations are exposed to earthquake in Albania, Croatia, Macedonia, Romania, Slovenia and Turkey, while in most countries, a large population is exposed to flood. Data on the population exposed to drought is available for a few countries like Bosnia and Herzegovina, Bulgaria, Moldova and Romania, which display substantially high levels of exposure. The exposed population data shows the countries' high vulnerability towards particular hazards; it is imperative that preparedness and prevention

measures should be a high priority. Drought, earthquake and flood in the region are transboundary in nature, a fact that emphasizes the need for transboundary cooperation and policy approaches [3].

Economic loss data available from different sources shows the countries' economic vulnerability to these hazards (**Table 5**). The economic loss data is compared with the country's GDP to understand the impact of the loss on the country's economy. In Turkey, the annual average economic loss is to the tune of 12% of the country's GDP, while for Romania it is 5%. Other countries like Bosnia and Herzegovina, Croatia, Macedonia, Moldova, Serbia and Montenegro also had substantial losses. The economic loss data complied from various sources, even though it is not complete, still shows an intense picture of loss in the region, with adverse impacts on the economy and on development of the countries.

Table 5 Economic loss in comparison to GDP in SEE countries, [1]

Country	Period taken for average	GDP per Capita 2005	Annual average economic loss due to all hazards (mill. USD)	% of GDP	Economic loss (mill. USD)			
					Drou-ght	Earth-quake	Flood	Tropical cyclone
Albania	1974 -2006	2755.3	68.67	2.49	2238	2 to 5	24.673	0
Bosnia-Hertegovina	1989 -2006	2384.0	22.94	0.96	408	>5	0	0
Bulgaria	1974 -2006	4733.9	14.76	0.31	0	5	260.23	0
Croatia	1989 -2006	6376.2	33.76	0.53	330	>5	0	0
Macedonia	1989 -2006	4467.7	24.59	2.13	0	5	353.6	0
Moldova	1984 -2006	2876.1	61.40	4.92	0	0	152.584	31.6
Romania	1974 -2006	5954.9	292.76	1.66	500	2756	3269.3	0
Serbia and Montenegro	1989 -2006	4936.0	82.0	0.05		2705	0	0
Slovenia	1984 -2006	13611.4	7.31	11.98	0	10	5	0
Turkey	1974 -2006	4680.8	560.56		0	15988	2511	0

6. CONCLUSIONS

The SEE region is highly vulnerable to flood, earthquake, landslide, forest fire and technological hazards. Poor land-use management, lack of land-use planning codes and river basin management practices, and deteriorating flood regulation infrastructure have all increased vulnerability to floods and landslides. A lack of early warning systems has also increased vulnerability to floods.

Some of the countries in the region have prepared national disaster management plans; these need to be reviewed and, if required, updated on a priority basis. Albania has developed a disaster management plan with the support of UNDP, and the plan is considered to be a comprehensive one. There is a lack of coordination between central and local-level authorities in disaster management activities in many countries. Even though there are premier institutes working on disaster-related activities in many countries in the

region, there is a lack of institutional coordination among these countries between the government departments who are responsible for implementing disaster risk management. There is a lack of capacity and training in disaster risk management and policy implementation at the government level in many countries. Private sector participation in disaster reduction is also not adequate in the region.

Base on this study, for further work some recommendations can be done. The recommendations that can be provided will be structured and deduced based on the reports reviewed and on available country-level historic data on hazards and their impacts. Both reports and data have limitations. Some of the recommendations can be generic for model disaster management activity, but most will be specific to the region, taking into account the sites and situation factors of the countries in the region.

7. REFERENCES

[1] UNISDR. „South Eastern Europe Disaster Risk Mitigation and Adaptation Initiative. Risk Assessment for South Eastern Europe - Desk Study Review", United Nations, Global Facility for Disaster Reduction and Recovery, http://www.unisdr.org, Geneva, 2008.
[2] World Health Organization (WHO), Millennium Development Goals. Available: http://www.undp.ro/mdg/.
[3] E.N. Gurenko, W. Zakout, "Mitigating the Adverse Financial Effects of Natural Hazards on the Economies of South Eastern Europe - A Study of Disaster Risk Financing Options", The World Bank, Sustainable Development Department Europe and Central Asia Region and UN/ISDR secretariat Europe, South Eastern Europe Disaster Risk Mitigation and Adaptation Programme, February 2008.
[4] UNDP (2004). A Global Report on Reducing Disaster Risk: A Challenge For Development, United Nations Development Programme, Bureau for Crisis Prevention and Recovery www.undp.org/bcpr
[5] International Federation of Red Cross and Red Crescent Societies, „World Disaster Report 2009 - Focus on early warning, early action", Available: http://www.ifrc.org
[6] EM-DAT Emergency Disaster Database. Available: http://www.emdat.be/
[7] UNEP,Available: http://www.nat-hazards-earth-syst-sci.net/9/1149/2009/nhess-9-1149-2009.html
[8] Natural Disaster Hotspots.Available: http://geohotspots.worldbank.org
[9] National Geophysical Data Center (NGDC). Available: http://www.ngdc.noaa.gov/
[10] Inter-American Development Bank (2005). „Indicators of Disaster Risk and Risk Management", Summary Report for World Conference on Disaster Reduction, Colombia.
[11] C. Pusch, „Preventable Losses: Saving Lives and Property Through Hazard Risk Management, A Comprehensive Risk Management Framework for Europe and Central Asia", Disaster Risk Management Working paper series 9, The World Bank, Washington, D.C., October 2004.
[12] UN/ISDR (2004). "Living with Risk: A Global Review of Disaster Reduction Initiatives", Inter-Agency Secretariat of the International Strategy for Disaster Reduction (UN/ISDR), United Nations, 2004, vols. I, II, and Annex.
[13] Guha-Sapir, D., Hargitt, P. H., „Thirty Years of Natural Disasters, 1974-2003: The Numbers", Centre for Research on the Epidemiology of Disasters, Brussels, 2004
[14] C. Filip, „Risk Assessment models for Natural Hazard as a Decision-Support Tool of Mitigation Strategy in Disaster Management", Management in the Worldwide Contemporary Challenges, ICMIE 2009, Politehnica University of Bucharest, 2009

Water management using falajs (man-made streams)

Ahmed A. Murad

Abstract **– The Al Ain area is located in the southeastern part of the UAE and characterized by low rainfall and high evaporation rate, which limits the availability of water for different uses. Ancient people in Al Ain built falajs (man-made streams or water paths) to enhance water availability throughout the year. The arid climate of the region played a major role in reducing the quantity of water flowing in the falajs and deteriorating water quality. In addition, human activities such as urbanization have negatively affected the quality and quantity of falaj water. It is observed that the salinity in the water increases as it flows from recharge areas to discharge areas. Presently, falajs are facing serious problems that threaten their existence. Due to deterioration of groundwater and reduction of groundwater availability, desalinated water has been used to maintain falaj systems.**

Keywords **– Falaj water, Al Ain, management, agricultural activities.**

1. INTRODUCTION

The people of Arabia, particularly in Oman and the United Arab Emirates (UAE) have used falajs (or aflaj) since ancient times to distribute groundwater to houses and cultivated areas. A falaj is a man-made stream or water path that connects the groundwater at the foot of mountain slopes and transports it to the surface for irrigation and other uses. The Royal Decree No. 3/94 of Oman defines a falaj as a canal built either above or below the ground to collect water from underground springs or the baseflow of wadis (ephemeral streams occuring throughout Arabia) for distribution and use for many purposes (Fig. 1) [1]. The falaj system in Arabia has been used for more than 3000 years, and is equivalent to the Qanat system of Iran [2].

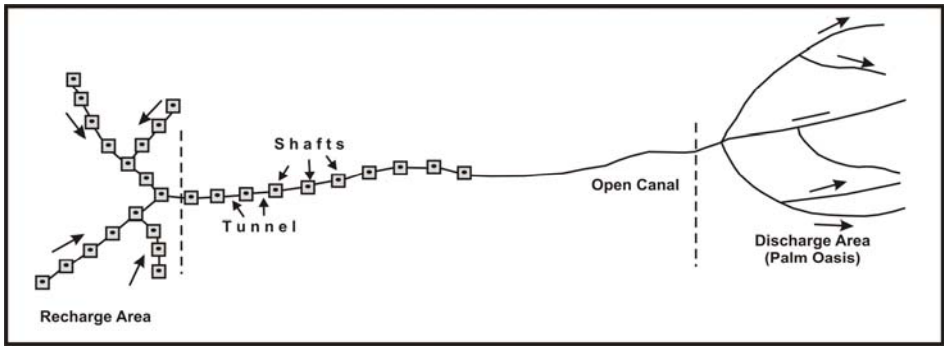

Fig. 1. Sketh showing the main parts of Falaj (Modified from [3], [4])

A. A. Murad is with UAE University, Department of Geology, P.O.Box: 17551, Al-Ain, United Arab Emirates (phone: +971-3-7134224; fax: +971-3-7671291; e-mail: ahmed.murad@uaeu.ac.ae).

ISSN-1584-5990

The maintenance of falajs is a responsibility shared by all persons belonging to a community. This, in addition to water-sharing activities, promote social harmony. **Using the falaj system for water distribution is a method of reducing water consumption through optimal use of water resources, including the control of groundwater pumping.** Most falajs in the region of Arabia are fully owned by farmers, while some are owned fully or partially by the relevant government. Each community is allocated some percentage of the falaj water [5]. In the UAE, all falajs are government owned.

Falaj systems have become a tradition, a continuing link to the history of the country. In the UAE, agriculture is considered as the most important use of land. Al Ain oasis, which is located 160 km east of Abu Dhabi, is mainly dependent on agricultural practices, which require large amounts of water to sustain them. The falaj is considered a conventional water resource. Traditionally, falaj systems have been a source of water for food production and income for farmers in the oasis.

Al Ain receives fresh water supply from the Northern Oman Mountains located in the east. Groundwater has been intensively used in the Al Ain area to irrigate date palms, which are the most abundant trees in the oasis. The harsh conditions coupled with heavy groundwater extraction have limited the functioning of the falaj system, in turn limiting the availability of water. The ancient people of Al Ain constructed the falajs to manage the limited water sources and to control water supply during drought periods.

Use of the falaj system is based on prioritization. Domestic supply has highest priority, with supply to permanently cultivated areas having secondary priority. Most falajs carry water for drinking, and the remaining water is conveyed to mosques, public baths, and finally to areas of washing [6]. Such management helps farmers save water for emergency purposes and to control water use during dry periods [7].

In the past, falaj water was utilized for all the abovementioned purposes, but currently it is mainly used for irrigation [4]. Three types of falajs are present in the Al Ain area: Ghaily, Daudi, and Al Aini (or Hadouri) [8]. All types are similar in their administration and management, but they have different sources of water [9]. The water of an Al Ghaily falaj comes from the baseflow of a wadi, a Daudi falaj receives water from a mother well, and a natural spring feeds Al Aini falajs. The Al Aini and Ghaily falajs are older than the Daudi falaj. The Daudi falaj is similar to the Qanat system of Iran [10].

This paper aims to assess the falaj system in the Al Ain area as a management tool for conserving water for agricultural activities. Also the challenges related to falaj water in the area are addressed.

2. PHYSICAL SETTING

Al Ain is the main city of the Emirate of Abu Dhabi and is located in its eastern region, about 160 km east of the city of Abu Dhabi (Fig. 2). Al Ain has an arid climate characterized by low rainfall and high evaporation rate.

The rainfall in Al Ain is scarce, and geographically and temporally irregular. In general, about 90% of the annual rainfall in the UAE occurs during winter, with about 60% of the rain falling during February and March [11]. The annual rainfall in Al Ain varies between 7.8 mm (in 1994) and 243.4 mm (in 1972) (Fig. 3) [12]. Surface water is absent or minimal and only some wadis carry runoff water for short periods during rare and intense rainstorms.

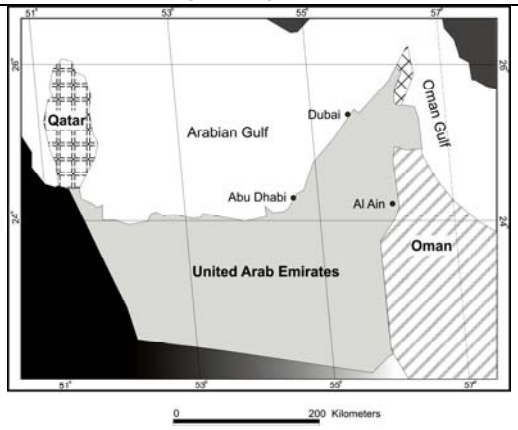

Fig. 2. Map showing the location of Al Ain

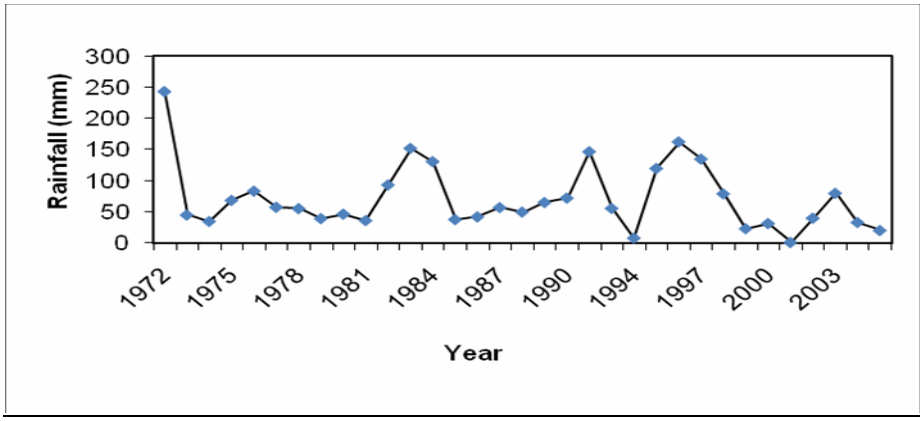

Fig. 3. Average annual rainfall in Al Ain area from 1972-2005 [12].

3. FALAJ WATER ASSESSMENT AND MANAGEMENT

Many falajs were built by ancient people in the Al Ain area to support agricultural activities, of which 24 falajs are documented [8], [2], [13]. The falajs in Al Ain and, more widely, in the UAE are confined to mountainous areas and gravel plains (Fig. 4). These sites were an intelligent choice for falaj construction because the mountainous areas are the main recharge areas. Noticably, agricultural activity and residential areas are concentrated in the west of the Al Ain area, near a recharge area. The direction of the Al Hili falaj is from the northeast to the southwest, while the Daudi falaj flows from the southeast to the northwest (Fig. 4). The Ain Sukhnah falaj runs from the south to the north, while the Maziad falaj goes from the north to the south.

The width, active area, depth, and length of Al Ain falajs are presented in Table 1. The width of these falajs varies from 0.65 m for the Al Hili falaj to 1.2 m for the Ain Sukhnah falaj. The active area (product of width and length) of the falajs differs from 1,500 m^2 for the Maziad falaj to 9,000 m^2 for the Buraimi falaj [8], [14]. The length ranges from 2,000 m for the Maziad falaj to 15,000 m for the Al Aini and Al Saroj falajs. As the width, ,active area and lenght of these falajs increase, the transit time (time taken for the falaj water to travel from recharge point to discharge point) increases (Fig. 5).

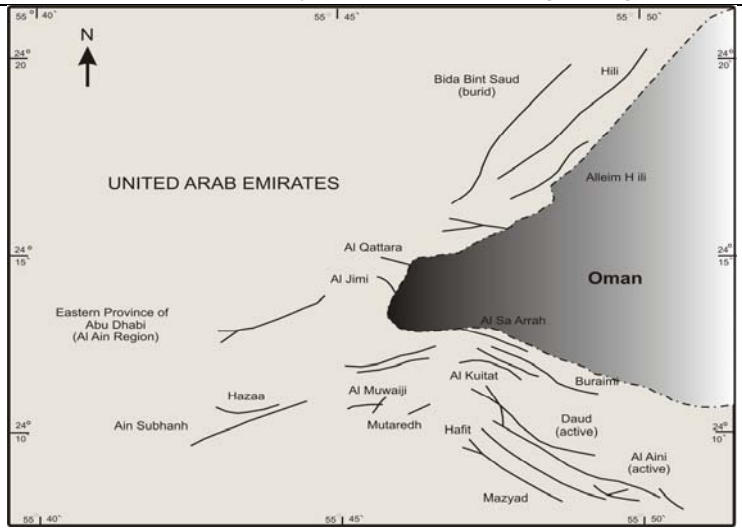

Fig. 4. Location map of major falajs in Al Ain area [8], [3].

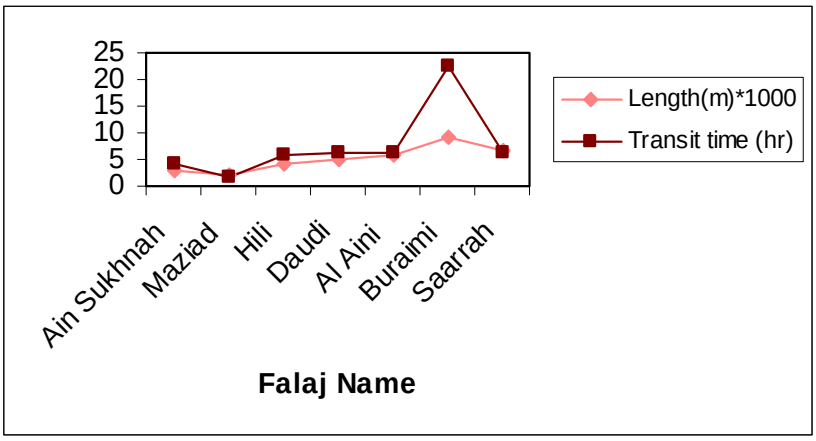

Fig. 5. The relationship between the length and transient time for some falajs in the Al Ain area.

Table 1. Physical properties of selected falajs in the Al Ain area [18[], [14].

Falaj Name	Width (m)	Active Area (m^2)	Depth (m)	Length (m)	Status
Ain Sukhnah	1.2	3600	-----	3000	-----
Al Hili	0.65	2600	30	10000	Supported by wells for irrigation
Al Aini or Al Saroj	0.80	4800	20	15000	Supported by wells for irrigation
Al Daudi	0.80	4000	20	7000	Supported by 87 wells for irrigation
Buraimi	1	9000	-----	9000	-----
Maziad	0.75	1500	24	2000	Supported by wells for irrigation

Sarrah	0.95	6175	-----	6500	-----

Water quality in the falajs is an important concern for the people in the Al Ain area because they constitute the main source of water for drinking and domestic uses. A previous study [8] showed that the electrical conductivity of water in the Ain Sukhanah falaj was 10,940 μS/cm (Fig. 6). The high salinity of this falaj might be attributed to the effect of the evaporite deposits in the Miocene Formation of Jabal Hafit and the dissolution of limestone, which contains some amount of gypsum. This study also indicated that the calcium (Ca^{2+}), sodium (Na^{+}), magnesium (Mg^{2+}), chloride (Cl^{-}), and sulfate (SO_4^{2-}) concentrations were high in the Ain Sukhanah falaj. It is clear that the water of the Ain Sukhanah falaj is of a lower quality than that of other falajs in the Al Ain area, and this might be related to the location of this falaj, being near Jabal Hafit, which, as mentioned, may have a significant impact on the water quality. Also, it has been found that falaj length has a significant impact on the salinity of the falaj water.

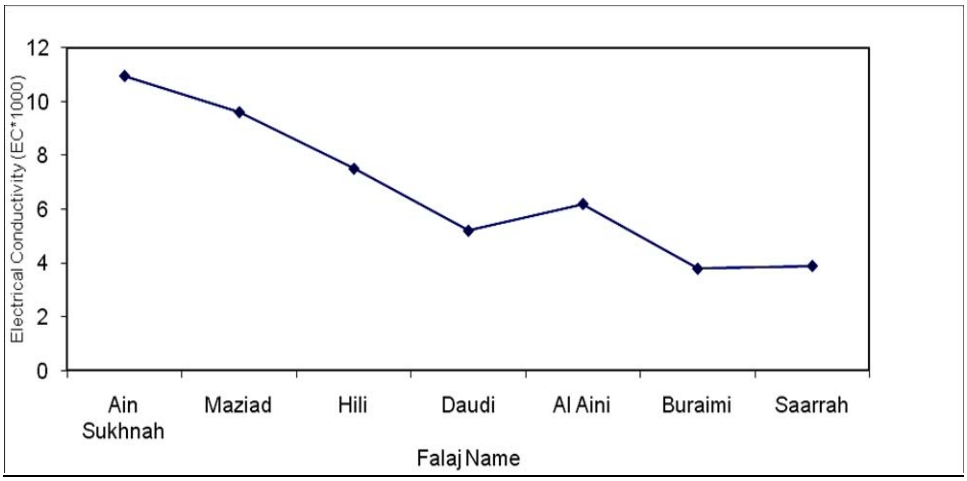

Fig. 6. Electrical conductivity (EC) for selected falajs of Al Ain area (Source of the Data: [8]).

The temperature of water collected from the extraction shafts of the falajs ranged from 32.7°C to 35.7°C. This temperature variation may be related to variation in the depth of the shafts. Total dissolved solids (TDS) in the water of the Al Aini falaj ranged from 268 mg/l to 914 mg/l, whereas TDS for the Al Daudi falaj ranged from 215 mg/l to 348 mg/l. It is clear that TDS of water in both falajs increases as water moves from the mother wells to the discharge area (Fig. 7). This is due to the fact that the location of the recharge area affects water quality. The salinity of the falaj water increases as water moves from the recharge area (mother well) and flows to the discharge area (sharaih), the location of oases or intense agricultural activities.

The falaj systems in Al Ain are presently facing serious threats, one of which is the reduction in water quantity and worsening water quality due to extensive pumping of groundwater for agricultural and other activities. Continuous pumping also increases the salinity of the water because of imbalance between recharge and discharge. Beside the reduction of quality, the quantity of water is also being reduced dramatically. This affects the runoff in the channel of these falajs. Many falajs have gone dry due to low rainfall coupled with excessive groundwater pumping. At the time of writing, about 50% of major

falajs in the area had gone dry, while 12.5% had been abandoned, and 37.5% are now supported by other wells in order to enhance the discharge of falajs (Fig. 8).

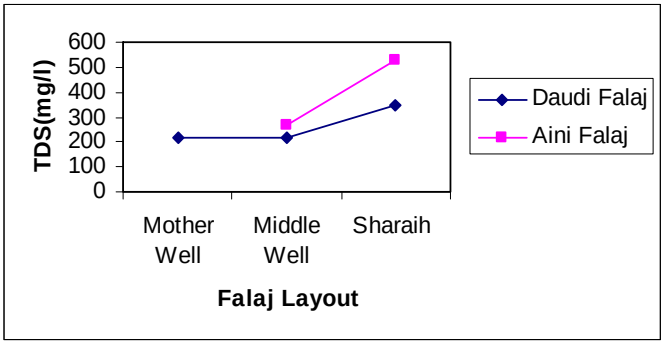

Fig. 7. Total Dissolved Solids (TDS) for water falaj collected from the mother well, middle well and sharaih for both Al Daudi and Al Aini falajs.

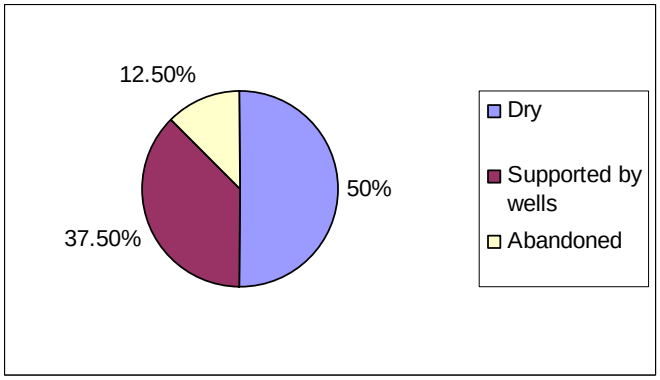

Fig. 8. The current situation of falajes in Al Ain area.

During the last few decades, many farmers have abandoned their farms to look for other jobs that provide higher income. As a consequence, the task of maintaining the falaj systems have been left to immigrants, who do not have sufficient knowledge about them. Other farmers have replaced the falaj system with new methods of water supply. **These new methods include electrical and diesel pumps to irrigate agricultural areas. In addition, drip irrigation techniques have been introduced in the area and are intensively used by farmers as a means to cope with water shortages. Presently, the distribution of water from groundwater wells is predominantly through plastic and steel pipes instead of open channels of falaj systems.** Another threat to falaj systems in the area is urbanization and development. Building and development in the area has led to a reduction in the area used for agriculture and is expected to cause chemical contamination of falaj water. Knowledge on building and maintaining falajs is limited to the elderly.

Water management is an essential tool in increasing the efficiency of water use, and conservation of the falaj system is essential in preserving the heritage of the area. Falaj systems supply water during drought periods and even for emergency purposes. Al Ain Municipality, which manages the area's falajs, conducts periodic maintainance because they are monuments of the tradition and history of the area, and not only help preserve the culture but also serve as tourists attractions. Maintenance of the falaj system involves

removing the accumulated sediments and silt from the channel; this helps reduce the travel time of the water from the mother well to the discharge area. In addition, such transporting of the water via falajs to cultivated areas is a management practice that saves water and distributes it wisely. Raising awareness of and educating the population about the importance of falaj systems would help transfer knowledge and skills of falaj construction and maintenance to future generations. The Ministry of Education could prepare awareness programs with emphasis on the value of falajs systems.

As the quality of the groundwater in the Al Ain area, which is the main source of water flowing in the falajs, is deteriorating currently, water from mother wells is being mixed with desalinated water in order to maintain required falaj discharge rates and improve water quality. Water mixing occurs after the groundwater leaves the mother well. One of the management strategies of the falaj system in the Al Ain area is to use a supporting well to maintain the regular discharge of falaj water to cultivated areas. This method is being employed by the Al Ain Municipality.

4. CONCLUSIONS

The falajs in the Al Ain area offer a means of **using groundwater efficiently and protecing it for future use through professional water distriubtion to irrigated areas.** Traditionally, falaj water was important for all people because it was used for domestic, agricultural, and industrial activities. The arid environment of the UAE has caused the quality and quantity of water of the falaj to reduce dramatically. Human activities have also had a significant impact on deterioration of the quality and reduction of the quantity of falaj water. The amount of local rainfall, which is the main source of water for the mother wells of the falajs, is very low. This affects the discharge and flow of falaj water to the Al Ain oasis. In addition, urbanization occuring near the falajs has negative impacts on the quality of falaj water. Increasing salinity is observed as the water flows from the recharge area to the discharge area. Periodic maintenance and assessment of falajs is essential in order to preserve the falajs in the area.

5. REFERENCES

[1] Institute of Public Administration. Organization and management of falajs in Oman (in Arabic), 1997,Oman.

[2] W. Y. Al-Tikriti, "The origin of the falaj: further evidence from the United Arab Emirates"Papers on the Archaeology and History of Mesopotamia and Syria, presented to David Oates in Honour of his 75th Birthday. L. Al-Gailani Werr, J. Curtis, H. Martin, A. McMahon, J. Oates and J. Reade (Eds.), pp. 339-355, NABU Publications.

[3] H. S. Al-Nuaimi, "Hydrogeological and geophysical studies on Al Jaww Plain, Al Ain area, UAE", 2003, UAE University, Faculty of Graduate Studies, M.Sc in Water Resources, Master thesis.

[4] A. S. Alsharhan, Z. A. Rizk, A. E. M. Narin, D. W. Bakhit, and S. A. Al Hajari, S. A., Hydrogeology of an arid region: the Arabian Gulf and adjoining areas. Netherlands: Elsevier Science, 2001.

[5] INPIM (International Network on Participatory Irrigation Management). (2006, May 21). Afalaj irrigation systems [online]. Available: http://www.inpim.org/leftlinks/FAQ/Newsletters/N12/n12a9

[6] A. S. Al-Ghafri, W. R., Norman, T., Inoue, T. and Nagasawa. (1999). "Traditional irrigation scheduling in aflaj irrigation systems of Oman, Case study of Falaj Al-Hageer,

Northern Oman," [First International Symposium on Qanat, 1999, vol. IV, pp. 37-42, Ministry of Energy, Yazd, Iran, may 8-11].
[7] J. C.Wilkinson, Water and tribal settlement in southeast Arabia: a study of the aflaj of Oman. Oxford, Clarendon Press, 1977.
[8] Z. S. Rizk, "Falajes of United Arab Emirates: geological setting and hydrogeological characteristics," The Arabian Journal for Science and Engineering, 1998, vol. 23, no. 1C, pp. 3-25.
[9] A. S. Al-Ghafri, T., Inoue and T. Nagasawa, "The way of water distribution," [The XIV Memorial CIGR World Congress, 2000m November 28-December 1, Tsukuba, Japan, pp. 1128-1133].
[10] A. S. Al-Ghafri, " Omani Falajes," Nizwa Journal, 2005, no. 44, pp. 11-20 (in Arabic).
[11] Z. S. Rizk' "A Review article on water resources in the United Arab Emirates," unpublished.
[12] Ministry of Communication-Meteorological Department, Data for Rainfall of UAE. 2005, Abu Dhabi, United Arab Emirates.
[13] Al Ain Municipality & Agriculture Department, "Al-Ain Falajes & Oases," 2004, Department of Prevention and Laboratories, Public Garden Administration.
[14] Environment Agency-Abu Dhabi (EAD), "The current status of Falajes in Al-Ain area, United Arab Emirates,", 2006 . Internal Report, (in Arabic).

New technologies for recovery and transformation of biogas. Case study.

Neculau Claudia, Thierry Nameche, Biali Gabriela

Abstract: **In this paper we will present shortly the techonology for the recovery and transformation of biogas in thermical and electrical energy.**

The case presented is about the landfill Anton, in Andenne, from Belgium.

We will analyse the need to apply this technology in this case, the parameters of installations, the analyses of the biogas outcome, the quantity of the thermical and electrical energy produced and the conclusions.

Keywords: **landfills, biogas, techonology, energy.**

1. INTRODUCTION

The problem of gases in the landfills

Household waste is composed of 50 to biodegradable organic matter 70%: green waste (damaged peelings, vegetables, meal leftovers etc), soiled paper, wood remains and other variable things related to the households. They start with being placed in discharges and burried under the following deposits their cycle of anaerobic biological breakdown: passing through a transformation under the action of numerous bacteria,resulting in mineral substances and gas. It's in fact the natural law of the recycling of the organic substances: in simple language is the decomposition of the alive cells and their handing-over into the natural circuit. It is said that the discharge is a bioreactor.

Biogas is thus the gas produced by the anaerobic digestion of the organic matters contained in waste. It is composed of methane (55%), carbonic gas (45%), the sulphur dioxide (H_2S), elements traces (sulphides, BTEX, COV). The elimination of biogas is a legal requirement. Several legal texts impose its recovery and its destruction (the Directive EEC of the 26/04/99, AGW of the 27/02/03, etc).

2. THE LOCATION OF RESEARCHES: LANDFILL ANTON, IN ANDENNE, BELGIUM

2.1. Presentation of the site: location, surface.

Located in the province of Namur, the landfill of Anton is on the commune of Andenne, Bonneville section, in the South of the national road N°90 connecting Huy to Namur. The site has a total surface area of 13.9 ha (5 ha for the landfill). The site occupies the excavations of an old calcareous career, installed with hillside, in overhang of the Meuse.

The landfill has been exploited since 1981 to receive waste from the town of Andenne and sludge from dredging resulting from the construction of a bridge stopping on the Meuse. From July 1983, its use intensified, because the landfill underwent an extension of the area of stocking and there was the permission to put household refuse of other origins there, so far as they are not of the nature of toxic waste. Several rather strict conditions

Neculau Claudia, ,SPAQUE SA ,Boulevard d'Avroy, 38/4,4000 Liège, Belgium,
Thierry Nameche, SPAQUE SA ,Boulevard d'Avroy, 38/4,4000 Liège, Belgium
Biali Gabriela,Technical University "Gheorghe Asachi" of Iasi, Romania Faculty of Hydrotechnics, Geodesy and Environment Engineering, Technical University of Iasi

ISSN-1584-5990

accompanied this authorization, in particular the obligation to pose an adequate sealing on the bottom and the side walls of the landfill. None of them appears to be respected.

Waste, main source of the agglomeration of Brussels, was poured at the level of the rock, without any special precaution. At the end of the lifetime, the landfill was simply covered with a layer of muddy and stony, non impermeable ground and of less than one meter thickness.

Since 1991, the Minister of Environment of the Walloon Region elected the SPAQuE Company in order to evaluate the site and to take the emergency measures which were essential. The first rehabilitation works began in 1993.

They were focused, in a first phase, on the management of the solid mass of waste, and that as well for reasons of stability of the slopes, and to manage the significant production of biogas. The first building site consisted of the installation of a capping in argillaceous silt, of a network of 5 air collectors, connected to 21 deep wells and several surface drains, drilled in the mass of waste.

In 1999, a device of cogeneration was installed in order to produce nearly 470 kW of electricity, while providing at least for part of the needs for heat for the 400 pensioners for the institute Saint-Lambert.

The implementation of a cogeneration on the biogas of landfill Anton constituted a first in the field in Walloon Region.

In 2000 and 2001, the rehabilitation works of water became full extensive with the installation of the waste water treatment plant at the bottom of the cliffs, edge of the black pond and the setting according to purification in the current of 2001.

Fig. 1 – Landfill Anton, in Andenne, Belgium

However, the percolation of the lixiviats in the fissured solid mass of lime stones does not allow its total recovery. The means of management implemented in this respect are multiple and complementary, namely:

- a systematic pumping of the lixiviats present in shaft bottom of degasification;
- recovery by drainage of the seepages on the face of exploitation;
- the startup in 2001 of a waste water treatment plant of the collected lixiviats and a mobile treatment unit of water of the black pond;
- the pond being completely emptied, the recovery and the treatment of the weak arrivals of lixiviats, in general very diluted, from now on are ensured by a module more adapted to the small quantities to treat.

The rehabilitated site is composed of a “high” part corresponding to the top of the career and of a “low” part, located at the level of the Meuse. It is in the high part of the site that the main part of the installations of SPAQuE is settled (office, network of degasification, installations of cogeneration). The grounds are turned and maintained. On the slopes of the discharge giving on the slope of the Meuse we found shrubby vegetation.

In the low part, below a cliff of almost 30 meters in height, there was a pond of 0.6 ha surface and a capacity of 50.000 m³.

In figure 1 is presented a photography air of the landfill Anton. In the left part you can see the installations of the SPAQuE company: offices, containers, etc.

2.1. Major gases and minor gases of landfills

A) Produced quantities of gas

On average each m^3 of household waste produces 200 m^3 of major gas but that is done during one long period which will depend on the conditions (MO content, moisture, volume of waste, pH, temperature, pressure, water content, type of management: covering, liming, etc) reigning in the landfill: in general from 10 to 30 years.

The figure no. 2 gives an idea of the evolution of the aggregate output of a domestic landfill named Anton.

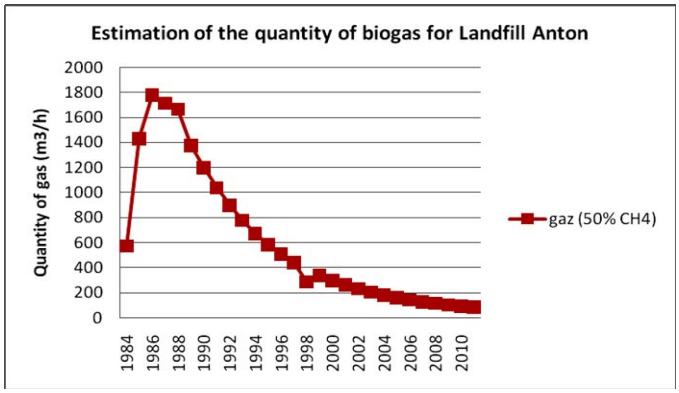

Fig. 2 – Estimation of the production of biogas for the landfill of Anton

The shape of the curve is completely characteristic and it is found for the majority of the discharges with old management.

We will noted that a landfill of 1 million m^3 will give during its degradation 200 million m^3 of normal gases; one Ha of landfill on 20 m of thickness of waste (average situation) will give 40 million m^3 of gas during the 20 years which will last its complete biological breakdown.

B) Propagation of landfills 'gases

In theory and under the action of the pressure that they generate from their production in the landfills, the gases follow the way of less resistance towards the free air by possibly cutting through a path in the mass of waste. It is in general the case of a traditional landfill without particular device: the gases migrate towards surface and it is by there that they escape himself by forming longitudinal cracks. So each time an awkward treatment of surface, or a sealed off thickness surfaces, or if a too great thickness of waste block the passage towards it, the gases will migrate laterally and spread into the neighboring grounds. If they meet channels of less resistance in the ground such as for example of the pipings deposited in sand or old galleries they can follow them on long distances and emerge very far from the landfill. A traditional case is their migration towards a bordering cellar while following conduits of water deposited in stones like it is often the case. The side migrations can also cause extensive damage with the cultures by the phenomenon of asphyxiates roots.

C) Major gases

C1) Composition and concentrations of major gases:

- H_2S depends on the quantity on suffers which is present. One generally finds from 0,1 to 1%. It is characterized by a strong odor "rotted eggs";

- CO_2 is very abundant during the first weeks of the decomposition: nearly 70%.Quickly will decrease not to represent during the long stage of degradation of the discharge approximately 30%. Of course its disappearance corresponds at the end of the process;

- methane CH4 is in the first weeks with regularly increasing concentrations: 20 to 30%. It reaches then a stage located towards the 55% to arrive at 60 70%. It varies to some extent conversely with the CO_2 concentration;

- the emissions proceed in the air and we will find inevitably oxygen concentrations and nitrogenizes which do not come directly from the methane – genesis;

In short, the relative concentrations of major gases vary in time and are elsewhere a good manner to appreciate the age of the landfill.

C2) Danger of major gases

- H_2S in theory is a pollutant gas. Nevertheless it is so malodorous even in weak concentration that in reality it is rather beneficial by informing presence in a place of gas of discharge;

- CO_2. It is inert. Nevertheless in substituent with oxygenate of the air, it can in buildings closed to lead to asphyxiations. Another harmful effect is, it, enough attends: in the event of side propagation of gas of discharge (see higher) CO_2 can replace on the level of the roots of the plants the oxygenated air and bring their fast deterioration. It is an effect often observed in cultures being next to the landfills. One sees zones of plants feeble and yellowing delimiting plumes of underground expansion of gases;

- the CH_4 has the same effects as CO_2 in substituent with oxygenate air. But methane constitutes together with the oxygen a high combustion mixture (it is in fact the firedamp of the coal mines). For certain concentrations it constitutes even an explosive mixture. In reality there are necessary two more conditions so that explodes: that the gas is in a closed place and that it's there a spark or a flame produced lighting. It is for example the case of a cellar where gas of landfill is infiltrated and where an electric switch is pressed or in a pocket within the waste when the accumulation becomes too thick: it is careless to exceed 25 m of layer of waste.

In addition, the generally combustible character of the mixture can lead to fires of the landfills especially which will damage the protective systems (geomembranes) and will cause the incineration at low temperature of other waste. It is well-known that the poured materials which contain chlorine (for example green waste, PVC or papers) are leading to an extremely toxic formation of dioxane and also a very corrosive hydrochloric acid in case of inhalation for the pulmonary cells. These fires are very difficult to extinguish and in certain discharges they prevail quasi permanently.

D) Minor gases

They were always present in gases of landfills but weren't highlighted in an indisputable manner as by the work of Wood and Porter (JAPCA May 1987 volume 37 n05) which weren't possible until the extraordinary development during the Eighties of the gas traces. Analysis techniques.

D1) composition and concentrations of minor gases

The minor gases are organic compounds that we can classify in families: alkanes, olefinic hydrocarbons, halogenous cycloalcanes, cycloalcénes, aromatic, compounds, sulphur compounds, alcohols, esters, ethers and of the various compounds. Certain analyses

detect some close of a hundred of species: in general one proceeds by “screening” of about sixty principal compounds.

The analyses are extremely variable in time following the precise circumstances of landfills. The exact origin of minor gases is very difficult to establish being given the multiplicity and the complexity of the reactions in question: it is enough to know that it is act of the secondary products of reactions of the decompositions which take place under the action of the micro-organisms in the landfills with strong organic fraction. II is essential to apprehend that these gases exist always even if the contents are varying permanently.

D2) dangers and harmful effects due to minor gases. Most of the components of minor gases are dangerous substances and poisons. The case of benzene for instance, currently prohibited in much of industrial uses, (but present, alas, in the unleaded gas) is well-known: his carcinogenic action, a slow toxicity (contrary to the acute toxicity of CO for example who is more spectacular) is allowed now by all.

3. TREATMENT OF LANDFILLS ‘GASES.

3.1.Gases collection

Before being able to treat gases they should be collected as close as possible from their place of production. It is thus on the level of the landfill that it is necessary to install an effective system of collection. Let us note that in general the output of the collection, even in the best cases, seldom exceeds 60 to 70% what it’s explain by the diffuse character of their production within the mass of waste and the very heterogeneous character of the propagation of gases in a discharge.

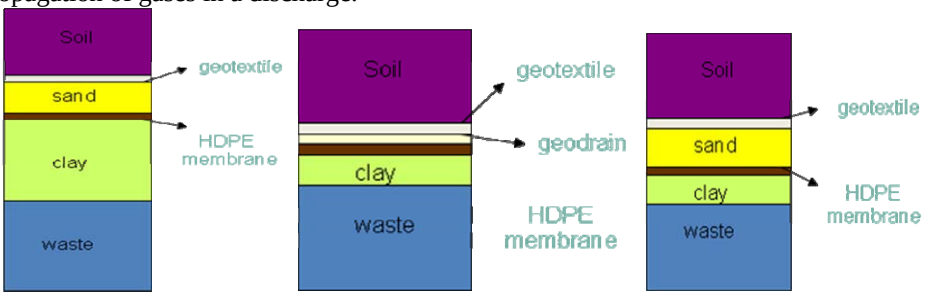

Fig. 3. Various alternatives to make a capping

One uses in general two collecting systems

- the network of surface. When the landfill is completed, each time that the cell is finished one poses on the surface a sandwich layer (see figure no. 3) intended to isolate the landfill from outside as well on the level of its effluents as of the elements which penetrate there normally (rainwater for example). This final layer (capping) comprises a network of drainage of gas located in lower part of the géomembrane in PEHD which is tight. This drain consists of channels of rollers in which one drowns tubes strainers (bored small holes) surrounded by felts. The whole system is connected to collecting tubes and by there to the device of treatment. A light depression is permanently maintained in the drains so as to aspire produced gases.

- the network of depth. It is necessary here to drill in the mass of waste of the wells (piezometers) strainers until the bottom of the deposit. Generally these piezometers are also used for taking away water sample. They are provided with a special head which collects gases and sends them through horizontal collectors located on the surface towards the treatment unit. One thus constitutes a grid of which more or less tight according to the output of collection that one wishes.

Fig. 4 – Example of wells drilling and degassing trenches

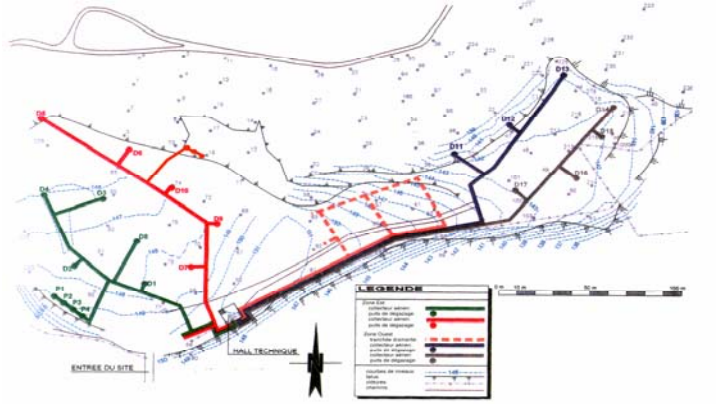

Fig. 5. Diagram of the network of degassification of the landfill Anton

In figure no. 5 it is shown the diagram of the network of degassification of the landfill Anton. It should be noted that the device could be assembled temporarily during the filling of a cell and "to go up" with waste: one then calls upon flexible tubes and piezometers with encasable elements with measurement of the advance of the embankment. You have to avoid the "aspired air". A form of sealing is created so that many gas the aspiration system taps. Thus it is not possible to collect "at free air".

3.2. Gases treatment

Incineration: generally it calls upon flares of the type we see used in oil installations. In figure no.6 you will find the diagram of a such burner. Initially this kind of pipe is satisfactory to the gripped end what ensured a certain combustion (at low temperature) of methane but left intact the question of indestructibles minor gases under these conditions.

To re-entry the flare it is placed a suction ventilator which creates the depression necessary. On the market flares exists from 100 to 2500 m3/hour of capacity of aspiration and gas incineration.

Fig 6 – Photo of a flare

Fixing the optimal temperature caused some controversies currently sliced in favour of 1200°C minimum for 0,3 seconds.

The reason of this choice is that it is required this temperature to ensure 100% destruction of minor gases, so their complete transformation into elementary molecules (H2O, CO2, N_{ox}) is fulfilled. The contrary case is: the organic molecules break up into other molecules complexes sometimes more dangerous as the ones of departure. There are also cases of recombination which form at the exit of the flare destroyed gases. To ensure that all occurs well it is necessary to carry out analyses "torch out".

A certain tendency marks elsewhere to replace the flares by installations for incineration more complete in particular involving a stage of capture for the acids.

Energy recovery. The gases of landfill contain very large quantities of energy that we could recover.

Among the modes of exploitation of biogas we can underline:

- production of warm water or vapor (boiler) - output of 90%;
- production of hot air (burner in vein of air);
- production of electricity using engines and the gas turbines - electric output between 30% and 40%;
- the cogeneration: electrical production to be sold on network (electric output between 30% and 40%) and production of heat (thermal efficiency 50 to 55%) for heating of the digester and other thermal valorizations - production of warm water, heating of buildings, drying, hygienisation, sterilization,…). (170KWh electric + 340 kWh thermal per ton of waste mechanized);
- Production of fuel (purification, compression, storage) used by the vehicles GNV (natural gas vehicles), which run on compressed methane;
- Injection in a gas distribution network (purification, compression).

One m^3 of gas produced 6 kWh is 0.6 liter of fuel.

Biogas has a natural energy in a native, potential state from 5 to 6 KWh/Nm^3. Its exploitation makes possible the saving of fossil energy sources and to reduce the gas emissions to greenhouse effect and to benefit from a renewable energy source which, without that would be lost in the free air.

Among these processes, the cogeneration is the only means of obtaining a total output of 85% if all produced heat is used. One also notes the profit increased on the production of CO_2.

4. RESULTS AND DISCUSSION

4.2. Estimation of the quantity of produced biogas

For the period September 1997-September 1998 the volume of biogas collected and incinerated in the flare with 1200°C reaches 3.555.779 Nm^3 in 8554 operating hours on 8700 hours a theoretical total.

The average volume output for the period of operation was of 415.68 Nm^3/h (405.91 Nm^3/h if we report flow to the theoretical duration of operation).

In terms of valorization, with an index of 97.64% and one biogas with 40% of CH_4 on average, the average annual methane flow available reached 166.27Nm^3 /h.

Based on this year of operation of the network of degasification, an evaluation was carried out. (fig. 7) of the methane potential available for the ten next years.

For reference, the quantity forecast out of methane is indicated by its content of energy in kilowatt (kW) in the following figure (fig 8).

In July 1997, the capacity of collection of each of the five collectors was successively tested also with a setting in depression ranging between 100 and 135 mbar, hang fifteen

minutes. Under the conditions of test, collected total volume reached 850N^3 /h instantaneous production.

On the basis of one year of operation of the flare, and after setting in balance of the network of degasification, the output at the end of the year 1997 is around 450 Nm^3/h, that is to say a volume higher than 10.000 Nm^3/day, with a high content in methane of approximately 40%.

Starting from a mathematical model, a modeling of the production of the biogas of the old landfill of Anton was carried out. The maximum of production was reached during the first 5 years of the landfill with a few 60 million m^3 of biogas.

In 1997, the quantity of biogas which will be to recover during the ten years following was estimated at 18 million m3, and to recover during the 10 years which follow, even more than 5 million m^3.

In 2023 the landfill should still produce more than 30m3/h with methane 40% against 450 m^3/h produced in 1997.

This justifies management with long term for this type of rehabilitation.

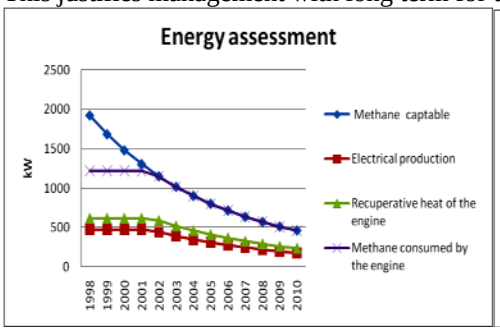

Fig. 7 – Estimation of quantity of biogas for Landfill Anton

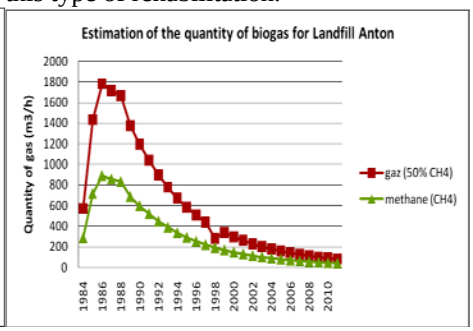

Fig. 8 – Energy assessment

On the basis of these estimates, the possibility of installing on the site a power station of electrical production and of heat by the valorization of the biogas of the landfill and an electric station of transfer to the network became real.

In 1998 was made an analysis for the supply, the installation, the startup and the maintenance of an engine running on the biogas of landfill coupled to an alternator (generator), of a power of 470 kW electrical, as well as cabin high voltage connected to the public network of electricity.

4.2. Installations for collecting and elimination of biogas - network of degasification and flares

In 1997 on the site were installed and made operational a network of degasification made up of 5 air collectors to which were connected 17 wells of degasification (Ø 1.00 m) established in the mass of waste on an average height of 26 m, a network of surface drains located in a zone with low thickness of waste (5 to 8 m), 4 microphone-wells of biogas recovery.

The existing flare of 250m3/h (installation in urgency in 1993) was replaced by a flare of 500m3/h with biogas 50% methane, corresponding to a thermal potential energy of 2.500 kW (1200°C during one minimum duration of 0.3 dryness).

In figure 5 (see chapter 3.1) the network of degasification of the discharge of Anton is represented.

4.3. Installations of recovery and valorization of biogas installed on the landfill Anton

With a methane concentration (CH4) higher than 40%, the volume recovered in 1998, requested a moment for decision-making of valorization of biogas, corresponded to more methane then 180Nm3/h, that is let's say more than 4.000 Nm3 per day. The LCV (lower caloric value) of the methane being of 35.900 kjoules per m3, either 8.577 kcal, the calorific value of the biogas recovered on the site of Anton reached close to 1800kWh, or the equivalent of 450kW electric (engine) to 600 kw electric (turbine) per hour.

It is on this basis that the technical concept,economic conditions and financial of the project of valorization of biogas were studied.

The unit aiming to treat/develop biogas is composed of a flare, a boiler in order to provide heat to the Institute Saint-Lambert and of a motor (see the figure no. 9 for the general principle of operation). These installations are annually controlled in order to make sure that the adopted standards of rejection are respected strictly (HCl, CO, SO_2 and Nox). The gas motor comprises an engine running on the biogas of landfill coupled to an alternator (generator) of a power of 470kW electric, as well as cabin with high voltage connected to the public network of electricity. In the following figure you can see the container of the gas motor which is on the site of Anton.

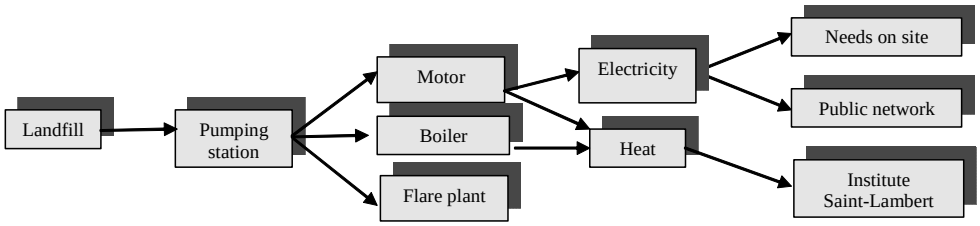

Fig. 9 – General principle of operation

The characteristics of the gas motor are: it is a Deutz MWM TBG616 motor , with 12 cylinders out of V and a supplying turbo compressed with exchanger. The thermal power is of 616 KW and the electric output of 470 KW. The total output is higher than 83%. Type of the alternator is STAMFORD 400 V.

The installation of heat supply comprises:

- a central boiler room, located in a metal container in the vicinity immediate of the Gas Motor container, which is intended to develop thermal recoveries available in the water and smoke of this one (see in the figure no. 11 a photo of the gas engine). It includes, in addition to the piping necessary to these recoveries, a composite boiler thermal biogases/light fuel of 600kW approximately intended for the emergency power supply of the Institute at the time of the breakdowns or of maintenance of the gas motor or the network of biogas as well as the two motor bike-circulators groups of warm water (2x100%). The fuel supply of the boiler will be carried out by means of a storage tank for 5 days of production of heat.

- a network of buried pipings crossing the road and the ground of the Institute and being used for the transport of heat towards the boiler rooms of the various houses, of a 2km length. This piping of the type isolated is prefabricated. The houses to be taken into account are 7. The boiler rooms of these houses must be adapted according to an identical principle each time: insertion of the plate heat exchangers in the return circuit of the water of heating (2 exchangers of 480kW and 6 of 264 kW), this allowing a pre-heating of this water before its passage in the boiler. The circuits of heating and medical warm water were

coupled both on the boiler of heating in order to also allow the medical production of warm water by means of this exchanger.

Fig. 10. Container of the gas engine

Fig. 11. Gas motor

5. CONCLUSIONS

5.1. Financial analysis

- Total cost of the installation: 670.000 € HTVA (unit of cogeneration: 288.000 € HTVA, cabin High voltage: 50.000 € HTVA, distribution network of composite heat + boiler: 332.000 € HTVA);

- Maintenance: an average of 35.000 € HTVA/year;

-Total financial income until 2008: 2.625.000 € HTVA (production of 18.000 MWh of electricity, Obtaining 14.000 green certificates, income cumulated of 965.000 € HTVA on the sale of electricity, income cumulated of 360.000 € HTVA on the sale of heat, income cumulated of 1.300.000 € HTVA on the sale of the green certificates).

Because of the production of biogas there is a risk of fire and explosion, bad smells, greenhouse effects, etc.

The advantages of biogas energy recovery systems are: to reduce greenhouse effect, to reduce the consumption of fossil energy sources.

The biogas presents an energy potential of 5-6 KWh/Nm^3.

The costs of the gas exploitation installations are recovered rather quickly (for example on the landfill Anton the installations were deadened over 3 years), but not the costs of rehabilitation of the entire andfill. This means that it is very interesting to install expoitation systems for biogas on landfills where rehabilitation was done, but it’s not recommended to create a landfill only for the biogas production and exploitation.

6. REFERENCE

[1] Tender dossier for the valorization of the heat of the gas motor - Research department GENERG
[2] Project of design, valorization - Reinhart Knop - June 1999
[3] Anton- valorization of biogas - state of the situation 1998 - SPAQuE SA
[4] The problem of gases in the discharges - Pierre Labeyrie
[5] Landfill rehabilitation presentation - Thierry NAMECHE, SPAQuE SA
[6 Modeling of production of biogas - Research department 3EI

Studies on landslides in Olanesti catchment, Valcea county

S. Rosulescu, F. Maracineanu, E. Constantin and N. Maracine

Abstract - **The paper presents the degradation of natural phenomena on a surface of approx. 400 ha, specific to the Mosoroasa Valley, Olanesti river basin, caused by excessive water erosion of surface and depth, especially landslides affecting the whole territory. For this reason, the category of specific traditional use - pasture and meadow, was replaced by unproductive land. Given the favorable natural environments for recreation activity, it is necessary to ensure stability of the ground to conserve the natural landscape feasible to exploit in future not only for animal husbandry and forestry but for recreation, thus contributing to improving living standards of people in the area. This paper presents studies appropriate to base planning solutions that will be subject to estate development project to restore the natural landscape and its ecological and economic functions.**

Keywords **– landslide, massif earth, versant.**

1. INTRODUCTION

Natural risks include different phenomena and are defined by estimating the probability of producing human loss and damage.

The risk associated with landslides refers to potential damage and human loss caused by the occurrence of this natural phenomenon.

Landslides and subsidence of the land are included in the category of natural risks and they associate with the vulnerability which reflects the degree of affectation of elements exposed to the action of natural phenomena generating damage. Landslides are natural risks which can cause disasters triggered by many factors that can lead to the disturbance of the balance of earth masses which compose the versant.

The elements exposed to specific risks are: population, animals, property, social-economic activities and environment. This risk is reflected by the envisaged level of losses estimated to victims, destroyed properties, interrupted economic activities, environmental impact. The areas of natural risk are geographically defined areas where the intensity characterizing destructive natural phenomena is highly probable to go beyond limits which will compulsorily cause damage and/ or human loss.

2. MATERIAL AND METHOD

Under the simultaneous or successive action of many factors which tend to modify the balance of forces existing in the massif, the versants decline, taking place a landslide which can be in furrows, in waves, in steps, with mounds, and flowing landslides, [1].

S. Rosulescu is with The Faculty of Land Improvement and Environmental Engineering, Bucharest, Romania (corresponding author to provide phone: +40-248-224191; fax: +40-248-213270; e-mail: serban.rosulescu@roconstructcenter.ro).

ISSN-1584-5990

Fig. 1. Settlement of the area of study

Active landslide has a length of almost 400 m starting from the watershed (photo 1) to the line of the valley Mosoroasa. The landslide front has a width of 91.5 m.

Fig 1. General view of the landslide

The conditions of formation and evolution of the relief in the Subcarpatii Getici determined that the whole geographical area present a natural inclination towards landslides. Therefore the area is known as one of the most vulnerable to landslides. Besides, the county of Valcea is on the first place at the national level from the point of view of

landslides (4.8t/ha per year), on the fourth place from the point of view of gully erosion (8.5 t/ha per year) and on the fifth place regarding surface erosion (12.0t/ha per year). (2)

These are the reasons why we approached in our studies the ecological reconstruction of an area characteristic for the processes of natural landscape degradation in order to reintegrate it harmoniously in the environment.

The area of study is settled in the perimeter of the locality Baile Olanesti, in the hydrographic basin Mosoroasa included in Depresiunea Getica, covering a surface of almost 500 ha. (fig.1), [3]

The land was used as pasture and was excessively exploited.

The purposes of the researches in this perimeter are:

- evaluate the impact of climatic conditions on the physical state of the versant
- establish the sources which produce water in excess in the area of study
- evaluate the geotechnical conditions by the bed of sliding
- determine the intensity of production of the sliding and the climatic factors which influence it.

3. RESULTS AND SIGNIFICANCES

In order to cover the objectives of the researches, visual and analytical systematic observations were organized. Based on these observations it is estimated that the main factor causing the sliding is represented by heavy rainfall.

Fig 2. Forms of dead water in the sliding area

During the period October 2009 – March 2010, in the area of study, these heavy rainfalls reached 646.2 mm, in comparison with the multi-annual average of 268,5 mm, in the same period, which means that in the cold season during the period 2009/2010 heavy rainfalls have increased by 2,41 times then the multi-annual average, especially in November and February (over three times more abundant).

Another factor causing the triggering slides is underground water. Underground water comes to surface at the top of the sliding from where it flows forming dead water and

muddy depositions in areas with slight slope (photo 2). The three drillings made in the area show that the depth of the phreatic water is between 0.8 – 1.7m, is basic-type and presents high carbonic aggression and low sulfate aggression.
Under these conditions are formed landslides in furrows (photo 3), landslides in waves (photo 4) and muddy landslides (photo 5).

Fig 3. Landslides in furrows

Fig. 4. Landslides in waves

The geotechnical study made on a median logitudinal route highlights the existence of eight layers of which the dominant layers are the flowing plastic dust, flowing plastic sandy dust and the flowing plastic shaly dust.

These layers form the natural covering of the versant disposed in an inclined way over the basic rock, represented by a layer of rough plastic dust with seams of yellow gritstone. The apparent density of lands is between 1.5 – 1.7 t/m.c., falling in the category of land-

type I and land-type II for mechanized works. The intern sliding angle is of 4º for the sandy dust and of 26 º for the rough plastic dust.

Fig 5. Flowing landslides (muddy)

The highlighting of the intensity of the earth mass displacement is made by setting telltales on a longitudinal alignment in the mass of sliding. The length of the profile on which this element is watched is of 130 m and has a difference in level between 509.90 and 466.86 m. The position of the telltales installed on this route is established by periodic topographic surveying in order to highlight the changes which take place in the earth mass. Although this objective is in an initial phase of achievement, preliminary observations shows that the earth mass continues to move.

4.CONCLUSIONS

The studies and researches regarding the landslides in the county of Valcea, especially in Olanesti catchment show that such landslides are natural hazards which happen because of natural causes favored by human activity.

From the researches made up to the present in the area of study result the following important problems:

- the landslide in the area of Mosoroasa is caused by the lithologic formation of the versant made of powdery lands which enter the category of gelive lands very sensitive at frost and thawing;
- the abundant pluviometrical regime from previous years favored the producing of the landslide by drenching the lands and reducing its' resistance parameters;
- the landslide is favored by ice formation from water in the rock pores which determine the destruction of lands structure;
- another factor for landslide is represented by underground water action which by flowing actions fine particles and creates plans with weak resistance that increase the versant instability;
- the water stagnating in the crevices and the unevenness produced by the landslide increases the moisture of the earth mass favoring the sliding in this way.

5. REFERENCES

[1] Maracineanu Fl., *Reconstrucția ecologică a terenurilor degradate – Note de curs*, 2009 FIFIM

[2] Roşulescu Ş. si colab., *Soluții tehnice constructive pentru ameliorarea alunecărilor de teren în spațiul Olt-Argeş*, Sesiune comunicari stiintifice Unversitatea Valahia,Targoviste 2009

[3] Tuas Mircea, Codreanu Mateiu, *Amenajări hidrotehnice pe versant,* 2008, Editura BREN, Bucureşti.

SECTION VIII

IRRIGATION AND DRAINAGE

Limitation of free air use in irrigation water pumping installation protection from water hammer

Anca Constantin, Claudiu Nitescu, Madalina Stanescu, Lucica Rosu

***Abstract* –Small amounts of free air dispersed throughout the pumped water is an efficient means of protection of a discharge conduit from water hammer. The extreme pressures during water hammer for a specific pumping installation are compared to those obtained in similar conditions, considering a biphasic water-air homogenous flow with small volume fraction of air. Disadvantages of this method are revealed as a non homogenous flow is taking into account.**

***Keywords* – biphasic flow, pumping installation, water hammer.**

1. INTRODUCTION

The activity of engineering design of a water supply pumping installation has always paid a special attention to the protection of the discharge duct from hydraulic shock. There were conceived a lot of devices and methods to avoid this phenomenon that may seriously damage the installation due to the extreme pressures it induces. Lately studies proved that small amounts of air spread through the pumped water could be a reliable means of protection from water hammer. The presence of small amounts of free air in the water results in a smaller celerity, due to the change of density of the biphasic fluid and to the gain in its compressibility.

The choice of this solution for protection must be well theoretically studied. The most eloquent and low cost method of study is numerical simulation, by the aid of special computer programs.

The main purpose of our study is to determine, by numerical simulation, how appropriate this protection method for a specific discharge duct is. The installation we focused on, **Fig.1**, is equipped with a centrifugal pump that operates at a discharge of $Q = 0.11\ m^3/s$ and a head of $H = 27.7\ m$. The geodetic head is $H_g = 20\ m$. The steel made discharge duct, with a diameter of $D = 300\ mm$ has $750m$ in length. The numerical simulation aims to point out:

-the attenuation of the extreme pressures during the hydraulic shock as the volume fraction of air of the biphasic fluid increases;

Anca Constantin, Ovidius University of Constanta, 22b Unirii Str, 900524-Constanta, Romania (aconstantina@univ-ovidius.ro).

Claudiu Nitescu, Ovidius University of Constanta, 22b Unirii Str, 900524-Constanta, Romania (claudiu.nitescu@univ-ovidius.ro).

Madalina Stanescu, Ovidius University of Constanta, 22b Unirii Str, 900524-Constanta, Romania (mada_x_dobre@yahoo.com).

Lucica Rosu, Ovidius University of Constanta, 22b Unirii Str, 900524-Constanta, Romania (lucirosu@yahoo.fr).

ISSN-1584-5990

-the variation range for the volume fraction of air in pumped water recommended for a good prevention of damages;

- technical and conceptual limitations of the method.

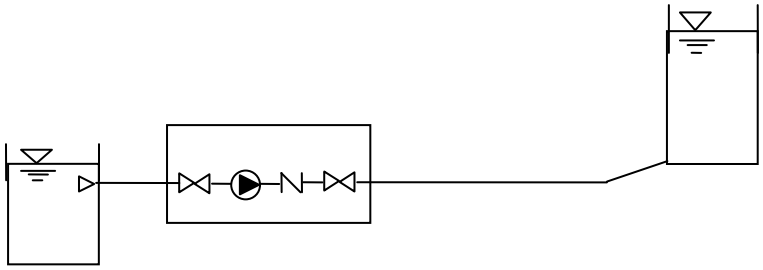

Fig. 1. Water supply pumping installation

2. MATHEMATICAL MODEL FORMULATION

2.1 MATHEMATICAL MODEL FOR HYDRAULIC SHOCK IN A DISCHARGE DUCT

The mathematical model for the hydraulic shock phenomenon, in the case of one dimension flow, is composed of the mass conservation equation (1) and momentum conservation equation (2):

$$\frac{\partial H}{\partial x} + \frac{c^2}{g}\frac{\partial u}{\partial x} = 0 \tag{1}$$

$$\frac{\partial H}{\partial x} + \frac{1}{g}\frac{\partial u}{\partial t} + \frac{\lambda u|u|}{2gD} = 0 \tag{2}$$

where: u-velocity, [m/s]; H-head, [m]; c-celerity, [m/s]; t- time, [s]; g-gravity acceleration, $g = 9.81\ {}^{m}/_{s^2}$; λ-Darcy's coefficient; D-pipe's diameter, $[m]$.

The rapid pressure variation during the hydraulic shock in the specified pumping discharge duct was determined by numerical simulation using a special computer program, based on the mathematical model of the water hammer phenomenon written in finite differences and solved by the method of characteristics [4].

The speed of wave propagation through pure water, considered as a single phase, is given by the relation:

$$c = \left(\frac{E_l}{\rho_l}\right)^{1/2}\left(1 + \frac{E_l}{E_c}\frac{D}{e}k\right)^{-1/2} \tag{3}$$

where ρ_l -water density, $\left[{}^{kg}/_{m^3}\right]$; E_l -modulus of elasticity of water, $\left[{}^{N}/_{m^2}\right]$; E_c -modulus of elasticity of the pipe wall, $\left[{}^{N}/_{m^2}\right]$; e-pipe-wall thickness, $[m]$; k-coefficient depending on the pipe's type of pose.

If a small amount of air is entrained by the liquid and the small bubbles of gas spread out homogenously, the celerity may be considerably reduced. As the volume fraction of air rises, the celerity decreases and may reach a value even less than the speed of sound in still air. Thus, the relationship (4) is recommended for celerity calculus in air–water biphasic homogenous mixtures [2]. Numerous studies pointed out a good agreement between this theoretical formula and experiment.

$$c_a = \left(\frac{E_l}{\rho_l}\right)^{1/2}\left[\left(1-\frac{m_a RT}{p}\right)\cdot\left(1+\frac{m_a RT}{p^2}\cdot E_l+\frac{E_l}{E_c}\frac{D}{e}k\right)\right]^{-1/2} \quad (4)$$

where R -air constant, $\left[{}^{J}/_{(kg\cdot K)}\right]$; T -absolute temperature, $[K]$;

p -absolute pressure, $\left[{}^{N}/_{m^2}\right]$; m_a -air mass on biphasic unit volume, $\left[{}^{kg}/_{m^3}\right]$.

Neglecting the air dissolution and liberation from water, the term $\frac{m_a RT}{p^2}\cdot E_l$ in relation (4) has an important weight on celerity only at pressures lower than 40 bar [3].

2.2. *MATHEMATICAL MODEL FOR REGIME BIPHASIC FLOW IN A DISCHARGE DUCT*

The flow into a discharge pumping conduit is characterized by large Reynolds number, turbulence being fully developed. The mathematical model uses the Reynolds-averaged Navier Stokes equations. Assuming the two phases are subjected to the same pressure field, the mass conservation for low volume fraction of air (5) and the momentum (6) equations become:

$$\nabla \boldsymbol{u}_l = 0 \quad (5)$$

$$\alpha_l\rho_l\frac{\partial u_l}{\partial t}+\alpha_l\rho_l\boldsymbol{u}_l\cdot\nabla\boldsymbol{u}_l=-\nabla p+\nabla\cdot\left[\alpha_l(\eta_l+\eta_T)\left(\nabla\boldsymbol{u}_l+\nabla\boldsymbol{u}_l{}^T-\frac{2}{3}(\nabla\cdot\boldsymbol{u}_l)I\right)\right]+\alpha_l\rho_l g \quad (6)$$

where u_l-speed of water, $[{}^{m}/_{s}]$; η_l-dynamic viscosity of water, $[Pa\cdot s]$; η_T-turbulent viscosity, $[Pa\cdot s]$; $\eta_T=\rho_l C_\mu\frac{k^2}{\varepsilon}$; α_l-volume fraction of water, $\left[{}^{m^3}/_{m^3}\right]$; α-volume fraction of air, $\left[{}^{m^3}/_{m^3}\right]$.

The relationship between the two volume fractions, expressed at normal pressure (101,3kPa) is:

$$\alpha_l = 1-\alpha \quad (7)$$

Taking ρ_g for air density and assuming there is no mass change between the two phases, the transport equation for the fraction of air is as follows:

$$\frac{\partial\rho_g\alpha}{\partial t}+\nabla(\alpha\rho_g\boldsymbol{u}_g)=0 \quad (8)$$

When we consider an homogenous flow, which means both phases have the same velocity, we have the relation:

$$\boldsymbol{u}_g=\boldsymbol{u}_l \quad (9a)$$

But if we take into account the difference between the velocities of the two phases, relation (9) becomes:

$$\boldsymbol{u}_g=\boldsymbol{u}_l+\boldsymbol{u}_s \quad (9b)$$

where the relative velocity $\boldsymbol{u}_s$ may be known assuming the balance of forces acting on the bubbles.

The mathematical model used for the non homogenous biphasic flow is extended by two more transport equations written for turbulent kinetic energy and for dissipation rate. The two equations include a new turbulence source term, due to the relative velocity [5].

The presence of air bubbles modifies the parameters of flow. The mathematical model presented above may be used for the study of pressure, velocities and volume fraction fields in different sections of the discharge conduit, in order to find out the difference from the single phase flow case. We focus on the pressure drop variation and volume fraction field.

3.RESULTS

The numerical simulation for the hydraulic shock in the above depicted installation was done by the use of *Hammer* programme, in a pipeline without any protection devices. There were considered either cases of single liquid phase or biphasic water-air fluid flow. In the later case, free air is deliberately introduced into the conduit, by a compressor, and the air volume fraction α is rigorously varied from 0,5 to10 %.

There was assumed a constant celerity along the pipeline.

In **Fig.2**. it is graphically represented the pressure variation in the conduit during hydraulic shock produced due to the sudden stop of the electrical power supply. The pumped water is assumed to be a single liquid phase.

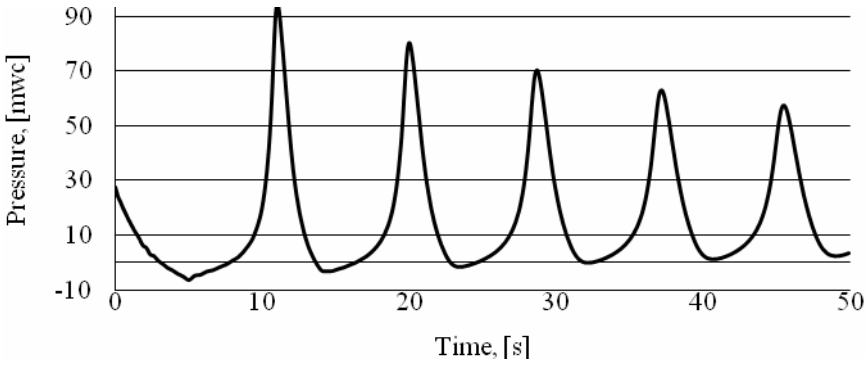

Fig.2. Pressure variation during hydraulic shock, in the unprotected discharge duct. First calculus node

It may be noticed that the extreme pressures, even if not dangerous for an usual pumping installation designed to resist at 100 mwc, are $p_{max} = 93\ mwc$ and $p_{min} = -6{,}4\ mwc$.

In the case of biphasic flow, the simulation of hydraulic shock takes into account the relation (4) for the celerity. Consequently the results with respect to the pressure variation may be seen in **Fig.3**. The volume fraction of air was taken as parameter. It may be easily noticed the attenuation of the extreme pressures as the volume fraction of air increases. An important attenuation is registered for the change of the volume fraction of air from 0 to 5%. The maximal pressure decreases to 37,38mwc and the minimal one increases to a positive value of 5,79 mwc. If the volume fraction of air increases more than 5 %, the attenuation is softer. For example, the maximal pressure attained for 7% air is 33,73mwc. We may conclude that 5% is the upper recommended value for the volume fraction of air in water.

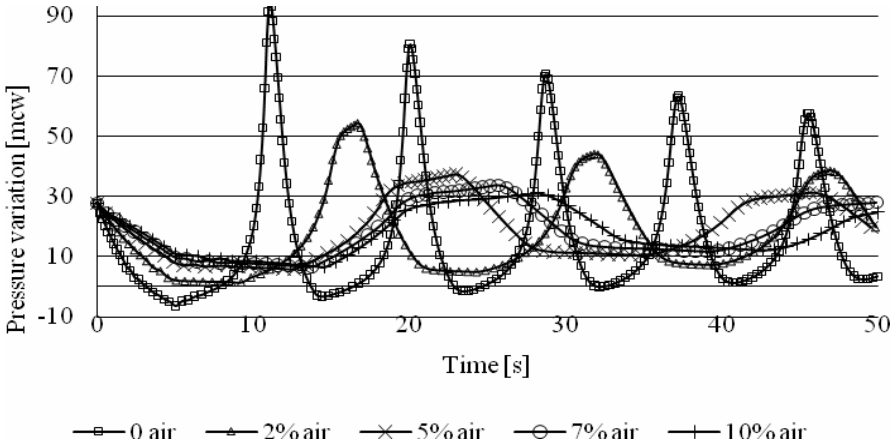

Fig.3. Pressure variation during hydraulic shock, in the discharge duct in the case of biphasic fluid at different volume fraction of air. First calculus node

The other aspect of our study is that of the flow parameter modification due to the presence of air in water. It may be exemplified by the flow around the check valve obturator. **Figure 4** shows the field of volume fraction of air, at local pressure, in the case of non homogenous flow model, in gravity field, as it was determined by the use of *Comsol* programme. The arrows, proportional to the air bubble speed, are pointing upward, indicating the direction of bubble flow. This simulation shows how air pockets occur inside the conduit.

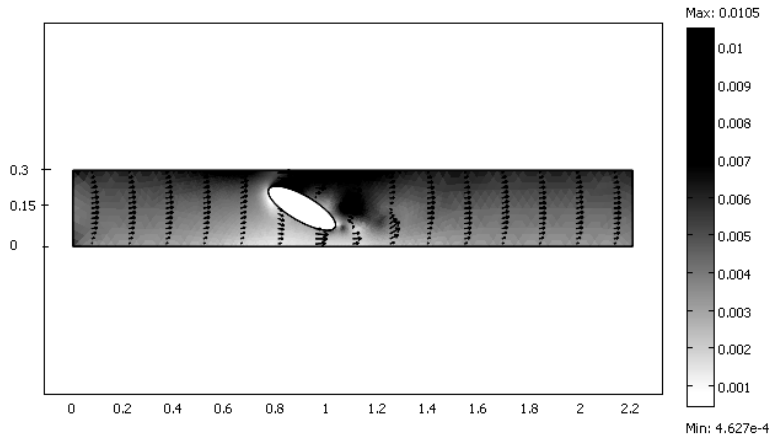

Fig.4. Surface: volume fraction of air, at local pressure; Arrows: air velocity

Turbulence induced by the air bubbles adds to the turbulence in single phase flow and influence the solid-fluid interaction. The resistance to the flow opposed by the obturator is defined as the ratio of the pressure drop to the mass flow rate. The pressure drop is calculated between the sections upstream and downstream the valve. In **Fig.5** there is represented the pressure drop variation with the increase of the volume fraction of air in water, in two cases: first, in the case of homogenous flow (9a) and second in the case of non homogenous flow - taking into account the relative velocity between water and air bubbles, (9b). It may be noticed the increase of pressure drop as the volume fraction of air increases.

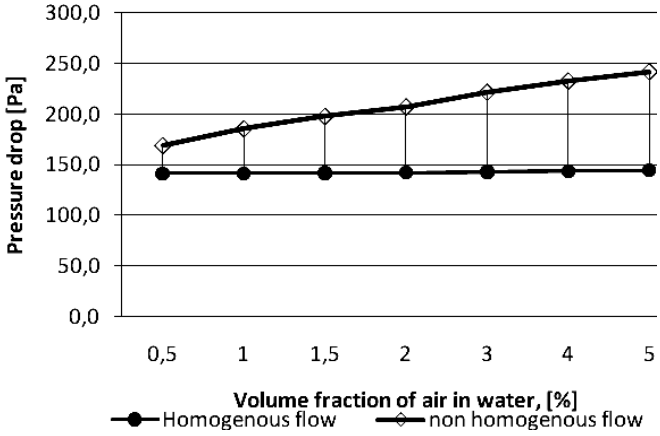

Fig.5. Pressure loss increase with air volume fraction

4. CONCLUSIONS

Gaseous air, in small amounts, deliberately and rigorously introduced in water, offers a good way to protect the duct from the extreme values of pressure, which occur during water hammer. The upper limit of volume fraction of air rationally results to be 5%. A greater value has no significance on the attenuation of the extreme pressures.

Free air method proved to be efficient in attenuating extreme pressures during hydraulic shock, but there are two main limiting aspects. First refers to the air bubbles that must be deliberately introduced into the hydraulic circuit by the help of a compressor, under a strict control of the volume fraction. The compressor implies additional power consumption. Second refers to air pockets formed in the upper sides of the duct, during normal operation of the installation. These pockets may become dangerous during water hammer. Consequently, the use of free air may be recommended only in installations where the configuration doesn't allow air accumulation in different sections. Numerical simulation using the non homogenous biphasic flow allows us to point out the sections of the conduit where air accumulates into pockets.

The presence of air might also be provoked by accident: by an incomplete evacuation, when the installation is put to work, or by the air valves during the first phase of water hammer, when the pressure in the duct decreases under the atmospheric value. Under these circumstances, the volume fraction of free air is hard to be estimated.

5. REFERENCES

[1] Brennen C.E., *Fundamentals on Multiphase Flow*, Cambridge University Press, 2005.
[2] Constantinescu Gh., *Contribuţii privind protecţia instalaţiilor sub presiune*, Teză de doctorat, Institutul Politehnic Timişoara, 1983, unpublished.
[3] Hâncu S., Marin G., *Hidraulică teoretică şi aplicată*, vol. I, II, Editura Universitară, Bucureşti, 2007.
[4] Popescu M., *Uzine hidroelectrice si statii de pompare. Functionarea hidraulica la regimuri tranzitorii,* Editura Universitară, Bucureşti, 2008.
[5] * * * *COMSOL MULTIPHYSICS*, tutorial, 2007.

Ovidius University Annals Series: Civil Engineering Volume 1, Issue 12, June 2010

Design discharge of irrigation pumping stations under reconstruction

Petar I. Filkov, Jordan D. Gerinski

***Abstract* – The political and economic changes in Bulgaria after 1989 seriously affected the agriculture – reduction of arable land, poor irrigation infrastructure maintenance, damaging of irrigation devices and structures, including pumping stations (PS), etc. Since 2001 the formation of Irrigation Associations has started and the reconstruction of irrigation fields and PS has begun. Considering pumping stations, usually their balancing reservoir is present and in some cases the pressure pipeline (penstock) is also usable. But the design discharge of the reconstructed PS is considerably smaller than the original one, due to decreased agricultural land and changed crop pattern, so the existing penstock is found to be oversized. As a result it is possible to vary the design discharge of the reconstructed PS to minimize the sum of energy consumption costs and machinery investments. Some specifics and directions for solving such kind of problems are considered in the article.**

***Keywords* – design discharge, irrigation, pumping station, reconstruction.**

1. INTRODUCTION

In current agricultural conditions in Bulgaria the design discharge of the reconstructed irrigation pumping stations (PS) is evaluated smaller than the original one and sometimes the difference is more than 20%. There are many reasons for the discharge decrease, but the most important one is the reduction of the actual irrigated area in the system.

Considering [1] and [2] the *original* design discharge Q_O of the PS has been usually estimated on the base of the PS operation time t_O = 24 h/d in the peak demand period T. The volume of the balancing reservoir (BR) of the PS has been determined as a result of the operation regimes analysis for the non-peak periods in the irrigation season. The penstock diameter and number, types and models of pumps have been selected after a complex optimization procedure [3].

In most cases of pumping stations reconstruction, the BR and penstock are in good technical condition and only pumps, pipes and valves are dismounted or stolen and sometimes the PS building is damaged or even demolished. If the existing PS was designed for 24 h/d operation the discharge is Q_O and the corresponding 24-hours-a-day *design* discharge for the reconstructed PS is $Q_{D,24}$. If Q_O is bigger than $Q_{D,24}$ it is possible, in above mentioned conditions of an existing BR and a penstock, to search for an optimal design discharge $Q_{D,t}$.

P. I. Filkov is with the University of Architecture, Civil Engineering and Geodesy, 1, Hristo Smirnensky Boulevard, 1046-Sofia, Bulgaria (phone: +359-887-385928; e-mail: filkov_fhe@uacg.bg).

J. D. Gerinski is with the University of Architecture, Civil Engineering and Geodesy, 1, Hristo Smirnensky Boulevard, 1046-Sofia, Bulgaria (e-mail: gerin_fhe@uacg.bg).

ISSN-1584-5990

The discharge $Q_{D,t}$ corresponds to t_{PS}-hours-a-day operation of PS and when t_{PS} is shorter than 24 h/d, the design discharge $Q_{D,t}$ is bigger than $Q_{D,24}$. The increase of $Q_{D,t}$ leads to higher head losses and greater energy consumption, but the average energy price $\overline{c}_e$ decreases, because shorter time t_{PS} allows avoiding pump operation during peak tariff periods. In the opposite, increased design discharge $Q_{D,t}$ may lead to bigger pumps or greater number of pump units which leads to increasing cost of investments *Inv* for the new PS equipment. Thus the aim of the present research is to find out if there is a positive economic effect of the PS design discharge increase.

2. RESEARCH DESCRIPTION

It is considered a PS with an existing BR and a penstock which are in good repair. For the PS under reconstruction it is assumed that the penstock and pipelines inside the PS remain the same. A theoretic research on the variation of energy expenses E_{exp} in function of PS daily operation time t_{PS}, i.e. of the design discharge $Q_{D,t}$ is made. The theoretical research is made using relative units – the 24-hour-a-day design values for the reconstructed PS are used as a base. As a result of the research the economic effect of the design discharge increase is obtained.

The economic effect analysis is not accomplished theoretically because the variation of *Inv* for new pumps, pipes and valves in PS cannot be presented as a mathematical function of $Q_{D,t}$. For that reason a practical example is presented.

In the practical example it is assumed that the original design discharge of the PS before the reconstruction Q_O is estimated for operation time of the PS t_O = 24 h/d. The discharge $Q_{D,24}$ for the reconstructed PS is assumed smaller than Q_O. Two variants of a design discharges are investigated. As a criterion for the best variant selection the *net present value* (NPV) of *Inv* and E_{exp} is used. The energy expenses E_{exp} are estimated only for a peak demand period T = 40 days. It is assumed a 10-year comparison period, 10% annual increasing of the electric energy price (i = 0,10) and a discount rate of 6% (r = 0,06). In the research Euro are used as a currency.

The relative discharge R of the PS is introduced as:

$$R = \frac{Q_{D,t}}{Q_{D,24}} = \frac{24}{t_{PS}} \tag{1}$$

The design total head of the PS for 24-hours-a-day operation is estimated via the equation:

$$H_{D,24} = H_G + h_{L,24}\text{, m,} \tag{2}$$

where H_G is the geodetic head, m;

$h_{L,24}$ are the head losses in the PS and penstock, m.

$$h_{L,24} = SQ_{D,24}^2\text{, m,} \tag{3}$$

where S is the resistant coefficient, s^2/m^5.

The design total head $H_{D,t}$ of the PS for t_{PS}-hours-a-day operation is estimated by (2) and the head losses are estimated by (3) using relevant $Q_{D,t}$. Because the penstock and pipelines are not a subject of the reconstruction, S is the same for every variant.

The electric energy consumed during the period of T days is:

$$E_{24} = \frac{0{,}002725 Q_{D,24} H_{D,24}}{\eta_{pump}\eta_{motor}} t_{PS} T \text{ , kWh,} \tag{4}$$

where t_{PS} = 24 h/d;

η_{pump} and η_{motor} are the pump and motor efficiencies.

When t_{PS} is less than 24 h/d the consumed energy is E_t and it is also estimated by (4). It is assumed that in every researched variant the pump impellers are reduced in order to equalize the pump head and hydraulic losses. Thus, in each case, the design and actual discharges are the same ($Q_D = Q_A$) and the design and actual heads are equal ($H_D = H_A$).

The relative consumed energy $\bar{e}$ is defined as a ratio between E_t and E_{24}. Regarding (1), (2), (3) and (4) $\bar{e}$ can be presented as follows:

$$e = \frac{E_t}{E_{24}} = \frac{K + R^2}{K + 1} \tag{5}$$

where

$$K = \frac{H_G}{h_{L,24}} \tag{6}$$

The average electric energy price for t_{PS}-hour-a day operation is estimated as follows:

$$\bar{c}_t = \frac{c_p t_p + c_d t_d + c_n t_n}{t_p + t_d + t_n} \text{ , €/kWh,} \tag{7}$$

where c_p, c_d and c_n are the energy prices for the peak, daylight and night tariff periods, €/kWh;

t_p, t_d and t_n are the operation times in the peak, daylight and night tariff periods, h/d.

Also

$$t_{PS} = t_p + t_d + t_n \text{ , h/d.} \tag{8}$$

The relative energy price c_e is defined as a ratio between the energy prices $\bar{c}_{24}$ and $\bar{c}_t$. The first one is estimated for 24 h/d operation of the PS and the second one – for t_{PS} h/d.

$$c_e = \frac{\bar{c}_t}{\bar{c}_{24}} \tag{9}$$

Relative energy expenses for the peak period are estimated as:

$$e_{exp} = \bar{e}.c_e \tag{10}$$

The criterion *Cr* is estimated using energy expenses for the first year $E_{exp,1}$ and the above presented parameters *Inv*, *i* and *r*. The following equation is used:

$$Cr = Inv + \sum_{j=1}^{10} E_{exp,1} \frac{(1+i)^{j-1}}{(1+r)^j}, \text{€}. \tag{11}$$

There are at least two constraints regarding possible values of $Q_{D,t}$, respectively *R* and t_{PS}. The first one concerns needed minimum cooling time of the pump motors t_{cool}:

$$24 - t_{PS} \geq t_{cool}, \text{ h}. \tag{12}$$

The cooling time t_{cool} varies between 2 and 4 h for big pumps, and thus, taking into account (1) and (12), there will be a gap of t_{PS} values between 24 h/d and 22 h/d. The values *R* = 1,043 and *R* = 1,091 are not included in the research.

The second constraint takes into account the existing balancing reservoir volume V_{BR}. It is an important constraint, because if $Q_{D,t}$ is too big an extra volume of BR may be needed. In accordance of the irrigation demand daily duration t_{IS} and the irrigation demand discharge Q_{dem} there are two possible cases – *A* and *B*.

Case *A* is observed when t_{IS} = 24 h/d and case *B* is defined when t_{IS} < 24 h/d. In case *A* $Q_{D,24} = Q_{dem}$ and it is possible only $t_{PS} \leq 24$ h/d, so $Q_{D,t} \geq Q_{dem}$ and $R \geq 1$. In case *B* it is possible both $Q_{D,t} \geq Q_{dem}$ ($R \geq 1$) and $Q_{D,t} < Q_{dem}$ ($R < 1$).

For case *A* the constraint regarding $Q_{D,t}$, t_{PS} and *R* is as follows:

$$\frac{R-1}{R} \leq \frac{V_{BR}}{86400 Q_{D,24}} \tag{13}$$

There are also conditions for avoiding peak tariff period operation. The maximum admissible stoppage time t_{stop} is estimated as follows:

$$t_{stop} = \frac{V_{BR}}{Q_{dem}}, \text{ h}. \tag{14}$$

During the day there are two peak tariff periods in Bulgaria – the first one is between 8:00 and 12:00 (4 h) and the second is between 20:00 and 22:00 (2 h). According to these data the conditions for avoiding peak tariff period operation can be defined as follows:

1) $t_{PS} \leq 18$, h/d; (15)

2) $t_{stop} \geq 4$, h; (16)

3) $t_{cool} \leq 20 - t_{PS}$, h. (17)

For case *B* when $Q_{D,t} < Q_{dem}$ and $Q_{D,t} = Q_{D,24}$ the constraint regarding V_{BR} is set as:

$$Q_{D,t} \le \frac{V_{BR}}{3600(24 - t_{IS})}, \text{ m}^3/\text{s}. \quad (18)$$

In case *B* the conditions for avoiding peak tariff period operation are similar to (15), (16) and (17).

3. RESULTS AND SIGNIFICANCES

The first part of the theoretical analysis is made using average values for the electric energy prices of the three main distributor companies in Bulgaria. The following prices for the tariff periods are used: c_p = 0,0869 €/kWh, c_d = 0,0562 €/kWh and c_n = 0,0307 €/kWh. The variation of the relative energy price c_e is presented in **Table 1**. The tariff period durations in Bulgaria for the whole day can be seen in the third column.

Table 1. Relative Energy Price c_e versus Relative Discharge R and PS Working Time t_{PS}

R	**-**	1,000	1,200	1,333	1,500	2,000	3,000
t_{PS}	**h/d**	24	20	18	16	12	8
t_p	**h/d**	6	2	0	0	0	0
t_d	**h/d**	10	10	10	8	4	0
t_n	**h/d**	8	8	8	8	8	8
Energy price $\bar{c}_t$	**€/kWh**	0,0554	0,0491	0,0449	0,0435	0,0392	0,0307
Rel. price c_e	**-**	1,000	0,886	0,810	0,785	0,708	0,554

The lowest value of the relative energy price c_e is 55,4% from the basic price. The lowest value of c_e is obtained at t_{PS} = 8 h/d, i.e. for R = 3, which means three times increase of the discharge. If the reconstructed PS has a discharge $Q_{D,24} = Q_O$ such kind of increase cannot be achieved without replacing the penstock. But if $Q_{D,24} < Q_O$, then the increased discharge $Q_{D,t}$ may be delivered through the existing penstock. For instance, if $Q_{D,24} = 0{,}5Q_O$ and R = 3, then $Q_{D,t} = 1{,}5Q_O$. If the peak period operation is avoided (t_{PS} = 18 h/d) the energy savings will be 19%, the relative discharge is R = 1,333 and, depending on the actual conditions, the increased discharge could be conducted through the same penstock.

It is evident from (5) that the ratio K between geodetic head H_G and head losses $h_{L,24}$ is very important for the value of the relative consumed energy $\bar{e}$. It is assumed that K will vary between 2 and 8, which is valid for most of the PS in Bulgaria. The relative energy expenses for K = 5 are presented in **Table 2**.

Table 2. Relative Energy Expenses e_{exp} versus Relative Discharge R and Head Ratio K

R	**-**	1,000	1,200	1,333	1,500	1,714	2,000
t_{PS}	**h/d**	24	20	18	16	14	12
Ratio $K = H_G / h_{L,24}$	**-**	5	5	5	5	5	5
Relative energy $\bar{e}$	**-**	1,000	1,073	1,130	1,208	1,323	1,500
Relative energy price c_e	**-**	1,000	0,886	0,810	0,785	0,752	0,708
Relative expenses e_{exp}	**-**	1,000	0,951	0,915	0,949	0,995	1,062

It is seen in **Table 2** that the effect of the design discharge increase is positive for the whole range of R between 1,0 and 1,714. The minimum value of e_{exp} is observed at

R = 1,333, i.e. at t_{PS} = 18 h/d, when the peak period operation is avoided. In that case the increase of the PS design discharge with 33,3% leads to 8,5% energy savings. Any further increase or decrease of R lessens the energy savings. Nevertheless nearly 5% savings are observed at R = 1,2 and R = 1,5. The former can be achieved with no penstock change, whereas the latter may be realized without replacing the penstock only if $Q_{D,24} < Q_O$.

The variation of the relative energy expenses e_{exp} in function of two main parameters R and K is presented on **Fig. 1**. The minimum values of e_{exp} are observed at R = 1,333 for the whole range of K between 3 and 8. It is evident from **Fig. 1** that the higher the ratio K the lower the relative energy price.

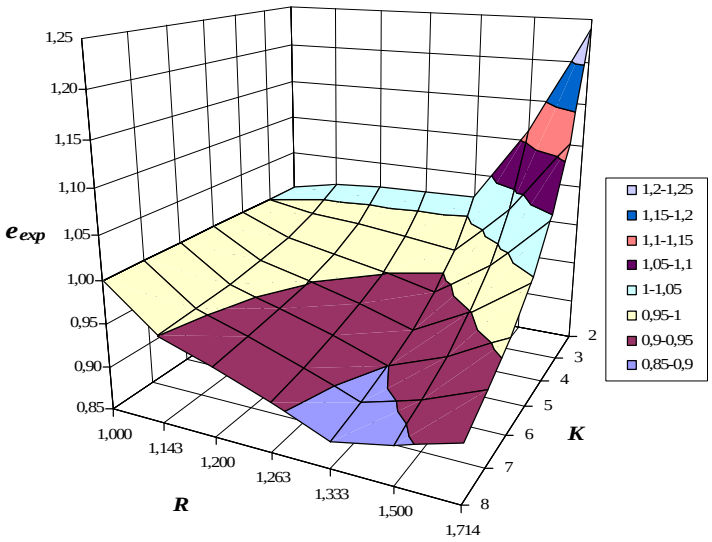

Fig. 1. Variation of relative energy expenses e_{exp} in function of parameters R and K

The example concerns an irrigation PS with a design discharge before reconstruction Q_O = 0,16 m^3/s, obtained for t_O = 24 h/d. Existing penstock has a length L = 500 m and a nominal diameter DN 300 mm. Geodetic head of the PS is H_G = 50 m and the design total head before reconstruction is $H_{D,O}$ = 60 m. The PS was equipped with 2 pumps (single stage, end-suction, centrifugal), provided for parallel operation, which are dismounted because of the worn out. Each pump line consists of 5 m long steel suction pipe with DN_s 300 mm and 10 m long steel discharge pipe with DN_d 200 mm, equipped with a check valve and a gate valve both with DN 200 mm. It is assumed that the constraint (13) and the conditions (14) - (16) are fulfilled.

The 24-hour design discharge for the PS under reconstruction is $Q_{D,24}$ = 0,12 m^3/s. The following variants are investigated:

Variant *I*: $Q_{D,24}$ = 0,12 m^3/s and 2 new pumps (n_p = 2).

Variant *II*: $Q_{D,18}$ = 0,16 m^3/s (t_{PS} = 18 h/d, R = 1,333) and 2 new pumps (n_p = 2).

Variant *III*: $Q_{D,18}$ = 0,16 m^3/s (t_{PS} = 18 h/d, R = 1,333) and 3 new pumps (n_p = 3).

For each of the variants the design total head of the PS is estimated by (1). For each of the variants the pump model is chosen using [4], the actual pump head and the actual discharge are obtained and the actual energy consumption is estimated. The type of new pumps is the same – single stage, end-suction, centrifugal pump are used.

The available pump models for each variant and their actual parameters are presented in **Table 3**. For variant *II* and *III* two sub variants (*a* and *b*) are investigated.

In **Table 3** needed input power for the pump is marked with $N_{p,A}$ and needed power for the PS is noted as N_A. The power N_A is estimated using an average motor efficiency η_{motor} = 0,95. The variant *IIIb* (3 pumps NK 100-400) has an actual discharge of 50 l/s instead of needed 53,3 l/s.

Table 3. Design and Actual Parameters of PS

Var.	Design			Pump model (Grundfos pumps)	Actual parameters			
	Q_D	n_p	Q_p		$H_{p,A}$	$\eta_{p,A}$	$N_{p,A}$	N_A
	l/s	-	l/s	-	m	-	kW	kW
I	120	2	60,0	NK 80-200 (2900 min^{-1})	56,5	0,80	41,6	87,6
II	160	2	80,0	NK 100-200 (2900 min^{-1})	60,5	0,82	57,9	121,9
				NK 125-400 (1450 min^{-1})	60,2	0,76	62,2	130,9
III	160	3	53,3	NK 80-200 (2900 min^{-1})	59,8	0,80	39,1	123,5
				NK 100-400 (1450 min^{-1})	56,7	0,72	41,2	130,1

The criterion values are estimated in **Table 4**. For variants *I* and *II* the suction and discharge pipes and valves are used without replacement, so only the pumps prices are taken into account in the value of *Inv* when NPV is estimated. The price $\bar{c}_t$ for the variant *IIIb* is calculated using the actual PS discharge and actual operating hours $t_{PS,A}$.

Table 4. Criterion values

Var.	Q_D	n_p	Pump model	E_t	$\bar{c}_t$	E_{exp}	*Inv*	*Cr*
-	l/s	-	-	kWh	€/kWh	€/year	€	€
I	120	2	NK 80-200	84096	0,0554	4658,0	12950	65160
II	160	2	NK 100-200	87768	0,0449	3939,2	14960	59110
			NK 125-400	94248	0,0449	4230,0	19710	67120
III	160	3	NK 80-200	88920	0,0449	3990,9	21425	66160
			NK 100-400	93672	0,0451	4229,1	27540	74940

It is evident from **Table 4** that the best variant is *IIa* – it has the lowest energy expenses and a relatively small cost of investments. Variants *I* and *IIIa* have almost the same criterion value, despite the additional pump, pipes, fittings and valves of the variant *IIIa*. Assumed constant 10% annual increase of the energy price lessens the advantage of the small energy expenses of the variant *IIIa*, compared to the variant *I*. In opposite to variant *IIIa*, variant *IIIb* is the worst one, besides the fact that it has second lowest pump head and the smallest PS discharge among variants *II* and *III*. The reason for the bad results of the variant *IIIb* is not only the high cost of investments – poor pump efficiency and high energy price are the two factors that worsen its criterion value. Comparison between *IIIa* and *IIIb* shows that it is possible to obtain better results for variants with extra pump(s) if the chosen pump models fit well to the actual conditions and the pump efficiency is high.

4. CONCLUSIONS

The above presented example of an existing PS having a BR and a penstock in good technical condition considers the case of a decreased 24-hour-a-day design discharge of the reconstructed PS. The following conclusions can be drawn from this research:

1. When peak period operation of the PS is avoided the energy expenses decrease between 5 and 15%, according to the weight of the head losses in the total design head of the PS.

2. It is more profitable to reconstruct existing PS to its original state for delivering a discharge near to or equal to its original one, instead of planning new technical decision for the decreased design discharge.

3. The reconstruction of the PS to its original design discharge should not be limited to a simple replacement of old pumps with new ones. A few variants with a different number of pumps should be investigated to obtain the best alternative.

It is stated in [2] that the design discharge should be determined considering operation regimes of the PS. The second conclusion raises a question: Are the energy savings enough to allow planning new PS for daily operation less than 24 h? Further research in that direction is necessary to obtain the weight of the energy expenses in the total sum of investments for a new PS.

5. REFERENCES

[1] Boyanov B., Irrigation and Drainage Systems and Pumping Stations. Sofia: ABC Tehnika, 2005, ch. 6. (in Bulgarian)

[2] KIPP Vodproject, Manual for planning of Irrigation and Drainage Pumping Stations. Designer's Library Nr.68, Sofia: KIPP Vodproject internal issue, 1996. (in Bulgarian)

[3] Kotov L., Irrigation and Drainage Pumping Stations. Sofia: Tehnika, 1994, ch. 6. (in Bulgarian)

[4] * * *. Grundfos Data Booklet "NB, NBE, NK, NKE", (PDF format style). Available: http://net.grundfos.com/Appl/WebCAPS/

Study on energy efficiency optimization through technological rehabilitation in Mircea Voda pumping station in Dobrudja

Gheorghe Iordache[*], Marian Dordescu[*], Anca Constantin[**], Lucica Rosu[**], Valeriu Cusnerenco

Abstract **– The paper presents a study on the implications of some rehabilitation works, carried on in a water supply pumping station in the irrigation system, over their energy efficiency. The case study looks at *Mircea Voda* pumping station from Mircea Voda irrigation system of Carasu Complex – Dobrudja, Romania. By this application, it is substantiated that, through minor works, with no significant changes to the main hydro-mechanical equipment of the station, but only by replacing the impellers of the existing pumps, significant energy savings and, consequently, financial savings can be obtained.**

Keywords **– energy efficiency, irrigation system, pumping station, rehabilitation**

1. INTRODUCTION

The irrigation water supply pumping station *Mircea Voda* is situated at the km 183 +720 on the left side of the channel Danube – Black Sea and absorbs the water from channel CA0 of Mircea Voda irrigation system.

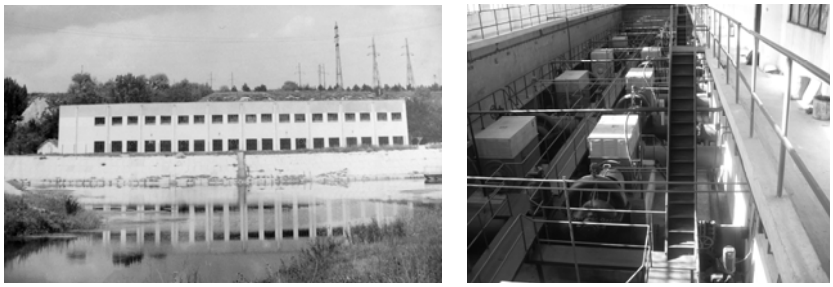

Fig. 1. Mircea Voda S.P. Baza pumping station –
View from the suction reservoir and from inside the station

Gh. Iordache is with the A.N.I.F. - R.A., Dobrogea Territorial Branch, Constanta, Str Zburatorului nr. 4, 900419-Constanta, Romania; e-mail: goguiord@yahoo.com).

A. Constantin is with Ovidius University of Constanta, Bd. Mamaia nr. 124, 900527-Constanta, Romania (e-mail: anca.constantin@ymail.com).

M. Dordescu is with the A.N.I.F. - R.A., Dobrogea Territorial Branch, Constanta, Str Zburatorului nr. 4, 900419-Constanta, Romania; e-mail: dordescu@yahoo.com).

L. Rosu is with Ovidius University of Constanta, Bd. Mamaia nr. 124, 900527-Constanta, Romania (e-mail: lucirosu@yahoo.fr).

ISSN-1584-5990

Currently, the pumping station (**Fig. 1.**) is served by 14 electro pumps type 24 NDS with Ø 950 mm rotors, each with a discharge of 1.8 m^3/s (6480 m^3/h), at a pumping head of 65 mCA, driven by asynchronous electric motors of 1600 kW in power with the rotation speed of 750 rpm, powered at 6 kV of electromotive force. Each pump sucks water from the suction reservoir through a pipe with the diameter Dn 1200 mm. The pumping station discharges water through two metal pipelines with Dn 1900 mm, and 1150 m in length.

The solution to the rehabilitation of the pumping station is relatively simple and it consists in the replacement of the Ø 950 mm impellers in 12 of the 14 existing pumps, type 24 NDS, with new Ø 1000 mm impellers. The other two pumps type 24 NDS will keep the existing Ø 950 mm impellers, but will be fitted out with frequency converters, which will allow them to function with variable rotational speeds, necessary for the supply of low discharges in frequent situations in the exploitation of irrigation facilities.

The main characteristics of *Mircea Voda* pumping station, calculated and analyzed in view of the optimization of energy efficiency, are:

- Station energy balance: energy efficiency; electric power consumption;
- Specific consumption of electric power.

2. DESCRIPTION OF THE THEORETICAL MODEL

2.1. Pumping energy efficiency

It is known that pumping energy efficiency can be determined with a relation of the following type:

$$\eta = \frac{P_h}{P_a} \tag{1}$$

with the meaning of the terms:

P_h [kW] – hydraulic power generated by the pumping unit;

P_a [kW] – the absorbed power of the electromotor.

The hydraulic power generated by the pumping unit is calculated with the relation:

$$P_h = \rho \cdot g \cdot H \cdot Q \tag{2}$$

in which:

ρ [kg/m³] – water density;

g [m/s²] – gravitational acceleration;

H [m] – pumping height;

Q [m³/s] –discharge.

The absorbed power of the electromotor (in the electric network), P_a, relative to the efficiency of the pump and of the electromotor, may be written as:

$$P_a = \frac{\gamma \cdot Q \cdot H}{\eta} = \frac{\gamma \cdot Q \cdot H}{\eta_p \cdot \eta_e \cdot \eta_c} \tag{3}$$

where:

γ [N/m³] – the specific weight of water, γ =9810 N/m³;

η_p [-] – efficiency of the pump;

η_e [-] – efficiency of the electromotor;

η_c [-]- coupling efficiency.

2.2. The consumption of electric power

The consumption of electric power, E_c [Wh], is calculated with the relation:

$$E_c = \frac{\gamma \cdot V \cdot H}{3600 \cdot \eta_p \cdot \eta_m \cdot \eta_c} \tag{4}$$

where:
V [m^3] -the volume of water pumped in 1h;
H [m] -pumping head;
η_p[-] - efficiency of the pump;
η_m [-]- efficiency of the electromotor .

2.3. The specific consumption of electric power

The specific consumption of electric power, C_e [Wh/m^3], calculated for one unit volume of pumped water, V=1 m^3, is:

$$C_e = \frac{\gamma \cdot 1 \cdot H}{3600 \cdot \eta_p \cdot \eta_m \cdot \eta_c}, \tag{5}$$

and for a volume V=1000 m^3 of pumped water (the most frequent way of expression for water volume used in irrigation systems due to the values are of the order of millions or billions of m^3 of water), from (5) an identical relation is obtained, but expressed in kWh/1000m^3:

$$\mathrm{C_e} = 2.723 \cdot \frac{\mathrm{H}}{\eta_\mathrm{p} \cdot \eta_\mathrm{m} \cdot \eta_\mathrm{c}} \tag{6}$$

(where, the coefficient *2.723* results from the transformation $\frac{\gamma}{3600} = \frac{9810\, N/m^3}{3600\, s} = 2.723$).

The difference between the specific consumption of electric power in the *proposed version,* C_{e_2}, in relation to the *existing situation,* C_{e_1}, will be:

$$D_{Ce} \text{ [kWh/1000m}^3\text{]} = C_{e_1} - C_{e_2} \tag{7}$$

2.4. The saving of electric power realized, by comparing the two analyzed variants, is**:**

$$E \text{ [kWh]} = D_{Ce} \cdot V_{total} \tag{8}$$

where:
V_{total} [m^3] – the volumes of pumped water, determined with the relation:

$$V = n \cdot Q \cdot T \tag{9}$$

n [pieces] – number of functioning pumps;

Q [m^3/s] – the pumped water discharge;

T [h] – the duration of functioning of the pumps.

3. RESULTS AND SIGNIFICANCES

3.1. Pumping station energy balance in the existing situation

In the existing situation, from the analysis of the characteristic curves of the pumps type 24 NDS-impellerΦ950 mm (**Fig. 2**), results that they function in the domain comprised between:

- the minimum manometric head, $H_{m.min}$=56m, with the discharge Q=2,1m³/s=7560m³/h and,
- the maximum manometric head, $H_{m.max}$ = 65m, with the discharge Q=1,8m³/s=6480m³/h.

For the maximum manometric pumping head, H_{mmax}=65m, from the characteristic curves of the pump results the pump's efficiency η_p =0.83, for the efficiency of the electromotor η_e =0.96. We assumed the coupling efficiency is included in η_e.

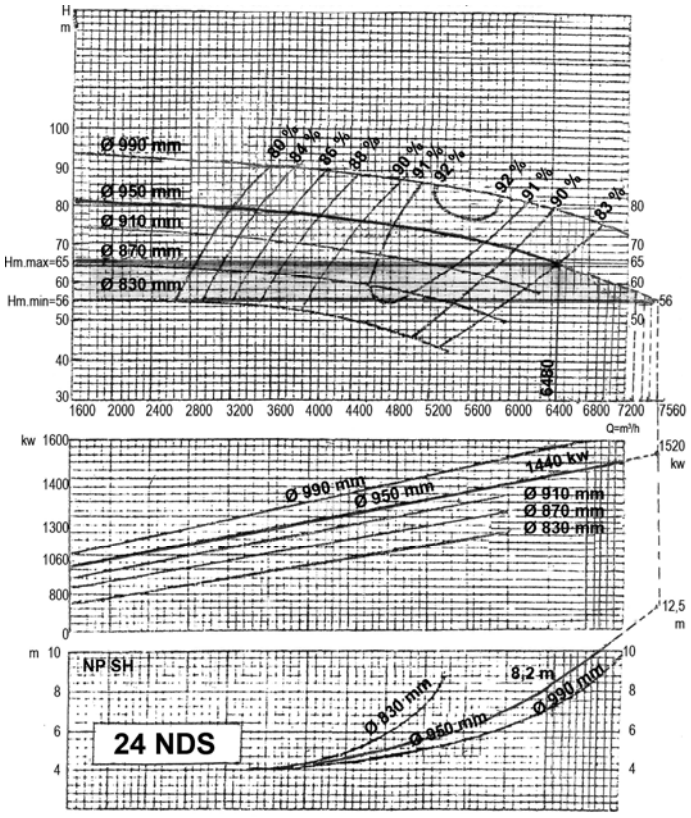

Fig. 2 – The characteristic curves of the pump type 24 NDS, impeller Φ 950 mm, in the existing situation

a) The absorbed power of the electromotor, in function of the efficiency of the pump and of the electric motor, calculated according to (3) is:

- For the maximum manometric pumping head, H_{mmax}=65m,

$$P_a = \frac{9810 \cdot 1.8 \cdot 65}{0.83 \cdot 0.96} \quad \Rightarrow \quad Pa = 1440 \text{ kW}$$

- For the minimum manometric pumping head**,** $H_{m.min}$= 56m,

$$P_a = \frac{9810 \cdot 2.10 \cdot 56}{0.79 \cdot 0.96} \Rightarrow P_a = 1520 \text{ kW}$$

b) The hydraulic power generated by the pumping unit calculated according to relation (3) for the two manometric heights, has the following values:

- for $H_{m.max}$ = 65 m:

$$P_{h1} = 1000 \cdot 9.81 \cdot 65 \cdot 1.80 = 1148\, kW$$

- for $H_{m.min}$ = 56 m

$$P_{h2} = 1000 \cdot 9.81 \cdot 56 \cdot 2.10 = 1154\, kW$$

c) The energy pumping efficiency, calculated according to (1) is:

- for $H_{m.max}$ = 65 m: $\eta = \frac{P_{h1}}{P_a} = \frac{1148}{1140} = 0.797$ =79,7%

- for $H_{m.min}$ = 56 m: $\eta = \frac{P_{h2}}{P_a} = \frac{1154}{1520} = 0.759$ =75,9%

d) The specific consumption of electric power, C_e [kWh /1000 m³], determined according to relation (6) was the result:

$$C_{e_1} = \frac{2.723 \cdot 59.8}{0.78 \cdot 0.96 \cdot 0.98} = 222 \text{ kWh /1000 m}^3$$

3.2. Pumping station energy balance in the proposed solution

For the operating domain of the pumps with the *maximum manometric head* H_m=65m and the *discharge* Q=6,480-6,500 m³/h the pump type 24NDS 800-600-1000 was chosen, with *new Ø 1000 mm impeller*. From the analysis of the characteristic curves of pump type 24 NDS, impeller Φ 1000mm (**Fig. 3**), results that it functions in the domain comprised between:

- the maximum manometric head*,* $H_{m.max}$ = 65 m, with the discharge Q=1.8m³/s=6480 m³/h;
- the minimum manometric head, $H_{m.min}$=56m , with the discharge Q=2.1m³/s=7560 m³/h**.**

In this variant, from the characteristic curves of the pump, for the maximum manometric pumping head, $H_{m.max}$ = 65m results: a pump *efficiency* η_p=0.90 while the efficiency of the electromotor ηe = 0.96.

a) The absorbed power of the electromotor, in function of the efficiency of the pump and of the electric motor, calculated according to relation (3) is:

- For the maximum manometric pumping head, H_{mmax}=65m,

$$P_a = \frac{9810 \cdot 1.80 \cdot 65}{0.90 \cdot 0.96} \cdot \Rightarrow P_a = 1328 \text{ kW}$$

- For the minimum manometric pumping head**,** $H_{m.min}$= 56m,

$$P_a = \frac{9810 \cdot 2.10 \cdot 56}{0.83 \cdot 0.96} \Rightarrow P_a = 1447 \text{ kW}$$

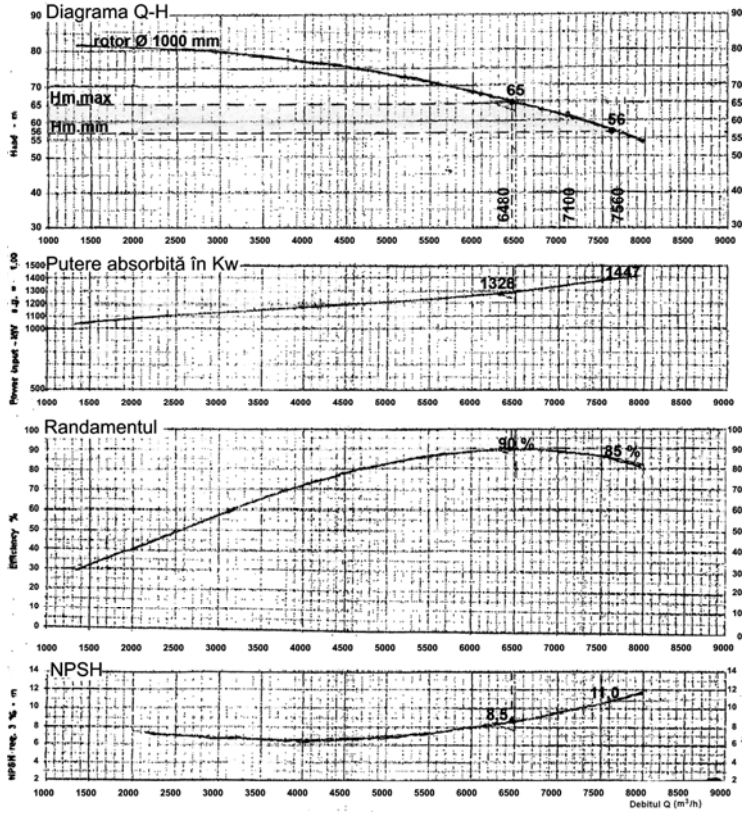

Fig. 3 – The characteristic curves of the pump type
24 NDS, impeller Φ 1000 mm, in the proposed solution

b) The hydraulic power generated by the pumping unit stays at the same values in the proposed variant because the value of the efficiency, for a certain manometric head, does not intervene in the calculations: $P_{h1} = 1148\,kW$, for $H_{m.max}$ = 65 m and $P_{h2} = 1154\,kW$, for $H_{m.min}$ = 56 m.

c) The energetic pumping efficiency, calculated according to (1) is:

for $H_{m.max}$ = 65 m: $\eta = \frac{P_{h1}}{P_a} = \frac{1148}{1328} = 0.865 = 86{,}5\%$

for $H_{m.min}$ = 56 m: $\eta = \frac{P_{h2}}{P_a} = \frac{1154}{1447} = 0.798 = 79{,}8\%$

d) The specific consumption of electric power, C_e [kWh /1000 m³], determined according to relation (6) resulted:

$$C_{e_2} = \frac{2{,}723 \cdot 59.8}{0.87 \cdot 0.96 \cdot 0.98} = 199 \text{ kWh /1000 m}^3$$

3.3. The comparative analysis, in the two analyzed situations, of the energy efficiency of Mircea Voda pumping station

a) The specific consumption of electric power

From the view point of the specific consumption of electric power, the difference between the specific consumption of electric power in the proposed variant (the values obtained under 3.2.d) compared to the existing situation (the values obtained under 3.1.d) is:

D_{Ce} [kWh/1000m^3] = $C_{e_1} - C_{e_2}$ = 23 kWh/1000 m³

This difference is in favour of the proposed variant, which emphasizes the fact that even from the point of view of the specific power consumption, the proposed solution is incomparably better than the existing situation.

b) The electric power consumption

In order to emphasize the electric power consumption, an example of calculation is presented, based on real data, from the records RAIF Constanta (the administrator of Carasu irrigation system), on the number of operating hours of the pumps type 24NDS, for a period of two years, 1998 and 1999, where the following recorded:

- *in the year 1998* functioned:
  - one pump at a time, with a total of 500 h;
  - 3 pumps at a time, with a total of 2600 h;
  - 4 pumps at a time, with a total of 2000 h.
- *in the year 1999* functioned:
  - one pump at a time, with a total of 300 h;
  - 3 pumps at a time, with a total of 1100 h;
  - 4 pumps at a time, with a total of 1500 h.

According to the data from the diagrams of the pump, at *medium pumping levels*, with the corresponding discharges, the following *manometric heads* H_m resulted:

- for 1 pump: H_{m_1} = 57.45 m and Q_1 = 7360m³/h (per pump);
- for 3 pumps H_{m_3} = 58.43 m and Q_3 = 7280 m³/h (per pump);
- for 4 pumps H_{m_4} = 59.,81 m and Q_4 = 7200 m³/h (per pump).

The values for the pumped water volumes, for the analyzed situations, (in the year 1998 and, 1999 respectively), were calculated with (9) (**Table 1.**):

Table. 1. - The volumes of pumped water in Mircea Voda pumping station

***n* [pieces]**	***Q* [m³/s]**	**1998**		**1999**	
		***T* [h]**	***V* [m³]**	***T* [h]**	***V* [m³]**
0	1	2	3	5	6
1 piece	7360	500	3 860 000	300	2 214 000
3 pieces	7280	2600	56 807 400	1100	23 760 000
4 pieces	7200	2000	57 600 000	1500	43 200 000
			V_{total} = 118 267 400		V_{total} = 69 174 000

The electric power saving, calculated by use of (8), for the years 1998 and 1999, shows substantial electric power savings, *greatly in favour of the solution proposed for the rehabilitation of the pumping*:

- in the year 1998: E = 23 kWh/1000m³ · 118 267 400 m³ = 2 720 150 kWh;
- in the year 1999: E = 23 kWh/1000m³ · 69 174 000 m³ = 1 591 002 kWh.

4. CONCLUSIONS

From the analysis of the data regarding the implications of some relatively simple solutions and with minimum investments (in the case study, the replacement of the existing impellers of the pumps) over the energy efficiency of the pumping station, we may conclude:

a) the pumping energy efficiency, in the solution proposed for the rehabilitation of Mircea Voda irrigation water supply pumping station, is incomparably superior to the current situation: for $H_{m.max}$ = 65 m, the efficiency rises to η = 86.5%, from η = 79.7%, and for $H_{m.min}$ = 56m, the efficiency rises to η = 79.8%, from η = 75.9%;

b) the difference, in favour of the proposed variant, between the specific electric power consumption in the proposed variant, in comparison to the current situation, is considerable: D_{C_e} =23kWh/1000m³;

c) due to the fact that the volumes of pumped water in an irrigation system are of the order of millions or billions of m³ of water a year, significant electric power savings are obtained. The given example reveals substantial electric power savings, greatly in favour of the solution proposed for the rehabilitation of the pumping station: 2 720 150 kWh (for the data of the year 1998), 1 591 002 kWh respectively (for the data of the year 1999).

5. REFERENCES

[1] Bartha, I., Javgureanu, V., Marcoie, N., *Hidraulica*, vol.II, Ed. Performantica, Iasi, 2004

[2] Giusca Radu Ioan, *Contribtii la optimizarea statiilor de pompare din cadrul amenajarilor de imbunatatiri funciare*, doctoral thesis, IANB, Faculty of Land Improvement, Bucharest, 1990

[3] Nicolaescu, Ion, *Bazele modernizarii sistemelor de irigatii in Romania*, Part II. Hidrotehnica Journal, 10/1993, Bucharest, 1993.

[4] Solomon Kenneth H., *Irrigation Systems and Water Application Efficiencies*, California State University, Fresno, Center for Irrigation Technology, 1988.

[5] Vermillion, D.L., *The emerging governance paradigm for irrigation management and development*, Int. J. Wat. Pol. Prac., 2003

[6] Weddington J., Canessa P., *Diesel Pumping Efficiency Program* - FINAL PROJECT REPORT, California State University Fresno, Center for Irrigation Technology, 2006

The results of drainage studies accomplished in Caras-Severin County

Man Teodor Eugen, Constantinescu Laura, Halbac-Cotoara-Zamfir Rares, Buran Claudia

***Abstract* – This paper presents the results of the drainage study made for the main types of soils with excess moisture in the Greoni-Ticvanu Mare area, Caras-Severin County. Also, the paper presents maps of agricultural potential of Caras-Severin County, soils map, map of land and improvement works in the county and map areas with excess water. Based on the pedological study and laboratory experiments to determine hydraulic characteristics of some kinds of drainage – according to the methodology known in technical literature – were established optimal economic and technical solutions recommended for the area taken in study.**

***Keywords* – drainage pipe, drainage study, filter material, horizontal drainage, silting degree**

1. INTRODUCTION

The establishment of optimum drainage solution for a specific type of soil requests a very good knowledge of the factors which determine drainage solution as are: drainage specific flow, drainage rate, soil's hydraulic conductivity, geometrical and hydraulically parameters of drain tube and of filtering material, the execution technology.

On the base of this data and on the base of technical-economical calculations we can establish the drainage solution and the distance between drains.

Belong the technical conditions, in the process of establishing the drainage solution, we must also take into account and a reduce consume of low valuable materials, a reduce consume of energy and fuels, a low consume of labor force, security in long time maintaining and exploitation, the utilization with priority of local materials and of some industrial wastes.

The drainage study, presented in this paper, was realized in Caras-Severin County. This is located in south-western Romania having a total surface of 851.794 ha, which represents 3.6% from national territory and place the county on top 3 in the hierarchy of Romania's counties. The agricultural surface represents 47% from the total surface of Caras-Severin County (fig. 1).

The main types of soils from Caras-Severin County are: luvosoil, entricombosoil, districombosoil, aluviosoil, vertosoil and preluvosoil (fig. 2). Analyzing the possibility to integrate the fields in quality classes, we can present the following situation (table 1):

M. T. E. Author is with "Politehnica" University of Timisoara, Hydrotechnical Engineering Faculty, 1A George Enescu Street, 300022-Timisoara, Romania (corresponding author to provide phone: +40-256-404084; fax: +40-256-404083; e-mail: eugentman@gmail.com).

L. C. Author is is with "Politehnica" University of Timisoara, Hydrotechnical Engineering Faculty, 1A George Enescu Street, 300022-Timisoara, Romania (e-mail: lauraconstantinescu_m@yahoo.com).

H. C. Z. R. Author is "Politehnica" University of Timisoara, Hydrotechnical Engineering Faculty, 1A George Enescu Street, 300022-Timisoara, Romania (e-mail: raresh_81@yahoo.com).

B.C. Author is "Politehnica" University of Timisoara, Hydrotechnical Engineering Faculty, 1A George Enescu Street, 300022-Timisoara, Romania

ISSN-1584-5990

Table 1. Quality classes of soils from Caras-Severin County [9]

Land use category	Surface	Quality class									
		I.		II.		III.		IV.		V.	
		S[ha]	NP	S [ha]	NP	S [ha]	NP	S [ha]	NP	S [ha]	NP
Arable	127.153	1232	81	14122	67	42929	50	45720	33	23150	15
Hays and pastures	257.684	8509	86	32559	70	103184	52	61279	35	52153	17
Plantation of vines	771	11	86	103	67	519	51	118	26	20	15
Orchards	11724	62	81	1244	65	3857	49	3963	33	2590	16

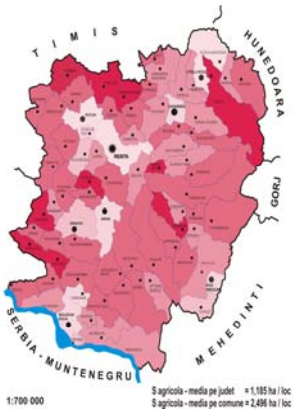

Fig. 1 Agricultural potential of Caras-Severin County [9]

Fig. 2 Soils map of Caras-Severin County [9]

Fig. 3 Areas with land reclamation and improvement works (blue areas are representing the communes with drainage arrangements while the areas with vertical lines are representing areas with surface drainage arrangements) [9]

We can conclude that the majority of agricultural fields, from the fertility class point of view, can be integrated in the III, IV and V classes.

The arranging potential with land reclamation and improvement works of Caras-Severin County's lands is:

- the arranging potential with surface drainage works covers 121.800 ha from which: 84.900 ha arable lands, 33.500 ha pastures and hays, 300 vines plantations, 3.100 ha orchards;
- the arranging potential with soil erosion control works covers 250.900 ha from which 45.600 ha arable lands, 193.200 ha pastures and hays, 800 vines plantations, 10.400 ha orchards;
- the arranging potential with dams works covers 28.800 ha. [9]

Actually, Caras-Severin County disposes of 28.637 ha with surface-drainage arrangements (23,5% from the arranging potential) and 43.910 ha with soil erosion control works (17,54% from the arranging potential). [9]

The land reclamation and improvement works were design and realized on hydrographic basins and sub-basins, in correlation with regularization works and dam works of the rivers which are crossing the county (fig. 3).

2. EXPERIMENT DESCRIPTION

The lab studies realized for Caras drainage arrangement, left bank, Greoni-Ticvanu Mare area, Caras-Severin county, comprise the following:

- a pedological study of soil in 3 points;
- silting degree study realized on stands with horizontal drains;
- calculation of distance between drains on the base of experimental lab studies.

Pedological studies are referring to soil texture, hydraulic conductivity determined in situ or in laboratory, stability indicator of mol drains, plasticity indicator and micro-structural indicator. These determinations were realized according to the Elaboration Methodology of Pedological Studies of ICPA Bucharest [1]. The studies and experimental researches for the determination of drain tubes, filtering materials and drain tubes with filtering material complexes hydraulic characteristics are referring to the determination of hydraulic resistance coefficient at water entrance in drains without filters or in drain tubes with filtering material complexes and at the determination of silting degree of drain tubes with filters. These laboratory experiments were realized according to the methodology known from technical literature [2] and were realized on vertical stands comprising drain tubes without filters or with various complexes of drain tubes with different filtering materials [2]. On horizontal stand were determined the silting degree, in time, of drain tube without filter or of the drains with filtering material complex and respective of hydraulic efficiency coefficient.

3. RESULTS AND SIGNIFICANCES

The pedological study is referring to 3 study points established by the beneficiary:
Probe 1: Ticvanu Mare
Probe 2: Fishery
Probe 3: Hays

Table 2. Soils physical properties [2]

No	Sample place	Texture	Hydraulic conductivity (m/day)	Mol drain indicator/ exploitation period	Micro-structural indicator	Plasticity indicator
1	Ticvanu Mare	Sandy-clay	1,99	0,09/ 1-2 months	0,88 unstable soil	18,48 unstable soil
2	Fishery	Dusty-sandy-clay	0,29	0,33/ 4 months – 1 year	0,52 insufficient stable soil	32,8 stable soil
3	Hays	clay	0,07	0,46/ 2 – 3 years	0,28 stable soil	58,76 stable soil

Table 3.

Graph 1 – Evolution in time of drained flows for tested variants from Ticvanu Mare area (fig. 4)				
Stand no.	Area and type of soil	Filtering material	Drain tube	q_i (l/min/ml) (initial flow)
1	Ticvanu Mare luvosoil	No filter	DPE Ø = 80 mm	1,204
2	Ticvanu Mare luvosoil	filter of polypropylene used bags enfolded on drain tube	DPE Ø = 80 mm	2,96
3	Ticvanu Mare luvosoil	Terasin filter enfolded on drain tube	DPE Ø = 80 mm	1,5

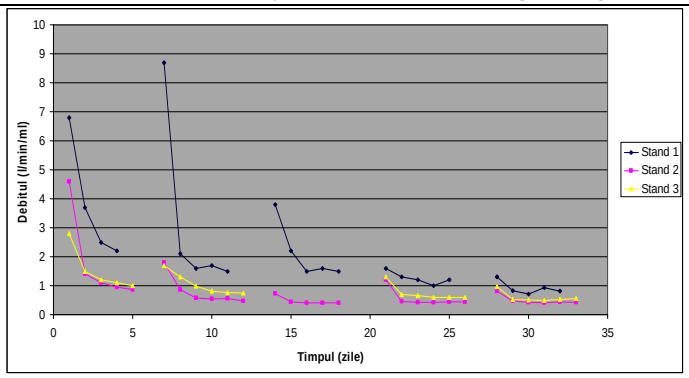

Fig. 4 [8]

The experimental results regarding the establishment of silting degree of drain tubes with different filtering materials complexes for Caras soil, left bank, Greoni – Ticvanu Mare area, Caras-Severin county involved the following tested variants:

Probe 1: Ticvanu Mare: Plastic drain of polyethylene (P.D.P) Ø 80 mm without filter, P.D.P. Ø 80 mm with filter of polypropylene used bags enfolded on drain tube, P.D.P. Ø 80 mm with Terasin filter enfolded on drain tube,

Probe 2: Fishery: P.D.P. Ø 80 mm with filter of polypropylene used bags enfolded on drain tube, P.D.P. Ø 80 mm with Terasin filter enfolded on drain tube

Probe 3: Hays: P.D.P. Ø 80 mm without filter, P.D.P. Ø 80 mm with filter of polypropylene used bags enfolded on drain tube

Daily experimental measures, realized for 33 days, with functioning periods without water of 2 days after each week, regarding the evolution in time of drain flows were graphical represented (tab. 3, 4, 5 and fig. 4, 5, 6):

Table 4.

Graph 2 – Evolution in time of drained flows for tested variants from Fishery area (fig. 5)				
Stand no.	Area and type of soil	Filtering material	Drain tube	q_i (l/min/ml) (initial flow)
4	Fishery Alluviosoil	filter of polypropylene used bags enfolded on drain tube	DPE Ø = 80 mm	4,65
5	Fishery Alluviosoil	Terasin filter enfolded on drain tube	DPE Ø = 80 mm	6,75

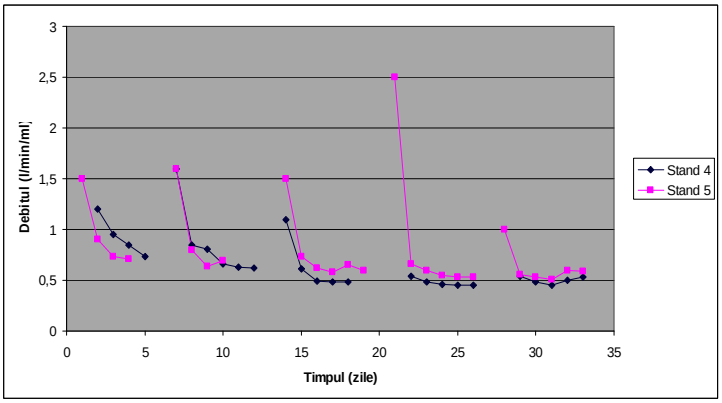

Fig. 5 [8]

According to the graphs 1, 2 and 3 and figures 4, 5 and 6 were realized the enfolded lines of flows discharges in time for the tested variants [2, 8] from which resulted the final flows determined after the silting process (q_c). Basing on the experimental results, presented in previous figures, were established the values of initial flow (q_i), of the final flow after silting process (q_c) and the values of silting coefficient. The hydraulic parameters which are characterizing the silting degree, in time, of drain tube without filter and of the complex formed by drain tube with filter, for the 3 tested soil samples from Ticvanu Mare area, presents a very favorable effect of filter of polypropylene used bags enfolded on drain tube and a good to a very good effect of Terasin filter. For establishing the final drainage solution for this arrangement, these results must be completed and corroborated with the results determined from the calculation of distance between drains which will decide the technical-economical solution according to the following tables (tables 5, 6 and 7):

Table 5.

Graph 3 – Evolution in time of drained flows for tested variants from Hays area (fig. 6)				
Stand no.	Area and type of soil	Filtering material	Drain tube	q_i (l/min/ml) (initial flow)
6	Hays Stagnogley preluvosoil	Without filter	DPE Ø = 80 mm	2,632
7	Hays Stagnogley preluvosoil	filter of polypropylene used bags enfolded on drain tube	DPE Ø = 80 mm	4,24

Table 6. The hydraulic parameters which are characterizing the silting degree of drain with and without filter complexes, for 3 tested soil samples from Ticvanu Mare area, Caras-Severin County [2]

Soil type and area	**Drain tube and filtering material**	**Drained flow (l/min/s)**		**Silting coeff. η_c**	**K_{sol} (m/ day)**	**Permeability coefficient (m/day)**		**Coeff. of hydraulic efficiency Ceh**
		q_i	**q_c**			**Kfi**	**Kfc**	
P1 – Ticvanu Mare, Stand 1, luvosoil	D.P.E. Ø 80 mm no filter	1,20	0,22	5,5	1,99	-	-	-
P1 – Ticvanu Mare, Stand 2, luvosoil	D.P.E. Ø 80 mm with filter of polypropylene used bags	2,96	0,55	5,4	1,99	246,4	45,6	22,9
P1 – Ticvanu Mare, Stand 3, luvosoil	D.P.E. Ø 80 mm with Terasin filter	1,5	0,52	2,9	1,99	33,5	11,55	5,80
P2 – Fishery Stand 4, aluviosoil	D.P.E. Ø 80 mm with filter of polypropylene used bags	4,65	0,50	9,3	0,29	246,4	26,5	91,4
P2 – Fishery Stand 5, aluviosoil	D.P.E. Ø 80 mm with Terasin filter	6,75	0,51	13,2	0,29	33,5	2,53	8,72
P3 – Hays, Stand 6, stagnogley preluvosoil	D.P.E. Ø 80 mm no filter	2,63	0,23	11,7	0,07	-	-	-
P3 – Hays, Stand 7, stagnogley preluvosoil	D.P.E. Ø 80 mm with filter of polypropylene used bags	4,24	0,42	10,1	0,07	246,4	24,4	348,5

Table 7. Geometrical elements of drains tubes used for Caras-Severin drainage arrangements [2]

Zone	Types of filtering material	Drain tube	Geometrical elements of drain tube (cm)					
			d_o	d_f	B	n	b	ℓ
Ticvanu Mare	filter of polypropylene used bags δ= 0,6 cm	Plastic	5 6,5 8	6,2 7,7 9,2	1,1 1,1 1,2	6 6 6	0,5 0,5 0,5	0,1 0,1 0,1
		Ceramic	7/9	10,2	33	-	-	0,1
	No filter	Plastic	5 6,5 8	5 6,5 8	1,1 1,1 1,2	6 6 6	0,5 0,5 0,5	0,1 0,1 0,1
		Ceramic	7/9	9	33	-	-	0,1
	Terasin δ =0,4 cm	Plastic	5 6,5 8	5,8 7,3 8,6	1,1 1,1 1,2	6 6 6	0,5 0,5 0,5	0,1 0,1 0,1
		Ceramic	7/9	9,8	33	-	-	0,1
Fishery	filter of polypropylene used bags δ= 0,6 cm	Plastic	5 6,5 8	6,2 7,7 9,2	1,1 1,1 1,2	6 6 6	0,5 0,5 0,5	0,1 0,1 0,1
		Ceramic	7/9	10,2	33	-	-	0,1
	Terasin δ =0,4 cm	Plastic	5 6,5 8	5,8 7,3 8,8	1,1 1,1 1,2	6 6 6	0,5 0,5 0,5	0,1 0,1 0,1
		Ceramic	7/9	9,8	33	-	-	0,1
Hays	filter of polypropylene used bags δ= 0,6 cm	Plastic	5 6,5 8	6,2 7,7 9,2	1,1 1,1 1,2	6 6 6	0,5 0,5 0,5	0,1 0,1 0,1
		Ceramic	7/9	10,2	33	-	-	0,1
	No filter	Plastic	5 6,5 8	5 6,5 8	1,1 1,1 1,2	6 6 6	0,5 0,5 0,5	0,1 0,1 0,1
		Ceramic	7/9	9	33	-	-	0,1

Table 8. The results of calculations of distances between drains for Caras-Severin County [2, 8]

Zone and type of soil	Types of filtering material	Drain tube	Hydraulic conductivity (m/day)		ς_i (ς_{if})	q mm / day	H m	Z m	h m	Cost unit. Lei/ km	Dist between drains l/m	Spec. Inv. lei/ha *
			K_{fc}	K_{sol}								
Ticvanu Mare luvos oil	filter of polypropylene used bags δ= 0,6 cm	Plastic	45,62 45,62 45,62	1,99 1,99 1,99	- ,481 -0,451 -0,448	7 7 7	3 3 3	0,8 0,8 0,8	0,6 0,6 0,6	16800 18300 20900	44 44,5 45	3814 4113 4658
		Ceramic	45,62	1,99	1,205	7	3	0,8	0,6	18500	45	4103
	No filter	Plastic	- - -	1,99 1,99 1,99	0,507 0,532 0,607	7 7 7	3 3 3	0,8 0,8 0,8	0,6 0,6 0,6	16700 17500 19900	44 44 45	3830 3987 4464
		Ceramic	-	1,99	3,973	7	3	0,8	0,6	18400	45	4105
	Terasin δ =0,4 cm	Plastic	11,55 11,55 11,55	1,99 1,99 1,99	-0,204 -0,184 -0,161	7 7 7	3 3 3	0,8 0,8 0,8	0,6 0,6 0,6	20100 20900 22800	44 44 45	4578 4709 5092
		Ceramic	11,55	1,99	1,765	7	3	0,8	0,6	21300	45	4733

Zone and type of soil	Types of filtering material	Drain tube	Hydraulic conductivity (m/day)		ς_i (ς_{if})	q mm / day	H m	Z m	h m	Cost unit. Lei/ km	Dist between drains l/m	Spec. Inv. lei/ha *
			K_{fc}	K_{sol}								
Fishery aluvio soil	filter of polypropylene used bags δ= 0,6 cm	Plastic	26,49	0,29	-0,515	7	3	0,8	0,6	16800	13	12690
			26,49	0,29	-0,495	7	3	0,8	0,6	18300	14	13474
			26,49	0,29	-0,484	7	3	0,8	0,6	20900	14	15063
		Ceramic	26,49	0,29	1,111	7	3	0,8	0,6	18500	14	13171
	Terasin δ =0,4 cm	Plastic	2,53	0,29	-0,254	7	3	0,8	0,6	20100	13	15302
			2,53	0,29	-0,234	7	3	0,8	0,6	20900	13,5	15486
			2,53	0,29	-0,215	7	3	0,8	0,6	22800	14	16522
		Ceramic	2,53	0,29	1,610	7	3	0,8	0,6	21300	14	15237
Hays Stagnogley preluvosoil	filter of polypropylene used bags δ= 0,6 cm	Plastic	24,39	0,07	-0,524	7	3	0,8	0,6	16800	4	38767
			24,39	0,07	-0,503	7	3	0,8	0,6	18300	5	40353
			24,39	0,07	-0,493	7	3	0,8	0,6	20900	5	44347
		Ceramic	24,39	0,07	1,087	7	3	0,8	0,6	18500	3	38373
	No filter	Plastic	-	0,07	0,507	7	3	0,8	0,6	16700	4	40283
			-	0,07	0,532	7	3	0,8	0,6	17500	4	40126
			-	0,07	0,607	7	3	0,8	0,6	19900	5	43523
		Ceramic	-	0,07	3,973	7	3	0,8	0,6	18400	5	39230

4. CONCLUSIONS

In the area of point no. 1, Ticvanu Mare, we are proposing a classic drainage with drain tubes at a distance of 44-45 m between them as function of used filtering material or without filter solution. In the other two points, Fishery and Hays, it can be adopted only the crossed drainage solution with respect for the distances between mole drains and tube drains. A special attention must be granted to the drain tubes with IFS or with a geotextil and the realization of a filtering trench with specific granular material in order to realize the hydraulic connection with the loosened soil and mole drains according to the normative. From the pedological studies it results that for Fishery and Hays areas, the deep loosened and mole drainage will be realized in every year until will be obtained the productions foreseen in project. The drainage effectiveness depends on the correct selection of filtering material, resulting that its nature and composition must be correlated with the soil conditions, water table, climate and drain tube characteristics. In the design process of drainage network must be foresees the study, analysis and testing of different filtering materials for the zone, type of soil and respective drainage situation, the analysis being realized as function of the following criterions: hydraulic, price, available quantities, available technologies, durability in time and other specific criterions of filtering materials. According to these criterions, the filtering materials will be selected in order to have the lowest price and in the same time a price lower than the drain tube. Also, will be selected filtering materials which can be found in sufficient quantities in the respective area and the analysis of filtering materials pores must be in correlation with the grading curve of drained soils. As a final conclusion, after the realization of the mentioned drainage study, were obtained optimum solutions from technical and economical point of view for arranging the areas affected by humidity excess, being used adequate drain tubes and filtering materials for each arrangement in part.

5. REFERENCES

[1] Man T.E., *Studiul rezistenţelor hidraulice ale drenurilor agricole*, 1983, Teză doctorat IPTV Timişoara;
[2] xxx - Studiu de drenaj pentru judeţele Timiş, Arad, Bihor şi Caraş-Severin, Colectiv: A. Wehry, E.T. Man, M. Orlescu, Gh. Rogobete, Beneficiar: I.E.E.L.I.F. Timiş, Contract 27/10.02.1986, Valoare 300000 lei;
[3] Bodog M.F., Interacţiunea irigaţii-drenaj şi impactul acestora asupra mediului din bazinul Crişurilor, Teză de doctorat, UP Timişoara, 2007;
[4] Stoica F., Studii de drenaj pentru stabilirea solutiilor tehnico-economice eficiente de amenajare a terenurilor cu exces de umiditate, Teza de doctorat, UPT, 2001;
[5] Wehry A., David I., Man T.E., 1982, Probleme actuale în tehnica drenajului, Ed. Facla, Timişoara;
[6] Man T.E., Wehry A., David I., Popescu F., Drainage Studies for Ground Arrangement Solutions of Soils with Humidity Excess from the Western Part of Romania (Timiş, Arad, Bihor, *Maramureş and Satu-Mare Counties),* International Drainage Symposium of ASAE Sheraton Grand Hotel & Sacramento Convention Center Sacramento USA, 21-24.03.2004, pp. 272 – 280;
[7] Man E.T., Halbac–Cotoara R., 2005, Metode clasice şi moderne de proiectare a amenajărilor de drenaje folosite în ţara noastră şi pe plan mondial, pag. 146 – 154, Buletinul Ştiinţific al Universităţii "Politehnica" Timişoara, Seria Hidrotehnica, Tom. 49 (63), Fasc. 1, ISSN 1224 – 6042, Ed. Politehnica;
[8] Halbac-Cotoara-Zamfir Rares, 2010, Studii de drenaj eficiente tehnico-economic pentru terenurile cu exces de umiditate, Teza de doctorat, manuscris.
[9] Planul de Amenajare Teritorială al Judeţului Caraş-Severin, Proiect nr. 97/4429/2003, SC Case SA Resita.

Ovidius University Annals Series: Civil Engineering Volume 1, Issue12, June 2010

A simple method for soil texture analyses

Al Shakarchi Sirwan, Ichinur Omer

Abstract **A simple method for soil texture analyses is used in Irak, especially for land characterization. Is a simplified version of the sedimentation method having the advantage of the work simplicity, no special equipement is require and is done in a short time .The disavantage of this method is unknowing result of the soil particles diameters.**

Keywords **– analyses, soil texture.**

1. INTRODUCTION

Ted Sammis method is very simple, not require too many devices, but it is important to check that the soil sample not have limestone ($CaCO_3$) and it is important to know the amount of clay, sand and silt, but we cannot find the diameter of each soil particules. Dry soil sample is placed in an container up to its half and 5 ml of Calgon is placed to separate soil particules. The content is mixed for 20 minutes and it is left to rest 40 minutes and after that the height of the sediment deposits is measured, which represent the sand content of the sample. The suspension remaining after 6 hours represent the silt content and than the clay content is calculated: 1 - (sand content + silt content). This method mentioned above, it wasn't applied in Romania before, but it is used in Iraq.

Five different soil samples was collected for soil texture analyses with this method.

2. EXPERIMENT DESCRIPTION

We used a glass container with a large mouth and we filled the glass container half full of soil (fig. 1).

Than we wet the soil to a mud consistency and tap the glass container to settle the soil.

Put 5ml calgon in the glass container to separate soil particles and add water to the top of the glass container and shake the soil water mix till the soil is all mixed up in the water.

Wait 6 hours and mark the level of the soil in the glass container. The difference between the bottom mark, which is the sand, and the second mark up is the silt portion of the soil.

Al Shakarchi Sirwan, engineer, PhD is with "Ovidius" University of Constanta, Bd. Mamaia nr. 124,

Ichinur Omer is with "Ovidius" University of Constanta, Bd. Mamaia nr. 124, 900356-Constanta, Romania (e-mail: ichinur.omer@univ-ovidius.ro).

ISSN-1584-5990

The total sand plus silt is the distance from the bottom of the glass container to the second mark.

The percent sand is the depth of the sand divided by the depth of the total soil

The percent silt is the depth of the silt divided by the depth of the total soil

The percent clay is 100 minus the percent sand plus silt.

3. RESULTS AND SIGNIFICANCES

To calculate the percent sand, silt and clay by measuring the depth of the soil by measuring the distance from the bottom to the first mark up in cm which is the sand fraction, the distance from the first mark up to the second mark up which is the silt fraction and the distance from the bottom to the third mark up from the bottom which is the sand plus silt plus clay fraction. Sometimes, when all the sand silt and clay has settled, the height of the soil is higher than when you marked the glass container after making a mud solution. This can only be determined by letting the glass container sit for several days.

For soil sand sample(fig. 2):

- height of glass container is 10 cm
- depth of soil sample in glass container is 5 cm
- The first reading after 40 seconds is 4.5 cm
- Second reading after 6 h is 0.4 cm

To obtain the sand, silt and clay percent the relations are:

Sand (%) =(first reading after 40 seconds / depth of soil sample)* 100

Silt (%)= { (Second reading after 6 h) / depth of soil sample }*100

Clay (%) =100-{ Sand (%)+Silt (%)}

To determine the soil texture knowing percent of sand, silt and clay we used USDA soil triangle.

Result of experiment for all soil samples by the Ted Sammis method is presented in Table nr.1

Table nr. 1. Result of experiment for all soil samples by the Ted Sammis method

Sample number	Clay	Silt	Sand
1	45%	50%	15%
2	40%	55%	5%
3	33.5%	52%	15.5%
4	34%	58%	8%
5	2.0	8%	90%

Fig. 1. Ted Sammis method - glass container with a large mouth(left) and filled half full with soil sample (right)

Fig 2. Ted Sammis method after 6 hours , The difference between the bottom mark, which is the sand, and the second mark up is the silt portion of the soil.

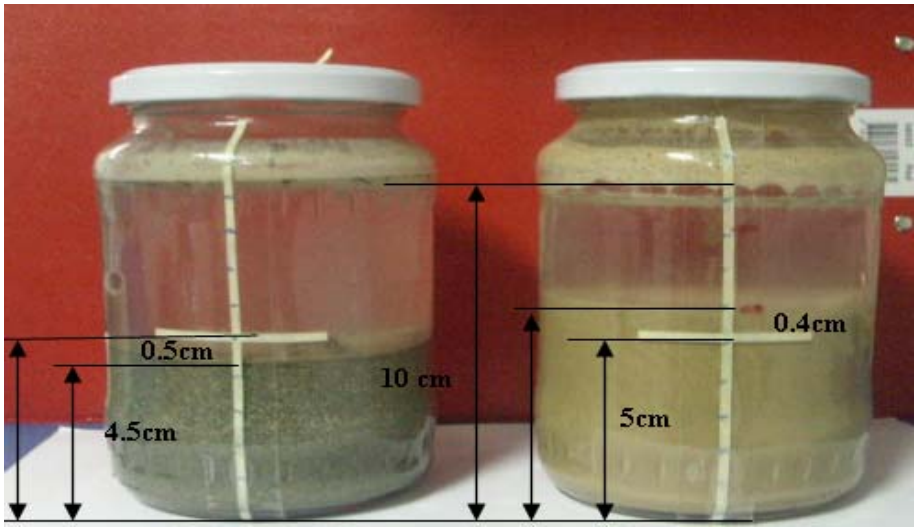

Fig 4. Ted Sammis method for 2 different soil samples: sand (right) and clay (left)

Table nr.2 Comparing the results between two soil texture analyses methods: Ted Sammis and Sedimentation method

Soil sample	Ted Sammis Method			Sedimentation method			Differences between methods		
	Clay	Silt	Sand	Clay	Silt	Sand	Clay	Silt	Sand
1	43%	46%	11 %	42%	45%	13%	1%	1%	2%
2	40%	55%	5%	38,4 %	51,4 %	10,2 %	1.6%	3.6%	5.2%
3	34%	52%	14 %	32,2 %	50,6 %	17,2 %	1.2%	1.4%	3.2%

4. CONCLUSIONS

For soil texture analysis we compare three methods: sieving method, sedimentation method and Ted Sammis method. Each of these methods has its specificity.

1. Sieving method is used to determine the soil texture analysis for sandy soil. If we use this method for the clay soil we didn't have the same results because the soil particule diameters of clay soil are very small and because the existence of organic matter. This method is more precise for sandy soil.

2. Ted Sammis method: This method is the simplest method, it does not require too many devices and can achieve results on the spot after 6 hours. But this method can not obtain the diameter of each soil particles in part as the sedimentation method, but can get the amount of each type of soil texture (clay soil, loam soil, and sandy soil). This method is used more for agricultural land.

3. Sedimentation method is the most accurate method for knowing the soil texture and soil particles diameters. This method is used for all soil types.

4. Using this method we obtained results for several soil types.

5. REFERENCES

[1] Ciurea C., Chirica A., *Geotehnica manual pentru lucrarile de laborator*, Ed. Ovidius University Press , 1999.
[2] Brown R.B., IFAS EXTENTION (soil texture), University of Florida ,
[3] Omer I., Arsenie D. I. , Buta C., Hidrogeologie, Ed. Ovidius University Press , 2008.
[4] Kharrufa D., *Irrigation and drainage (Irak and arab homeland)* , BAGDAD 1994.
[5] Abdulan. Al –Ani, *Elements of soil science*, University of Bagdad , 1980.
[6] Ted Sammis – *Soil texture analyses*, webmaster@weather.nmsu.edu, Mexico State University, 1996.

Experimental research on sloping land drainage

Al Shakarchi Sirwan, Ichinur Omer

***Abstract* – The paper considers the sloping land drainage in two variants: when slope has the same direction as the sense of infiltration (positive slope) or when slope has an opposite direction to infiltration sense (negative slope). The experimental box scheme used for this research is presented in this paper. It has expanded for the following slopes of 3%, 5%, 7%, 10% and 15%, having the same absolute value for negative slopes too. Seven soil types, starting from a sandy soil to a loamy soil were used. During experiments we have determined the adequate flow rates for stationary regimes, the time while the stationary regimes have been made and the piezometric curves respectively. The results are presented in tabular form.**

***Keywords* – sloping land drainage, experimental research.**

1. INTRODUCTION

Sloping land drainage may be in two ways: (1) - normally sloping drainage, when slope> 0, and (2) - backwards sloping drainage (slope <0). To obtain results from soil tests to sloping drainage in different directions (slope> 0, i.e. slope <0), a device (box) for sloping drainage at constant level was built. In nature this drainage system is specific to a river passing near a road, when the drainage system is intended lowering the groundwater.

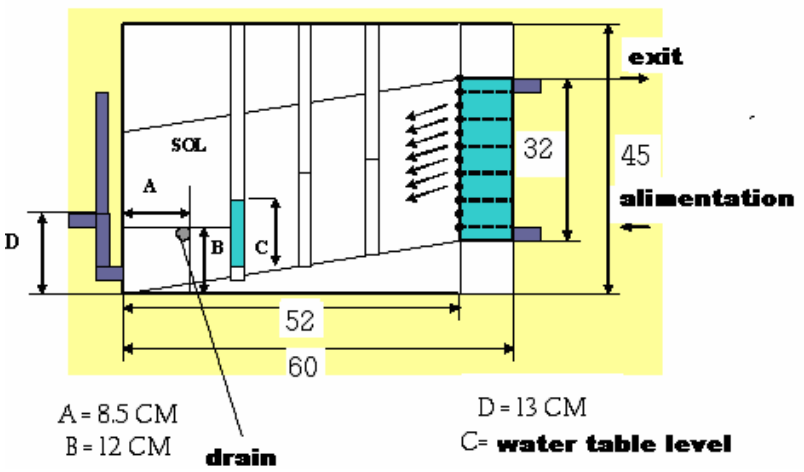

Fig. 1.

Al Shakarchi Sirwan, engineer, PhD is with "Ovidius" University of Constanta, Bd. Mamaia nr. 124,
Ichinur Omer is with "Ovidius" University of Constanta, Bd. Mamaia nr. 124, 900356-Constanta, Romania (e-mail: ichinur.omer@univ-ovidius.ro).

ISSN-1584-5990

Training device will be made from a box (parallelepiped) of glass, with dimensions L = 60 cm, l = 20 cm and h = 45 cm. This device is like a basin where water will enter. Right wall of the box has two holes: one located at a height of 3 cm from the base, which makes power pool, and a hole placed at 32 cm height from the base, to stabilize the water level in the tank (if the amount of water in the tank exceeds 32 cm, water flows to the channel and the basin water level remains constant and equal to the soil layer in the device).

In the basin, at a distance of 8 cm from the right wall is inserted a vertical grid from a geotextile material, through which the water will infiltrate from the basin to soil box.

At the bottom of the device will enter an impermeable material with a slope of 3%. It will be several devices, with several slopes, namely 5%, 7%, 10% and 15%- a total of 5 devices. At 12 cm height from the base of the box will fit a drainage tube with a diameter of 18 mm and a length of 20 cm. (Fig. 1).

In front of the device, 3 glass capillary tubes (piezometers) will be placed at a distance of about 10 cm between them. These piezometers are intended to read the highest points on the depression curve. During the experiment we can see the water level rises in tubes; water tube height is h, and distance between tubes is L. (Fig. 2 and 3).

Fig.2. Sloping drainage device before the beginning of the experiment

Fig.3. Sloping drainage device during the experiment

2. EXPERIMENT DESCRIPTION

Following this experiment, we determine the flow through that soil (amount of water discharged by the drain).

Seven soil samples were available. Each of these seven soils which are following to be analyzed should be left first to dry approximately 24 hours at a temperature of 20°C to separate the granules (to loose moisture content). This aspect is important to avoid formation of holes (vacuum) when samples are introduced into device.

After 24 hours, we introduce small amounts of that sample in the device, and then spill water supply through the hole at 3 cm height then waits until the water level in the tank is constant. During this time, water seeps through the permeable wall of basin to the soil.

We wait 30 minutes to drain water until it stabilizes the flow (every 3 or 5 minutes we measure the amount of water drained; when several consecutive amounts are equal, then flow are stabilized).

After stabilizing the flow, we measure the amount of water discharged over a given period of time (3 to 3 minutes). The operation is repeated seven times. Gather all the results divided by 7 and get average results for a random sample of known size distribution of soil particles and known slope.

The results are tabulated in Table 1 and Table 2, Fig. 4. The experiment is repeated with the same order of operations for all slopes (5%, 7%, 10% and 15%).

In the case of backward sloping drainage we proceed in the same way. Total number of devices that will be built is 10.

Table 1

Results obtained Sample 5-2			Time (min)	Time (s)	Water volume discharged	q_{20} (m3 /s)	q (m^3/s)
Point	l(m)	Slope(m/m)					
0	0	0,03	3	180	172	9,55556E-07	4,7778E-06
1	0,1	0,05	3	180	162	0,0000009	0,0000045
2	0,2	0,07	3	180	159	8,83333E-07	4,4167E-06
3	0,32	0,1	3	180	156	8,66667E-07	4,3333E-06
D	0,41	0,15	3	180	150	8,33333E-07	4,1667E-06

Table 2

Results obtained Sample 5-1			Time (min)	Time (s)	Water volume discharged	q_{20} (m3 /s)	q (m^3/s) l(m)
Point	l(m)	panta Slope(m/m)					
0	0	0,03	3	180	410	0	0
1	0,1	0,05	3	180	400	1	0,1
2	0,2	0,07	3	180	396	2	0,2
3	0,32	0,1	3	180	390	3	0,32
D	0,41	0,15	3	180	370	D	0,41

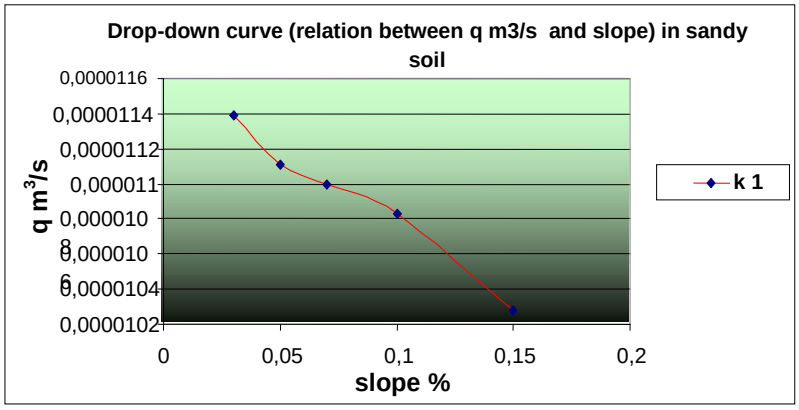

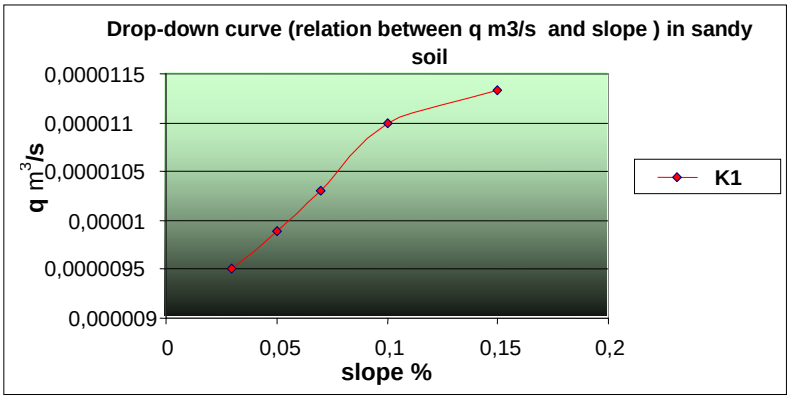

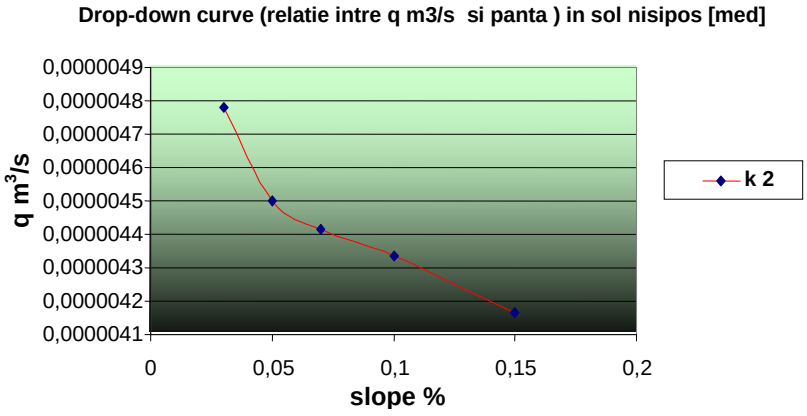
Drop-down curve (relatie intre q m3/s si panta) in sol nisipos [med]
0,0000049
0,0000048
0,0000047
0,0000046
0,0000045
0,0000044
0,0000043
0,0000042
0,0000041
q m3/s
0
0,05
0,1
0,15
0,2
slope %
k 2

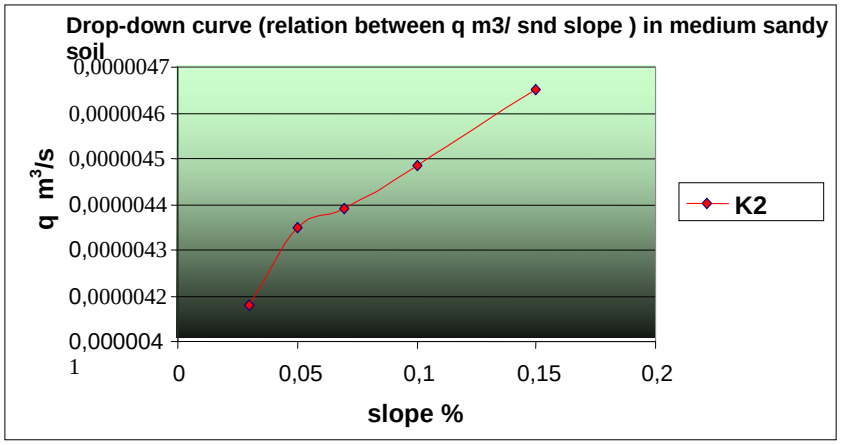
Drop-down curve (relation between q m3/ snd slope) in medium sandy soil
0,0000047
0,0000046
0,0000045
0,0000044
0,0000043
0,0000042
0,000004 1
q m3/s
0
0,05
0,1
0,15
0,2
slope %
K2

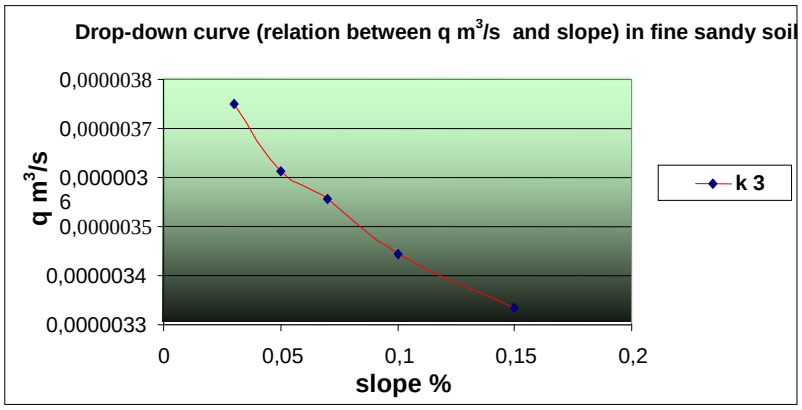
Drop-down curve (relation between q m3/s and slope) in fine sandy soil
0,0000038
0,0000037
0,000003 6
0,0000035
0,0000034
0,0000033
q m3/s
0
0,05
0,1
0,15
0,2
slope %
k 3

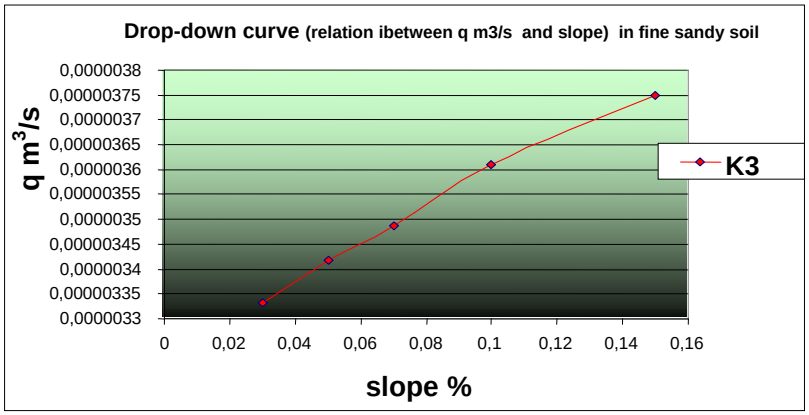

Fig.4. Relationship between slope drainage with different direction from the two random soils (same size distribution of soil particle)

a) Discharged water quantity decreases depending on slope (as the slope is greater as the water volume decreases)

b) Discharged water quantity increases depending on slope (as the slope is greater as the water volume increases)

Unsteady flow regime

$$q = kiA = -kih_u \tag{1}$$

$$q = -k\frac{dh}{dx}A = -k\{\frac{d(z+h)}{dx}\}h \tag{2}$$

Equaling

$$kih_u = k\left[\frac{dz}{dx} + \frac{dh}{dx}\right]h \tag{3}$$

We record

$$\eta = \frac{h}{h_u} \rightarrow i = \left(-i + \frac{dh}{dx}\right)\eta = \left(-i + h_u\frac{d\eta}{dx}\right)\eta \tag{4}$$

$$\frac{d\eta}{dx} = \frac{d\eta}{d\ell}\cdot\frac{d\ell}{dx} = \frac{1}{\cos\varphi}\cdot\frac{d\eta}{d\ell} = \frac{1}{\sqrt{1+i^2}}\cdot\frac{d\eta}{d\ell} \Rightarrow i(1+\eta) = h_u\eta\frac{d\eta}{d\ell}\sqrt{1+i^2} \tag{5}$$

$$\frac{\sin^2\eta}{\cos^2\eta} = tg^2\eta = i^2 \rightarrow \frac{1}{\cos^2\eta} = 1+i^2 \tag{6}$$

Differential equation of the curve of depression

$$\frac{id\ell}{h_u\sqrt{1+i^2}} = h\eta\frac{\eta}{1+\eta}d\eta = \frac{1+\eta-1}{1+\eta}d\eta = d\eta - \frac{d\eta}{1+\eta} \tag{7}$$

Integrates equation

$$\rightarrow \frac{i}{h_u\sqrt{1+i^2}}\left(\ell - \ell_0\right) = \eta - \eta_0 - h_u\frac{1+\eta}{1+\mu_0} \tag{8}$$

Depression curve equation as the final

$$\frac{i}{\sqrt{1+i}}\ell = h - h_0 - h_u\frac{1+\eta}{1+\eta_0} \tag{9}$$

Basic equation for the opposite

$$\frac{-i}{\sqrt{1+i^2}}\ell = h_0 - h + h_u\ln\frac{h_u+h}{h_u+h_0} \tag{10}$$

3. EXPERIMENTAL RESULTS

For obtain the value of h we use the equation:

$$\frac{i(l-l_0)}{\sqrt{1+i^2}} = h - h_0 + h_u\ln\frac{h_u-h}{h_u-h_0} \tag{11}$$

This equation is valid for normal sloping drainage (slope> 0).

We have the value of flow determined above and permeability obtained before, and we obtain:

$$h_u = \frac{q}{K*i} \tag{12}$$

This equation is inserted into Excel for each slope, flow and permeability, resulting hcalculation. After obtaining hmesure by experimental results, we can get $h_{calculation}$ (line device), and we make a comparison between $h_{calculation}$ and h_{mesure} by equation:

$$\frac{h_{calc} - h_{mes}}{h_{calc}} * 100\,(\%) \tag{13}$$

After results, values in the table are used to establish a relationship between the amount of water discharged and the slope to see that the volume of water discharged from a

sandy soil is much greater than the volume of water discharged from a loamy soil and the piezometer read ground clay, , $h_{column} > h_{sandy\ soil}$, shown in fig. 5. The contribution of this experiment: get some relations between q/k and slope.

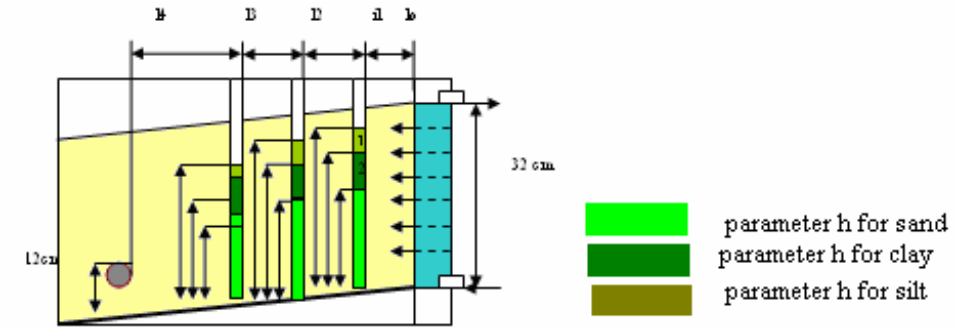

Fig. 5 Depression curve for the three type of soil

We supose an equation that describes the curve (that line):

$$f_2(i) = i^x[y + z\frac{h}{l} + t(\frac{h}{l})^2] \tag{14}$$

This equation further we will call a basic equation.
Known: i, h/l, q/k * d
Unknowns: x, y, z, t.

$$i^x[y + z\frac{h_1}{l_1} + t(\frac{h_1}{l_1})^2] = \frac{q}{K * d} \tag{15}$$

$$i^x[y + z\frac{h_2}{l_2} + t(\frac{h_2}{l_2})^2] = \frac{q}{K * d} \tag{16}$$

$$i^x[y + z\frac{h_3}{l_3} + t(\frac{h_3}{l_3})^2] = \frac{q}{K * d} \tag{17}$$

$$i^x[y + z\frac{h_4}{l_4} + t(\frac{h_4}{l_4})^2] = \frac{q}{K * d} \tag{18}$$

Using the Mathcad software, we obtain the values (x, y, z, t) for all soils and for all slopes from 0.03 to 0.15.

For the slope of 0.03 we are using the equations:

$x = a*I + b$ (19)
$y = a * I + b$ (20)
$z = a * I + b$ (21)
$t = a * I + b$ (22)

We replace in the first equation the slope (I) to 0.03, and results:

$$x=a*0,03+b \tag{23}$$

For the following equation, the slope will have a value of 0.1.

We add the first and the second equation, and multiply them by (-1), and we get the value of the a:

$$x=a*0,03+b \tag{24}$$
$$x=a*0,1+b \tag{25}$$

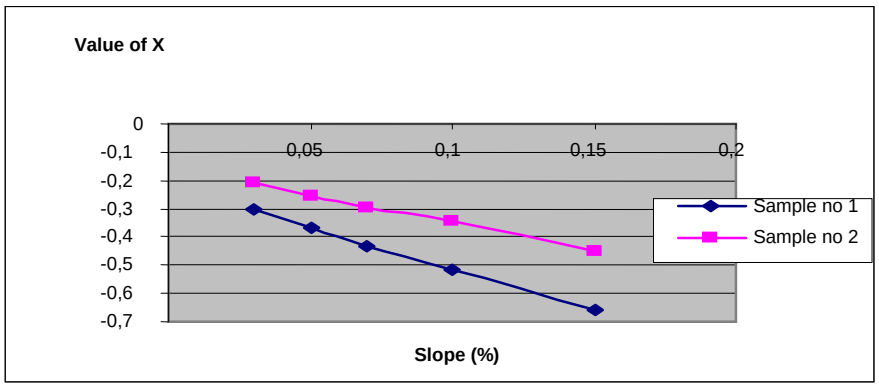

Fig. 6 Relation between slope and the values of x

After we find the value of a, we replace it in one of the two equations and we find and the value of b. The procedure to obtain the other values (x, y, z, t) is the same. In the basic equation, we replace the mean values a, b and c (for sandy soil), at the same slope for all soil samples. In the same way it works for clay soil too. After replacing in the equation the values of a, b and c, these following four equations result:

Basic equation

$$i^{x}\left[y+z\frac{h}{l}+t\left(\frac{h}{l}\right)^{2}\right]=\frac{q}{K*d} \tag{26}$$

We obtain the following final equation for backwards sloping drainage in clayey soil:

$$i^{1.025i-0.328}\left[\left(0.753i+3.452\right)+\left(1.035\cdot10^{-6}\cdot i-4.95\cdot10^{-6}\right)\cdot\left(\frac{h}{l}\right)+\left(2.208\cdot10^{-6}\cdot i+1.126\cdot10^{-6}\right)\cdot\left(\frac{h}{l}\right)^{2}\right]=\frac{q}{K*d} \tag{27}$$

Equation for normal sloping drainage in clayey soil

$$i^{2.6i-0.313}\left[\left(1.235i+3.452\right)+\left(-8.403\cdot10^{-6}\cdot i-4.79\cdot10^{-6}\right)\cdot\left(\frac{h}{l}\right)+\left(1.771\cdot10^{-6}\cdot i+1.091\cdot10^{-6}\right)\cdot\left(\frac{h}{l}\right)^{2}\right]=\frac{q}{K*d} \tag{28}$$

Equation for backwards sloping drainage in sandy soil

$$i^{-0.971i-0.253}[(-1.476i+2.943)+(3.066\cdot10^{-6}\cdot i+2.379\cdot10^{-6})\cdot\left(\frac{h}{l}\right)+(-2.143\cdot10^{-5}\cdot i-1.05\cdot10^{-7})\cdot\left(\frac{h}{l}\right)^2]=\frac{q}{K*d} \quad (29)$$

Equation for normal sloping drainage in sandy soil

$$i^{1.238i-1.333}[(-0.8\cdot i+4.770)+(-5.762\cdot10^{-6}\cdot i+1.837\cdot10^{-5})\cdot\left(\frac{h}{l}\right)+(1.242\cdot10^{-6}\cdot i-4.29\cdot10^{-6})\cdot\left(\frac{h}{l}\right)^2]=\frac{q}{K*d} \quad (30)$$

If we consider that the slope value is 0.04, then the equation is the following:
First equation

$$0.04^{-0.2875}[3.422+5.4\cdot10^{-6}\cdot\left(\frac{h}{l}\right)+1.21\cdot10^{-6}\cdot\left(\frac{h}{l}\right)^2]=\frac{q}{K*d} \quad (31)$$

Second equation for backwards sloping drainage in clayey soil (clay 37.6%, silt 51.0%, sand 11.4%):

$$0.04^{-0.209}[3.403-5.1\cdot10^{-6}\cdot\left(\frac{h}{l}\right)+1.16\cdot10^{-6}\cdot\left(\frac{h}{l}\right)^2]=\frac{q}{K*d} \quad (32)$$

Third equation for normal sloping drainage in clayey soil (clay 37.6%, silt 51.0%, sand 11.4%):

$$0.04^{-0.214}[2.884+2.5\cdot10^{-6}\cdot\left(\frac{h}{l}\right)-9.6\cdot10^{-7}\cdot\left(\frac{h}{l}\right)^2]=\frac{q}{K*d} \quad (33)$$

4. CONCLUSIONS

From the experimental results is observed these novelties:

1. On effect angled drainage is normally seen as the slope increases, the volume of water discharged is greater:

2. In drainage bent backwards with the larger slope as the water volume discharged is less.

3. In depression curve, h in sandy soil value is less than silty soil and smaller than the loamy soil, result from the grain diameter is less so as porosity is greater in this case is seen in Fig 5.

4. The soil density increases as the value h (reading piezometer) increases.

5. REFERENCES

[1] Ciurea C., Chirica A., *Geotehnica manual pentru lucrarile de laborator*, Ed. Ovidius University Press, 1999.
[2] Brown R.B, IFAS EXTENTION (soil texture), University of Florida ,
[3] Omer I., Arsenie D. I. , Buta C., Hidrogeologie, Ed. Ovidius University Press , 2008.
[4] Kharrufa D., *Irigation and drenage (Irak and arab homeland)* , BAGDAD 1994.
[5] Abdulan. Al –Ani, *Elements of soil science*, University of Bagdad , 1980.

SECTION IX

SURFACE AND GROUNDWATER HYDROLOGY

The influence of the hydro-geological conditions and the nature of the contaminants in the behavior of natural attenuation

Ioan Bica, Alexandru Dimache and Iulian Iancu

***Abstract* – For the remedy of the polluted aquifers three management options are now used: (i) containment; tracing boundaries for the extension of the polluted area, which even though it doesn't mean that the polluted area shall be remedied, it limits the pollution to strictly one area, preventing the plume of pollution to extend; (ii) remedy; mechanical, chemical physical or biological processes will be applied in order to remedy the polluted area or the decrease of the concentration of the pollutant up to acceptable levels; (iii) if no techniques are to be applied in the area, monitoring the evolution of pollution in time and in space and quantifying the natural processes which contribute to the decay of the pollutants is a process known as natural attenuation. Natural attenuation employs the physical-chemical and biological processes, in order to reduce the concentrations of the pollutant so that it accepts levels in the subterranean environment.**

The success of using natural attenuation as a restoration method for contaminated aquifer strata implies careful monitoring of different parameters during the entire process, parameters which dictate the time necessary for the natural attenuation process to take place in order to reduce the mass of contaminant to restoration levels accepted by the health and environmental standards. The required time for natural attenuation differs significantly depending on hydro-geological conditions, the nature of the contaminants and their quantity.

The evaluation of the potential for natural attenuation is a necessary stage in the design of remedy systems. The paper presents a model for the calculation in order to estimate the spatial and temporal trends of the pollution, respectively of the natural attenuation taking into account the characteristics of the pollutants and parameters of the polluted strata.

***Keywords* –aquifer strata, monitoring, natural attenuation, remedy systems.**

1. INTRODUCTION

Natural attenuation combines physical, chemical and biological processes – dilution, volatilization, biodegradation, adsorption, chemical reactions between aquifer components

Ioan Bica is with Technical University of Civil Engineering of Bucharest, Bd.Lacul Tei, nr. 124, 020392 Bucharest, Romania (corresponding author to provide phone: +40-021-2433660; fax: +40-021-2433660; e-mail: bica@utcb.ro).

Alexandru Dimache is with Technical University of Civil Engineering of Bucharest, Bd.Lacul Tei, nr. 124, 020392 Bucharest, Romania (e-mail: aldi@utcb.ro).

Iulian Iancu is with Technical University of Civil Engineering of Bucharest, Bd.Lacul Tei, nr. 124, 020392 Bucharest, Romania (e-mail: iancuiulian@hidraulica.utcb.ro).

ISSN-1584-5990

resulting in the reduction of the pollutant's concentrations to accepted values in the aquifer strata.

The use of natural attenuation as a method for the restoration of contaminated aquifers implies estimating the required time for the natural attenuation process to take place in order to reduce the mass of contaminant to levels accepted by health and environment standards [1].

Natural attenuation does not mean doing nothing, the method being known as monitored natural attenuation.

The success of using natural attenuation as a restoration method for contaminated aquifer strata implies careful monitoring of different parameters during the entire process, parameters which govern the time necessary for the natural attenuation process to take place in order to reduce the mass of contaminant to restoration levels, accepted by the health and environmental standards.

The required time for natural attenuation differs significantly depending on hydro-geological conditions, the nature of the contaminants and their quantity.

Estimating the time period necessary for the natural processes to reduce a certain contaminant within the groundwater is essentially a mass balance problem. Let it consider M_0 the initial mass of contaminant and R_{AN} the diminishing or elimination rate of the contaminant through natural attenuation processes. The masic balance equation can be written as:

$$\left[M_0 - \left(R_{AN} \cdot t\right)\right] = M_{rez} \tag{1}$$

where:

t – time;

M_{rez} – the residual mass concentration after the natural attenuation at a certain time t.

The conclusion is that the time for concentration reduction for a certain contaminant below a certain value (M_{lim}) results from the mass balance equation [1]:

$$\left[M_0 - \left(R_{AN} \cdot t\right)\right] = M_{\lim} \tag{2}$$

$$t_{rem} = \frac{\left[M_0 - M_{\lim}\right]}{R_{AN}} \tag{3}$$

in which the remediation time t_{rem} refers to the time period necessary for an initial contaminant mass to be reduced below a certain value through natural physical, chemical and biological transformation processes [2].

In practice however, the problem is more complex because the rate of natural attenuation processes varies over time ($R_{AN} \times t \neq constant$). That is why it is necessary for the problem of estimating the time of remediation to be treated as three different, yet interconnecting problems (**Fig. 1.**).

The first problem refers to the stabilization distance, and implies estimating the maximum spread of the pollutant plume, from a continuous pollution source with constant concentration, that has reached a stationary form. This maximum spread of the pollutant plume is given by the geometrical position of the points for which $t_{rem} \neq 0$, where by restoration refer to reaching a certain level of remediation that has been set beforehand.

This estimation of the stabilization distance may be used for determining the required measures for diminishing/eliminating the contamination.

The second problem refers to the stabilization period. This is the period of time necessary for the expansion of a contaminant plume to shrink towards an accepted spread considering the remediation level, if the contamination source had been totally or partially removed.

The third problem refers to the reduction of NAPL (non-aqueous phase liquids). The reduction of pollutants that are non-miscible with water or sparingly soluble implies estimating the time needed for the NAPL contaminants to dissolve and to biodegrade, thus reaching lower levels than those set by quality standards.

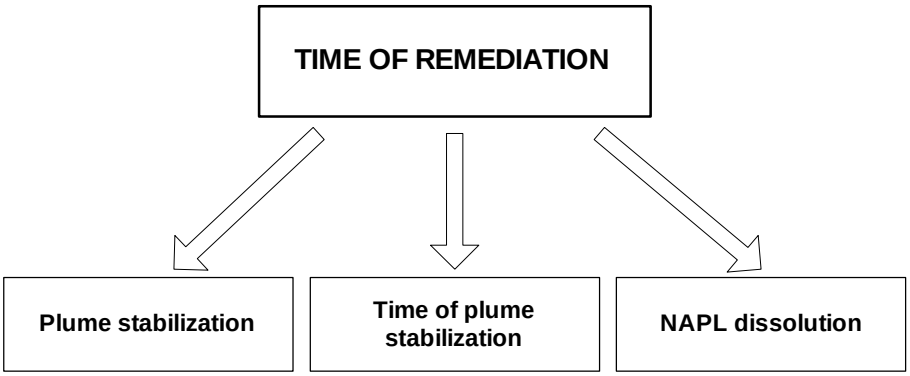

Fig. 1. Conceptualization of the remediation time estimation problem [3]

The capacity for natural attenuation to reduce the contaminant concentrations within the underground environment depends on the diminishing or elimination rate of the contaminant with regard to the mass of contaminant that comes from the contamination source during a certain amount of time.

If the contaminant mass that comes from the pollution source is greater than the transformation rate ($M > R_{AN} \times t$), than the contaminant plume will expand. If the contaminant mass is equal to the transformation rate ($M = R_{AN} \times t$), the contaminant plume will be stable. If the contaminant mass is smaller than the transformation rate ($M < R_{AN} \times t$), the contaminant plume will subside and the concentrations will diminish [2].

The location characterization must offer information about hydro-geological parameters, potential migration pathways towards receptors (ecological or human), geochemical information and data about the expansion and contaminant concentrations.

2. SPATIAL AND TEMPORAL TRENDS ESTIMATION OF NATURAL ATTENUATION

Models are used for the calculus in order to estimate the spatial and temporal trends of the pollution, respectively of the natural attenuation taking into account the characteristics of the pollutants and parameters of the polluted strata. In order to create those models, specialized software programs are used that can simulate the diminishing /elimination processes to which the contaminant is subjected to during the natural attenuation.

These programs estimate the time of remediation, as well as compare this method to other restoration methods for the same location.

In this paper a model for the calculus is presented in order to estimate the spatial and temporal trends of the pollution, respectively of the natural attenuation time to achieve the

proposed goals of remediation, taking into account the characteristics of the pollutants and the parameters of the polluted strata.

For study, it is taken into account a site contaminated with petroleum hydrocarbons (BTEX) – see **Fig. 2.**

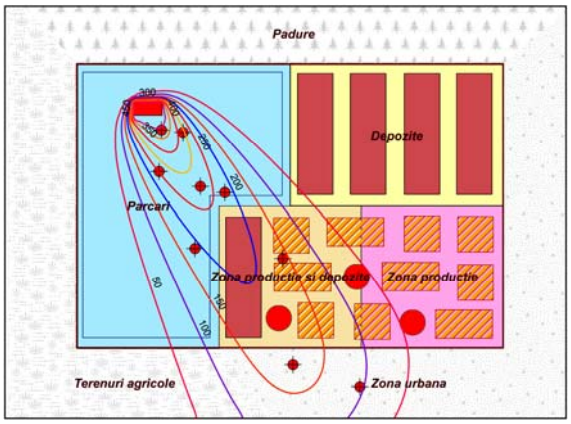

Fig. 2. Contaminated site with petroleum hydrocarbons and position of characterization wells

Evaluation of the effectiveness of natural attenuation requires an assessment of hydro geological characteristics. The following information must be obtained:

- hydraulic conductivity, who is a critical parameter that influences fate and transport of contaminants;
- hydraulic gradient;
- effective porosity.

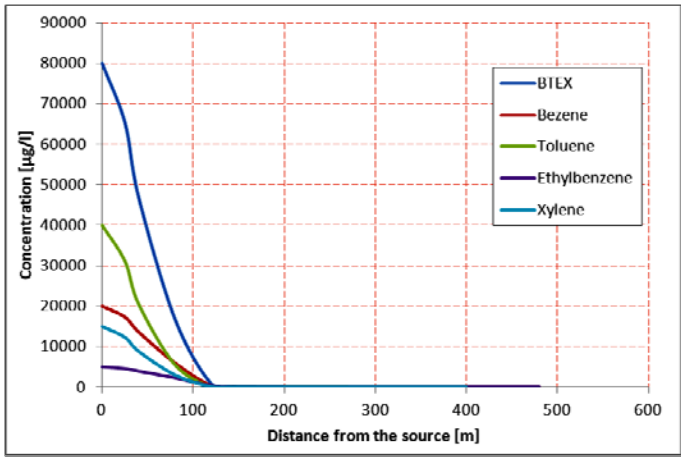

Fig. 3. Spatial distribution of contaminants along the centerline of plume

These three values are used to calculate the groundwater flow velocity and to estimate the extension of the pollution. In the study, it is simulated, based on the site characterization data, the extension of the pollution, with help of mathematical modeling using Groundwater Modeling System (**Fig. 2.**).

From the modeling and from the characterization boreholes, information about the contaminant concentration along the centerline of the plume have been obtained (**Fig. 3.** and **Table 1).**

Table. 1. Contaminant concentration measured at each monitoring well.

Well ID	Distance (m)	BTEX (µg/l)	Benzene (µg/l)	Toluene (µg/l)	Ethylbenzene (µg/l)	Xylene (µg/l)	MTBE (µg/l)
0	0	80000	20000	40000	5000	15000	175000
1	25	65401	17330	31170	4581	12320	169900
2	40	47059	13650	20580	3960	8869	161700
3	80	16828	5968	5546	2304	3010	132000
4	120	776.4	319	56.9	333	67.5	63410
5	145	89.4	24.6	1	61.4	2.4	33400
6	270	17.27	2.7	0.03	14.4	0.14	19270
7	400	2.92	0.21	BD	2.7	0.01	10150
8	480	0.39	0.01	BD	0.38	BD	4878

In order to estimate the time of reduction of the contaminant concentration Natural Attenuation Software program was used.

Natural Attenuation Software (NAS) is a screening tool to estimate remediation timeframes for monitored natural attenuation (MNA) to lower groundwater contaminant concentrations to regulatory limits, and to assist in decision-making on the level of source zone treatment in conjunction with MNA using site-specific remediation objectives.

NAS is designed for application to groundwater systems consisting of porous, relatively homogeneous, saturated media such as sands and gravels, and assumes that groundwater flow is uniform and unidirectional. NAS consists of a combination of analytical and numerical solute transport models. Natural attenuation processes that NAS models include are: advection, dispersion, sorption, non-aqueous phase liquid (NAPL) dissolution, and biodegradation [4].

The data regarding the location includes hydro-geological data (hydraulic conductivity, hydraulic gradient, porosity and aquifer thickness), location of the monitoring wells, as well as a characterization of the contaminated area.

In the study it is used various values for hydraulic conductivity, hydraulic gradient and took into consideration all four constituents form BTEX: benzene, toluene, ethyl benzene and xylene.

3. RESULTS OF NATURAL ATTENUATION TIME ESTIMATION

To estimate time required for contaminants to in the source area to attenuate to a predetermined target source concentration, NAS uses groundwater flow code (MODFLOW), for simulate flow in the aquifer, in conjunction with SEAM3D code, to solve the solute transport equation.

MODFLOW is a code that numerically solves the three-dimensional groundwater flow equation for porous structure by using finite difference method. The equation that describes the groundwater flow and MODFLOW solve [5], is:

$$\frac{\partial}{\partial x}\left(k_{xx}\frac{\partial h}{\partial x}\right)+\frac{\partial}{\partial y}\left(k_{yy}\frac{\partial h}{\partial y}\right)+\frac{\partial}{\partial z}\left(k_{zz}\frac{\partial h}{\partial z}\right)-W=S_s\frac{\partial h}{\partial t} \quad (4)$$

where:

k_{xx}, k_{yy} and k_{zz} are values of hydraulic conductivity along *x, y* and *z* coordinate axes;

h is the potentiometric head;

W is a volumetric flux per unit volume and represents source and/or skins of water;

S_S is the specific storage of porous material;

t is time.

SEAM3D (Sequential Electron Acceptor Model, 3 Dimensional), is a numerical model and code for solute transport with aerobic and sequential anaerobic biodegradation and dissolution of compounds from non-aqueous phase liquids (NAPLs). SEAM3D consists of a series of modules for simulating the fate and transport of multiple constituents in a three-dimensional, anisotropic, heterogeneous domain [6].

Modeling natural attenuation estimated time of reducing the contaminant concentration under a certain value using NAS, was made with the following series of data:

- maximum time of analysis: 10 years;
- NAPL mass: 10 kg;
- source has been removed;
- total porosity: 0.35;
- effective porosity: 0.3;
- contaminated aquifer thickness: 5 m.

NAS requires the calculations' site data, including hydro geologic parameters, contaminant source delineation and characterization, monitoring well locations, and concentrations of contaminants.

Two scenarios were analyzed. In the first scenario the hydraulic gradient was assumed to 0.002 m/m and hydraulic conductivity to: 10 m/d, 20 m/d and 30 m/d. In the second scenario hydraulic conductivity was assumed to 10 m/d and hydraulic gradient to: 0.002 m/m, 0.003 m/m and 0.005 m/m.

Those scenarios were made to see the influence of hydraulic conductivity and hydraulic gradient upon the time of reducing the concentration of contaminants (BTEX), to a certain value: BTEX – 7 µg/l, benzene – 3 µg/l, toluene – 2 µg/l, ethyl benzene – 1 µg/l, xylene – 1 µg/l at 480 meters from the source.

The results are presented in **Fig. 4.** and **Fig. 5.**

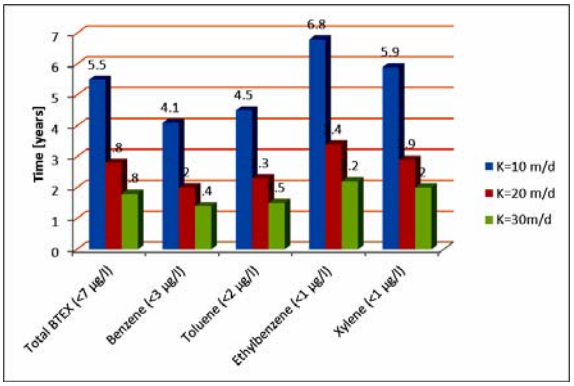

Fig. 4. Hydraulic conductivity influence upon the time of remediation associated with natural attenuation

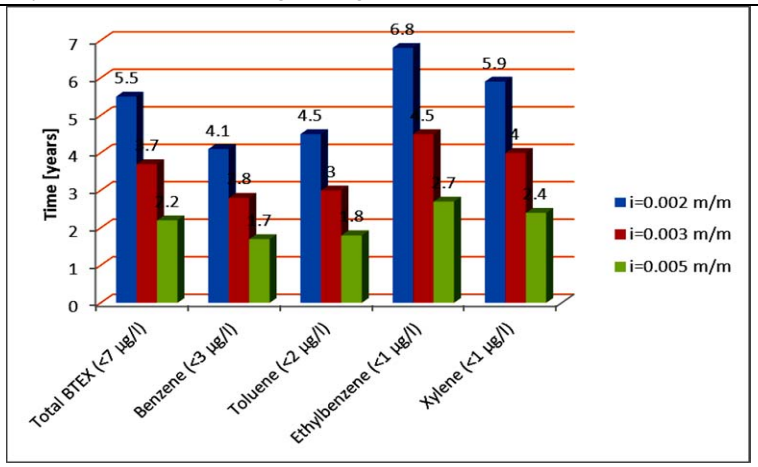

Fig. 5. Hydraulic gradient influence upon the time of remediation associated with natural attenuation

NAS also calculated the estimate plume length – 1580.4 m. The dispersion parameters estimated by the model, used in calculations were:

- longitudinal dispersivity: 13.74 m;
- transversal dispersivity: 0.69 m;
- dispersivity ratio: 20.

In the study have been also estimated the time necessary for reducing the concentration of contaminants to a certain value using pump and treat remediation technology, by using in the calculus a well situated at 200 meters from the contaminant source, with a pumping rate of 3 l/s (around 260 m^3/day). For an assumed hydraulic conductivity of 10m/day and hydraulic gradient of 0.002, using Pump and Treat Technology of Remediation. The time was reduced with approximative75% (**Table 2.**).

Table. 2. Time of remediation using Natural Attenuation and Pump and Treat methods of remediation (years).

Method	BTEX	Benzene	Toluene	Ethylbenzene	Xylene
Natural Attenuation	5.5	4.1	4.5	6.8	5.9
Pump and Treat	1.3	1	1.2	1.4	1.4

4. CONCLUSIONS

In order to decide what contribution natural attenuation can make to meeting site remediation goals, very detailed site investigations must be carried out and it is necessary to know the location and concentration of the contaminants source, and how the contaminants move in the ground [7].

Natural attenuation presents some advantages in comparison with other methods of remediation: generating a less volume of wastes, reducing the potential for cross media transfer of contaminants associated with ex situ treatment, reducing disturbances to ecological receptors, possible use in conjunction with active remedial measures. Natural attenuation also has some potential disadvantages: more complex and costly site characterization, possibly longer time frames to achieve remediation goals and objectives, need for more extensive education and outreach efforts to gain public acceptance [8].

The decision to use monitored natural attenuation requires being supported by a specific site characterization plan, that can provide hydro-geological data that can be used to demonstrate the natural attenuation processes active on the site, and evaluate the time at which that processes will reduce contaminant concentration to required levels.

The success of using natural attenuation as a remediation method for contaminated aquifer strata implies careful monitoring during the entire process, as well as estimating the time necessary for the natural attenuation processes to take place.

The evaluation of the time necessary for natural attenuation processes to take place is a necessary stage in the design of remediation systems, even if eventually another method of the remediation will be chosen based on site specific conditions.

5. REFERENCES

[1] Iancu I., Bica I., Dimache A., *Estimation of Remediation Time Associated with Natural Attenuation of aquifers*. 2009, Buletinul Stiintific al Universitatii Tehnice de Constructii Bucuresti, Nr.2, pag. 51-58.

[2] Bica I., Iancu I., Dimache A., Alboiu N.,. *Evaluation of natural attenuation as a remediation method of contaminated aquifers*. 2008, Buletinul Stiintific al Universitatii Politehnica din Timisoara, Tomul 53(67), Fascicola 2, pag. 219-222.

[3] *Guidance on Remediation of Petroleum-Contaminated Ground Water By Natural Attenuation.* Washington State Departament of Ecology Toxics Cleanup Program, 2005.

[4] Widdowson M.A., Mendez E, s.a., *Natural Attenuation Software (NAS) – User manual*, Version 2.

[5] *A Modular Three-Dimensional Finite-Difference Groundwater Flow Model,* USGS, 1988.

[6] *SEAM3D – A numerical Model for Three-Dimensional Solute Transport Coupled to Sequential Electron Acceptor-Based Biological Reactions in Groundwater*, Virginia Tech, Technical Report, June 2002.

[7] *Monitored Natural Attenuation of Petroleum Hydrocarbons,* U.S. EPA Remedial Technology Fact Sheet.

[8] *Subsurface Contaminant Focus Area: Monitored Natural Attenuation (MNA) – Programmatic, Technical and Regulatory Issues,* Pacific Northwest National Laboratory, U.S. Departament of Energy, July 2001.

Mathematical model applied to rainfall-runoff on a sub- watershed, part of a larger catchment area

Florentina Ioniță, Nicolai Sîrbu and Virgil Petrescu

***Abstract* – The main source of water within the catchment area is the rainfall. A part of rainfalls on a watershed evaporates, another part leach into the soil, and the rest flows to the river network forming its liquid discharge. The last amount of water flows at the surface area on the shortest possible way to the channel network, which collects and transports to the catchment outlet.**

In this paper one tries to model rainfall-runoff with the aid of a mathematical model and numerical simulation for a given sub-watershed, part of a larger catchment area.

The mathematical model takes into consideration a specific rainfall-runoff model with some parameters that simulate the surface runoff, hypodermic flow and interflow by means of some virtual retention reservoirs. In this way, we can get the diffuse and point water sources in the hydrodynamic routine used in flood risk analysis.

***Keywords* – catchment; flood risk, mathematical model, rainfall-runoff.**

1. INTRODUCTION

Floods are among the natural phenomena that marked and deeply marke the evolution of human society. They are being the most common disasters in the world and also the largest producer of property damage and human victims. Floods are caused especially by hydro meteorological events, but should be considered anthropogenic interference, too (for instance, irrational impoundments lead to the increase of downstream floods) [1], [2].

For the environmental protection and in particular human lives against such disasters it resort to structural or, preferably, non-structural measures. The efficient applications of these measures are based on a priori knowledge of the potential flood areas expansion and of the flow rates during high water periods.

The main source of water within the catchment areas is the rainfall. Knowledge only of the total precipitation is not sufficient for determining a hydrograph since not all the rainfall participate to the leakage in the rivers. The fraction of the total rainfall that

Florentina Ioniță, Eng. PhD Student, Technical University of Civil Engineering of Bucharest, Bd. Lacul Tei, nr. 124, 020396- Bucharest, Romania (phone: +40-21-2433630; fax: +40-21-2433630; e-mail: ionitamflorentina@gmail.com).

Nicolai Sîrbu, Lecturer, PhD, Technical University of Civil Engineering of Bucharest, Bd. Lacul Tei, nr. 124, 020396- Bucharest, Romania (phone: +40-21-2433630; fax: +40-21-2433630; e-mail: nsirbu@utcb.ro).

Virgil Petrescu, Professor, PhD, Technical University of Civil Engineering of Bucharest, Bd. Lacul Tei, nr. 124, 020396- Bucharest, Romania (phone: +40-21-2433630; fax: +40-21-2433630; e-mail: virgil.petrescu2007@gmail.com).

ISSN-1584-5990

participates to the flow is called net rain. Other parts evaporate, or leach into the soil (**Fig. 1**).

The modeling of the rainfall-runoff process aims to generate the inputs for the hydrodynamic model used in flood risk analysis. A common practice in the river network modeling is to couple a hydrodynamic routine with a rainfall-runoff model. This coupling serves as a faithful reproduction of the phenomena like in the nature.

The most studies in hydrology are related to the development and the application of mathematical models and numerical simulation for different purposes, such as: forecast, data extrapolation in time and space, determination of the characteristic hydrological parameters for design. In hydrology, the models are a necessity which takes into account the very complex nature of processes occurring in catchments and river networks, which are subject to changes over time and space due to natural factors and human actions.

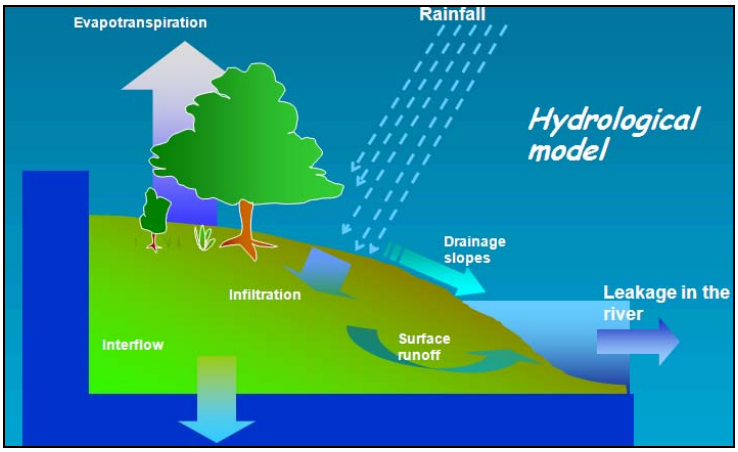

Fig. 1. Terrestrial phase of hydrological cycle processes

2. RAINFALL-RUNOFF MATHEMATICAL MODELS

The rainfall-runoff models divide the major components of leakage - each flow is treated separately as a reservoir - such that the phenomena are judged by relationships more or less empirical among reservoirs. In these relationships occur parameters whose values must be established.

The identification of the rainfall-runoff parameters is based on the balance equations that consider the precipitation (liquid or solid) as inputs and the flow hydrograph as outlets. Thus, considering a sub-watershed which ends at a hydrometric station, and rainfall on this area, the values of parameters are obtained by calibration. Accepting these values for a particular sub-watershed, they are also valid for similar areas where is a quasi-constant morphological, hydrological and meteorological characteristics. In this way, we can generate the flow hydrograph.

One of these models is N.A.M., a model with concentrated parameters which simulates surface flow, interflow and hypodermic flow, based on the amount of moisture in three retention areas (reservoirs). N.A.M. is the abbreviation for the Danish „Nedbør-Afstrømnings-Model", meaning Rainfall-Runoff-Model. This model is part of the Mike 11 sofware produced by Danish Hydraulic Institute (DHI). The N.A.M. model includes a number of optional extensions such as a complex mode of snow melting and the hydrology of irrigated areas.

The one-dimensional equations used in MIKE11 package are [3], [4]:

- Continuity Equation:

$$\frac{\partial Q}{\partial x}+\frac{\partial A}{\partial t}=q \tag{1}$$

- Equation for conservation of momentum:

$$\frac{\partial Q}{\partial t}+\frac{\partial\left(\alpha\frac{Q}{A}Q\right)}{\partial x}+gA\frac{\partial h}{\partial x}+g\frac{Q|Q|}{C^2RA}-gAi=0 \tag{2}$$

where:

Q is river discharge;

q - lateral inflow on unit lenght as e.g. calculated by the rainfall-runoff model;

A - cross-sectional area;

x - longitudinal coordinate;

t - time;

α - non-uniform velocity distribution coefficient;

g - gravitational acceleration;

h - water depth;

i - bottom slope;

C - Chézy coefficient;

R - hydraulic radius.

These equations are solved using an implicit finite difference scheme, applying a Double Sweep algorithm (Abbott-Ionescu 6-points scheme).

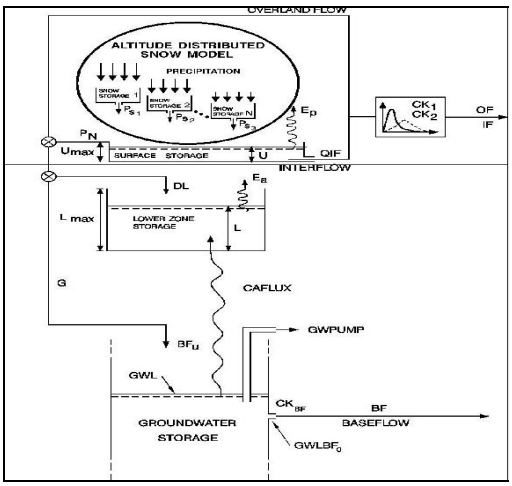

Fig. 2. Structure of the N.A.M. model

The global error given by R_2 - Nash-Sutcliffe coefficient is, after [3], [4]:

$$R_2=\frac{\sum_{i=1}^{N}\left[Q_{obs,i}-Q_{sim,i}\right]^2}{\sum_{i=1}^{N}\left[Q_{obs,i}-\overline{Q}_{obs}\right]^2} \tag{3}$$

where:

Q_{sim} - simulated discharge and Q_{obs} - observed discharge

The N.A.M. model can be applied independently for one basin or for several sub-basins which drain the water to the river network.

The rainfall-runoff N.A.M. model requires as input time series precipitation data, evapotranspiration and temperatures, but also GIS (Geographic Information Systems) data. In addition, for the model calibration must be used time series of flow rates.

The necessary data for the model are:

- Meteorological data: liquid precipitation, potential evapotranspiration, temperature, solar radiation;
- Hydrological data: river flow rates, water quantities for irrigation, groundwater flow;
- Geometric and topographic data: Basins area and/or sub-basins, Altimetric data.

The most important meteorological data are precipitation and potential evapotranspiration. In the case of melting snow module we must add temperature and, optionally, solar radiation.

N.A.M. model also simulates human activities as irrigation and groundwater extraction. In this case the corresponding time series are needed.

The GIS rapid development and diversification of application areas allowed its use in hydrological modeling, primarily in pre and post processing [5].

The GIS data required for modeling the rainfall-runoff are: DTM (Digital Terrain Model) for study area; Grid data format: fill, flow direction, flow accumulation, stream grid, catchment grid, slope gridand Data in vector format: the hydrographic network, the catchment, the sub-catchments.

All these data are useful for defining the hydrological model, starting from the DTM. The watershed delineation is made in ArcMap using a DTM, with a resolution of 50 - 100 m. The catchments are built with surfaces around 500 - 1,000 km^2 and they are ended in hydrometric stations.

3. STUDY CASE FOR SUB-WATERSHED CIUCEA-VADU CRIŞ

This paper presents the results of modeling the rainfall-runoff phenomena with N.A.M. code for the Ciucea-Vadu Criş sub-watershed, which is part of the Cri□ul Repede catchment (**Fig. 3**). This sub-watershed has an area of 497.11 km^2 and the river network has a total length of around 35 km.

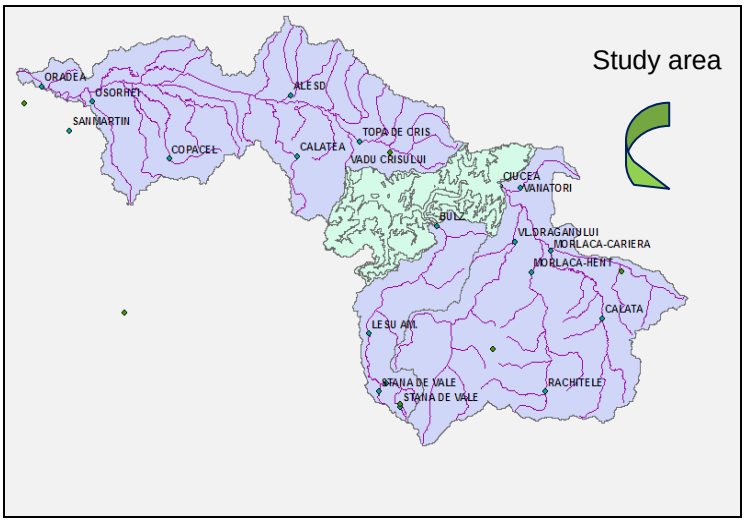

Fig. 3. Crişul Repede catchment with Ciucea-Vadu Criş sub-watershed

Time series of data precipitation are prepared and corrected preliminarily for each hydrometric station, using measurements between 2001 and 2006 years. These data were corrected with 5 - 10% due to uncertainties of the measurements. We also checked the variation of rainfall with respect to elevation, representing the linear regression, too (**Fig. 4**). Data from hydrometric stations located in similar climatic regions have normally such a linear correlation, with an increase in rainfall of 2 to 10% at 100 m.

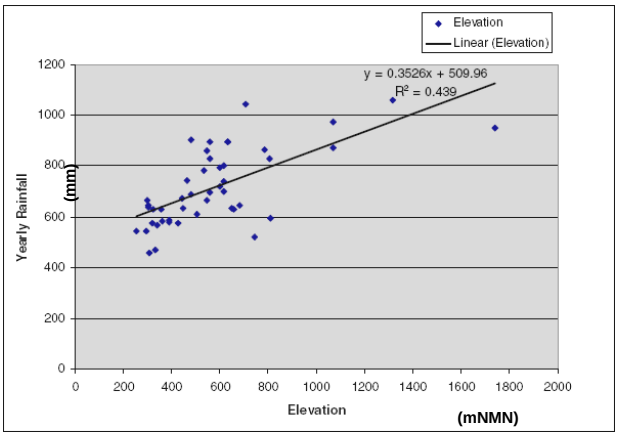

Fig. 4. The linear regression of rainfall versus elevation for Cri□ul Repede catchment

Similarly, the temperature data has been analyzed by linear correlation between the annual average temperature and the altitude.

The average rainfall for the study area was calculated with Thiessen polygons method used by N.A.M. model (**Fig. 5**). This method is most commonly used because it is simple and it gives good results, especially when the network is not homogeneous in space.

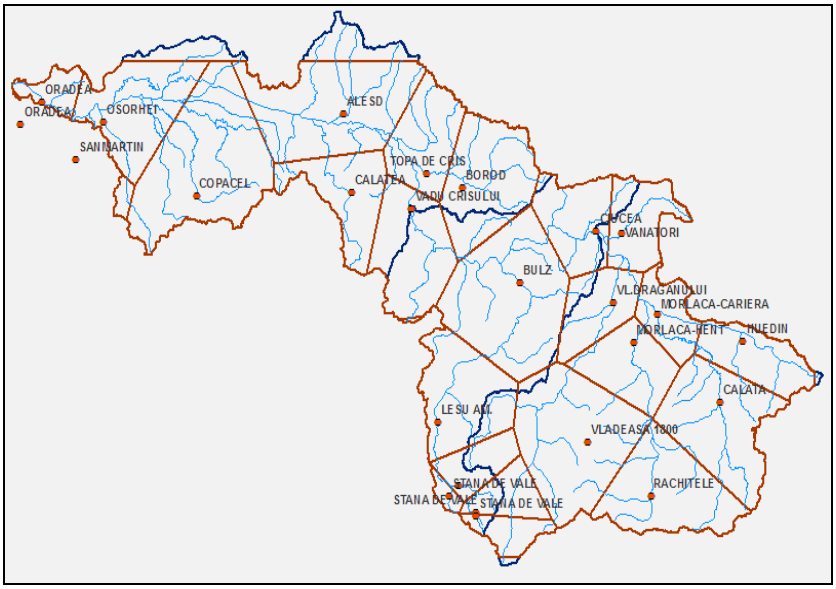

Fig. 5. Thiessen polygons for Crişul Repede catchment

The calibration was done starting from the parameters file, so it is very important to choose a good initial conditions. It is recommended to start the simulation at a moment without snow deposits and with low leakage, say late September or early October. In this conditions, it is sufficient to specify only three initial conditions:

- Maximum contents of surface storage: normally 0,5 – 0,8;
- Maximum contents of root zone storage: normally 0,5 – 0,8;
- Baseflow (ground water storage).

In order to simulate daily data with the observed rainfall at 7:00 am and the observed discharges at 12:00 am, it was proposed a 6 hours time step (**Fig. 6**).

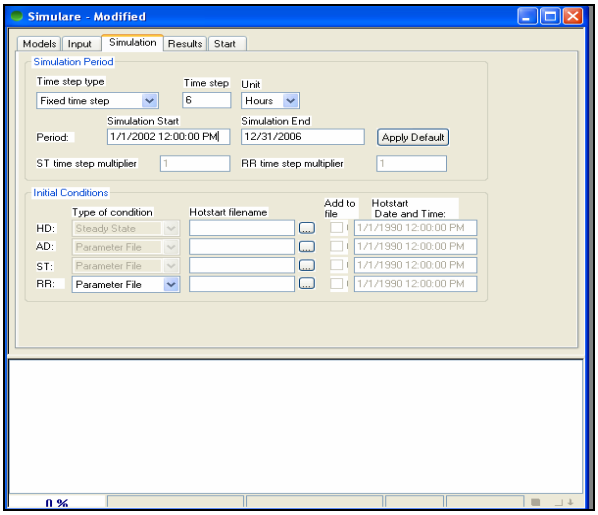

Fig. 6. Mike simulaton file with the time step and the simulation period

The model calibration must consider the following objectives:

- Consistency between the simulated runoff and the observed one;
- Consistency between the simulated hydrograph and the observed one;
- The peak flow consistency regarding the match of the time, the frequency and the water volume;
- Low-water level consistency between the simulated and the observed values.

N.A.M. model has also an important tool: it allows autocalibration procedure of 9 important parameters. In **Table 1** are shown these parameters obtained by autocalibration and manual calibration for the Ciucea-Vadu Cri□ sub-watershad.

Table 1. N.A.M. parameters and their calibrated values

Umax	Maximum contents of surface storage	30
Lmax	Maximum contents of root zone storage	150
CQOF	Overland flow coefficient	0.9
CKIF	Time constant for interflow	400
TOF	Root zone threshold value for overland flow	0.9
TIF	Root zone threshold value for inter flow	0.9
TG	Root zone threshold value for recharge	0.9
CKBF	Time constant for routing base flow	5,000
CK1,2	Time constant for routing overland flow	35

After this procedure, a calibration plot which compare the observed/simulated discharges, and the cumulative water volumes observed/simulated was built (**Fig. 7**). This is very useful to check the overall calibration result. It is very important that the WBL (Water Balance – the difference between the calculated average runoff and the observed one) be within 10%, and the overall hydrograph shape given by the Nash-Sutcliffe coeficient R2 has a value close to 1 (between 0.7 - 0.9).

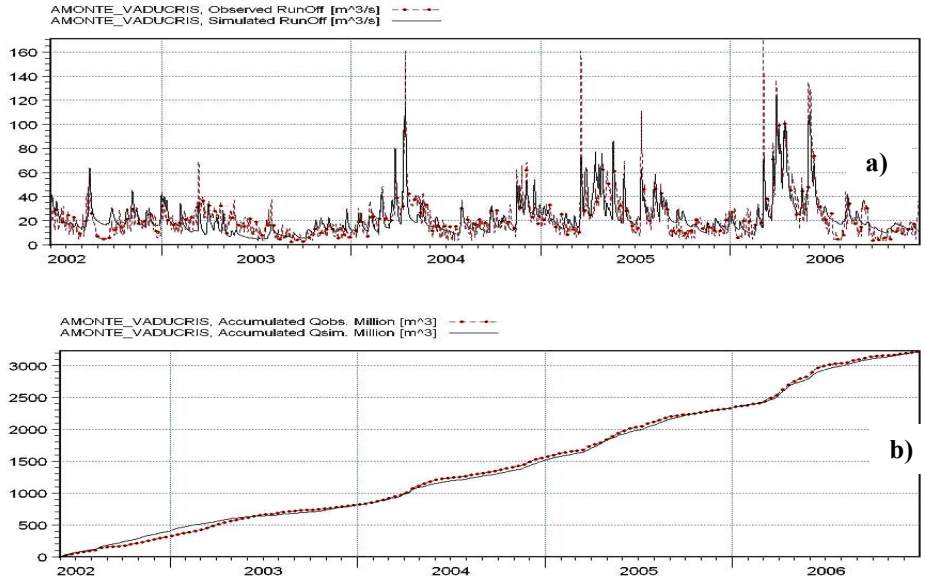

Fig. 7. Calibration plot for Ciucea – Vadu Criş sub-watershed:
a) discharges; **b)** water volumes

From the calibration plot, one can choose the necessary discharges for further computation with the hydrodynamic model.

On the calibration plot we can add additional results from the N.A.M. such as overland flow, interflow and baseflow.

4. CONCLUSIONS

The rainfall-runoff model is used primarily to generate diffuse or punctual entries in the hydrodynamic model used especially for flood risk analysis.

The use of a such rainfall-runoff model needs a good hydrological phenomenology understanding. The N.A.M. product is more attractive with respect to other similar models. Graphic interface easily allows the calibrated parameters introduction, the geometry data, Thissen polygons distribution etc. The view of the results allows the image composition in overlapping of the observated and the simulated flows, as shown in the paper for Ciucea – Vadu Cri□ sub-watershed.

The performance of the hydrological model shows that the simulated streamflow reflects the variation in temperature and precipitation as well as the moisture interaction between the surface, subsurface and the groundwater storages.

5. ACKNOWLEDGMENTS

The authors wish to thank PhD Department of the Technical University of Civil Engineering of Bucharest for assistance in achieving this paper.

6. REFERENCES

[1] Stănescu A. V., *Hidrologie urbană.* Bucureşti: Editura Didactică şi Pedagogică, 1995.

[2] Constantinescu Şt., *Observaţii asupra unor indicatori morfometrici determinaţi pe baza MNAT*. Bucureşti, geo-spatial.org, 2006.

[3] *** MIKE 11 – *A Modelling System for Rivers and Channels – User Guide,* DHI, Agern Alle 5, Denmark, DK-2970, Horsolm, 2006.

[4] *** MIKE 11 – *A Modelling System for Rivers and Channels – Short Introduction Tutorial,* DHI, Agern Alle 5, Denmark, DK-2970, Horsolm, 2006.

[5] Moore I. D., Grayson R. B., Landson A. R., *Digital Terrain Modeling: A Review of Hydrological, Geomorphological and Biological Applications,* Hydrol. Proc., 5, pp. 3–30, 1991.

Floodplain delineation

T. Hraniciuc

Abstract – **This study demonstrates how to perform a floodplain delineation with WMS, and how to delineate a floodplain based on water surface elevations for a river and a TIN which represents the topography for the area. We must provide an elevation TIN (Triangulated Irregular Network) and a scatter point data set with river stage values. TIN elevations might be obtained from survey data, or by converting DEM (Digital Elevation Model) points to TIN vertices. River stage files can be assembled manually, or read in from a HEC-RAS project file. This study will familiarize us with how to delineate a floodplain based on water surface elevations for a river and a TIN which represents the topography for the area.**

Keywords – **Floodplain, flood impact maps, flood barrier coverage.**

1. INTRODUCTION

This study will familiarize us with how to delineate a floodplain based on water surface elevations for a river and a TIN which represents the topography for the area.

The objectives in this study will be:

- Experiment with the various floodplain delineation options, including input data, search radius, flow path, and quadrants;
- Perform floodplain delineations with water surface elevations;
- Use a Flood Barrier coverage to restrict flood waters;
- Generate flood depth, impact, and extent coverages.

We can choose from several different delineation options, which in turn affect how the floodplain is computed. Options include Search Radius, Flow Path, and Quadrants.

2. EXPERIMENT DESCRIPTION

To make simulation with WMS we must have the terrain data digitized. If we have not yet digitized the terrain WMS allow doing this. In our application the terrain data is ready digitized as well as showed in figure 1.

Digital Elevation Models (DEM's) are the most commonly available digital elevation source and therefore an important part of using WMS for watershed characterization.

A DEM is a rigid data structure that contains a two-dimensional array of elevations where the spacing between elevation is constant in the x and y directions.

The next step it's to make the hydrographic network and delineate the basin for our application using the WMS tools. From the hydrographic network we will chose the river or

T. Hraniciuc Technical University "Gheorghe Asachi" of Iasi, Department of HydrotechnicaConstructions and Sanitary Engineering, D. Mangeron Blvd., 65-67, Iasi Romania, (email: hraniciuc_tomi@yahoo.com).

ISSN-1584-5990

a part of the river for our study. Using the tools from WMS we just must put the section on the river, this point representing the outlet point for the basin.

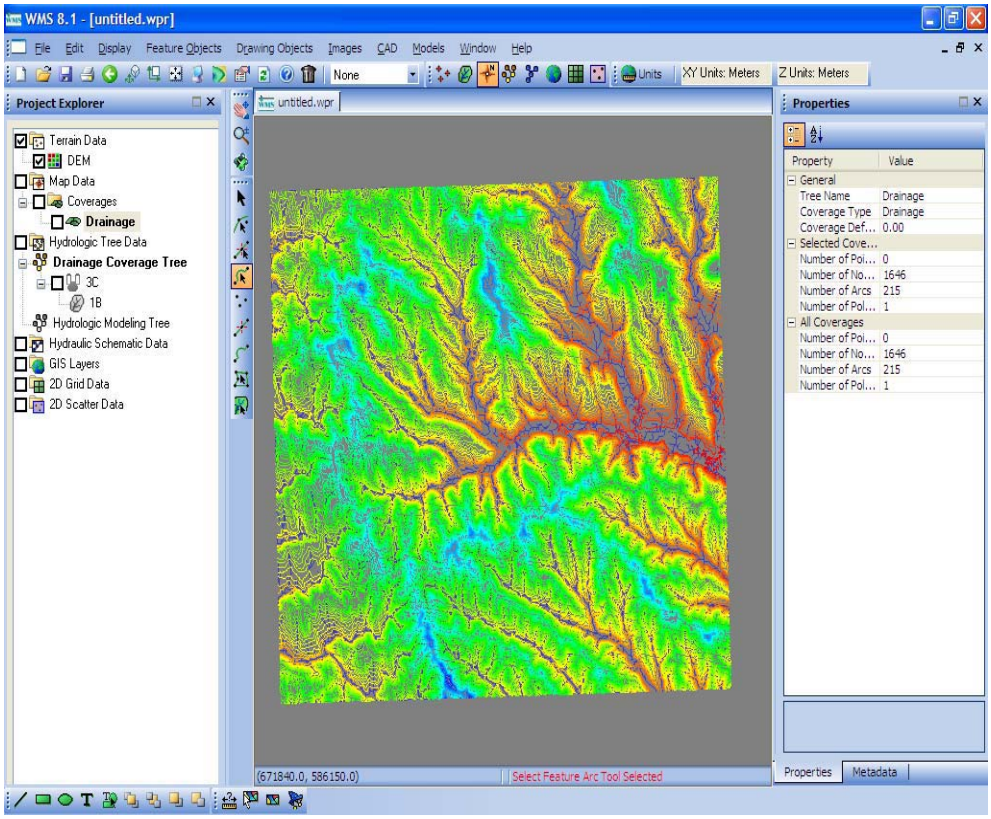

Fig. 1 DEM

The basin surface that will result will be our area for the next steps where we will make the flood simulation. The soft allow us to choose measurement system. We can choose to be in hectares or acres for area and meters, feet or something else for the length. The basin delineation will be marked automatically by the soft depending on the Digital Elevation Model. WMS is able to merge multiple DEM files that span quad sheets.

Triangulated Irregular Networks (TIN) is constructed from a scattered set of xyz vertices. They can be used for visualization, as background elevations maps for generating new TIN's or DEM's, or to perform basin delineation and drainage analysis. Now we have the basin. The next step will be to editing TIN. WMS has automated methods of editing TIN's so that they provide a representation of terrain that is useful for drainage analysis.

These methods include selecting thin boundary triangles, transforming data and eliminating flat triangles and pits.

Data transformations are especially useful for converting elevations between feet and meters. Flat triangle need to be eliminated from drainage analysis. Inaccurate basin delineation can result from pits because water flows into the pits rather than to the actual outlet. After we finished editing TIN, we need to create centerline coverage for our reaches and cross section coverage for our cross sections.

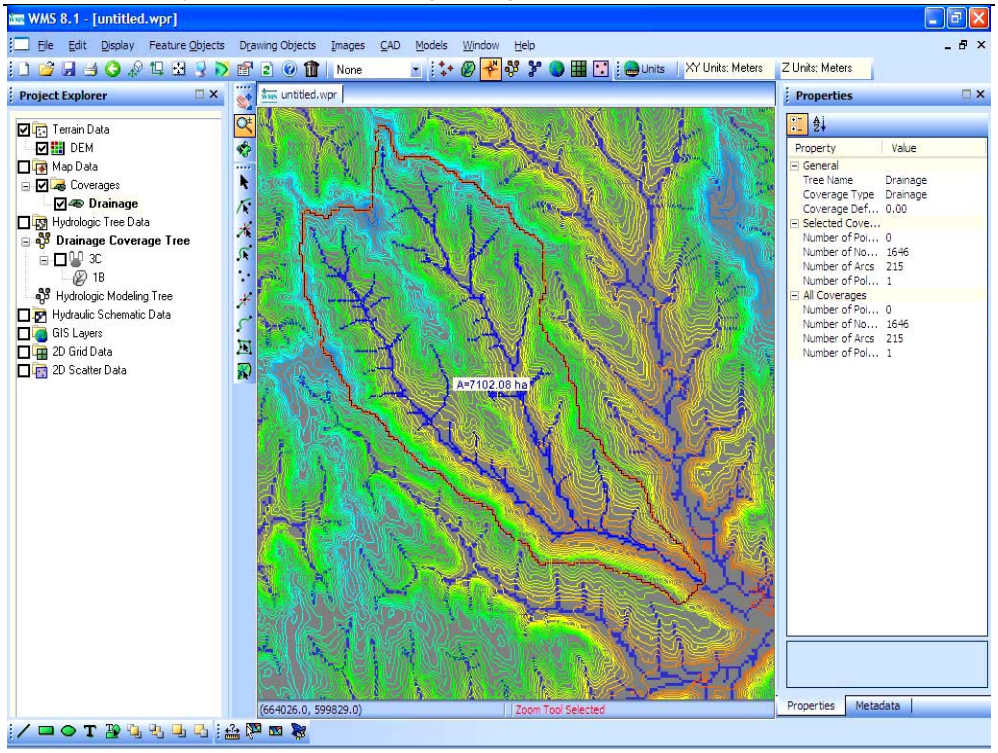

Fig. 2 Basin delineation

This will form the core of our conceptual model. Centerline arcs are used to define the location and lengths of the study reaches and assign their attributes. This defines the centerline for the model in this simulation. It will consist in two reaches in the main channel (divided by the tributary) and one reach in the left tributary. Bank arcs are used to define the location of the banks and the over-bank distances. Reaches are stream sections where the flow rates and other hydraulic conditions are assumed to be constant. A river can be comprised of one or more reaches but only one flow path. When we finished drawing the river channels and the banks, we need to create the Land use (Materials coverage). We know what land use is located in our basin, so we must draw the polygons who we will assign the material type to each polygon. After that we must assign the roughness to each material type, and to make difference we can color this in different colors. The material coverage is very important for our modeling because the flow and the results depend of this material and their roughness. If we don't introduce this data's the soft will confirm an error when we will compute the model and the results can't be read.

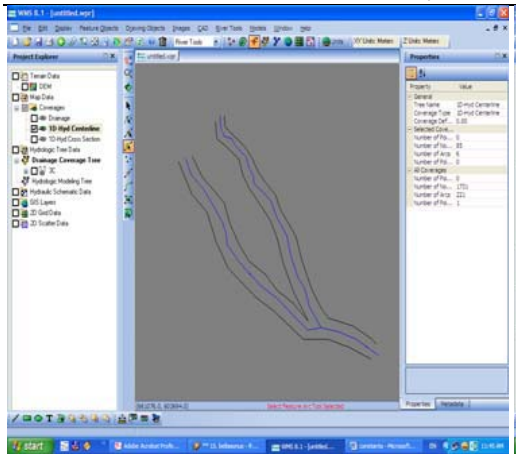

Fig. 3 The banks and the river reaches

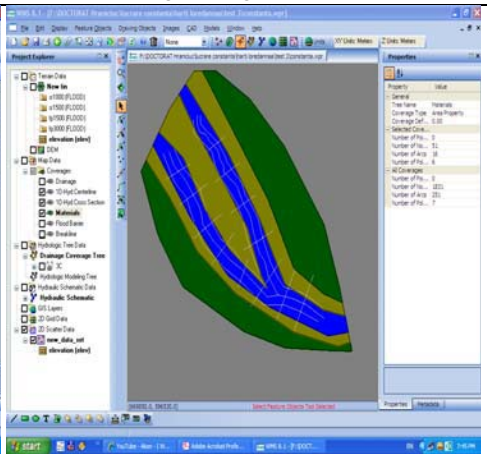

Fig.4 Materials coverage

At this point we need to crate the cross section on the river and the tributary. We must create at least two cross sections on each reach by clicking a point on one side of the reach than double-clicking a point on the other side of the reach. In the cross section coverage, all arcs are cross section arcs. Their position and orientation define the location of the cross section in the system, but they do not have any data assigned. We want to assign elevation data, materials and point property locations to the cross sections.

This information will be extracted from the TIN, the area property coverage and the centerline coverage. WMS will extract an elevation point at every triangle edge along the cross section arc. If we give double clicking on every cross section we can see their properties and it form.

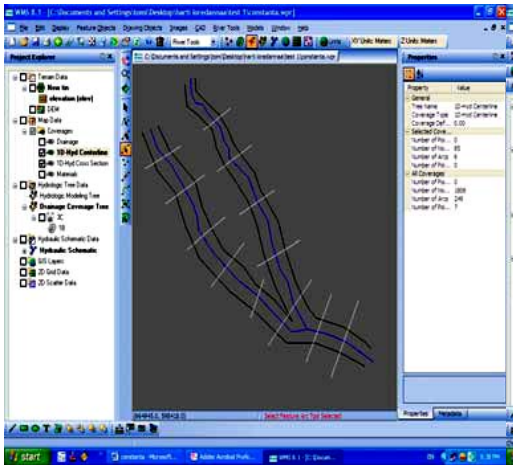

Fig. 5 Cross sections positions

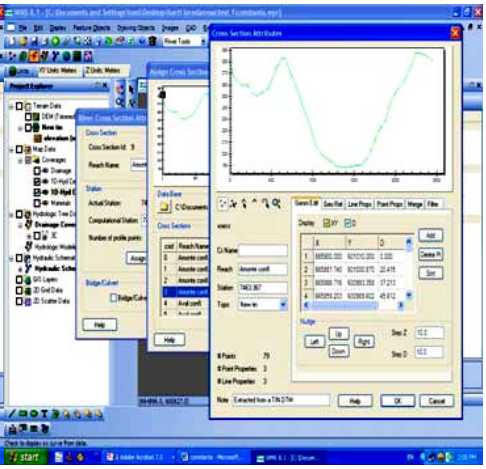

Fig.6 Cross sections properties

The Channel Calculator is a good tool for approximating channel flows or flow depths. Given a flow rate, the Calculator can compute a flow depth, and vice versa. As we calculate flow depths, we need to jot down the depth values so we can recall them later when we create the 2D scatter points. The cross section displays in the small graphics window. With the cross section selected we are ready to set necessary parameters to perform calculations for depths.

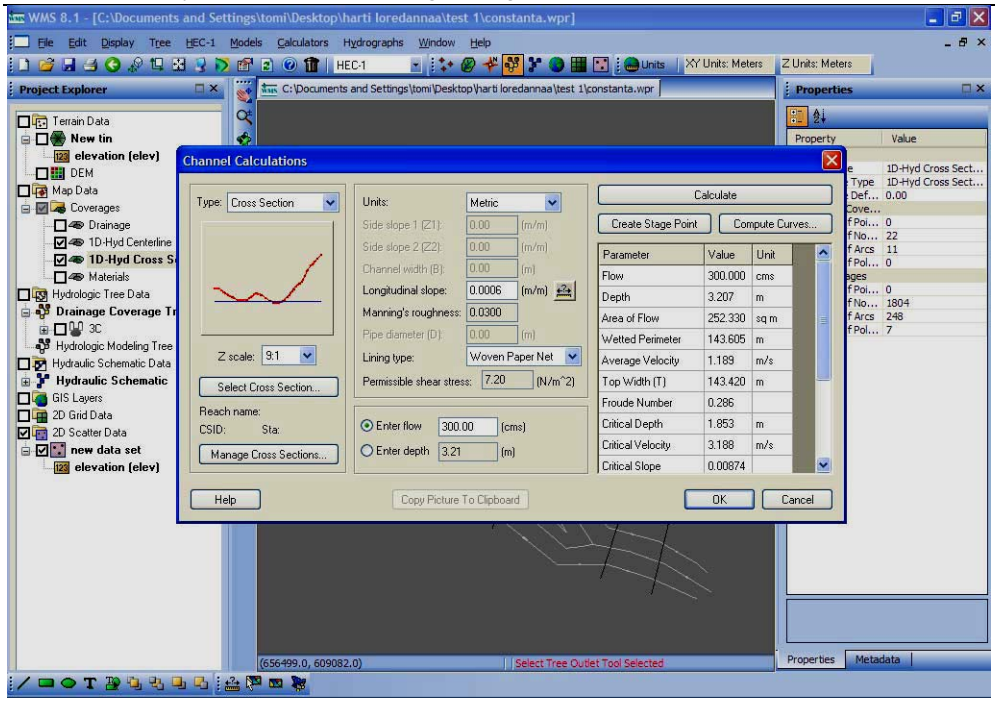

Fig. 7. Calculations depths based on cross sections properties

3. RESULTS AND SIGNIFICANCES

Delineate the Floodplain

We have finished delineating a floodplain based on the water elevations that we calculated on our own.

These color-filled contours shown in Figure 8 represent the varying water surface elevations in the computed floodplain. The next Figure (Fig. 9) will show the varying water depth in the computed floodplain.

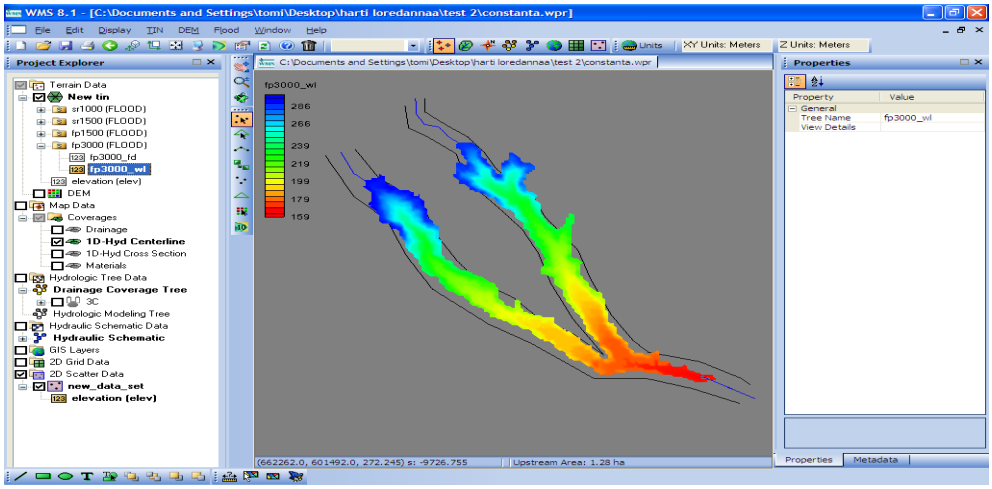

Fig. 8. Water surface

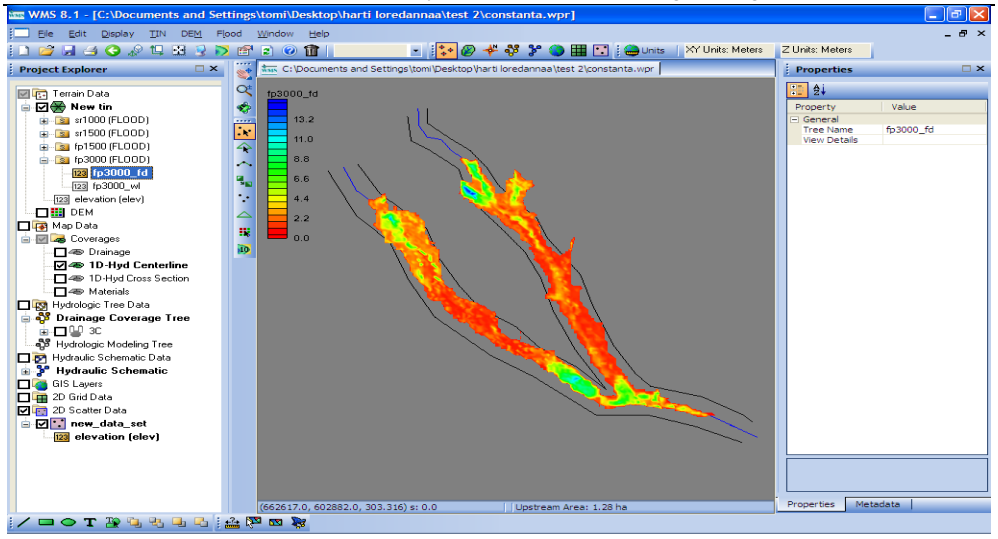

Fig. 9. Water depth results

Creating a Flood Impact Map

WMS can use two separate floodplain delineations to generate a Flood Impact coverage. A Flood Impact coverage shows the difference between two flood depth or water level sets. The differences are divided into ranges or classes. Using the floodplains delineated in the previous steps, we will create a Flood Impact coverage in order to investigate the difference in flooding with and without the proposed levee. Double-click on any one of the polygons, the dialog that opens shows the amount of change from the original data set to the modified data set, as well as the impact class ID and name.

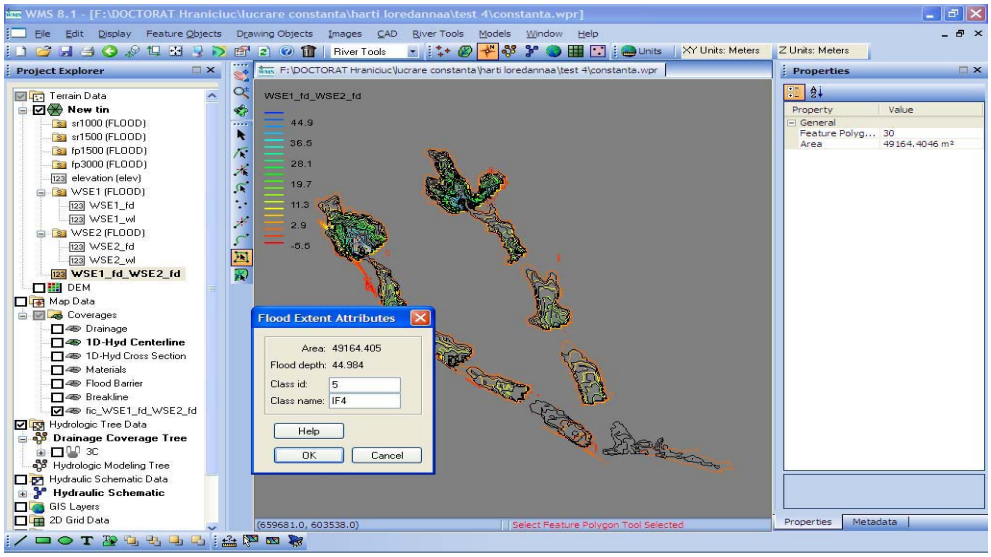

Fig. 10. Flood Impact Map

Using a Flood Barrier Coverage

WMS allows users to "confine" a delineation from the given elevation data by creating a flood barrier coverage. Arcs representing ridges or levees (existing or proposed) may be created in the model, and these in turn alter the floodplain delineation by restricting interpolation of the floodplain so that values on the "dry" side of the levee are not interpolated. In this exercise, a map file of arcs representing a proposed levee will be used to demonstrate the effects of incorporating a flood barrier coverage.

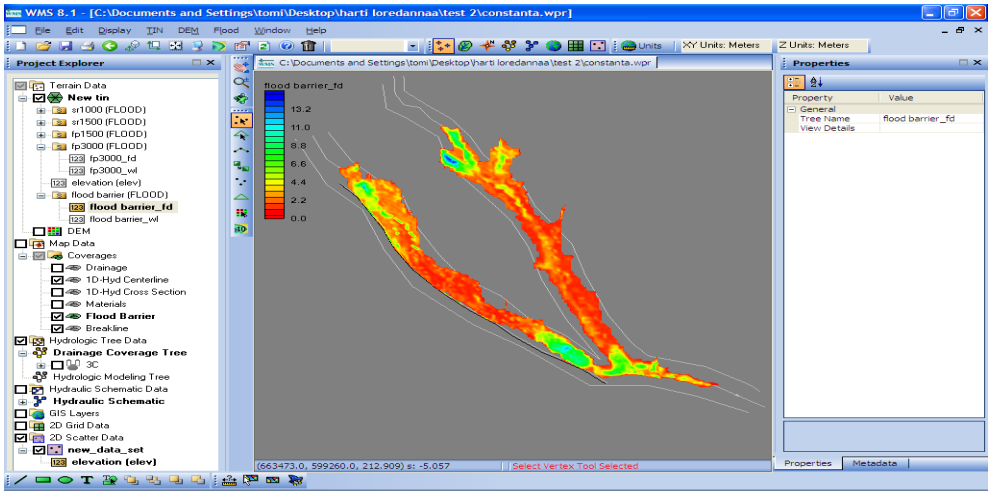

Fig. 11. Flood Barrier Coverage

Creating a Flood Extent Coverage

Flood depth and water level information are stored with the TIN, but WMS allows for the creation of feature objects from this data. In floodplain delineation, it may be useful to create a flood extent coverage. This coverage defines the boundary of the flood and may be exported for use in GIS applications.

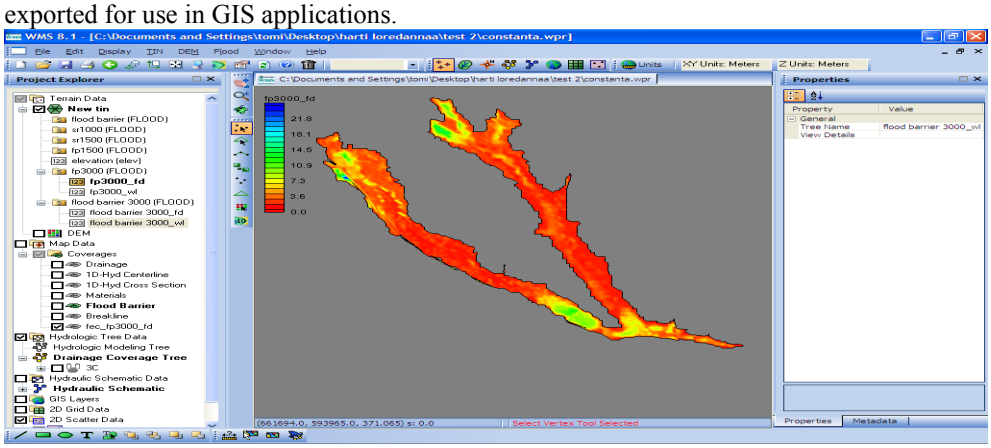

Fig. 12. Flood Extent Coverage

Creating a Flood Depth Coverage

The flood extent coverage essentially divides the watershed area into two parts: flooded and not flooded. However, it is often necessary to know not only if an area is flooded but also how much flooding has occurred. Double-click inside a few of the

polygons that have been created. This will bring up the flood extent attributes, which include the average flood depth for the zone.

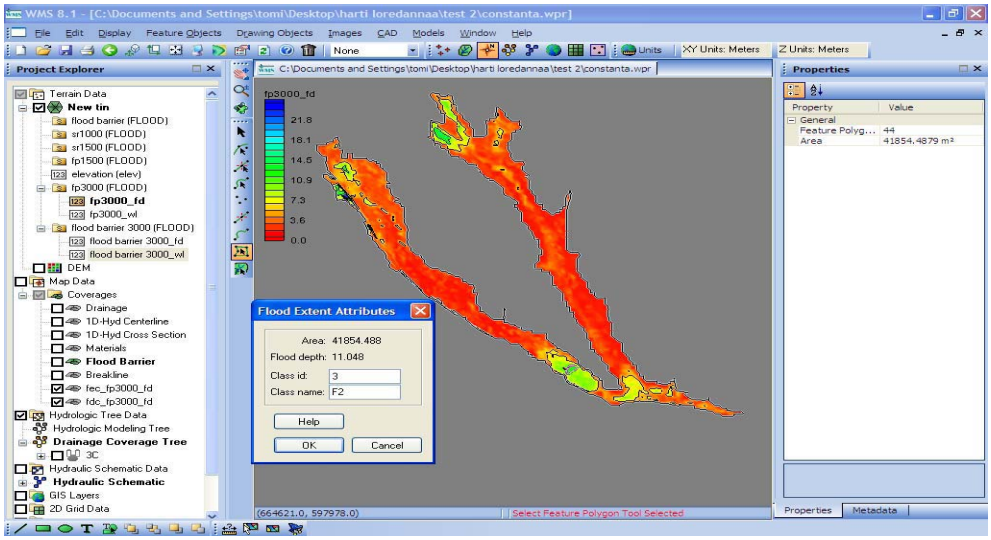

Fig. 13. Flood Depth Coverage

4. CONCLUSIONS

Increased flood risk due to the use of land and climate change are already manifest must be recognized and fully understood and taken into account in schemes of risk management decisions and planning. Flood risk to life and human activities can be minimized through a controlled development flooding areas such as: floodplains delineation (hazard maps), land use regulation, plans planning and preservation of areas of mobility water courses. Regarding the use of modern software in management of flood, was a considerable evolution that helps very much specialists in the field, creating a scheme in the basin in a record time and analyze the evolution of flood depending on the type of work considered.

Using such software may not be just one more ace in the fight against disasters caused by floods. However, it should be paid great attention on the data entered in the program and how to insert, because any disparity or vagueness of data entered may lead to results that do not reflect reality and may mislead the specialists, it has adverse consequences on the basin planning and management of floodplains.

6. REFERENCES

[1] Giurma I. (2000), "Sisteme de gospodărirea apelor", Editura Cermi Iasi.
[2] Giurma I. (2003), Viituri şi măsuri de apărare", Editura Cermi Iasi
[3]Chiriac, V., ş.a. (1980), "Prevenirea şi combaterea inundaţiilor", Editura Ceres Bucuresti.
[4] Leopold, L.B. (1994) "A view of the River" Harvard University Press, Cambridge, Mass.
[5] Chow, V.T., Maidment, D.R. and Mays, L.W. (1988) "Applied Hydrology" Mc Graw-Hill Book Co, New York.

Floodplain Mapping Delineation in Beshar River by Using Arcview Techniques and HEC-RAS Model

A. Salemian* and H. Moosavi Jahromi

Abstract – **The aim of this paper is determine the flood bed of Beshar River in the domain of 650 meters from upstream the Beshar bridge in Yasooj to the 9 kilometers downstream it. The return periods of the floods are 2, 25, and 500 years. The study of the results of the presented mapping in this paper shows that for a flood with 2-years return period about 923359.21 m^2, with a flood with 25-years return period about 1539685.14 m^2, and for a flood with 500 years return period about 1991374.621 m^2 of the left and the right banks of the river under study, are exposed to flood.**

Keywords – **floodplain, return period, mapping, backwater, HEC-RAS.**

1. INTRODUCTION

A floodplain is the normally dry land area adjoining rivers, stream, lakes, bays, or oceans that is inundated during flood events. Flooding is caused by the overflow of streams and rivers and abnormally high tides resulting from severe storms. The floodplain can include the full width of narrow steep stream valleys, or broad areas along streams in wide, flat valleys. The floodplain carries flow in excess of the channel capacity. The greater the discharge, the greater is the extent of inundation.

The aim of this paper is analysis the effect of flood on the left and right banks of Beshar river. The effect of flood with different return periods on the riverbanks is investigated and characteristics of flood mapping (left and right bank) for different return periods are obtained. The surface, surrounding, and the average height of flood mapping for different recurrence periods are also studied.

Considering the erosiveness of Beshar River, and its banks being destroyed in some locations as the result of the floods in this area, the authorities of the office of water affairs in Kohgiloye & Boyer Ahmad province, Iran, have done operations for preserving the river in its critical locations including the distance from 2600 meters from its right with 320 meters long, and 2920 meters distance from the bridge with 280 meters long. The results of this paper can be used for preventing and controlling the erosion of river bed and banks [1-2].

In Section 2 we will briefly review the data and metodology of analysis. Section 3 will give the main result of our work. For simulation and floodplain mapping, the Arcview Techniques and HEC-RAS Model are used.

Manuscript received March 9, 2010

Amirreza Salemian is with Civil Engineering Department, Islamic Azad University of Dehdasht, Dehdasht, Iran, phone: +98-744-3227172; e-mail: el_amirreza@yahoo.com

Habib Moosavi Jahromi is with Water Sciences Engineering, Shahid Chamran University of Ahwaz, Ahwaz, Iran.

ISSN-1584-5990

2. DATA AND METHODOLOGY

The equations ruling the flow are Saint-Venant equations which include continuity, momentum, and energy equations.

Continuity equation: $$T\partial y/\partial t + A\partial v/\partial x + v\partial A/\partial x = \pm q_l \quad (1)$$

Momentum equation: $$\partial v/\partial t + v\partial v/\partial x + g\partial y/\partial x = g(S_0 - S_f) \quad (2)$$

Energy equation: $$p/\rho g + z + v^2/2g = H \quad (3)$$

Where T is the top width, y is the depth of flow section, A is the cross section of flow, v is the mean velocity of flow, S_f is the change of energy with longitudinal distance, S_0 is the channel bottom slop, $p/\rho g$ is the pressure head, $v^2/2g$ is the velocity head, z is the elevation head, H is the total head q_l is the lateral discharge in unit length. These equations do not have analytical solutions, and should be solved by using numerical methods [3].

Surface flow in open channels is always governed by energy head, velocity head, and pressure head [4]. The HEC-RAS simulates open channel flow and is able to operate with sub-critical, super-critical, and mixed flow regimes. For instance, the following two equations are used for modeling sub-critical flow using an iterative procedure for the downstream (Equation 4) and upstream (Equation 5) sections respectively,

$$WS_2 + (\alpha_2 V_2)/2g = WS_1 + (\alpha_1 V_1)/2g + h_e \quad (4)$$

$$h_e = L S_f + C[(\alpha_2 V_{22})/2g - (\alpha_1 V_{12})/2g] \quad (5)$$

where WS_1 and WS_2 are the water surface elevations at ends of reach, V_1 and V_2 are the mean velocities at ends of reach, and α_1 and α_2 are the velocity or energy coefficients for flow at ends of reach, h_e is the energy head loss, g is the gravitational constant, L is the discharge-weighted reach length, S_f is the representative friction slope for reach, and C is the expansion or concentration loss coefficient[5].

Fig. 1: Yasooj city on the map

Solving Saint-Venant equations simultaneously, leads to the creation of kinematics, diffusive, and dynamic waves [6] Solving these waves numerically by using explicit and implicit methods, the equations of flow could be solved, and the unknown parameters like discharge and cross section of flow can be obtained. In this study, HEC-RAS software by using the dynamic wave model has solved the equations of flow and found the unknown parameters [7].

The domains of left and right banks of the River exposed to flood with different discharges in different return periods will be determined by mapping. Beshar River has the geographical location 510 to 520 east length and 300 to 310 north width. This domain is 4300 high, and its lowest height is 1740m. Its surface is 2737 km^2. Yasooj as the provincial capital of Kohgiloye & Boyer Ahmad is the most populated city of this province which has surrounded Beshar River [1-2]. The studied domain includes 650 meters from upstream Beshar located in Yasooj to 9 km downstream (Shahmokhtar bridge) This domain is between two stations of Ghalat and ShahMokhtar . the location of Yasooj city on the map is shown in figure 1. The Hydrography network and hydrometry stations of Beshar river watershed zone is given in figure 2 and topography of the river is displayed in figure 3.

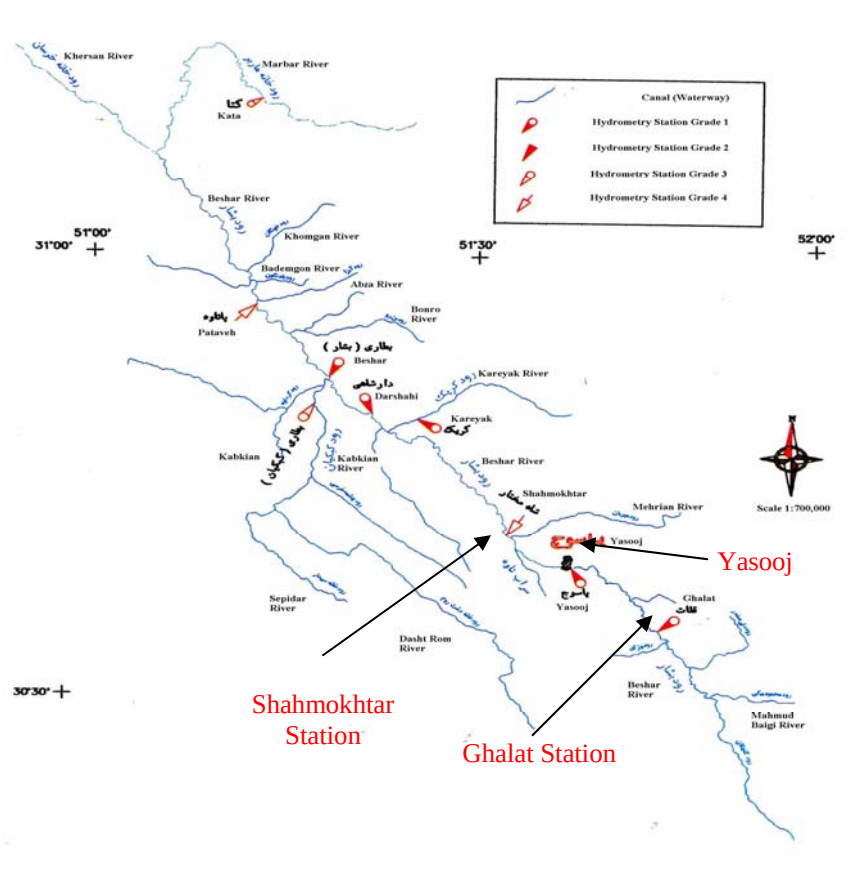

Fig. 2: Hydrography network and hydrometry stations of Beshar river watershed zone

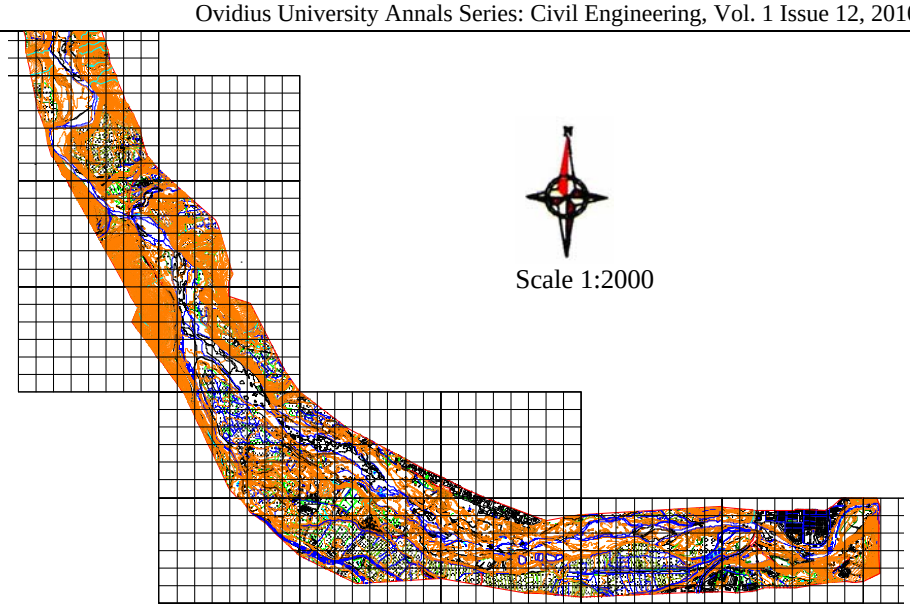

Fig. 3: Topography of the Beshar River (Scale 1:2000)

The direction of the study in this part is based on the hydrology of surface waters, and the conditions of hydrometric stations. The stations studied in this study are Shahmokhtar and Ghalat.

The analysis of the statistics and information of surface water, and making use of its results in other parts of the project is of great importance. Hence, in this part of the study, the amount of annual precipitation is studied, and the amounts of discharge with return periods of 2, 25, and 500 years have been used. The given discharges have been obtained by hydrologic methods [8].

Table1: amounts of discharge with different return periods [1]

discharge	**return period**
$Q=282.3m^3/s$	2-year
$Q=7363m^3/s$	25-year
$Q=1215.6m^3/s$	500-year

After calibration roughness coefficient For Ghalat and Shah Mokhtar Stations n= 0.045 is acceptable [9].

In a GIS environment, the best available digital topographic data for the subject area is used in conjunction with an automated hydrologic and hydraulic tool to extract the watershed geometry characteristics into a conventional hydraulic modeling platform. For the purposes of this paper, the automated method is assumed to be GeoRAS exporting to/from a current version of HEC-RAS (i.e. version 3.1.3).

Using the GeoRAS tool, layers representing the spatial alignment of the stream centerline, bank station locations, flow paths (for determining the left overbank, right overbank, and channel distances), and cross sections are created. The geometry and spatial attributes are extracted and exported to HEC-RAS[10].

If the general structure dimensions (height from channel invert, width of opening, opening type, etc.) are known, the structure can be added to the model geometry. While not required, the inclusion of even the most basic structure geometry helps ensure that its

hydraulics effects are factored into the calculated floodplain and water surface elevations (WSELs). This minimal amount of additional input helps provide a much more accurate calculation of the floodplain for the amount of extra effort required. It is important to note that if structure data is to be incorporated, the location of all applicable structures should be identified at the initial stages of the GeoRAS layer creation, such that the appropriate bounding cross sections can be placed. This will ensure that the natural channel geometry is reflected in the HEC-RAS model at the locations where structure data is to be entered. If no structure data is available, the road crossing can be modeled as a weir, which typically results in a more conservative floodplain

After completion of the HEC-RAS model, the output is then exported back to a GIS environment, and the calculated WSELs are compared to the topographic data. At each cross section, areas where the calculated WSEL is higher than the ground elevation are determined to be within the floodplain, and a spatially referenced, polygonal shapefile is created representing the floodplain boundaries which can then be utilized for any number of applications and is easily transferable to other digital formats [11].

3. RESULTS AND DISCUSSION

An instance of the results of mapping for different return periods is given in figures and charts below.

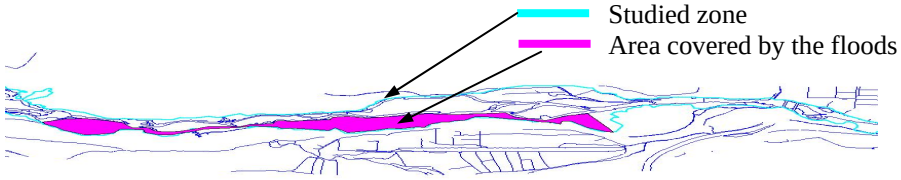

Fig. 2-1: two – year mapping

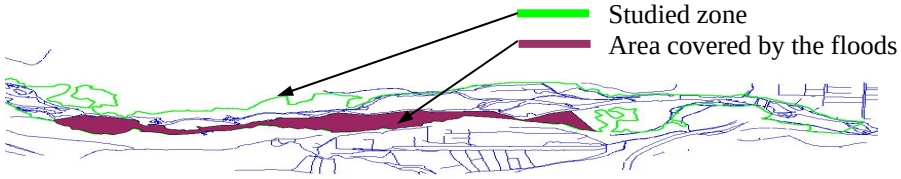

Fig. 2-2: 25 – year mapping

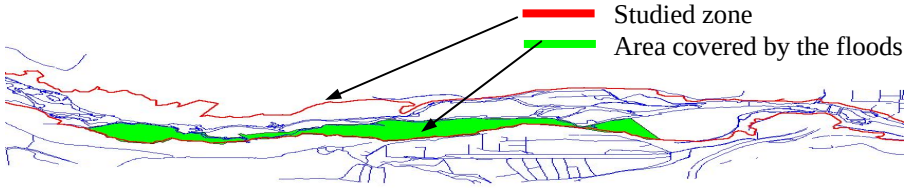

Fig. 2-3: 500 – year mapping

Figure 2: The comparison of flood mapping (left bank) for different return periods.

Figure 2 is the representation of the flood mapping of the River in the domain of this project for 2, 25, and 500- year return periods. As it is seen in the figure the location of the left bank mapping of Beshar River is in the 989 meters distance downstream the bridge located in Yasooj.

The studies show that surface, surrounding, and the average height of flood mapping for different recurrence periods are as follows.

Table 2: the characteristics of flood mapping (left bank) for different return periods (989 meters distance downstream the Beshar bridge in Yasooj).

Return period	**The Average Height of flood(m)**	**The surrounding of mapping (m)**	**The area of mapping (m^2)**	**The distance from Beshar bridge(m)**	**Location of mapping**
2years	1.046	5984.367	2l0903.l01	989 meters downstream the bridge	Left bank
25 years	1.76	6155.917	275934.635	989 meters downstream the bridge	Left bank
500 years	2.30	6160.601	316997.928	989 meters downstream the bridge	Left bank

Table 2 characteristics of flood mapping (left bank) in the domain of the project for different return periods (in the 989 meters distance downstream the Beshar bridge in Yasooj). Considering the table above the surface of a 25 years flood in Comparison to a 2 years flood had 31 percent of increase, the 500 years in comparison to the 2 years had 51 percent of increase, and the 500 years in comparison to the 25 years had 15 percent of increase. Whenever the reduction of the width of the river is so that the special energy in the contracted point is lass than the minimum energy in that point, because no point on the curve E-Y will be the answer to the problem, this is not physically possible. So, if the condition of the flow in the upside the given point is critical the result will be a backwater, and the specific energy in the beginning of the contraction increases so much that the flow in the contracted area is possible with the least possible specific energy . This is done by the increase of the depth of the river in the upstream of the river. In this case the depth in the contracted area will be fitted on the critical depth in that area [12-13].

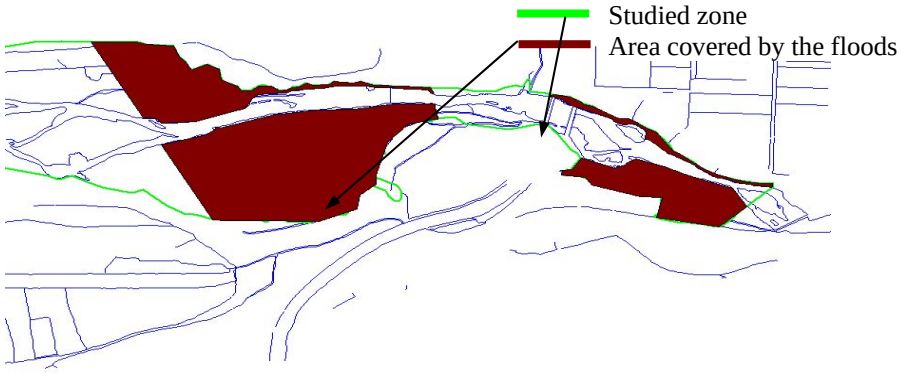

Fig. 3-1: 25 years mapping before backwater

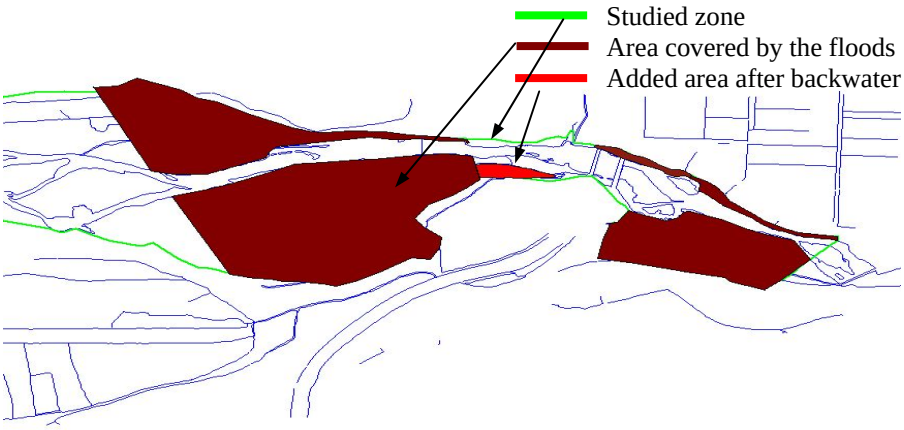

Fig. 3-2: 25 years mapping after backwater
Figure 3: the comparison of the 25 years mapping before and after the backwater in the area of the project.

The comparison of the results of this study for different return periods is done, and for the flood with 25 years return period the results of the comparison of the results before and after backwater are as follows.

Considering the previous figure, the comparison of the surface of flood mapping with the 25 years return period before and after backwater, the table below is given.

Table 3: The comparison of the surface of flood mapping with the 25 return periods before and after the backwater

return Period	**The percentage of the increase in area after backwater in comparison to before it**	**The area of mapping (m^2)**	
		Before backwater	**after backwater**
25	28.7	254397.872	327430.09

It should be said that the red area is only under flood because of backwater and its area is 5086.848 m^2.

4. CONCLUSIONS

The study of the results of the presented mapping in this paper shows that for a flood with 2-years return period about 923359.21 m^2, with a flood with 25-years return period about 1539685.14 m^2, and for a flood with 500 years return period about 1991374.621 m^2 of the left and the right banks of the river under study, are exposed to flood. Results show that the surface of a 25 years flood in Comparison to a 2 years flood had 31 percent of increase, the 500 years in comparison to the 2 years had 51 percent of increase, and the 500 years in comparison to the 25 years had 15 percent of increase.The comparison of the surface of flood mapping with the 25 years return periods before and after the backwater shows 28.7 percen of the increase in area after backwater.

Considering the presented results it is found that a great portion of the left and right banks of Beshar River are exposed to flood that it is a consequence of the decrease in the

right and left heights , the decrease in the width, and the occurrence of backwater in the contracted areas of Beshar River.

6. REFERENCES

[1] The center for basic studies of water affairs of Kohgiloye & Boyer Ahmad.
[2] The center for planning and development of water affairs in kohgiloye & Boyer Ahmad
[3] V.T. Chow, 1959 "open channel hydraulics" McGraw-Hill, New York
[4] Hwang and Hita, 1987, "Fundamentals of Hydraulic Engineering Systems"
[5] R. Abdalla, C. Vincent Tao, Q. Cheng, and Jonathan Li, "A Network-centric Modeling Approach for Infrastructure Interdependency" ASPRS 73 (6) 2007, pp.681-690
[6] V.M. Ponce, R.M. Li and D.B Simsons, "Applicability of kinematics and diffusion models," J. hydraulics division 104 (HY3) 1978, pp.353-360
[7] R.J. Fennema and M.H. Chaudhry, "Numerical solution of 2-D free surface flow: Explicit methods" J. Hyd. Eng., ASCE, 116 (8) 1990 pp.1013-1034
[8] W. Viessman, J.W Kapp, G.L Lewis, and T.E Harbaugh, 1972, "Introduction to hydrology" 2nd ed., Harper & Raw, New York.
[9] W.L Cowan, "Estimating hydraulic roughness coefficient" Agricultural engineering 37 (7) 1956 pp.473-75
[10] http://www.hec.usace.army.mil/software/hec-ras/hec-georas.html
[11] M. Urisko, J. Urisko, M. DePue, "Revision techniques incorporated in the Georgia map modernization program" Proceedings of the 2007 Georgia Water Resources Conference, March 27–29, 2007, University of Georgia
[12] C.J Kiefer and H.H Chu, "Backwater functions by numerical integration" Trans. American Soc. Civil Eng., 120, 1995, pp.429-442
[13] R.H. French, 1985 "open channel hydraulics" McGraw-Hill, New York

Parametric models for the soil hydraulic functions

Florian Stătescu, Dorin Cotiuşcă Zaucă, Vasile Lucian Pavel and Constantin Victor Stătescu

Abstract – **Water flow in unsaturated or partly saturated soil is traditionally described with the Richards equation. The unsaturated soil hydraulic functions in this equation are the soil water retention curve θ(h), the hydraulic conductivity K(h) or K(θ), and the soil water diffusivity function D(θ). Using SoilPara software, based on the two models (Mualem and Burdine), a study was conducted concerning the hydraulic characteristics of several textural soil specimens with different compaction degrees. This software made possible a selective use of the two models, and the results were comparatively analyzed depending on their characteristics.**

The paper is a theoretical study and includes: the presentation of the most used mathematical models describing the hydraulic properties of the soils, a software which can calculate these properties, and a simulation for showing some of its using conditions.

Keywords – **conductivity, diffusivity, model, retention curve, soil.**

1. INTRODUCTION

Water flow in unsaturated or partly saturated soil is traditionally described with the Richards equation [4] as follows:

$$C\frac{\partial h}{\partial t}=\frac{\partial}{\partial z}\left(K\frac{\partial h}{\partial z}-K\right) \tag{1}$$

where h is the soil water pressure head (with dimension L), t is time (T), z is soil depth (L), K is the hydraulic conductivity (LT^{-1}) and C is the soil water capacity (L^{-1}), approximated by the slope ($d\theta/dh$) of the soil water retention curve, θ(h), in which θ is the volumetric water content (L^3L^{-3}). Equation (1) may also be expressed in terms of the water content if the soil profile is homogeneous and unsaturated ($h \le 0$):

$$\frac{\partial \theta}{\partial t}=\frac{\partial}{\partial z}\left(D\frac{\partial \theta}{\partial z}-K\right) \tag{2}$$

Florian Stătescu, Prof. Gheorghe Asachi" Technical University of Iasi, Bd. D. Mangeron nr.65, 700050- Iasi, Romania (phone: +40-232-477553; fax: +40-232-231041; e-mail: fstatesc@hidro.tuiasi.ro).

Dorin Cotiusca Zauca, Conf. "Gheorghe Asachi" Technical University of Iasi, Bd. D. Mangeron nr.65, 700050- Iasi, Romania; e-mail: cotiusca@hidro.tuiasi.ro).

Vasile Lucian Pavel, Asist. "Gheorghe Asachi"Technical University of Iasi, Bd. D. Mangeron nr.65, 700050- Iasi, Romania; e-mail: pvlpavel@yahoo.com.

Constantin Victor Statescu, Ma Student, Katholieke Universiteit Leuven, Belgium; e-mail: victorstatescu@yahoo.com.

ISSN-1584-5990

where D is the soil water diffusivity (L^2T^{-1}), defined as:

$$D = K\frac{dh}{d\theta} \tag{3}$$

The unsaturated soil hydraulic functions in the above equations are the soil water retention curve θ(h), the hydraulic conductivity K(h) or K(θ), and the soil water diffusivity function D(θ) (can be calculated from θ(h) and K(h) curves). Parametric models of these functions are reviewed in detail below.

Several functions have been proposed to empirically describe the soil water retention curve. One of the most popular functions is the equation of Brooks and Corey [1]:

$$\theta = \begin{Bmatrix} \theta_r + (\theta_s - \theta_r)(\alpha h)^{-\lambda} & ,(\alpha h \succ 1) \\ \theta_s & ,(\alpha h \le 1) \end{Bmatrix} \tag{4}$$

where θ_r and θ_s are the residual and saturated water contents, respectively; α is an empirical parameter (L^{-1}), whose inverse is often referred to as the air entry value or bubbling pressure, and λ is a pore-size distribution parameter affecting the slope of the retention function. For notational convenience, h and α for the remainder of this report are taken positive for unsaturated soils (i.e., h denotes suction).

Equation (4) may be written in a dimensionless form as follows:

$$S_e = \begin{Bmatrix} (\alpha h)^{-\lambda} & ,(\alpha h \succ 1) \\ 1 & ,(\alpha h \le 1) \end{Bmatrix} \tag{5}$$

where S_e is the effective degree of saturation, also called the reduced water content ($0 \le S_e \le 1$):

$$S_e = \frac{\theta - \theta_r}{\theta_s - \theta_r} \tag{6}$$

Close results can be obtained using the equation of van Genuchten [1980]:

$$S_e = \frac{1}{\left[1 + (\alpha h)^n\right]^m} \tag{7}$$

where α, n and m are empirical constants affecting the slope of the retention curve.

Typically, m and n will then become strongly correlated, leading to poor convergence and ill-defined parameter values, with large confidence intervals. More stable results are generally obtained when the restrictions m=1-1/n or m=1-2/n [7] are implemented for these incomplete data sets. Another, more pragmatic consideration for selecting one of the restricted m, n cases is the rather complicated form of the predictive

equation for the unsaturated hydraulic conductivity when the variable m, n case is combined with one of statistical pore-size distribution models.

The model of Mualem for predicting the relative hydraulic conductivity [3], K, may be written in the form:

$$K(S_e) = K_s S_e^{\ell}\left[\frac{f(S_e)}{f(\ell)}\right]^2 \tag{8}$$

where $$f(S_e) = \int_0^{S_e} \frac{1}{h(x)}dx \tag{9}$$

in wich S_e is effective degree of saturation (given by equation 6), K_s is the hydraulic conductivity at saturation, and ℓ is a pore-conectivity parameter.

When the Brooks and Corey retention function (5),i.e.,

$$h = \frac{1}{\alpha S_e^{1/\lambda}} \tag{10}$$

the hydraulic conductivity function becomes

$$K(S_e) = K_s S_s^{\ell+2+2/\lambda} \tag{11}$$

or as a function of pressure head (αh>1)

$$K(h) = \frac{K_s}{(\alpha h)^{\lambda(\ell+2)+2}} \tag{12}$$

The soil water diffusivity function becomes in this case

$$D(S_e) = \frac{K_s S_e^{\ell+1+1/\lambda}}{\alpha\lambda(\theta_s - \theta_r)} \tag{13}$$

Equations (10) trought (13) also represent the limiting equations for the van Genuchten model [6] with variable m,n when $n\to\infty$ while keeping the product $\lambda = mn$ finite.

The model of Burdine [2] can be written in a general form as follows:

$$K(S_e) = K_s S_e^{\ell}\frac{g(S_e)}{g(\ell)} \tag{14}$$

where $$g(S_e) = \int_0^{S_e} \frac{1}{[h(x)]^2}dx \tag{15}$$

Results analogous to those for Mualem 's model can be derived also for Burdine's model. Since the derivations for both models are very similar we give here only a brif synopsis. Substituting the inverse $h(S_e)$ into (15) and using $x=y^m$ gives:

$$g(S_e) = \alpha^2 m \int_0^{S_e^{1/m}} y^{m-1+2/n} (1-y)^{-2/n} dy \tag{16}$$

The hydraulic conductivity function is given by the expression:

$$K(S_e) = K_s S_s^{\ell+2+2/\lambda} \tag{17}$$

or as a function of pressure head ($\alpha h>1$)

$$K(h) = \frac{K_s}{(\alpha h)^{\lambda(\ell+2)+2}} \tag{18}$$

and the diffusivity function becomes in this case:

$$D(S_e) = \frac{K_s S_e^{\ell+1+1/\lambda}}{\alpha\lambda(\theta_s - \theta_r)} \tag{19}$$

Equations (17) through (19) are the classical equations of Brooks and Corey.

The soil water retention curve, $\theta(h)$, contains 5 parameters, i.e., θ_r - the residual water content, θ_s - the saturated water content, and the shape factors α, m, n – empirical parameters. The predictive equations K and D introduce two additional unknowns: ℓ – the pore connectivity parameter and K_s – the saturated hydraulic conductivity.

2. SIMULATION

Using SoilPara software [7], based on the two models as well (Mualem and Genuchten), a study was conducted concerning the hydraulic characteristics of several textural soil specimens with different compaction degrees. This software made possible a selective use of the two models, and the results were comparatively analyzed depending on their characteristics.

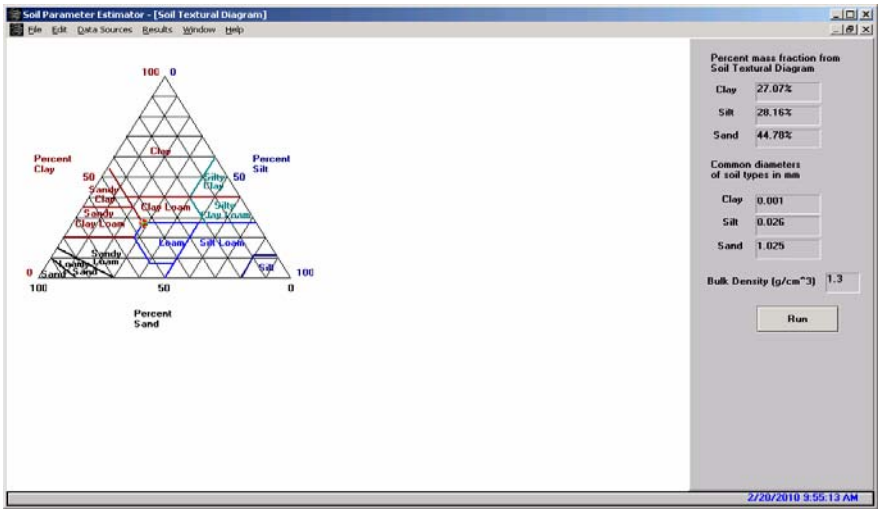

Fig. 1. Soil texture diagram

The SoilPara Estimator allows the selection of the following parameters:

a) Soil texture and bulk density (DA) (**Fig. 1.**);

b) A model type determines the conductivity model and the constraints imposed on van Genuchten parameters during the analysis (**Table 1** and **Fig. 2**).

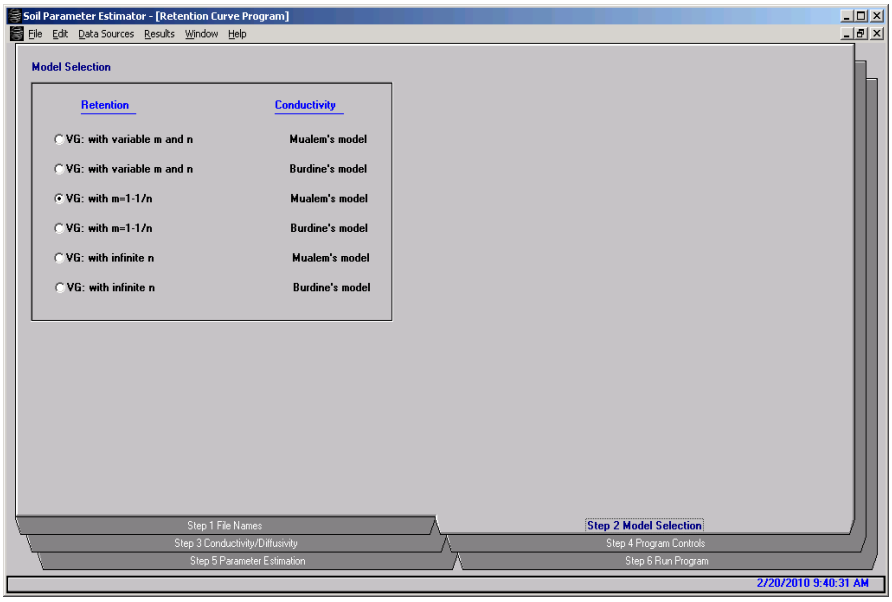

Fig. 2. Model selection

After running the program, we obtain the final values of the studied parameters (θ_r, θ_s, α, n, ℓ) and suction curve (**Fig. 3.**).

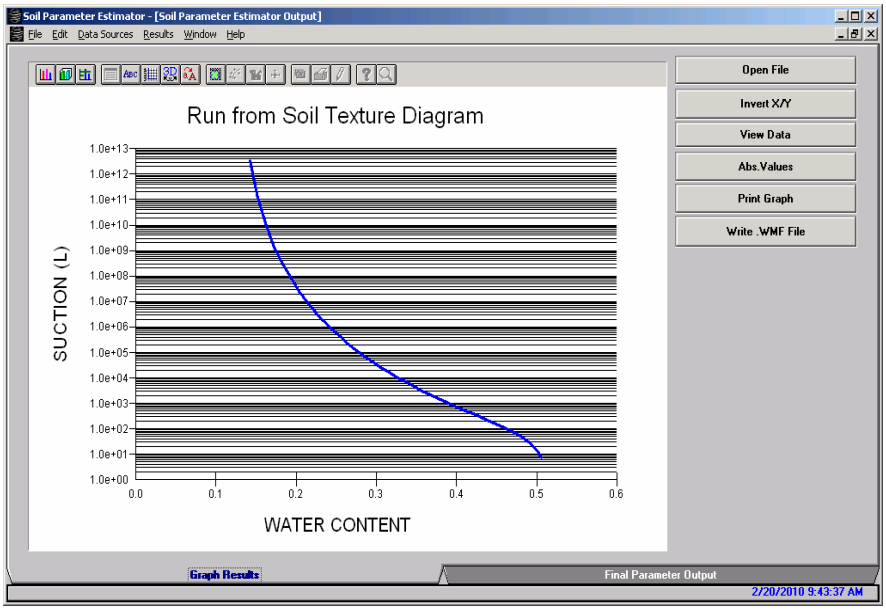

Fig. 3. Output file

Table 1. - Type of retention and conductivity models implemented as a function of the input variable MTYPE

MTYPE	Retention model	Conductivity model
a	Eq. 7 with variable m,n	Mualem 's model (Eq. 8)
b	Eq. 7 with variable m,n	Burdine's model (Eq. 14)
c	Eq. 7 with variable m=1-1/n	Mualem 's model (Eq. 8)
d	Eq. 7 with variable m=1-2/n	Burdine's model (Eq. 14)
e	Eq. 7 with $n \rightarrow \infty^+$	Mualem 's model (Eq. 8)
f	Eq. 7 with $n \rightarrow \infty^+$	Burdine's model (Eq. 14)

3. RESULTS AND DISCUSSION

Using SoilPara program, the hydraulic functions of soils were determined, for classes of texture and bulk density presented in **Tables 2** and **3**.

Table 2. Textural class

Code	Type	Clay (%)	Silt (%)	Sand (%)
01	Sandy	10	30	60
03	Sandy Clay Laom	25	30	45
05	Clay	45	30	25

Table 3. Bulk density (DA)

Code	DA (g/cm^3)	Code of texture	Characterisation
1	1.28	01	Very loose
		03	Not settled
		05	Poor settled
2	1.36	01	Loose
		03	Not settled
		05	Moderate settled

We have analyzed 36 variants [5], derived from the combination of the 3 textured classes, 2 classes of bulk density and the 6 types of retention and conductivity models, as seen in **Table 1.**

The values obtained for θr (WCR), with the distribution presented in **Fig. 4.** and θs (WCS), with distribution shown in **Fig. 5.**, were statistically processed, establishing media (Xm), standard deviation (s) and coefficient of variation (Cv) (**Table 4**.).

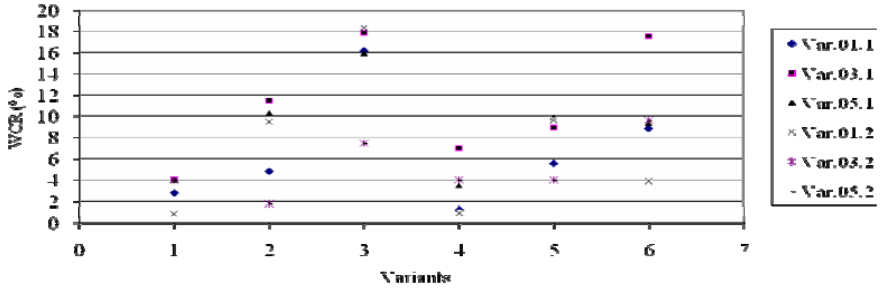

Fig. 4. Distribution values θr (WCR), for the 6 variants

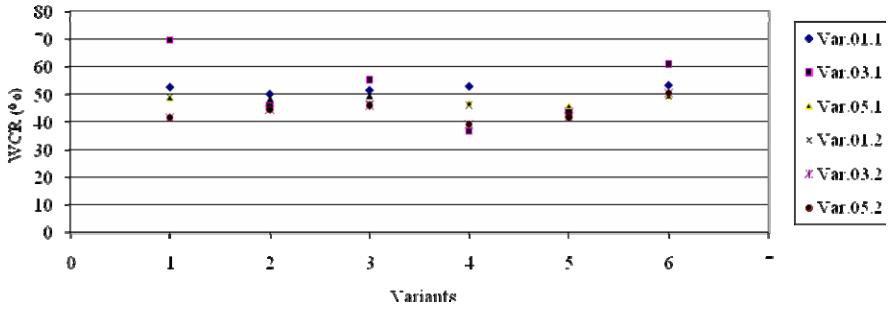

Fig. 5. Distribution values θ_s (WCS), for the 6 variants

Tabel 4. Results obtained

Variants	θ_r (%)			θ_s (%)		
	X_m (%)	s	C_v (%)	X_m (%)	s	C_v (%)
01.1.a…f	3.75	0.54	14.52	46.69	5.76	12.33
03.1.a…f	9.02	2.91	32.26	46.45	2.32	4.99
05.1.a…f	17.05	1.22	7.17	49.10	2.98	6.06
01.2.a…f	4.62	1.60	34.63	44.81	5.84	13.03
03.2.a…f	8.5	2.01	23.64	44.00	2.38	5.40
05.2.a…f	9.34	0.11	1.17	50.51	1.72	3.40

Analysis of obtained results pointed out the following aspects:

a) the pore connectivity parameter was $\ell = 0.5$ in all studied variants;

b) values obtained for the parameters θr - the residual water content and θs - the saturated water content range within stipulated values;

c) coefficient of variation calculated for θr values enroll in the limits of 1.17-34.63;

d) coefficient of variation calculated for θs values are inscribed in the limits 3.40 - 13.03;

e) The range of obtained results being relatively large, shows that it is also necessary an experimental and detailed study to compare the results and get relevant conclusions.

The SoilPara Estimator has three methods to calculate soil water retention parameters: using soil texture diagram, using typical USDA values (there are up to 12 different soil types included in this section) and using laboratory data available.

4. CONCLUSIONS

The Software SoilPara is easy to use and to calculate soil water retention parameters. This can be applied to four broad classes of problems:

a) May be used to calculate the unsaturated soil hydraulic functions if the model parameter vector b = (θ_r, θ_s, α, n,m, ℓ , K_s) is specified by the user.

b) Predicting K/D from observed θ(h) data. This option permits one to fit the unknown retention parameters (with or without restricted m,n values) to observed soil water retention data. The fited retention parameters are subsequently used to predict the hydraulic conductivity and diffisiviti functions by making use of the models of Mualem or Burdine.

c) Predicting θ(h) from observed K/D data. May be used to fit the unknown hydraulic coefficients to observed conductivity data using one of the available predictive conductivity or difussivity models.

d) Simultaneos fit of retention and K/D data. This option results in a simultaneous fit of the model parameters to observed water retention and hydraulic conductivity or difussivity data.

The use of Software SoilPara proves to be a handy alternative for various on site studies.

5. ACKNOWLEDGMENTS

This work was supported by the C.N.C.S.I.S., research project ID_1887, entitled: Innovative Research of Monitoring the Dynamics of Hydraulic Soil Properties, Generated by Climate Changes.

6. REFERENCES

[1]. Brooks, R.H. and Corey, A.T., *Properties of porous media affecting fluid flow*, Journal Irrig. Div. Am. Soc. Civ. Eng., 92(IR2):61-88, 1966.
[2]. Burdine, N.T., *Relative permeability calculations from pore-size distribution data*, Petrol. Trans. Am. Inst. Min. Eng., 198:71-77, 1953.
[3]. Mualem , Y., *Hydraulik Conductivity of unsaturated soils: Prediction and formulas*, In A. Klute (ed.), Methods of Soil Analysis, Part1. Physical and Mineralogical Methods, American Society of Agronomy , Madison, Wisconsin, p. 799-823, 1986.
[4]. Richards, L.A., *Capillary conduction of liquids through porous mediums*, Physics, 1:318-333, 1931.
[5]. Stătescu, Fl., *Tehnici inovative de monitorizare a dinamicii caracteristicilor hidraulice ale solului, generate de schimbările climatice*, proiect ID_1887, finanţat de CNCSIS, 2009.
[6]. Van Genuchten, M.Th., *Indirect methods for estimating the hydraulic properties of unsaturated soils*, Proc. Int. Workshop, University California, 1991.
[7]. SOILPARA, *Software to determine hydraulic properties of unsaturated/saturated soils*, License Resource & systems International Inc., 1995.

Floodplains determination based on mathematical models and measurements

Adelina Elena Stoica, Nicolai Sîrbu and Virgil Petrescu

***Abstract* – Floods are natural phenomena with profound implications on the human society development, as they are some of the most widespread disasters. Floods together with their consequences lead inevitably to the need for suitable management of risk and for determination of floodplains**.

This paper aims to determine areas susceptible to flooding of one river basin, on the basis of measurements and mathematical models simulating the open channel flow, and finding technical solutions for the management of these areas in the catchment.

Setting the floodplain boundaries was done by generating specific maps according to the river flow rates with different probabilities of expedience. Based on these maps it is possible to define to what extent are affected areas, population, economic and social objectives, etc.

As a result of this work the boundaries of floodable areas obtained for a given perimeter, and their spatial extension as function of the river discharge are presented.

The work is part of the concerns at national and international level for identification of areas susceptible to flooding, and it is the starting point in drawing up flood risk maps.

***Keywords* – flood maps, floodplain, river basin, risk maps.**

1. INTRODUCTION

Floods are the most geographically widespread disasters around the world and also the largest producer of damage and fatalities. Large river flows, and thus flooding, generally cannot be avoided but can be managed. Their effects can be reduced by a set of measures and actions to help mitigate the risk associated with these phenomena. Floods with their consequences make the necessary management and assessment of flood sensitive areas. These are challenges frequently addressed nationally and internationally levels, trying to find the best strategies and solutions in the field.

Assessment of flood susceptible areas is done by setting limits to flooding with simulation models with free surface flow, taking into account the influence of the hydraulic

Adelina Elena Stoica, Eng. PhD Student, Technical University of Civil Engineering of Bucharest, Bd. Lacul Tei, nr. 124, 020396- Bucharest, Romania (phone: +40-21-2433630; fax: +40-21-2433630; e-mail: adelinastoica@gmail.com).

Nicolai Sîrbu, Lecturer, PhD, Technical University of Civil Engineering of Bucharest, Bd. Lacul Tei, nr. 124, 020396- Bucharest, Romania (phone: +40-21-2433630; fax: +40-21-2433630; e-mail: nsirbu@utcb.ro).

Virgil Petrescu, Professor, PhD, Technical University of Civil Engineering of Bucharest, Bd. Lacul Tei, nr. 124, 020396- Bucharest, Romania (phone: +40-21-2433630; fax: +40-21-2433630; e-mail: virgil.petrescu2007@gmail.com).

ISSN-1584-5990

structures (bridges, culverts, weirs, dams, spillways, etc.). European approach to flood risk management as a subchapter of the integrated management of water resources is done in accordance with:

• Water Framework Directive (2000/60/EC), adopted on October 23, 2000, which establishes a framework for Community water policy, aiming to achieve sustainable water management in all Member States.

• Framework Directive on floods (2007/60/EC), approved by Parliament on October 23, 2007, which requires all Member States to conduct a preliminary assessment by 2011 to identify streams in flood risk, 2013 to draw maps of flooding and property at risk and also in 2015, to take appropriate and coordinated measures to reduce flood risks through risk management plans focused on flood prevention, protection and preparedness.

In Romania, the flood risk management is established through the norms on the elaboration and content of flood risk maps, to be completed National Strategy for flood risk management.

2. MATHEMATICAL MODELING OF FLOODING LIMITS

Setting limits of flood for a given area is made by mathematical modeling with specialized programs, and then all results will be integrated into a geospatial database linked to a GIS (Geographical Information System) for the preparation of flood risk maps**.**

There are many mathematical models that simulate the open channel flow given by software like MIKE 11. It provides a library of computational methods for steady and unsteady flows in branched and looped channel networks, as well as quasi two-dimensional flow simulation on floodplains. Other software used in modeling the floodplains is SMS package (Surface Water Modeling System), which use the model presented by HEC-RAS (Hydrologic Engineering Center for River Analysis System) for the one-dimensional case.

HEC-RAS simulates the hydraulics of water flow in rivers and channels. The program is one-dimensional, meaning that there is no direct modeling of the hydraulic effects of cross section shape changes, bends, and other two- and three-dimensional aspects of the flow. The program was developed by the United States Department of Defense, Army Corps of Engineers in order to manage the rivers.

The Hydrologic Engineering Center (HEC) in Davis, California, developed the River Analysis System (RAS) to aid hydraulic engineers in channel flow analysis and flood control. It includes numerous data entry possibilities, hydraulic analysis components, data storage and management capabilities, and drawing and reporting performances.

The basic computational procedure of HEC-RAS for steady flow is based on the solution of the one-dimensional energy equation [1], [3]:

$$Y_2 + Z_2 + \frac{\alpha_2 V_2^2}{2g} = Y_1 + Z_1 + \frac{\alpha_1 V_1^2}{2g} + h_e \tag{1}$$

where:

Z_1, Z_2 are the bottom elevations in (1) and (2) consecutive cross sections;

Y_1, Y_2 - the water depths;

V_1, V_2 - the average velocities (total discharge/ total flow area);

α_1, α_2 - the Coriolis coefficients;

g - the gravitational acceleration;

h_e - the energy loss.

The energy loss is evaluated by friction and flow area contraction or expansion:

$$h_e = L\overline{S_f} + C\left|\frac{\alpha_2 V_2^2}{2g} - \frac{\alpha_1 V_1^2}{2g}\right| \quad (2)$$

where:

L is the reach length;

$\overline{S_f}$ - the average friction slope between the two sections;

C - expansion or contraction coefficient.

The momentum equation may be used in situations where the water surface profile is rapidly varied. These situations include hydraulic jumps, hydraulics of bridges, and evaluating profiles at river confluences.

For unsteady flow, HEC-RAS solves the full, dynamic, Saint-Venant equation (3), using an implicit, finite difference method. The unsteady flow equation solver was adapted from Dr. Robert L. Barkau's UNET package.

$$\frac{\partial Q}{\partial t} + \frac{\partial QV}{\partial x} + gA\left(\frac{\partial z}{\partial x} + S_f\right) = 0 \quad (3)$$

where:

Q is the river discharge;

A - the flow area;

t - time;

x – one-dimensional coordinate.

HEC-RAS is equipped to simulate hydraulics of a channel network, a dendritic system or a single river reach. Certain simplifications must be made in order to model some complex flow situations using the HEC-RAS one-dimensional approach. It is capable of modeling subcritical, supercritical, and mixed flow regime together with the effects of bridges, culverts, weirs, and other hydraulic structures [5], [6].

3. THE MODELING PROCESS AND RESULTS

This paper aims to determine the floodable areas of the Buzău river basin, on the basis of measurements and mathematical models simulating the water motion, and finding technical solutions for the land protection and the management of these phenomena.

Fig. 1. The Buzău catchment and the study area

The paper presents a case study which shows floodplains for different flow rates, considering a steady motion and applying one-dimensional model of the flow.

For this study we used the following software: ArcGIS, for pre-processing and post-processing, HEC-RAS for numerical modeling of the flow, and HEC-GeoRAS in order to obtain the inlet data for HEC-RAS.

The study area is part of the Buzău river basin (**Fig. 1**), between the hydrometric stations Vama Buzău and Sita Buzău, on a length of 14.3 km (**Fig. 2, a**). A detail area around a bridge is presented in **Fig. 2, b**.

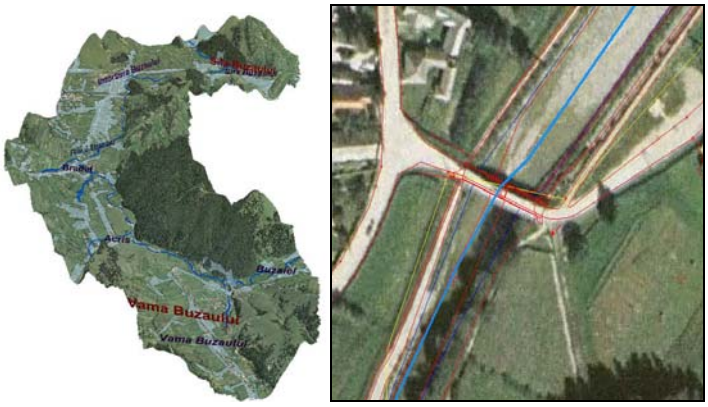

Fig. 2. a) 3D view of the study area: from Vama Buzău to Sita Buzău;
b) a bridge over the Buzău river

The hydrodynamic model used the following data: digital terrain model (DTM), data on average daily flow rates and the flash floods for this river reach recorded in 1991 and 2005 years.

Digital terrain model was obtained by processing LIDAR data in raster format with 2 m resolution and with an accuracy of 0.25 m [4]. According to its definition, a buffer of 1.5 km for the river Buzău and its tributaries and hydraulic structures were used (**Fig. 3**).

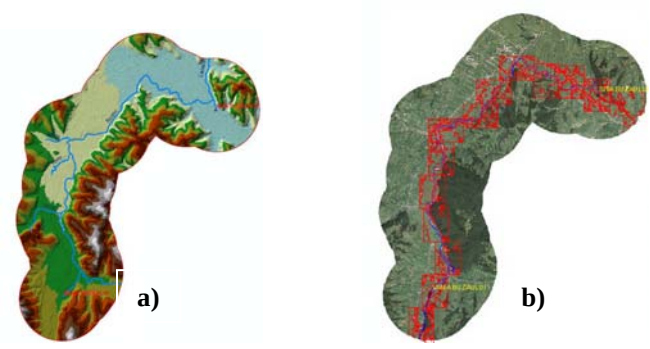

Fig. 3. a) DTM of river Buzău and its tributaries;
b) the bridge locations on the river Buzău

The flow modeling and setting the limits of the floodable areas at different flow rates values in a large range (between 0.1 and 600 m^3/s) were done for steady motion state, using available information stored during 1991 and 2005 floods. The hydrodynamic modeling has also taken into account the existence of 10 bridges. Thus, we proposed several scenarios,

depending on the flow rate values. As expected, the widest zones correspond to the scenario with the highest flow rates (600 m^3/s). By numerical simulation were obtained the flood limits and the water levels next to a bridge (**Fig. 4**).

Upstream of the bridge the water level increases due to narrowing the flow area and downstream a descendent water level is produced by local growth of the velocities [2].

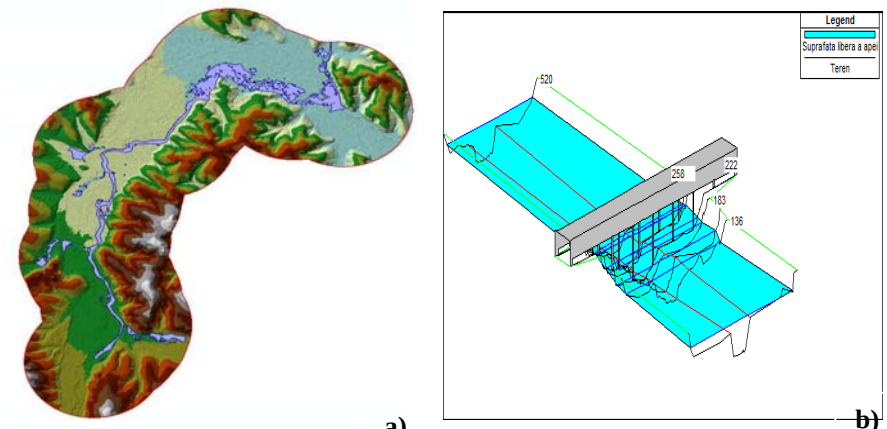

a) **b)**

Fig. 4. a) Floodplain limits on study area; **b)** a bridge section

To identify areas susceptible to flooding was made a detailed study near the city Întorsura Buzăului. In one last examined scenario, it was opted for a much higher flow rate than those registered or usual considered, i.e. 600 m^3/s. It is noted that in this condition the numerical simulation shows that a huge area, including a part of the city, is covered by water (**Fig. 5**). Therefore, based on flood risk maps, structural measures and, especially, non-structural flood control must be considered.

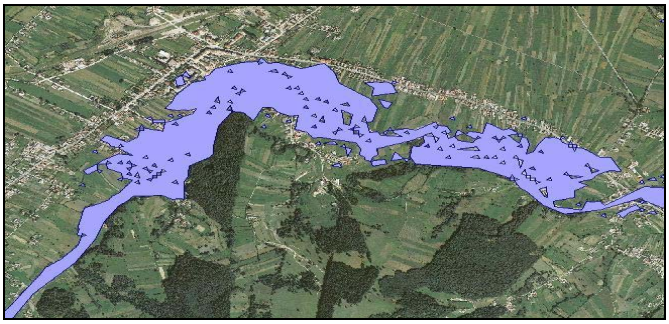

Fig. 5. Intorsura Buzăului - detail flood map

4. CONCLUSIONS

The flood risk maps are useful tools to indicate the material and human damages and, as a result, the required structural and non-structural measures for flood control.

In order to define the areas susceptible to flooding it must generate these specific maps, according to the river flow rates with different probabilities of exceedance. This can be done by mathematical modeling and numerical simulation with specialized software, and then all results will be integrated into a geospatial database linked to a GIS system.

HEC-RAS simulation program, used in this paper for a case study, is a powerful tool in defining problems and establishing the flooding limits, with some advantages and disadvantages. Although HEC-RAS is based only on one-dimensional model flow, it is and will remain a long time favorite program for hydraulic engineers for its efficiency in open channel flow modeling, under steady and/or unsteady state, because of its consistent documentation, simplicity in use, and especially for the fact that it is not expensive.

5. ACKNOWLEDGMENTS

The authors wish to thank the PhD Department from Technical University of Civil Engineering of Bucharest for assistance in achieving this paper.

6. REFERENCES

[1] Cioc D., *Hidraulică.* Bucure□ti: Editura Didactică şi Pedagogică, 1983.
[2] Dimache A., Mănescu M., *Retele edilitare*. Bucure□ti: Editura Matrix, 2006.
[3] Hâncu S., *Hidraulică teoretică şi aplicată.* Bucure□ti: Editura Tehnică, 2008.
[4] Nițu C., Nițu C. D., Tudose C., Vişan, M. C., *Sisteme informaționale geografice şi cartografie computerizată*. Universitatea din Bucureşti, ISBN 973-575-650-1, 2002.
[5] *** US Army Corps of Engineers, *HEC-RAS - River Analysis System User's Manual*. Institute for Water Resources, Hydrologic Engineering Center, Davis, CA 95616-4687, 2008.
[6] *** US Army Corps of Engineers, *HEC-GeoRAS GIS - Tools for Support of HEC-RAS using ArcView GIS User's Manual.* Institute for Water Resources, Hydrologic Engineering Center, Davis, CA 95616-4687, 2008.

Some considerations about risk phenomenas which are registred in Dobrouja

Dacian Teodorescu

Abstract **– In this analysis, it is propuse to describe some specific meteorological and hydrological phenomenas which are registred in Dobrouja, based on a registred dates. It want to present some cases study wich are registred more than 50 years perioad. Also, it was analized the effects who are generated by floods and produced very important materials disasters and losing human lifes. In the finale analysis it was present the antrophic influences which are increase to produce these risk phenomenas.**

Keywords **– alluvial discharge, discharge, flood, hydrograph, mud flood (sel), monitor well.**

1. INTRODUCTION

The maximum flow is generating by an interaction between of many factors such as in a first place climates, especially liquid precipitations and solid which are decisive factors. Beside of these a very important influence have active basin area and also the shape of this; the earth initial moisture measure; permeability and temperature soil; vegetation, lacquer units presence. It's very important to tell that the soil structure is consist of sedimentary deposits (*loess, laimstone and clay*) which have a reduced permeability. And last we can add the human works influence (deforest, water hydrotechnicals etc.)

The precipitations torrential regim is specific for this region, for year specific periods, which are not the same, it registred very important water rising stages. These are manifest like a momentary flood wave and some time are very dangerous. It's call *sel* (Moslem name). The period of manifestation is in spring and summer time, when the river bed process is accelerated.

This surface flow are registred in a very short priod of time, water rising stage are increase only the rainfalls quantity is bigger in a relativ short time, when the rainfalls intensity is fast outrun by infiltration.

The floods genesis of Danube and Littoral drainage basins from Dobrouja are generate in principal by precipitations. All these majority was produced as outcome of some torrential rainfalls with intensity and higher water layer (rainfall floods), again rainfalls-melting snow floods and melting snow floods with a reduced frequency.

So, indirect, human is responsible for all these phenomenas, because he permanent altered environment with uncontroled deforest and unsuitable works on slope fields (stoping and unconsolidation earthworks).

2. STUDY DESCRIPTION

For study it was taken two drainage basins with closely same parameters such as: Topolog have 342 km^2 active basin area, 50 km meander length, 5 $^0/_{00}$ slope, 0,15 drainage

Dacian Teodorescu, engineer, PhD is with Romanian Water Dobrouja-Littoral Basins Administration, Hydrological and Hydrogelogical Office, Bd. Mircea cel Batran nr. 127, -Constanta, Romania (e-mail: tdacian@)gmail.com).

ISSN-1584-5990

density and 1780 hectares afforest surface; Casimcea have 740 km^2 active basin area, 69 km meander length, 4 $^0/_{00}$ slope, 0,09 drainage density and 1042 hectares afforest surface.(**fig. 1 and fig. 2**)

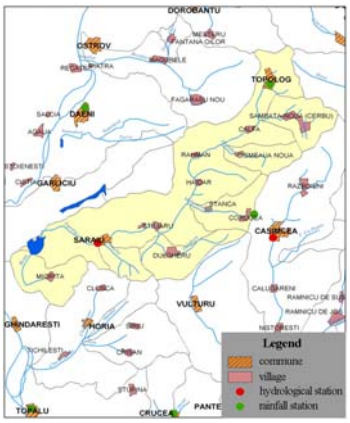

Fig. 1. Casimcea drainage basin

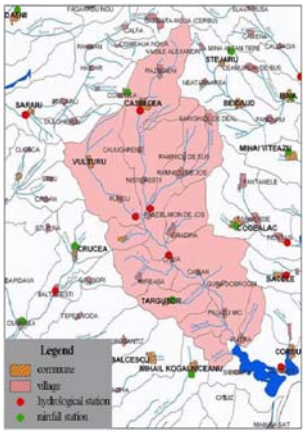

Fig. 2. Hydrological and meteorological phenomenas isohyets map registred into august 28, 2004

Both drainage basin have below 1000 km^2. Casimcea have two important affluents Cartal on the right side and Ramnic on the left side. Cartal have 128 km^2 active basin area, 26 km meander length, 6 $^0/_{00}$ slope, 0,20 drainage density. Ramnic have 87 km^2 active basin area, 20 km meander length, 9 $^0/_{00}$ slope, 0,23 drainage density. The maximum flow are produced not in particularly order it is difficult to predict the moment and water volume runoff. The time for peoples warning are very short, it depend how large is drainage basin, flow velocity and how performance are the communication devices. These extreme phenomenas have also major finally through erosion process and mobility of river bed.

To cause of these precipitations was cloudburst torrential rainfalls from august 28, 2004 which are produced between collision of tropical sea air mass, wet and warm. These are pushed by mediteranean drawdown centers which are coming from south-east Europe and polar air mass, still wet, but cold. These are coming in our regions or through the Azoric anticyclone, or to one barometric maximum which are center some where in north of Europe. (**fig. 3**)

It was created two precipitation poles one above Casimcea Plateau and other above perimeter between south of Constantza City and north of Eforie City. The precipitations amount was between upper 300 mm above Casimcea Plateau and upper 200 mm above Eforie City.

These precipitations amount has generated flash floods in Topolog and Casimcea drainage basins between 28 and 30 August, 2004.

In Topolog drainage basin maximum discharge was 7,45 m^3/s and it was registred at 23:00 hour on august 28, 2004. The high water was 360 cm and precipitations quantity registred was 107 mm. Time of increse was 6 hous and time of decrese was 17 hours. It was destroyed 30 family houses and 50 households, 400 animals died like pigs, cows and sheeps and more then 200 hectares was flooding .(**fig. 4**)

In Casimcea drainage basin maximum discharge was 50 m^3/s on Ramnic and it was registred at 17:00 hour on august 28, 2004. At 18:00 hour on Cartal it was registred a maximum discharge about 102 m^3/s on august 28, 2004. And at 20:30 hour on Casimcea (Cheia) the maximum discharge was about 287 m^3/s.(**fig. 4**) The high water was 450 cm at

Cheia, 350 cm at Ramnic and 550 cm at Cartal. The precipitations quantitys registred was 312 mm at Pantelimonu and 87 mm at Cheia.

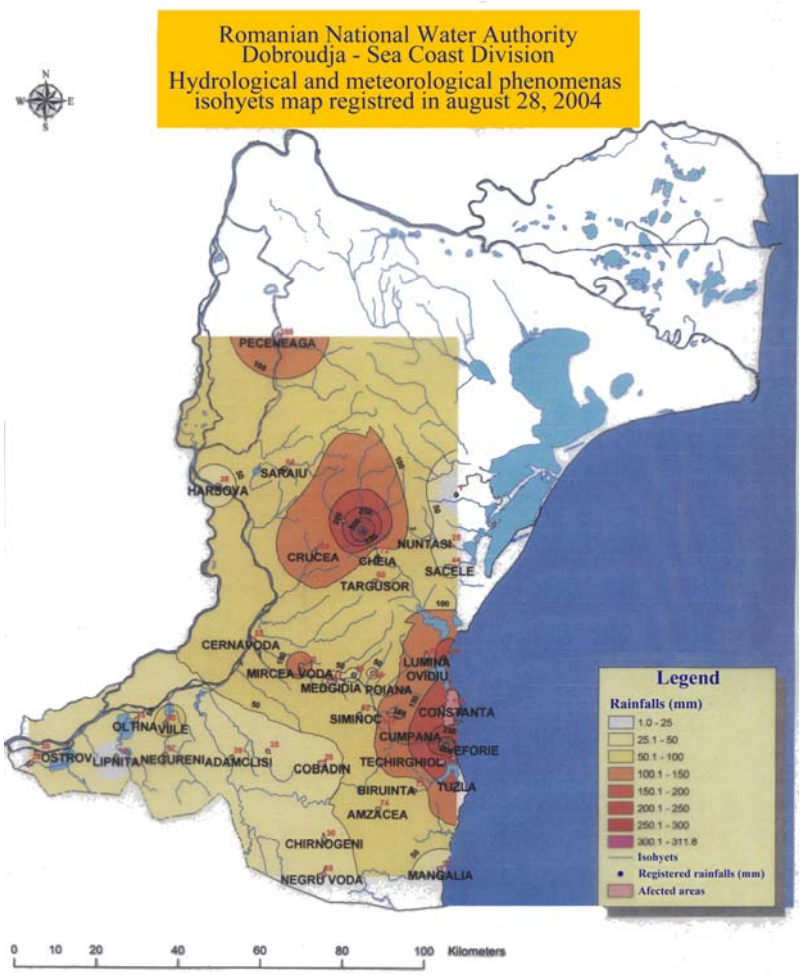

Fig. 3. Topolog drainage basin

3. RESULTS AND SIGNIFICANCES

These correlation diagrams was made in agreement with monitoring and censored datum of hydrogeological network, which is compused more then 200 monitor wells. These monitor wells are sorted in the *first order* (variation between of piezometric water head in correlation with water level of a river or lake from drainage basin) and *second order* (variation between of piezometric water head in correlation with rainfall quantitys which are registred at rainfall station situated on drainage divide). (**fig. 5**)

In (**fig. 5**) it was given correlation diagrams between the first order freshwater heads monitor wells F1 Nuntasi and water levels Nuntasi river and also precipitations registred at Nuntasi hydrological station. The unsequence are since there are some unlicense pumpsengine who take water for irrigation crops. Very important to tell that between august 25-30, 2004 Black Sea Coast long it was registred big quantity of rainfalls upper 200 mm on 24 hours (at Constantza meteorological station was 201 mm). So, the water volumes surface runoff in Siutghiol Lake drainage basin given us

more then 20 cm increase of gauge heights. In *first order* monitor wells F1 Aurora increase more then 40 cm of freshwater heads. As it's present at *second order* monitor well F1 Vadu the upper freshwater heads was more then 15 cm in a second part of september 2004

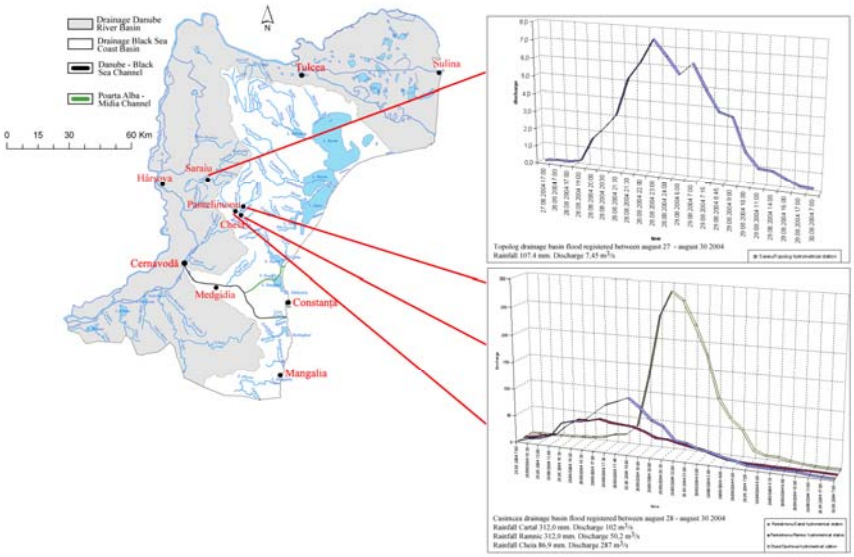

Fig. 4. Topolog and Casimcea floods hydrographs registred into august 28, 2004

From diagrams which are present in (**fig. 6**) it can fix specific feature of surface runoff regim. As we can see multi-annuals mean monthly liquid discharge in percentage are rich in february-march and april-may periods (the surface runoff it's given by precipitations which are decrease from vest to east, and also decrease with altitude). These liquid discharges from this months are rich because rainfalls and snows melt are bigger than other months.

The maximum surface runoff, can be registred every month of the year, but it have specific intensitys, causes and different spatial distributions.

The alluvial surface runoff depend from temporary and spatial varation. The errosion are higher intensity on Topolog and Casimcea drainage basin. These are influence by permeability and waterproof rock features. Because the lower velocitys and slopes in fields, the quantity of alluvial is bigger and the sediment bed of river are increase. These are given to river an increase number branchs and built a delta.

As we can see, in Dobrouja, the alluvial surface runoff are influence by climatic conditions and surface runoff.

In (**fig.7**) the alluvial surface runoff values are upper in february and june-september when rainfalls quantitys are rich. The liquid and solid precipitations are very important because these are given big quantitys of alluvial surface runoff (as we can see in **fig. 7**). About the minimum surface runoff, it can be observed that also have a zone character. This was influenced by mean altitude of drainage basin and local factors such as: rocks, vegetation cover degree and human.

The decay rivers create a lot of troubles for human society. It is also a risk phenomena. These phenomena created problems in irrigations system because river discharge is not sufficient to give the soil moisture for crops. In South of Dobrouja the rivers are decay all year period (such as: Iris Valley, Urluia Valley and Albesti Valley). Only time to time clodsbuster give up surface runoff for some day or hours in spring or autum period.

The values of surface runoff discharge (liquid) are between 1 to 10 l/s in dry period for the North Dobrouja rivers. These are registred in upper Taita and Telita drainage basins.

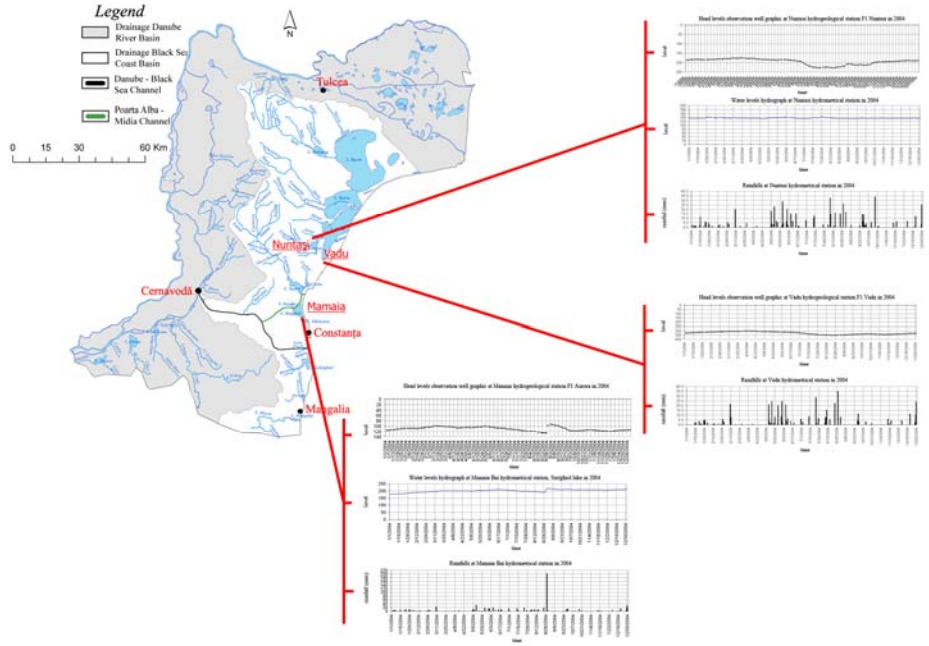

Fig. 5. Correlation diagrams between rainfalls, freshwater heads monitor wells and gauge heights registred into august 28, 2004 at Mamaia Bai and Nuntasi hydrometrical station and Vadu hydrogeological station

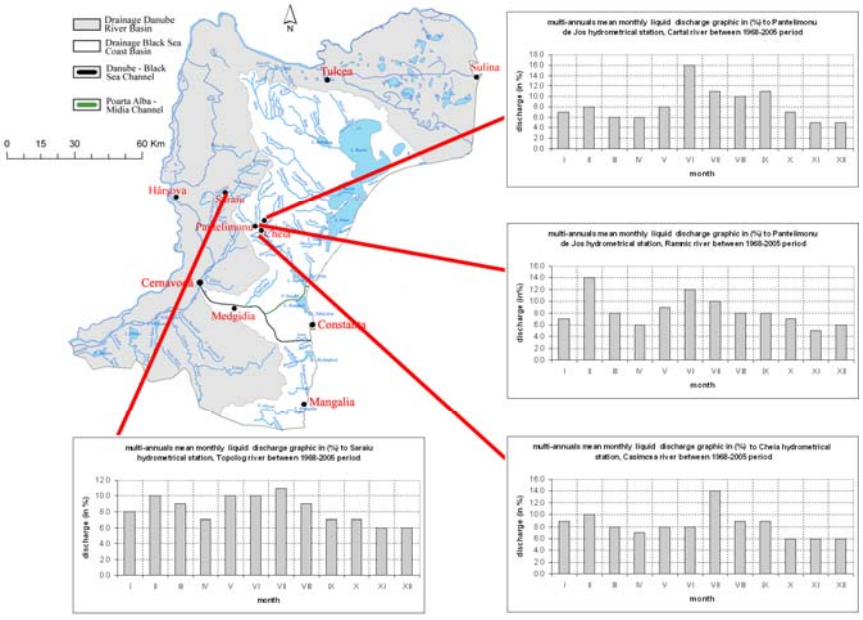

Fig. 6. Multi-annual mean monthly liquid discharge in (%) registred into different hydrological station between 1968-2005 period

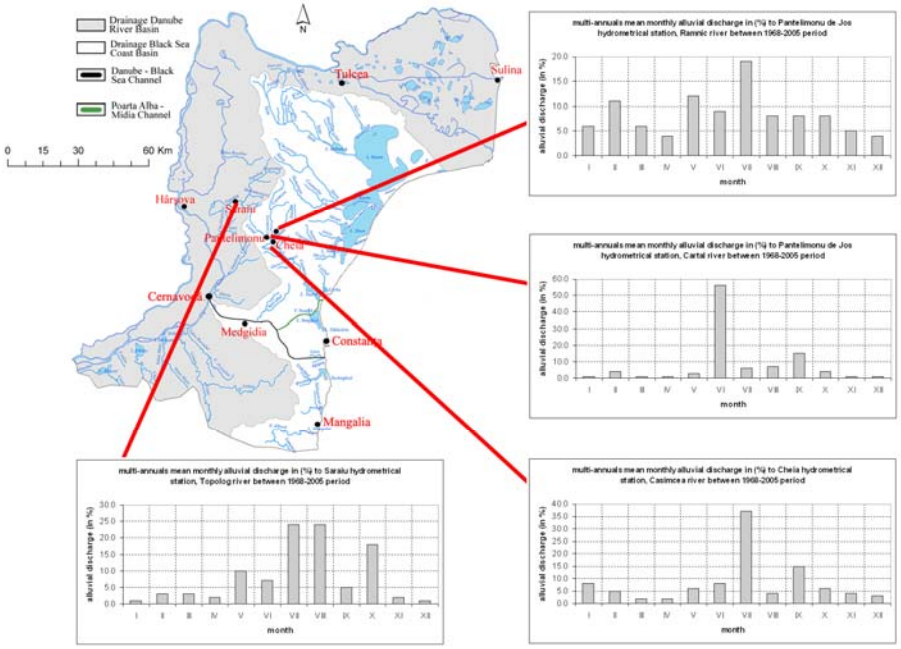

Fig. 7. Multi-annual mean monthly alluvial discharge in (%) registred into different hydrological station between 1968-2005 period

4. CONCLUSIONS

For surface water and groundwater evolution it's necessary to know some important elements such as: Surface and groundwater variation regim; sediment yeld regim; physical-chemical and biological qualitys of water units; one of them alter the valley micromorphology; underground aquifer interdependent relations with geological structure, surface water and available meteorological conditions; to know the action of human factors about water zone system, it's necessary to develop some numerical models for study of this impact. When it will create and develop these numerical models it's easely find the best solution for protection and employment water resources; afforest is solution to reduced the influnce of dry winds; also this can create a necessary hydrological regim for growing up plants; it will be create a steady climate and air and soil moisture conditions.

5. REFERENCES

[1]. Maftei, C. (2004), Applications into Hydrology, Editura Ex Ponto, Constanta
[2]. Mustatea, A. (2005), Historical flood in Romania, Editura Institutului National de Hidrologie si Gospodarirea Apelor, Bucureşti
[3]. Ujvari, I. (1959), Romanian hydrology, Editura Stiintifică, Bucuresti.
[4]. Ujvari, I. (1972), The Romanian water geography, Editura Stiintifica, Bucureşti.
[5]. Zavoianu, I. (1999), Hydrology, Editura Fundatiei *Romania de Maine*, Bucuresti
[6]. ***(1968),The hydrologycal studies XXIII- The hydrologycal Monography of the Dobrouja rivers and lakes, Bucureşti.
[7]. ***Data Archiving – National Administration of Meteorology Bucureşti
[8]. ***Data Archiving – National Intitute of Water Management Bucureşti
[9]. ***Data Archiving – Romanian Water Dobrouja-Littoral Basins Administration

SECTION X

CIVIL ENGINEERING

Disinfection of drinking water by ozonation

Ildikó Bartalis, Ilie Siminiceanu, Enikő Fazakas, Zsuzsanna Turóczy

***Abstract* – Since a long time, natural processes have not been able anymore, to rectify the environmental load caused by the ever-increasing world population. Our water reserves are a main issue of interest, because pollution from both the atmosphere and soil will eventually enter the aqueous phase by deposition and percolation respectively.**

Ozone has greater disinfection effectiveness against bacteria and viruses compared to chlorination. In addition, the oxidizing properties can also reduce the concentration of iron, manganese, sulfur and reduce or eliminate taste and odor problems. Ozone oxides the iron, manganese, and sulfur in the water to form insoluble metal oxides or elemental sulfur.

***Keywords* – chemical oxidant, ozonation, ozone, ozone generators, quality water.**

1. INTRODUCTION

The classic procedures of water disinfection are generally realized with chemical substances, which on their turn produce secondary disinfection products, which pollute in certain limits. The limitation and elimination of these problems can be solved by the treatment of the water with ozone on large scale, and this paper approaches the treating procedures of the drinking water with ozone, and this method's advantages confronted with the disinfection of drinking water with chlorine.

The 20th century brought an unimaginable development of technology and science, but besides this development, the environmental pollution, especially water pollution has reached huge rates on Earth. This way, advanced procedures (especially ecological ones) are required for the disinfection of water.

In these days, thousands of specialists and scientists are working in order to reduce the process of pollution and to diminish the effects of pollution with modern procedures.

Water is an indispensable factor of life; it occupies ¾ of the Earth's surface. It represents the main factor in supporting, maintaining and developing life, it is a part of us – 2/3 of the human body consists of water. Water is the most wide-spread substance on the surface of the globe; however, the volume of the water which can be used by people is relatively small. This way, approximately 1 billion people don't have access to water of proper quality, and 2 billion people don't have acceptable sanitary conditions.

I. Bartalis is with „Babeş - Bolyai" University, Cluj – Napoca, Saint George University Extension, Stadionului str., Nr.5, Saint George, Romania (e-mail: kimildi59@gmail.com).

I. Siminiceanu is with Technical University „Gh. Asachi", Faculty of chemical engineering, Mangeron Blvd., 71, 700050, Iasi, România (e-mail: isiminic@ch.tuiasi.ro).

E. Fazakas is with Chemi Ceramic Ltd., Saint George, Ciucului str., Nr.163, Romania (e-mail: chemicer@clicknet.ro).

Z. Turóczy is with Chemi Ceramic Ltd., Saint George, Ciucului str., Nr.163, Romania (e-mail: chemicer@clicknet.ro, turoczyzsuzsi@yahoo.com).

ISSN-1584-5990

As a percentage, the volume of sweet water of the rivers, lakes and underground waters (bilge) represents approximately 0,7%, the water of the seas and oceans represents 97%, and the rest, approximately 2,3% can be found in glaciers and ice caps. Our connection to water is not only bio-physical, but also economical.

The urbanization, industrialization and the intensive development of agriculture led to the substantial growth of water consumption. In the present, a population of over 6 billion people is consuming 8.109 m^3 water daily, of which 12% is used as domestic water, 39% in agriculture and 49% in industry. The average water consumption of the population is of 160l/day, including drinking water, domestic water, and water of public usage.

The daily individual water consumption is an indicator of the modern quality life. Through their natural formation, the environmental agents are organically connected, one's deterioration has an effect on others (soil, air, water). Man is a part of the environment, not necessarily the most important, but surely the most destructive.

In the assurance of the premises for the durable development, the quality management of the environmental agents occupies a very important role, all of the long term or short term society developing programs compulsory including these aspects. Through the perspective of actual water consumption and through the correlation with the existent quantity of resources, the water quality management represents a fundamental component of environmental agents' management, due to some aspects regarding water treatment for drinkability and industrial consumption, and due to aspects regarding the engendering and the possibilities of purifying raw sewage [2].

The main components of water quality management are [2]:

- cost analysis for the pretreatment of the water necessary for the consumption of the population or for production processes
- the monitoring of the effluents produced through domestic and industrial consumption
- the disparagement of pollutants at the source and the reduction of wastes resulted in the industrial processes, this way avoiding the impurification of water supplying natural sources
- the utilization of a technology which doesn't pollute among the industrial processes of production and among water treatment processes and raw sewage purification
- the introduction of more strict quality standards for the industrial effluents, this way imposing the final purification of the effluents resulted in the production processes

The surface, subterranean and marine waters' treatment with the aim of obtaining drinking and industrial water is absolutely necessary, its purpose being: the removal of the impurities and the pollutant compounds of organic and inorganic origin, the removal of the micro-organisms which are existing in the water naturally or which appeared due to an accidental pollution, the assurance of the drinking and industrial water necessity, correlated with the necessities of the human society's development.

2. WATER DISINFECTION

Water disinfection is a physical or/and chemical procedure of water treatment which consists of destroying the common and pathogenic micro-organisms. Although, usually this is the last step in the water treatment scheme, its efficiency can be influenced by any of the processes upstream and, especially by the decantation process, in which the bacteria content reduces through the sedimentation of solid materials in suspension. Similarly, the absence of turbidity and the limitation of the organic compounds' content –

with a diminishing character during the first stages of treatment, through the optimization of the coagulation-flocculation process, contribute to the growth of disinfection efficiency and to the diminution of secondary product forming potential [2].

The disinfection procedures can be classified in the followings:

- chemical procedures: treatment with oxidizing agents (chlorine and its compounds, bromine, iodine, potassium permanganate, oxygenated water, ozone, or heavy metal ions - Ag^{2+}, Cu^{2+}),
- physical procedures: water boiling (more than 10 minutes), irradiation with UV radiations,
- combined procedures: low filtration on sand, combined procedures on semi-permeable membranes and chlorination.

Side by side with the action on pathogenic micro-organisms, the disinfection agents also react with the natural organic substances, which are present in the water, in this way takes place the formation of the so-called secondary disinfection products (PSD). The natural organic components which are present in the water are represented in a proportion of 50-65% by humic substances (humic and fulvic acid), derived from humus and aquatic plants. The secondary disinfection products have been identified in the 1970's, as being toxic and even cancerous; in the treated water the most frequent products that can appear are the following:

- trihalomethanes: chloroform, bromodichloromethane, dibromochloromethan, bromoform
- haloacetic acids: mono-, di- and trichlorine acetic acids, mono- and dibromoacetic acids
- bromide ion and chlorate ion
- aldehyde resulted from the chlorination of some amino acids

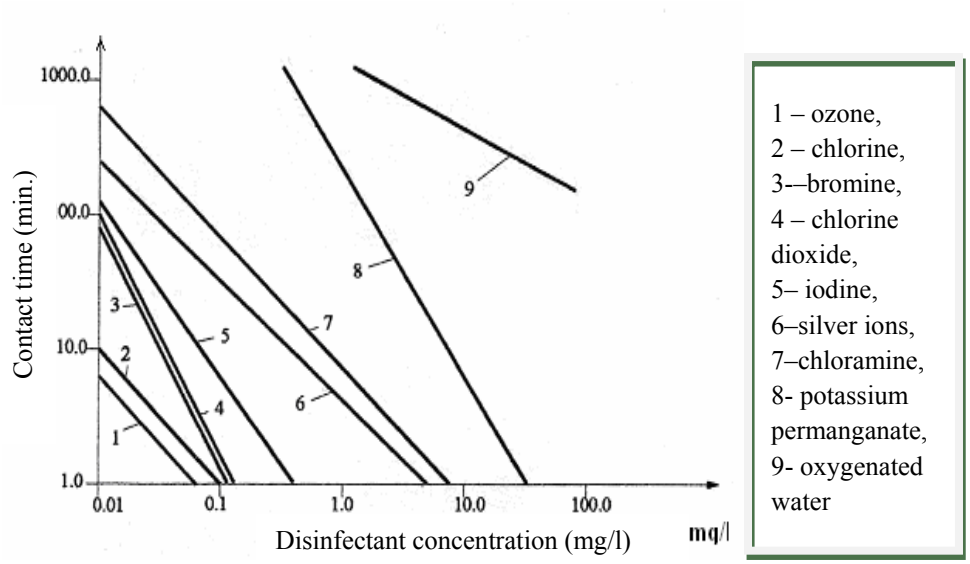

Fig. 1. The efficiency of different disinfection agents

As a result, in the case of chemical disinfection processes, a special attention has to be given to microbiological decontamination and to the forming potential of the secondary disinfection products. For this reason several standards have been elaborated, referring not only to the presence of the pathogenic agents, but to the residual

concentrations of disinfection agents and also to secondary disinfection product concentrations.

From the point of view of the disinfectants' efficiency of destroying the micro-organisms in a proportion of 99,99%, it can be found that this decreases in the following order:

O_3 > Cl_2 > Br_2 > ClO_2 > I_2 > Ag^{2+} > cloramine > $KMnO_4$ > H_2O_2

The oxidizing agents' efficiency, in accordance with contact time and concentration, determined in the same conditions (pH = 7,5; t =5^{o}C), is represented in fig. 1. (Buiteman, 1995). In this figure it can be noticed that in order to obtain a proportion of 99,99% in the efficiency of destroying the micro-organisms, when working with ozone, the contact time is 7 minutes at a concentration of 0,07 mgO_3/l, and for Cl_2 the contact time is 10 minutes at a concentration of 0,1 mg Cl_2/l.

3. THE OZONATION OF DRINKING WATER

The ozone is one of the most used disinfection agents, besides chlorine, its main advantage being the absence of the formation of halogenized secondary products, which are specific during the treatments with chlorine. In 1893, the first treatment installation with ozone has been built in Oudshoorn, Netherlands, and after that this procedure was introduced in Germany (in 1898) and France (in 1906) [2].

The principle of disinfection with ozone is given in the 2nd figure.

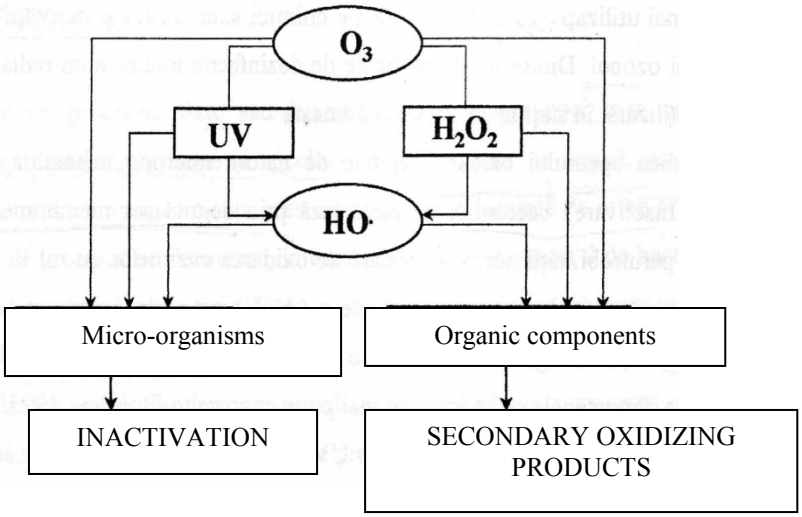

Fig.2. The principle of the disinfection with ozone

Although it is used as a disinfectant in the final stage of treatment, the ozone has proved to be very efficient in pre-ozonation processes, for the oxidation of the organic compounds and the micro-organisms, and then, in the final stage of the treatment, little quantities of chlorine will be added in order to maintain the residual disinfectant effect in the distribution network.

The advantages of ozone:

- ecological oxidizing agent
- great oxidation power (short reaction time)
- doesn't require depositing operations, being produced in the place where is used

- confronted by other water disinfection agents it doesn't produce secondary halogenated components
- doesn't produce specific taste and smell
- enriches the treated water in oxygen

The organic and inorganic substances' oxidation effect – present in the treated water –contributes to the elimination of the water's colour, taste and smell. The efficiency of colour-elimination is assured at doses of more than 2 g/m^3 and at a contact time of 3-15 minutes. The colour-elimination speed depends on temperature, on the water's pH and on the presence of some substances (ex. iron compounds and reductive organic materials), which react with the ozone, diminishing the dose affected by colour-elimination.

The elimination of the iron occurs with the formation of the ferric-hydroxide precipitate at higher speed reactions than the oxidation of the organic substances:

$$2Fe^{2+} + 7/3O_3 + H_2O \rightarrow 2Fe^{3+} + 3O_2 + 2HO^- \quad (1)$$

$$2Fe^{3+} + 6H_2O \rightarrow 2Fe(OH)_3 + 6H^+ \quad (2)$$

$$6HO^- + 6H^+ \rightarrow 6H_2O \quad (3)$$

Through the self-destruction of the residual ozone, the treated water enriches in oxygen and it has a pleasant taste. Turbidity is also influenced by the presence of the ozone through the decrease of particles of small size, at small doses, and through the increase of the number of the particles at high doses, due to the flocculation phenomena that could occur.

Among the inorganic substances which oxidize in the presence of ozone, we can cite the following: chlorites (at chlorates), nitrites (at nitrates), halogens (at chlorates, bromates, iodates), ammonia (at nitrates), urea, hidrazines, chloramines, bromamines. The organic substances which oxidize in the presence of ozone are: hydrocarbons, aromatic compounds, amino acids, mercaptans, phosphoric esters.

Both for drinking water and treated water are necessary the toxicity tests. The waters' toxicity is measured with EC50 which means the concentration (mg/l) at which 50% of the aquatic species die (fish, algae), being exposed to a certain amount of time [1].

Toxicity tests, applied to one sample of treated water, allow the evaluation of the efficacy of the applied procedure. Ozone is a toxic, oxidizing gas. The ways of penetration in the organism are: inhalation, through skin and eyes. Acute effects: ozone at a concentration of tens of ppm (ppm = 2mg/m^3), at 20 ^{o}C, 101,3kPa causes discomfort; at individual exposure it causes headaches, the drying of the throat and the nasal mucous membranes.

The smell starts to feel at approximately 0,02 ppm, however desensibilisation occurs in time. The exposure to high concentration can provoke headaches, pressure sensation, anorexia. It is estimated that the lethal dose is approximately 50 ppm at an exposure of 30 minutes. The areas, in which the ozonizing installations are found, have to be very well ventilated and equipped with sonorous or luminous alarms, in the case of exceeding the maximum acceptable concentration (the maximum acceptable dose is from 0,1 cm^3 to 1 m^3 air) [4].

4. THE CHEMICAL MECHANISM OF OZONATION

Ozone is an unstable gas from the point of view of both production and utilization. The large variety of the gas-liquid contact, through which the transfer of the ozone to the water occurs, it happens instantaneously with the chemical reactions. Ozone can react with the substances of the water in two ways, directly and indirectly, which leads to the

differentiation in the process' kinetics. In the 3rd fig. the ozonation's direct and indirect mechanisms are presented [5].

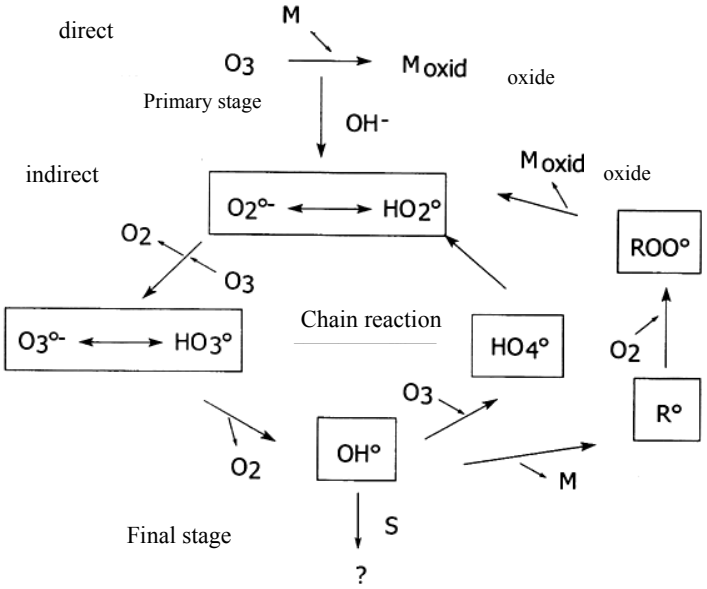

Fig. 3. The ozonation's direct and indirect mechanisms

Simple ozonation

$$O_3 + HO^- = HO_2^- + O_2 \quad (4)$$

$$HO_2^- + O_3 = O_2^{-\cdot} + O_2 + HO^{\cdot} \quad (5)$$

$$O_2^- + O_3 = O_3^{-\cdot} + O_2 \quad (6)$$

$$O_3^{-\cdot} + H^+ = O_2 + HO^{\cdot} \quad (7)$$

$$3O_3 + H_2O = 4O_2 + 2HO^{\cdot} \quad (8)$$

5. EXPERIMENTAL EQUIPMENT

The drinking water's treating procedures should also be applicable in the case of residual water and backwards. The installation of the experimental equipment is dependent on the reaction mechanisms and the experimental observations. It must be clear what kind of equipment and procedures will be chosen.

The ozonation system is made of the following components, which are presented in the 4th fig. [4]:

- ozone generator, measuring instruments which are necessary to measure the ozone concentration is gas and liquid phase; the reactor system, where the ozonation process effectively takes place.

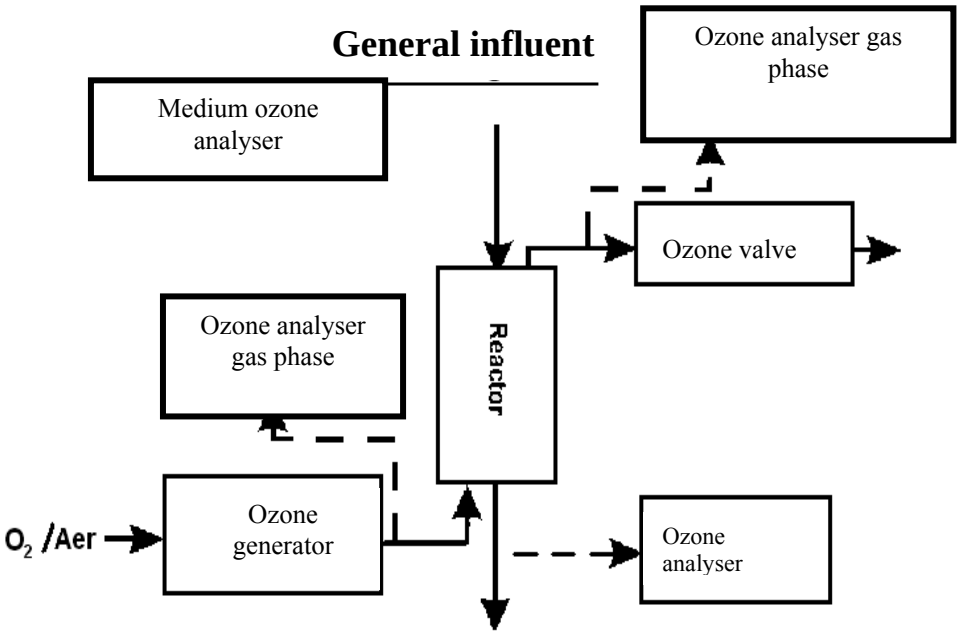

Fig.4. The ozone system

6. THE OZONE GENERATOR

The ozone generator with tubular electrodes, realized by S.C. ICPE Bistrita S.A., is made out of a horizontal metallic body (stainless steel), equipped with a certain number of steel-stainless steel tubes, representing electrodes' mass, cooled with water in the middle, its ends being separated in order to prevent any contact between the gas and the water. In the steel tubes dielectric tubes are installed, made out of special glass, being interiorly metalized, forming high tension electrodes.

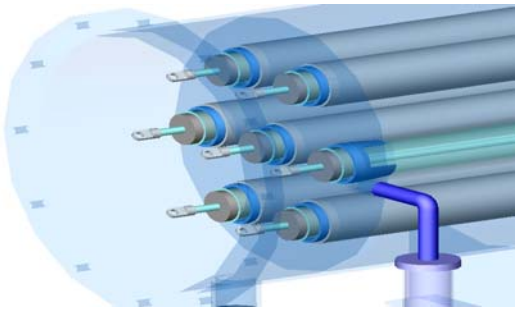

7. PARTIAL VIEW OF S.C. ICPE BISTRITA S.A.

Fig. 5. Ozone generator body

Every metallic tube forms a basic electrode inside which a cylindrical and coaxial tube is fixed to the glass, behaving like a dielectric, and its metalized interior face is connected to high tension. The dielectric tube is sealed at one end, and adjusted on the steel tube with adjusting dielectric rings, which allow the circulation of air in the space formed of the glass tube with and

external diameter of 50 mm and the unoxidable steel tube with an internal diameter of 54-57 mm. Through this circular space a luminous discharge produces, of Corona type, which is stabilized and which passes over the oxygen from the air directly in the ozone. This ozonizer is capable of enduring a unique pressure, max. 15 atm, which can be used to introduce ozone at the working-point. The last tubular element of the apparatus can produce more than 15g/h on the tube at a concentration of 20 g ozone on cubic meter of a specific energy consumption of 17 watts per hour per gram.

8. CONCLUSIONS

The tendency of replacing chlorine is a progressive process, considering the utilization of ozone instead of chlorine. In the last 80 years ozone has been used permanently in France, its utilization extended in Germany, in the Netherlands, in Switzerland and even in Hungary.

If in the water the organic nitrogen or the free ammonia is present, the chlorine compounds leave a characteristic smell behind and the water can become even toxic; a concrete case is that phenol, even in a small quantity, the phenol chloride resulted from the reaction with chlorine gives a bad taste. Even with a content of 0,1 mg/l from these substances, water becomes undrinkable.

During the last few years the utilization of chlorine, as a disinfection agent is put under the question mark, not only regarding its resistance to micro-organisms, but also regarding the great number of disinfection residual products in the case of waters treated with chlorine.

9. REFERENCES

[1] Siminiceanu I.,"Procese fotochimice aplicate la tratarea apei",Ed. Tehnopres, Iaşi, 2003.
[2] Teodosiu C.,"Tehnologia apei potabile şi industriale",Ed. Matrix Rom, 2001, Bucureşti.
[3] Buiteman J.P."Water Treatment Methods and Processes",IHE lecture notes,Delft,The Netherlands, 1995.
[4] Gottschalk, J.A. Libra, A. Saupe "Ozonation of Water and Waste Water", Wiley-VCH, Weinheim, 2000.
[5] Staehelein J., Hoigne J. "Reactionsmechanismus und Kinetik des Ozonzerfalls in Wasser in Gegenwart organischer Stoffe" , Vom Wasser 61: 337-348. (1983)
[6] Crăciun M, Vlad G, Bocskai Z, Ciceiu A, Bălan A „Creşterea eficienţei de epurare biologică prin catalizarea cu oxigen activ", Revista Ecoterra, nr. 6, an II, Ed. Facultatea de Ştiința Mediului, UBB-Cluj Napoca, (2005)

Pollution in Timisoara City

Constantinescu Laura, Man Teodor Eugen

Abstract – **The paper presents types of pollutants for environmental factors (air, water and soil) in Timisoara City. For air the measurements were made in two locations namely the center of the city and the southern industrial zone where were measured the concentration of SO_2, NO_2, O_3, CO, NH_3, powder suspended.**

For water analysis were performed on samples of water from the distribution network of Timisoara City, from local sources distribution of water (public water wells) and private water wells. The soil is subject to action of air and water pollution as the meeting place of the pollutants: powder in the air and toxic gases dissolved by the rain in the atmosphere return to the soil, infiltration water permeates the soil with pollutants by training it to deep. Looking at the results exceedances occurred in powder suspended and sedimentation and partly to groundwater. The soil is taken up by industrial waste, household waste.

Keywords – **air, maximum allowable concentration, pollution, soil, waste, water.**

1. INTRODUCTION

Pollution is the change of environmental factors under the action of pollutants which can be chemical substances, physical factors and biological factors. Pollution is a consequence of human activity following has grown with increasing its population and the development of new technologies. Soil, water and air are environmental factors that are interdependent. Soil is the meeting place of pollutants. Of the soil quality depends the protection of water sources, both the surface and groundwater. Powder in the air and toxic gases dissolved of rain in the atmosphere return to the soil. Infiltration water impregnates the soil with pollutants training them to deep, and polluted rivers infect the flooded or irrigated areas. Most solid waste is stored on the soil. At the same time the soil is really complex and effective remediation, neutralization, recycling and recovery of waste laboratory. Environmental protection in our country is a matter of national interest to preserve the ecological balance, maintaining and improving the quality of natural factors, to ensure conditions of living and working ever better current and future generations, ensuring sustainable development.

2. MATERIAL AND METHOD

To establish air quality in Timisoara city, Timis Environmental Protection Agency made measurements in 2007, in the two points, namely: the downtown and industrial area

L. C. Author is is with "Politehnica" University of Timisoara, Hydrotechnical Engineering Faculty, 1A George Enescu Street, 300022-Timisoara, Romania (corresponding author to provide phone: +40-256-404131; fax: +40-256-404132; e-mail: lauraconstantinescu_m@yahoo.com).

M. T. E. Author is with "Politehnica" University of Timisoara, Hydrotechnical Engineering Faculty, 1A George Enescu Street, 300022-Timisoara, Romania (e-mail: eugentman@gmail.com).

ISSN-1584-5990

in the south. Analysis undertaken followed concentrations of SO_2, NO_2, ammonia, powder suspended and sedimentation powder and were performed according to the methodology. [1].

In the surveillance and control program on water quality for human consumption, in 2007, Public Health Department of Timis County analyzed samples of drinking water of distribution network of Timisoara city, from public water wells and private water wells. Soil pollution in Timisoara city manifests as indirect contamination with industrial pollutants (air pollutants brought on the ground by rainfall), pollutants resulting from automobile traffic, pollution of surface waters, but also by direct contamination (introduction in soil of materials from demolition and construction, various uncontrolled waste deposited on land, etc.). Chemical properties of soil (ph, humus, heavy metals) were determined according to the Methodology development studies soil. [2]

3. RESULTS AND DISCUSSION

3.1. Concentrations results of SO_2, NO_2, ammonite powder suspended and sedimentation powder for Timisoara, 2007

Analysis undertaken by the Environmental Protection Agency referring to the concentrations of SO_2, NO_2, ammonia, powder suspended and sedimentation powder are presented in Tables 1 and 2.

Table 1. The concentrations of SO_2, NO_2, ammonia, powder suspended, Timisoara, 2007 [3]

Analysis / Location	SO_2		NO_2		Ammonia		Powder suspended	
	Measured	MAC	Measured	MAC	Measured	MAC	Measured	MAC
Central zone								
Annual average concentration (mg/m3)	0.002	0.06	0.013	0.013	0.013	0.30	0.050	0.075
Maximum daily value (mg/m3)	0.023	0.25	0.052	0.052	0.084	0.10	0.222	0.15
Southern industrial zone								
Annual average concentration (mg/m3)	0.002	0.06	0.010	0.010	0.040	030	0.077	0.075
Maximum daily value (mg/m3)	0.025	0.25	0.068	0.068	0.099	0.10	0.332	0.15

Analysis of data from Table 1 shows the following conclusions:

- It is noted that there were no exceedances of the maximum allowable concentration (MAC) for measurements of SO_2 in Timisoara city. According to the STAS 12574/87 maximum permissible concentration has the following values: 0.06 mg/m3 for annual average and 0.25 mg/m3 for maximum daily value. The same conclusion is for NO_2 concentration, too, taking into account the maximum allowable concentration has the value

0.04 mg/m3 value for annual average and 0.10 mg/m3 for maximum daily value. Regarding the concentration of ammonia in the air, it was found that there were no exceedances of maximum allowable concentrations.

- Daily maximum allowable concentration is 0.10 mg/m3, which shows that in the industrial area south of the city have been very close values of maximum allowable concentration (0.099). For this reason it requires careful monitoring to identify the source of pollution. The presence of particles in air is linked to the natural environment and human activity. Anthropogenic sources powder generator includes all activities based on combustion of liquid, solid and gaseous fuels and activities related to road transport.

- At powder suspended is found exceeding the annual average concentration (maximum allowable concentration is 0.075 mg/m3) in the industrial area in southern city and the high percentage that the daily highs exceeding the daily maximum allowable concentrations (0.15 mg/m3) both the center and the south of the city. Powder suspended has an effect of impaired respiratory function which is even stronger as the particles are smaller. In addition to this effect appears the carcinogenic and mutagenic effect caused by heavy metals of powder. According Ord.592/2002, the annual limit value for human health protection is 0.040 mg/m3, and daily limit value for human health protection is 0.050 mg/m3. Therefore, it is found exceedances of limit values imposed, both the mean annual and maximum daily values.

Table 2. Sedimentation powder concentrations, 2007 [3]

Location	Maximum value (mg/m2/month	% of MAC
Central zone	38.50	226.47
Southern industrial zone	32.61	191.82

Measurements of sedimentation powder (Table 2) of Timisoara show large excesses maximum allowable concentration in the central area and in the south of the city.

3.2. Results of surveillance and control daily program on the quality of drinking water, for Timisoara, 2007

Under the surveillance and control daily program of water quality for human consumption were analyzed water samples from the distribution network of Timisoara city, from public water wells and private water wells. At the public water wells of Timisoara city (of 80) found a rate of 12.35% of inadequate samples for indicator Fe, 10.25% at turbidity, and 5% bacteriological. Groundwater quality in most drilling executed in phreatic aquifer, have exceeded the maximum allowable limit at least one indicator of water quality characterization. [4].

3.3. Results on the degree of pollution of the soils for Timisoara, 2007

Soils of Timisoara city are the type of aluviosoils, usually in parks near watercourses, and entiantroposoil in built-up areas. Soils pollution in the city of Timisoara is manifested by:

a). Soil pollution by direct deposit, uncontrolled of various wastes such as in the Danube area, Kuntz district, Ronaț Triaj area, ring Arad Route – Torontal Route;

b). Soils pollution by storage of raw materials (kaolin) in improper deposits - deposits from Timisoara Terracotta Factory, which currently is no longer a problem because the factory was closed and demolished. Pending future constructions on the land released are stored materials resulting from demolition;

c). Soils pollution through household wastewater such as Subuleasa Channel and Behela Channel;
d). Soils pollution by industrial waste water from ponds UMT – FZT;
e). Soils pollution through water contaminated with hydrocarbons, such as oil pollution from pond Azur;
f). Soils pollution by storage of inorganic chemical substances (carbide) – pond of the Banat Sugar Factory, which currently is not a problem, the factory was dismantled.

For chemical characterization of soils were selected 6 points where were collected soil samples that were analyzed. The test results including chemical characteristics and heavy metal contents are summarized in Table 3:

Table 3. Chemical characteristics of soil for the 6 points studied in Timisoara, 2007

Nr. Sample Analysis	**1**	**2**	**3**	**4**	**5**	**6**
Ph	7.24	6.85	7.63	7,79	7.57	7.71
Humus (%)	2.58	3.47	3,53	5.26	1.4	2.4
Cobalt (ppm)	0.76	0.54	0,61	0.75	0.73	0.60
Copper (ppm)	22	19	22	22	22	48
Manganese (ppm)	220	264	250	300	352	310
Zinc	28	26	27	29	29	30
Cadmium	1.3	1.7	1,3	0.9	0.5	0.9
Nickel	6	11	5	6	10	3
Lead	7	16	7	8	13	5

Analysis of results presented in Table 3 show the following conclusions:
- ph soil is from slightly acid to neutral and slightly alkaline and the reserve of humus is medium;
- the content of heavy metals fall within acceptable limits except for cobalt which has higher values for maximum allowable limit and cadmium and lead where the values of soil approach to the alert threshold. These higher values are due to traffic and the presence of some ash deposits of Colterm.

3.4. Conclusions on the main types of waste for the city of Timisoara, 2009 [5]

-Household waste, following the study [5] has the following composition:

Table 4. Medium waste composition collected in Timişoara (2008) (%)

Paper, cardboard	**Glass**	**Metals**	**Plastic**	**Composite**	**Fine waste < 40 mm**	**Construction/ demolition**	**Organic materials**	**Others**
6	11	2	9	1	9	9	43	10

In Timişoara, a new system for collecting household waste was starting in 2007. This system consists of a recycling bin and a waste bin for residual waste.

The recycling bin includes recyclable materials like plastic, glass, paper, metals, aluminium or composites. The waste bin contains biodegradable waste like organic kitchen waste, gardening waste or pet waste.

The waste sorting campaign, launched by the Universität Sttutgard and the „Politehnica" University Timişoara in May 2008, made encouraging results. But some open-ended questions also show that it will be a long way to get an effective and efficient

waste management system. Impurities and hazardous waste will still reduce the chance to get proper secondary raw materials from the household waste in Timişoara.

In the waste structure the recyclable materials have a share of 29% and the biodegradable component of 43%.

-Waste resulting from medical activities are classified as hazardous waste (resulting from activity of health services, medical and technical services, administrative, accommodation, food blocks and food distribution offices) and dangerous waste (anatomic-pathological and anatomical parts, infectious waste , sharp-cutting, chemicals and pharmaceuticals). [6]

Dangerous waste given the highest possible impact on human health and the environment and therefore it is necessary a rigorous management from production to final disposal. According to the principle "the polluter pays" the producers of dangerous waste are responsible for management of dangerous waste generated.

In addition to dangerous medical waste, in Timisoara there are dangerous waste from waste oils, spent solvents, various materials containing solvents, coffee waste from the manufacture of paints, grease and oil mixtures of fat separators, waste adhesives and sealants, batteries and lead acid batteries.

These dangerous wastes were disposed of by incineration or were temporarily stored for incineration. [7]

In Timisoara city operating medical waste and other dangerous waste incinerator of SC Pro Air Clean SA Timisoara, this has a capacity of incinerating 9.8 tons / day. For dangerous waste resulting from medical activities, during temporary storage must not exceed 72 hours, of which 48 hours inside unit, 24 hours for transport and final disposal.

Increased living standards of Romanians and the evolution of society resulted in the emergence of more and more new types of waste, more heavily polluted. These include waste from electrical and electronic equipment.

Therefore Romania has adopted the Government Decision no. 448 / 2005 on the management of electrical and electronic equipment waste, by which any manufacturer, distributor and consumer electrical and electronic equipment is required by law, as the end of the life of the product, to deliver the waste to authorized agents, are prohibited throwing these wastes with the household waste. The levels of Timisoara, there are 4 points for WEEE collection sites.[8]

4. CONCLUSION

By analyzing the results of quality monitoring activities of environmental factors in Timisoara city are found most frequently exceeded the values for the year 2007 (2009) were recorded in powder (air, water, soil) powder suspended and sediment. Mean annual PM10 powder suspended measured in the center of the represents 126.46% of limit value and the measured in the industrial area south of the city is 102.67%.

Sedimentation powder measured in the central zone and southern industrial area of the city has exceeded the monthly maximum allowable concentration, namely 226.47% in downtown and 191.82% in industrial area south of the city.

In the SO_2 and NO_2 were not exceeded annual average concentrations, hourly and monthly limits according to the Order 592/2002. Ammonia concentrations measured in the south of Timisoara city approached the maximum allowable concentration.

Reconstruction of geological environment and terrestrial ecosystems affected is to bring them as close to natural state, by measures for cleaning, repair and / or ecological reconstruction, complementary and compensatory, and eliminating any significant risk of impact on them, according to the land use category.

Remediation process of geological environmental is to remove sources of contamination from the site, in isolation and decontamination of contaminated areas, limitation and elimination of opportunities for the spread of pollutants in the geological environment and in meeting the limits allowed for concentrations of pollutants. Assessment of soil quality correlates with the concept of biodiversity having regard to the links which exist between pollutant compounds and the effect of these compounds on organisms, including humans. Caution is advised in the cultivation of lands with vegetables and harvesting of plants, flowers or leaves for teas from perimeters affected by pollution. It should also be identified temporary deposits with various waste located on the area of Timisoara city.

Were identified and evaluated in terms of degree of pollution of rivers (Bega, Behela) and stagnant (ponds, lakes, ANIF and SNIF channels, Subuleasa channel), activity that should continue.

Studies effectuated in the area of urban waste deposit of Timisoara (Gate SAG) shows a massive release of methane, a phenomenon that favors fire outbreak and the formation of gas pockets. Noxious emissions adversely affect air quality in the area.

In addition, drillings made in the area showed up groundwater pollution at a depth of 2,5-3,5 m with organic substances, ammonium salts and chlorides.

Regarding soil, it was found pollution by oil land heavy metals within a radius of 50m.

5. REFERENCES

[1] STAS 12574/87.
[2] The methodology of developing soil studies, ICPA, Bucharest, 2003.
[3] Environmental Protection Agency Report In Timis County, 2008.
[4] Law 311/2004 regarding drinking water.
[5] I.Mirel, C.Staniloiu, I.Olaru, Ghe.Moldovan, M.Berechet, M.Kranert, G.Hafner, O.Shiere, Waste Management in Romania, Buletinul Stiintific al „Universitatii" Politehnica din Timisoara, Seria Hidrotehnica, Tom 53(67), Fascicula 2, 2008.
[6] Council Directive 91/689/CEE on dangerous waste (as amended by Council Directive 94/31/CE).
[7] Directive 2000/76/EC regarding waste incineration.
[8] Government Decision nr.448/19.05.2005 regarding waste electrical and electronic equipment

Optimization of wastewater treatment in meat processing industry

Dragoş Dracea, Loredana – Mihaela Dobre

***Abstract* – Water treatment is a stupendous field which needs many complex technologies for reducing environment pollution. Water purifying stations represent a collateral activity in agricultural and food industry and involve huge technical and economical effort which is hard to accept by investors. In this paper are presented the tests accomplished in laboratory that evidence the efficiency of purifying wastewater from meat industry. There were used different treatment recipes and were studied the results. Reducing costs due to energetic and reagent consumption from a wastewater treatment plant should be harmonized with environmental impact.**

***Keywords* – chemical treatment network, optimization, water treatment station**

1. INTRODUCTION

Water is our most vital form of sustenance. It is important that we return the water we borrow from nature in such a condition that it does not cause pollution. Clean water will be an important economic and political issue in the future. The availability of clean water will be crucial for mankind's development in many important respects.

Water from many industrial processes is usually so contaminated that it cannot be released directly into a recipient waterway, or, as in many cases, sent to a municipal treatment plant without first undergoing some form of pre-treatment. In contrast to municipal wastewater, the contaminants that have to be removed vary widely, depending on the type of industry the water comes from. The advantage of treatment at source is that we usually know what contaminants are present in the wastewater and there for know what has to be removed.

The choice of process clearly has a big influence on the operating economics of different treatment processes. The investment cost (per volume), energy consumption, chemical precipitants and costs of sludge processing all affect operating economy [1].

Treatment stations represent important objectives of the society because of the complex impact that they generate on the environment. Environmental pollution generates a complex impact over society, which is easily to quantize on short term, but with major possible consequences on long periods of time. The short term social impact is represented by water alteration, which is an important resource for all fields. Quality control of water resources is assured by a law which takes into account the actual technological restrictions of all cleaning systems from economical agents.

Dragoş Dracea is with USA-MV, FIFIM Bucharest, Bd Marasti nr. 4, e-mail: dragosdrac@yahoo.com

Loredana – Mihaela Dobre is with the Politehnica University of Bucharest, Chemical Engineering Department, Polizu 1-3, Bucharest, 011061, Romania, tel: +40214023870 (e-mail: Loredana.Dragne@gmail.com).

ISSN-1584-5990

The general situation in our country regarding the quality of water, air and soil can be considered:

- by law: minimal obstructions for the quality and the quantity of discharges;
- by economy: limited resources of economical agents;
- by industry: development of an improperly field for the local market requirement, as for the equipment and also for consumables;
- by society: assuring the resources needed for a healthy climate.

Quality and quantity of water are drastically and fast being reduced and there for is needed a good management of the existing resources. The global crises of water resources impose a good intendance of these by optimizing the consumption and the treatment processes.

The aim of this work is to present the results obtained in some cases of treatment stations from food industry.

2. EXPERIMENT DESCRIPTION

2.1. Quality of analyzed wastewater

The tests have been made with wastewater from a meat processing factory. The instant characteristics of the analyzed waters [3], were: turbidity 461 NTV, MS 550 mg/L, pH 6.8, chemical oxygen demand (COD) 1854 mg/L and a conductivity of 3.96 mS/cm. These waters can be characterized as having a medium grade of pollution and they are cleaned in a classical treatment network: homogenization – mechanical-chemical stage – biological stage. The cleaning processes are realized in automated treatment stations with the possibility of adjusting the interest parameters (flow rates, doses, etc.) depending on chemical indicators monitorized online: pH and dissolved oxygen.

2.2. Treatment technologies recommended

The reagents producers for wastewater treatment recommend the chemical treatment with coagulant salts of iron combined with an organic polymer as flocculant. The coagulant removes larger suspend particles, fats, colloidal particles, proteins and some dissolved organic substances. The commonest method of separating sludge is by flotation, since the nature of the sludge makes it suitable for this method.

In order to achieve satisfactory treatment results it is important to have the right pH during the precipitation stage. The optimum pH when the coagulant is added is around 5. After a few seconds the pH should be raised to between 6 and 6.2 to achieve optimal coagulation. Coagulation is both physical and chemical process. The reaction between particles and coagulant will allow the formation of aggregates and their subsequent sedimentation [2]. Cationic coagulants neutralize the negative charge of colloids and form a spongy mass called microflocs. The bridging action of polymers is important in flocculation. Anionic coagulants although gives good mechanical strength to flocs they are not recommended in wastewater treatment from meat industry because of the big volume of the generated sludge. The experts recommend cationic coagulants for organic particles because they permit agglomeration of the sludge in low volume (compacting the sludge).

2.3. Coagulation tests

Coagulation tests of analyzed wastewater were accomplished using a KEMIRA jar test equipment.

At the entry of the cleaning station the wastewater had the following characteristics: temperature – 20 .9 ^{0}C, pH – 6.8, turbidity – 461 NTU, conductivity – 3.98 mS/cm, suspension content – 550 mg/L and chemical oxygen consumption – 1854 mg COD/L.

The tests were realized using coagulants type PIX113 (iron (III) sulfate solution 42 %) and anionic flocculant type A 1883 RS or cationic flocculant type C 2240 from KEMIRA WATER. The aim of the study was to establish the optimum dose of coagulant and flocculant and also the flocculant type adequate for the optimum dose of reagents and for the water quality.

3. RESULTS AND SIGNIFICANCES

The results obtained at the chemical treatment of analyzed wastewater are presented in table 1. It can be observed that cationic flocculant has proved to be more appropriate for reducing turbidity. It reduced turbidity up to 75% more than the anionic floccculant for doses higher than 400 µl/L. Also, another observation is that adding flocculants does not change pH of the treated water, but the low values has to be adjusted by adding a base (NaOH or $Ca(OH)_2$) after decantation. The cationic flocculant reduces the content of organic matter and nutrients with a higher efficiency than the anionic flocculants. This phenomenon is explained by the fact that for low doses the electric charges of the colloids are annulled by the cationic flocculant which compact the sludge.

Table 1. Characteristics of treated wastewater using different types of flocculants.

Sample No.	Iron(III) sulfate 42%	Flocculant solution		Turbidity	pH	CCD	Nitrogen Ammonia	Total phosphor
	µl/l	ml	µg/l	NTU	-	mg/l	mg/l	mg/l
1	300	Cationic C 2240	2	73	6.1	734		
2	400		2	24	6.1	713		
3	500		2	24	5.9	693		
4	600		2	23	5.8	668	32.75	0
5	700		2	26	5.5	665		
6	800		2	29	5.2	674		
7	900		2	30	4.9	652		
8	1000		2	30	4.8	635	35.75	0
9	300	Anionic A 1883	2	109	6.1	885		
10	400		2	85	6	810		
11	500		2	57	5.8	767		
12	600		2	27	5.7	723		
13	700		2	22	5.4	723		
14	800		2	18	5.2	693		
15	900		2	25	5.1	683		
16	1000		2	20	4.8	689	38.75	0

The coagulation – flocculation processes for both types of flocculants used are depictured in figure 1, respectively figure 2.

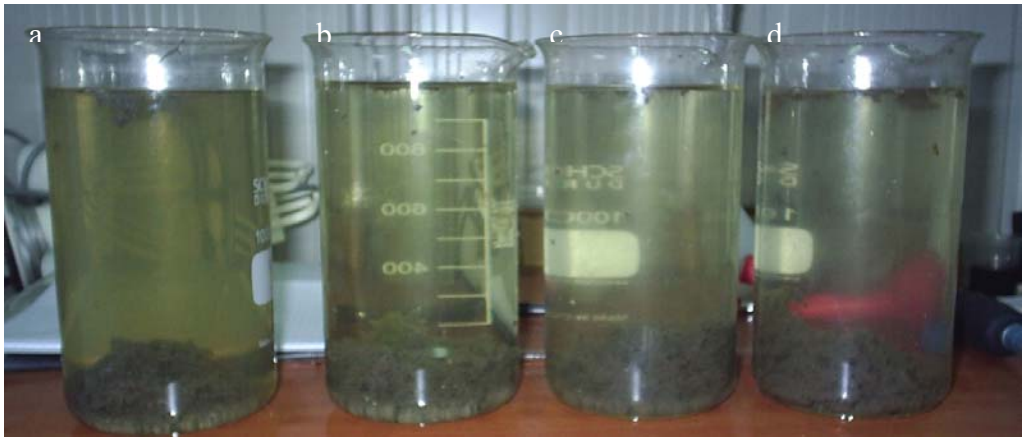

Fig. 1. Coagulation – flocculation process using a cationic flocculant and iron(III) sulfate 42% in different doses: a – 500 µl/l; b – 600 µl/l; c – 700 µl/l; d – 800 µl/l.

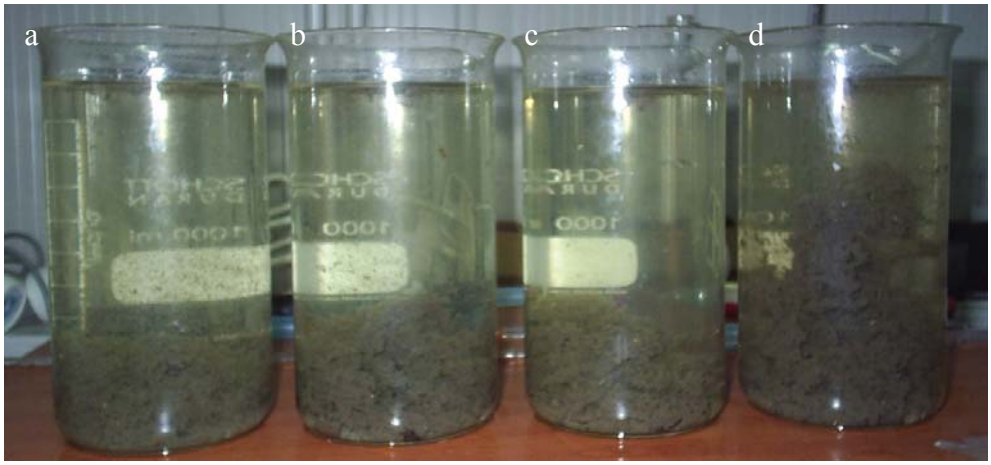

Fig. 2. Coagulation – flocculation process using a anionic flocculant and iron(III) sulfate 42% in different doses: a – 700 µl/l; b – 800 µl/l; c – 900 µl/l; d – 1000 µl/l.

It observes a better coagulation – flocculation when using the cationic flocculant, even for lower doses of coagulant. Also, the turbidity, the content of organic matter from analyzed wastewater and the sludge compactness are improved in this case.

Figure 3 presents the organic matter content and turbidity variations depending on coagulant and flocculant doses. The efficiency of reducing these two parameters depending on the coagulant and flocculant doses is presented in figure 4.

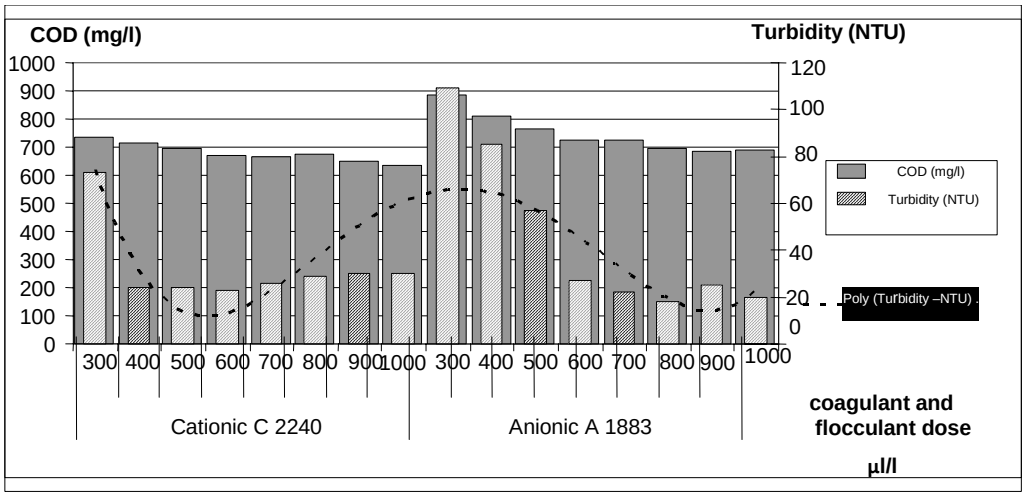

Fig. 3. Dependence of turbidity and organic matter content on coagulant and flocculant dose

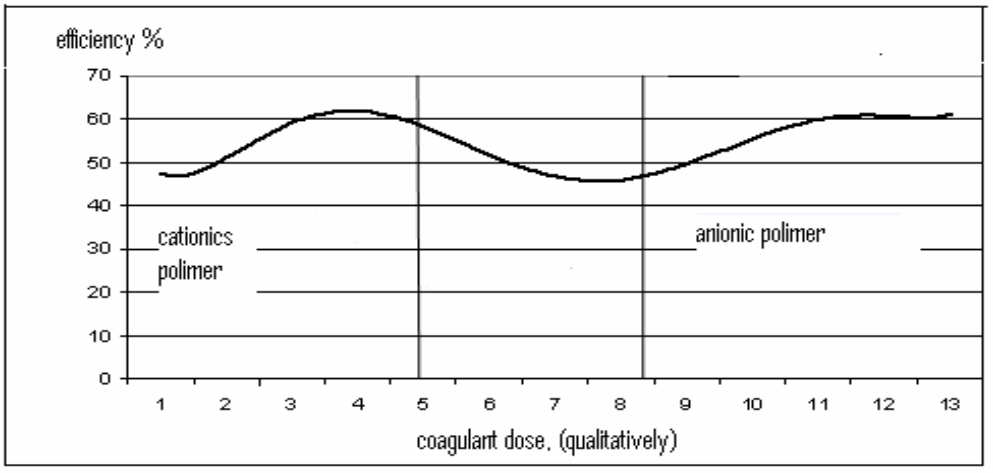

Fig. 4. Coagulation – flocculation zones depending on the coagulant concentration

4. CONCLUSIONS

For reducing the impact of wastewaters over environment caused by industry and by treatment field it is necessary to reduce the effort and to raise the efficiency of cleaning.

To adopt solutions for an efficiency exploitation of these treatment stations it is necessary to assure a homogenous flow which will permit using some standard recipes with minimum consumption of reagents.

Treatment of medium polluted wastewaters with cationic coagulant and polyelectrolyte assures minimum doses of these substances. The reliability of processes must be assured by a good supervising.

5. ACKNOWLEDGMENTS

The authors thank ing. Mioara Dragne for her technical assistance during experiments.

6. REFERENCES

[1] About water treatment, Kemira Kemwater, 2003 Sweden, pag 35- 112.
[2] G.Racoviteanu, Teory of and filtration water. 2003, Ed. Matrix ROM, Bucuresti, pag 21-63.
[3] V. Dean Adams, Water and wastewater Examination manual. New York: CRC Press, 1990.

Green buildings – a new and less known concept

Draghici Gabriela, Cotes Adriana Florentina and Cotes Dan

***Abstract* –Is the green house a building made from burned clay and covered with reed? Not at all; the green house is a modern concept where the building wisely puts in good use the natural potential and friendly interacts with the environment.**

***Keywords* – building, concept, energy saving, green house**

1. COULD ANY BUILDING BECOME A GREEN BUILDING?

Of course it can. We consider useful to remind that the main function of a building is, on one hand to assure to its occupants a healthy environment, nice and comfortable, fairly less dependent on te external conditions, especially weather and acoustic conditions, and on the other hand, it has to be friendly in domains as: production and collection of the wastes, air, water and soil pollution, noise, energy and natural resources consumption, its effects on the ecosystems.

Present demands regarding this aspect, are more restrictive than those accepted in the previous historical periods because of the changes that happened in the nature and complexity of the actions (internal and external) that exerted on the buildings on one hand, and on the other hand because of the evolution of users' requirements. The satisfaction of these exigencies, directly connected to the energy consumption is as much important as those exigencies regarding the safety and stability to mechanical actions, architectural and aesthetic aspect or the inclusion in the surroundings.

Based on the information gathered from the studies made by the Romanian Agency for Energy Preserving, the energy consumption on Romanian residencial buildings represents 1/3 of the total Romanian energy consumption – and there is an increasing tendency. This high consumption has as a result, besides increasing the costs of the residencial buildings, the production of a higher amount of toxic and "green house" effect products that affect the environment and that can be responsible of the climate change.

The saving of the energy brings some good things both for the environment and for the one who is exploiting the building. That's why the client is interested not only about the construction costs, but also about the maintenance costs of the building. Certainly, a green building will be more expensive than a classical building. The real estate specialists appreciate that the costs for a green building are only with 17% higher than the price of a classical one. But, the maintenance and exploitation costs are tending to 0, fact that makes the green building more attractive to the owner or tenant.

G. Draghici, lecturer, PhD is with Ovidius University of Constanta, Bd. Mamaia nr. 124, 900356-Constanta, Romania (e-mail: g_draghici_univ@yahoo.com).

A. F. Cotes, ecologist, is with the Youth Association for Excellence, 9 Mai street, no.16, Eforie Sud, Romania.

D. Cotes, PhD eng., is with the Youth Association for Excellence, 9 Mai street, no.16, Eforie Sud, Romania (e-mail: dan_cotes@zappmobile.ro).

ISSN-1584-5990

2. WHAT IT BEGINS WITH?

In the early stage of land acquisition, an environmental evaluation of the location (site) is needed. SR ISO 14015:2005 standard provides guidance on how this analysis should be performed. This is an opportunity to get information regarding:

- Soil structure (physical, chemical, mechanical);
- Risk of landslides;
- Rainfall levels, hydrostatic levels; flooding and snowing risks;
- Air currents, their direction and intensity, air's humidity and salinity;
- Artificial electro-magnetic fields;
- Release of smells, gases, dust and smoke;
- Noise, vibrations and shock production
- Sunlighting and shading degree;
- Existence of favourable habitats for insects, rodents, etc.
- Local seismic degree;
- Access in case of emergency;
- Legal and other charges.

Then, this review will be taken into account in all the phases of construction of the green building, from stage to the maintenance and dismantling stage of the green building. After completion of the construction, this study will be periodically resumed in order to see how the construction has caused changes regarding: higrotermic system (releases), atmospheric regime (currents); smells, gases, dust releases, acoustic regime (noise, vibrations, shocks source), brightness (light reflexions, shading), artificial electrical or magnetical fields, releases of biological agents (laboratories, hospitals), flora or fauna changes (deforestation, water drainage), soil and subsoil changes (soil quality, declivity), etc.

The architect should know the results of this study. The contact surface between the building and external environment influences both heat contributions and loss. A smaller outer surface will increase the efficiency of the thermic-insulation, the compactness index being one of the most important parameters in determining of the energy indicators.

The glazed surfaces, properly dimensioned and oriented, help to reduce heat loss and recovery of the solar contributions. The judicious orientation against prevailing winds and cardinal points is very important for controlling air infiltrations and to provide a convenient route of air circulation during the summer for air conditioning facilities.

The energy saving requirements and of other shortcomings related to the mechanical ventilation and especially air conditioning, led to a shift to controlled natural ventilation, not only in residencial buildings, but also in multistaged public buildings, new or rehabilitated, where the ventilation is achieved naturally. A couple of systems have been developed to increase the „basket" effect, using some architectural elements as courtyards or atriums or to make possible a rational use of the solar energy and wind pressure (active facades, double-peau facades).

The important thermal mass of the soil causes a gradual attenuation of the diurnal and annual variations of the outdoor air temperature with the depth, along with a time lag. These can be exploited to achieve the construction of an underground or partially burried building, in the design and development of the seasonal solar energy stocking systems and of the newly introduced fresh air preheating/ pre-cooling systems through buildings' ventilation process.

The passive solar energy recovery systems, consisting of greenhouse type spaces, walls that assure the greenhouse effect, different kinds of solar facades, etc., have entered the basic vocabulary of the contemporary architecture. Their operation is based on the:

greenhouse effect, thermal inertia, thermal natural convection airflow. A higher level of development is the introduction of photovoltaic panels integrated into high performance facades.

Turning these principles resulted in the development of some solutions and complex systems based on several overlapping effects and integration with overall architecture concept. The passive solar energy recovery systems, associated with heat recovery systems from the vicious air, air conditioning systems through ground-air heat exchanging systems, or evaporative cooling systems for summer, lead to significant energy savings within the greenbuildings, with real adaptability characteristics to the fluctuation of the external environmental parameters.

The technological developments regarding the building materials and products offer the designers some complex technical solutions, with a higher efficiency such as: transparent insulations, thermal insulating windows with selective optical qualities, active facades, assets involved in space ventilation process, photo-voltaic surfaces, etc.

Planner's task is to choose the environmentally friendly materials for the future construction and, where possible, the materials used should be locally extracted and processed, near to the future construction site, in order to save the energy used in their transportation. Here are a couple of construction materials considered to be „green": plants that are quickly regenerating (bamboo, which is growing very quickly), straw, wood from certified forests, processed rocks, recycled metal, paper flakes, compressed soil, clay or sand.

In this context it should be mentioned the fact that Romania made an agreement so that, for the new construction works, the ecological material weight should increase from 7% in 2009 to 11% till 2013, and that 50% of the lighting equipments will be ecological.

Basement's floor must be isolated because of its poor thermal isolation leads to increased energy consumption for heating. It's more convenient to install the thermic isolation along with a phonic isolation system in the floor. Also, the best solution for isolation is to be made by placing extruded polystyrene plates under the foundation. In this case, the resistance to pressure is equal to that of the ground. The use of hydro-thermal insulation materials is creating the premises of an energetically cheap basement.

Since the outer surface of basement walls are in a permanent contact with the wet soil, the insulating materials used should be insensitive tomoisture, as the extruded polystyrene plates are. In addition, it should be built a drainage system and the basement external walls should be isolated with two layers of bituminous membrane.

The basement insulation can save 30% in heating costs. If the basement is unheated, but is crossed by the heating pipes, these should be isolated.

About 20% of the total heating energy is lost through an uninsulated attic. Since the roof is relatively thinner than the external walls, it is recommended, especially for residencial buildings' attics extension, to insulate the attic in a professional and efficient way. The attic offeres a nice and pleasant living place if the climate is adequate. But the attic is particularly exposed. Scorching summer heat, winter low temperatures and strong winds are felt much more if the thermic isolation is not adequate. Additional costs for using a strong insulating material are low compared with the resulting economic costs of energy. Even if the attic is uninhabited and its expansion of was not planned, it must still be isolated. This will turn the unheated attic in a hovercraft, with an insulating role.

Inside the building is not necessary to achieve the same temperature in all rooms. In the entrance hall would not be normal to have the same temperature as in the bathroom. At low temperatures in the bathroom we won't feel well. A well-being state is achieved. It is recommended to use a delay heating system for the bathroom. In unused condition the bath should be heated at a lower temperature as it does not cool completely and the high energy

consumption to raise the temperature will not be needed. Therefore, there should be a centralized system for temperature control during the day, in each room. Thus we can save energy and yet not cool the room completely. A decrease in room temperature by 10C is already an energy saving of around 6%.

The insulation of the facade plays an important role in energy savings of up to 35%. When the external temperature is -100C and the themic insulation is poor, the inner walls temperature at surface reaches temperatures of approximately + 100C. Even though room temperature is +220C, it won't make us feel comfortable because human body's thermic radiations are absorbed by the inner walls. If using thermal insulation, inner wall's surface temperature is increasing to about 180C, air temperature can be lowered to 200C, and yet the comfort state will increase.

After commissioning of the building, the repartition of the heat on the inner part of the house can be checked using an "infrared camera", so that the weaknesses of the thermal insulation can be accurately indicated. Thus, we will know whether and where to intervene. The cracks should be removed as soon as possible. Some crack types can be repaired but only after the deformation processes that made them were finished. In other cases we can act quicker: for example, an improperly applied thermal insulation system (missing or inadequate diagonal reinforcement of the corner areas) can lead to shrinkage cracks in windows sills.

For the facades the thermal insulation systems are used. As insulating materials the most indicated ones are expandable polystyrene plates or mineral wool available in slabs or rolls. These insulation systems are called systems becuse the providers only deliver the isolating materials along with all the necessary assemblying, soldering and coating materials. The reliability of insulation systems is given only when the materials used are aligned with each other. It is not recommended to combine materials from different groups of systems.

There are also materials with superior thermal properties, less known, pending to be introduced into practice:

Insulating materials as thin layers associated with refective foils, which are designed to reflect the infrared radiation and thus to suppress heat transfer by radiation;

Insulating materials obtained by vacuum venting of a fibrous or cellular support packed into a tight sheet; among these the silicon Nanogel has special properties, being less conductive than air at normal pressure.

The efficiency of the thermal isolation implies its continuity over the entire surface of the tire. Any physical or geometric discontinuity generates a thermal bridge characterised by additional heat loss and condens and discomfort risks. These thermal bridges can be avoided or treated in an adequate manner, if possible, when they cannot be avoided.

Windows have to meet numerous functinos such as: natural light entering the house, maximize the solar heat, minimizing the heat loss and resistance to the numerous requests caused by wind, rain, heat, cold, etc. During the winter, window energy losses consist in losses of heat through the glass, frames and through frame's bridges that appear at the junction with window's borders. Opposite to the heat losses are energy gains from the sunlight on Eastern, Southern and Western sides. Energy gains that are welcomed during the winter, are transforming, under certain conditions, in disadvantages during the summer, if the shading or ventilation was not predicted. The result is the overheating during the summer. Solar protection and shading facilities (shutters and rolls) have to be mounted where they are most efficient, respectively, to the outside of the building, before the heat reaches the rooms.(nu are logica deci am tradus fara partea cu "sa se monteze de exterior). This is the most efficient way and saves the energy that would otherwise be necessary to lower the room temperature with air conditioning.

The windows are products of high technique. It Windows are best suited for two or three glass panes with metal coating and gas filling between the panes, techniques that reduce heating costs through an optimal thermal insulation and that are improve the quality of life through noise protection. Break-resistant windows are recommended especially for ground floors. For safety purposes, in special cases, safetu glasses used in cases of fire are recommended. When opening the windows a system should be installed so that it automatically stops the air conditioning/ radiators.

Planning the construction of the house windows is very important for the later convenience of its residents. The most efficient windows are considered to be those that, through their placing, are capturing as much natural light as possible, decreasing that way the electrical illumination needs.Thus, large windows on the Southern side of a new building creates rooms bathed in light. The windows situated on the Eastern and Western sides of the building will be optimized for a sufficient illumination. Northern side won't have windows at all, or if it will have, they will be small windows, for example for stairwells and toilets. Northern side of the building will always reach energy losses.

Reducing the energy amount for lighting involves the extent of daylight usage, which is achieved mainly through architectural measures: choose of the adequate shapes and sizes for the windows, avoidance of windows obstruction with trees, buildings or plants, paint the surfaces that are situated opposite to the windows in light, refelctoring colours, expand the window openenings to the outsidein order to increase the area of visible sky, position some anidolic systems, that consist in some windows with a special shape and structure with the role to focus and lead the light beam to less bright areas of the room, during a certain time of the day. In this way we'll obtain an uniform illumination and we'll reduce the duration of artificial light usage.

The illumination of a building represents about 10% of the total electrical energy consumption If a building is equipped with energy saving bulbs as light sources, it can it can reduce energy costs. A 20W energy saving bulb illuminates around 6000 hours using only 1200kWH. An equally bright incandescendent bulb of 100 W has an estimated life time of only 1000 hours During the lifetime of an traditional bulb we need only 10 traditional bulbs and 5 times more energy. Despite higher acquisition costs, the total costs for energy saving bulbs are two thirds lower. That is how an 80% economy is achieved using energy saving lighting sources. Only about 10% of the total energy consumption is up to illumination, in case of using a traditional incandescendent bulb, the rest of it is turning into heat. There are economical energy sources, of different sizes, shapes and types. They may have adjustable luminosity, light sensors for external illumination and even motion sensors for halls or other common areas. Motion sensors and automatic switches ensure that the lamp lights only when it's dark and when someone is within the action range of the sensor.

On the equipping of the house with electrical equipments, the energetical efficiency class of the equipment and especially the consumption in stand-by mode should be monitored. However applicances are consuming more power even in they are in standby function, so you can choose to use programmable outles. One third of the power consumption in residential buildings is due to the household appliances.

Generally, the products purchased in a green home should be mainly from the category of eco-labeled products because these have the advantage of: reduced energy consumption, being energetically efficient, reduced water consumption, a longer life time, are recyclable, reduce the pollution of the environmental parameters, are not containing toxic or dangerous chemical substances and have a high protection levels for human life.

This category includes for the moment:

- Electrical house eqipmeents: washing machines (laundry and dishes), frigorific equipments, televisios, electrical lamps, vacuum cleaners;
- Cleaning products: for dish washing machines, laundering machines, bathrooms, universal detergents, absorbant paper;
- Office supplies: notebooks, personal computers, graphic paper and self copying paper;
- House and garden products: rigid floor materials, bed mattresses, crops' soil and subsoil improving products;
- Lubricants;
- "CE" marking sign is also a guarantee that the product is environmentally friendly.

The building should assure proper facilities for the selective capitalization of plastic, metal, glass, paper and cardboard wastes. Then, these will be recycled through the authorized companies.It is not excluded that the money made with these wastes may cover the costs of the domestic wastes. The "Wastes= raw materials" sign should be visibly displayed. For soft organic wastes (bread, vegetables, fruits, etc., excluding meat products or any other animal origin products) we can use a little chopping machine in the kitchen, so that these wastes could be undertaken in the sewerage network. It is a way to highly reduce the quantity of wastes delivered to the salubrity company. This is how the costs that have to be paid to the salubrity company will decrease. The building should also be foreseen with a modality to collect the dangerous wastes (like used cooking oil).

The sunlight lamps will be used in order to illuminate the garden, the terrace, the garage entrance or the building's front way (usually made in pressed gravel instead of asphalt or concrete). The two separate systems (solar unit and separate lamps) will facilitate lamp's positioning even in shade, if the day solar cell will be placed in other location. The solar cell should store up a couple of day light hours in the accumulator so that the lamp can function 12 hours during the night.

The solar panels can be used to obtain hot water. For a good dimensioning of the solar installation the hot water consumption should be calculated. For a householding, as an informative value will be used a 40-60 litres/person/day consumption.

Daily water consumption for an individual is between 120 and 150 litres. 40% of it is slooping through toilet's basin and almost the same quantity is used for bath or shower. The loads from toliet's basin are limiting the water quantity from it. It is recommended to equip the building with some reservoirs foreseen with an economy switch. Water's flow in the wash bowl is around 12litres/minute, but half of it is enough for washing the hands. There can be installed some adjustable flow regulators. Flow regulators will reduce the flow, saving this way up to 50% of fresh water. There are even electronic systems that can save around 70%, because they are opening only when the button is pushed and are closing back immediately.

In water's usage both ecological and economical aspects should be considered. Both in houselholdings and offices, only 3-4% of the fresh water supplies are used for cooking and drinking.

In this case, the opportunity of making a small purification station has to be considered. These small station can be made in a compact shape using different materials (concrete steel, glass fibers, plastic), usually having 4 rooms:

- Primar levigation with fat's separation;
- Primar levigation being used as a septic tank;
- Bacterian bed with plastic granules that assures the secondary aerobic treatment;
- Secondary levigation.

Another water source except the free one is the rain water. Besides this advantage, rain water does not have to be processed, offers protection against calcification (example: for washing machines), helps plants to undertake the minerals, etc. The rain water is usually collecting on the roof. A pipe system and preliminary comuted filters will lead the rain water in the reservoir. The reservoir is up or under ground or it may be installed in the cellar. Using a pump and a re-circulating filter rain weater is leaded through the pipes to the consumption places. During dry periods, fresh water supplying is assured through an automatic system. There are no doubts regarding the hygiene of the rain water. Recent studies confirm that the modern rain water using plants guarantee the adequate filtration of the water.

In the arrangement of the gardens, concerning the water consumption, we should have in view some aspects. First of all, the plants chosen for the garden should need water in the same period of the day an in approximately equal amounts. There should be consulted a specialist because some of the plants are likely to suffer from water shortages and others suffocate from too much water. Once established this aspect it can be reduced by up to 40% water consumption for watering the garden by practicing an automatic watering system – the correct amount at the right time. Automatic watering is not only comfortable but also contributes to the optimum plant growth and to the economic use of water resources. Water should penetrate the soil well. The applicable principle is: better watered less often, but intensively. During the dry phases, the insallation of artificial rain should stand around 20 minutes in one pace in order to ensure about 10 liters of water per square meter. Then will be sufficient to spray the water every four hours. Too much water will wash the fertilizers and nutrients from the roots and will prevent the distribution of oxygn in the sooil. If in the upper soil layers there is no water, the roots will seek the moisture themselves from the deeper layers. If it is too hot during the day, it's preferable to avoid watering, because every water drop has the glass effect and will burn the plants. Besides this, the sun evaporates the water faster.

The consequences are: higher water consumption and a low efficiency of watering. The best time for watering is the early morning. If the watering is made between 9.00 and 10.00 pm, 25 -30% of the water still evaporates. If the owner of the garden waters the lawn in the morning, between 2.00 and 4.00 am, the evaporation percent is under 10%. That is how much water can be saved. But, because nobody wakes up happily at this tme just to open the water tap in the garden at this hour, watering is possible through an automatic computer controlled watering. Computer watering is indicated for a fully automatic control of the artificial rain installations and of the spray irrigation systems. If the owner of the garden has the possibility to connect a sensor to the computer watring system, the watering will be doneonly when it is absolutely necessary.

For residential heating, as the case, it canalso be chosen an alternative method as: heat pumps, the heating using the pellets, etc. However, fossil fuels should be avoided.

Wodden pellets are some small pieces of pressed wooden chips. They are ecologically burned in the stoves and modern heating boilers specially designed for this purpose. Heating with pellets is also economic and they have a more secure future than the oil, gas or coal. Another advantage is that wood is a renewable raw material.

The heat pump collects the energy through a collector. This is placed in the drilling made in the ground. Drilling depth ranges from 90 to 200 meters, depending on the size of the selected heat pump. This system can be used for all possible types of buildings, large or small, public or private. It requires less space and the probe drilling can be done even in the smallest gardens.

If we're talking about water, sewerage or heating systems of a building, if it already exists, it have to be checked regarding the tightness along the entire length of the property,

and if it's newly made, a higher attention should be given to all the measures needed in order to eliminate any kind of loss.

A comprehensive analysis of the relationship between the energy consumption and indoor environmental quality, both for residential and administrative buildings, was performed in the European Project "HOPE" (Health Optimization Protocol for Energetically Efficient Buildings), conducted among 14 participants from 12 European countries during 2002 – 2005. There have been investigated more than 160 residential and administrative buildings, half of them presenting relatively low energy consumption. The investigation consisted of a general inspection, a discussion with building's manager and the distribution of questionnaires to the inhabitants (occupants). It was found that the energy consumption depends not only on the internal temperatures' value, the rigors of climate and ventilation, but it also highly depending on the architectural and structural solutions used and on the ecploitation manner.

3. CONCLUSIONS

The reduction of the energy consumption for building exploitation can not be separated from the indoor and outdoor environment quality or from the influence on the outdoor environment, and all of these are the result of the simultaneous action of a complex of factors which are essentially defined by the structural and architectural features, location, weather conditions, facilities' operational state, users behaviour. The interaction between these components may influence the effectiveness of each energy efficiency measure or complex of measures on building's behaviour as a whole.

4. REFERENCES

[1]. Roulet C.-A., Ostra B., Foradini F., Cox Ch. - Designing healthy, comfortable and energy efficient buildings: lessons from enquiries within the European HOPE Project. CISBAT 2005

[2]. Roulet C.-A. - Sante et qualite de l'environnement interieur dans les batiments, Presses Politechniques et Universitaires Romandes, Lausanne, 2003

[3]. Bliuc I., Rotberg R., Dumitrescu L. - Simulation and performance analysis of hygrothermal behaviour of buildings in transient regime, Proceedings of the International Conference "PBE 2004: Performance Based Engineering for 21st Century", Ed. Cermi Iasi, 2004, ISBN 973-667-063-5, pag. 43-48

[4]. Bliuc I., Rotberg R. - The impact of some dwelling energy - efficiency raising measures on the inner ebvironnment quality. Evaluation methodology. CISBAT 2005

[5]. Bliuc I., Baran I. - Metodologie pentru adoptarea soluției optime de reabilitare termică a clădirilor. Simpozion Internațional Materiale, elemente şi structuri compozite pentru construcții, Timişoara 2005

[6]. De Wilde P., ş.a. - A strategy to provide computational support for selection of energy saving building components. A VII-a Conferință Internațională IBPSA, Rio de Janeiro, 2001

[7]. Mansoury Y., Allard F. ş.a - Conceptual implementation of natural ventilation strategy. AVIII- a Conferință Internațională IBPSA, Eindhoven, Netherlands, 2003

[8]. * * * Asigurarea calității mediului interior cu consumuri energetice minime – atribut al arhitecturii durabile. Grant CNCSIS 2004-2006

Some issues concerning technical procedures of treating sewage sludge in wastewater treatment plants in order to capitalize in agriculture

Dinu Ilinca, Gheorghita Oana

Abstract – **With the progress of civilization, the urban and rural development, same as the evolution of consumption patterns, wastewaters have evolved considerably in terms of quantity and quality. The need to protect natural water quality requires the operation of wastewater treatment plants near communities for wastewater treatment. Wastewater treatment plants inevitably generates a by-product known as sewage sludge. In this context, based on thorough theoretical studies, the authors analyze the possibility of environmental protection by capitalization in agriculture as organic fertilizer of sewage sludge from municipal treatment plants.**

Keywords – **capitalization, thickening process, sewage sludge, wastewater treatment plants**

1. INTRODUCTION

Yearly, in the world, are generated hudges quantities of sewage sludge as a result of wastewaters treatment. So, for many years, wastewater sludge has posed disposal problems. The safe disposal of the sewage sludge is one of the major environmental concerns throughout the world. Disposal alternatives that have been tried include soil application, dumping in waters, landfilling and incineration. Landfilling and land application of the sewage sludge are suggested to be the most economical sludge disposal method.

1.1. Actual stage of the use of sludge from wastewater purification stations

The waste water treatment stations release meaningful amounts of urban sludge and decant water that required for evacuation high costs. Increasingly quantity and the high content of fermentable organic substances of the mud resulted from purification of wastewater were the determiners of the direction in agriculture. Sludge usage in agriculture ensures biological recycling of nutrients and reduces the costs for chemical fertilizers.

In England this waste is being used in agriculture since 1543, and in 1992, in France and Spain, 50-60% of the quantity of sludge was directed towards agriculture, lower quantities are recorded in Germany (27%), Luxembourg Ireland (12%), Greece (10%) etc.

Dinu Ilinca is with Technical University " GH. ASACHI" Iasi, Hydrotechnics, Geodesy and Environmental Engineering Department, Bd.Mangeron nr. 67 - Iasi, Romania, e-mail: illinka_d@yahoo.com.

Gheorghita Oana is with Technical University " GH. ASACHI" Iasi, Hydrotechnics, Geodesy and Environmental Engineering Department, Bd.Mangeron nr. 67 - Iasi, Romania.

ISSN-1584-5990

(table 1). According to the European Commision, a general increase in the sludge quantity is foreseen in the future, but this increase does not reflect the situation in each country.

France, UK, Luxembourg, Germany and the Netherlands plan to further develop incineration. Agricultural use of sewage sludge will also increase in Ireland, Finland, UK and Portugal. It should concern about 55% of sludge produced in the European Union, whereas land filling should concern about 19% and incineration 23%.

Table 1. Situation of urban sludge usage in agriculture in the European Community in 2007

Country	**Agriculture**		**Overall**
	tone d.s/year	%	tone d.s./year
Belgium	17114	29	59198
Denmark	92500	54	170300
France	500000	60	852000
Germany	728300	27	2681200
Greece	4820	10	48200
Ireland	4518	12	36682
Italy	269000	33	81600
Luxembourg	946	12	7876
Netherlands	84683	26	322879
Spain	175000	50	350000
England	490000	44	1107000
Portugal	7500	30	25000
EEC	2374678	37	6476375

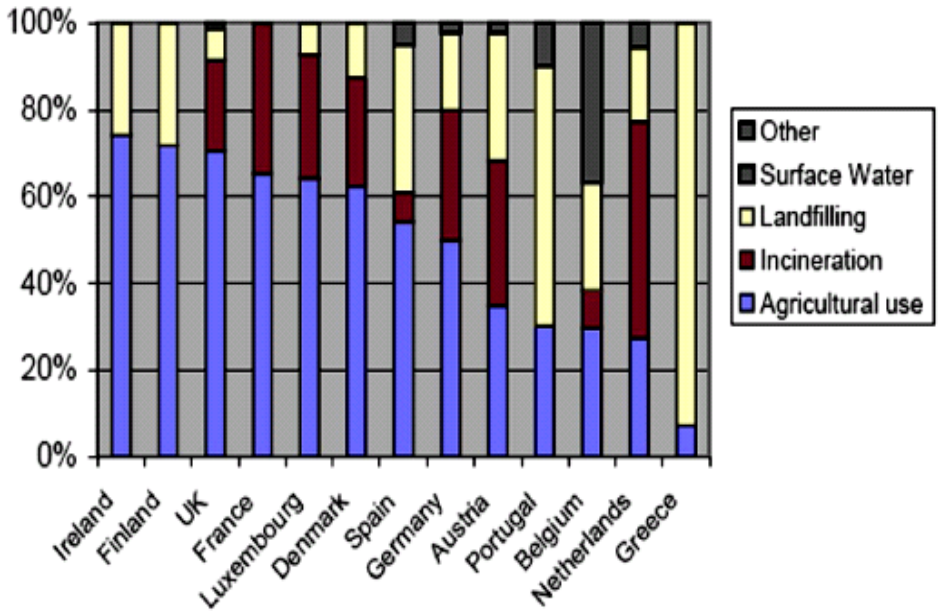

Fig.1. Destination of sewage sludge in the member states of EU in 2005 (Renner 2000)

In Romania, are considerable amounts of city sludge, from urban activities, and the crisis in organic fertilisers asks for the use of this sludge in the agricultural production circuit. There is a database for 5 years (2003, 2004, 2005, 2006 and 2007) with data on the

sludge from purification stations, which could lend to agriculture use. The analysis of data from the five years led to following results:

Table 2. Situation of urban sewage sludge in Romania between 2003 - 2007

	Generated sludge (dry sludge) tone/year	**Used in agriculture (dry sludge) tone/year**	**%**
2003	460222	54856	**12**
2004	403039	55990	**14**
2005	377 209	63336	**17**
2006	347121	48898	**14**
2007	172529	1127	**0.65**

2. TECHNICAL SOLUTIONS FOR PREPARING THE ORGANIC SLUDGE FOR AGRICULTURE

METHODS FOR REDUCING SLUDGE VOLUME

2.1. Sludge Thickening

The processes used to reduce the volume of the sludge resulting from purification processes, in order to use it as organic fertilizer in agriculture are: sludge thickening processes and those of its dehydration. Sludge thickening is the simplest and most widespread method of its concentration, resulting in volume reduction and improvement of specific resistance to filtration.

The degree of thickening depends on several variables, among which most important are: the type of sludge (primary,digested, active, etc.), initial concentration of solids, temperature, use of chemical agents, thickening time etc. By thickening, sludge volume can be reduced by almost 20 times compared to the initial volume, but is deepening the economic and technical efficiency to a solid concentration of 8-10%.

Thickening processes most commonly used are gravity thickening, thickening by flotation or centrifugation. The method is applied to gravity thickening.

Table 3. Comparative data between different processes of sludge thickening

Technology	**Obtained dry matter content (%)**	**Energy consumption kWh/m3 sludge**	**Features**
Gravity Thickening	4 – 6	0,1 – 0,3	Simple low operating costs, require large space, high construction costs, is not affected by solids present in the sludge.
Centrifugation	5	0,7 – 2,5	Convenient for biological sludge (without abrasive substances), space-saving and low construction cost
Thickening by flotation	4 – 6	0,3 – 0,6	Space-saving, low construction costs, sophisticated technology, high operating costs

2.2. Sludge dehydration

Retained sludge dehydration process in wastewater treatment plants is one of the most important stages of their processing considering the problems faced by most operators in terms of handling and transport of significant volumes of sludge. The dehydrated sludge is understood process that reduces their moisture so they can be easily manipulated. In small wastewater treatment plants (small flows of sludge), dehydration is achieved through natural processes (platforms for drying sludge or sludge bed) if space is available and are provided with the protection of the environment (protection of groundwater , human settlements, air, etc.). Mechanical drying methods are widely applied for different types of sludge (mud raw, digested, precipitation, etc.). To obtain an efficient separation of phases required preconditioning sludge.

3. SEWAGE SLUDGE MANAGEMENT ON ITS APPLICATION IN AGRICULTURE IN THE CONTEXT OF ENVIRONMENTAL PROTECTION

At the European level, the recovery in agriculture of sewage sludge produced in urban wastewater treatment stations has been the subject of common regulations (The European Council-1986) known as the EEC Directive 86/278, which aims to regulate the use of sludge in agriculture so as to avoid harmful effects on soil, air, water groundwater, vegetation, animals and humans. To ensure health protection, the sludge must be treated biological, chemical or thermal by long-term storage or by any process leading to significant reduction of the power of fermentation and concentration in pathogens. Storage period of at least 60 days is required for finishing the process of stabilization and disinfection because it is known that anaerobic fermentation does not destroy all pathogens and parasites. In addition to the nutrients in sludge there are variable quantities of heavy metals which accumulation in soil, over certain limits, may adversely affect the life of soil, plant life, quality of food products and the whole environment. These must fall within limits required by legislation to allow the use of sludge as fertilizer on agricultural land. In table 4 are presented maximum permitted concentration of heavy metal in sludges used in land application, in Romania.

Table 4. Maximum allowed content of heavy metal in sludges used in land application, in Romania

Parameter	Maximum allowed content (ppm)
Cd	10
Cu	500
Ni	100
Pb	300
Zn	2500
Hg	5
Cr	500
Co	50
As	10

To avoid any adverse effects of the sludge application on agricultural land should be taken into consideration aspects such as: physical, chemical and biological characteristics of sludge and soil properties, the ability of sludge loading, the ability of plants to exploit these nutrients from organic waste and the danger of environment

pollution. Sludge application on agricultural land has the advantage of being the least expensive method of neutralization and recycling of these organic wastes, while consistent with the general concept of ecological recycling, neutralization and improvement in some ecosystems.

4. MATERIAL AND METHOD

Research carried out aimed at valorising sewage sludge from the wastewater treatment plant from Iasi and its effects on potato, winther wheat and maize yield cultivated in rotation, and soil property modification.

The objective of this study was to evaluate the effectivenes of sewage sludge as phosphorus and nitrogen amendment for cambic chernozem soils in comparation with mineral fertilizers (NH_4NO_3 and KCl). The experiment were conducted during 10 years in two rotations: 1) potato – winther wheat – maize and 2) maize – potato – winther wheat.

Sewage sludge applied in potato was 65, 130 and 195 t/ha respectively, and in maize 30, 60 and 90 t/ha, sewage sludge rates applied alone or in combination with N and K as mineral fertilizers.

5. RESULTS AND DISCUSSIONS

The results led to the following conclusions:

- The air – dried sewage sludge from plot Iasi contained about 200 kg organic matter, 6 kg N, 8 kg P, 2 kg K, 30 kg Ca and 10 kg soluble salts in 1000 kg. The heavy metals content was under the maximum limits allowable, excepting Zn which was found between 4140 and 5378 ppm Zn.

Table 5. Contents of heavy metals in sewage sludge obtained from wastewater treatment station in Iasi

Sludge origin	Cd ppm	Cu ppm	Ni ppm	Pb ppm	Zn ppm	Cr ppm	Co ppm	Mn ppm	Fe %
Settling tank	0,66	73	77	179	5378	68	32	235	3,01
Batches	0,98	74	75	207	4140	63	33	336	4,20
LMA (CE)	10	1000	300	750	2500	1000	-	-	-
LMA (Ro)	10	500	100	300	2000	500	50	-	-

LMA (CE)= maximum allowed limits by the Directive 86/278;
LMA (Ro)= maximum allowed limits in Romania.

- At potato crops resulted in an yield increase of 100 tubers for one ton sewage sludge in case of rate of 65 t/ha, at higher rates the yield increase being lower. Annual rainfall had a significant influence on yield increase.
- The nitrogen utilization from sewage sludge was of 8,5 %at a rate of 65 t/ha and 2,5 % at a rate of 195 t/ha. From 100 kg N as mineral fertilizer, potato used 30 % and produced 60 kg tubers/l kg N applied in soil. The yield increase at 1 kg N from sewage sludge was of 17 kg tubers at a rate of 65 t/ha. Therefore, the nitrogen

efficiency from mineral fertilizer was about three times higher compared to N from sewage sludge.

- Applied in maize crop, resulted an yield increase of 23,2 kg grains for 1 ton sewage sludge at a rate of 30 t/ha and only 13,2 kg/ 1 t at a rates 90 t/ha. By comparing to manure, the yield increased was lower. The nitrogen utilization from sewage sludge by maize was of 11 % at 30 t/ha and 6,6 % at 90 t/ha. From mineral fertilizer, maize used 25,9 % of 100 kg N/ha.

Table 6. Direct effect of sewage sludge applied in moderate doses on the production of potato (average yields of two years)

Sewage sludge (t/ha)	Fertilizers								
	N_0K_0			$N_{96}K_0$			$N_{96}K_{120}$		
	t/ha	Dif., t/ha	%	t/ha	Dif., t/ha	%	t/ha	Dif., t/ha	%
0	17,1	-	100	0,2	3,1	118	20,4	3,3	119
30	19,7	2,6	115	21,4	4,3	125	21,5	4,4	126
60	21,4	4,3	125	21,8	4,8	127	22,1	5,0	129
90	22,4	5,3	131	22,4	5,3	131	22,6	5,5	132

DL 5%=1,6; 1 %=2,1; 0,1 %=2,8 t/ha.

Table 7. Direct effect of sewage sludge applied on corn grain yield (average two years)

Sewage sludge (t/ha)	Fertilizers								
	N_0K_0			$N_{100}K_0$			$N_{100}K_{50}$		
	kg/ha	Dif., kg/ha	%	kg/ha	Dif., kg/ha	%	kg/ha	Dif., kg/ha	%
0	5292	-	100	6155	863	116	5952	660	112
30	5988	692	113	6544	1252	123	6262	970	118
60	6126	827	115	6685	1393	126	6482	1190	122
90	6482	1190	122	6750	1458	127	6608	1316	125

DL 5%=658; 1 %=881; 0,1 %=1140 kg/ha.

- Residual effect of sewage sludge in second year in wheat crop was of 7,1 kg/t sewage sludge applied in the previous year at a rate of 65 t/ha and only 3,7 kg/t at 195 t/ha. At a rate of 100 kg N/ha mineral fertilizer resulted in an yield increase of 4,9 kg grains/1 kg N. Maize yield in the third year after sewage sludge application increase by 11 kg grains/ton at a rate of 65 t/ha and only by 3,8 kg/t at rate of 195 t/ha. Ammonium nitrate alone increased yield maize by 10,6 kg grains for 1 kg N. Plant utilization of N from sewage sludge during 3 years was of 17,5 % at a rate of 65 t/ha sewage sludge and only 6,5 % at rate of 195 t/ha.

- The sewage sludge has increased soil pH by 0,2 units 3 years after the application of 65 t/ha, due to high amounts of Ca present in it. The content of accessible phosphates from soil fertilized by 65 t/ha sewage sludge increased significantly, existing the danger of soil overphosphatizing, with negative consequences on the plant nutrition. The total content of Cu, Ni, Pb, Co and Mn from soil had easily increased on plots amended by 60 – 90 t/ha sewage sludge, doubled or tripled in case of Zn and remained unchanged in case of Cd.

Table 8. Content of heavy metals (total forms) in soil fertilized with sewage sludge, cultivated with wheat alternatives

Sludge t/ha	Cd ppm	Zn ppm	Cu ppm	Pb ppm	Cr ppm	Ni ppm	Co ppm	Mn ppm
0	0,8	75	32	20	16	20	26	950
30	0,8	105	34	20	17	20	27	1015
60	0,8	203	37	22	18	20	28	1075
90	0,8	223	41	25	20	22	28	1150
LMA *)	3,0	300	100	50	100	50	-	-

LMA *)= maximum allowed in soil.

- Soil contamination by pathogenic germs remain low, Salmonella was absent, existing only the contamination with eggs of intestinal worms.

- Sewage sludge between 30 – 60 t/ha had residual effect for at least 3 years. Periodical soil analyses on Zn and P_{AL} content are indispensable, in order not exceed the allowable maximum limits. The data have showed that the rate of sewage sludge on chernozem must exceed 400 kg P/ha.

6. CONCLUSIONS

Sewage sludge is considered an organic fertilizer that results especially from the water waste treatment plants. On short and middle time, agricultural utilization of sewage sludge is a solution for the future, in purpose to depolute the environment and to improve the soil's properties.

Sewage sludge application on agricultural lands can have the next benefits effects: supplying the nutritive elements (N, P, K, secondary macro elements, microelements), improvement of physical properties of soil and the rising of the humus content in soil.

On the other hand exists a serial of inconvenient, such as: contaminant potential of nitrates and phosphates; destructive potential on the health of the heavy metals and pathogens potential transfer.

This disadvantage depends on the inter relations between a few factors: sludge composition, the dose and the frequency of application on soil, soil characteristics and the plant. Sludge composition, and the relation between the soil and this, influences the chemical form of metals and the accessibility for the plant.

A method to estimate the accessibility of metals regarding the soil needs must be tested in field conditions, on different soil types, and with sludge having a different composition. It must be taken in considerate any chemical modification of metals from sludge.

7. REFERENCES

[1]Dima M.,*Urban wastewater treatment*, 2005, Ed. Tehnopress, Iasi.

[2] Singh R.P., Agrawal M., *Potential benefits and risks of land application of sewage sludge*, 2008, Waste Management 28 (2008), pp 347-358.

[3] Berbecea A., Radulov I., Sala F.,*Agriculture use of sewage sludge pros and cons,* Universitatea de Ştiinţe Agricole şi Medicină Veterinară a Banatului Timişoara.

[4] NP 118 – 06, *Normative for the construction design and installations of urban wastewater treatment plant*, 2006, Part Five: Sludge Processing.
[5] Lixandru Gh., *Folosirea namolurilor de canalizare ca ingrasamant in agricultura,* 2005, Universitatea de Stiinte Agricole si Medicina Veterinara, Iasi, Factori si procese Pedogenetice din Zona Temperata, 4 S. noua 41-45.

Contributions to the influence of moisture on the natural stone resistance structure of the patrimony buildings

Gramescu Ana Maria, Dragoi Mihaela, Pericleanu Dan

***Abstract* – In this paper we presented the results of studies and researches conducted by the authors regarding the rehabilitation of historical monuments. The paper deals with changes of behavioral parameters of natural stone masonry subject to the phenomenon of moisture.**

***Keywords* – heritage buildings, moisture, stone masonry.**

1. INTRODUCTION

Stone masonry is a material widely used in Dobrogea area and beyond, both in residential construction and Orthodox workships places. According to recent population and housing census in Romania, in terms of materials used and with reference to urban residential buildings, the construction of brick, stone or substitutes represent about 50% of the buildings.

These arguments were the basis for the initiative to strengthen existing building fund in order to use efficiently these resources. In local, national and even international (UNESCO) heritage there are included buildings with main structure made of local materials - stone - constructions that are characterized by the value of assets over which the society must work in order to promote conservation and restoration of architectural-historical value. Such buildings generally have an appreciated value, being characterized by a remarkable functional and relevant compliance for the period in which they were made through the materials and technologies that had an important contribution to the criteria for quantifying the amount of reserves and protected monuments.

The most important fact is that the materials used are generally local area resources and that technologies express a tradition of centuries in terms of buildings. In time such structures have been exposed to destructive factors of physical, chemical and mechanical processes which in conjunction with rheological parameters have led to lower mechanical behavior of the constituent material. Within this paper presents the studies and research conducted by the authors on the influence of moisture in all aspects of natural stone construction, based on the results of detailed investigations on stone constructions made in the SE area of the country.

Gramescu Ana Maria is with Ovidius University of Constanta, Bd. Mamaia nr. 124, 900356-Constanta, Romania (phone: +40-241-619040; fax: +40-241-618372; e-mail: gramescu_am@yahoo.com).

Dragoi Mihaela is with Ovidius University of Constanta, Bd. Mamaia nr. 124, 900356-Constanta, Romania (e-mail: dragoi.mihaela@gmail.com).

Pericleanu Dan is with Ovidius University of Constanta, Bd. Mamaia nr. 124, 900356-Constanta, Romania (e-mail: pericleanu_dan@yahoo.com).

ISSN-1584-5990

Construction of natural stone can be made from the following types of masonry:

- rough stone;
- processed stone (carved, quarry stone, polygonal, waist);
- mixed.

Rough stone masonry are composed of irregularly shaped stones as extracted from the quarry or riverbed, the thickness of bearing walls is at least 60cm for irregurlary raw stone and river rocks and at least 50cm for the raw one with two flat gross and parallel faces. This type of masonry is used for foundations, pedestals, walls for buildings, retaining walls, stone packing, vaults.


(a)

(b)

Fig. 1. (a) Rough stone masonry with mortar; (b) Polygonal rough stone masonry


Fig. 2. Dry stone masonry (without mortar)

Processed stone masonry are detailed in fig. 3.

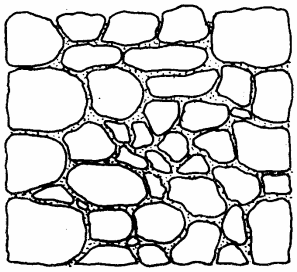
(a)
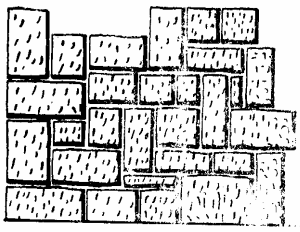
(b)

Fig. 3. (a) cut stone masonry, which has two seen faces (it is kept the row correspondence one the two seen faces, observing the same row as a short tail of a match against a long tail on the opposite side); (b) modern masonry it is permiteed the vertical joints coincidence on a maximum height of two rows; for uniform pressure distribution, at each 2m height, it is made a continuous horizontal joint.

.

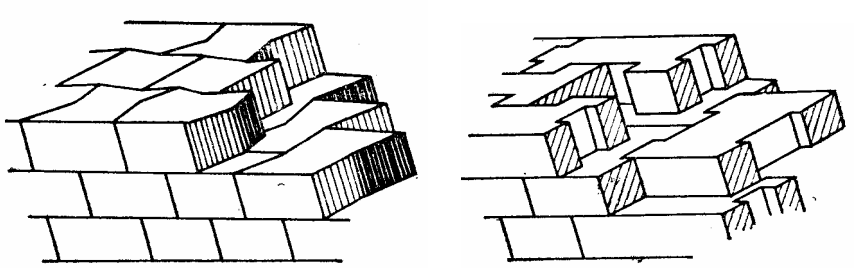

Fig. 4. Size stone masonry blocks in the shape of dovetail joints and blocks with right threshold (used in elevation masonry works of art, monuments, columns, vaults, breakwaters, quays,etc).

In case of masonry with high joints, the compressive strength of the assembly is on lime mortar, less durable than stones; if there are thin joints, the compressive strength tends to the stone one.

The overall analysis of the behavior of these constructions highlights a high-risk (vulnerable) to the action of destructive factors, factors which may manifest as:

a) degradation of masonry visible at the surface of contact with the environment, demonstrated by:

- substance accumulation (accumulation of substances or formation of cruts);
- deformation (loss of the surface's smoothness);
- disruption of continuity (the formation of cracks in the material);
- color changes (variations in color, tone or bright of the materials);
- substance loss (separation of the material);
- grain variations (changes in the characteristics of the material causing the loss of native tactile roughness).

b) the action of natural processes:

- succesive expansion and contraction of the material affected by thermal variations, generating internal tensions;
- mechanical action of water, by changing the state of aggregation (freezing, evaporation), generating tensions which produce separation, surface weathering, porosity;
- mechanical action of salt crystallisation in aqueous solution by increasing volume associated stress inducing process that produces similar degradation as frost;
- abrasive action of wind that produces the progressive erosion of surfaces exposed; the wind has also a transport effect (carrier of water molecules, the wind is a factor of amplification by amplifying the effects of water volume and pressure impregnation phase fluid flow; depending on its direction it may cause wetting for ussually protected portions), acceleration (which accelerates the cycles of evaporation, which in drying phase it enhance moisture migration from inside to outside) and scratchy distribution of rain and dust on surfaces exposed - compared with speed, direction and turbulence caused by obstacles;
- physical wear, normal or premature, due to operation conditions, normal or unreasonable;
- natural aging process that produces slow changes in the structure and properties of certain materials.

c) the action of chemical processes is based on chemical reactions between compounds present in the constituent material, in water and in various pollutants compounds from

water or in atmosphere. These reactions lead to the formation of salts with different characteristics and effects on the masonry:

- changes in solubility;
- crystallization;
- color;
- changes in volume with similar effects as frost;
- changes in the strength of materials.

2. MOISTURE – STONE DETERIORATION FACTOR

Moisture represents a major factor for initiating and contributing to stone weathering especially in rocks such as limestone, dolomite and marbles.

Moisture can occur both in direct contact with water from precipitation, maximum and minimum humidity, which in many cases can be combined with variations in temperature, freeze-thaw processes, prevailing winds, smoke and gases aggresive containing. It was established by experts that over 10 years of exposure to 100 cm column of rainfall the limestone rocks can reduce their thickness with 0.2 mm. If rain and especially drizzle are acidic, the process of "corrosion" is more intense. The water of the crystalline marbles can dissolve sulfates and includes bacteria, following which the final result is the appearance of stone with small caves, called "grain of sand displaced". This effect could be found on Hagieni mosque building.

Fig. 5. Hagieni mosque / Hacĭlar Camisi

Regarding infrastructure made of natural stone a potential risk is represented by the quality of groundwaters and how they can help to initiate a chemical degradation process.

Fig. 6. Nicolae Balcescu mosque – Foundation stone impaired by moisture rising land

In order to know how moisture affects the mechanical processes of rock there is necessary a detailed analysis of physical and mechanical properties of stone masonry.

Fig. 7. Details on stone degradation due to moisture

When the mortar is soaked with water, its plasticity significantly increases, while its resistance decreases.

Traditional masonry are even more sensitive and degraded through regurlalry watering, by failure of protection devices against rain, and/or irrigation of land rise.

Due to the fact that mortar porosity is higher than the stone, the largest evaporation occurs in the mortar and the design of efflorescence significantly reproduces the masonry structure.

Moisture can directly affect the adhesion between stone and mortar connection (which can be heavily eroded many times). Absorbed water for more than 20-25% of total capacity leads to serious reduction of adherence. The water penetrates into the pores and ceramic blocks, similar to natural stones. Stagnant water in ceramic structure represents damp masonry. In these conditions, on the exterior walls it was observed a repeated freeze-thaw phenomenon in a large number of cycles. The volume changes of water in pores during a changeover state of aggregation lead to internal tensions in the bricks. The old bricks, being porous, will be more easily exposed to this phenomenon, thus often results outside grinding blocks. The picture below shows quite convincingly the cumulative effects of moisture on an old masonry wall of brick and weak mortar.

Fig. 8. The effect of grinding brick masonry caused by repeated freeze-thaw phenomenon of stagnant water wall surface

When the temperature falls, the stone tends to contract while the water contained solidify by amplifying its volume with about 1/10 and producing a pressure of about 165 kg/cm^2. The two pressures are adding up, causing internal tensions, very high at local level, which produce disintegration of mineral texture.

Aqueous solutions of mineral salts deposited in the pores will crystallize in the same time with water evaporation. Thus, it appears tensions in areas that limit the pores due

to crystallized salts. Referred as "efflorescence of stone", the phenomenon of crystallization of salts in the stone building is a great danger for the sustainability of historic structures. The most common salts in efflorescence phenomena encountered in the examined buildings are: sulphate, carbonates and nitrates (sodium, magnesium, calcium, potassium).

Fig. 9. Nisipari mosque – Limestone construction – efflorescence caused by mineral salts

The impact of moisture on stone masonry:

- reducing mechanical resistance :

Replacing the air with water in the pores of a material is equal to replacing the elastic behaviour of air by relative incompressibility of water. When placed under load material, the effect of interstitial water expulsion induces additional efforts, added to vertical or axial compression through natural discharge of loads, thus determining the occurrence of destructive horizontal components (masonry) or radial and tangential (woodwork). For example: a limestone rock with 36% porosity, strength resistant is reduced from 126kg/cm^2 for dry stone to 48kg/cm^2 for saturated stone. It is also affected the mechanical resistance of the wall by the growth of its own weight, thus a wall with 30% moisture has to bear an extra weight of 300 kg for each cubic meter of masonry (an overload of 10% in case of an building P+4E). Thus, generally an over moisture of 10% reduces the masonry strength by 60%.

- dimensional variations of material:

Passing the material from dry condition to wet may cause dimensional growth that are reduced in stone cases (35 – 180 microns/ml).

- degradation of materials by physical, chemical and biological processes as those listed above;
- increased thermal conductivity;
- environmental degradation.

3. METHODS FOR REMOVING THE EFFECTS PRODUCES BY MOISTURE

The methods to eliminate the destructive effects of moisture products are based on:
- eliminating the sources;
- dry masonry;
- cleaning masonry;
-masonry waterproofing with materials: the solution must be determined based on the behavioral characteristics of natural stone (limestone) in conjuction with the environment (area with constant salt aggression).

In order to remove the moisture that climbs by capilarry there has been used in stone masonry methods such as under-masonry and isolation of foundation, the design of ventilations holes and lately – electronic drain. This method consists in binding the building by ground sockets, type lightening rod by introducing in masonry a hidden installation, made of copper conductors. As a result, the water from the material capillaries is

eliminated through own weight. The average ratio between evaporation surface and absorption, deduced from various observations on wet masonry is the following:

- to exterior walls: 3 .... 8;
- to interior walls: 4 .... 10.

Also in literature the index is defined as the ratio between maximum height rise of moisture and masonry thickness:

- to exterior walls: 1.5 .... 4;
- to interior walls: 2 .... 5.

It has been noticed that the greatest climb heights are found in brick walls, during winter, on the walls exposed to north, in an environment with water with high salt content, average with saturated air or near saturation.

In general, the evaporation of water contained in masonry depends on the drying coefficient specific to each type of masonry and proportional to its thickness. The drying period of masonry varies with the square of the thickness of masonry walls. For example, for brick masonry the average drying ratio is 0.28, 1.2 for lime mortar, 0.25 for fat lime mortar and 1.6 for concrete.

In order to remove salts from water, which are re-crystallizing on the stone surface with an exfoliated effect, it is used the washing of masonry with fresh water when the stone is brittle. Parts of smaller stone, located in a precarious state, are dressed with absorbent filter paper, which scutch by wetting. Moisture penetrates the material and when it evaporated the process train the salts remain soaked in paper.

For washing the stone, dirt of dust or smoke, it is used various detergent dilluted in warm water, rubbing the material with a soft brush so as not to cause destruction of protective crust. The surface clogging dust can be removed by blowing compressed air (process used to clean the front of Military Club in Bucharest). The oil paint, placed over the stone can be removed only by using organic solvent, avoiding the burning paint, which can cause destruction of protective crust.

Research conducted to find methods of stone conservation degraded, exposed in the open air, did not led to the development of secure solutions. The process with silicating stone surface has proven ineffective. By preventing the exchange of moisture between the material and exterior, silicating caused actually a speedy decay of stone. As a result, many solutions developed for the conservation of stone have a small scope, limited to stone elements to be preserved in museums, in particular air-conditioned spaces and small components of stone buildings, which can be detached, treated in laboratory conditions and then put back into operation (statues, reliefs, modern elements).

If for the parts that will be kept in museums, in special conditions of climate, it can be done protective films with wax or silicone resin, in case of the parts which are to remain or to be brought outdoors in open air, the treatment refers to strengthen measures that do not affect the exchange of steams between the inside and outside and also leads in restoring the protective crust.

Natural protective crusts are the results of the following process: the water penetrates from outside through the pores of the stone filled with carbon dioxide, causing a dissolution of its superficial layer. When evaporating, water comes out the same way, but dissolved limestone is deposited in a more compact form, the crust, which plays an important protective stone. The destruction of the crust is particularly harmful, as well as its recovery represents means of conservation.

For stone treatment, that has reached the stage of degradation, the following methods are used:

- Impregnation: the stone is placed in a bath with protective substance;
- Injecting the substances are introduced under pressure inside the stone;

- Vacuum: the stone is placed in a bath that produces a vacuum; the air exits the pores, its place being took by the liquid introduces in the bath.

In order to carry out these operations, from case to case, it can be choose the resin or solvent with a suitable viscosity, depending on the nature and porosity of the stone. From the wide range of synthetic resins, there have been experiments with epoxy resins and polyester, dissolved in various organic solvents.

Fig. 10. Masonry restored and being restored using existing components

4. CONCLUSIONS

The moisture in building materials or buildings plays an important role by creating a climate conducive to the maintenance of living and health of people, and by ensuring the sustainability of buildings and building elements in order to reduce heating costs, etc. The damage caused by moisture not only influence the optical image of the building, but strongly influence the substance and constructive climate as well as energy balance.

The problems caused by moisture in all its forms do not have a standardized solution, absolute, each case must be studied and solved independently and solved, by correctly identifying the causes that have induced pathology. The study of stone characteristics before designing and executing an intervention works on the existing structure is of great importance in understanding the behavior of that structure in different scenarios (seismic action, additional weights, replacing some elements of resistance, changing the methodology for handling, etc.) It is important to investigate nondestructive methods and to take all necessary data for a more realistic calculation of material.

5. REFERENCES

[1] Balint SZABO: Introduction to the theory of the resistance on historic structures, Cluj
[2] CR6 - 2006 - Code design for masonry structures.
[3] Crisan Rodica: Recommendations on the analysis, conservation and structural restoration of architectural heritage, „Ion Mincu" University Publishing House, Bucharest, 2002.
[4] Crisan Rodica:Traditional masonry. Characteristics and specific degradation processes, „Ion Mincu" University Publishing House, Bucharest, 1996.
[5] Curinschi Vorona George: Architecture, Planning, Restoration, Technical Publishing House,Bucharest,1996.
[6] Gramescu Ana Maria, Barbu Daniela a.m.: Repairing and strengthening the constructions, AGIR Publishing House, Bucharest, 2008.
[7] Gramescu Ana Maria: Projects restored for historic monuments - case studies.

Study on coagulation properties and efficiency of polyaluminum chloride (E-PAC) prepared by electrolysis process

A. Păcală, I. Vlaicu, M. Anghel, C. Radovan

***Abstract* – Alternative coagulants based on prehydrolyzed forms of aluminium, known as polyaluminium chlorides (PAC), with general formula $Al_m(OH)_nCl_{3n-m}$ have been developed rapidly. The electrolysis process could produce effective PAC, conventionnaly named electrochemical-PAC (E-PAC). This paper presents the efficieny of Bega River water treatment oriented to drinking water production management by using of different series of electrochemical E-PAC, prepared in our laboratory by electrolysis process in the electrochemical reactor with aluminium as anode, stainless steel plates as cathode, and Al Cl_3 aqueous solutions as the electrolyte. Effect of preparing conditions of E-PAC and coagulation properties were investigated through jar-tests in the various raw water quality conditions.**

***Keywords* – coagulation-flocculation, drinking water treatment, electrochemical polyaluminiumchloride (E-PAC), electrochemical reactor.**

1. INTRODUCTION

One of the most important long-term management tasks related to a water treatment process is the proper treatment to obtain a „clean and healthy drinking water".

Coagulation and flocculation is widely used in drinking water treatment and these techniques form an important step in the treatment process. To achieve the best treatment performance, the best type of coagulant and coagulation conditions need to be selected [1].

As well as traditional coagulants, such as aluminium sulphate ("alum"), there are now many commercial products that contain prehydrolyzed forms of the metals, mostly in the form of polynuclear species. In the case of Al, most materials are formed by the controlled neutralization of aluminium chloride solutions and are generally known as polyaluminium chloride (PAC) [2].

Because they are already partially neutralized, they have a smaller effect on the pH of water and so reduce the need for pH correction.

The mechanisms of action of PAC and similar products are still not well understood. Most explanations are in terms of the high charge associated with species such as Al_{13} ($[AlO_4Al_{12}(OH)_{24}(H_2O)_{12}]^{7+}$) and the consequent effectiveness in neutralizing the negative charge of colloids in water [2]-[4].

A. Păcală, I. Vlaicu, M. Anghel are working at Water Treatment Company - AQUATIM, Str. Gh. Lazar nr.11/A, 300081-Timisoara, Romania (contact author's coordinates: T: +40-256-208823; fax: +40-256-294753; e-mail: apacala@yahoo.com).

C.Radovan is Professor at the West University of Timisoara, Chemistry, Biologie and Geography Faculty, Department of Electrochemistry, Bd. Pestallozi nr.22, Timisoara, Romania.

ISSN-1584-5990

The so-called "Al_{13}" polymer, $Al_{13}O_4(OH)_{24}^{7+}$ has the Keggin structure, with one tetrahedral Al surrounded by 12 Al octahedra with shared edges. Beside the characteristic of a higher positive charge (+7) and resultant strong ability to bind to particles, Al_{13} polymer possesses fairly stable structure against hydrolysis before adsorption to particle surfaces. These properties contribute to their superior behavior in coagulation. In recent years has been demonstrated that the PAC products give better coagulation than alum at low temperatures and produce a higher quality of final treated waters (for example lower turbidity and reduced organic content) and with a greater reliability (less sensitivity to changes in temperature and pH) [2], [4].

In these specific circumstances, the new reagents on polyaluminium chloride (PAC), available on the Romanian market were tested, as a possible alternative to aluminum sulphate and sodium aluminate used today in Bega River water treatment process [5]-[8]. Recent research has shown that the electrolysis process could produce effective PAC [3].

It has been explored several aspects and illustrated the principle of PAC preparation by electrolysis and demonstrated that the electrolysis process could provide favorable conditions for polyaluminum formation. Our research followed this approach, so we managed to introduce a new and effective method for preparation of PAC-electrolysis process (E-PAC) [7].

This paper presents the efficieny of Bega River water treatment oriented to drinking water production management by using of different series of electrochemical E-PAC, prepared in our laboratory by electrolysis process in the electrochemical reactor with aluminium as anode, stainless steel plates as cathode, and $AlCl_3$ aqueous solutions as the electrolyte.

The experiments concerned with the determination of the effect of preparing conditions on quality of E-PAC and the coagulation properties, comparatively with the traditionally applied coagulant, aluminum sulphate ("alum") and sodium aluminate, as a classical reference.

2. EXPERIMENT DESCRIPTION

2.1. Raw water characteristics

The water used in the experiments was surface water from Bega River, used as raw water in the municipal Bega water treatment plant of Timisoara, Romania. The quality of the raw water was different during the experimental investigation; the general characteristics of the raw water quality are presented in **Table 1**.

Table. 1. Parameters of raw water quality

Parameter	Unit	Min.value	Max.value
Turbidity	NTU	20	50
pH		7.56	7.67
Temperature	°C	1.5	5.5
Alkalinity	mmol/L	1.7	1.9
Conductivity	μS/cm	259	319
DOC	mgC/L	4.66	5.785
UV_{254}	m^{-1}	0.317	0.542
Al	mg/L	0.00	0.01

2.2. Electrochemical preparation of E-PAC

A schematic view of electrochemical reactor (ECR) for E-PAC preparation is illustrated in **Fig. 1**. It consisted on a D.C. Power Supply (HY 3000D, China), an electrolyzer made out of organic glass (rectangular size 76 x 51 x 70mm) equipped with 6 parallel plain-plate electrodes, 3 anodes and 3 cathodes disposed in a mono-polar arrangement with 10 mm anode-cathode distance. Three sheets of Al (95 x 50 mm) were used as anodes while the cathodes were three sheets of stainless steel plates (95 x 50 mm). The system is completed by the electrolyte (200ml aqueous solution $AlCl_3$ 0.5M) and stirring apparatus (IKA, Germany) [3], [7]. An ammeter and a voltmeter (not presented in the simplified schema) were used for electrical characteristics control. Electrolysis was carried out in galvanostatic conditions at various current densities (i_A, A/m^2) and quantity of electricity (Q, Ah).

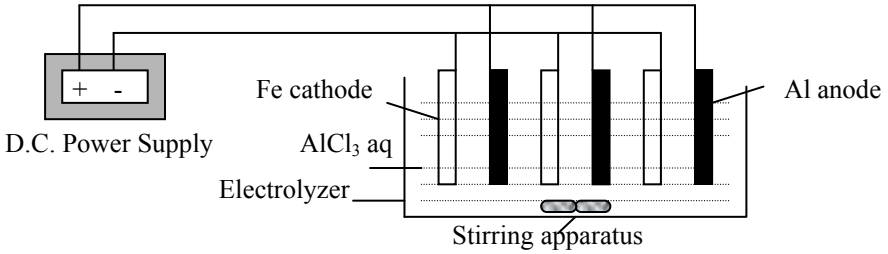

Fig. 1. The schematic view of electrochemical reactor (ECR)

2.3. Jar tests

Coagulation studies were performed in the laboratory as Jar tests, a common procedure for studying coagulation [9]. Jar tests experiments were performed using Jar test equipment manufactured by Velp Scientifica (Model FC6S, Italy), characterized by an electronic speed control with an independent speed settable for each place (six posts), aimed to optimise the result of settling reducing chemical consumption. The selected applied procedures for experimental series consisted in 2 min rapid mixing at 150 rpm (G = 86.05 s^{-1}), slow mixing at 45 rpm (G = 12.7 s^{-1}) for 8 min, and settling for 30 min (which are comparable to current plant conditions at the Timisoara Waterworks).

Tests were carried out on 0.8 L water samples and the temperature was 2-5°C for all experiments. Coagulants dosage was measured by a calibrated pipette (Multipette stream Electronic hand dispenser, Eppendorf, Germany*).*

Treated water samples were taken after settling for later analyses.

2.4. Analytical methods

For 30 min after settling, supernatants were collected to measure residual turbidity using a Turbidimeter (HACH 2100N, USA).

Dissolved Organic Carbon (DOC) is fraction of TOC that passes through a filter (0.45 micron pore size) and was determined from preserved (acidified) samples using a TOC Analyzer (TOC-V CPH, SHIMADZU, Germany). The UV_{254} was measured by a Spectrophotometer UV-VIS (UV-VIZ T90+, PG Instruments Ltd, SUA).

Total and dissolved Al concentrations were measured before and after sample filtration through 0.45 membrane, respectively, using Spectroquant kits for Aluminium test Merck

and a photometer SQ 118 Merck (Germany). pH and conductivity were determined on a laboratory multi-parameter analyser (Consort C863, Consort, Belgium).

3. RESULTS AND SIGNIFICANCES

3.1. Active species formation in E-PAC preparation

The principle of E-PAC preparation by the electrolysis process was illustrated in recent studies [3], [7]. When the electrolysis is carried out with direct current in the reactor, Al^{3+} and OH^- are generated at the anode and cathode, respectively.

Reactions taking place at the electrode surface are:

$$\text{Anode: } Al \rightarrow Al^{3+} + 3e^- \quad (1)$$

$$\text{Cathode: } 3\,H_2O + 3e^- \rightarrow 3/2\,H_2\uparrow + 3OH^- \quad (2)$$

The reaction then taking place in the bulk of the electrolit, is :

$$Al + H_2O + AlCl_3 \rightarrow Al_m(OH)_nCl_{(3m-n)} + H_2\uparrow \quad (3)$$

In eq. (3), $Al_m(OH)_nCl_{(3m-n)}$ represents the intermediate product of Al species which continues to hydrolyze to $Al(OH)_3$. If the generation and reaction of ionized OH^- and Al^{3+} are regulated at a proper rate, it is possible to control the ensuring processes of hydrolysis, polymerization, gelation and precipitation of aluminum species, in order to obtain PAC containing as much Al_{13} as possible.

$$Al^{3+} \rightarrow \text{monomeric} \rightarrow Al_{13}\text{ polymer} \rightarrow \text{colloid or precipitated Al} \rightarrow Al(OH)_3\downarrow \quad (4)$$

It is assumed by several authors that the process of Al_{13} formation requires the presence of $Al(OH)_4^-$ as a precursor. Some researchers assumed a very rapid $Al(OH)_4^-$ production under the inhomogeneous conditions at the solid-solution interface [3], [4]. During the electrolysis, OH^- was generated at the surface of the cathode sheets that were arranged throughout the electrolysis reactor, leading to formation of $Al(OH)_4^-$ at the metal-solution interface with subsequent formation of Al_{13} polymers.

The different total Al concentrations (Al_T) in the E-$PAC_{(1-8)}$ solutions, obtained as a function of various i_A current density (A/dm^2) tested, is shown in **Table 2.** Concentrations of Al total in the electrolyte were analyzed after stopping of the electrolysis [11].

Table 2. The influence of the current density on Al_T formation (initial aqueous solution $AlCl_3$ 0.5 M; distance between the electrodes: 10mm; quantity of electricity Q = 1.5 Ah)

Samples	***Current density,*** A/dm^2	***pH_f***	***Al_T,*** g/L
1. (E-PAC_7)	0.185	3.05	17.48
2. (E-PAC_5)	0.37	3.17	18.45
3. (E-PAC_1)	0.55	3.1	18.61
4. (E-PAC_3)	0.74	3.05	18.7
5. (E-PAC_4)	0.92	3.15	18.8
6. (E-PAC_2)	1.1	3.06	19.02

The maximum Al_T yield (19.02 g Al/L) in the E-PAC_2 was obtained using current density of 1.1 A dm^{-2}, stirring rate 600 rpm (parameters were selected by experiments).
Tables 3 show the working conditions and results for these working conditions: current densities of 1.1 A/dm^2 and different quantity of electricity Q (Ah).

Table 3. The influence of the quantity of electricity Q (Ah) on Al_T formation (initial aqueous solution $AlCl_3$ 0.5 M; distance between the electrodes: 10mm; current intensity I = 1.5 A)

Samples	***Q*** Ah	***pH_f***	***Al_T,*** g/L
1. (E-PAC_8)	0.5	2.98	14.73
2.	1.0	3.07	15.23
3. (E-PAC_6)	2.0	3.11	17.79

Although at higher current densities the process had been more intensive, the cell voltage was high enough to determine disadvantageous specific energy consumption. In addition to the electrode processes, reactions in the bulk of solution influenced the processes that occurred at the adsorption surface of the electrochemically-generated coagulant.
From these series of solutions obtained in our laboratory we selected for testing their effectiveness as coagulants, the E-$PAC_{(1-8)}$ solutions.

3.2. Efficiency of the coagulants

It was determinated the ability of the coagulants to reduce turbidity and remove the natural organic matter (NOM) from the raw water of Bega River. The investigation has been oriented toward the study of the effects of preparing conditions on quality of E-PAC solutions obtained in laboratory, conventionnaly named electrochemical - PAC (E-PAC), and with the traditionally applied coagulant aluminum sulphate (”alum”) and sodium aluminate, used today in Bega River water treatment process.

The raw water samples were treated with these coagulants, using the so-called „Jar test" procedure, according to the water treatments standards [9].

In the selected procedures applied, comparable with the current plant conditions at the Timisoara Waterworks, six water samples were always treated and controlled simultaneously in the apparatus. The dose range of the applied coagulant was the same to that used in alum of Waterworks, for all coagulants compared [6], [8].

The controlled water quality parameters, for the raw and the treated water samples, were: turbidity which conceive suspended solids content (the data are expressed in nephelometric turbidity units, i.e.in NTU); UV-absorbency measured at λ=254 nm (expressed as absorbency m^{-1}) to characterize the concentration changes of organic compounds; dissolved organic carbon (DOC) to emphasize the removal of (NOM), expressed as mgC/L; the total aluminum (Al_T) and dissolved (Al_{diz}) concentrations. The measurements were accomplished before and after sample filtration through 0.45 membrane. Temperature, pH and specific conductivity data of water samples were also checked during the experiments.

Water quality parameters of raw water and treated water after coagulation/flocculation process and 30-min sedimentation are presented in **Table 4** (representative data, selected from a set of experiments).

For turbidity removal, polymer bridging plays an important role, which is facilitated by high molecular weight polymers with relatively low charge density. For NOM removal, charge neutralization plays a dominant role.

Table 4. Water quality parameters of raw water and treated water with alum and sodium aluminate, respectively E-PAC$_{(1-8)}$ solutions

Parameter, unit	***Raw water***	***Alum and sodium alumi-nate***	***E-PAC 1***	***E-PAC 2***	***E-PAC 3***	***E-PAC 4***	***E-PAC 5***	***E-PAC 6***	***E-PAC 7***	***E-PAC 8***
Turbidity, NTU	24.5	4.17	1.95	2.23	2.81	2.13	2.40	3.29	3.19	3.33
Temperature, °C	3.5	4	4	4	4	4	4	4	4	4
pH	7.56	7.30	7.11	7.06	7.15	7.08	7.09	7.03	7.07	7.04
DOC, mg C/L	4.66	3.053	2.66	2.76	2.91	2.88	2.77	2.67	2.80	2.95
Conductivity, µS/cm	319	309	316	315	313	321	316	323	322	328
Al_T, mg/L	0	0.29	0.18	0.21	0.31	0.21	0.20	0.23	0.21	0.18
$Al_{diz.}$ mg/L	0	0.06	0.01	0.04	0.08	0.03	0.03	0.05	0.04	0.02
UV-254, m^{-1}	0.317	0.071	0.046	0.041	0.053	0.046	0.042	0.042	0.045	0.051

Generally, aqueous NOM is negatively charged and the coagulant demand for neutralizing the negative charge is much higher than that for neutralizing the charge of mineral particles. Therefore, E-PAC proved to be the most efficient coagulant in terms of NOM removal (DOC, UV absorbency) and turbidity removal.

The distribution of residual Al in water and the sediment after coagulation with this applied coagulants showed that the higher residual dissolved Al is obtained when using alum and sodium aluminate, fact expected by us. Better results were obtained with E-PAC$_1$ solution prepared.

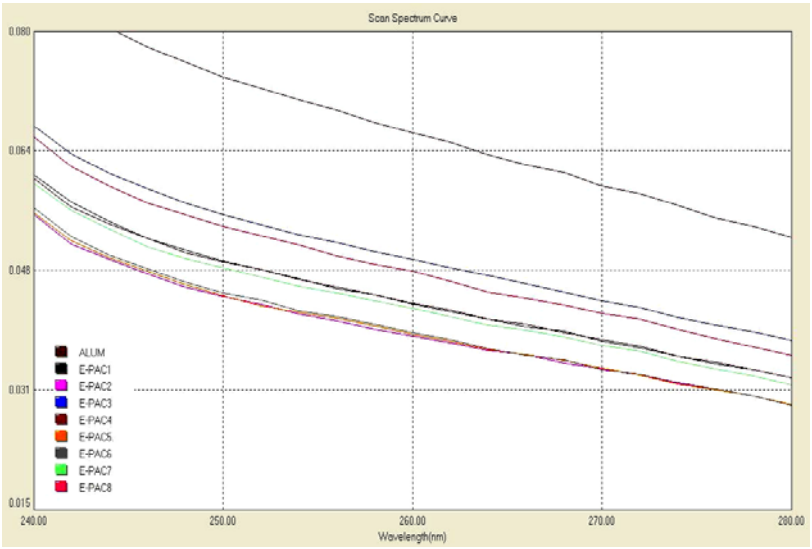

Fig. 2. UV absorbency spectrum curve

Scan Spectrum Curve for domaine 240-280 nm wavelength have been rendered with UV absorbency in **Fig. 2**.

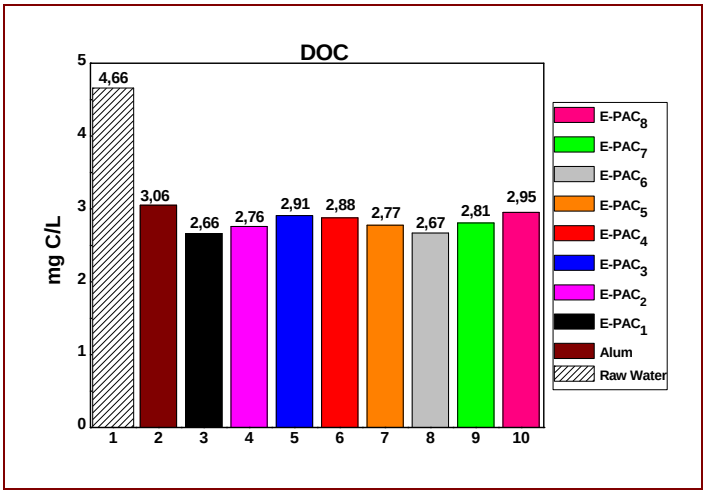

Fig. 3. DOC removal of raw water (1) and treated water with aluminium sulphate and sodium aluminate (2), respectively E-PAC$_{(1-8)}$ solutions

In **Fig. 3** is presented DOC removal of raw water and treated water with aluminium sulphate and sodium aluminate, respectively E-PAC$_{(1-8)}$ solutions.

Summarizing the obtained data, it can be concluded that the best values (lower residual concentrations) were achieved while using E-PAC$_1$, produced by an electrochemical synthesis method.

4. CONCLUSIONS

A comparative investigation of water treatment efficiencies by using E-PAC coagulants, generated in our laboratory, and the traditionally applied coagulant, aluminum sulphate (”alum”) and sodium aluminate, as a classical reference, was carried out.

A new method for the preparation of E-PAC in an electrochemical reactor, equipped with plain-plate Al anodes and stainless steel cathodes, and $AlCl_3$ aqueous solution as electrolyte was successfully applied. Although the process was complex; it was easily controlled and preparation conditions needs to be studied in detail.

Optimum data regarding residual turbidity, UV-254 absorbance and concentration of organics compounds were obtained when E-PAC$_1$ has been utilized as coagulant.

It can be estimated that the electrochemical production of polyaluminium chloride might be developed at a larger scale and the product will be applied in the drinking water plants.

5. REFERENCES

[1] J.Q. Jiang, N.J.D. Graham, “ Pre-polymerised inorganic coagulants for treating water and waste water,” Chem&Ind., no. 10, 1997, pp.389-395.

[2] J. Gregory, J. Duan, “ Hydrolyzing metal salts as coagulants,” Pure Appl. Chem., vol. 73, no. 12, 2001, pp.2017-2026.

[3] J. Qu, H. Liu, " Optimum conditions for Al_{13} polymer formation in PACl preparation by electrolysis process," Chemosphere, vol. 55, 2004, pp.51-56.
[4] W. Stumm, J.J. Morgan, Aquatic Chemistry - Chemical Equilibria and Rates in Natural Waters. New York: Wiley Interscience, 1996, pp. 823-832.
[5] K. Bodor, A. Păcală, I. Vlaicu, D. Marsavina, A. Anghelina, "Pilot Plant Treatment of Water for Drinking Purpose by PAC," Environ. Eng. and Manag. Journal, vol. 5, no.6, Sept./Oct. 2007, pp.401-403.
[6] I. Vlaicu, A. Păcală, C. Bogatu, " Prehydrolysed coagulants - a laboratory study concerning their using in water treatment from Bega River," In Proceedings of the International Symposium " The environment and industry", 25-27 October 2007, Bucharest, Romania, pp. 119-120.
[7] I. Vlaicu, A. Păcală, C. Bogatu, " Prehydrolysed coagulants - a laboratory study concerning their using in water treatment from Bega River," In Proceedings of the International Symposium " The environment and industry", 25-27 October 2007, Bucharest, Romania, pp. 119-120.
[8] K. Bodor, A. Păcală, R. Borogu, I. Vlaicu, " The use of PAC for treating water from the Bega river for drinking purpose," Proceedings of the 13th Symposium on Analytical and Environmental problems, Sept. 2006, Szeged, Hungary, pp. 186-190.
[9] N. Lindqvist, S. Korhonen, J. Jokela , T. Tuhkanen, "Comparison of Iron and Aluminium Based Coagulants and Polymeric Flocculant Aids to Enchance NOM Removal," Chemical Water and Wastewater Treatment, vol. VII, 2002, pp.133-142.
[10] K. Barkacs, I. Bohuss, A. Bukovszky, I. Varga, G. Zaray, " Comparison of polyelectrolytes applied in drinking water treatment," Microchemical Journal, vol. 67, 2000, pp.271-277.
[11] SR EN 1302:2000- Chemicals used for treatment of water intended for human consumption- Aluminium-based-coagulants-Analytical methods.

Ovidius University Annals Series: Civil Engineering Volume 1, Issue 12, June 2010

Gabion structures for the protection of banks and slopes

Stancu Popescu, Florin Mărăcineanu, Elena Constantin

***Abstract* – The work deals with the issue of checking the resistance of gabions walls to forces exerted upon them; walls with leveled internal and external side are considered, and the methodology of checking to overturning, slipping and pressure on foundation is presented. In order to see whether the assembly behaves as a monolith, the strain status is verified in all the areas where changes of section are noticed. If there are no tensions in any section, the assembly is considered to behave as a unit and the verification regarding slipping on the foundation base is made, determining the safety coefficient. The stabilizing forces, opposing the slide of the support wall, are the friction, the cohesion, the passive pressure and the anchoring forces.**

***Keywords* – active pressure, gabions, overturning moment, resistance moment, support wall.**

1. GENERALITIES. ADVANTAGES

Individual gabions boxes or mattresses used in hydrotechnical arrangements as construction blocks. They are used for building dams, river banks protection, infrastructure of bridges or railroad or highway embankments, corrections and diversions of water courses, either for industrial or agricultural puposes. They have a wide application especially in water courses where rocks and gravel can be extracted from the bed. Placing gabions side by side or one upon another elastic works can be made; being firmly attached to the bottom and having a considerable mass, they provide a great resistance to water fury. Gabion protected banks have the advantage of a high permeability which removes the subpressure effect of water seepage, harmful for concrete structures; this high permeability acts as as a selfdrainage reducing the hydraulical load of groundwater[1]. The gaps between the stones filling the gabions dissipate the flow energy and wave action, the entire structure is aired and requires no additional drainage works. During the exploatation, gabions incur practically no maintenance expenses . Water penetration into the gaps between the gabions determines a decrease of the kinetic energy. This work should be subject to reliability checks to the forces acting upon them; these checks cannot be done in the design phase.

S. Popescu is with University of Agronomy Sciences and Veterinary Medicine Bucharest, Faculty of Land Improvement and Environment Management, Marasti Bdlv., nr.59, 011464-Bucharest, Romania (phone: 0040723198299; e-mail: stancu_popescu@hotmail.com).

F. Maracineanu is with University of Agronomy Sciences and Veterinary Medicine Bucharest, Faculty of Land Improvement and Environment Management, Marasti Bdlv., nr.59, 011464-Bucharest, Romania (phone: 0040735868716; e-mail: florin_maracineanu@yahoo.com).

E. Constantin is with University of Agronomy Sciences and Veterinary Medicine Bucharest, Faculty of Land Improvement and Environment Management, Marasti Bdlv., nr.59, 011464-Bucharest, Romania (phone: 0040745751328).

ISSN-1584-5990

Therefore, based on the international literature available, we adapted a design methodology conferring the gabion structures the necessary reliability.

2. FORCES ACTING ON BANKS CONSOLIDATION

Gabion retaining walls are elastic structures behaving differently than conventional concrete or bricks retaining walls that give a monolith charater to the assembly

They are interpreted as gravity walls, as they use their own weight to resist lateral earth pressure.

The own weight of the gabion depends mainly on two factors:

- Volumic weight of the material from which the filling stone comes;
- The material layout inside the gabion, leading to a higher or lower use of space

The earth push (active pressure) may be calculated as follows:[2]

$$P_a = K_a \times D_a \times \frac{H^2}{2} \quad \text{or} \tag{1}$$

$$p_a = \frac{1}{2} D_a \times H^2 \times tg^2(45^0 - \frac{\varphi}{2}) \tag{2}$$

Ka - active pressure coefficient
Da - apparent density of the earth
H - height of the retaining wall
φ - earth internal friction angle

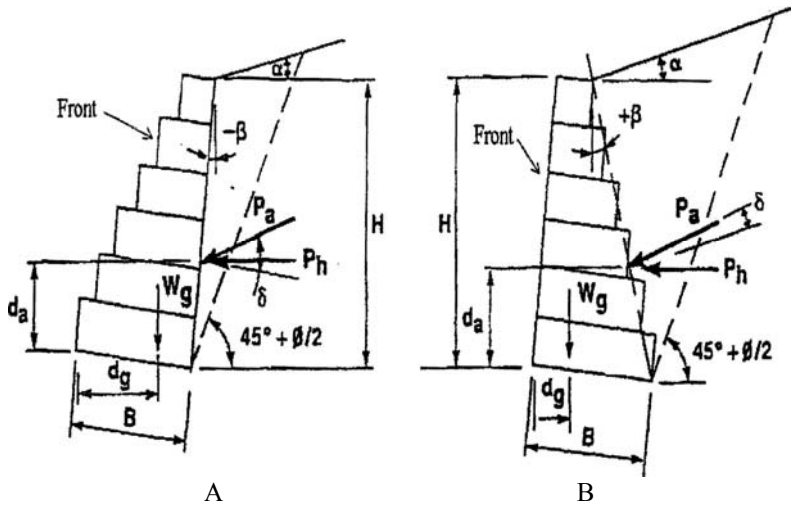

A B

Fig.1. Designing gabion walls[2]. A. stepped outer side. B. stepped inner side

Designing gabion walls with outwards or inwards steps follows the same principles, starting with choosing the sizes of verification.

The following steps are to be made:

- finding the forces acting on the wall;
- checking that the resistance moment exceeds the overturning moment;

- checking that the sliding resistance exceeds the horizontal active force
- checking that the resultant vertical force is in the middle third of the wall and the maximum pressure is within allowed limits

Forces acting on the wall

The main forces acting on the wall are the vertical force produced by the gabions weight and lateral pressure (push) of the earth.

Wall weight per length unit (Gg) is calculated multiplying the gabion cross with the density of the stone filled gabion. The value of 1600 kg/m3 Gg may be used for common materials.

Lateral earth pressure is determined by the equation of Columbus, based on the balance of the earth mass, considered rigid, but facing friction force and its own weight.

According to this equation, the total active force for a triangular distribution of pressure acting on the wall will be:

$$P_a = K_a \times D_a \times \frac{H^2}{2} \tag{3}$$

Ka = active pressure coefficient
Da = apparent density of the earth (often 1.9 t/m3)
H = wall height

If uniformly distributed overload (q) occurs on the surface filling, the issue may be dealt as an equivalent layer of soil which produces a uniform pressure over the entire height of the wall, so the equation (3) becomes:

$$P_a = K_a \times (D_a \times \frac{H^2}{2} + qH) \tag{4}$$

The active pressure coefficient is given by:

$$K_a = \frac{\cos^2(\varphi - \beta)}{\cos^2\beta \times \cos(\delta + \beta)[1 + \sqrt{\frac{\sin(\varphi - \beta)\sin(\varphi - \alpha)}{\cos(\varphi + \beta)\cos(\eta - \beta)}}]} \tag{5}$$

α = surface slope
β = sharp angle of the tilted surface of the filling with the vertical
φ = internal friction angle of the earth
δ = coefficient of friction between wall and earth

Since the wall friction force is small, δ is currently regarded as having zero value.
The horizontal component of the active pressure is Ph

$$Ph = Pa \times \cos\beta \tag{6}$$

The vertical component of the active pressure is usually neglected, as it reduces the turnover moment and increases sliding resistance.

3. METHODOLOGIES FOR CHECKING THE STABILITY OF GABION WALLS

MECHANISMS OF STRUCTURE FAILURE IN THE GABION RETAINING WALLS

In case of massive structures for water retention (dams) or for taking over the earth push (retaining walls) the failure mechanisms are considered: overturning towards downgradient toe, sliding on the foundation plate, pressure on foundation.

OVERTURNING CHECKING

Pressure force of the earth tends to overturn the wall that must remain in balance with the force of resistance due mainly to the wall weight.

Based on the principles of statics, moments are considered in the area of the downgradient toe of that wall. Verification has the expression:

$$M_r = SF_0 M_0 \tag{7}$$

M_r = resistance moment
M_0 = overturning moment
SF_0 = factor of safety to overturning

Neglecting the wall friction, the active force normally acts on the tilted surface of the filling at a H / 3 distance from the basis. If overpressure occurs, the total active force will act at a distance:

$$d_a = \frac{H(H \times 3 \times \frac{q}{D_a})}{3(H \times 2 \times \frac{q}{D_a})} + B\sin\beta \tag{8}$$

The overturning moment will be:

$M_0 = d_a$ x PH (9)

The weight of the gabion wall acts vertically through the center of gravity of its cross section, located at a distance d_g .

The resistance moment is the sum of the products of vertical forces (W) per unit length and distance (d)

$$M_r = \sum dW \tag{10}$$

For simple weight walls, the resistance moment is got multiplying the weight wall and the distance:

$$M_r = G_p \times d_p \tag{11}$$

SLIDE CHECKING

Active pressure earth tends to cause horizontal sliding of the wall to which the resistence of the wall base must be opposed and it is expressed by:

$$\mu G_t \geq SF_s \times P_h \tag{12}$$

μ - friction slide coefficient (tangent of the angle of friction of the earth)

G_t - sum of vertical forces, in this case Gg

SF_s – sliding safety factor

PRESSURE CHECKING ON FOUNDATION

In this case you should check firstly if the vertical force occurs within the middle third base. If B is the base width, the eccentricity of the vertical force on the half width is:

$$e = \frac{B}{2} - (M_r - M_0) \times G_t \tag{13}$$

At 1 / 3 of half power base occurs:

$$-\frac{B}{6} \le e \le \frac{B}{6} \tag{14}$$

Maximum pressure basis will be:

$$p = \frac{G_t}{B(1 + \frac{6e}{B})} \tag{15}$$

This pressure must not exceed the allowable pressure soil P_b:

$$p \le P_b \tag{16}$$

Safety factor is included in P_b.

SUMMARY ON CHECKING CALCULATIONS OF THE GABION RETAINING WALLS

Overturning towards downstream leg can be determined by the formula:

$$C \ge \frac{M_r}{M_0} \tag{17}$$

M_r – time setting (resistance)
M_0 – overturning moment

Sliding the sole foundation is determined with the formula:

$$C \ge \frac{\mu G_t}{P_h} \tag{18}$$

μ - friction coefficient between solid and foundation soil (0.25 to 0.35);

G_t – sum of vertical forces, in this case, the weight of gabion wall;

P_h – horizontal component of active pressure

• Checking the status of efforts the relationship of critical sections is determined with the formula:

$$\sigma_{am},\sigma_{av} = \frac{G_t}{\Omega} \pm \frac{\sum M}{W} \tag{19}$$

$\sigma_{am};\sigma_{av}$ [3] - value of the pushing pressure in the critical sections

Ω - active section

$\sum M$ - sum of moments in relation to the axis section

W – resistance modulus

$$W = \frac{1}{6} bh^2 \tag{20}$$

b,h [cm] – size of the gabion's base

4. CONCLUSIONS

From calculations and field experience results that the structures generally don't resist while sliding the base foundation, but the examination has to be done regarding all actions. To see if the ensemble can be considered to be acting as a monolith, there is supposed to be done the examination of the status of efforts in all areas where changes of the riverbed section are observed.If there are no tensions in one of the sections, the emsemble is considered to be acting as a whole and the next step is to proceed to the examination of the sliding on the foundation base, so that there can be obtained the safety factor.Stability of the supporting walls inside the gabions is about to be verified using structural calculations in order to determine the stability of hydraulic construction. The friction forces, cohesion forces at the sliding surface, passive pressure at the wall base and the anchoring forces from the upper wall are stabilizing forces opposing to the sliding and this fact is a specific character of the gabion walls.[4] The methodology presented in the paper provides a greater reliability for those constructions based on it.

5. REFERENCES

[1] Raffaele A & col.Ouvrages flexibles pour les trincons torrentiels et fluviaux,Premiere partie S.P.A Officine Maccaferri Bologna 1983

[2] Nistreanu Mircea Contributii la modernizarea tehnologiilor de executie si exploatare durabila a lucrarilor de amenajare a cursurilor de apa din vestul tarii .Teza de doctorat USAMV Bucuresti 2002

[3] Banut V Ivan M. Vulpe A. Statica stabilitatea si dinamica constructiilor Ed. Didactica si Pedagogica Bucuresti 1982

[4] Maracineanu Florin & col Modern Tehnology in Share Consolidation by Using Gabions.Buletinul Institutului Politehnic Iasi, vol. XLXII (I) 2001

Aspects related to hydrological phenomen a incurred at metro tunnels construction and operation

Ioan Sebeşan, Ionel Voinescu

Abstract **– The paper describes problems of hydrological nature encountered during tunnels and subway stations construction and during their exploitation / operation. The authors will present sealing and waterproofing systems for this type of constructions.**

Keywords **– hydrological problems, subway stations, tunnels, waterproofing systems**

1. HYDROLOGICAL ASPECTS INCURRED DURING THE TUNNELS AND METRO STATIONS CONSTRUCTION

In the early ‘70s, the state management decided to set up a multidisciplinary committee assigned to study the opportunity of building an underground metro network in Bucharest, the capital of Romania, which today, such study we may call (pre)feasibility study. Therefore, in February 1972 the committee started its activity and at the end of 1973 the study had been completed and conclusions submitted.

For this reason, in November 1974 it started the first metro line design execution about to link two major equipment factories, Semănătoarea and Timpuri Noi, on a parallel route with Dâmbovița River.

Hence, in September 1975, the construction works of the first metro line along the hereinabove mentioned route had started. There were taken into consideration the soil conditions in Bucharest since the underground waters were located only at 2-3m depth and on the route about to be built this first metro line there were no buildings. The technical method chosen for the construction of the tunnels and metro stations was “cut & cover”.

This type of underground construction with rectangular section, walls, foundation and floor lines are called gallery, method agreed both by the Bucharest metro designer, contractor and operator, and also recognized by designing documents and legislation.

Later on, as the metro network expanded in other districts, but at the ground level there were buildings that couldn’t be totally demolished, it had been used another method for the tunnels construction called „tunnel boring” at 15 m depth compared the ground level.

The underground constructions resulted using this method were called tunnel, whose section is totally a circular/oval, concept found both in the designing, construction and operating activities of the Bucharest metro network, and in the underground constructions technical literature.

I. Sebesan is with “Politehnica” University of Bucharest, Bucharest, Romania (e-mail: ioan_sebesan@yahoo.com).

I. Voinescu is with Administration of Public Domain, sector 1, Bucharest, Romania (e-mail: iovo2003@yahoo.com).

ISSN-1584-5990

The first metro line was opened on 16 November 1979, between Semănătoarea and Timpuri Noi having 8,63 km length and 6 stations. The execution of these metro stations was performed using the "moulded walls enclosure with lid" method, based upon the idea of using the station floor roof and the moulded walls as a supporting element during the construction.

Shortly after the works related to the second extension Timpuri Noi - Republica had started, the construction rhythm increased at about 4 km of tunnel/year, because it has been used the tunnel boring machine instead of „cut & cover". The designing and construction of this boring machine was a national premiere, both as design and construction. The design was issued by I.P.C.F. (Rails Designing Institute) and the supposed construction was performed by Uzinele "23 August" in Bucharest, presently named S.C. "FAUR" S.A.

On short, the other metro lines' construction was performed in stages, as following:

- in December 1984 it was opened Semănătoarea - Crângaşi (towards Gara de Nord) inter-station, in total length of around 1 km, to the Republica – Semănătoarea extension was being added one more station (Crângaşi);
- in January 1986 it was opened Piața Unirii 2 - I.M.G.B. Depot extension of around 10 km in length, 8 stations and a depot, I.M.G.B Depot.;
- in October 1987 it was opened Piața Unirii 2 – Pipera extension, of around 8,7 km length and 5 stations; later on the 6th station was added, Piața Romană, built by metro gallery drilling with an external extension;
- in December 1987 the route from Republica to Crângaşi was extended up to Gara de Nord, with 2, 8 km and a new station Gara de Nord (1); besides the usual double track for the trains operation, there were also executed 4 parking lines. Although Basarab station was designed to be part of this route, this one had been later completed;
- in August 1989 it was opened Gara de Nord 1 - Dristor 2 extension of 7,8 km length and 6 stations;
- in January 1990 it was opened Republica – Pantelimon inter-station, of 1,5 km length, 1 station and 2 depot, Pantelimon Depot;
- in March 2000 it was opened Gara de Nord 2 - 1 Mai extension, of 3,6 km length and 4 stations;
- in November 2008 it was opened Nicolae Grigorescu - Linia de Centură extension, derived from Dristor 2 - Republica (Pantelimon), of 4,75 km length and 4 stations.

The construction of the hereinabove was not very easy, the contractors were confronting in time with several issues, such as the soil composition, especially those hydrological related: water leaks from the drinking water and sewage pipes, sewage discharged pipes, natural springs, some excessive ground waters etc.

For all of these, after serious analysis, there were approved and adapted technical solutions which were finally successful: redirecting water losses from the city's water and sewage pipes, creating metal or concrete dams and water pumping to the ground using high capacity equipments, usage of special concrete with fast solidifying degree etc.

Such major issue and not simple at all was confronting the contractors, in February 1985, at Dâmbovița River under crossing, when they dug the tunnel from Tineretului area to Piața Unirii, located on the present Metro Line 2. They had to capture the entire flow of this river, upstream the related diggings, via three giant pipes of around 1,6 m diameter and to discharge this water downstream the works using high capacity pumps. Let's not forget to mention that it was winter season and the temperature reached sometimes -23º C, the ground water being frozen and created major problems to those trying to pump it. The

solution chosen and carefully analyzed by the engineers was a successful one for that time being recorded as a premiere in Romania and the second in Europe.

One of the great issues of this type encountered nearby Titan park, where today is located the Centru Titan metro station. This place contained huge water springs and the existing pumps at that time couldn't face the related flows. The digging of deep and thick storage wells failed to be a solution. After several attempts, it was chosen the soil and water freezing solution (clay, sand) by introducing deep drilling bores into the soil. They were connected to high capacity cold producer equipment, the solution being successful.

2. HYDROLOGICAL ISSUES INCURRED WITHIN THIS PERIOD OF TIME

The seepages were generally incurred during the entire period of metro operation, for 30 years, respectively. These current problems varied and varies depending the wet or dry seasons of the year, the hydrological level at a certain moment of objects partially or totally immersed, or depending the existence and water losses discharge from the city drinking water and sewage distribution pipes, either further any failures, or heavy rains, when these water pipes cannot take over the flows and are discharged in favourable free areas.

The most dangerous seepages which could appear inside the constructions (tunnels, galleries, metro stations) from the source point of view are the following:

- the ones appearing from the underground water which involve major quantities of solid material (sand, clay) from the external side of the tunnel to be inserted into the tunnel inner side; if not discharged, they can facilitate in time the occurrence of some holes outside, the "cooperation" between the structure (concrete) - ground (soil) can be weakened, that can lead, for instance, to the appearance of distortions in the tunnel circular section, with major implications both from the self construction strength point of view, but especially of its operation when the metro trains will run by the affected zone.
- the high flow seepages caused by massive losses from the city heating network, and/or cold and hot water pipes and water sewage systems, either further certain damages incurred at these equipments, or several heavy rains exceeding the transport/collecting capacity of this system pipes. Additional to the possible damages that may appear, as mentioned before, these seepages can create both damages to the electrical installation and equipments in the tunnel and stations, and discomfort for the passengers using the metro transportation and the metro staff.
- the high and non controlled flows seepages caused by major earthquakes/explosions, by the modification (displacement) of the reinforced concrete structures positions or even to minor or major destruction of them.

From the quantitative point of view, the seepages in the metro network are the following:

a) damping;
b) drops;
c) trickles;
d) with measurable flow;
e) input of suspended soils (sand, clay etc.).

In order to keep under control these seepages and to avoid or limit, if any case, their consequences, within the operation activity of the metro network, it is necessary to be included programs of continuous and special surveillance and also intervention programs to cope with the hydrological issues that may appear.

Therefore, within the frame of the current surveillance program there will be taken into consideration, the following aspects:

- visual examination of the non immersed parts of the constructions, installation and equipments, located under the underground water level;

- visual examination of the immersed parts of the constructions, installation and equipments, located under the underground water level;

- visual examination using simple means of hydrological regime modification and of the investigated ground area morphological modifications.

The special surveillance program is applied to the constructions and areas with hydrological high risk. More accurate, within this program, a special surveillance will be granted to the following aspects:

- the level of underground water located on the backside of the structure;
- the underground water temperature;
- underground water chemical degree of aggression;
- water pressure acting upon the resistance walls of the underground structures in the metro network;
- seepages incurred within the construction;
- the humidity and air temperature within the underground metro constructions influenced by the existing seepages in that area;
- the condition, bed soil damaging and underground construction structure from the hydrological point of view.

3. SEALING AND WATERPROOFING METHODS USED FOR METRO UNDERGROUND CONSTRUCTIONS

The sealing system is a major component of an underground construction designed to provide a proper indoor area for a normal operation activity, both from the safety conditions point of view, the construction integrity, and passengers' comfort and normal working conditions for the metro staff.

The construction waterproofing is mainly obtained when waterproof materials are used (concrete with waterproofing degree P>8), but also by elastic sealing in the concrete structure joints.

The sealing is a relative concept because it cannot be totally complied; therefore are accepted certain values of the infiltrated flows. The underground constructions of the metro are considered properly protected against water intrusion (waterproofed) when admitting minor infiltrations not produced in a single point that lead to a total infiltrated flow smaller than the admissible flow for each type of underground construction:

- for the metro stations and galleries max. 1,0 l/s·km;
- for the metro tunnels max. 2,0 l/s·km.

The special sealing measures applied to the underground constructions against water infiltrations suppose two modalities of performing the sealing screen:

a) Sealing on the structure external side - by injecting in the surrounding area different suspensions (clay-concrete, clay, concrete-silicate etc.), mixed solutions of sodium silicate with or without reagents (organic or non organic) or synthetic resins (polyurethane);

b) Sealing in the structural element depth - by injecting in the concrete's depth, in fissures, cracks or joints chemical substances providing a reaction in contact with water and turn into a sealing screen (mainly polyurethane resins).

The special sealing measures are applied further their tracking on the construction zone considered as belonging to certain water infiltrations exceeding the above mentioned admissible flows.

The injections with clay-concrete suspensions at the external side of structure are generally applied to the metro tunnels (circular section).

The injections with chemicals (mainly raisins) in the concrete structure are applied for all underground construction types of reinforced concrete: metro stations, depots, galleries (rectangular section), tunnels, shunt backs, ventilation equipment and pumping installation located on the zone between two metro stations (inter stations).

3.1 Metro tunnels sealing

For the proper execution of the metro tunnels underground construction, in the related designs were provided sealing constructive measures of such underground construction type, as follows:

- Tunnel ring arch bricks are equipped right from the mounting with neoprene foam gaskets (12 x 50 mm) and with strips of fibreglass cloth impregnated with bitumen;
- Arch bricks joints, at the internal side are closed with putty thyocol protected with mortar of expansive concrete or with rapid sealing special mortars.
- Final treatment is intended to obtain a durable structure, with low sealing degree for underground water infiltrating inside the tunnel.

By applying such measures on arch bricks it is readjusted the concrete in the exfoliated areas, with rags, dangerously cracked or there are closed the in order to protect the trimming against corrosion. The cracks closure by sealing also allows the structural element waterproofing. Injecting joints and bolt holes suspect of water infiltrations and plugging injections holes lead to infiltration decreasing in the arch bricks ring under the above mentioned admissible values.

The holes plugging with injections are made with mortar of expansive mortar or rapid waterproofing mortar without breaking the bed previously obtained by filling injection. If any water infiltrations appear in the injection hole, there can be used injections with chemicals based on polyurethane resins or similar, after the hole's closing using the above modality.

The results of the final treatment works are the following:

certain subsequent reinforced concrete structure corrosion phenomena is stopped;

the infiltrated water is redirected so that not to affect the third rail ort he metro train;

the infiltrated flow is limited so that it could be collected and channelled towards the pumping stations in order to be evacuated.

The fluids currently used for the underground constructions injecting are needed to:

- seal by injection the external side of tunnel: stable suspensions based upon cement-clay (CC) and bentonite cement (BC);
- seal in structural elements depth: chemicals based upon polyurethane resins or similar.

The injection works are included in the set of constructive measures carried out in order to decrease the infiltrations in the tunnel main and to provide:

- durability of the structure made of precast reinforced concrete arch bricks;
- normal operation of the tunnel and the related endowments.

In order these fluids to meet their efficiency in the injected zones, accurate recipes are set for the stable CC and BC suspensions. These must indicate the main components quantities, added substances and the report water-solid, as well as the variations quantitative limits.

The fluids (substances) designated to stop the infiltrations have to meet the following conditions:

- to be stable (not to separate or deposit one of the water components);
- to be homogenous;
- to be resistant to water movement immediately after injection;
- to be fluid enough to be injected;
- not to be degraded by the action of water aquifers.

Given the variations of the hydrostatic level which mostly depends on the wet or dry seasons of the year, the sealing material behind the tunnel may perform or not the assignment for which was injected (sealing on the external side of arch bricks ring). It is possible after a long dryness period to occur major infiltrations on extended areas, when the hydrostatic level is restored, and for this reason, the initial sealing is being applied again by injections with clay-cement.

3.2 Sealing of the metro galleries and stations

Starting with the designing stage, during the metro galleries and stations construction, it was provided to be mainly performed by using high waterproof reinforced concrete P4, P8 or even P12 to the elements entering in contact with the underground water. These constructions are also protected by bituminous waterproofing sheets located on the upper ceiling. The compression and casting joints between the structural elements are provided with elastic sealing elements (gaskets at the prefabricated elements, sealing strips and sheets in the monolith reinforced concrete elements).

The existing joints and cracks suspect of infiltrations from the underground water are treated by chemicals injections (usually, polyurethane resins or similar).

Hence, because:

- the upper ceilings of the accesses and metro stations or underground depots are located close to the ground surface being exposed to the weight and vibrations of the ground transport (trams, cars and high tonnages equipments etc.),
- the rain waters, sewages and accidental leaks from the urban water distribution and heat system seep into the filling sheets over the stations upper ceiling,
- the waterproofing materials (bitumen sheet over the station, lamination sheets or rubber strips at the construction joints) lost a great part of their properties during the construction, both because they became obsolete and the related weakening further usual mechanical actions (earthquakes, vibrations etc.),
- the external shafts of deep wells, ventilation system, electric cables, and discharge waters installation are not properly waterproofed or the existing piping corroded so that the rain waters could easily infiltrate inside the stations,
- the works performed at the moment of construction stage for the metro network hadn't always been of the best quality (cracks, concrete segregations), therefore there were encountered infiltration issues starting with the metro commissioning, no matter their status was,
- the existing sealing materials at the construction stage (except tunnels for which the used methods proved to be efficient), couldn't provide a very good sealing,
- a part of the waters collecting and discharging system in the stations and inter-stations (pipes embedded in the structure, hidden weepers, chutes performed behind the walls etc.) is obsolete and hard to reach or inaccessible in some areas,
- the leaks in the areas destined to commercial activities in the metro are not always directed until pumping stations, but they discharge somehow uncontrolled into the weepers, whose unsilting is very difficult,

- the infiltrations cannot be fully eliminated, but they can be maintained within the admissible levels set by the design engineers.

The current joints and cracks suspect of underground waters infiltrations are treated by chemicals injections (usually, polyurethane resins or similar).

The filling of the fine cracks located above the underground waters level (not suspected of water infiltrations) is being made with cement paste, adding polyvinyl acetate or chemicals injections based upon concrete high adherent epoxy resins.

Based upon an accurate infiltrations survey, there can be also performed sealing on the structure visible side by applying special waterproofing plasters with rapid hardening cement mortars.

The clay-cement suspensions applied for injections must be easy to use, stable, hard to be washed by the waters behind the tunnel structure, waterproof, and after hardening to have a higher mechanical resistance compared with the one of the clay met during the tunnel boring.

Often after the injections are finished on some areas, due to the balance restoration and water increasing pressure behind the sealed structural element, it is possible to appear new infiltrations on nearby areas which were not initially suspected of infiltrations and consequently couldn't had been treated by injections. This could be explained because once the water pressure increased, it must support the superficial tension in the nearby pores or cracks and previously free of infiltrations. After a few days of survey, it may proceed to their sealing using the same injection technology until the phenomenon is stabilized and the structural element is completely sealed.

The inner underground construction structure can be sealed by applying on the inside some thin waterproof plaster (layers) of homogenous pulverous materials, fine grained, which in contact with water may form a waterproof system of concrete by a crystal barrier in the pillars system and of cracks with opening smaller than 0,25 mm, resulted from the concrete contraction and relaxing. Compared with the metal or plastic waterproof membranes which provide only a superficial barrier, the mortars applied in layers, in the presence of water, continue to crystallize with the concrete. They can be "dry" applications, for porous concretes or mixed with water, for concrete walls and ceilings.

The applicability of these waterproof products covers a wide range of objectives such as: bases (of any kind), dams, sewage systems of concrete pipes, treatment stations of waste waters, concrete tanks, tunnels, shafts, hydrological constructions etc. Such products can be used directly on the concrete bed and as final waterproofing lay, over the currently used mortars.

The main elements, components of the waterproofing products applicable in layers are: Portland cement, fine mineral aggregates with high quartz level (silica) and special chemicals which in the presence of moisture become active, penetrate the concrete and chemically react with the calcium oxide in its internal mass and finally produce non soluble crystals.

Hence, the admissible infiltrations limits were revised on timely basis, and they reduced significantly in time, as follows:

- from 5l/sec.·km to 2 l/sec.·km – for tunnels (for each simple tunnel/rolling track);

- from 2l/sec.·km to 1 l/sec.·km – for galleries and stations (for each side of the station/gallery).

Such cases are careful kept under strict control and surveillance by the specialized staff, and the waters are collected and guided via the discharging system existing at the metro. This is possible so long the infiltrated waters are not aggressive and to not contain large quantities of solid material from the outside of the construction. Such event may have

as result the weakening of the cooperation between the building and ground. If sand are brought into the tunnels and such phenomenon is not properly controlled by sealing and consolidation works, there may also appear distortions of the circular section, the construction stability, all installation and activities being put into danger.

4. CONCLUSIONS

In order to prevent such unpleasant situations with major possible prejudices, in addition to the permanent observation of the hydrological phenomena appeared inside the metro underground constructions, there are permanently performed land surveys of the metro constructions geometry.

Such situation was met at Centru Titan metro station where the underground water is very dense and aggressive. A lot of problems incurred in this area, as mentioned in chapter 1 above, the soil texture being sandy. Therefore, the soil (sand) under the tunnel foundation frame was moved in time, on a small distance, leaving practically the foundation frame in suspension. Although over this frame the metro trains were running, luckily its geometry hadn't bee modified compared with the other underground construction elements (tunnel), and hen such very dangerous nonconformity was ascertained, there were immediately taken protecting measures of the area and involved remedies.

Until now, and except this situation, there were not ascertained significant modifications of the reinforced concrete geometry metro underground constructions, the cooperation between the structural elements of the metro underground constructions and the soil being stable.

5. REFERENCES

[1] Boieru P., Asupra unor rezultate privind curgerea bifazică apă-aer în conducte. 1972, Hidrotehnica Nr.1, vol. XVIII, pag 23-29.
[2] Wylie E.B. Free air in liquid transient flow. Third International Conference on Pressure Surges. BHRA Fluid Engineering, Conterburz, England.
[3] H. Poor, An Introduction to Signal Detection and Estimation. New York: Springer-Verlag, 1985, ch. 4.
[4] B. Smith, "An approach to graphs of linear forms (Unpublished work style)," unpublished.
[5] E. H. Miller, "A note on reflector arrays (Periodical style—Accepted for publication)," IEEE Trans. Antennas Propagat., to be published.
[6] J. Wang, "Fundamentals of erbium-doped fiber amplifiers arrays (Periodical style—Submitted for publication)," IEEE J. Quantum Electron., submitted for publication.
[7] C. J. Kaufman, Rocky Mountain Research Lab., Boulder, CO, private communication, May 1995.
[8] Y. Yorozu, M. Hirano, K. Oka, and Y. Tagawa, "Electron spectroscopy studies on magneto-optical media and plastic substrate interfaces(Translation Journals style)," IEEE Transl. J. Magn.Jpn., vol. 2, Aug. 1987, pp. 740–741 [Dig. 9th Annu. Conf. Magnetics Japan, 1982, p. 301].
[9] J. Jones. (1991, May 10). Networks (2nd ed.) [Online]. Available: http://www.atm.com

OUR SPONSORS

R.A.T.C. CONSTANTA

OIL DEPOL SERVICE S.R.L.

TOP GEOCART

AKDEMIR PROD S.R.L.
S.C. CEPLINSCHI COM S.R.L.
S.C. CLEAN CONTROL I.T.C. S.R.L.
S.C. DOBROGEA GRUP S.A.
S.C. GTF PROSPECT S.R.L.
SINDICATUL LIBER AL S.C. RAJA S.A. CONSTANTA
S.C. VMB LUX CONSTRUCT S.R.L.

Sustainability, a new field of research and communication in Romania

Nicolae Postavaru

Abstract – **In Romania, for the moment, sustainability is just an academic term, which can not be found in our daily language, even if it should be.**

This leads to miscommunication between "technicians" and users on one site and between technicians and those who should advertise this term, on the other side.

But what is sustainability?

It is a new approach of the development in terms of 3 essential elements: environment – social – financial. This means that any technical solution has to meet three demands, in order to be sustainable:

- **To be friendly with the environment; for example without any unregenerative energy or water consumption, with few gas emissions or if it is possible with zero carbon emissions.**
- **To be efficient from the financial point of vie w, namely, costs for the entire life cycle of the development should be minimum, and the basic investment should not engage supplementary funds.**
- **To be close to people's payment capabilities and in the same time to resolve some social problems like: railway, sewerage systems etc.**

Keywords – **sustainability**

1. INTRODUCTION

Why Sustainable Development?

The start point was a simple observation: we have only one planet and an alarming statistic: an increasing population. Statistically speaking, population is growing and in 2050 will reach 15 billion compared with 1 billion in 1900.

2. ARGUMENTS

Another statistic is showing that some of us consume more then others:

- The richest 20%, own 86% of the worlds resources
- Half the global population lives on 2% of the land and consumes 75% of it's resources
- Most of the world will not have sufficient freshwater in 30 years.

Scientist showed us that:

Nicolae Postavaru, Dipl. Eng. M.S.Ph.D is with Technical University of Civil Engineering Bucharest / Ove Arup & Partners International Consultant, Bucharest, Romania (phone: +40-241-619040; e-mail: author@univ-ovidius.ro).

ISSN-1584-5990

Are in growing:

- Population
- CO_2 emissions
- Desertification
- Global temperature
- Sea level
- Deforestation

Are decreasing:

- Biodiversity
- Non-renewable resources
- Resources
- Natural Environment

Taking into account that we have only one planet where we can live, we have two options:

- ✓ We should change our mentality and way of living

Or

- ⛔ Our planet will disappear

What are the key external driving forces that will be important to our business and life in the next 10 years?

- *Social,*
- *Technological,*
- *Economic,*
- *Environmental,*
- *Political*

Driving forces:

- imminently serious
- potentially huge
- uncomfortably predictable
- conceptual
- irrational
- unknowns….

- water
- hydrogen economy
- demographic change
- global connectivity
- spirituality
- climate change

WATER:

- 70% of the earth
- 97% too salty to drink
- most of the rest is ice
- we contaminate it
- we throw it away
- we dissipate it
- 4.5 litres per day in Gambia; 150 lpd in the UK.
- from 17,000 cubic meters per annum [1950] to 7,300 cubic meters per annum.
- By 2020, 25 developing nations with over 250,000,000 people are expected to experience high water stress.
- it is considered to be a “full-scale emergency”.

Solutions:

- changing lifestyle
- new technological solutions for : desalinisation, purification, reutilisation

HYDROGEN:

- reduce pollution
- is an important resource for energy
- a solution for cars, planes and ships
- Hydrogen-fuelled FedEx fleet in Tokyo
- bus fleet in Iceland
- Boeing is planning a hydrogen fuelled aircraft

Solutions:

- is very dependent upon the development of technologies for efficient production of hydrogen, its storage as well as its safe transfer
- starting with 2025 majority of vehicles should run with hydrogen

Demographic changes:

- increasing population
- fertility rates are falling and are predicted to continue to fall for the next 30 – 40 years
- the global population will age faster in the next 60 years than ever before
- the number of people aged 60 will triple by 2050 and the world median age is predicted to increase from 27 today to 36 in the same amount of time
- if we believe that the earth is a closed system, then at some point, standards of living will have to change to adapt to the change

Solutions:

- Later retirement ages are already being discussed as one solution

Global connectivity:

- The global population has adapted this technology very rapidly with a multitude of new terms permeating our vocabulary
- Connection no longer means a wire.
- New hierarchies for achieving collective solutions that belies, or even goes against those in power.[LINUX – individuals vs corp] MoveOn.org:A network of on-line activists which, with more than 2 million members, builds electronic advocacy groups virtually + ‘instantly’.
- SARS was one of the first very public successes of knowledge sharing to combat a shared threat. Information was exchanged at an incredible rate. But then again, the connectivity presented the threat to begin with.
- The changes that global connectivity is bringing are as yet difficult to quantify since they are deeply profound and continue to play themselves out every day.

Spirituality:

- There is an apparent rise, especially in wealthier societies, in question of meaning and belief
- Economists are attempting to measure happiness in a data drive to assess satisfaction.
- Changing expectations are being felt in the desire for a new work-life balance.

Implications:

- Some are equating this with environmentalism that was first seen decades ago and views as the domain of the radicals and quacks.

Unknowns:

- Climate changes
- Anti-capitalism

3. CONCLUSIONS

Sustainable means to be educated so as to keep account of all aspects of personal and social life. Your way of living affects everybody: people, nature, technology etc.
Gro Harlem Brundtland, (1987) Director General of World Health Organisation said:
"Development that meets the needs of the present without compromising the ability of future generations to meet their own needs"
And Kofi Annan, (2001) Secretary General of the United Nations:
"*Our biggest challenge in this new century is to take an idea that seems abstract – sustainable development - and turn it into a reality for all the world's people****".***
We have to have an equilibrate agenda:

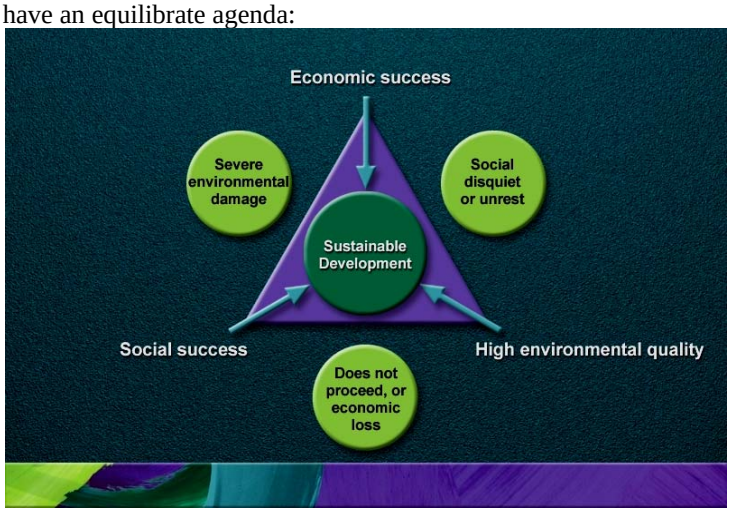

Fig. 1.

To understand complexity**:**

Fig. 2.

ARUP applies a series of sustainable projects in:
Building design:

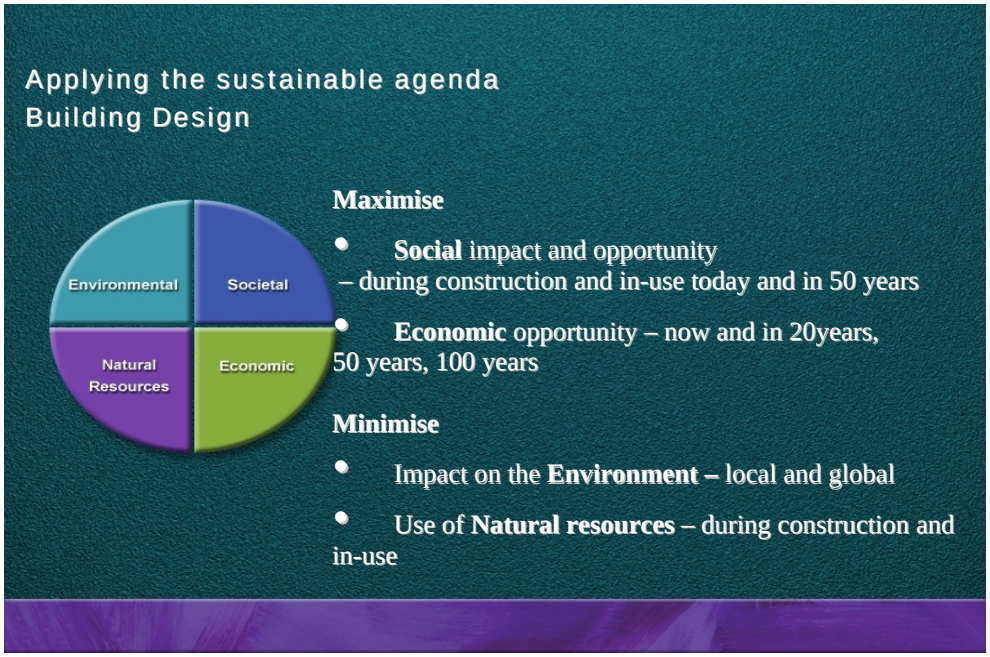

Fig. 3.

A Holistic Approach

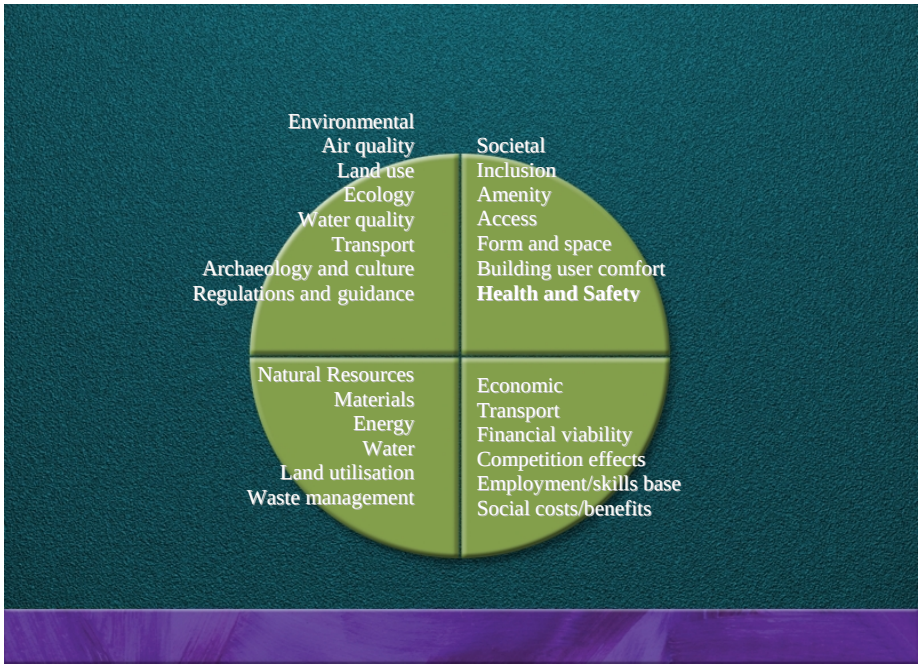

Fig. 4.

We have indicators for the whole system:

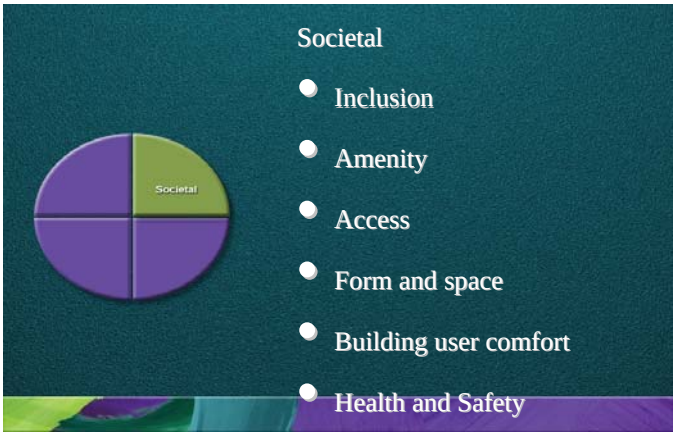

Fig. 5.

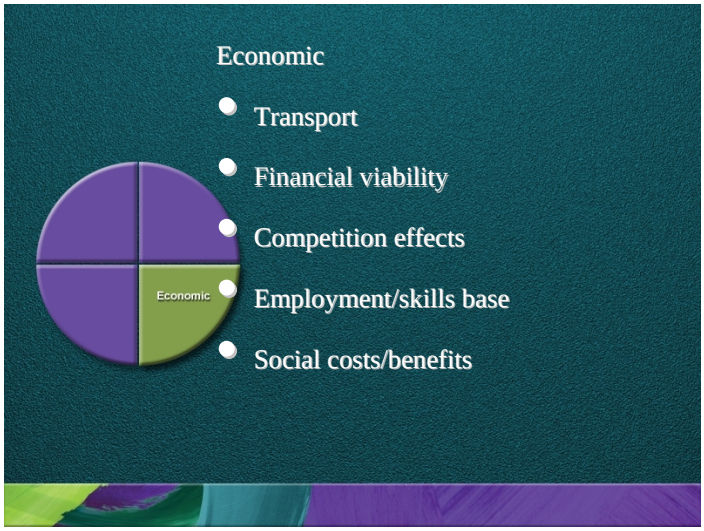

Fig. 6.

We do not have indicators for the political field, but we know that we are interested in a stable way with sustainable views.
Arup's healthy concepts were formed by the man who established the firm, Sir Ove Arup , philosopher and engineer:

THE ARUP LEGACY

What should our designs try to achieve? We must take a critical look at the brief, make it more comprehensive. We must look beyond the narrow object and ask ourselves: What will be the ecological consequences?
"*A design team which produces a total, balanced, efficient design can help to produce a better environment****"***
*"To strive for quality in only a part is almost useless if the whole is undistinguished****"***

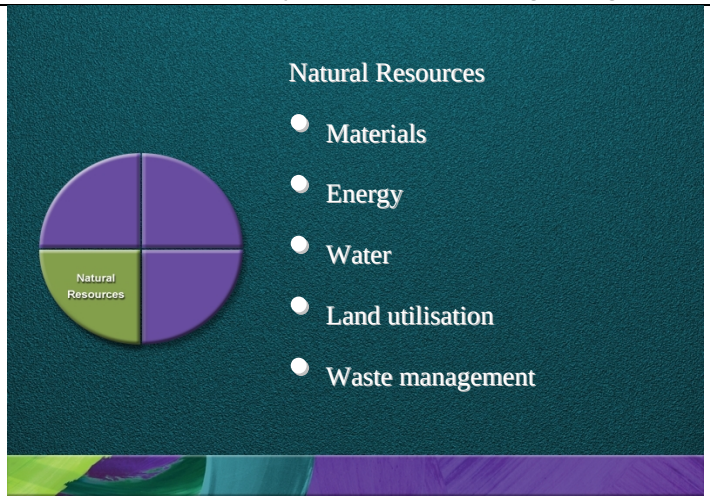

Fig. 7.

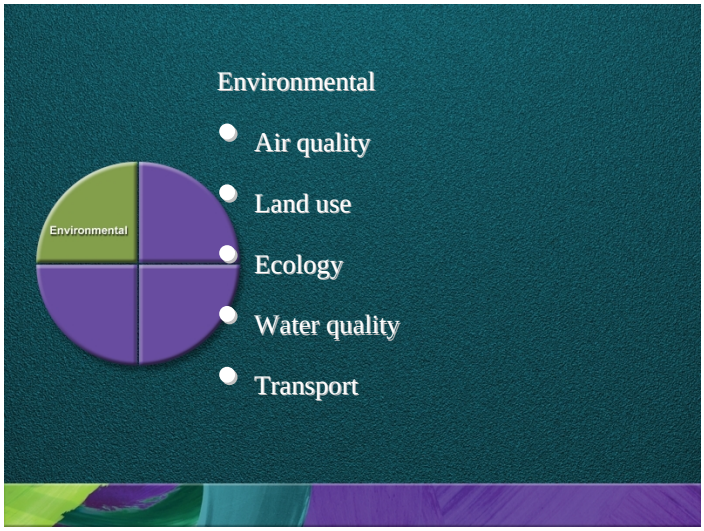

Fig. 8.

4. REFERENCES

[1]. Roulet C.-A., Ostra B., Foradini F., Cox Ch. - Designing healthy, comfortable and energy efficient buildings: lessons from enquiries within the European HOPE Project. CISBAT 2005

[2]. Roulet C.-A. - Sante et qualite de l'environnement interieur dans les batiments, Presses Politechniques et Universitaires Romandes, Lausanne, 2003

[3]. Bliuc I., Rotberg R., Dumitrescu L. - Simulation and performance analysis of hygrothermal behaviour of buildings in transient regime, Proceedings of the International Conference "PBE 2004: Performance Based Engineering for 21st Century", Ed. Cermi Iasi, 2004, ISBN 973-667-063-5, pag. 43-48

[4]. Bliuc I., Rotberg R. - The impact of some dwelling energy - efficiency raising measures on the inner ebvironnment quality. Evaluation methodology. CISBAT 2005